PULLOUT BEHAVIOR OF INCLINED ANCHORS IN REINFORCED COHESIVE SOIL UNDER STATIC AND CYCLIC LOAD

Thesis submitted by

ARUNASHIS MAJUMDER

DOCTOR OF PHILOSOPHY IN ENGINEERING

CIVIL ENGINEERING DEPARTMENT

FACULTY COUNCIL OF ENGINEERING & TECHNOLOGY

JADAVPUR UNIVERSITY

KOLKATA-700032, INDIA

2024

INDEX NO.: 186/17/E

1. **Title of the Thesis:**
   PULLOUT BEHAVIOR OF INCLINED ANCHORS IN REINFORCED COHESIVE SOIL UNDER STATIC AND CYCLIC LOAD

2. **Name, Designation and Institution of the Supervisors:**

(1) Prof. (Dr.) Sibapriya Mukherjee
Ex. Professor,
Department of Civil Engineering,
Jadavpur University

(2) Prof. (Dr.) Sumit Kumar Biswas,
Associate Professor,
Department of Civil Engineering,
Jadavpur University,
Kolkata-700032, India.

(3) Prof. (Dr.) Subhadeep Banerjee,
Professor,
Soil Dynamics Laboratory,
Geotechnical Engineering Division,
Department of Civil Engineering
Indian Institute of Technology Madras,
Chennai- 600036, India.

3. **List of Publications:**

a) Journal Papers

i) Majumder, A., Banerjee, S., Mukherjee, S., Ray, S., & Biswas, S. K. (2023). "A Numerical Study on the Pullout Behavior of Inclined Square Anchor Plates in Soft Clay Under Cyclic Loading". Indian Geotechnical Journal, pp-1-16. (ISSN-2277-3347)

b) Book Chapter

i) Majumder, A., Roy, R., Banerjee, S., Mukherjee, S., & Biswas, S. K. (2021). Pullout behavior of plate anchors in geotextile reinforced soft clay. In Proceedings of the Indian Geotechnical Conference 2019: IGC-2019 Volume V (pp. 285-296). Springer Singapore.

c) Conference Proceedings

i) Majumder, A., Roy, R., Banerjee, S., Mukherjee, S., & Kumar Biswas, S. (2023). "Pullout Characteristics of Inclined Square Plate Anchors in Geotextile Reinforced Soft Clay". National Seminar on Geotechnics-Recent Advancement in Research and Practice (GEO RARP), 12th -15th May, 2023, Organised by Kolkata Chapter of Indian Geotechnical Society.

ii) Majumder, A., Roy, R., Banerjee, S., Mukherjee, S., & Kumar Biswas, S. (2019) "Pullout Behavior of Plate Anchors Embedded in Geotextile Reinforced Soft Clay". National Seminar on Geotechnics for Infrastructure Development and Urbanisation (GEOIndus), 19th -21st December, 2019, Organised by Surat Chapter of Indian Geotechnical Society.

STATEMENT OF ORIGINALITY

I, Arunashis Majumder, registered on 06.08.2017 do hereby declare that this thesis entitled "**Pullout Behavior of Inclined Anchors in Reinforced Cohesive Soil Under Static and Cyclic Load**" contains literature survey and original research work done by the undersigned candidate as part of Doctoral studies.

All information in this thesis have been obtained and presented in accordance with existing academic rules and ethical conduct. I declare that, as required by these rules and conduct, I have fully cited and referred all materials and results that are not original to this work.

I also declare that I have checked this thesis as per the "Policy on Anti Plagiarism, Jadavpur University, 2019", and the level of similarity as checked by iThenticate software is below 10%.

Signature of Candidate: Arunashis Majumder

Date: 03.07.24

Certified by Supervisor(s): (Signature with date, seal)

1. Sibaprija Mukhopadhyay 03.07.24

Professor (Retd.)
CIVIL ENGINEERING DEPARTMENT
JADAVPUR UNIVERSITY
KOLKATA-32

2. Sunir Kr. Bhowmick 03/07/24

Associate Professor
Department of Civil Engineering
Jadavpur University
Kolkata-700 032

3. Subhadeep Banerjee 03.07.24

Dr. SUBHADEEP BANERJEE
Professor
Department of Civil Engineering
Indian Institute of Technology Madras
Chennai - 600 036, India

CERTIFICATE FROM THE SUPERVISOR(S)

This is to certify that the thesis entitled "**Pullout Behavior of Inclined Anchors in Reinforced Cohesive Soil Under Static and Cyclic Load**" submitted by **Shri Arunashis Majumder**, who got his name registered on 06.08.2017 for the award of Ph.D. (Engineering) degree of Jadavpur University is absolutely based upon his own work under the supervision of **Prof. (Dr.) Sibapriya Mukherjee, Prof. (Dr.) Sumit Kumar Biswas, and Prof. (Dr.) Subhadeep Banerjee,** that neither his thesis nor any part of the thesis has been submitted for any degree/ diploma or any other academic award anywhere before.

Sibapriya Mukherjee 03.07.24
Professor (Retd)
CIVIL ENGINEERING DEPARTMENT
JADAVPUR UNIVERSITY
KOLKATA-32

1. _____
Signature of the Supervisor
and date with Office Seal

Sumit Kr. Biswas 03/07/24
Associate Professor
Department of Civil Engineering
Jadavpur University
Kolkata-700 032

2. _____
Signature of the Supervisor
and date with Office Seal

Subhadeep Banerjee 03/07/24

3. _____
Signature of the Supervisor
and date with Office Seal

SUBHADEEP BANERJEE
Professor
Department of Civil Engineering
Indian Institute of Technology Madras
Chennai - 600 036, India

ACKNOWLEDGEMENT

It is with great pleasure and a profound sense of privilege that I express my heartfelt gratitude to my research supervisors, Prof. Sibapriya Mukherjee, Prof. Sumit Kumar Biswas and Prof. Subhadeep Banerjee. Their unwavering inspiration and support were pivotal to the completion of this thesis. I am deeply grateful for their patience, detailed and constructive feedback, continuous encouragement, and invaluable guidance throughout my research journey.

I would like to offer thanks to Prof. Partha Bhattacharya (Present HOD) of Civil Engineering Department, Jadavpur University for his valuable support and cooperation in my research work.

I would like to express my gratitude to Prof. Ramendu Bikas Sahu, Prof. Gupinath Bhandari, Prof. Pritam Aitch, Prof. Narayan Roy, Prof. Arghadeep Biswas and Prof. Obaidur Rahaman of Geotechnical Engineering Division of Civil Engineering Department, Jadavpur University for their insightful suggestions and valuable advice. I also wish to express my immense gratitude to all faculty members, staff members, and research colleagues of Civil Engineering Department, Jadavpur University for their constant encouragement and cooperation.

I would like to extend my sincere thanks to Shri. Rabin Paul, Shri Apurba Banerjee and Shri. Ranjit Kushari of Soil Mechanics Laboratory for their support to perform laboratory tests.

I would like to thank Ratul Roy, Sushovan Ray, Zakirul Biswas, Azfar Hossain for their unwavering assistance, support, and encouragement throughout the work.

I would like to express my gratitude to my sister, Ms. Anindita Majumder, for her continuous encouragement and support throughout my entire thesis work.

I would like to express my sincere gratitude to my grandmother, Ms. Bharati Bose for her encouragement and motivation.

Furthermore, I am immensely grateful to Mr. Rajesh Nandi, Faculty of the Civil Engineering Department, Narula Institute of Technology, Kolkata, for his unwavering encouragement and support during times of need.

I would like to express my deepest gratitude to my parents, Mr. Ashis Majumder and Mrs. Kanika Majumder. They have stood by me through every high and low, sharing my joys and also comforting me in moments of frustration. Their boundless love and understanding have been instrumental in my success.

Place: Jadavpur University

Arunashis Majumder
Arunashis Majumder

DEDICATED TO

MY BELOVED PARENTS

ABSTRACT

Some structures, including tall buildings, towers, underground reservoirs, and offshore or waterfront structures, are subjected to uplift loads. These loads arise from overturning moments caused by lateral forces such as wave action, wind, and earthquakes. Under these conditions, both tensile and compressive reactions occur on two opposite sides at the foundation level. Therefore, anchors must be designed to resist uplift forces effectively. Plate anchors are utilized in both offshore and onshore structures to counteract such forces.

This study aims to determine the ultimate uplift capacity of model plate anchors measuring 25 mm × 25 mm, 50 mm × 50 mm and 75 mm × 75 mm in both reinforced and unreinforced soil bed with embedment ratios of 1, 2, and 3 and anchor inclination angles 30°, 45°, and 60° with vertical under static and cyclic loading. The soil bed has been made of locally available clay and the anchors are of mild steel. The geotextile layer has been placed as reinforcement, at a distance of 0.25 times the embedment depth from the bottom of the anchor and extended up to four times the anchor width. The properties of clay, mild steel and geotextile have been obtained by conducting prior testing appropriately. Numerical analyses have been performed on models of inclined anchors with finite element method using ABAQUS, for both static and cyclic loading. To support the numerical study, a few model anchor tests have been conducted by applying monotonic load with the help of a pulley arrangement, with displacements recorded using a Linear Variable Differential Transformer (LVDT). The experimental results have closely agreed with the numerical ones.

The ultimate pullout capacity under of inclined anchors has been found to increase significantly with the increase in the dimensions of the plate, the embedment ratio, and also the angle of inclination of the anchor with vertical. It has also been found that for inclined anchor that pullout load capacity increases with the application of geotextile in soft clay soil when all other parameters remain same. Finally, a prediction model for ultimate pullout capacity of anchors in unreinforced and reinforced soil has also been proposed by carrying out regression analysis with the help of machine learning on the data obtained from numerical simulations.

Keywords: Inclined anchor, Geotextile reinforcement, Cyclic loading, Reinforced soil bed, Finite element method.

INDEX

LIST OF TABLES

LIST OF FIGURES

LIST OF ABBREVIATION

CLR	Cyclic Load Ratio
FE	Finite Element
FEA	Finite Element Analysis
GFR	Grid Fixed Reinforcement
LL	Liquid Limit
LVDT	Linear Variable Differential Transformer
MAE	Mean Absolute Error
MAPE	Mean Absolute Percentage Error
ME	Max Error
MEMS	Micro Electrical Mechanical System
MSE	Mean Squared Error
NC	Normally Consolidated
PL	Plastic Limit
RE	Reinforced
SNAC	Solid Nonlinear Analysis Code
UR	Unreinforced

LIST OF SYMBOLS

3D	Three Dimensional
2D	Two Dimensional
A	Area of Plate Anchor
B	Width of Plate Anchor
C_u	Undrained Cohesion
E	Young's Modulus
F	Pullout Load in Unreinforced Soil Bed
F_c	Uplift Capacity Factor
F_g	Uplift Factor
F_r	Pullout Load in Unreinforced Soil Bed
F_γ	Uplift Capacity Factor
H	Embedment Depth of Anchor
I_P	Plasticity Index
K	Coefficient of Earth Pressure
K_P	Passive Earth Pressure Coefficient
N_C	Limiting Capacity Factor
N_{CO}	Pullout Capacity Factor
Q_u	Maximum Uplift Capacity
S	Shape Factor
W	Weight of Soil Above Anchor
W_L	Liquid Limit
W_P	Plastic Limit
R^2	Coefficient of Regression

LATIN

β	Angle of Inclination of Plate Anchor
γ_{anchor}	Density of Anchor Plate Material
γ_d	Maximum Dry Density
$\gamma_{Geotextile}$	Density of Geotextile Material
γ_{Soil}	Density of Soil
∅	Angle of Internal Friction

μ	Poisson's Ratio

UNIT

Hz	Hertz
kN	Kilo Newton
kg	Kilogram
MPa	Mega Pascal
mm	Millimeter
N	Newton

CHAPTER 1
INTRODUCTION

1.1 OVERVIEW

This chapter brings out the background of the study, depicts the present study itself, and brings out the organization of the thesis.

1.2 BACKGROUND

Foundation system of some structures, such as, tall buildings and towers, underground reservoirs, offshore or waterfront structures experience uplift load. This occurs due to overturning moments developed due to lateral loads induced by wave action, wind and/or earthquake. Under such circumstances, both of tension and compression reactions take place at the foundation level. This element, that is, the anchor, needs to be designed in such a way that they can resist uplift. A comparison of anchor with plant roots in Nature may be drawn in this respect. The roots basically act as anchors and acts against the action of wind. When the roots cannot resist the action of overturning, the trees or plants fall down.

In other words, the anchors are a thin system of foundation that is especially made to withstand any force that can pull a structure out or cause it to overturn. They are used to transfer uplifting forces from an anchor foundation to the soil. The resistance to pullout is developed from the shear strength of the surrounding soil and dead weight of the anchor itself.

In practice there are some cases where the anchor has to be placed with some inclinations. While inclined anchors are more suited for resisting overturning moments, both horizontal and vertical anchors can withstand pullout forces (Ghaly and Clemence, 1998). The literature has stated that, in comparison to horizontal anchors, the pullout capability of anchors increases with inclination.

Examples of some of the various types of anchors used in geotechnical engineering: 1. Grout system 2. Soil hook system, 3. Plate system. 4. Helical system. Fig 1.1 to 1.4 represents different types of anchors.

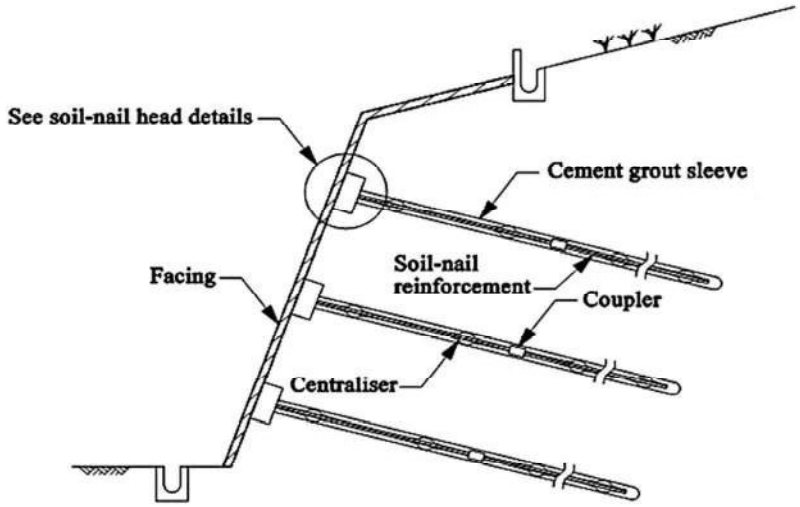

Fig. 1.1: Grouted Anchor (After Niroumand et al., 2010)

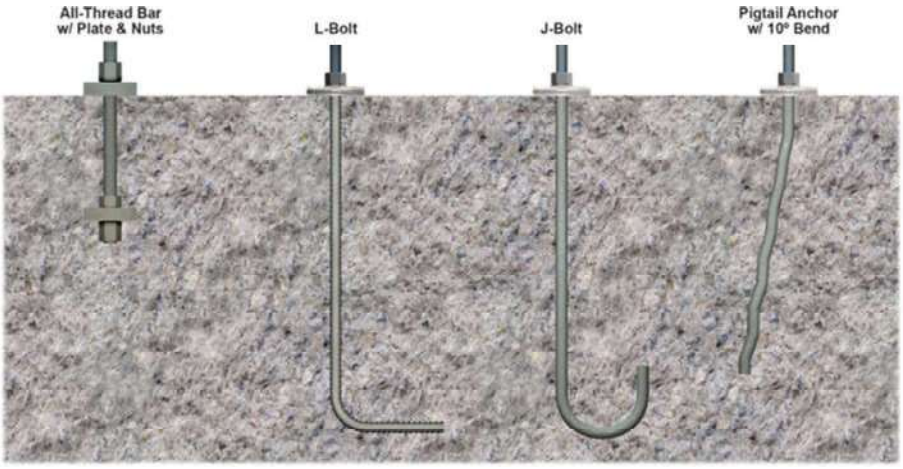

Fig. 1.2: Soil Hook system (After Williams Form Engineering Corp)

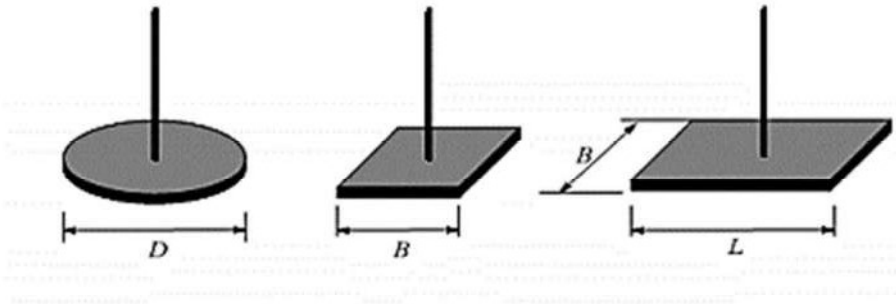

Fig. 1.3: Plate Anchors (After Niroumand et al., 2010)

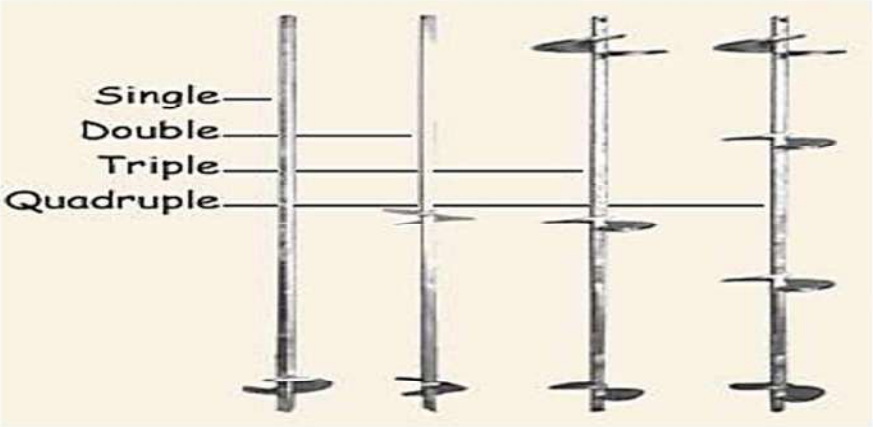

Fig. 1.4: Helical Anchors (After Niroumand et al., 2012)

Grout System Anchors are used to stabilize slopes, retaining walls, and deep excavations by injecting grout into drilled holes, creating a strong bond with the surrounding soil or rock. They are also ideal for providing additional support to foundations and counteracting uplift pressures in waterlogged areas.

Soil Hook System Anchors are suitable for reinforcing loose or unstable soils, particularly in slope stabilization projects. They are commonly used to secure temporary excavation walls and shallow foundation systems where quick installation is required.

Plate System Anchors are applied in retaining walls and earth retention systems, utilizing large flat plates to distribute loads over a wider area. They are effective for stabilizing shallow foundations and structures on soft soils by enhancing load-bearing capacity.

Helical System Anchors are ideal for deep foundations, especially in soft or expansive soils, where screw-like helical plates anchor deep into stable layers. These anchors are commonly used for wind turbines, communication towers, and structures that require resistance to both uplift and lateral loads.

The design of soil anchors must consider both compressive and tensile criteria for effective response of foundation, with a greater emphasis on the tensile criterion. To meet these requirements, anchor plates are commonly used due to their simplicity compared to other anchor types. These plates can be cast in place through excavation. Installing anchor plates in non-cohesive soils is generally easier than in cohesive soils. As the use of cast-in-place anchor plates

to counteract uplift forces becomes more widespread, the need for developing a systematic procedure for design of anchor plate against uplifting forces is essential.

The anchors are likely to be subjected to cyclic loading due to action of wind, wave action and earthquake.

In some situations, it may happen to adopt some soil reinforcements, say, in the form of geotextiles or geocell to increase the soil strength to resist the required uplift load **(Banerjee and Nagaraju, 2017).**

With all these aspects in view, an attempt has been made to carry out the present study as detailed below:

1.3 THE PRESENT STUDY

The current investigation has been done to get an insight on the pull-out behaviour of inclined anchors (at different inclinations of square anchor plates with vertical) in soft clay under both static and cyclic loading. The study has been done for different sizes of anchors, different embedment depths under both static and cyclic loading (at stipulated frequencies and amplitudes). The objective and scope of work in respect of the present study have been reached after identifying the research gap with a thorough literature review presented in Chapter2.

1.4 ORGANISATION OF THE THESIS

The thesis has been organized with eight different chapters in the following order: -

Chapter 1: Introduction presents the background and brief description of the present study.

Chapter 2: Literature Review describes in brief the works of the past researches in the context of the present research in chronological order. The works have been divided in different subsections of the chapter namely- Anchor in unreinforced soil under (i) static load and (ii) dynamic load and anchor in reinforced soil under (i) static load and (ii) dynamic load. This chapter also brings out objectives and scope of the present research.

Chapter 3: Materials and Methods describe property of materials ((soil, geotextile and anchor plate) used for the study. This chapter also describes the methodology used for the numerical and experimental studies.

Chapter 4: Numerical study depicts the procedure, input and output and finally presents the results obtained.

Chapter 5: Experimental Study focuses on limited number of model anchor test in different (unreinforced and reinforced) soil bed.

Chapter 6: Response of inclined anchors presents observations and analyses of the results of numerical study and compares the results of the experimental study. It also presents regression analysis based on machine learning using the numerical data available from this study. This has been executed in order to generate a model that can assess the pullout capacity of the inclined anchors.

Chapter 7: Summary, Conclusions, Limitation and Future Scope of Study summarizes the present study and draws conclusions from it, and also suggests some guidelines for further research.

CHAPTER 2

LITERATURE REVIEW

2.1 OVERVIEW:

The behaviour of horizontal, vertical and inclined anchors embedded in different types of soil has been investigated in details during the previous few decades. These investigations have encompassed experimental studies as well as numerical and analytical approaches. However, most of these studies have concentrated on analysing the behaviour of vertical and horizontal anchor in different soils. This chapter aims to provide a comprehensive review of the available literature about the present topic. The research on the behavior of vertical, horizontal, and inclined anchors embedded in various soils under various loading conditions will be sequentially summarized in the subsequent sections, with an emphasis on the key developments in recent times. Furthermore, this chapter will address at the end, the rationale behind the current investigation, as derived from the insights gathered from the literature review.

2.2 ANCHORS IN UNREINFORCED SOIL

2.2.1 Under Static Load:

Bhattacharya and Kumar (2016) conducted some investigations to study the uplift capacity of strip and circular plate anchors horizontally embedded in a layered sandy medium using finite-element limit analysis combined with linear programming. The soil medium below the anchor plate was composed of loose sand and considered different combinations of internal friction angles for the sand layers above the anchor. The study found that pullout resistance increased steadily with the relative thickness of the dense sand layer (H_{dense}) compared to the embedment depth (H) of the anchor plate. For a given embedment ratio (H/B), uplift resistance was higher when the dense sand layer was placed directly above the plate rather than closer to the ground surface. Additionally, circular anchors consistently had higher pullout capacity factors than strip anchors. An increase in the embedment ratio resulted in a corresponding rise in pullout resistance. It was also noted that an increase in the ratio of the unit weights of dense to loose sands caused a slight decrease in the uplift factor (F_g) when the dense sand layer was above the anchor plate. The numerical results from the study estimated slightly higher uplift resistance compared to experimental data available in the literature.

In their detailed investigation, Bhattacharya and Kumar used various coefficients and parameters to linearize the yield function and compute the ultimate pullout pressure at failure. They validated their numerical results by comparing them with theoretical and experimental data available in the literature. This comprehensive approach provided new insights into the behavior of anchors in layered sandy mediums and highlighted the importance of considering the relative positioning of dense sand layers to optimize uplift resistance

Singh and Mistri (2011) conducted an extensive study to evaluate the load capacity of horizontal and inclined plate anchors in sandy soils. The researchers reviewed various experimental, theoretical, and numerical approaches for estimating the load capacity of these anchors. They performed a detailed parametric analysis by varying embedment ratios for horizontal anchors and inclination angles for inclined plate anchors. To compare the load capacities of horizontal and inclined plate anchors, Singh and Mistri conducted calculations for a strip anchor of 2 meters width and unit length, varying the embedment ratio for horizontal anchors and the inclination angle for inclined anchors.

Experimental and theoretical studies showed that the load capacities for horizontal plate anchors in loose and medium dense sands are highest according to Balla's correlation, whereas Andreadis and Harvey provided the lowest values. For dense sand, Hanna et al.'s relationship yielded the maximum values. In loose sand at an embedment ratio of 3, experimental values of vertical uplift capacities reached up to 4000 kN, surpassing theoretical values which did not exceed 2500 kN. However, for medium dense and dense sands, both experimental and theoretical values were comparable. Inclined load capacity for anchors in loose sand ranged from 500 kN to 1000 kN for vertical orientation, with the values increasing exponentially beyond 40° inclination angle. A similar trend was observed for medium dense and dense sands.

Overall, the study provided a comprehensive analysis of the load capacity of horizontal and inclined plate anchors in sandy soils, highlighting the variations in capacity based on anchor orientation, embedment depth, and soil properties. Their findings were crucial for designing effective anchoring systems in various engineering applications.

Mistri and Singh (2011) conducted a study using PLAXIS to evaluate the load-carrying capacity of rectangular anchor plates in a horizontal orientation with different embedment ratios in clay. A parametric study was conducted to compare the load-carrying capacity of these anchors in clay

through finite element modelling using PLAXIS. In the analysis, an elastic-plastic Mohr-Coulomb model and 15-noded triangular elements were used for the soil. The results were compared with those obtained from established methods, showing good agreement for shallow anchors, while some divergence was observed for deeper anchors. It was proposed that the rate of increase in uplift capacity changed at the depth of transition where the behavior of the surface anchor shifted to that of a deep anchor. However, this transitional behavior was not distinctly observed in clay with increased shear strength. With increased soil consistency, the variation in the final uplift capacity also increased.

Displacement contours of shallow and deep plate anchors in soft, medium, and stiff clays, as demonstrated in Fig. 2.1 and observed in tests by Mistri and Singh, clearly showed the pattern of anchor/soil interaction during the uplift of the anchor plate, indicating that deeper anchors required more force to mobilize the plate.

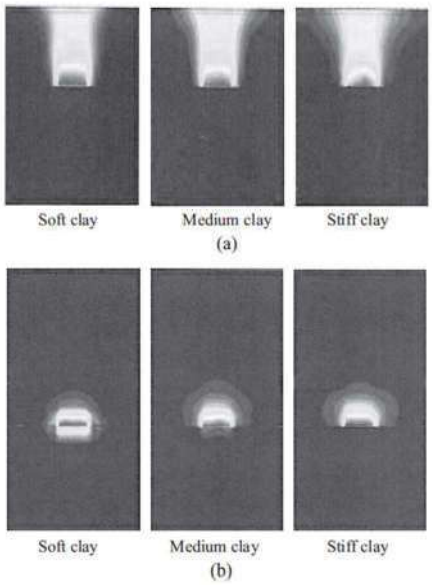

Fig. 2.1: Displacement contours of (a) shallow plate anchors in clay; (b) deep plate anchors in clay (After Mistri and Singh)

Yu et al. (2011) in their numerical study on plate anchor stability in clay, analyzed the pullout capacity of strip plate anchors in uniform and normally consolidated (NC) clays. Various factors were accounted for in the study, including anchor inclination, anchor embedment ratios, clay non-homogeneity and clay self-weight. Results were presented in both graphical and numerical forms to aid practical design solutions, and a systematic design procedure was proposed. Key findings from the study indicated that anchor inclination significantly affected the pullout capacity factor.

In weightless clay, the vertical anchor had the highest pullout capacity factor (N_{co}), while the horizontal anchor had the lowest at a given embedment ratio. Conversely, when the soil overburden stress ratio ($\gamma H/s_u h$) was sufficiently large, the horizontal anchor had the highest pullout capacity factor, and the vertical anchor had the lowest.

The assumption of superimposing the overburden pressure for vented plate anchors in both NC and uniform clays was also validated by the study. The ultimate pullout capacity factor (N_c) was observed to decrease with increasing embedment ratio and increasing anchor inclination until reaching a maximum value (N_c, max). The effect of anchor inclination on N_c was more pronounced in NC clay compared to uniform clay.

For attached anchors, the pullout capacity factors were the same as those for vented anchors with a large soil overburden stress ratio. The degree of soil non-homogeneity had a linear negative effect on anchor pullout capacity in weightless clay, with up to a 50% reduction for horizontal anchors and a 30% reduction for vertical anchors. Moreover, for horizontal anchors, increasing the degree of clay non-homogeneity increased the ultimate pullout capacity factor for shallow anchors ($H/B < 1.5$) but decreased it for deeper anchors ($H/B > 2$).

Wang et al. (2010) examined plate anchor capability during vertical pullout using three-dimensional large deformation finite-element calculations. Model test data, plastic limit solutions and small strain FE results were used to compare the large deformation results for rectangular, circular and strip anchors. Continuous pullout of plate anchors was simulated. The impacts of anchor roughness, aspect ratio, soil characteristics, and overburden pressure were studied. The results showed that the roughness of the anchor had little bearing on its performance. After tensile stresses are created, the soil beneath the anchor base separates from the anchor at a specific embedment depth close to the mud line. It was found that the ratio of separation depth to anchor width was independent of the initial anchor embedment depth and the increment was linear with the ratio of soil undrained shear strength to the product of anchor width and soil effective unit weight. The maximum uplift capacity of rectangular plate anchors was expressed as follows in the study:

$$\mathbf{Q_U = A\, C_U\, N_C} \quad \text{..... (2.1)}$$

$$\mathbf{N_C = N_{C0} + (\Upsilon H/C_U)} \quad \text{..... (2.2)}$$

Where Q_U =maximum uplift capacity H= pre-embedded depth of the anchor; A= area of plane N_c=limiting capacity factor for deeply embedded anchors and N_{co}=anchor capacity factor in weightless soil.

Khatri and Kumar (2009) investigated the vertical uplift resistance of horizontally placed circular plate anchors in an undrained setting, within a clay layer where cohesiveness increased linearly with depth. The axisymmetric static limit analysis framework, along with finite elements, was used for the analysis. The impact of gradually increasing cohesiveness on the vertical uplift resistance of horizontally embedded circular plate anchors in clay was examined. The axisymmetric static limit analysis framework for foundations immersed in clays under undrained conditions was used. For a variety of embedment ratios and rates of increase in soil cohesiveness with depth, the uplift factor (F_c) was found. Assuming that there was no uplift resistance on the lower surface of the anchor plate, the magnitude of F_c was calculated under immediate breakaway conditions. Failure patterns from various scenarios were also looked at. The impact of the roughness of the anchor plate on pullout resistance was examined. The outcomes of this investigation were closely compared to those that were previously available in the literature. Furthermore, to validate the proposed static limit analysis formulation, the analysis was performed on two additional simple problems: the assessment of stability numbers for vertical circular excavations and the measurement of collapse pressure magnitude for vertical cylinders under compression. The magnitude of Fc increased continuously with an increase in H/B up to a certain critical embedment ratio (H_{cr}/B), beyond which F_c became almost constant. For H/B > H_{cr}/B, the magnitude of F_c remained unchanged with respect to changes in the value of m, which defined the rate of cohesion increase with soil depth. The suggested axisymmetric formulation offered a satisfactory comparison for issues related to determining stability numbers for circular vertical excavations and the collapse pressure magnitude for a vertical circular cylinder under compression.

Merifield et al. (2005) assessed the stability of inclined strip anchors in undrained clay using displacement finite-element analysis and numerical limit analysis. In this study both lower and upper bound limit analysis techniques were utilized, as well as displacement finite-element analysis, to evaluate anchor stability. Additionally, the Solid Nonlinear Analysis Code (SNAC) was employed, which improved the accuracy of predicting collapse loads and mitigated the locking problems. The problem considered inclined anchors placed at angles of 22.5°, 45°, and

67.5° to the vertical in purely cohesive soil. The true value of the breakout factor was found to be within a ±7% error bound for these inclinations in weightless soil using the lower and upper bound limit theorems. The displacement finite-element (SNAC) results generally fell within ±5% of the upper bound solutions. The study examined how anchor inclination influences pullout capacity and proposed a straightforward empirical equation that estimates collapse loads with an average accuracy of ±5%. The ultimate anchor capacity showed a linear increase with overburden pressure until reaching a threshold, indicating a shift from a nonlocalized to a localized failure mechanism. For deep anchors, the average limiting breakout factor (N_c*) was found to be between 10.8 (lower bound) and 11.96 (upper bound).

Key findings indicated that the ultimate anchor capacity increased linearly with overburden pressure up to a certain limit, reflecting a transition from nonlocalized to localized failure mechanisms. The research also demonstrated that upper bound velocity diagrams and SNAC displacement plots could effectively depict the failure mechanisms of inclined anchors. These diagrams helped visualize the expected patterns of soil movement around the anchors under load Furthermore, the study proposed an empirical equation for predicting the collapse load of inclined anchors, which provided estimates within ±5% of the actual values. This empirical relationship was significant for practical design applications, offering a reliable method for engineers to estimate the capacity of inclined anchors based on various geometric and soil parameters.

Goel et al. (2005) examined the breakout resistance of inclined plate anchors in sandy soil by utilizing a limit equilibrium method. The breakout resistance was obtained for various soil friction angles, considering different anchor inclinations and relative depth ratios. The study considered an inclined plate of diameter B embedded at depth D in a soil medium, inclined at an angle i to the vertical. For evaluating the resistance, an elemental length of anchor cable was considered. The lateral pressure and normal components of pressure acting on different sections of the anchor were calculated. The uplift resistance was evaluated using these pressures, considering an elliptical distribution along the anchor's horizontal section. The study observed that as the anchor inclination increased, the breakout factor consistently increased. When comparing the predicted breakout resistance values from this analysis with experimental data from other researchers, there was reasonably good agreement. The suggested breakout factor was:

$$\mathbf{N_q = \frac{4D}{\pi B} K \tan\Phi I_i \, Sec^2 i} \quad \text{..... (2.3)}$$

where N_q =break out factor in sand, K = coefficient of earth pressure, I_i = coefficient of inclination, i = inclination angle of plate anchor, Φ= angle of shearing resistance of the soil. Theoretical results showed that the coefficient I_i increased with the inclination angle of the anchor, peaking at 35-45 degrees before decreasing to zero at 90 degrees. Higher values of the lateral earth pressure coefficient (K) had minimal effect on the coefficient Ii. The breakout factor Nq increased continuously with anchor inclination and with the relative depth ratio (D/B), being higher for greater soil friction angles. The proposed model provided a reliable prediction of ultimate breakout capacity, validated against various experimental and field test results. The necessity of using a factor of safety, ranging from 2.5 to 4, was emphasized to account for uncertainties in soil properties and changes due to anchor installation.

Merifield et al. (2003) used a novel three-dimensional numerical method based on the finite element approach of the lower bound analysis theorem to compute the maximum pull-out strength of various anchor shapes in clay. From the analysis, an estimate of the lower limit of anchor failure factor (N_c) was obtained for square, circular and rectangular anchors, as shown in Fig. 2.2 to 2.4. The estimated capacities were encouraging compared to the results of published and available laboratory tests. The study discovered that the anchoring capacity of strip anchor increased as the overburden pressure reached a critical point, indicating a shift from shallow to deep anchoring behavior. In addition, according to them, at a given depth of anchorage, an anchor may behave as shallow or deep, depending on the dimensionless overload ratio H/C_u. From their analysis, simple parametric equations for avoidance factors, as indicated below, were suggested to determine the capacity of square and circular anchors in a homogeneous soil profile for different anchoring depths.

$$\mathbf{N_{co} = S\,[2.56\ \ln\,(2\ H/B)]} \quad \ldots\ldots\ldots\ldots\ldots\ldots\ldots\ldots\ldots\ldots\ldots\ldots\ldots\ldots \mathbf{(2.4)}$$

Where, N_{co}= break out factor

S= shape factor for square or circular anchor

H/B= embedment ratio

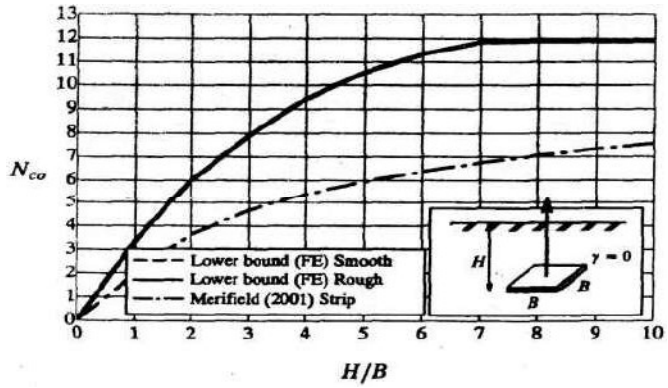

Fig. 2.2: Breakout factor for square anchor in clay (After Merifield et al. 2003)

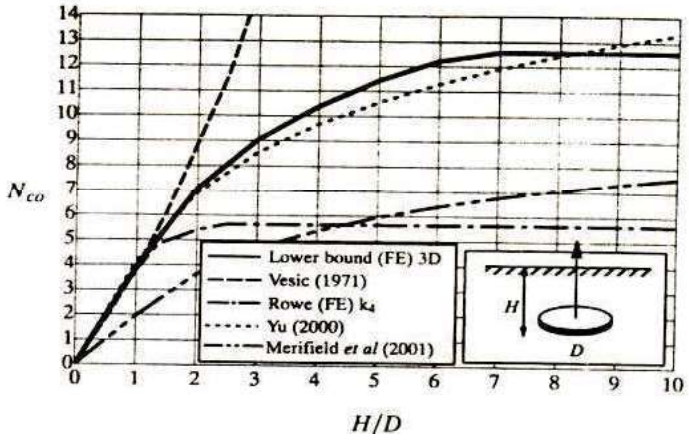

Fig. 2.3: Breakout factor for square anchor in clay (After Merifield et al. 2003)

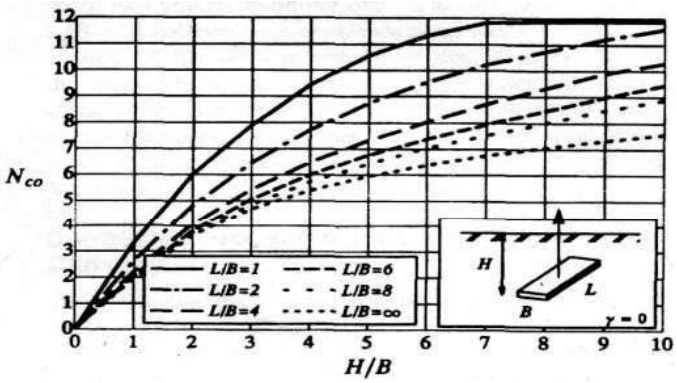

Fig. 2.4: Breakout factor for square anchor in clay (After Merifield et al. 2003)

Ilamparuthi et al. (2002) studied how circular plate anchors with diameters up to 400 mm behaved when embedded in loose, medium-dense, and dense dry sand, focusing particularly on

their uplift characteristics. The study found that uplift capacity was significantly influenced by anchor diameter, embedment ratio, and sand density.

A 100 kN capacity loading frame was specifically designed for the investigation, comprising a setup with two portal frames connected by steel I sections. Pullout load was applied through a loading yoke consisting of steel plates connected by threaded rods. Failure mechanism tests on half-cut models were conducted in a tank with a perspex front face to allow observation of rupture surfaces, while full-shaped model tests were conducted in a rigid cylindrical steel tank.

Model anchors were fabricated from 6 mm thick mild steel plate, with half-cut anchors used for some tests and circular plate anchors of varying diameters used in others. Uniformly graded medium Palar River sand was employed, with sand beds prepared through controlled pouring and tamping techniques to achieve reproducible densities. Friction angles for the sand at different densities were measured using direct shear tests.

Instrumentation included a 50 kN capacity strain gauge type load cell for recording pullout load and a linear variable displacement transducer (LVDT) for measuring vertical displacement. Thirteen tests on half-cut models and 98 tests on full-shaped models were conducted, revealing that uplift capacity depended strongly on anchor diameter, embedment ratio, and sand density. Shallow anchors exhibited uplifted frustums of soil, while deep anchors formed balloon-shaped rupture zones.

The load–displacement behaviour was observed to be three-phase for shallow anchors and two-phase for deep anchors. Different methods for determining the critical embedment ratio were considered, proposing values of 4.8, 5.9, and 6.8 for loose, medium-dense, and dense sand, respectively. These findings were supported by empirical equations that produced breakout factors similar to those from many published laboratory and field studies. In testing on shallow half-cut models, a smoothly curved rupture surface appeared from the top edge of the anchor to the sand surface at about $\varphi/2$ to the vertical, where φ represents the angle of shearing resistance. For deeper anchors, a balloon-shaped rupture surface formed at 0.8φ to the vertical within the sand bed.

Merifield et al. (2001) investigated the stability of horizontal and vertical strip anchors in undrained clay. By employing two numerical approaches based on finite element formulations of the upper limit and lower limit analysis theorems, the ultimate pullout capacity was obtained. Assuming a stiff plastic clay model with a Tresca Yield criterion, these formulations generated

linear programming problems in accordance with established methodologies. By obtaining estimates of the upper and lower limits of the shrinkage capacity, the actual tensile strength was bracketed from above and below. The results obtained for both homogeneous and inhomogeneous clay were presented in terms of avoidance factors, as shown Fig.2.5 and Fig.2.6 for horizontal and vertical bands and a single parametric equation for avoidance factors for horizontal and vertical anchors were suggested.

The bound solutions were compared with existing numerical solutions as well as with published results from small laboratory tests. Based on their analysis they concluded

- The related solutions were able to predict the exact anchorage capacity within ± 5% and compare well with the results of small-scale laboratory tests.
- Existing digital solutions might differ by up to ± 25% with bonded solutions in homogeneous soil, with a slight reduction of the error for homogeneous soil whose resistance increases with depth. For a H / B integration rate> 4, the existing solutions were usually the ones that make the biggest mistake.
- It was found that anchor roughness affected the ultimate capacity of vertical anchors as it increased, while the ultimate capacity of horizontal anchors was less affected.

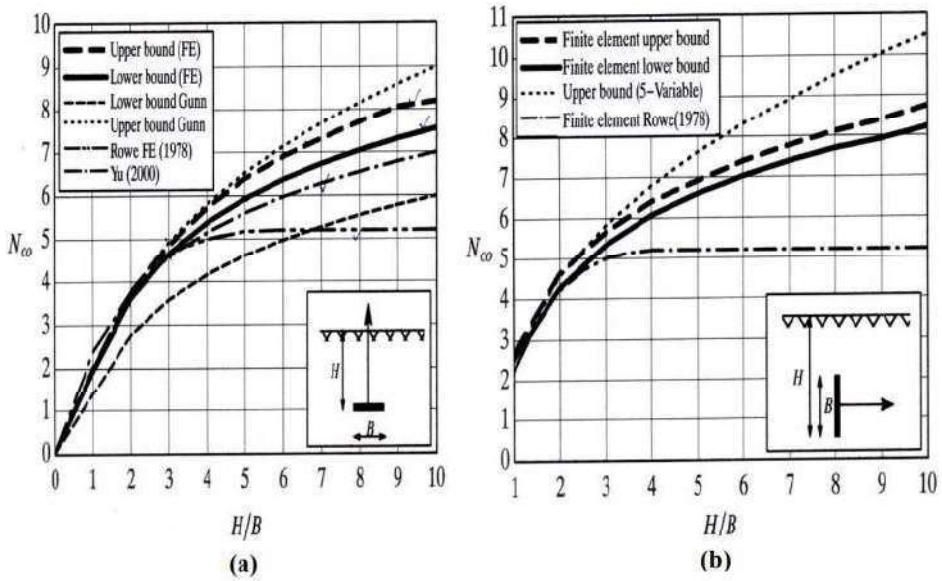

Fig. 2.5: Break out factors for horizontal and vertical anchors in homogeneous soil (After Merifield et al. 2001)

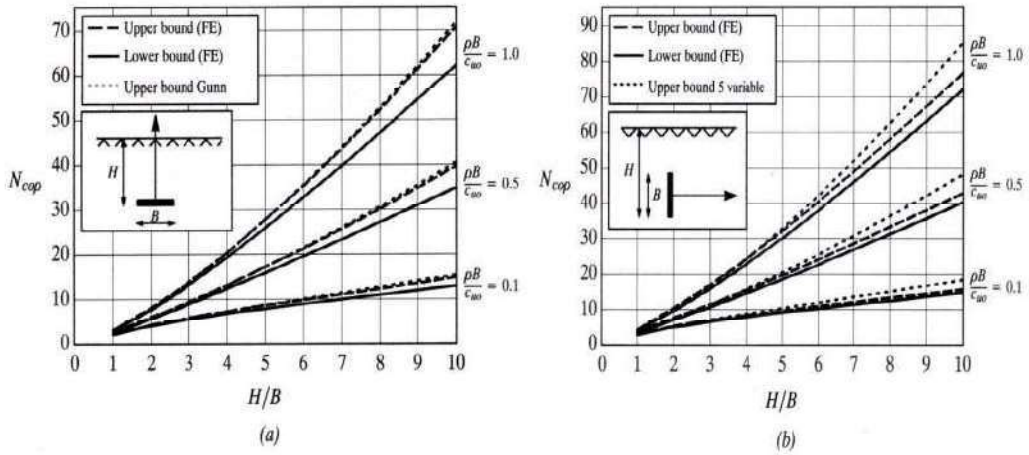

Fig. 2.6: Break out factors for horizontal and vertical anchors in non-homogeneous soil after (Merifield et al. 2001)

Ghalay and Clemance (1998) presented experimental and theoretical studies on the pullout performance of inclined helical screw anchors. The anchors used in the experimental program were positioned in loose, medium and dense sands with angles of 15, 30, and 45 degrees relative to the vertical. Specific tests were performed on anchors set into coloured-layered sands at an angle of 45° and 60° in order to identify the rupture surface and failure mechanism. These studies confirmed that the rupture surface was asymmetrical and extremely complicated; yet, it could be represented by logarithmic spiral curve segments. In order to correlate the pullout capacities of inclined and vertical anchors set to the same depth in identical sand conditions, the notion of a conjugate anchor and auxiliary rupture surface was developed and implemented.

Helical screw anchors were inserted into the ground by rotating their shafts with torque. This method applied similarly to both vertical and inclined anchors. The helical shape of the anchors facilitated their self-propulsion and created drag forces that aided in soil penetration. Occasionally, a downward force on the shaft was necessary in shallow installations to compensate for insufficient surcharge and ensure adequate soil contact. For inclined anchors, this force needed to be applied axially to maintain their direction and minimize soil disruption. Inclined helical screw anchors were preferred for their straightforward installation using light equipment and ability to maintain the desired angle. While both vertical and inclined anchors could resist pullout forces and overturning moments, inclined anchors were particularly effective against overturning moments.

The pullout capacity of inclined helical screw anchors was influenced by several factors: installation depth, relative depth ratio, sand characteristics, and the angle of inclination. Representation of the rupture surface of these anchors posed challenges due to its intricate geometry. The boundaries of the rupture surface consisted of segments resembling logarithmic spirals, with varying poles around its perimeter. In shallow anchors embedded in sand, the rupture surface extended to the ground surface, while in deeper anchors, it remained localized. The pullout force caused the rupture surface to deform asymmetrically, elongating towards the horizontal pull direction and contracting oppositely. For an anchor inclined at an angle α, the axis linking the anchor plate and sand surface formed an angle of α/3 with the vertical, passing through the point of maximum sand surface deformation, which was the centre of the circle of deformation. Theoretical development included a coefficient of embedment depth, derived from relative depth and inclination angle, aiding in calculating pullout capacity. Comparative analysis of theoretical, experimental, and field results demonstrated consistent findings, validating the proposed theory.

Ghaly (1997) examined the load-displacement behavior of vertical anchor plates that are horizontally loaded and implanted in sands, based on 128 published field and laboratory studies. Both a geometry factor and a pullout capacity factor were established. These dimensionless factors included all of the variables that had significant effects on how vertical anchor plates behaved when they were loaded horizontally. Several attempts were made to plot the gathered data so that an overall pattern could be seen. The final horizontal pull-out resistance of vertical anchor plates was predicted using this data in a generalized manner based on the influencing factors. The following expressions were proposed for ultimate load capacity:

For circular anchors:

$$\left(\frac{Q_u}{\gamma AH}\right)\tan\emptyset = 5.5(H^2/A)^{0.31} \quad \text{(2.5)}$$

For square and rectangular anchors:

$$\left(\frac{Q_u}{\gamma AH}\right)\tan\emptyset = 3.3(H^2/A)^{0.39} \quad \text{(2.6)}$$

The laboratory and field results described in the literature were acquired for shallow anchor plates with various configurations implanted in different types of sands. This data was applied to forecast the overall horizontal pullout strength of vertical anchor plates, considering various

influencing factors. Additionally, another equation was provided to determine the displacement associated with the applied load magnitude. The suggested formulations were helpful to the practice since they offered a simple approximation for quantities that were somewhat complex, such the displacement that goes along with the ultimate pullout resistance. These expressions were reasonably accurate, especially given that they were based on laboratory and field results from testing in a wide range of sands conducted by various investigators under a variety of locations and conditions.

Rao & Kumar (1994) developed a theory for the vertical uplift capacity of shallow horizontal strip anchors in a general C-Ø soil using a log-spiral failure surface. The methodology was similar to that used to determine the bearing capacity of foundations under compression, separating the impacts of cohesion, surcharge, and density on uplift capacity. The theory was demonstrated to accurately predict anchor pullout behavior in clays, as well as loose and medium-dense sands.

The suggested formula for the ultimate pullout strength per unit length of the strip anchor in clay was:

$$\mathbf{Q_{U,net} = CF_C + qF_q + 0.5\Upsilon BF_\Upsilon} \quad \text{..... (2.7)}$$

Where C= cohesion of soil, γ = unit weight of soil, B = width of plate anchor, and F_C, F_q, F_Υ= uplift capacity factors which are functions of embedment ratio and soil friction angle.

Ghaly et al. (1991) conducted a study examining spiral screw anchors in cohesionless soils through both experimental and theoretical approaches. A testing regime was implemented that encompassed 56 tests on five model anchors placed in loose, medium and dense dry sands. The experimental setup was equipped to record the pullout force, anchor uplift, and sand surface deformation. The findings revealed that the failure mode and pullout force were influenced by the angle of shearing resistance of the sand and the installation depth of anchor. The maximum load capacity of screw anchors primarily depended on anchor diameter, sand characteristics, and installation depth. Screw anchors were classified based on their failure modes: shallow, transitional, and deep. The transitional failure mode was observed across all sand conditions, indicating a gradual rather than sudden transition from shallow to deep behavior. There was no specific failure pattern associated with a particular relative depth ratio for any type of sand. The

range of relative depth ratios for each failure mode varied with the density of the sand; denser sand allowed for deeper failure modes compared to looser sand.

The diameter of the failure circle on the sand surface, caused by uplift, increased with the embedment depth up to a certain point. Beyond this depth, the diameter remained constant during transitional failure modes. The resistance against pullout loads was primarily provided by the shear strength mobilized along the failure surface of the soil mass that broke out. Fig.2.7 represented failure surface obtained in this study for different screw anchors. Using the reported failure mechanism of the anchor and the limit-equilibrium technique of analysis, a mathematical model was developed. Based on the experimental data, a simple equation was constructed that incorporates the degree of shear mobilization into the coefficient of passive earth pressure. A comparison of the derived theory with the experimental results of the current inquiry and field results reported in the literature revealed good agreement.

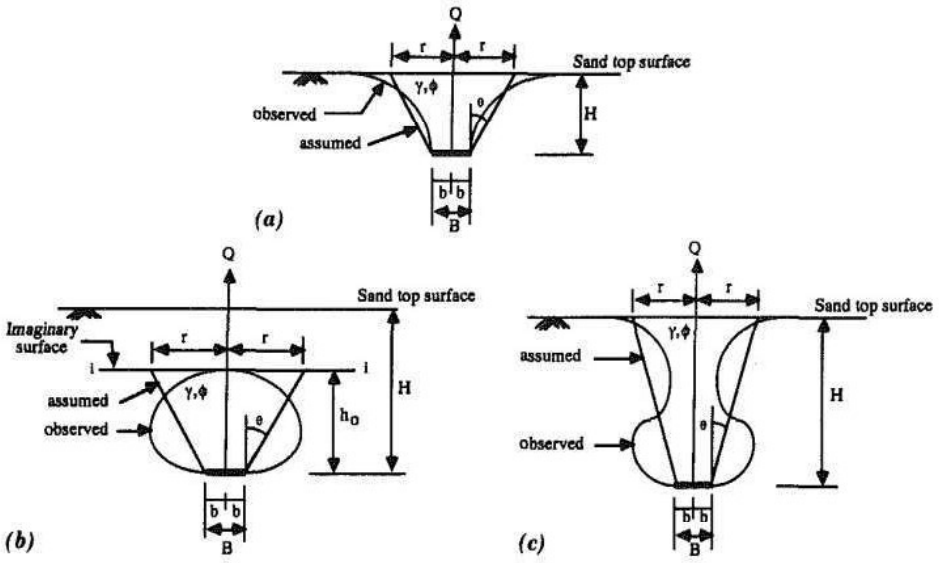

Fig. 2.7: Failure Surface for (a) Shallow Screw Anchor; (b) Deep Screw Anchor;(C) Transit Screw Anchor (After Ghaly 1991)

Murray & Geddes (1989) scrutinized the passive resistance exhibited by inclined anchor plates in sand, focusing on laboratory experiments conducted to evaluate the ultimate passive resistance and associated displacements. The study compared experimental results with theoretical solutions derived from upper and lower bound limit theorems of soil plasticity.

Experimental tests involved rectangular anchor plates of varying length-to-breadth ratios (L/B) and depth-to-breadth ratios (H/B), loaded at angles ranging from 0° to 90°. The results indicated that the ultimate passive resistance and displacements increased with depth and angle of loading, particularly within the range of 45 to 90 degrees.

Theoretical solutions for strip anchors (L/B) were developed using upper and lower bound limit analysis, considering soil obeying an associated flow rule. While a poor lower bound solution was formulated, upper bound solutions demonstrated favourable agreement with experimental evidence, particularly when accounting for interface friction between sand and anchor plates.

Comparison with previous studies revealed good alignment between upper bound solutions and experimental data, as well as with equivalent free surface stress characteristic solutions. However, discrepancies emerged when comparing with finite element analyses for horizontally pulled strip anchors in elastic-plastic soil.

Ultimately, the findings suggested that upper bound solutions could effectively estimate the ultimate passive resistance of inclined anchors in dry sand, providing valuable insights for engineering applications.

Das & Puri (1989) investigated the pull-out capacity of inclined anchors embedded in compacted clay. Pull-out tests were performed on anchors with inclinations between 0° (horizontal) and 90° (vertical) for embedment ratios up to 4. laboratory tests utilized a square anchor (50.8 mm x 50.8 mm) in a test box filled with compacted clay soil. The soil had specific properties (e.g., liquid limit of 38%, plastic limit of 21%) and was prepared and compacted to simulate field conditions. The anchors were pulled out at various inclinations, and the results were recorded.

The net ultimate load was determined from load-displacement diagrams, with adjustments made for adhesive forces between the anchor rod and clay. The breakout factors were calculated for each test and compared against empirical relationships for horizontal and vertical anchors. The tests showed that the breakout factor increased with embedment ratio up to a maximum value, aligning well with previous empirical relationships.

An empirical relationship for inclined anchors was proposed, considering the breakout factors for different inclination of pull-out load based on model tests. Fig 2.8 shows the nature of failure of soil mass for horizontal, inclined, and vertical plate anchors in clay subjected to ultimate pull-out load. The net ultimate holding capacity can also be expressed as given by

$$\mathbf{Q_u = (Q_g - W_a \cos\beta) = AC_uF_c + W\cos\beta} \quad \text{..... (2.8)}$$

Where, Q_g = Gross ultimate load, Wa = Self weight of the Anchor

Q_u = Net Ultimate Load, A = Area of Anchor Plate

Cu = Undrained Cohesion, Fc = Breakout Factor

W = Weight of Soil immediately above the anchor plate

β = Inclination of anchor with the horizontal as shown in Fig 2.9

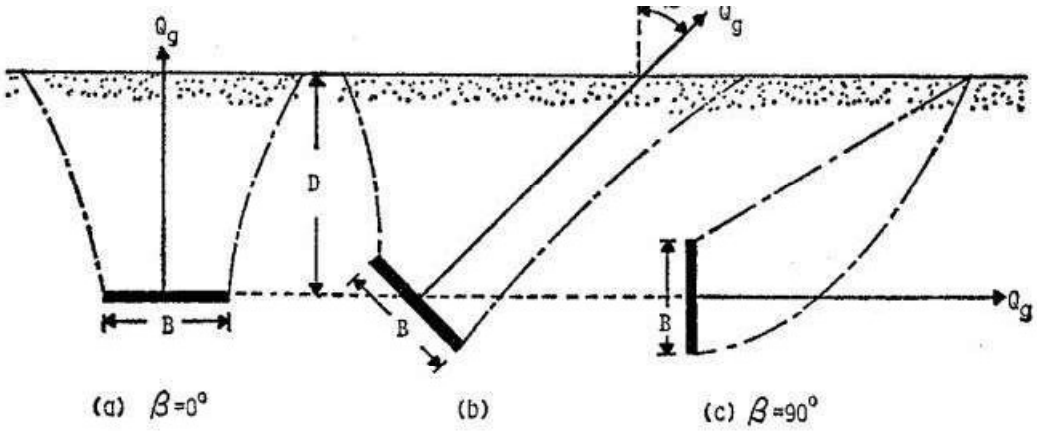

Fig. 2.8: Nature failure surface in soil at Ultimate load after (Das & Puri, 1989)

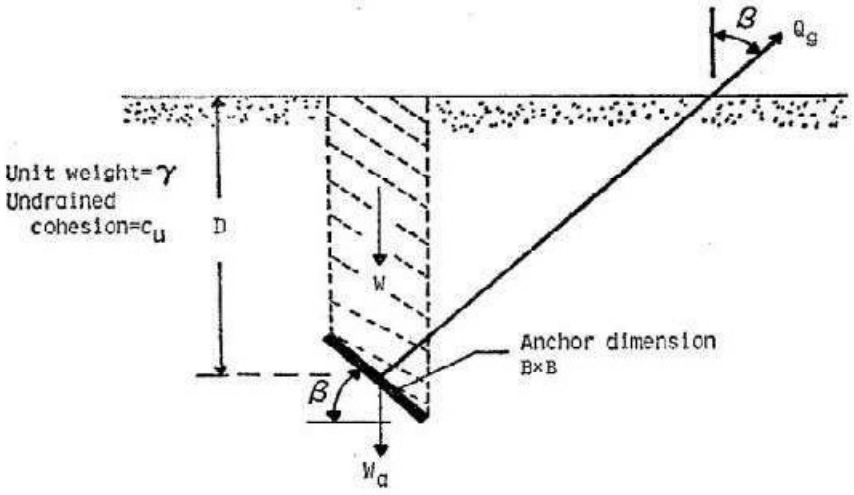

Fig. 2.9: Geometric parameters of inclined anchor in clay (Das & Puri, 1989)

Now based on model test they derived breakout factor for horizontal, inclined and vertical plate anchors with the help of Eq. 2.8 given above. They observed that for a given inclination of anchor the breakout factor increases with average embedment ratio up to a maximum value

afterwards remains constant as exhibited in Fig 2.10.

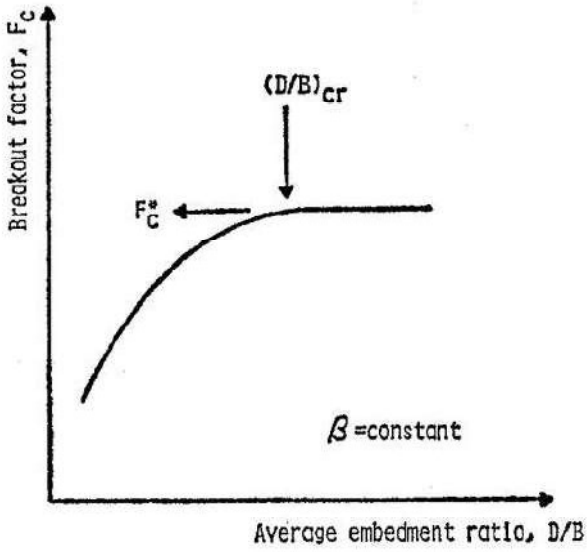

Fig. 2.10: Nature of variation of Fc with D/B for a given anchor inclination (After Das and Puri,1989)

Tagaya et al. (1988) investigated the pullout resistance of buried anchors. Empirical formulas for estimating pullout resistance were developed based on extensive experimental data, offering practical methods for calculating anchor performance under various conditions. It was identified that pullout resistance increases with burial depth due to the confining pressure of the overlying sand, though the rate of increase diminishes at greater depths, indicating an optimal burial depth for efficiency. The influence of sand density on pullout resistance was also demonstrated. Denser sand was found to provide greater resistance due to higher frictional forces and interlocking of sand particles around the anchor, while loose sands exhibited lower pullout resistance, emphasizing the importance of soil compaction in anchor design.

Anchor shape and size were shown to play significant roles in pullout resistance. Larger anchors were observed to exhibit higher resistance due to increased surface area in contact with the sand. Additionally, the shape of the anchor, whether fluke, plate, or helical, was found to affect stress distribution and failure modes in the surrounding sand. Different failure mechanisms depending on anchor type and soil conditions were identified. Shallow anchors were often found to fail by surface rupture, while deeper anchors typically failed through a combination of soil shear and anchor-soil interface failure. These mechanisms are crucial for predicting anchor behavior and designing anchors to withstand expected loads.

Hanna et al. (1988) analyzed the behavior of shallow inclined plate anchors embedded in sand. Their study, which was analytical in nature, investigated how the ultimate holding capacity of these anchors varied with different inclination angles ranging from 0° to 60°. The findings revealed that the pullout capacity of the anchor plate increased as the inclination angle increased. In Fig. 2.11, a shallow strip anchor was depicted, with its actual failure surface nearly parallel to lines ab' and cd'. As shown in the figure, the passive forces per unit width of the anchor were denoted by P1 and P2 along the planes of ab and cd, respectively, with the angle δ representing the deviation between the normal of each plane and the direction of each force. The following equations were derived in this study:

$$W=1/2\ (L_1 + L_2)\ h\gamma\ \cos\varphi \quad \text{..... (2.9)}$$

$$P_1=1/2\ R_\gamma K_P \gamma L_1^2 \quad \text{..... (2.10)}$$

$$P_2=1/2\ R_\gamma K_P \gamma L_2^2 \quad \text{..... (2.11)}$$

Where, K_p =passive earth pressure coefficient with δ=φ &R_γ=reduction factor for K_p which is a function of δ/φ.

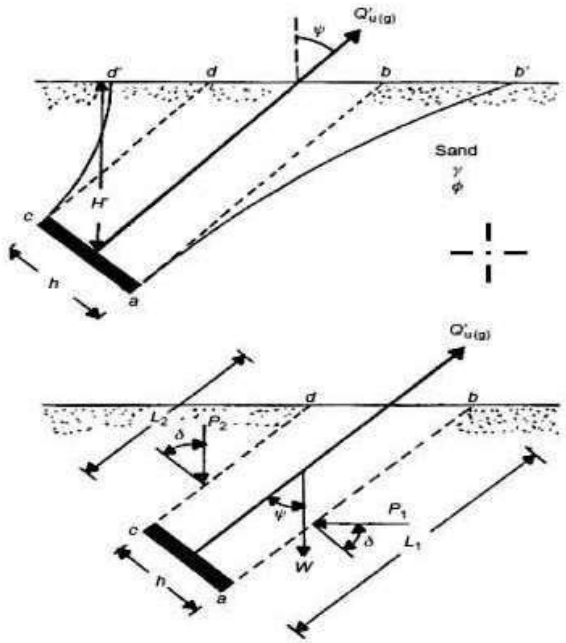

Fig. 2.11: Shallow inclined strip anchor

Chattopadhyay and Pise (1986) investigated the breakout resistance of horizontal anchors in sand. Their research was focused on understanding the factors that influence the force required to dislodge an anchor embedded in sandy soils. The significance of this work lied in its application to civil engineering, particularly in the design and installation of anchoring systems used in various structures such as retaining walls, offshore platforms, and transmission towers. A series of experimental tests were conducted to determine the breakout resistance of horizontal anchors. These tests were carried out in controlled conditions using different types of sand to evaluate how grain size, density, and moisture content affect the resistance. The experimental setup involved a test tank filled with sand, where horizontal anchors were embedded at various depths and subjected to vertical pullout forces until failure occurred.

Key findings from their experiments indicated indicates that the existence of a characteristic relative depth, beyond which breakout factor approaches a constant value. The value of characteristic relative depth depends on the angle of shearing resistance of the soil as shown in Fig. 2.12.

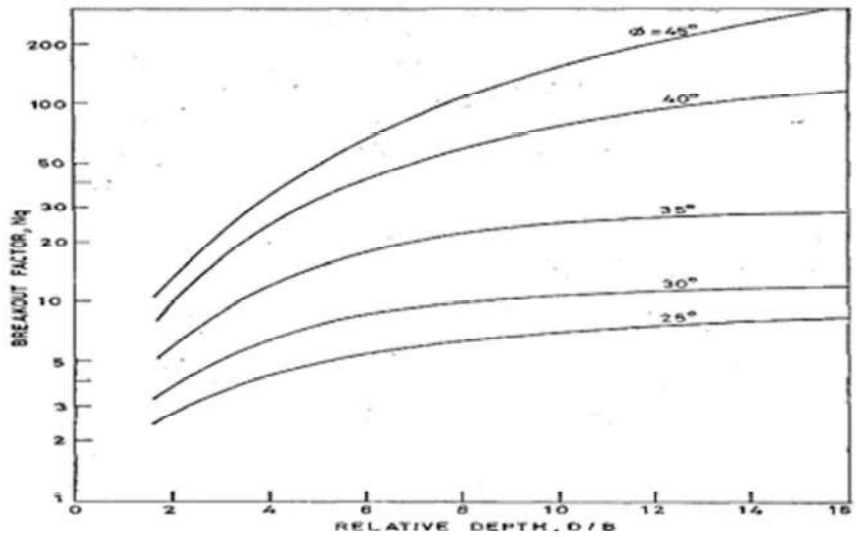

Fig. 2.12: Theoretical values of break out factor N_q in sand (After Chattopadhyay et al 1986)

Additionally, the density of the sand significantly had an impact on the breakout force, with denser sands providing higher resistance. The grain size distribution also played a crucial role; sands with a well-graded distribution tend to offer greater resistance compared to uniformly

graded sands. The study further explored the theoretical aspects of anchor resistance by comparing the experimental results with existing theoretical models. It had been found that while some models could predict the breakout resistance with reasonable accuracy, others tended to underestimate the resistance, particularly at greater depths and in denser sands. This discrepancy highlighted the need for refining current theoretical approaches to better account for the complex interactions between the anchor and the surrounding soil. This work underscored the necessity for further research to develop more accurate predictive models and to explore the performance of anchors in different soil conditions and configurations.

Saran (1986) performed a study aiming to forecast the critical pullout load, breakout load, and load-deformation behavior of soil anchors. This analysis utilized hyperbolic stress-strain relationships of soils as the constitutive model. The research covered various anchor shapes such as square, circle and strips. Comparisons between the analytical findings and existing experimental data demonstrated good agreement.

Earlier methods computed critical pullout load and breakout load separately using limit equilibrium approaches, while deformation behavior studies utilized finite element techniques. This paper proposed a new method for obtaining complete load-deformation characteristics by adopting a suitable rheological or mathematical model. Parameters for these models were derived from the soil's stress-strain relationship obtained from triaxial tests. The analysis assumed the anchor was buried at shallow depth in a homogeneous, isotropic medium of semi-infinite extent, the anchor plate was rigid with negligible weight, and the pullout force was resisted by a linear soil wedge increasing in height with load. Critical pullout load was defined when the wedge height equalled the depth of embedment. For loads less than the critical pullout load, soil strength mobilized fully at the anchor level and decreased linearly to zero at the top of the wedge. For loads between critical pullout and breakout load, strength mobilized fully at the anchor level and partially at the ground level. Forces on the soil wedge were computed, and equilibrium conditions were used to derive equations for critical depth and pullout load. For deformations, the soil wedge was divided into horizontal slices, and stresses on elements were calculated to determine strains and resultant vertical displacement. Model tests on anchors made of brass sheets were performed to validate the analytical method. The anchors included strip, square, and circular shapes, tested in Dhanauri clay. The tests showed that the analytical predictions matched well with experimental results, indicating the proposed method's reliability in predicting anchor behavior under load.

In conclusion, the study successfully developed a method for predicting the complete load-deformation behavior of shallow soil anchors using hyperbolic stress-strain curves, validated through analytical and experimental comparisons.

Das et al. (1985) proposed methodologies based on model laboratory tests for estimating the ultimate uplift capacity of rectangle, square and strip anchors, placed vertically or horizontally in clay. The width-to-height ratio of the anchor plates utilized in the experiments ranged between one and five. The ultimate pullout load of an anchor might be described as a nondimensional breakout factor (N_c^*). Based on the experimental results, an empirical equation for determining the ultimate pullout load was proposed. For shallow anchors, the breakout factor increased with the embedment ratio. For a given value of embedment ratio, the breakout factor increased with the decrease of the width-to-height (B/h) ratio of the anchor. Based on the experimental results, an empirical relation (Eq. 2.12) for the ultimate pullout resistance of shallow vertical anchors was presented.

$$P_u = 2SBhc_u\ (H/h)^{0.74}\ (\text{For } H/h \leq 5) \quad \text{..... (2.12)}$$

Rowe and Davis (1982) conducted a theoretical investigation into the behavior of anchor plates in sand, considering factors such as anchor embedment, friction angle, dilatancy, initial stress state, and anchor roughness. Their theoretical results were compared with their model tests and other experimental data, showing encouraging agreement and providing reasonable predictions of anchor capacity. The study extended theoretical results for sand to cohesive-frictional soils and presented them in influence charts for hand calculations to estimate anchor capacity for various geometries and soil types.

Previous theoretical research into anchor behavior primarily focused on elastic response and ultimate capacity, using either limit equilibrium concepts or the method of characteristics, often with empirical corrections. These approaches involved arbitrary assumptions regarding the shape of the failure surface or the influence of the soil above the anchor. Rowe and Davis's study considered the effects of anchor roughness, initial stress state, and soil dilatancy, which were generally overlooked by previous researchers.

The finite element analysis used in the study allowed for the consideration of plastic failure within the soil, anchor breakaway from the soil, and shear failure at a soil-structure interface. It was found reasonable agreement between the finite element results and available elastic and plasticity

solutions, with finite element collapse loads accurate to within 6%. The load-deformation relationships showed that true elastic response was limited to low load levels, followed by pseudo-elastic behavior at working loads, and elasto-plastic behavior at higher loads. Shallow anchors showed small displacements before collapse, while deeper anchors exhibited more extensive plastic deformation. Anchors with a horizontal axis showed larger regions of plastic failure and higher collapse loads compared to those with a vertical axis. The anchor capacity factor increased linearly with embedment ratio for vertical anchors, while the relationship for horizontal anchors was not linear but could be approximated by linear interpolation. It was also noted that dilatancy during plastic deformation caused the soil in front of the anchor to lock up, requiring a larger plastic region for collapse to occur. This effect increased anchor capacity, which they expressed in terms of a correction factor to the basic anchor capacity factor. The study provided a comprehensive analysis of anchor plate behavior in sand and cohesive-frictional soils.

Andreadis and Harvey (1981) focused on the design and performance of embedded sea bed anchors subjected to repeated loading. The researchers highlighted that installation procedures that disturb the adjacent soil can drastically reduce the anchor's life under repeated loading, although such anchors might perform adequately under static loading. For instance, it was noted that an anchor embedded in dense soil, which was then disturbed to a lower density, demonstrated only 70% of the ultimate static capacity of an anchor in undisturbed dense soil under static loading. However, under repeated loading, the disturbed anchor's life, in terms of load repetitions to failure, was reduced by a factor of 250 compared to the undisturbed anchor.

It also observed that repeated loading significantly influenced the resistance to movement during subsequent static loading. The research suggested that the total permanent cyclic movement experienced by the anchor could predict its load-displacement behavior under static loading.

Their study proposed that the ultimate static capacity of an embedded anchor could be related to the breakout factor, which depends on several variables including soil parameters, relative depth, anchor size and shape, and soil disturbance during installation. They found that deeper anchor installations mitigated inaccuracies in the designed ultimate static capacity and reduced the adverse effects of changes in the sea bed's topographical features. The research concluded that their design approach, based on medium-scale laboratory tests and some prototype test results, was preliminary.

Harvey and Burley (1973) explored the behavior of inclined and vertical anchors embedded in dry sand. Fig. 2.13 shows a vertical section through the failure zone corresponding to the major axis of the ground surface failure ellipse. The shape of the failure surface is considered to be an arc of a circle perpendicular to the plate and making an angle of $(\frac{\pi}{4} - \frac{\emptyset}{2})$ with the horizontal free surface. The researchers found that for values of H/D (the ratio of embedment depth to anchor diameter) less than 6, there was good agreement between theoretical predictions and experimental results. For H/D ratios greater than 6, theoretical results tended to overestimate the experimental pull-out capacities due to the lack of consideration for the tunnelling effect that reduces the failure cone's size.

When comparing vertical and inclined anchors at the same embedment depth, the pull-out forces were found to be similar, although slight differences increased as the H/D ratio increased. This indicated that anchor inclination had a limited effect on pull-out capacity for deeper anchors. The study showed a significant increase in capacity for shallow inclined anchors compared to vertical ones, which was attributed to the greater surface area of the failure cone in cohesive soils.

The study also highlighted the theoretical and practical implications of critical depth, defining "deep" and "shallow" anchors based on the H/D ratio. For "shallow" anchors (H/D < 6), the theoretical models were validated by experimental data, but for "deep" anchors, the models tended to overpredict the pull-out resistance.

Overall, the research indicated that while the existing theoretical models were effective for shallow anchors, further investigation was needed for deep anchors, particularly to account for the effects of cohesion and other variables not included in the initial theoretical framework.

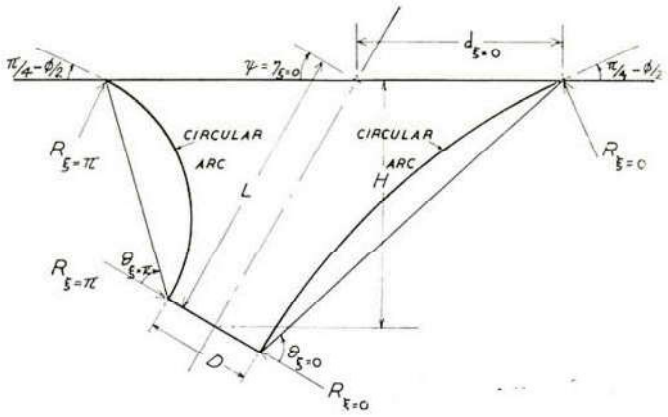

Fig. 2.13: Vertical Section through failure zone for inclined anchor (After Harvey and Burley 1973)

Vesic (1971) developed an analytical method based on solutions to the expanding cavity problem near the surface of a semi-infinite stiff plastic solid for estimating the pullout capacity of horizontal plate anchors. These solutions provided the maximum radial pressure required to cause a spherical or cylindrical hollow implanted at a depth below the surface of the solid to break free. Pullout capacities for strip and circular anchors were then evaluated by assuming that the pullout load was equivalent to the ultimate cylindrical or spherical cavity pressure, plus the weight of earth acting directly above the anchors.

. The ultimate pullout capacity was given by:

$$Q_u = A\,(\Upsilon H F_q + c F_c) \quad \text{..... (2.13)}$$

Where A = Area of plate, H = embedment depth, c = cohesion of soil, F_q and F_c= breakout factors.

Meyerhof & Adams (1968) observed a disagreement in uplift-capacity theories for foundations resting on slip surfaces, primarily due to challenges in predicting the failure zone's geometry. Through model tests, a semi-theoretical relationship was proposed applicable to rectangular, circular and strip footings in both sandy and clayey soils. Their findings indicated that the long-term uplift capacity in clay could significantly differ from the short-term capacity, especially at shallow depths. This difference over time was attributed to the dissipation of negative pore water pressures, leading to soil softening. The long-term capacity in clay was estimated using theories applicable to sandy or frictional materials. By combining the short-term capacity relationship for clay and the long-term capacity relationship for sand, they demonstrated that the capacity reduction was most notable in stiff clays at shallow depths, with a critical depth where long-term capacity exceeded short-term capacity for each clay type.

An empirical approach was developed using a coefficient (N_u) linking the uplift coefficient of clay to its undrained strength. These uplift theories were validated through full-scale field tests in sands and clays, showing practical correlations. The theories were also adjusted to account for group effects in square and rectangular arrangements of piles or footings. Here, the maximum group capacity was determined as the sum of individual unit capacities, while the minimum capacity was treated as that of the entire group as a single unit. Intermediate capacities were interpolated based on unit spacing. Model tests in both sand and clay provided a basis for calculating efficiency factors. Initially derived for strip footings, their theory was later adapted for circular and rectangular footings, as well as plate anchors. The proposed relationship for ultimate pull-out capacity of strip footings was:

$$Q_u = 2cH + \Upsilon H^2 K_p \tan\delta + W \quad \ldots\ldots\ldots\ldots\ldots\ldots\ldots\ldots\ldots\ldots \quad (2.14)$$

where δ = Ø/2 to 2Ø/3, KP = coefficient of passive earth pressure, and W = weight of soil above the footing.

(Mariupolskii L.G., 1965) proposed the mathematical equations related to the uplift response of circular anchor plates to examine shallow anchor behavior without assuming a "quick condition" of the soil has been proposed. In their study an extracting load was applied to an anchor plate, it was pressed against the base of an earth column, forming a circular cylinder. Initial soil compaction occurred above the anchor, with the most intense deformations near the anchor plate and diminishing upward. The reactive forces included the dead weight of the earth column and the friction and cohesion forces along the cylinder's surface. As soil compaction increased, friction forces rose due to the increasing vertical compressive stresses, leading to enhanced radial stresses.

As the earth column moves upward, adjacent soil rings are entrained by friction and cohesion forces, leading to tensile stresses and probable failure in the form of a cone with a curvilinear generatrix. Full-scale tests and model experiments had confirmed this scheme, showing a gradual increase in extracting force to a limiting value, beyond which a continuous internal crack formed along the separation surface. This results in the breakdown of the raised earth into individual parts.

The ultimate load on the anchor, designated as Pz, can be expressed as:

$$P_z = O_1 + G_2 + \gamma V + Q \quad \ldots\ldots\ldots\ldots\ldots\ldots\ldots\ldots\ldots\ldots\ldots\ldots\ldots\ldots\ldots\ldots \quad (2.15)$$

where O_1 is the weight of the anchor, G_2 is the weight of the earth column above the anchor plate, V is the volume of the conical part of the entrained earth, and Q is the total cohesive force along the lateral surface of the separation cone.

Field and laboratory tests, including the placement of painted strips in a trough, revealed characteristic vertical "steps" at failure sites but did not show the formation of a conical soil wedge above the anchor plate, which typically accompanies bulging phenomena. These observations supported the hypothesis of soil failure through a separation cone rather than bulging.

The investigation into the behaviour of shallow anchors under withdrawal forces highlighted the complexity of soil mechanics in this context. The proposed hypothesis and subsequent experimental validation indicate that the formation of a separation cone, rather than traditional

bulging, better describes the failure mechanism. The developed formulas for ultimate load calculation align well with experimental data, providing a robust framework for understanding and predicting the performance of anchor foundations in various soil conditions. The importance of considering unique soil-structure interaction conditions in geotechnical design has been underscored

Balla (1961) was first to undertake a systematic model study on the problem of anchors. The tests were conducted on circular anchors embedded in sand. In laboratory tests, a glass container measuring 60.5 x 51.5 x 36 cm was used. The mushroom foundation models had diameters of 6, 9, and 12 cm, and shaft lengths of 2.5, 10, 15, 20, 25, and 30 cm such that maximum depth to diameter ratio Was 3.33. The soil was sand, layered in an air-dry state. In some tests, the sand was wetted, with a moisture content of 10-12 percent. The voids ratio was established to be 0.55-0.58. The slope angle of the sand, according to shear and compressive tests, was 36°-38°, and its cohesion in a wet state was 0.05 kg/cm² (0.5 t/m²). These tests investigated many aspects, but the paper focused on the breaking out resistance of mushroom foundations in natural, unaffected homogeneous soil. Analysing the laboratory tests, it was observed that the failure wedge was a solid of revolution such that its meridian section was circle. He derived an expression for breakout load by calculating dead weight of soil in the failure wedge and resultant shear force on the sliding surface. The proposed expression Was

$$\boldsymbol{Q_{bkt} = \gamma H^3 \left[F1(\emptyset,\lambda) + \frac{c}{\gamma H} F2(\emptyset,\lambda) + F3(\emptyset,\lambda) + W_f\right)} \quad \text{..... (2.16)}$$

where F_1, F_2, F_3 are non-dimensional constants, to be obtained from charts of table. c, γ , Ø are values of unit cohesion, unit Weight and angle of internal friction. 2B and H were the width and depth of anchor respectively and λ is depth to width ratio. Rest of the notations are shown in the list of notations. Breaking out resistance was found to be proportional to the third power of the foundation depth, dependent on the physical characteristics of the soil and the relationship between foundation depth and the diameter of the foundation slab. Balla compared the results of model test with the predicted values. A good agreement was reported. However, Balla gave the values of F_1, F_2 and F_3 for depth ratios up to 4 only.

2.2.2 Under Dynamic Load:

Beirne et al. (2017) investigated field data from reduced scale anchor tests at two sites to validate a new release-to-rest model for dynamically installed anchors. The investigation focused on evaluating the penetration resistance experienced by dynamically installed anchors in both normally consolidated and over consolidated clay. Through a series of centrifuge tests, the study utilized a model anchor equipped with a micro electric mechanical system (MEMS) accelerometer to capture its full motion response during installation.

Data obtained from these tests were employed to validate an anchor embedment model, which accounted for strain-rate-dependent shearing resistance and fluid mechanics drag resistance. The model's predictions, based on a database of over 100 anchor installations compiled from the study and existing literature, demonstrated a close agreement with measured anchor embedment depths, falling within ±15% of the actual measurements.

A notable finding across the entire database was the observed strain rate dependency on frictional resistance relative to bearing resistance. The study suggested that this dependency might be higher for frictional resistance, particularly when considering a soil strength lower than the fully remoulded strength as the reference strength. This phenomenon hinted at the potential entrainment of water along the anchor-soil interface during installation.

Further validation of the anchor embedment model was conducted through additional centrifuge tests in both normally consolidated and over consolidated clay samples. These tests allowed for the application of the model across a range of over consolidation ratios and strength profiles.

Overall, the study highlighted the potential of dynamically installed anchors as a cost-effective solution for mooring floating facilities and pipelines. Reliable prediction of anchor capacity hinges on accurate estimation of embedment depth, which poses challenges due to the assessment of soil shearing at extremely high strain rates and consideration of hydrodynamic effects during installation. However, the findings suggested that the developed anchor embedment model could accurately describe anchor motion in both normally consolidated and over consolidated clay, provided appropriate scaling considerations were taken into account.

Nouri et al. (2016) investigated the undrained response of plate anchors subjected to combined translational and torsional loading using three-dimensional finite element (3D-FE) analysis. The study aimed to predict the ultimate bearing capacity and understand the interaction between shear and torsional resistances. Their research was motivated by the need to address anchor

performance in offshore environments, particularly under extreme loading conditions that may involve complex load orientations beyond the intended loading plane.

The study utilized plastic limit analysis to establish benchmark solutions for ultimate translational resistance, which showed satisfactory agreement with the FE values. They found that while plate thickness significantly impacted the maximum shear and torsion resistance, it minimally affected the shape of the failure envelope. A simple three-degree-of-freedom interaction equation was developed, curve-fitted to FE failure data points, and introduced representative interaction relationships for square and rectangular plates. The study built on these foundations by modifying the plastic limit solution to better predict the torsional collapse load and failure envelopes for plates with finite thickness.

In their numerical modelling, Nouri et al. used ABAQUS software and assumed the plate was deeply embedded, leading to localized plastic flow around the plate anchor. They modelled clay as a linear elastic perfectly plastic material using the Von Mises failure criterion and assumed the plate as a rigid body. They highlighted the challenges of numerical modelling, particularly stress concentration at the plate edges, and addressed these by refining the mesh and using contact pairs along the plate corners.

Their analysis showed that mesh refinement improved results but did not significantly change the bearing capacity values after a certain degree of refinement. It was found that using contact interfaces in the soil along the plate corners enhanced stress distribution, leading to more accurate FE results for shear bearing capacity. Their findings were validated against plastic limit analysis values, showing minor discrepancies, and confirmed that the interface coefficient of friction had a negligible impact on the ultimate shear capacity for values greater than one.

The study concluded that the 3D-FE analysis effectively predicted the translational and torsional ultimate bearing capacities of plate anchors and provided a robust method for evaluating the interaction between these two loading modes. The findings offered valuable insights for designing and analyzing plate anchors in offshore environments, considering complex loading conditions and anchor geometries.

Yu et al. (2015) conducted a detailed experimental study on the stability of plate anchors in clay under cyclic loading. The primary focus was to understand the effects of cyclic loading on the bearing capacity of plate anchors, a subject previously studied extensively under monotonic conditions but less so under cyclic conditions. The study utilized 1g model tests to evaluate how

cyclic loading influences the ultimate pullout capacity of plate anchors. The study included a thorough examination of load-displacement curves and discussed how overburden stress and cyclic loading amplitude affected strain-softening behavior.

Yu et al. detailed their experimental setup, which included a consolidation tank for kaolin clay and a cyclic loading apparatus. They conducted three tests at different stress levels. In Test 1, the plate anchor experienced low overburden pressure, resulting in cavity formation behind the anchor and a significant reduction in residual bearing capacity after several cycles. The cyclic loading caused notable softening of the resistance, as indicated by load-displacement curves and maximum bearing capacity factors. In Test 2, with higher overburden pressure, the anchor showed more pronounced hysteresis behavior in its resistance response. Numerical simulations using the strain-softening model in FLAC confirmed the experimental findings, showing good agreement with the observed strain-softening behavior. The study highlighted the importance of the fully localized soil flow mechanism, which was evident in the high stress level tests. Test 3 explored the effects of varying cyclic loading amplitudes. The results indicated that larger amplitudes led to more hysteresis in the load-displacement response, and the resistance stabilized at a certain displacement, reflecting fully plastic failure. The key conclusions from Yu et al.'s study were:

- At low stress levels, cavities formed beneath the anchor after initial pullout, significantly reducing residual bearing capacity after several cycles. This reduction was attributed to the strain-softening behavior of the clay under cyclic loading
- At high stress levels, bearing capacity decreased with accumulated plastic shear strain due to clay strain-softening. The fully localized soil flow mechanism caused the resistance to show significant hysteresis under cyclic loading.
- The amplitude of cyclic loading greatly influenced the load-displacement curve shape, with higher amplitudes mobilizing more hysteresis.

This study provided valuable insights into the behavior of plate anchors under cyclic loading, emphasizing the role of strain-softening in reducing bearing capacity and highlighting the importance of considering cyclic effects in the design and analysis of plate anchors in clay.

Singh and Ramaswamy (2008) investigated the response of embedded circular plate anchors to varying frequencies of cyclic loading. The study highlighted the significant influence of static and cyclic load ratio levels on the permanent movement and post-cyclic behavior of deep anchors in soft saturated soil. In their experimental program, Singh and Ramaswamy subjected anchors to cyclic load ratio levels of 0.30 and 0.45, with time periods of 2, 6, 12, and 24 seconds, and recorded cumulative anchor movements over 1000 cycles. In a second phase, they recycled the anchors at various load levels after an unloading period of 22 hours and performed monotonic pullout tests to assess post-cyclic capacity. The tests used an 80 mm diameter circular plate anchor buried at a depth of 480 mm in saturated clay with a moisture content of 57.3%.

The soil used in the experiments was high-plasticity commercial clay, consisting of fine sand, silt, and clay, with a liquid limit of 75% and a plasticity index of 44%. The presence of kaolinite, chlorite, illite, vermiculite, and quartz particles was confirmed through X-ray diffraction. Test samples were prepared by thoroughly mixing pulverized clay with water and allowing for moisture equilibrium before filling the test tank, which had a diameter seven times that of the anchor to prevent boundary effects. The meticulous preparation ensured uniform consistency and reliable test results. The study found that higher frequency cycles caused more movement in the anchors compared to lower frequency cycles for the same duration of loading. Pre-loading reduced anchor movement in subsequent loading stages, especially when the recycling load ratio was less than the pre-cycling load. However, if the recycling load was higher, the anchors exhibited behavior similar to those not subjected to prior cyclic loading. Anchors that underwent cyclic loading followed by monotonic pullout showed an increase in initial stiffness, although the peak pullout load decreased marginally compared to anchors that did not experience cyclic loading. The post-cyclic stiffness of the anchors varied between 1.169 and 1.327 times the original stiffness.

Thorne et al. (2004) studied the uplift behaviour of horizontal strip anchors in clay under fast loading. The possible failure mechanisms were reviewed, including failure due to shear and traction in the soil and the development of suction in the porous fluid. The analysis was made using the finite element program AFENA. The analyses assumed a thin, perfectly rigid strip,

progressively displaced until failure occurred. Based on their findings the following conclusions were drawn:

- The behaviour of the strip anchors in the pull-out capacity are functions of the nondimensional parameters H/B, ϒH/C, U_C/C, where H is the embedment depth, C is the cut resistance without drainage, U_C is the magnitude of the maximum tensile stress of the pore water in the soil and ϒ and B are the unit weight and width of plate.
- Shallow anchors in relatively strong soil tend to fail due to the development of a tensile failure in the soil that is above the anchor and the ultimate capacity is a function of the undrained shear strength of the soil, its own weight and the tensile capacity of the porous fluid
- The failure mechanism of the deep anchors where the initial vertical total stress in the plate exceeded seven times the resistance without draining involved only one cut fault located around the anchor. The ultimate capacity in such a case becomes a function only of the resistance without draining the soil.

2.3 REINFORCED SOIL

2.3.1 Under Static Loading

Banerjee and Nagaraju (2017) investigated the pullout behavior of square anchor plates in reinforced soft clay using numerical simulations. Their study aimed to determine the uplift capacity of anchor plates in cohesive soils with geosynthetic reinforcement. Finite element software ABAQUS had been used to model three different sizes of square anchor plates. The simulations considered material non-linearity through a hypo elastic model and included a single layer of geosynthetic placed at three different positions relative to the anchor plate. Parameters such as embedment ratio, position of reinforcement, and width of reinforcement were analyzed. The results showed that the pullout load increased with the embedment ratio and the presence of reinforcement. Specifically, the ultimate pullout load was higher in reinforced soil compared to unreinforced soil for all depths of embedment and positions of reinforcement. This increase in pullout capacity was attributed to the additional frictional forces developed between the soil and the geosynthetic reinforcement. The maximum increase in pullout capacity due to reinforcement ranged from 52% to 72% for square anchors. The effect of reinforcement was most significant when the reinforcement was placed close to the anchor plate.

The study also included a comparison of numerical results with previously published experimental data by Bhattacharya et al. The numerical analysis closely matched the experimental results, validating the accuracy of the simulations. The researchers concluded that geosynthetic reinforcement significantly enhances the pullout capacity of anchor plates in soft clay and provided design curves to predict breakout factors based on various parameters

Niroumand et al. (2013) studied various factors affecting the uplift response of symmetrical anchor plates embedded in sand were investigated. The inclusion of geogrid and grid-fixed reinforcement (GFR) was found to significantly improve the uplift capacity of the anchor plates. It was observed that a single layer of GFR directly resting on top of the anchor plate was more effective in enhancing the uplift capacity compared to multiple layers. The inclusion of geogrid alone improved the uplift capacity by 19%, while the addition of GFR further increased this improvement to 29%.

The effectiveness of reinforcement varied with the number of layers and their proximity to the anchor plate. A single layer of geogrid provided better results than multiple layers due to the additional anchorage offered by the GFR system. The uplift capacity was significantly increased in both loose and dense sand when geogrid with GFR was used, reducing the need for higher embedment ratios.

The study also showed that the optimal spacing for multiple GFR layers was 0.5 times the width of the anchor plate. Both laboratory and numerical analysis results agreed in terms of the breakout factor and failure mechanism pattern. The uplift capacity increased with the sand unit weight and embedment ratio. Symmetrical anchor plates in dense sand exhibited higher uplift capacities than those in loose sand, and the uplift capacity increased non-linearly with the embedment ratio.

The geogrid reinforcement extended the contact zone between the soil and the laboratory box, resulting in a longer failure surface and increased uplift force. The inclusion of GFR layers enhanced the anchor plate response more effectively than soil reinforcement alone. The study concluded that using a single layer of GFR was more effective than multiple layers in improving the uplift capacity of symmetrical anchor plates.

Bhattacharjee et al. (2008) studied the behavior of square plate anchors under uplift load in reinforced clay using a three-dimensional finite element displacement model with ANSYS software. The analysis of anchor behavior was generalized into two categories: 'Immediate

Breakway' and 'No Breakway.' The 'Immediate Breakway' case was used, wherein upon loading, the vertical stress below the anchor became zero, and no contact between the anchor and the soil occurred. The ultimate pullout capacity in undrained homogeneous clay was expressed in terms of the breakout factor Nc, a function of embedment ratio H/B and overburden pressure. In reinforced clay, the reinforcement mobilized additional shear stress in soils due to tensile forces in the geotextile. The breakout factor for reinforced clay was derived from the ultimate pullout capacity determined from the finite element model, validated by experimental findings for different sizes of square plate anchors in reinforced clay. The soil-anchor system was modelled with 8-noded isoparametric brick elements and the geotextile with two-noded spar elements. Material nonlinearity of soil and geometrical nonlinearity of the geotextile were considered, adopting the Drucker-Prager model for material nonlinearity. The analysis was carried out using incremental-iterative procedures following the modified Newton-Raphson method with ANSYS Software. Model tests investigated the effect of geosynthetics on load displacement behavior of square plate anchors of different sizes in a square tank. The soil used was dry kaolin mixed with water to fill the test tank to the required height. The anchor was placed centrally on a soil cushion, and a filter paper was used to eliminate soil adhesion. The anchor shaft was connected to a cable, passing over two frictionless pulleys, attached to a hanger for pullout loads. Tests were conducted with square anchor plates of sizes 50mm x 50mm and 75mm x 75mm for embedment ratios of 2, 3, and 4, and at different positions of geotextile layers. The properties of soil and geotextile were specified, with kaolinite as the soil and woven geotextile.

Load-displacement curves for a 50mm x 50mm anchor for an H/B ratio of 2, with and without reinforcement, showed that displacement was less for reinforced anchors compared to unreinforced cases with increased uplift load. Both experimental and theoretical values agreed well, with a variation of 10 to 12%. For reinforced clay, both displacement and uplift load increased with embedment ratio H/B. Displacement vectors at failure for different embedment ratios indicated that with increasing H/B from 2 to 4, slight bulging of the soil surface occurred at H/B = 4, while larger zones of heave were noticed for H/B = 2 and 3. The plastic zones extended laterally for H/B = 2 and 3, but displacement vectors were nearly vertical for H/B = 4. The ultimate pullout load for reinforced clay was expressed in terms of pullout capacity factor, with the cross-sectional area of the anchor plate being a critical parameter.

Nene and Garg (1991) investigated the behaviour of shallow plate anchors in reinforced cohesive soil using both woven and non-woven geotextile. The breakout loads were computed by limit equilibrium method. In order to validate the analytical method, model laboratory tests were conducted in cohesive soil with circular and square anchors with geo-synthetic placed at a distance of B/2 and B, B being the width of anchor, from the top of the plate anchor and width four times the width of model footing. The research focused on understanding the interaction between the anchors and the reinforced soil, specifically examining how different reinforcement types and configurations influence the ultimate pullout capacity of the anchors. Experimental tests were conducted using plate anchors of different sizes and shapes embedded in cohesive soil samples reinforced with materials such as geotextiles and geogrids. The results indicated that soil reinforcement significantly enhances the pullout resistance of shallow plate anchors. Key findings demonstrated that the increase in pullout capacity was dependent on the type, orientation, and density of the reinforcement used. Additionally, the study provided insights into the failure mechanisms of reinforced soil-plate anchor systems, highlighting the role of soil-reinforcement interaction in improving the overall stability and load-bearing capacity. These findings had practical implications for the design and optimization of anchoring systems in geotechnical engineering, particularly for applications requiring enhanced stability in cohesive soils.

2.3.2 Under Dynamic Load

Ravishankar et al. (2022) evaluated plate anchors, which are extensively employed in foundation systems to resist static and cyclic pullout stresses from superstructures. It was discovered that the anchor's ultimate pullout capability was lowered by a brief period of cyclic disturbance brought on by wind, waves, or tide. Due to the soil's decreased undrained shear strength following a period of cyclic loading, the post-cycle pullout load that the plate anchor could withstand under actual circumstances was frequently lower. The ultimate static and cyclic pullout capability of the anchor was significantly impacted by the geotextile reinforcement positioned above the horizontal anchor plate, which also addressed the post-cycle shear strength deterioration. The results of several experimental tests on plate anchors embedded in both unreinforced and reinforced soft clay were reported in the study. At various embedment depths, plate anchors were subjected to strain-controlled monotonic and cyclic pullout tests. The outcomes showed that the strengthened system had less anchor displacement and a greater static and cyclic pullout capacity. The anchors buried in reinforced soil demonstrated a better post-

cycle pullout resistance than the anchors in unreinforced soil because of the improved cyclic resilience capability of woven geotextile.

Biradar et al. (2019) examined the pull-out behavior of anchor plates in reinforced soft clay subjected to cyclic loading. It was found that cyclic loading significantly influences the pull-out behavior, but factors such as the size of the anchor plates, different loading frequencies, and amplitudes were not extensively explored.

The study utilized numerical modelling to analyze the pull-out behavior of anchor plates of different sizes under cyclic loading conditions. The findings indicated that the pull-out load of anchor plates increased with the size of the anchor, embedment ratio, amplitude, and frequency of the cyclic loading. For instance, the pull-out capacity increased by about 40% when the size of the square anchor plate increased from 50 mm to 100 mm. Additionally, the pull-out load was observed to increase with the embedment ratio.

The study also revealed that the presence of geosynthetic reinforcement significantly enhanced the pull-out capacity of anchor plates. The additional frictional forces developed between the soil and the geosynthetic material contributed to the increased pull-out loads. The optimum increase in pull-out capacity was achieved when the reinforcement was placed close to the anchor plate, at approximately 0.25 times the embedment depth. Moreover, the width of the reinforcement also played a crucial role, with the pull-out capacity peaking when the reinforcement width was about four times the width of the anchor plate.

Parametric studies confirmed that the pull-out load increased significantly with higher embedment ratios and larger amplitudes of cyclic loading. Specifically, the pull-out load for all plate anchors increased by more than 100% when the embedment ratio varied from 1 to 6. The study proposed a semi-empirical formulation for the breakout factor of square anchors in reinforced soil based on regression analysis of the numerical simulation data. This formulation is expected to aid practicing engineers in designing anchor plates for soft clay under cyclic loading conditions.

Overall, the study provided valuable insights into the pull-out behavior of anchor plates in reinforced soft clay, highlighting the significant impact of cyclic loading and the beneficial effects of geosynthetic reinforcement. The findings underscored the importance of considering various parameters, such as anchor size, embedment ratio, and reinforcement characteristics, in the design and analysis of anchor plates subjected to cyclic loading.

Tafreshi et al. (2018) in their study of cyclic and post-cycling anchor responses in geocell-reinforced sand, a series of near-full-scale experimental tests were conducted to investigate the influence of geocell reinforcements on the cyclic uplift capacity of plate anchors. The experiments included both geocell-reinforced and unreinforced conditions, with anchors buried at various embedment depths and subjected to cyclic loading followed by monotonic post-cycling loading.

The findings revealed that the unreinforced system cyclically failed under a load approximately 70% of its ultimate uplift capacity (P_u). In contrast, the use of geocell reinforcement enabled the system to resist cyclic loads exceeding 100% P_u stably. A cyclic displacement rate of less than 0.05 mm per cycle indicated a stable response. It was observed that under cyclic loading, the load transmission through the soil near the anchor increased over time for unreinforced systems, whereas geocell-reinforced systems were less prone to this phenomenon.

Further, it was found that the post-cycling monotonic capacity of both reinforced and unreinforced anchors decreased after cyclic loading. However, the unreinforced scenario demonstrated a more significant reduction in capacity, particularly in residual capacity. The reinforced cases exhibited a more consistent post-peak ductile response and considerable displacement without significant strength loss, unlike the unreinforced cases which showed substantial reductions in residual capacity.

Two general types of load-displacement behavior were observed under cyclic loading: stable and unstable responses. Stable responses, characterized by decreasing rates of uplift displacement accumulation and reducing hysteresis loop areas, were noted in most reinforced tests and unreinforced cases subjected to lower loading levels. A cyclic load ratio (CLR) of 40% was identified as the threshold between stable and unstable responses for unreinforced conditions.

The study also concluded that accumulated displacement increased with cyclic load ratio and decreased with embedment depth ratio. Reinforced systems prevented excessive displacements even under high cyclic loads, with the maximum anchor upward displacement being lower compared to unreinforced scenarios. Notably, failure was not observed in reinforced conditions subjected to CLR of 40%, 50%, 60%, and 70%, except for one test at D/B = 1.5 under CLR = 70%. Unreinforced conditions under certain cyclic load levels (D/B = 1.5, 2, 2.5 under CLR = 40%) displayed excessive anchor upward displacement, causing significant heave of the soil surface local to the anchor rod. The reinforced beds, on the other hand, maintained higher

resistance against high cyclic loads and showed less pronounced post-cyclic loss of anchor capacity, which is beneficial for long-term applications in environments prone to frequent cyclic loading.

Ravichandran et al. (2008) investigated the uplift behavior of plate anchors under monotonic and cyclic loading in geogrid-reinforced sand beds. The study focused on how reinforcement affects uplift capacity under submerged conditions, considering parameters like reinforcement width, sand packing unit weight, and embedment depth. It was found that geogrid reinforcement significantly enhances uplift capacity under monotonic loading. For cyclic loading, anchor displacement increased initially but stabilized after about 350 cycles, with post-cyclic peak pullout loads slightly higher than those under monotonic conditions.

The investigation showed that the breakout factor, representing pullout capacity, increased with the embedment ratio and sand density, with reinforced conditions yielding higher breakout factors compared to unreinforced conditions. The friction angle's increase also contributed to a higher breakout factor, particularly for deeper and denser sand conditions. Vertical reinforcement was noted to be more effective than horizontal reinforcement due to better interlocking resistance.

Experiments revealed that anchor movement under cyclic loading was influenced by cyclic load amplitude, sand bed density, and embedment depth. Movement per cycle decreased with more cycles, stabilizing after 350 cycles, and was higher in denser sand beds due to higher absolute cyclic loads. Post-cyclic monotonic pullout loads were marginally higher than monotonic pullout loads, although the rate of resistance increase post-cyclic loading was lower due to disturbances and particle rearrangements. The study also confirmed that vertical geogrid reinforcement provided higher uplift capacity compared to horizontal reinforcement.

Dickin and Leung (1983) investigated the stress-displacement behavior of vertical anchor plates and continuous anchor walls in dense sand when subjected to horizontal pull-out forces. They conducted numerous centrifugal model tests on 25 mm and 50 mm models at accelerations up to 40 g. The study aimed to evaluate the errors that arise when extrapolating results from conventional small model tests to field-scale situations. Their findings revealed significant overpredictions of pull-out resistance and underestimations of failure displacements in small-scale models compared to actual field conditions. Despite these discrepancies, the effects of anchor geometry, defined by dimensionless shape factors, remained consistent across different scales.

The researchers compared centrifugal test results with conventional small model test outcomes and recent theoretical and semiempirical design formulas. They used shear strengths derived from plane strain compression tests at appropriate stress levels for this comparison. Their results underscored the importance of using centrifugal modelling to simulate prototype stress levels accurately, thereby eliminating scaling issues associated with conventional small-scale tests.

The study highlighted the limitations of applying small-scale test results directly to field situations without appropriate modelling laws. The complex stress-strain behavior of soils, influenced by factors such as density, stress level, stress path, and strain rate, further complicated the accuracy of predictions based on small-scale tests.

The study demonstrated the applicability of centrifugal testing for vertical anchors and provided insights into the potential errors when using small-scale models to predict field behavior. Their findings emphasized the necessity for appropriate scaling laws and validated the use of centrifugal models to achieve more accurate predictions in geotechnical engineering.

2.4 SUMMARY

This previous section has presented a comprehensive review of the available literature about the behaviour of horizontal, vertical and inclined anchors embedded in different types of soil. The response of horizontal, vertical and inclined anchors embedded in different types of soil has been investigated in details during the previous few decades. These investigations have encompassed experimental studies as well as numerical and analytical approaches. However, most of these studies have concentrated on analysing the behaviour of vertical and horizontal anchor in different soils. From the review of literature, it has been found that only few studies have been made for anchors in reinforced soil (Banerjee and Nagaraju, 2017, Niroumand et al. 2013, Bhattacharjee et al. 2008), and most of the works have comprised of vertical anchors only. The pullout behaviour of anchor due to cyclic loading has been investigated by only few researchers (Biradar et al. 2019, Tafreshi et al. (2018), as per available literature. So, it becomes evident that the behaviour of inclined anchors in both unreinforced and reinforced soil bed is not well addressed in the available literature.

2.5 RESEARCH GAP

Although prior studies have analyzed vertical and horizontal anchors in various soil conditions, the response of inclined anchors in both reinforced and unreinforced soils is not well-documented. The pullout behavior of anchors under cyclic loading has only been explored in a

few cases. Thus, there is a clear gap in understanding how inclined anchors perform, particularly in soft clay environments with or without reinforcement, under cyclic loads.

2.6 NOVELTY OF THE PRESENT RESEARCH

This study aims to bridge the existing research gap by investigating the response of inclined anchors embedded in soft clay, both with and without soil reinforcement, under cyclic loading conditions. The current research offers a novel exploration into how these anchors behave in challenging soil conditions, providing insights that were previously underexplored in geotechnical studies. Based on this, the objective and scope of the work have been obtained for the current research and presented in subsequent sections.

2.7 OBJECTIVES:

The aim of the present study has been focussed to investigate the pull-out behaviour of inclined square plate anchors of different widths and embedded in soft clay with different inclinations Hence the determination of pull-out capacity for different sizes of square anchor plates has been envisaged with different embedment depths with different angles of inclination and different combination of frequency and amplitude in soft cohesive soil. With the above in view, the following objective has been identified for the present study:

To study the pull-out behavior of inclined anchors in unreinforced and reinforced soft clay.

2.8 SCOPE OF WORK:

The scope of the present study is outlined below:

1. Numerical analysis of the respective anchor models (inclined model anchor plates having dimensions of 0.025 m × 0.025 m, 0.050 m × 0.050 m, and 0.075 m × 0.075 m with embedment ratios of 1, 2 and 3 and inclination angles 30°, 45°, and 60° with vertical, in unreinforced and reinforced soft clay under static and cyclic loading have been done using ABAQUS (version 6.14), a finite element software. Comparison of numerical models following the present way of analysis has been made with the available results from the already executed study by some earlier researchers to validate the numerical model of the present study.

2. Experimental investigation which encompasses carrying out model tests relating to pull-out behaviour of inclined model anchor plates having dimensions of 0.025 m × 0.025 m, 0.050 m × 0.050 m, and 0.075 m × 0.075 m with embedment ratios of 1, 2 and 3 and inclination angles 30°,

45°, and 60° with vertical, in unreinforced soft clay. For reinforced clay, inclined model anchor plates having dimensions of 0.025 m × 0.025 m and 0.050 m × 0.050 mm with embedment ratios of 1, 2 and 3 and inclination angles 30°, 45°, and 60° with vertical have been considered.

3. Finally, compilation of the results after comparing the numerical and experimental results and carrying out a parametric study to understand the influence of the relevant parameters (plate size, inclination angle, embedment ratio, soil type, frequency and amplitude of the cyclic load) on ultimate pullout capacity and also to develop a regression model based on the available results, to predict ultimate pullout capacity.

CHAPTER 3

MATERIALS AND METHODS

3.1 OVERVIEW

The study investigates the behaviour of inclined anchor plate in unreinforced and reinforce clay. Materials and main methods used for this have been discussed in this chapter.

3.2 MATERIALS

The following materials have been used in the entire test:

1.Soil for foundation bed.

2. Mild steel for anchor plate

3.Geotextile for soil reinforcement

Tests have been carried out for each of these materials to determine their respective properties. These properties have been used in the experimental and numerical studies. The tests are as follows:

3.2.1 Tests for Clay

Locally available clay collected from Jadavpur, West Bengal, India has been used in this study. In order to find out engineering properties of the Clay routine standard laboratory tests were conducted for index properties, compaction characteristics and undrained shear strength. The experimental procedure for routine tests on Clay used was followed according to IS specification in which tests like Grain Size Distribution (IS: 3104-1965), Atterberg Limit (IS: 2720 Part V, 1965), Standard Proctor Test (IS: 2131-1963) and Undrained Shear Strength were conducted. For undrained shear strength, the test was done with Clay compacted to a water content of 19.5% and dry density 16.5 KN/ m^3. For the present study water content for compaction was fixed at OMC+4 %, based on literature study done previously (Sengupta et. al., 2017) as it would resemble to the field condition that would require improvement through the use of plate anchors.

- **Properties of Clay**: **-** Laboratory test conducted over clay showed following results
  - Liquid Limit (LL) = 37.7 %
  - Plastic Limit (PL) = 23.8 %
  - Optimum Moisture Content = 14 %
  - Maximum Dry Density (Υ_d) = 1.70 T/m^3

- Average water content during testing = 18%
- Unit wt. of compacted soil during testing = 19.38 kN/m^3
- Undrained cohesion, C = 2.5 T/m2
- Angle of internal friction, ϕ = 0
- Grain size: Sand = 0%, Silt = 75%, Clay = 25%

Based on the test data, grain size distribution, Proctor compaction and Unconfined compressive strength of clay used in the present investigation are exhibited in Fig. 3.1 to 3.4.

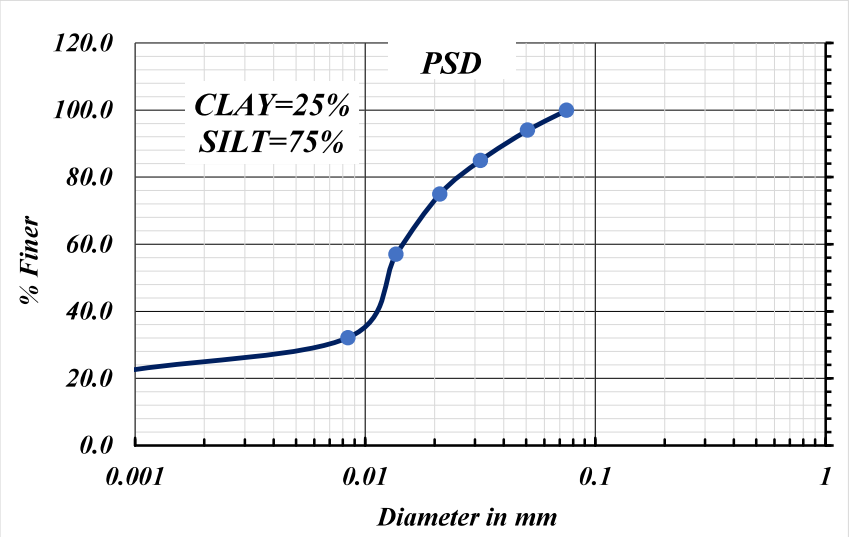

Fig. 3.1: Particle Size Distribution through Hydrometer Analysis

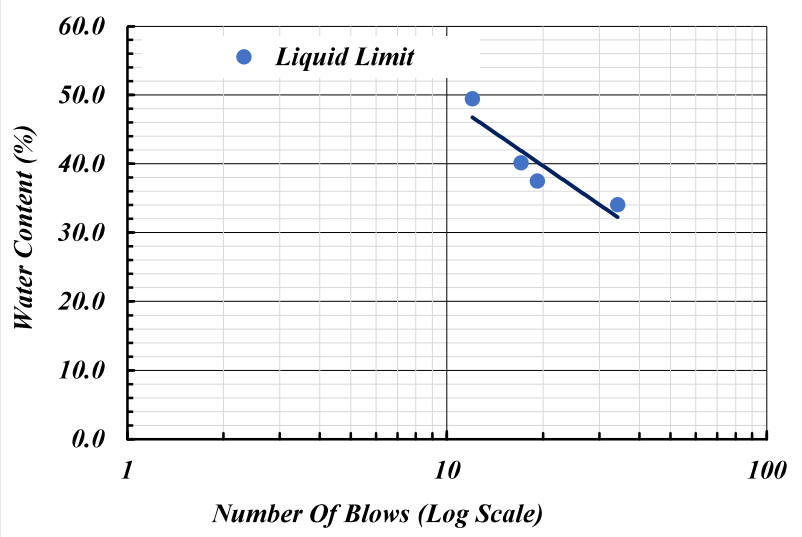

Fig. 3.2: Liquid Limit Determination

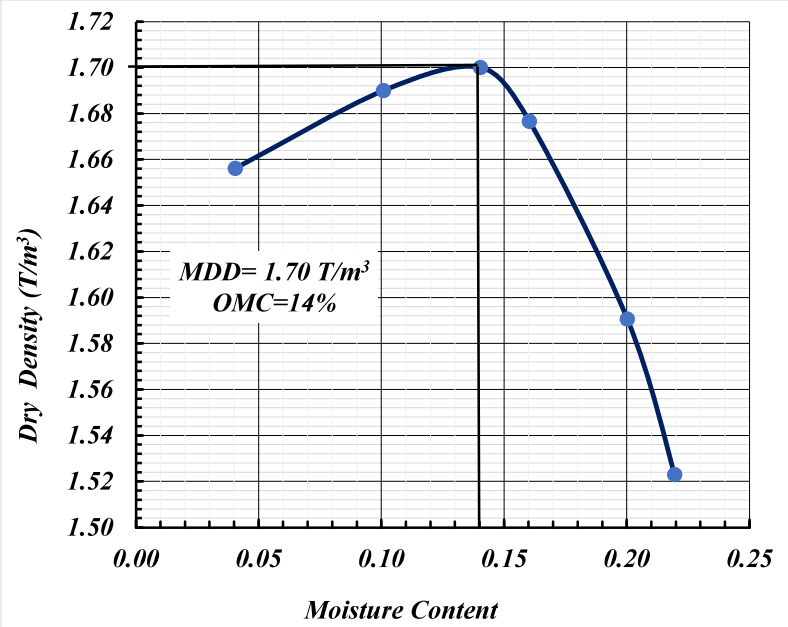

Fig. 3.3: Determination of Proctor Density

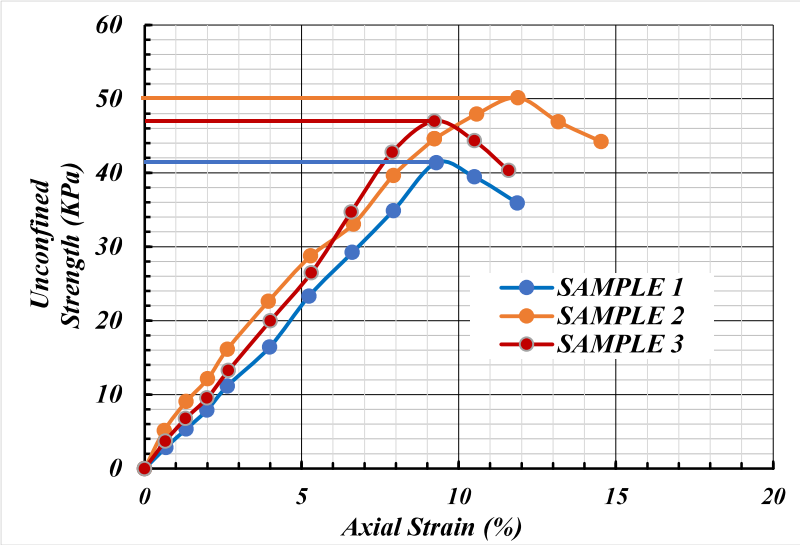

Fig. 3.4: Determination of Unconfined Compressive Strength

3.2.2 Tests for Geotextile*:*

Woven geotextile of permeable polystron fabric has been used in the present investigation as reinforcing material. Tests were conducted on geotextile material used in the present study to determine the thickness (ISO 9863), mass per unit area (ISO 9864), Apparent opening size (ISO 12956). Tensile Strength at 10% elongation (ISO 10319) as well as the breaking load was

estimated. The obtained results of the tests conducted over the geotextile material showed more or less similar values that are obtained from Manufacturer's manual.

- Properties of Geotextile: - Physical and mechanical properties of the geotextile obtained from the standard tests as discussed above are given below:
  - Thickness = 0.36 mm
  - Mass per unit area = 146 gm/m^2
  - Tensile strength (Machine Direction) = 27.6 KN/m
  - Elongation at maximum load = 28.6%
  - Load at 10% elongation = 15 KN/m
  - Interface adhesion between Soil and Geotextile = 0.17

The Tensile stress characteristics of the geotextile has been shown in Fig. 3.5

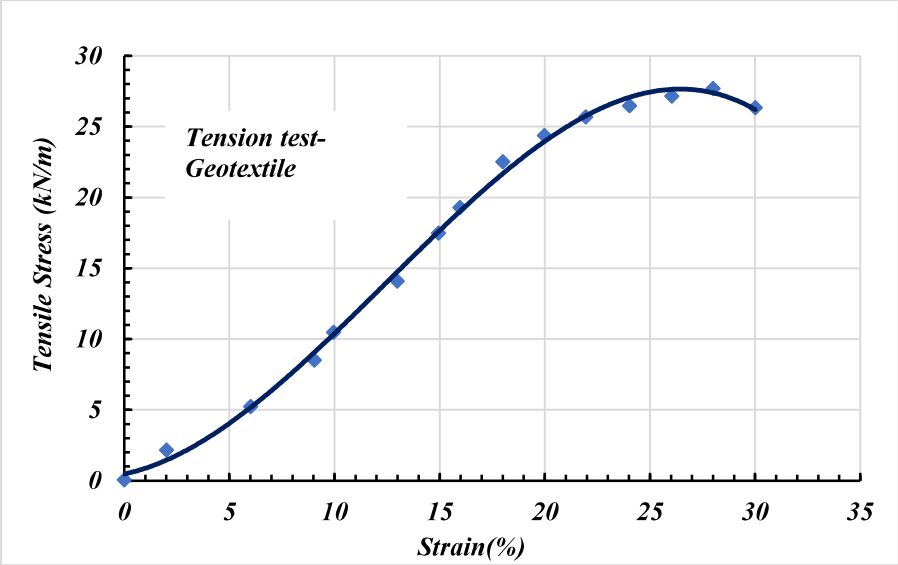

Fig. 3.5: Tension Test of Geotextile

3.2.3 Test for Mild Steel (Material of Anchor Plate):

In the ongoing investigation square anchor plates made of mild steel has been used. To determine the properties of the mild steel plates to be used a Tension test was conducted with a round tensile specimen made from mild steel and tested in UTM at a strain rate of 0.05 mm/sec. Typical Stress Strain graph obtained from tension test of mild steel specimen has been exhibited in Fig. 3.6 to Fig. 3.9.

- Properties of Anchor Material: - Physical and mechanical properties of the Anchor material obtained from the Tension tests as discussed above are given below:
  - Young's Modulus (E) = 200 GPa
  - Mass per unit volume (ϒ) = 7850 Kg/m^3
  - Poisson's Ratio (μ) = 0.33

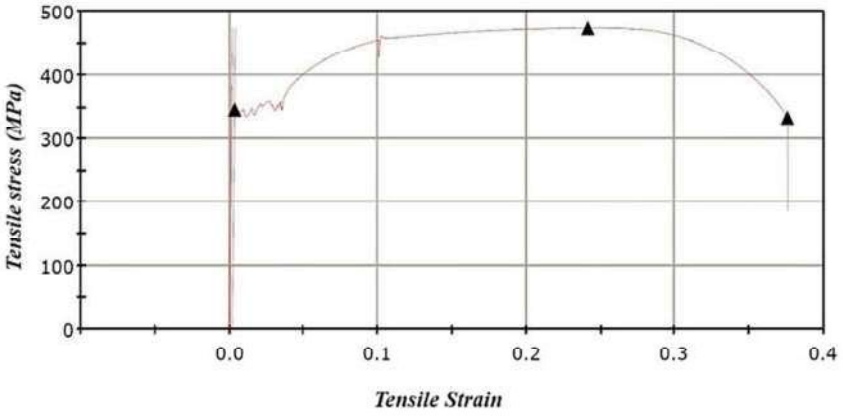

Fig. 3.6: Tension Test of Mild Steel Specimen

Fig. 3.7: Tension Test of Mild Steel Specimen

Fig. 3.8: Tension Test of Mild Steel Specimen

Fig. 3.9: Tension Test of Mild Steel Specimen

3.3 METHODS

Methodology adopted for the numerical and experimental studies has been briefly illustrated in this section.

3.3.1 Numerical Study:

Several numerical techniques have been developed to analyze the behaviour of the plate anchors in clay soils. The numerical modelling of the plate anchors is associated with important input data of sizes of anchor plates, depth of embedment, inclination angle of anchor plate and frequency & amplitude of load. Finite element analysis software ABAQUS v6.14 is used for the numerical modelling. The square plate size of 25 mm, 50 mm, and 75mm has been used at three different embedded ratios of 1, 2 and 3 at inclination angles of 30, 45 and 60° with the vertical in soil. For the numerical study analyses have been carried out under monotonic loading by providing a definite displacement in vertical and horizontal direction according to the inclination angle at the anchor plates. Direct method of equation solver with unsymmetrical matrix storage is specified in analysis step. Mohr Coulomb failure model has been adopted for inclusion of non-linearity of soil, which has been considered as an isotropic strain hardening material. When material and mesh deform together, the Lagrangian domain is normally used. On the contrary, the Eulerian domain is being used when the mesh remains in fixed position while the material undergoes deformation. Geometric nonlinearity is taken into consideration in the Lagrangian domain. Furthermore, the material boundary and an element boundary overlap in the Lagrangian domain since all of the Lagrangian elements are composed of a single material. Here, only the Lagrangian domain has been employed to conduct the current study. This part of the study has been done for static as well as cyclic loading. In case of cyclic loading, the anchor plate has been subjected to two cycles of sinusoidally varying displacement with the amplitudes of 2 mm, 5mm at the plate surface. Load displacement behaviour of the anchor plate-soil system has been explored by applying loading frequencies of 0.2 Hz, 0.5 Hz. Subramaniam and Banerjee (2013 and 2014) reported that beyond 1st five cycles the reduction in strength of soil is not significant. Hence it was decided to consider the first two cycles, where the majority of reduction is taking.

3.3.2 Experimental Study:

The test programme for model anchor tests has been done for unreinforced and reinforced clay using different embedment depths and position of geotextiles above the bottom level of plate (0.25 times the depth of embedment from bottom of anchor plate) in embedded soil. For

unreinforced bed, total twenty-four numbers of tests have been carried out covering three different plate sizes (0.025 m × 0.025 m, 0.050 m × 0.050 m, and 0.075 m × 0.075 m) with different embedment depth for each case. In case of reinforced bed, eighteen model tests have been carried out for 25 mm and 50 mm square plate having a fixed width of geosynthetics and positioned at a distance of 0.25 times the depth of embedment from bottom of anchor plate.

3.4 SUMMARY

The present chapter has detailed the materials and methodology to be adopted in this study. It has also described the basic engineering properties of the materials to be used in the study. Finally, a brief description of numerical and experimental modelling technique is also included.

CHAPTER 4

NUMERICAL STUDY

4.1 OVERVIEW:

In this chapter numerical study has been performed to investigate the behavior of inclined plate anchors in unreinforced and reinforced clay soil under static and cyclic loading. Details of the study have been divided into following four sub sections: -

1. Inclined anchors in unreinforced clay under static loading.
2. Inclined anchors in reinforced clay under static loading.
3. Inclined anchors in unreinforced clay under cyclic loading.
4. Inclined anchors in reinforced clay under cyclic loading.

4.2 FINITE ELEMENT ANALYSIS:

Several numerical techniques have been developed to analyze the behaviour of the plate anchors in clay soils. The numerical modelling of the plate anchors is associated with important input data of sizes of anchor plates, depth of embedment, inclination angle of anchor plate and frequency & amplitude of load. Finite element analysis software ABAQUS v6.14 has been used for the numerical modelling of reinforced analysis.

The square plate size of 25 mm, 50 mm, and 75mm has been used at three different embedded ratios of 1, 2 and 3 at inclination angles of 30, 45 and 60°s with the vertical in unreinforced soil.

4.2.1 Use of ABAQUS for the Present Study:

The methodology of the current work mainly is comprised of Finite element modelling in ABAQUS software which is illustrated as follows:

The numerical modelling of the plate anchors is associated with important input data of sizes of anchorplates, depth of embedment, inclination angle of anchor plate and frequency and amplitude of load. Finite element analysis software ABAQUS v6.14 has been used for the numerical modelling. The square plates of size 0.025 m, 0.050 m, and 0.050 m have been used at three different embedded ratios of 1, 2 and 3 at inclination angles of 30, 45 and 60°s with the vertical in reinforced clayey soil.

The software has been used to generate the model graphically, run the program, and then obtain the results. The numerical analysis of soil-anchor models has been carried out using general-purposefinite element analysis software ABAQUS v 6.14.

The Lagrangian domain is generally used when material and mesh both deform with each other. On the other hand, Eulerian domain is used when mesh stays in fixed position as the material deforms. In Lagrangian domain, geometric non linearity is considered. Moreover, in Lagrangian domain, Lagrangian elements are totally of a single material, so the material boundary overlaps with an element boundary. Here the present study has been carried out using only the Lagrangian domain.

It has been considered that, at failure of soil, there should not be any deformation or distortion of anchor plate. Soil body has been discretized with 4- nodded quadrilateral plane strain elements and modelling of soil has been done by Mohr-Coulomb plasticity model. The anchor plate and geotextile has been modelled as 2-D wire elements.

Numerical analysis using ABAQUS has been carried out based on 2D plain strain condition. The modelling of square anchor plates in a 2D plane strain model brings limitations, because plate-soil interaction isa strongly 3D phenomenon. However, 3D model of the anchor plates with contact pairs would require significant computing resources. Similar observations have also been made by other researchers (O'Kelly et al. 2013; Nouri et al. 2016)

Interaction at the soil-anchor interface has been considered with soil as slave surface and anchor as master surface. Node to surface discretization due to the rigidity of anchor material than the deformable soil has been modelled with small sliding behaviour accounting for the cohesive property.

The energy of the wave increases with both frequency and amplitude. Further with increase of frequency and amplitude dynamic amplification increases. This may reflect in foundation stiffness. In the present numerical analysis, an attempt has been made to carry out behavioural study of plate anchors under cyclic loading with variation of amplitude and frequency. Therefore, they have been considered to be subjected to low frequency and low amplitude leading low to moderate strain and large-scale nonlinearity of the system has been averted. Uniform displacement was applied uniformly across all nodes of the anchor plate, subjecting it to two cycles of sinusoidally varying displacement with amplitudes of 2 mm and 5 mm. The

load-displacement behavior of the anchor plate-soil system was explored by applying loading frequencies of 0.2 Hz and 0.5 Hz. Further it may be noted that Biradar et al. (2019) also carried out their study with similar frequencies and amplitudes.

The present study considers soil anchor system in two parts; the soil and the anchor. The soil has been modelled using Mohr-Coulomb criterion available in the software. The anchor has been modelled as linear-elastic material. Total three-square anchor plates of size 0.025 m, 0.050 m and 0.050 m have been considered for analysis. The domain of soil medium defined is 1m x 1m, as from pilot study this was found to be enough to minimize the influence of boundary constraints on the behaviour of anchor plates. Clayey soil in reinforced condition has been used for this study.

Initially pilot studies have been carried out to finalise the dimensions of domain and anchor model for the numerical study. In this context, it may also be noted that mesh refinement is a crucial aspect of numerical analysis, particularly in the context of finite element analysis (FEA). Here for this numerical study, meshes have been refined with utmost effort. Some pilot studies in respect of refining the mesh, have also been carried out to ensure accurate results. The final mesh size for both main domain and interface elements have been obtained after a good number of such pilot studies. The interface elements have been considered to take into account so that no slip occurs within the region of change of material near the interface of anchor and soil.

4.2.2 Constitutive Model and Property Used:

In the model adopted for the present study Mohr- Columb failure criterion has been used for soil. The anchor plate has been considered as elastic structural element. Various properties of soil, anchor plate and geotextile used for numerical study have been given in Table 4.1. Those values have been obtained from the laboratory tests conducted in Soil Mechanics and Foundation Engineering laboratory, Department of Civil Engineering, Jadavpur University.

Table 4.1: Properties of Material

SOIL	
Constitutive Model	Mohr- Columb Plasticity model
Property	**Value**
Density (γ_{soil}) (kN/m^3)	19.42
Cohesion (C_u) (kN/m^2)	24.517
Angle of Internal Friction (ϕ) (Degree)	5
Tensile Cut-off Stress (kN/m^2)	49.033
Liquid Limit (W_L) (%)	37.7
Plastic Limit (W_p) (%)	23.8
Plasticity Index (I_p)	13.9
Poisson's Ratio (μ)	0.33
Young's Modulus (E_s) (kN/m^2)	11×10^3
ANCHOR PLATE MATERIAL	
Constitutive Model	2-D wire elements
Density (γ_{anchor}) (kN/m^3)	76.982
Poisson's Ratio (μ)	0.33
Young's Modulus (E_s)(kN/m^2)	2×10^8
PROPERTIES OF GEOTEXTILE	
Constitutive Model	2-D wire elements
Thickness (m)	0.0036
Density ($\gamma_{Geotextile}$) (kN/m^3)	0.00143
Poisson's Ratio (μ)	0.42
Young's Modulus (E_s)(kN/m^2)	4.2×10^5
Mass per unit area	146 gm/m^2
Tensile strength (kN/m)	27.6
Elongation at maximum load	28.6%
Load at 10% elongation	15 KN/m
Interface adhesion between Soil and Geotextile	0.17
NB.: Tests were conducted on geotextile material to be used in the present study to determine the thickness (ISO 9863), mass per unit area (ISO 9864), Apparent opening size (ISO 12956). Tensile Strength at 10% elongation (ISO 10319) as well as the breaking load was estimated. The obtained results of the tests conducted over the geotextile material showed more or less similar values that are obtained from Manufacturer's manual.	

Note: Poisson's Ratio (μ) of the soil has been obtained from relationship mentioned in Annexure I

4.3 INCLINED ANCHORS IN UNREINFORCED CLAY UNDER STATIC LOADING:

4.3.1 Boundary Conditions:

Boundary conditions have been created in the step specified for analyses. Mechanical, displacement/rotation boundary conditions have been chosen, defining hinge and roller conditions as shown in Fig 4.1.

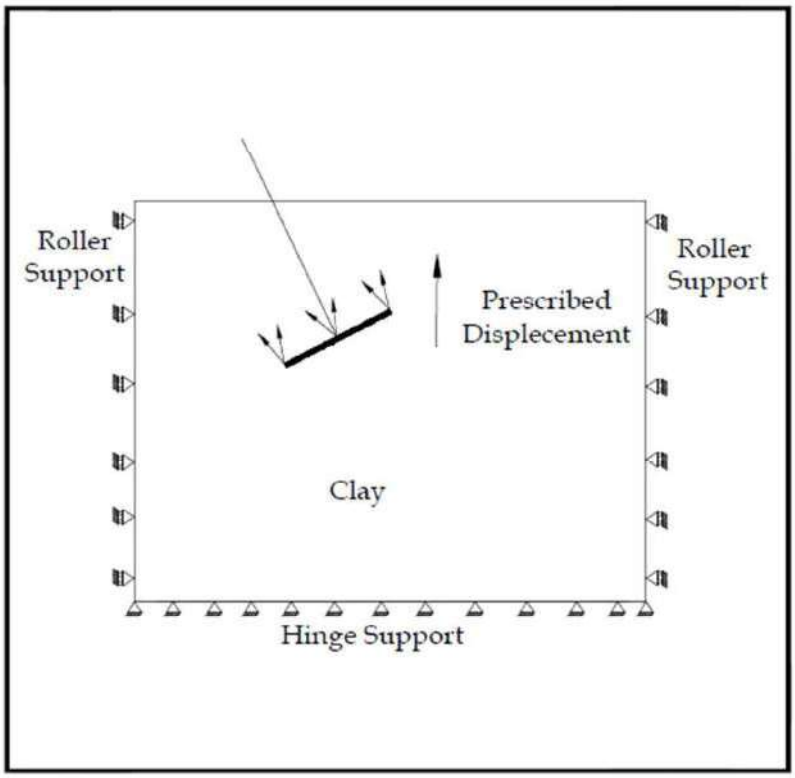

Fig. 4.1: Schematic Representation of Boundary Condition specified in ABAQUS

4.3.2 Solution Procedure:

For the present numerical study analyses have been carried out under monotonic loading by providing a definite displacement in vertical and horizontal direction according to the inclination angle at the anchor plates. Direct method of equation solver with unsymmetrical matrix storage is specified in analysis step. Full newton method of solution technique with linear extrapolation is considered for the present study. Mohr Coulomb failure model has been adopted for inclusion of non-linearity of soil, which has been considered as an isotropic strain hardening material.

4.3.3 Validation of Numerical Model

In order to extend the numerical study for inclined anchors in geotextile reinforced soft clay, an attempt has been made to validate the result obtained by Das and Puri (1989) for inclined anchor in soft clay. Ultimate load has been observed to increase with embedment ratio for any particular plate size because of higher embedment ratios soil resists pullout displacement of the plate. The increase in ultimate load has been observed to correspond with the increasing inclination for a specific embedment depth (Das and Puri, 1989), as depicted in Fig. 4.2. The size of the plates is 50.8 mm x 50.8 mm x 9.5 mm embedded in clay having the value of $c_u = 42.45$ KN/m^2. Table 4.2 represents experimental parameters for anchor Plate Tests conducted by Das and Puri (1989).

Table 4.2: Experimental Parameters for Anchor Plate Tests (After Das and Puri, 1989)

Parameter	Values/Description
Anchor Types	Horizontal, Vertical, Inclined
Embedment Ratio (D/B)	1, 2, 2.5, 3, 4, 5, 6, 7, 8
Angle of Inclination (in Degree)	Horizontal: 0°, Vertical: 90°, Inclined: 20°, 30°, 40°, 45°, 60°, 70°
*Soil Unit Weight (r)**	21.02 kN/m³ (±6% variation)
Moisture Content (w)	17.4%
Degree of Saturation (Sr)	98%
Undrained Cohesion (Cu)	42.45 kN/m²
Specific Gravity of Soil (G_s)	2.7
Triaxial Test Condition	U-U triaxial tests conducted at a strain rate of 1% per minute

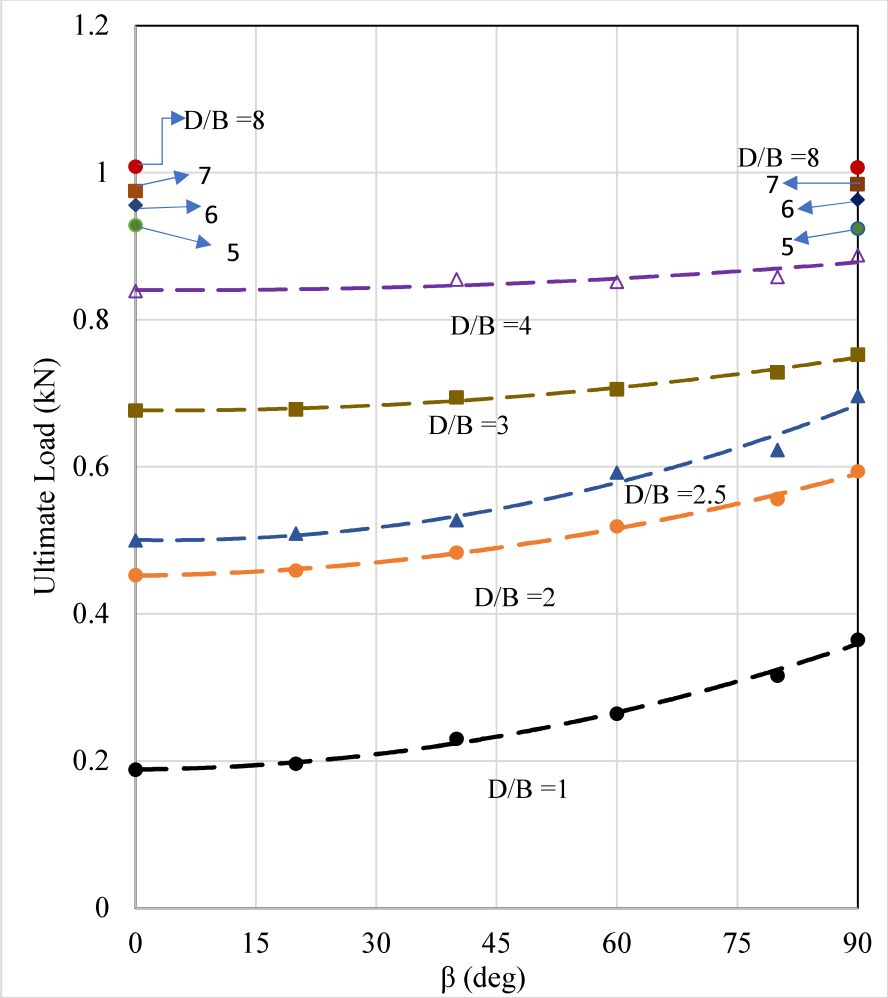

Fig. 4.2: Ultimate load vs inclination angle (After Das and Puri, 1989)

The same trend also has been observed in the present study using the numerical approach made in the present study with the input of same properties obtained from the paper of Das and Puri (1989). Fig. 4.3 shows the superimposed comparative graphs obtained from the values generated from numerical models of present study and from the values obtained from the paper of Das and Puri (1989).

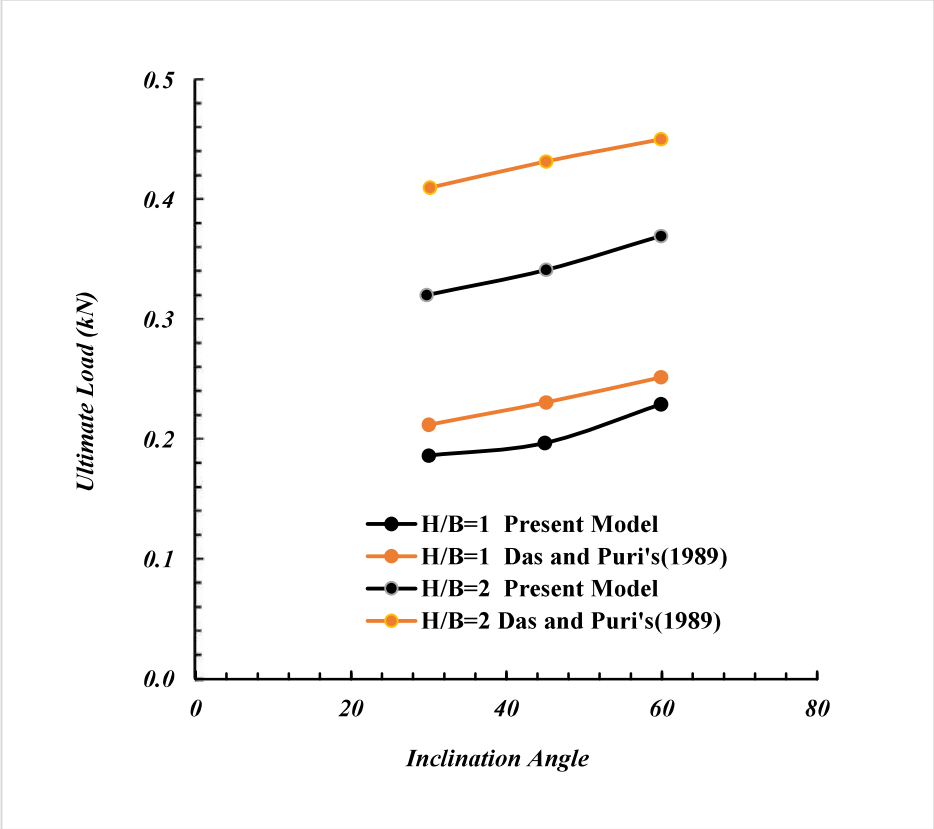

Fig. 4.3: Comparative study of Ultimate load vs Degree of inclination from paper of Das and Puri's (1989) to present model

The maximum deviation of the value from present study with respective value from the paper of Das and Puri (1989) is almost 24.44% (i.e. [{(0.45-0.34)/(0.45)} x 100%]).

The minimum deviation of the value from present study with respective value from the paper Das and Puri (1989) is almost 12% (i.e. [{0.25-0.22)/(0.25) x 100%]).

More over graphs obtained from the study of Das and Puri (1989) (with some inputs of specific parameters) and graphs generated from the present study (with same inputs of same specific parameters), are showing the same trend. So, this particular resemblance has indicated that the present model can be extended for the studies on inclined anchors embedded in geotextile reinforced soft clay.

4.3.4 Numerical Cases in Unreinforced Soil Condition

The total numerical case studies in unreinforced soil condition with plate sizes,embedment ratio and inclination angle has been given in Table 4.3.

Table 4.3: Programme for Numerical Study in Unreinforced soil condition

SL NO.	Plate Size (mm)	Embedment Ratio(H/B)	Inclination Angle w.r.t Vertical	Nomenclature
1	25mm X25mm	1	30°	25-01-30
2			45°	25-01-45
3			60°	25-01-60
4		2	30°	25-02-30
5			45°	25-02-45
6			60°	25-02-60
7		3	30°	25-03-30
8			45°	25-03-45
9			60°	25-03-60
10	50mm X50mm	1	30°	50-01-30
11			45°	50-01-45
12			60°	50-01-60
13		2	30°	50-02-30
14			45°	50-02-45
15			60°	50-02-60
16		3	30°	50-03-30
17			45°	50-03-45
18			60°	50-03-60
19	75mm X75mm	1	30°	75-01-30
20			45°	75-01-45
21			60°	75-01-60
22		2	30°	75-02-30
23			45°	75-02-45
24			60°	75-02-60
25		3	30°	75-03-30
26			45°	75-03-45
27			60°	75-03-60

4.3.5 Presentation of Results of Numerical Analysis:

4.3.5.1 Pullout load vs displacement graphs:

Fig. 4.4 shows the variation of the pull-out load with the progressive increase in the displacement. As can be seen for the figure, the load increases almost linearly with the displacement up to a displacement of 0.25mm followed by a nonlinear plastic behaviour. The

double tangent method results in an ultimate load of 3.5 kg. Similar results have been obtained for different inclination of plates and H/B ratios as shown from Fig. 4.5 to Fig. 4.30, which have been presented in Annexure II. The pull-out load according to the model condition is given in Table 4.3.

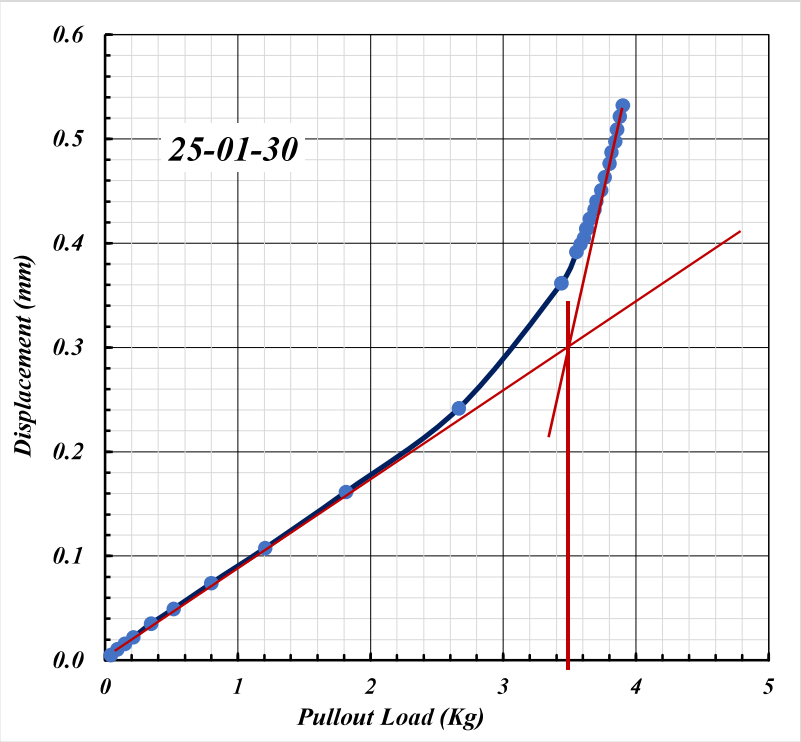

Fig. 4.4: Load vs Axial movement for 25 mm Square Plate with (H/B=1) inclined at 30° with vertical in unreinforced soil

4.3.5.2 Stress Contour of Numerical Analysis:

Fig. 4.31 shows the variation of stress contours at maximum load capacity. As can be seen for the figure, there are changes in the stress pattern (due to deformations generated in the soil-anchor system due to application of pull over the anchors) in each stress contours and the changes have been indicated by different colour combinations. In each and every stress contour, red colour indicates high stressed zone and blue colour indicates the unaffected zones from stress. Similar results have been obtained for different inclination of plates and H/B ratios as shown from Fig. 4.32 to Fig. 4.57, presented in Annexure II.

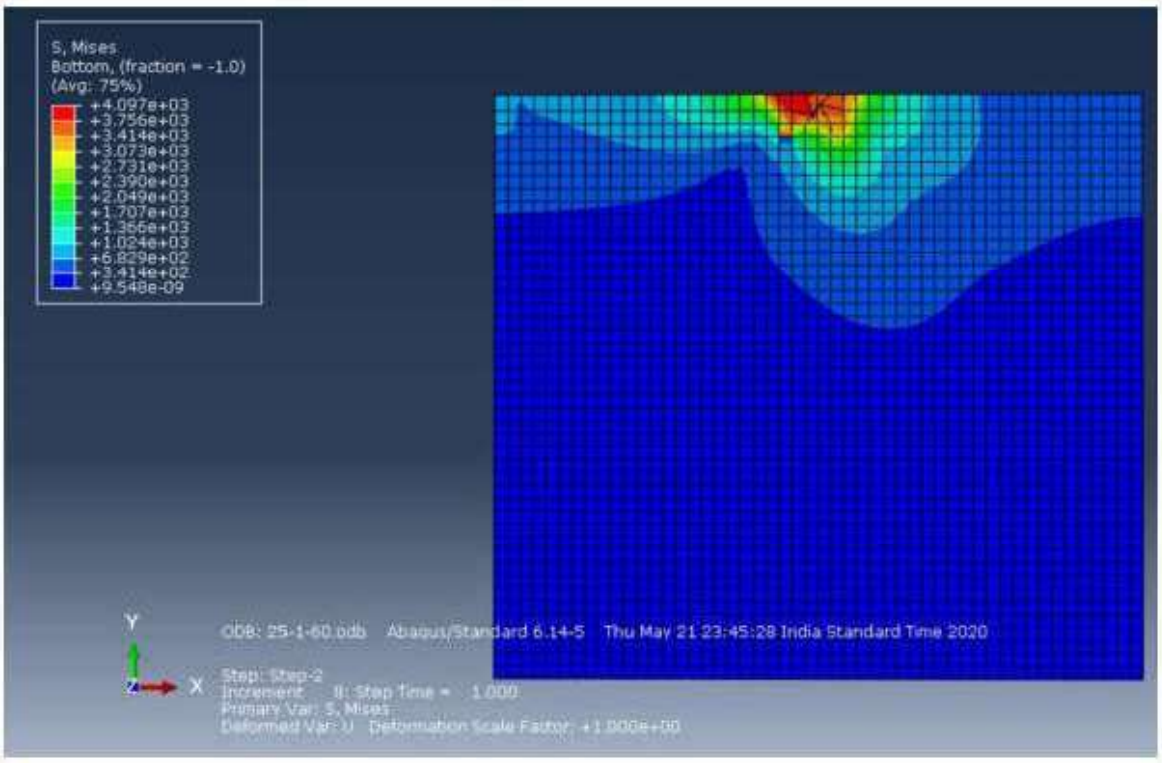

Fig. 4.31: Stress Contour for 25mm Square Anchor Plate with (H/B =1) inclined at 30° with vertical in unreinforced soil

Table 4.4 has been based on the failure load as obtained from load-displacement curves presented from Fig. 4.4 to 4.30, by double tangent method.

Table 4.4: Results from Numerical Analysis in unreinforced soil

SL NO	Nomenclature	Pullout Load (kg)
1	25-01-30	3.5
2	25-01-45	4
3	25-01-60	4.3
4	25-02-30	4.4
5	25-02-45	5.2
6	25-02-60	5.8
7	25-03-30	4.7
8	25-03-45	5.8
9	25-03-60	6.2
10	50-01-30	6.2
11	50-01-45	7.6
12	50-01-60	12.2
13	50-02-30	8.8
14	50-02-45	10.1
15	50-02-60	15.2
16	50-03-30	10
17	50-03-45	12.4
18	50-03-60	17.6
19	75-01-30	17
20	75-01-45	19.5
21	75-01-60	24.5
22	75-02-30	20.5
23	75-02-45	27
24	75-02-60	30
25	75-03-30	27.5
26	75-03-45	32.5
27	75-03-60	38

4.4 INCLINED ANCHORS IN REINFORCED CLAY UNDER STATIC LOADING:

4.4.1 Boundary Conditions:

Boundary conditions were created in the step specified for analyses. Mechanical, displacement/rotation boundary conditions were chosen, defining hinge and roller condition as shown in Fig. 4.58.

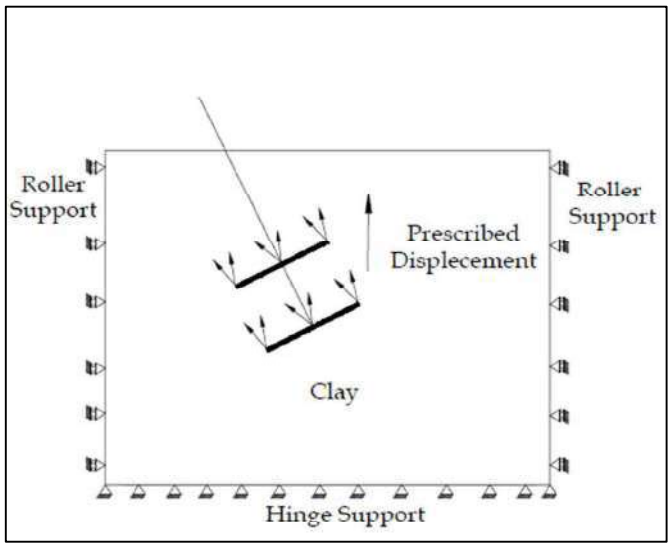

Fig. 4.58: Schematic Representation of Boundary Condition specified in ABAQUS

One typical mesh generated in ABAQUS for analysis of numerical models has been shown in Fig. 4.59.

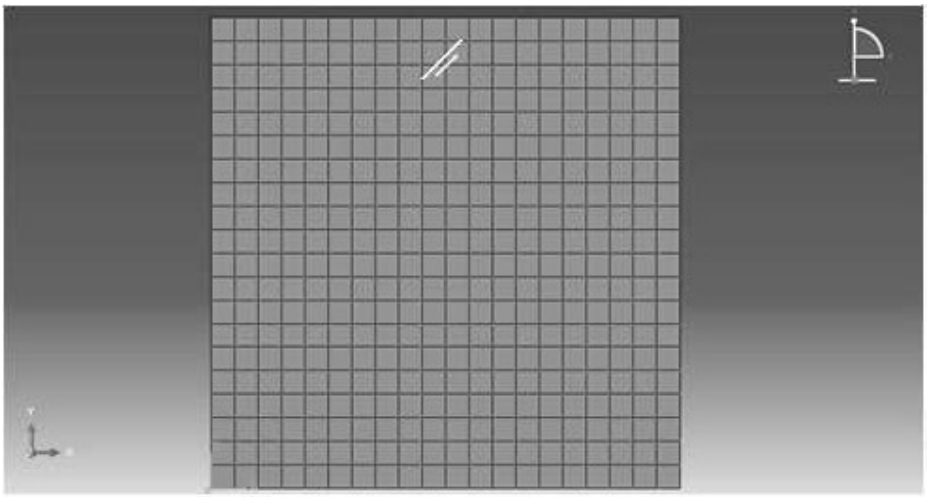

Fig. 4.59: Typical Finite Element mesh developed in ABAQUS

4.4.2 Numerical Cases for Reinforced Soil Condition

The total numerical cases for unreinforced soil condition with plate sizes,embedment ratio and inclination angle have been given in Table 4.5.

Table 4.5: Programme for Numerical Study in reinforced soil condition

Sl No.	Plate Size (mm)	Embedment Ratio(H/B)	Inclination Angle w.r.t Vertical	Nomenclature
1	25mm X25mm	1	30°	25-01-30(RE)
2			45°	25-01-45(RE)
3			60°	25-01-60(RE)
4		2	30°	25-02-30(RE)
5			45°	25-02-45(RE)
6			60°	25-02-60(RE)
7		3	30°	25-03-30(RE)
8			45°	25-03-45(RE)
9			60°	25-03-60(RE)
10	50mm X50mm	1	30°	50-01-30(RE)
11			45°	50-01-45(RE)
12			60°	50-01-60(RE)
13		2	30°	50-02-30(RE)
14			45°	50-02-45(RE)
15			60°	50-02-60(RE)
16		3	30°	50-03-30(RE)
17			45°	50-03-45(RE)
18			60°	50-03-60(RE)
19	75mm X75mm	1	30°	75-01-30(RE)
20			45°	75-01-45(RE)
21			60°	75-01-60(RE)
22		2	30°	75-02-30(RE)
23			45°	75-02-45(RE)
24			60°	75-02-60(RE)
25		3	30°	75-03-30(RE)
26			45°	75-03-45(RE)
27			60°	75-03-60(RE)

4.4.3 Presentation Of Results of Numerical Analysis in Reinforced Soil

4.4.3.1 Pullout load vs displacement graphs:

Fig. 4.60 shows the variation of the pull-out load with increasing displacement for anchor in reinforced soil bed. As seen in the figure, the load increases approximately linearly with displacement up to 0.8 mm, after which it exhibits nonlinear plastic behaviour. The double tangent approach produces an ultimate load of 4.8 kg. Similar findings have been obtained for varying plate inclinations and H/B ratios, as illustrated in Fig. 4.61-4.86 in Annexure III. Table 4.5 shows the pull-out load based on model conditions.

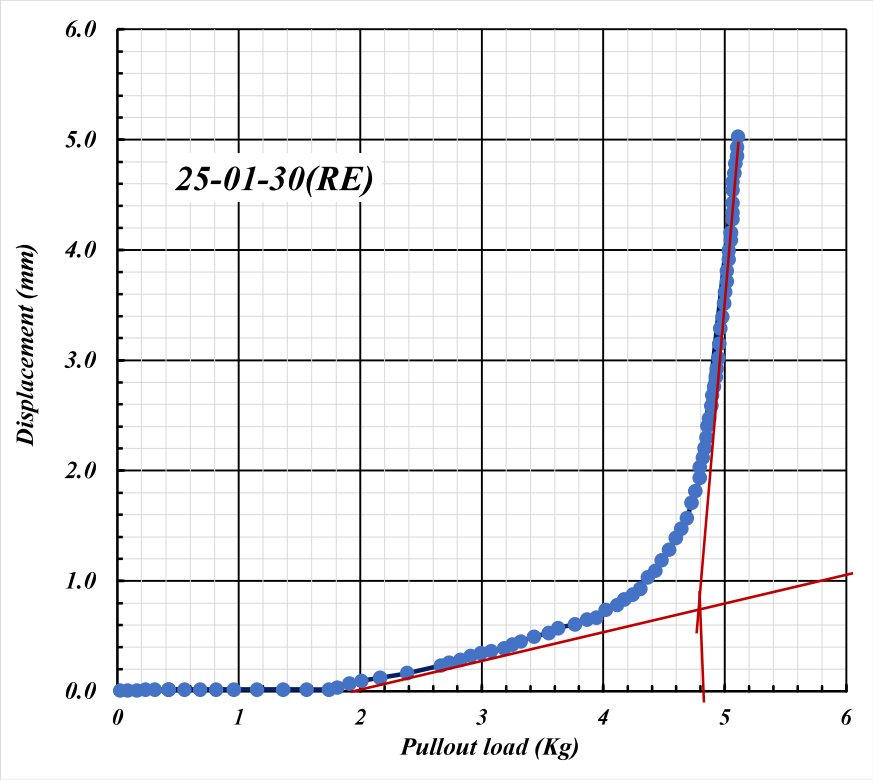

Fig. 4.60: Load vs Axial Movement for 25mm Square Plate with (H/B=1) inclined at 30° with vertical in reinforced condition

4.4.3.2 Stress Contour of Numerical Analysis:

Figure 4.87 shows the change in stress contours at maximum load capacity. As shown in the figure, there are changes in the stress pattern (due to deformations formed in the soil-anchor system as a result of pulling on the anchors) in each stress contour, which are shown by different colour combinations. In each stress contour, red denotes a highly stressed zone while

blue indicates unaffected zones from stress. Similar findings have been obtained for various plate inclinations and H/B ratios, as illustrated in Figs. 4.88-4.113 in Annexure III.

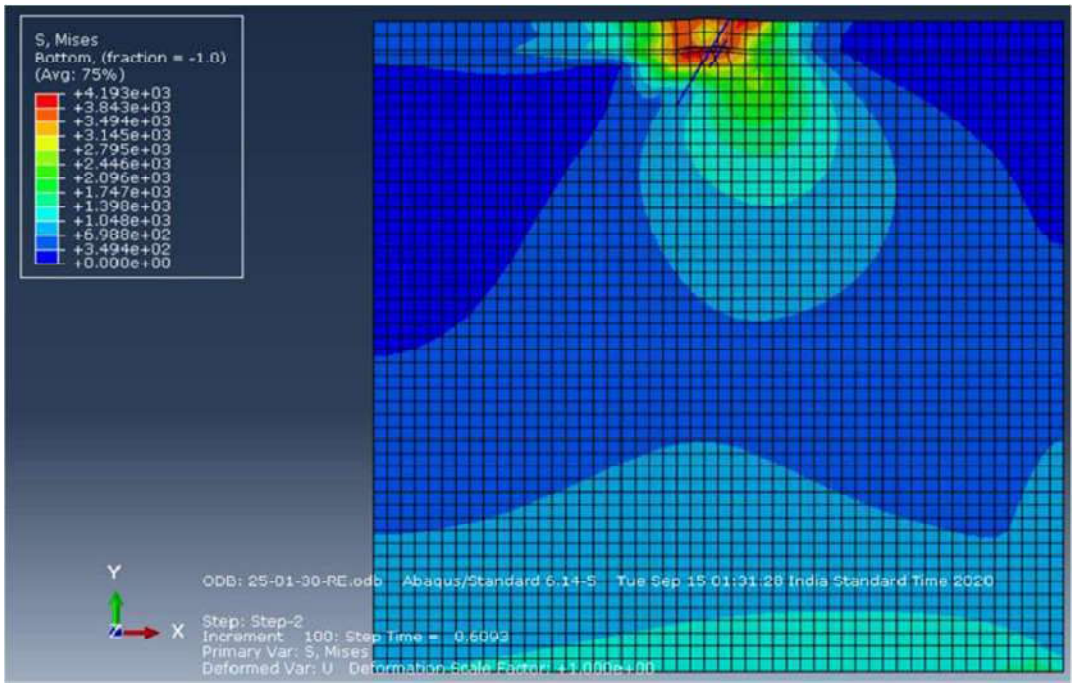

Fig. 4.87: Stress contour for 25mm Square Anchor Plate with (H/B=1) inclined at 30° with vertical in reinforced soil

Table 4.6 has been based on the failure load obtained from load-displacement curves presented from Fig. 4.61 to 4.87, by double tangent method.

Table 4.6: Results from Numerical Analysis in Reinforced Soil

SL NO	Nomenclature	PULL OUT LOAD (kg)
1	25-01-30(RE)	4.8
2	25-01-45(RE)	6.0
3	25-01-60(RE)	6.4
4	25-02-30(RE)	5.8
5	25-02-45(RE)	7.1
6	25-02-60(RE)	8.3
7	25-03-30(RE)	6.8
8	25-03-45(RE)	9.1
9	25-03-60(RE)	9.4
10	50-01-30(RE)	7.7
11	50-01-45(RE)	9.6
12	50-01-60(RE)	14.6
13	50-02-30(RE)	17.0
14	50-02-45(RE)	22.0
15	50-02-60(RE)	23.5
16	50-03-30(RE)	21.0
17	50-03-45(RE)	28.0
18	50-03-60(RE)	33.5
19	75-01-30(RE)	22.5
20	75-01-45(RE)	27.0
21	75-01-60(RE)	32.0
22	75-02-30(RE)	31.0
23	75-02-45(RE)	35.0
24	75-02-60(RE)	43.0
25	75-03-30(RE)	33.5
26	75-03-45(RE)	43.0
27	75-03-60(RE)	50.0

4.5 INCLINED ANCHORS IN UNREINFORCED CLAY UNDER CYCLIC LOADING:

4.5.1 The Present Model

Boundary conditions have been created in the step specified for analyses. The horizontal and vertical movement of the bottom boundary of soil model has been restrained whereas side boundaries are restrained in horizontal direction only. Anchor model is restrained in both directions. Mechanical, displacement/rotation boundary conditions are chosen, defining hinge and roller condition as shown in Fig 4.114.

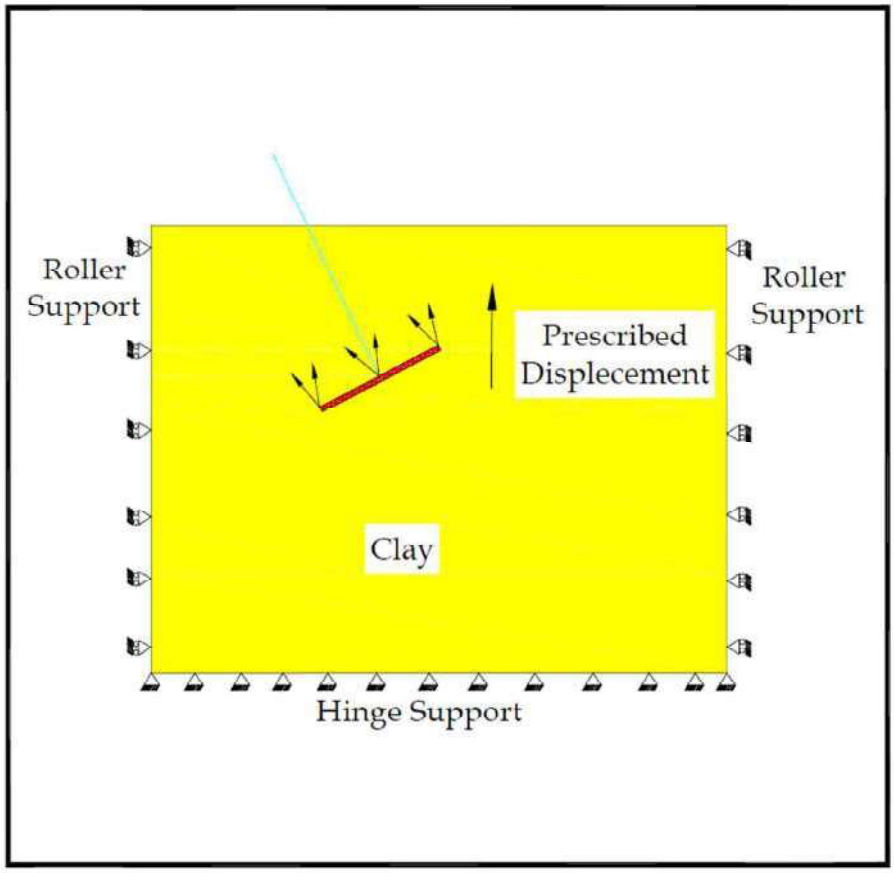

Fig. 4.114: Schematic Representation of Boundary Condition specified in ABAQUS 6.14

4.5.2 Solution Procedure

The present numerical analysis has been carried out under cyclic loading by providing a definite displacement in vertical and horizontal directions. Direct method of equation solver with unsymmetrical matrix storage is specified in analysis step. Mohr Coulomb failure model has been adopted for inclusion of material non-linearity of soil, which has been considered as an isotropic strain hardening material.

4.5.3 Validation Of the Present Model:

The validation of the present model has been done base on the work of Yu et al. (2015). In the study of Yu et al. (2015), tank of dimensions 800 mm in height, 700 mm in length, and 220 mm in width had been used to conduct the tests. The anchor plate had the dimensions of 50 mm width, 210 mm length and 20 mm thickness. The cohesion was found to be 25 kPa. The liquid and plastic limits of kaolin clay had been found to be 58% and 27% respectively. The sinusoidal loading with 0.1 Hz frequency and 48 mm amplitude had been induced to plate anchor in Test 2 whereas the concerned embedment ratio was 10 which implied the embedment depth was 510 mm from the surface. Numerical simulations had been carried out in their study with the use of the strain-softening model of 'FLAC' for comparison with the experimental results. The corresponding load-displacement behaviour had been attained as seen in Fig 4.115 and Fig 4.116. Break out factor 'F/AC_u' had been considered in the study, where F is the Load, A is the area of plate anchor and C_u is the undrained cohesion of kaolin clay.

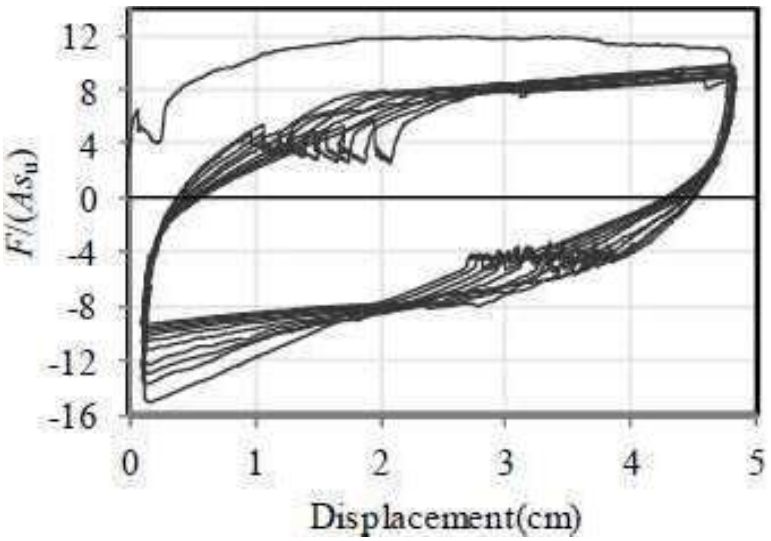

Fig.4.115: Breakout Factor vs Normalized Displacement curves of Test 2 (after Experimental Study of Yu et al. (2015))

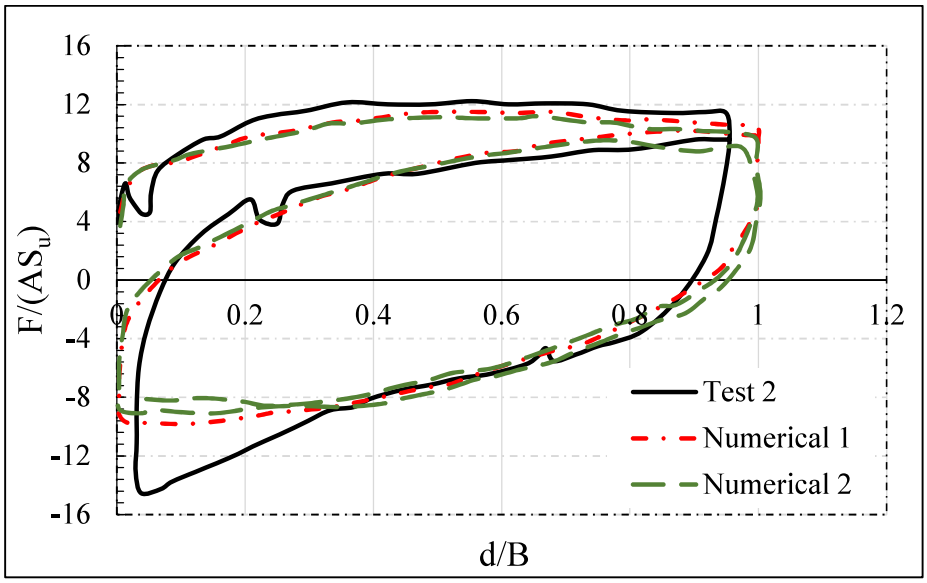

Fig. 4.116: Comparison between the breakout Factor vs Normalized Displacement curves of model test result and the numerical result for Test 2 (after numerical study of Yu et al. (2015)

In the current study, the numerical models have been developed by 'ABAQUS'. In this context,it is to be noted that the model has been made for 25 mm × 25 mm inclined square anchor and inclination angle has been kept at 60°s with the vertical and embedded at depth 25 mm i.e., embedment ratio 1. That particular model with that particular area of plate is transformed into amodel with the area of plate anchor with size 102mm × 102 mm and inclination angle of 90° and soil-anchor interaction surface is transferred to the depth 510 mm from 25mm so that it maintainsembedment ratio 5. The plate anchor modelled as linear elastic material and soil as Mohr- Coulomb model. In the study, the angle of internal friction was adopted as 5^O and young's modulus of Kaolin clay was adopted as 0.2 MPa. The square type of anchor plate had been used for modelling with side length 102 mm. The anchor plate of size 102 mm × 102 mm had almost equal area of that of plate size 50 mm × 210 mm which had been used in experimental study. But shape of anchor also had effect on the load-Displacement behaviour. Bhattacharya (2010) observed the influence of shape of plate anchor on the load displacement behaviour. The researchers noted that the same areas of anchors viz 50mm × 100mm, 75 mm × 75 mm and 50 mm × 200 mm, 100 mm × 100 mm sizes with same embedment depth shows approximately similar pullout load in spite of their various embedmentratios and various shapes as presented in Fig 4.117.

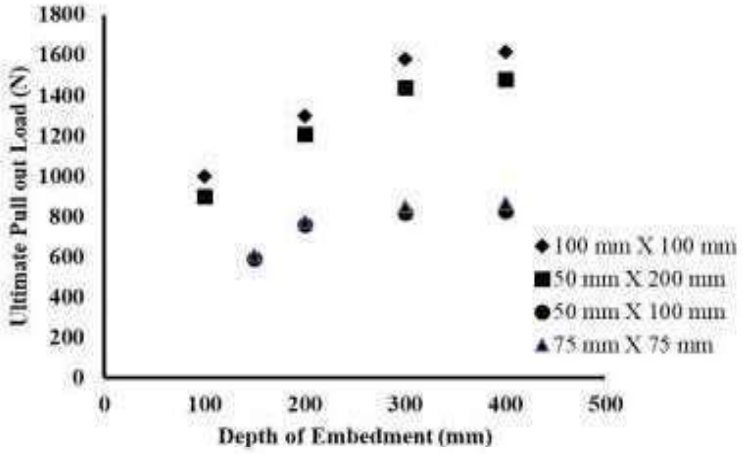

Fig. 4.117: Ultimate pullout load for equal anchor area at same embedment depth (After Bhattacharya, 2010)

The embedment ratio considered as 5, which will confirm the identical embedment depth of 510mm with that of experimental study. The first two cycles of sinusoidal loading had been applied with 0.1 Hz frequency and 48 mm amplitude. These same considerations have been adopted by the Biradaret al. (2019) in the respective study. Following Fig 4.118 and Fig 4.119 are associated with the study of the Biradar et al. (2019).

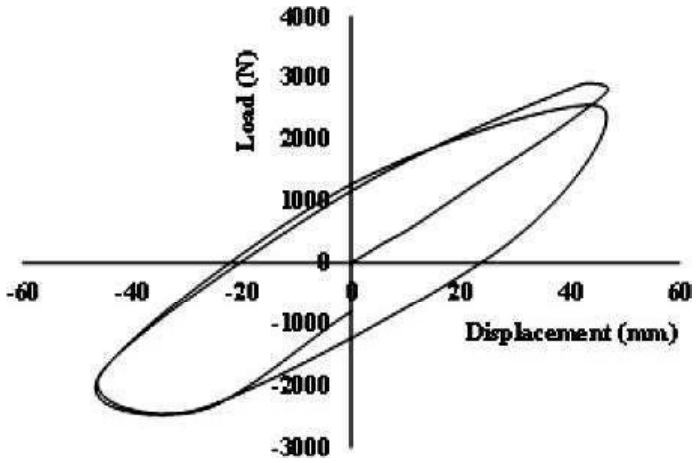

Fig. 4.118: Load-displacement behaviour for 0.1Hz Frequency, 48 mm amplitude and embedment ratio (H/B) of 5 for plate size 100mm × 100mm (after Biradar et al. (2019))

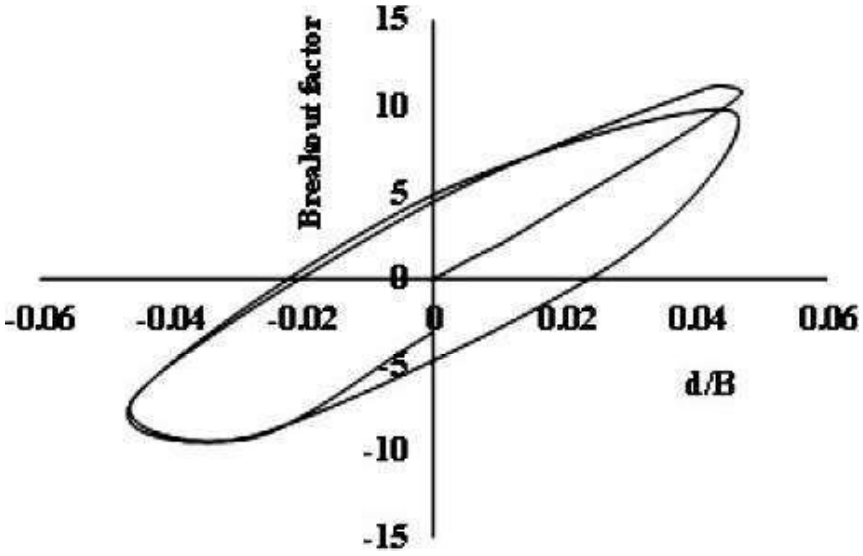

Fig. 4.119: Breakout Factor vs Normalized Displacement behaviour for 0.1Hz Frequency, 48 mmamplitude and embedment ratio (H/B) of 5 for plate size 100mm × 100mm (after Biradar et al. (2019))

Following Fig 4.120 and Fig 4.121 have been attained from the present study:

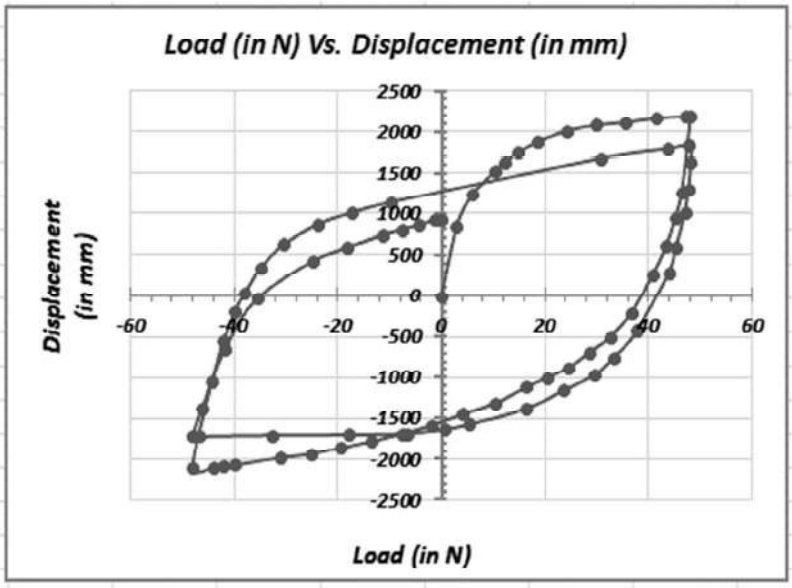

Fig. 4.120: Load-displacement behaviour for 0.1Hz Frequency, 48 mm amplitude and embedmentratio (H/B) of 5 for plate size 102mm × 102mm (in present study)

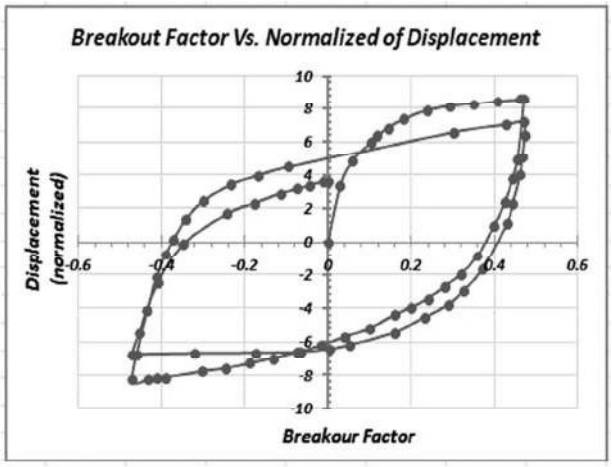

Fig. 4.121: Breakout Factor vs Normalized Displacement behaviour for loading frequencies with 0.1 Hz frequency and 48 mm amplitude and embedment ratio (H/B) of 5 for plate size 102mm x102mm (in the present study)

Comparison of breakout factors of current study with the experimental and numerical analysis results attained by Yu et al. (2015) and Biradar et al. (2019) have been done. It may be noted that the shapes of the figures are of similar nature for the present study and the above mentioned two studies. The breakout factors were evolved out for first two cycles as shown in Table 4.7.

Table 4.7: Comparison of Breakout factor obtained in present analysis with reported by Yu et al. (2015) and Biradar et al. (2019)

	Embedment Ratio	**Embedment Depth (mm)**	**Break Out Factor (F/AC_u)**	
			1st Cycle	**2nd cycle**
Experimental Study (Yu et al.,2015)	10	500	10.36	9.42
Numerical Analysis (Yu et al.,2015)			10.32	9.67
Numerical Analysis (Biradar et al., 2019)	5	510	11.1	9.76
Present Study	5	510	8.61	7.19
% Deviation with respect to present study	w.r.t Experimental Study of Yu et al., 2015		20.26	31.02
	w.r.t Numerical Study of Yu et al., 2015		19.80	34.49
	w.r.t. Biradar et al., 2019		28.85	35.75

Comparison between experimental results with corresponding numerical simulations of first two cycles had shown in Fig 4.116 and based on the above Fig.4.116 to Fig. 4.117 and

Fig.4.119 to Fig. 4.121 and Table 4.6, it is evident that the Break out Factor obtained from present study, has agreed well with the Break out Factor obtained from the method proposed by Biradar et al. (2019) and with both the numerical and experimental studies of Yu et al. (2015) for the same parametric considerations. Also, the values obtained from current approach are slightly lesser than those obtained from the studies (experimental and numerical) of Yu et al. (2015) and study of after Biradar et al. (2019) but they are reasonably close to each other. Pullout load of cycle-1 has been considered as the ultimate pullout capacity of the anchor, in line with the approach used by Biradar et al., 2019. In Table 4.6, for the 1st cycle, the observed variation ranges between 20-28%, which may not be considered excessively high. Despite this variation in absolute values, the trend of both the curves aligns closely. The deviations can be attributed to factors such as test conditions, model assumptions, and potential inconsistencies during testing. For instance, slight differences in material properties, boundary conditions have contributed to the discrepancies observed in comparison to the numerical model. Nonetheless, the overall consistency in the trend of results supports the reliability of the findings of the study. Thus, the present model has been validated for carrying out the present research under cyclic loading.

4.5.4 Numerical Cases Considered for The Study:

The total numerical case studies in soil condition with various plate sizes, embedment ratio, inclination angle, frequency and amplitude has been given in Table 4.8 to 4.11. Here respective nomenclature is also introduced.

Table 4.8: Numerical Model Considered in Present Study for 0.2 Hz Frequency and 2 mm Amplitude

Case No.	Frequency (Hz)	Amplitude (mm)	Plate Size (mm)	Inclination Angle (^{O})	Embedment Ratio	Code Name
Case-1	0.2	2	25	30	1	25P-1E-30A-0.2Hz-2Mm
Case-2					2	25P-2E-30A-0.2Hz-2Mm
Case-3					3	25P-3E-30A-0.2Hz-2Mm
Case-4				45	1	25P-1E-45A-0.2Hz-2Mm
Case-5					2	25P-2E-45A-0.2Hz-2Mm
Case-6					3	25P-3E-45A-0.2Hz-2Mm
Case-7				60	1	25P-1E-60A-0.2Hz-2Mm
Case-8					2	25P-2E-60A-0.2Hz-2Mm
Case-9					3	25P-3E-60A-0.2Hz-2Mm
Case-10			50	30	1	50P-1E-30A-0.2Hz-2Mm
Case-11					2	50P-2E-30A-0.2Hz-2Mm
Case-12					3	50P-3E-30A-0.2Hz-2Mm
Case-13				45	1	50P-1E-45A-0.2Hz-2Mm
Case-14					2	50P-2E-45A-0.2Hz-2Mm
Case-15					3	50P-3E-45A-0.2Hz-2Mm
Case-16				60	1	50P-1E-60A-0.2Hz-2Mm
Case-17					2	50P-2E-60A-0.2Hz-2Mm
Case-18					3	50P-3E-60A-0.2Hz-2Mm
Case-19			75	30	1	75P-1E-30A-0.2Hz-2Mm
Case-20					2	75P-2E-30A-0.2Hz-2Mm
Case-21					3	75P-3E-30A-0.2Hz-2Mm
Case-22				45	1	75P-1E-45A-0.2Hz-2Mm
Case-23					2	75P-2E-45A-0.2Hz-2Mm
Case-24					3	75P-3E-45A-0.2Hz-2Mm
Case-25				60	1	75P-1E-60A-0.2Hz-2Mm
Case-26					2	75P-2E-60A-0.2Hz-2Mm
Case-27					3	75P-3E-60A-0.2Hz-2Mm

Table 4.9: Numerical Model Considered in Present Study for 0.2 Hz Frequency and 5 mm Amplitude

Case No.	Frequency (Hz)	Amplitude (mm)	Plate Size (mm)	Inclination Angle (^{O})	Embedment Ratio	Code Name
Case-28	0.2	5	25	30	1	25P-1E-30A-0.2Hz-5Mm
Case-29					2	25P-2E-30A-0.2Hz-5Mm
Case-30					3	25P-3E-30A-0.2Hz-5Mm
Case-31				45	1	25P-1E-45A-0.2Hz-5Mm
Case-32					2	25P-2E-45A-0.2Hz-5Mm
Case-33					3	25P-3E-45A-0.2Hz-5Mm
Case-34				60	1	25P-1E-60A-0.2Hz-5Mm
Case-35					2	25P-2E-60A-0.2Hz-5Mm
Case-36					3	25P-3E-60A-0.2Hz-5Mm
Case-37			50	30	1	50P-1E-30A-0.2Hz-5Mm
Case-38					2	50P-2E-30A-0.2Hz-5Mm
Case-39					3	50P-3E-30A-0.2Hz-5Mm
Case-40				45	1	50P-1E-45A-0.2Hz-5Mm
Case-41					2	50P-2E-45A-0.2Hz-5Mm
Case-42					3	50P-3E-45A-0.2Hz-5Mm
Case-43				60	1	50P-1E-60A-0.2Hz-5Mm
Case-44					2	50P-2E-60A-0.2Hz-5Mm
Case-45					3	50P-3E-60A-0.2Hz-5Mm
Case-46			75	30	1	75P-1E-30A-0.2Hz-5Mm
Case-47					2	75P-2E-30A-0.2Hz-5Mm
Case-48					3	75P-3E-30A-0.2Hz-5Mm
Case-49				45	1	75P-1E-45A-0.2Hz-5Mm
Case-50					2	75P-2E-45A-0.2Hz-5Mm
Case-51					3	75P-3E-45A-0.2Hz-5Mm
Case-52				60	1	75P-1E-60A-0.2Hz-5Mm
Case-53					2	75P-2E-60A-0.2Hz-5Mm
Case-54					3	75P-3E-60A-0.2Hz-5Mm

Table 4.10: Numerical Model Considered in Present Study for 0.5 Hz Frequency and 2 mm Amplitude

Case No.	Frequency (Hz)	Amplitude (mm)	Plate Size (mm)	Inclination Angle (^{O})	Embedment Ratio	Code Name
Case-55	0.5	2	25	30	1	25P-1E-30A-0.5Hz-2Mm
Case-56					2	25P-2E-30A-0.5Hz-2Mm
Case-57					3	25P-3E-30A-0.5Hz-2Mm
Case-58				45	1	25P-1E-45A-0.5Hz-2Mm
Case-59					2	25P-2E-45A-0.5Hz-2Mm
Case-60					3	25P-3E-45A-0.5Hz-2Mm
Case-61				60	1	25P-1E-60A-0.5Hz-2Mm
Case-62					2	25P-2E-60A-0.5Hz-2Mm
Case-63					3	25P-3E-60A-0.5Hz-2Mm
Case-64			50	30	1	50P-1E-30A-0.5Hz-2Mm
Case-65					2	50P-2E-30A-0.5Hz-2Mm
Case-66					3	50P-3E-30A-0.5Hz-2Mm
Case-67				45	1	50P-1E-45A-0.5Hz-2Mm
Case-68					2	50P-2E-45A-0.5Hz-2Mm
Case-69					3	50P-3E-45A-0.5Hz-2Mm
Case-70				60	1	50P-1E-60A-0.5Hz-2Mm
Case-71					2	50P-2E-60A-0.5Hz-2Mm
Case-72					3	50P-3E-60A-0.5Hz-2Mm
Case-73			75	30	1	75P-1E-30A-0.5Hz-2Mm
Case-74					2	75P-2E-30A-0.5Hz-2Mm
Case-75					3	75P-3E-30A-0.5Hz-2Mm
Case-76				45	1	75P-1E-45A-0.5Hz-2Mm
Case-77					2	75P-2E-45A-0.5Hz-2Mm
Case-78					3	75P-3E-45A-0.5Hz-2Mm
Case-79				60	1	75P-1E-60A-0.5Hz-2Mm
Case-80					2	75P-2E-60A-0.5Hz-2Mm
Case-81					3	75P-3E-60A-0.5Hz-2Mm

Table 4.11: Numerical Model Considered in Present Study for 0.5 Hz Frequency and 5 mm Amplitude

Case No.	Frequency (Hz)	Amplitude (mm)	Plate Size (mm)	Inclination Angle (^{O})	Embedment Ratio	Code Name
Case-82	0.5	5	25	30	1	25P-1E-30A-0.5Hz-5Mm
Case-83					2	25P-2E-30A-0.5Hz-5Mm
Case-84					3	25P-3E-30A-0.5Hz-5Mm
Case-85				45	1	25P-1E-45A-0.5Hz-5Mm
Case-86					2	25P-2E-45A-0.5Hz-5Mm
Case-87					3	25P-3E-45A-0.5Hz-5Mm
Case-88				60	1	25P-1E-60A-0.5Hz-5Mm
Case-89					2	25P-2E-60A-0.5Hz-5Mm
Case-90					3	25P-3E-60A-0.5Hz-5Mm
Case-91			50	30	1	50P-1E-30A-0.5Hz-5Mm
Case-92					2	50P-2E-30A-0.5Hz-5Mm
Case-93					3	50P-3E-30A-0.5Hz-5Mm
Case-94				45	1	50P-1E-45A-0.5Hz-5Mm
Case-95					2	50P-2E-45A-0.5Hz-5Mm
Case-96					3	50P-3E-45A-0.5Hz-5Mm
Case-97				60	1	50P-1E-60A-0.5Hz-5Mm
Case-98					2	50P-2E-60A-0.5Hz-5Mm
Case-99					3	50P-3E-60A-0.5Hz-5Mm
Case-100			75	30	1	75P-1E-30A-0.5Hz-5Mm
Case-101					2	75P-2E-30A-0.5Hz-5Mm
Case-102					3	75P-3E-30A-0.5Hz-5Mm
Case-103				45	1	75P-1E-45A-0.5Hz-5Mm
Case-104					2	75P-2E-45A-0.5Hz-5Mm
Case-105					3	75P-3E-45A-0.5Hz-5Mm
Case-106				60	1	75P-1E-60A-0.5Hz-5Mm
Case-107					2	75P-2E-60A-0.5Hz-5Mm
Case-108					3	75P-3E-60A-0.5Hz-5Mm

4.5.5 Presentation Of Results of Numerical Analysis in Reinforced Soil Under Cyclic Loading:

4.5.5.1 Pullout load vs displacement graphs:

In the present chapter, an attempt has been made to interpret the results obtained from the numerical modelling (done by the ABAQUS software; Version 6.14). Pull-out load vs. Displacement curves generated from the output from numerical modelling in the present study, have been plotted in this chapter. Here the inclination angles indicated in the figures are inclination angles with respect to vertical and this convention has been followed throughout.

Typical Load vs displacement curves obtained from numerical study have been illustrated in Fig 4.122. whereas Fig 4.123 to Fig 4.229 have been presented in Annexure-IV.

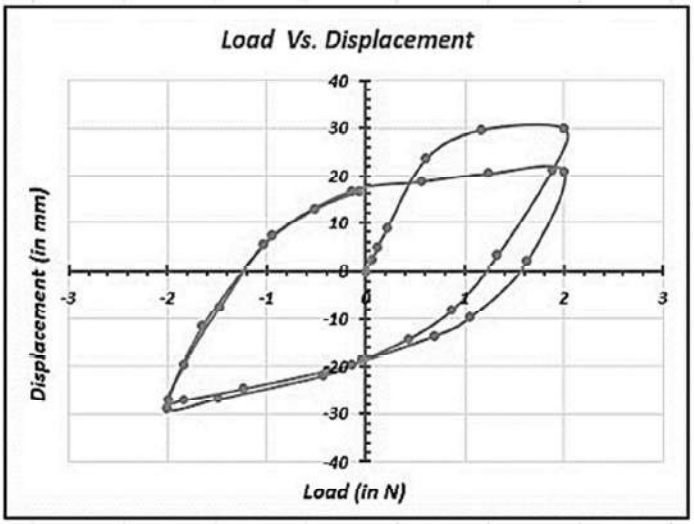

Fig. 4.122: Load vs. Displacement for 25 mm Square Plate with (H/B =1) at 30° inclination under 0.2 Hz frequency and 2mm amplitude

4.5.5.2 Stress contour obtained from numerical analysis

Typical Stress Contours obtained from numerical analysis has been presented in Fig 4.230. Rest of the stress contours have been presented from Fig. 4.231 to Fig. 4.337 in Annexure IV. It can be noted that there are changes in the stress pattern (due to deformations generated in the soil- anchor system dueto application of pull over the anchors) in each and every stress contour and the changes have been indicated by different colour combinations. In in each and every stress contour, red colour indicates the mostly stressed zones and blue colour indicates the unaffected zones (from stress).

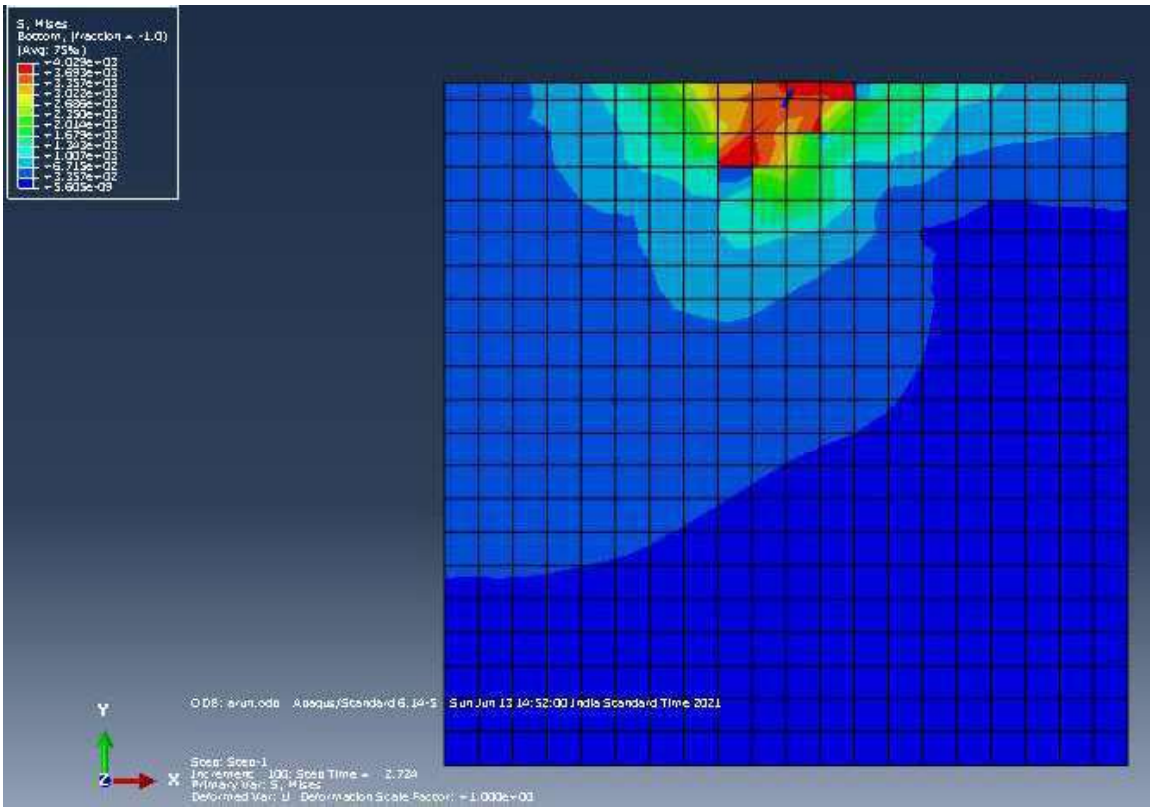

Fig. 4.230: Stress Contour for 25 mm Square Plate with (H/B =1) at 30° inclination under 0.2 Hz frequency and 2mm amplitude

4.6 INCLINED ANCHORS IN REINFORCED CLAY UNDER CYCLIC LOADING

4.6.1 Boundary Conditions and Loading

The model consists of three parts; the soil, the anchor and the reinforcement. The soil has been modelled using Mohr-Coulomb model available in the software. The anchor and Geotextile have been modelled as linear-elastic materials.

Total three-square anchor plates of size 50mm, 75 mm and 100mm have been considered for analysis. The width of reinforcement has been kept four times the width of anchor plate in the model. The position of reinforcement is 0.25 times the embedment depth which is proved to be generating more load carrying capacity of anchor as described in literature. Single layer of geotextile reinforcement used for the analysis. The size of soil medium defined is 1m x 1m which is enough to minimize the influence of boundary constraints on the behaviour of anchor plates. Clay soil has been used for the study on plate anchors; with square shape anchor plates in reinforced and unreinforced soils.

Boundary conditions have been created in the step specified for analyses. The horizontal and vertical movement of the bottom boundary of soil model has been restrained whereas side boundaries are restrained in horizontal direction only. Anchor model is restrained in both directions. Mechanical, displacement/rotation boundary conditions were chosen, defining hinge and roller condition as shown in Fig 4.338. The loading has been applied at right angle to the axis of the inclined anchor plate at its centre.

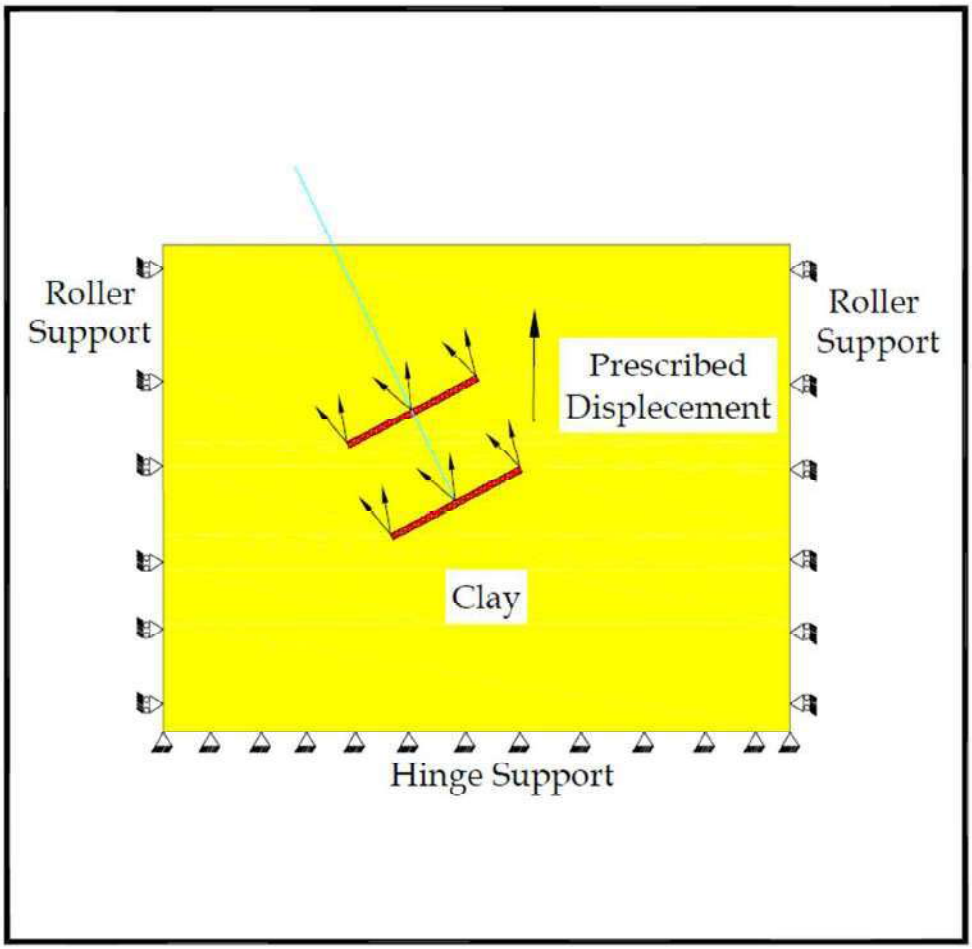

Fig. 4.338: Schematic Representation of Boundary Condition specified in ABAQUS

One typical mesh generated in ABAQUS for analysis of numerical models has been shown in Fig.4.339 represents typical finite element meshing of the model in reinforced bed.

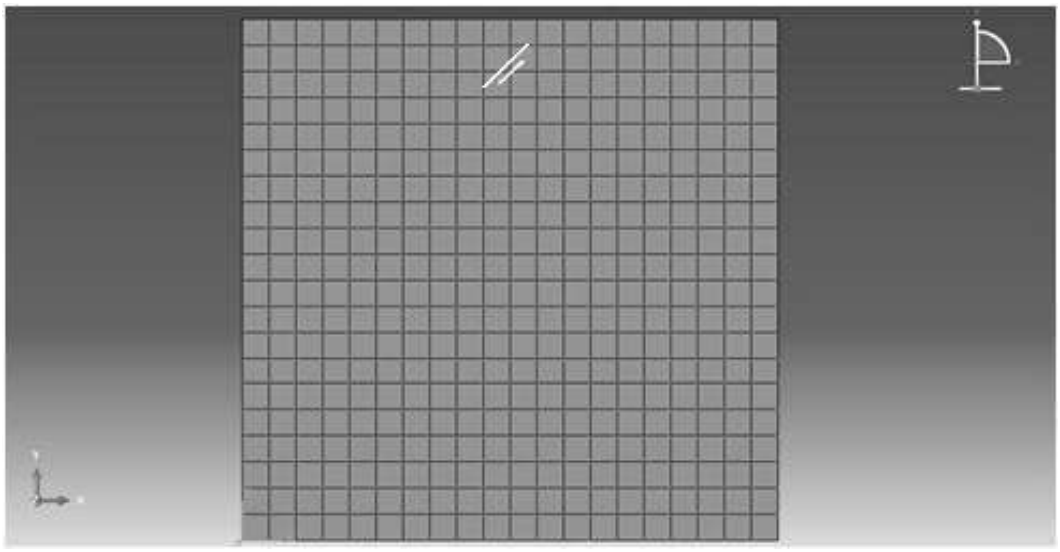

Fig. 4.339: Typical Finite Element mesh developed in ABAQUS

4.6.2 Analysis Conditions

The following salient aspects have been considered in Numerical Analyses:

1) Numerical analysis is carried out based on 2D plain strain condition

2) Geotextile is modelled as linear elastic material

3) Soil is modelled with Mohr-Coulomb plasticity model with specific Tension Cut-off value, which proved to be a very important parameter for calculation of Pullout capacity. Although the effect of this parameter was noted to be pronounced for larger plate sizes and higher embedment depth.

4) Interaction at the soil-anchor interface is formulated considering soil as slave surface and anchor as master surface with Node to Surface discretization due to the rigidity of anchor material than the deformable soil, with small sliding behaviour accounting for the cohesive property used in the interaction property. The tangential and Normal behaviour at the soil-anchor interface was specified as Penalty (Standard) provided with coefficient of friction obtained from Direct Shear Test. Separation of anchor plate from initial slave surface was allowed with non-linear stiffness effects in normal behaviour.

5) The Soil-Geotextile interface is formulated considering soil as slave surface and geotextile as master surface with Surface-to-Surface discretization due to the flexibility of geotextile with respect to deformable soil body. Small sliding behaviour accounting for the cohesive

property and tangential as well as normal behaviour, similar to that specified in soil-anchor interaction, was specified with no separation allowed for the geotextile from initial slave surface.

The present numerical analysis has been carried out under cyclic loading by providing a definite displacement in vertical and horizontal directions. Direct method of equation solver with unsymmetrical matrix storage is specified in analysis step. Mohr Coulomb failure model has been adopted for inclusion of material non-linearity of soil, which has been considered as an isotropic strain hardening material. The variations of different parameters considered in the present study are shown in Table 4.12.

Table 4.12: Variation of parameters

Anchor			**Loading**	
Plate Size (m)	Inclination Angle (°)	Embedment Ratio	Frequency (Hz)	Amplitude (mm)
0.025m×0.025m, 0.050m×0.050m & 0.075m×0.075m	30°, 45°, 60°	1, 2, 3	0.2Hz, 0.5Hz	0.002 m and 0.005 m

Thus, it appears that there is total 108 numbers of cases which have been studied in the present work.

4.6.3 Validation of the Present Model:

The acceptability of present numerical analysis has been verified with results of Ravishankar et. al. (2022) where anchor plate with size 0.100 m × 0.100 m was embedded at an inclination angle of 90° and soil-anchor interaction surface was located to 0.2 m depth so that it maintained embedment ratio 2. The first two cycles of sinusoidal loading had been applied with 0.1 Hz frequency and 2.5mm amplitude.

In this context, it is to be noted that the model has been made for 0.1 m × 0.1 m Horizontal square anchor and inclination angle has been kept at 90°s with the vertical and embedded at depth 0.2 m (i.e., embedment ratio 2). That particular model with that particular area of plate is transformed into a model with the area of plate anchor with size 0.100 m × 0.100 m and inclination angle of 90° and soil-anchor interaction surface is transferred to the depth 0.2 m (embedment ratio of 2). Table 4.13 represents parameters used in the study of Ravishankar et al. (2022).

Table 4.13: Consolidated Properties of Soil, Anchor Plate, and Geotextile used in the of Ravishankar et al. (2022)

Property	Value
Soil Properties	
Grain size distribution (Clay, %)	60
Grain size distribution (Silt, %)	30
Soil classification	CH
Specific gravity	2.70
Liquid limit, WL (%)	73
Plastic limit, WP (%)	31
Plasticity Index, IP	42
Anchor Plate Properties	
Unit weight (kN/m³)	78.5
Poisson's ratio	0.3
Thickness (mm)	10
Young's modulus (GPa)	210
Geotextile Properties	
Type of geotextile	Woven
Material	Polypropylene
Mass per unit area (g/m²) (ASTM D5261)	220
Thickness at 2 kPa pressure (mm) (ASTM D5199)	0.6
Ultimate tensile strength (kN/m) (ASTM D4595)	42
Elongation at ultimate tensile strength (%) (ASTM D4595)	12
Strength at 5% strain (kN/m) (ASTM D4595)	20
Aperture opening size (microns) (ASTM D4751)	< 75

Fig.4.340 presents load displacement behaviour for model of Ravishankar et. al. (2022). Fig. 4.341 has been obtained from the present model and it shows similar variation for the present model.

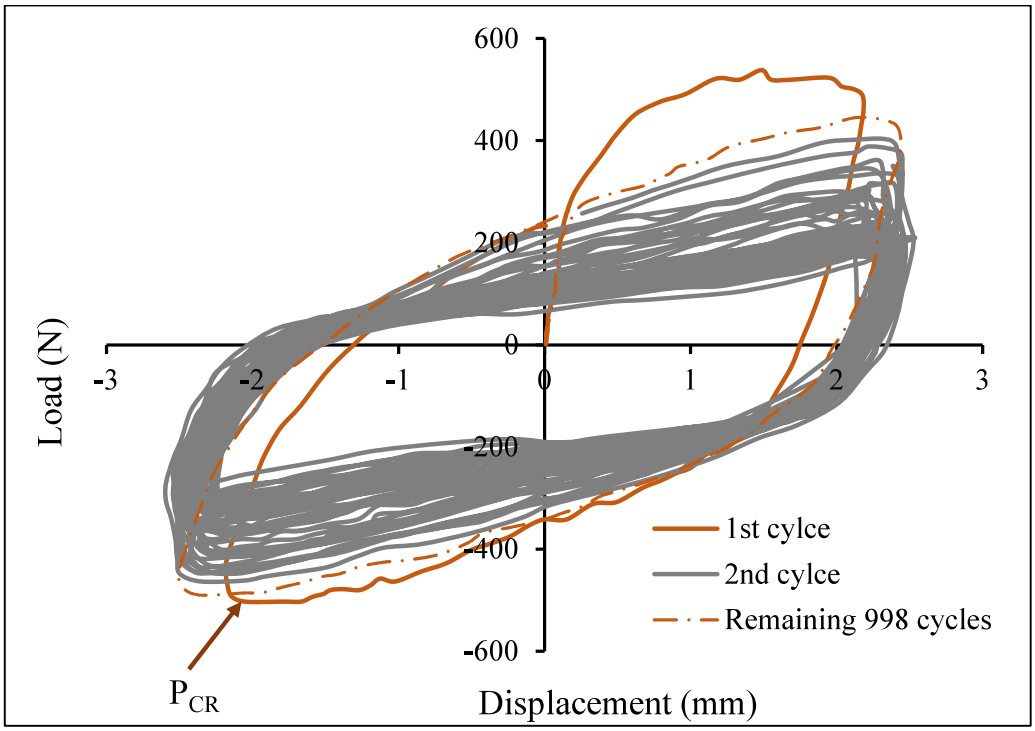

Fig. 4.340: Load-displacement behaviour for 0.1Hz Frequency, 2.5 mm amplitude and embedment ratio (H/B) of 2 for plate size 100 mm (0.1 m) × 100 mm (0.1 m) (Ravishankar et. al. (2022)

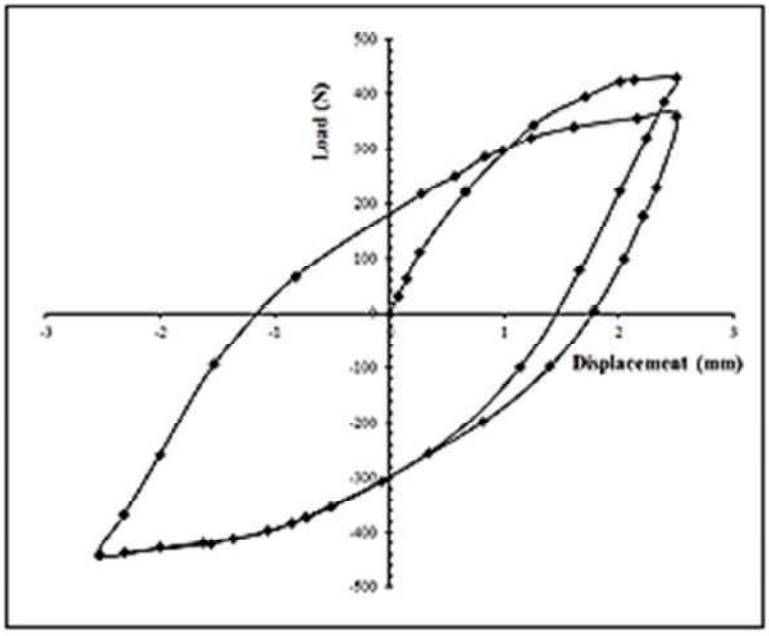

Fig. 4.341: Load-displacement behaviour for 0.1Hz Frequency, 2.5 mm (0.0025m) amplitude and embedment ratio (H/B) of 2 for plate size 100mm (0.100 m) × 100mm (0.100 m) (as per present model)

Ravishankar et. al. (2022) considered that the ultimate pull out is the peak load corresponding to adisplacement equal to each of the considered maximum amplitudes of a given frequency for the first two cycle in respective study to account for the resonance effect between soil and the applied cyclic loading. According to the present model, pull out load for 1st two cycle is the maximum load corresponding to 2.5mm amplitude i.e., 429.431 N, which has been obtained in a similar way.

Comparison of pull-out load for 1st two cycle of current study with experimentally analysis results attained by Ravishankar et. al. (2022) has been done. It may be noted that the shapes of the figures are of similar nature for the present study and the above-mentioned study. The pull-out load for 1st two cycle evolved out for 1st two cycle are furnished in Table 4.14.

Table 4.14: Comparison of pull-out load for 1st cycle of current study with experimentally analysis results attained by Ravishankar et. al. (2022)

	Embedment Ratio	**Embedment Depth (m)**	**Pull out load (N)**	
			1st Cycle	**2nd cycle**
Ravishankar et. al. (2022)	2	0.2	490	433
Present Study	2	0.2	429.431	359.263
% Deviation with respect to Ravishankar et. al. (2022)			12.361	17.029

Comparison between numerical results of present study with those of corresponding numerical simulations of first two cycles based on data shown in and Table 4.12, it is evident that the pullout load for first two cycle obtained from the present study, has agreed well with that obtained from the method proposed by Ravishankar et. al. (2022) for the same parametric considerations. Also, the values obtained from current approach are slightly lesser than those obtained on the basis of the study of Ravishankar et. al. (2022) but they are reasonably close to each other.

So, the present model has been used to extend the study for inclined anchors with different numerical cases.

4.6.4 Numerical Cases Considered for The Study:

The total numerical case studies in soil condition with various plate sizes, embedment ratio, inclination angle, frequency and amplitude has been given in Table 4.15 to 4.18. Here respective nomenclature is also introduced.

Table 4.15: Numerical Model Considered in Present Study for 0.2 Hz Frequency and 2 mm Amplitude

Case No.	Frequency (Hz)	Amplitude (mm)	Plate Size (mm)	Inclination Angle (^{O})	Embedment Ratio	Code Name
Case-1	0.2	2	25	30	1	25P-1E-30A-0.2Hz-2Mm
Case-2					2	25P-2E-30A-0.2Hz-2Mm
Case-3					3	25P-3E-30A-0.2Hz-2Mm
Case-4				45	1	25P-1E-45A-0.2Hz-2Mm
Case-5					2	25P-2E-45A-0.2Hz-2Mm
Case-6					3	25P-3E-45A-0.2Hz-2Mm
Case-7				60	1	25P-1E-60A-0.2Hz-2Mm
Case-8					2	25P-2E-60A-0.2Hz-2Mm
Case-9					3	25P-3E-60A-0.2Hz-2Mm
Case-10			50	30	1	50P-1E-30A-0.2Hz-2Mm
Case-11					2	50P-2E-30A-0.2Hz-2Mm
Case-12					3	50P-3E-30A-0.2Hz-2Mm
Case-13				45	1	50P-1E-45A-0.2Hz-2Mm
Case-14					2	50P-2E-45A-0.2Hz-2Mm
Case-15					3	50P-3E-45A-0.2Hz-2Mm
Case-16				60	1	50P-1E-60A-0.2Hz-2Mm
Case-17					2	50P-2E-60A-0.2Hz-2Mm
Case-18					3	50P-3E-60A-0.2Hz-2Mm
Case-19			75	30	1	75P-1E-30A-0.2Hz-2Mm
Case-20					2	75P-2E-30A-0.2Hz-2Mm
Case-21					3	75P-3E-30A-0.2Hz-2Mm
Case-22				45	1	75P-1E-45A-0.2Hz-2Mm
Case-23					2	75P-2E-45A-0.2Hz-2Mm
Case-24					3	75P-3E-45A-0.2Hz-2Mm
Case-25				60	1	75P-1E-60A-0.2Hz-2Mm
Case-26					2	75P-2E-60A-0.2Hz-2Mm
Case-27					3	75P-3E-60A-0.2Hz-2Mm

Table 4.16: Numerical Model Considered in Present Study for 0.2 Hz Frequency and 5 mm Amplitude

Case No.	Frequency (Hz)	Amplitude (mm)	Plate Size (mm)	Inclination Angle (^{O})	Embedment Ratio	Code Name
Case-28	0.2	5	25	30	1	25P-1E-30A-0.2Hz-5Mm
Case-29					2	25P-2E-30A-0.2Hz-5Mm
Case-30					3	25P-3E-30A-0.2Hz-5Mm
Case-31				45	1	25P-1E-45A-0.2Hz-5Mm
Case-32					2	25P-2E-45A-0.2Hz-5Mm
Case-33					3	25P-3E-45A-0.2Hz-5Mm
Case-34				60	1	25P-1E-60A-0.2Hz-5Mm
Case-35					2	25P-2E-60A-0.2Hz-5Mm
Case-36					3	25P-3E-60A-0.2Hz-5Mm
Case-37			50	30	1	50P-1E-30A-0.2Hz-5Mm
Case-38					2	50P-2E-30A-0.2Hz-5Mm
Case-39					3	50P-3E-30A-0.2Hz-5Mm
Case-40				45	1	50P-1E-45A-0.2Hz-5Mm
Case-41					2	50P-2E-45A-0.2Hz-5Mm
Case-42					3	50P-3E-45A-0.2Hz-5Mm
Case-43				60	1	50P-1E-60A-0.2Hz-5Mm
Case-44					2	50P-2E-60A-0.2Hz-5Mm
Case-45					3	50P-3E-60A-0.2Hz-5Mm
Case-46			75	30	1	75P-1E-30A-0.2Hz-5Mm
Case-47					2	75P-2E-30A-0.2Hz-5Mm
Case-48					3	75P-3E-30A-0.2Hz-5Mm
Case-49				45	1	75P-1E-45A-0.2Hz-5Mm
Case-50					2	75P-2E-45A-0.2Hz-5Mm
Case-51					3	75P-3E-45A-0.2Hz-5Mm
Case-52				60	1	75P-1E-60A-0.2Hz-5Mm
Case-53					2	75P-2E-60A-0.2Hz-5Mm
Case-54					3	75P-3E-60A-0.2Hz-5Mm

Table 4.17: Numerical Model Considered in Present Study for 0.5 Hz Frequency and 2 mm Amplitude

Case No.	Frequency (Hz)	Amplitude (mm)	Plate Size (mm)	Inclination Angle (^{O})	Embedment Ratio	Code Name
Case-55	0.5	2	25	30	1	25P-1E-30A-0.5Hz-2Mm
Case-56					2	25P-2E-30A-0.5Hz-2Mm
Case-57					3	25P-3E-30A-0.5Hz-2Mm
Case-58				45	1	25P-1E-45A-0.5Hz-2Mm
Case-59					2	25P-2E-45A-0.5Hz-2Mm
Case-60					3	25P-3E-45A-0.5Hz-2Mm
Case-61				60	1	25P-1E-60A-0.5Hz-2Mm
Case-62					2	25P-2E-60A-0.5Hz-2Mm
Case-63					3	25P-3E-60A-0.5Hz-2Mm
Case-64			50	30	1	50P-1E-30A-0.5Hz-2Mm
Case-65					2	50P-2E-30A-0.5Hz-2Mm
Case-66					3	50P-3E-30A-0.5Hz-2Mm
Case-67				45	1	50P-1E-45A-0.5Hz-2Mm
Case-68					2	50P-2E-45A-0.5Hz-2Mm
Case-69					3	50P-3E-45A-0.5Hz-2Mm
Case-70				60	1	50P-1E-60A-0.5Hz-2Mm
Case-71					2	50P-2E-60A-0.5Hz-2Mm
Case-72					3	50P-3E-60A-0.5Hz-2Mm
Case-73			75	30	1	75P-1E-30A-0.5Hz-2Mm
Case-74					2	75P-2E-30A-0.5Hz-2Mm
Case-75					3	75P-3E-30A-0.5Hz-2Mm
Case-76				45	1	75P-1E-45A-0.5Hz-2Mm
Case-77					2	75P-2E-45A-0.5Hz-2Mm
Case-78					3	75P-3E-45A-0.5Hz-2Mm
Case-79				60	1	75P-1E-60A-0.5Hz-2Mm
Case-80					2	75P-2E-60A-0.5Hz-2Mm
Case-81					3	75P-3E-60A-0.5Hz-2Mm

Table 4.18: Numerical Model Considered in Present Study for 0.5 Hz Frequency and 5 mm Amplitude

Case No.	Frequency (Hz)	Amplitude (mm)	Plate Size (mm)	Inclination Angle (^{O})	Embedment Ratio	Code Name
Case-82	0.5	5	25	30	1	25P-1E-30A-0.5Hz-5Mm
Case-83					2	25P-2E-30A-0.5Hz-5Mm
Case-84					3	25P-3E-30A-0.5Hz-5Mm
Case-85				45	1	25P-1E-45A-0.5Hz-5Mm
Case-86					2	25P-2E-45A-0.5Hz-5Mm
Case-87					3	25P-3E-45A-0.5Hz-5Mm
Case-88				60	1	25P-1E-60A-0.5Hz-5Mm
Case-89					2	25P-2E-60A-0.5Hz-5Mm
Case-90					3	25P-3E-60A-0.5Hz-5Mm
Case-91			50	30	1	50P-1E-30A-0.5Hz-5Mm
Case-92					2	50P-2E-30A-0.5Hz-5Mm
Case-93					3	50P-3E-30A-0.5Hz-5Mm
Case-94				45	1	50P-1E-45A-0.5Hz-5Mm
Case-95					2	50P-2E-45A-0.5Hz-5Mm
Case-96					3	50P-3E-45A-0.5Hz-5Mm
Case-97				60	1	50P-1E-60A-0.5Hz-5Mm
Case-98					2	50P-2E-60A-0.5Hz-5Mm
Case-99					3	50P-3E-60A-0.5Hz-5Mm
Case-100			75	30	1	75P-1E-30A-0.5Hz-5Mm
Case-101					2	75P-2E-30A-0.5Hz-5Mm
Case-102					3	75P-3E-30A-0.5Hz-5Mm
Case-103				45	1	75P-1E-45A-0.5Hz-5Mm
Case-104					2	75P-2E-45A-0.5Hz-5Mm
Case-105					3	75P-3E-45A-0.5Hz-5Mm
Case-106				60	1	75P-1E-60A-0.5Hz-5Mm
Case-107					2	75P-2E-60A-0.5Hz-5Mm
Case-108					3	75P-3E-60A-0.5Hz-5Mm

4.6.5 Presentation Of Results of Numerical Analysis in Reinforced Soil Under Cyclic Loading:

4.6.5.1 Pullout load vs displacement graphs

In the present section, an attempt has been made to interpret the results obtained from the numerical modelling (done by the ABAQUS software; Version 6.14). Pull-out load vs. Displacement curve for 25 mm Square Plate with (H/B =1) at 30° inclination under 0.2 Hz frequency and 2mm amplitude generated from the output from numerical modelling in the present study, have been plotted in this chapter in Fig.4.342. For rest of the cases, Pull-out load vs. Displacement curves is plotted from Fig 4.343 to Fig.4.449 in Annexure V.

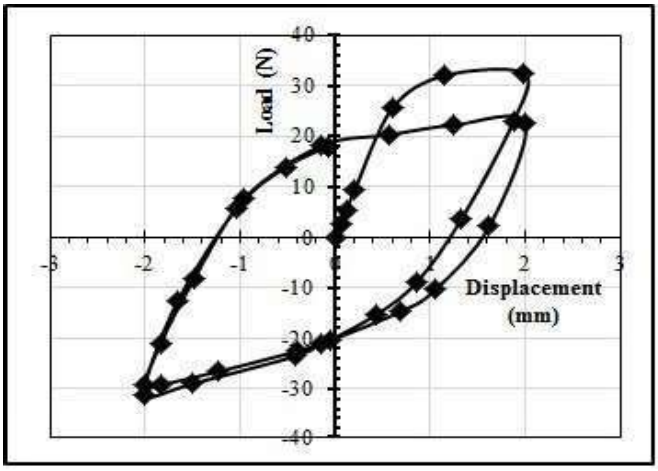

Fig. 4.342: Load vs. Displacement for 25 mm Square Plate with (H/B =1) at 30° inclination under 0.2 Hz frequency and 2mm amplitude

4.6.5.2 Stress contour obtained from numerical analysis

Stress Contours obtained from numerical analysis have been shown with the figures from Fig.4.450 to Fig.4.557. A typical stress contour plot is shown in Fig. 4.450, while the remaining stress contours are presented in Figs. 4.451 to 4.557 in Annexure V. Here, the inclination angles indicated in the figures are inclination angles with respect to vertical and this convention will be followed throughout as already mentioned earlier.

When the stress contours are studied, it can be noted that there are changes in the stress pattern (due to deformations generated in the soil- anchor system due to application of pull over the anchors) in each and every stress contour and the changes have been indicated by different colour combinations. In in each and every stress contour, red colour indicates the mostly stressed zones and blue colour indicates the unaffected zones (from stress).

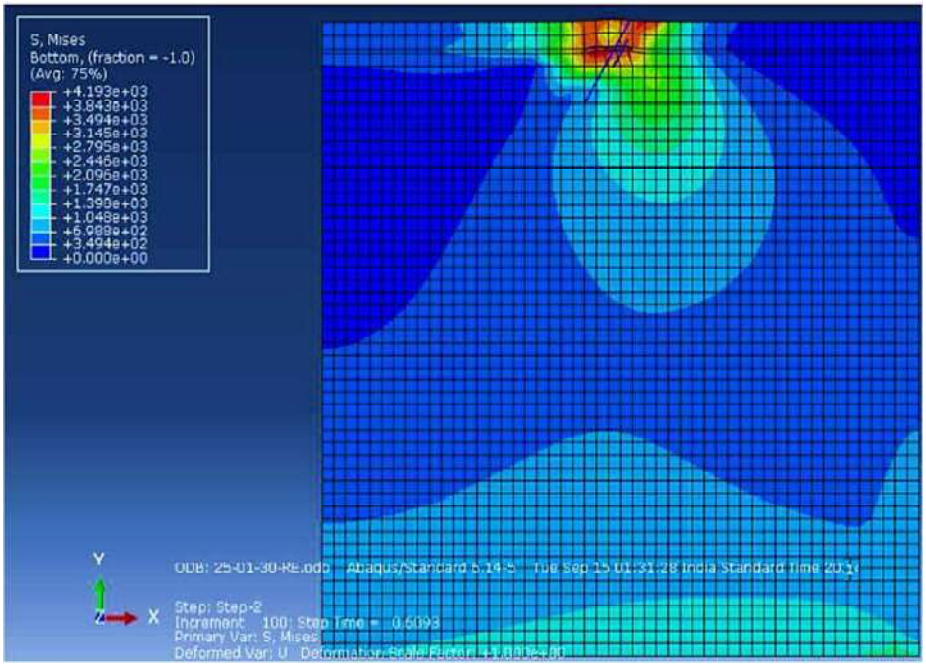

Fig. 4.450: Stress Contour for 25mm Square Plate with (H/B =1) at 30° inclination under 0.2 Hz frequency and 2mm amplitude

4.7 SUMMARY

This chapter has presented constitutive model, boundary conditions and properties of different materials used for numerical analysis of inclined anchors. Pullout behaviour of inclined anchors in unreinforced and reinforced clay soil bed has been observed for different plate size, embedment ratio and inclination angle and presented through pullout load-displacement graph in first two subsections of this chapter for static loading. It has also included the response of inclined anchors in unreinforced and reinforced clay bed due to different amplitude and frequency of cyclic loading. This chapter has also presented stress contours obtained at maximum load capacity during numerical analysis of inclined anchors in unreinforced and reinforced clay soil bed for both static and cyclic loading. This has been done to obtain pullout capacity of inclined anchors in both unreinforced and reinforced soil bed under both static and cyclic loading. The values of pullout capacity of inclined anchors, as obtained from relevant load-displacement curves, have also been presented in this chapter.

CHAPTER 5

EXPERIMENTAL STUDY

5.1 OVERVIEW

In order to supplement the numerical study presented in chapter 4, the experimental study for the current investigation has been performed in two stages. In the first stage, the uplift capacity of inclined anchors in unreinforced clay for static loading has been investigated, while in the second phase, the same has been investigated with the inclined anchors embedded in reinforced clay. These have been illustrated in the following sections of this chapter.

5.2 INCLINED ANCHORS IN UNREINFORCED CLAY UNDER STATIC LOADING

5.2.1 Model Anchor Tests

The model anchor test programme in unreinforced clay under static loading has been shown in Table 5.1 for different embedment depth and inclination position of different sizes of anchor plate in unreinforced soil. In this study total twenty-four numbers of tests have been carried covering three different plate sizes with three different embedment depths for three different anchor inclination angle cases. Different parameters involved in model test are shown in Fig. 5.1.

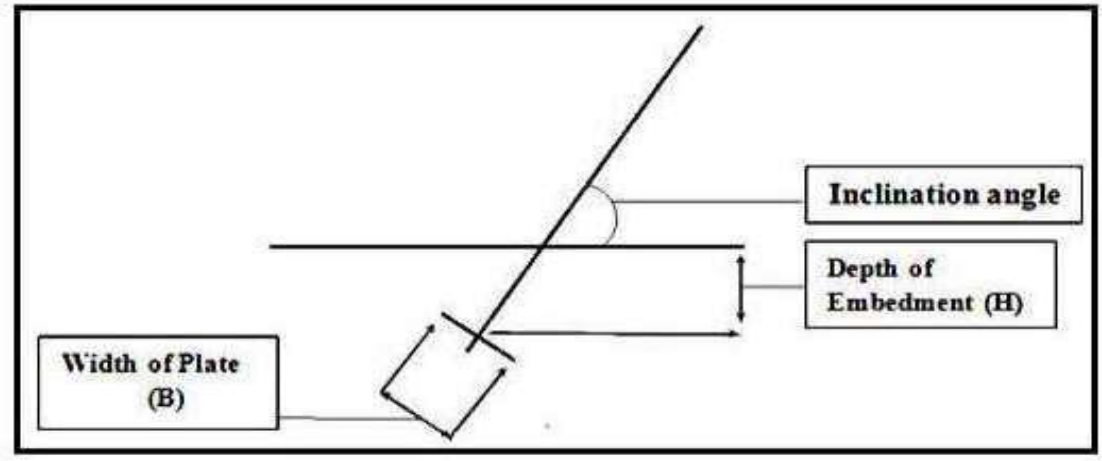

Fig. 5.1: Schematic Representation of Model Anchor Test in Unreinforced Condition

Table 5.1: Test Programme – Model Anchor Plate Test

Sl. No.	Plate Size (mm)	Embedment Ratio(H/B)	Inclination Angle w.r.t Vertical	Nomenclature
1	25mm X 25mm	1	30°	25-01-30
2			45°	25-01-45
3			60°	25-01-60
4		2	30°	25-02-30
5			45°	25-02-45
6			60°	25-02-60
7		3	30°	25-03-30
8			45°	25-03-45
9			60°	25-03-60
1	50mm X 50mm	1	30°	50-01-30
2			45°	50-01-45
3			60°	50-01-60
4		2	30°	50-02-30
5			45°	50-02-45
6			60°	50-02-60
7		3	30°	50-03-30
8			45°	50-03-45
9			60°	50-03-60
1	75mm X 75mm	1	30°	75-01-30
2			45°	75-01-45
3			60°	75-01-60
4		2	30°	75-02-30
5			45°	75-02-45
6			60°	75-02-60

5.2.2 Model Test Set Up

It has also been mentioned in the Chapter 4 of Numerical study that pilot studies have been considered to finalise the dimensions of the domain and the anchor model. The experimental model has been fabricated to properly simulate the numerical model used in the present study. The model test set up comprises of different equipment assembled in order to achieve suitability in conducting experiment. A brief overview of the equipment used in model test has been furnished herein. Also, a schematic representation of the test set up has been shown in Fig. 5.2, whereas Fig. 5.3 represents the test set up.

The model set up consists of the following equipment described as follows

a) Foundation Tank

b) Loading Frame and Pulley Arrangement

c) Displacement Measurement

d) Anchor Plates and Dead Weight for Pull-out Test

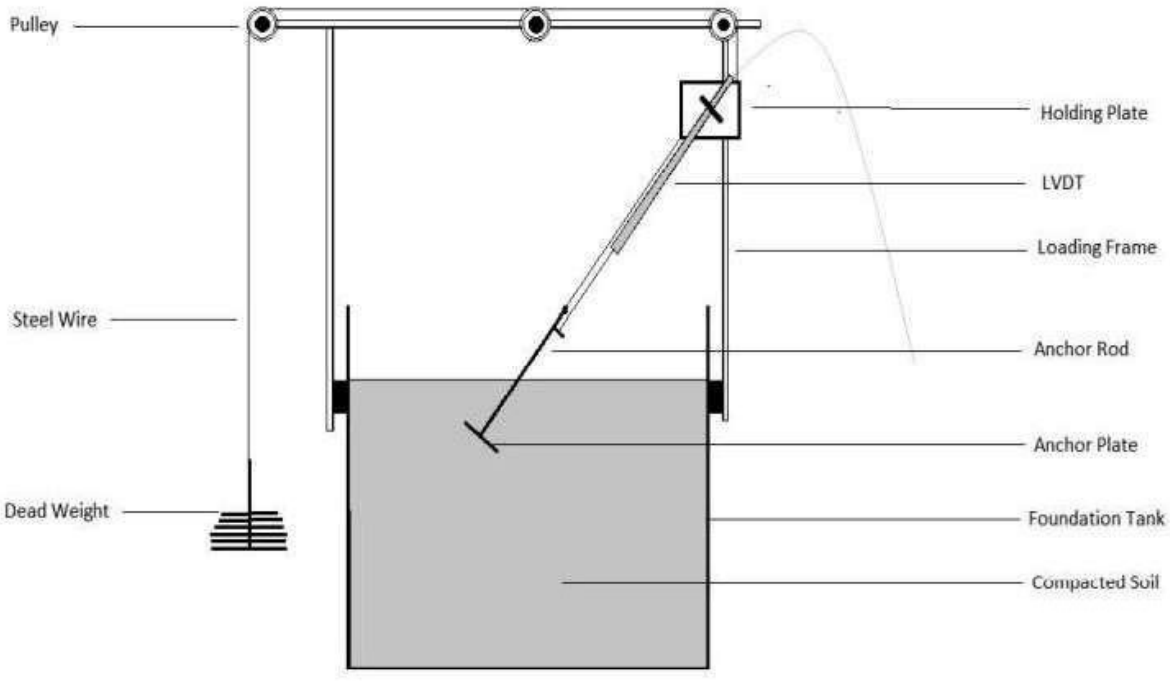

Fig. 5.2: Schematic Representation of Test Set Up

Fig. 5.3: Test Set Up

a) Foundation Tank

In the present investigation foundation tank of plan dimension 1.0 m X 1.0 m and 1.0 m depth is used for carrying out pull-out tests. The dimension of tank is chosen in such a way that the

effect of boundary on pull-out capacity is negligible for the square anchor plates tested. A schematic view of the foundation tank has been shown in Fig. 5.4.

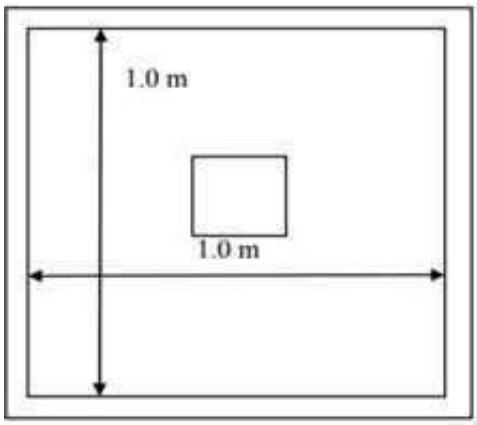

Fig. 5.4: Plan view of Tank

The set up has been fabricated according to the model developed for numerical analysis. Results obtained from Numerical analysis also showed that by having a dimension of soil 1.0m X 1.0m X 1.0m, the stress contour reaching to ground surface also finishes well before the soil boundary.

b) Loading Frame and Pulley Arrangement

To apply the monotonic pull-out, load a loading frame is constructed over the foundation tank forming two angles (2L50X50X6) placed back-to-back. The anchor plate is attached with a straight rod and pulled through a steel wire by turning over pulley arrangement as shown in Fig 5.2.

c) Displacement Measurement

In the present investigation axial movement of anchor plate is measured by Linear Variable Differential Transformer (LVDT) by welding a horizontal flat plate on the straight rod and fixing the LVDT over that plate. Least count of LVDT is 0.01 mm. LVDT is supported with the help of an arrangement as shown Fig 5.2 from the loading frame and fixed in its position with proper fastening.

d) Anchor Plates and Dead Weight for Pull-out Test

In the present investigation Square Anchor plates of mild steel is used. As shown in Fig. 5.5 for the ongoing investigation three different sizes of square anchor plates of width 25 mm, 50 mm and 75 mm with respective embedment ratio are used to estimate the Pull-out capacity required up to a certain specified axial movement of anchor plates. For carrying out model test pull-out load is applied through dead weights of different increment given as 180 gm, 360

gm, 575 gm, 1412 gm, 1960 gm, 2270 gm and 4500 gm as exhibited in Fig. 5.6. During pull-out test anchor plate is attached with a 10 mm diameter shaft through a slotted hole at the middle of anchor plate, which in turn is tied with the steel wire used for pulling arrangement through pulley mechanism. During preparation of embedded soil after placement of anchor the loading arrangement supports a minimum load to keep the anchor-shaft assembly in proper alignment. This minimum load is taken as the zero load for model test results.

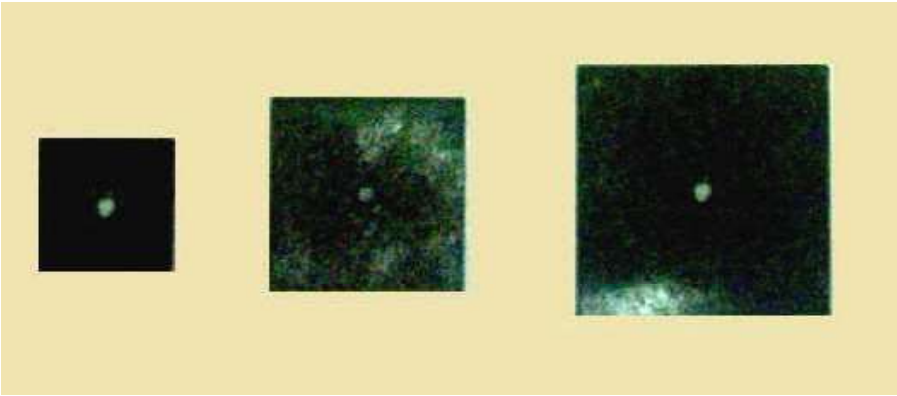

Fig. 5.5: 25mm, 50 mm and 75 mm Square Anchor Plates used for Pull-out Test

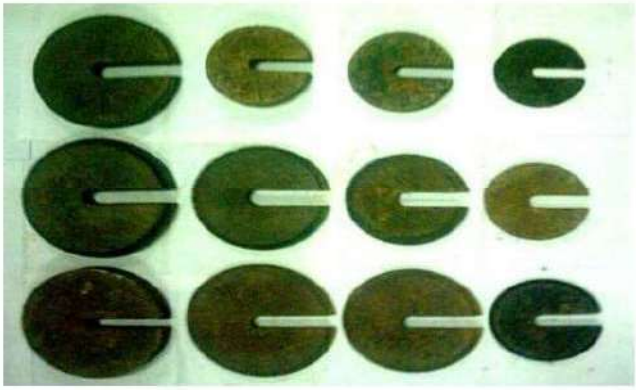

Fig. 5.6: Dead Weight used for Pull-out test

5.2.3 Experimental Procedure:

Pull-out test for the three different size square anchor plates has been carried out under different embedment condition for unreinforced as well as for reinforced case. For all the model test foundation tank described earlier of size 1.0m x 1.0m x 1.0m is used following the steps mentioned below. To carry out pull-out test of anchor plates in cohesive soil, one of the critical points is compaction control and to achieve for homogeneity in the system. The steps for the experimental procedure are as follows: -

a. Calibration curve for finding number of blows of rammer per unit volume: For the present investigation an effort was made to calibrate between number of blows required to achieve a certain degree of compaction and the corresponding dry density and shear strength achieved. Calculation for number of blows required to achieve standard proctor density is specified below. The need of calibration curve arrived due to the problem involved in achieving required density and strength in the foundation tank with the number of blows counted from Standard Proctor method. The difference in the number of blows required to achieve a certain degree of compaction is due to the change in the volume of soil involved in standard laboratory procedure of Standard Proctor test with the volume of soil involved for model test.

As per the Indian standard equivalent of the Standard Proctor procedure for laboratory testing of compaction, called Light Compaction Test (IS: 2720, Part VII-1974),

Volume of mould = 1000 cc

Weight of Hammer = 2.6 Kg

Height of Drop = 310 mm

Soil is compacted in three layers with each layer tamped for 25 times.

Total Compactive Effort required to compact 1000 cc of soil = $3\times25\times2.6\times9.81\times0.31$ N-m

= 593.0145 N-m

In present investigation for 50 mm square anchor plate with embedment ratio one (H/B =1) the volume of soil required to be compacted = $0.05\times1.0\times1.0 = 0.05$ m^3 = 50000 cc

Total Compactive Effort required = 593.0145×50 = 29650.725 N-m

Weight of Rammer used in model test = 4.5 Kg

Average Height of Drop = 250 mm

Total Number blows required for 0.05 m^3 of soil = $29650.725/ (4.5\times9.81\times0.25)$

$= 2686.67 \approx 2687$

Total Number of blows required as per Light Compaction per m^3 of soil = 2687/0.05 = 53740

As mentioned above, calibration curve for different embedment volume is established based on the number of blows and achieved strength and density and expressed in terms of Number blows of rammer required per 1 m^3 of soil is as shown in Fig. 5.7 and Fig. 5.8.

Based on the calibration plot obtained in this study, the dry density and strength showed little increments with increase in compactive effort at a water content of OMC+4 %, which was 18% in this present study. To achieve the required amount of compaction, control a particular range of number of blows per 1 m^3 of soil is specified which in this present study is 100,000 to 150,000. The obtained number of blows per m^3 of soil from calibration curve is

approximately double the numbers required from interpolated results of light compaction. This can be accounted on the basis of quality control required during compaction. As stated earlier the volume of soil to be compacted differs from the standard light compaction considerably, thus the quality control needed during compaction to achieve a certain degree of strength for cohesive soil must be ascertained.

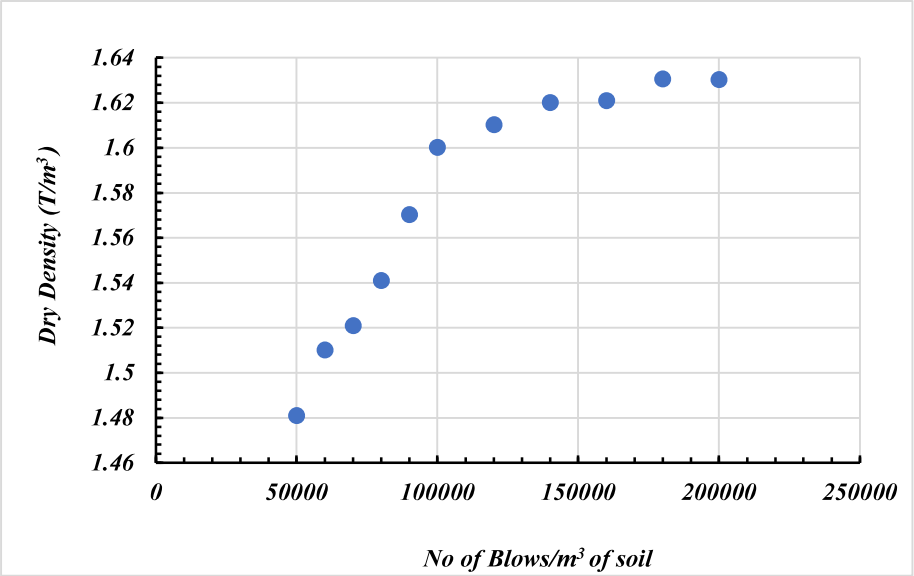

Fig. 5.7: Calibration Plot of Dry Density and Number of Blows

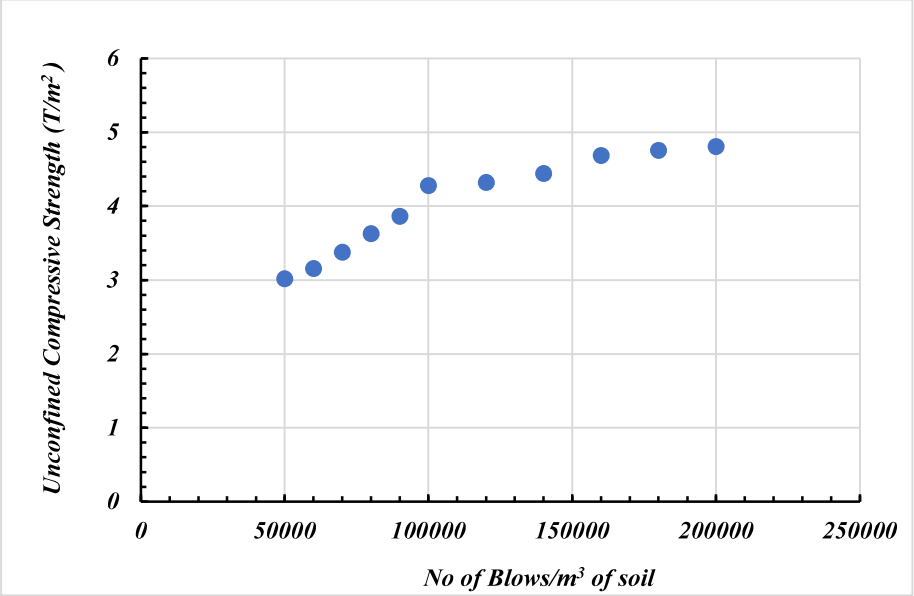

Fig. 5.8: Calibration Plot of Unconfined Compressive Strength and Number of Blows

b. Preparation of Soil Bed: Before placing the anchor plate a soil bed minimum thickness of 200 mm was provided. In the present study, the tank-filling procedure focused on

compaction rather than the conventional method of filling with clay slurry and subsequent consolidation. Specifically, consolidation was not performed; instead, compaction was done at a controlled moisture content (OMC + 4%, with an average water content of about 18%) to ensure the homogeneity of clay strength. This approach was chosen to align with the primary objective of validating numerical analysis, where only short-term effects were considered, thus avoiding the complexities introduced by long-term consolidation. The compaction process involved layering the clay in the tank and compacting each layer using a set number of blows determined from laboratory compaction tests. This ensured uniform soil density and strength throughout the test setup. By controlling moisture content during compaction, the procedure achieved consistent soil properties, thereby providing a reliable simulation of the conditions modelled in the numerical study. Thus, the soil of that bed has been compacted same as the soil of upper side of anchor to maintain the homogeneity of the whole soil system.

c. Placement of Anchor & Preparation of Embedded Soil: After the preparation of soil bed anchor plate is placed horizontally at the middle of soil bed along with a 10 mm diameter shaft attached vertically to the anchor plate. This arrangement is tied through a steel wire to the counterweight by pulley arrangement as discussed earlier in this chapter. With sufficient precautions to keep the anchor – shaft assembly vertical, embedded soil is prepared depending on the number of blows referring to Table 4.2. The entire volume of soil is compacted in 2 to 3 layers depending on which approximate number of blows per layer is calculated. After preparing the embedded soil total number of blows for the entire volume of soil is noted.

d. Arrangement for displacement measurement: A horizontal plate was welded to the anchor rod. A holding plate has been installed on the load frame to hold the LVDT as shown in Fig 6.2 to measure the movement of anchor rod axially. The initial reading of the LVDT was taken as zero. The least count of that instrument is .01mm.

e. Pull-out Test: Pull-out test is carried out by different incremental loading through dead loads placed on the hanger attached to the steel wire and pulley arrangement. For each load increment the LVDT reading at the end of fluctuation is recorded and afterwards next load increment is applied. This load increment is continued until indicated by observed failure or the displacement exceeds 10% of plate dimension, whichever occurs earlier. The Load vs Displacement curves obtained through the model tests are used to find out the ultimate pull-out capacity by using double tangent method, as the double tangent method allows for a more accurate determination of pull-out capacity. It takes into account nonlinearities that may exist in the curve and provides a more detailed analysis of the load-displacement behaviour. Table 5.2 represents comparison of number of blows.

Table 5.2: Comparison of Number of Blows

TEST CONDITION			NUMBER OF BLOWS			
PLATE SIZE	EMBEDMENT RATIO	VOLUME OF SOIL	LIGHT COMPACTION	CALIBRATION PLOT RANGE		Actual Value Adopted(*)
				MINIMUM	MAXIMUM	
25 mm	1	0.025 m^3	1344	2500	3750	2700
	2	0.05 m^3	2687	5000	7500	5400
	3	0.075 m^3	4031	7500	11250	8100
50 mm	1	0.05 m^3	2687	5000	7500	6300
	2	0.1 m^3	5374	10000	15000	10700
	3	0.15 m^3	8061	15000	22500	16700
75 mm	1	0.075 m^3	4031	7500	11250	8200
	2	0.15 m^3	8061	15000	22500	17300
	3	0.225 m^3	12092	22500	33750	24200

(*) To achieve the desired strength of soil

5.2.4 Presentation of Model Anchor Test Results:

The pull-out variation in load with the progressive increase in displacement is displayed in Fig. 5.9. As seen in the picture, until a displacement of 0.15 mm, the load increases approximately linearly with displacement; after that, a nonlinear plastic behavior occurs. The ultimate pullout load 3.2 kg has been obtained using the double tangent approach for this case. Figures 5.10 to 5.32 illustrate similar outcomes for various plate inclinations and H/B ratios, which have been shown in Annexure VI. Table 5.3 provides the pull-out load based on the model conditions.

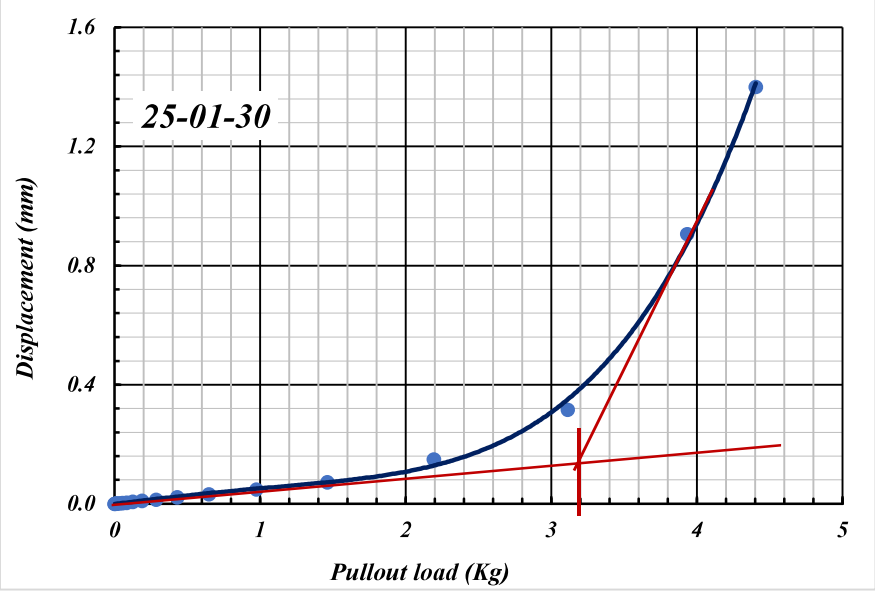

Fig. 5.9: Load vs Axial Movement for 25 mm Square Plate with (H/B =1) at 30^0 inclination

Table 5.3 has been based on the failure load obtained from load-displacement curves presented from Fig. 5.9 to 5.32, obtained by double tangent method.

Table 5.3: Model Test Results

SL NO	Test Nomenclature	Ultimate Pullout Load (F)(Kg)
1	25-01-30	3.2
2	25-01-45	3.4
3	25-01-60	3.8
4	25-02-30	4.2
5	25-02-45	4.5
6	25-02-60	6.2
7	25-03-30	4.7
8	25-03-45	5.3
9	25-03-60	6.8
10	50-01-30	6.2
11	50-01-45	6.9
12	50-01-60	11.6
13	50-02-30	8.8
14	50-02-45	10.5
15	50-02-60	17.5
16	50-03-30	10
17	50-03-45	15
18	50-03-60	20.5
19	75-01-30	17.5
20	75-01-45	20.5
21	75-01-60	23
22	75-02-30	20.8
23	75-02-45	27
24	75-02-60	29

5.3 INCLINED ANCHORS IN REINFORCED CLAY UNDER STATIC LOADING

5.3.1 Model Anchor Tests:

The model anchor test programme has been shown in Table 5.4 for different embedment depth of 50 mm x 50 mm anchor plate in reinforced soil. In this study total eighteen tests have been carried out. Different parameters involved in model test are shown in Fig. 5.33.

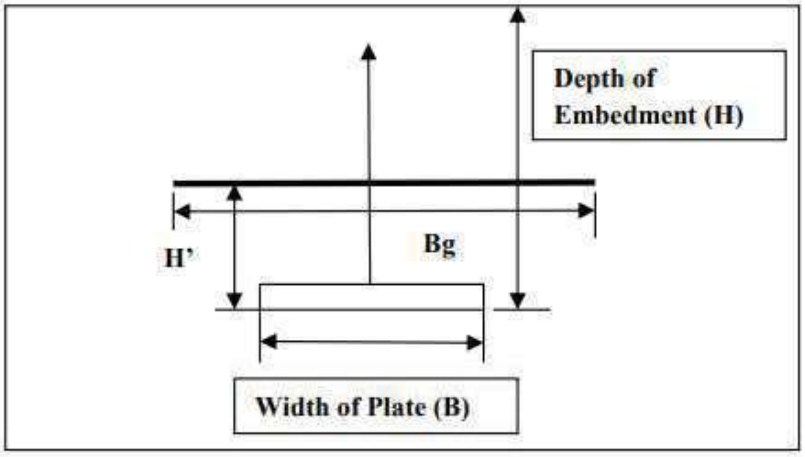

Fig. 5.33: Schematic Representation of Model Anchor test in Reinforced Condition

Table 5.4: Test Programme – Model Anchor Plate Test

Sl. No.	Plate Size (mm)	Embedment Ratio(H/B)	Inclination Angle W.R.T. Vertical	Nomenclature
1	25mm X 25mm	1	30°	25-01-30(RE)
2			45°	25-01-45(RE)
3			60°	25-01-60(RE)
4		2	30°	25-02-30(RE)
5			45°	25-02-45(RE)
6			60°	25-02-60(RE)
7		3	30°	25-03-30(RE)
8			45°	25-03-45(RE)
9			60°	25-03-60(RE)
1	50mm X 50mm	1	30°	50-01-30(RE)
2			45°	50-01-45(RE)
3			60°	50-01-60(RE)
4		2	30°	50-02-30(RE)
5			45°	50-02-45(RE)
6			60°	50-02-60(RE)
7		3	30°	50-03-30(RE)
8			45°	50-03-45(RE)
9			60°	50-03-60(RE)

5.3.2 Experimental Procedure:

In this case the only difference in the experimental procedure from the previous case is to place the reinforcement.

In the present study, reinforcement in the form of geotextile of width four times the width of plate is used, and placed at a distance of 0.25 times the depth of embedment from the bottom of anchor plate (Bhattacharya, 2008). A hole of 10 mm is made at the centre of the sheet to allow the shaft, connected to the anchor. After the placement of geotextile horizontally over the desired level the embedded soil left, are compacted in layers.

5.3.3 Presentation of Model Anchor Test Results:

Fig. 5.34 depicts how the pull-out load varies as the displacement increases gradually. As seen in the figure, the load increases approximately linearly with displacement up to 0.2 mm, after which it exhibits nonlinear plastic behaviour. The double tangent approach produces an ultimate load of 5 kg. Similar findings have been obtained for various plate inclinations and H/B ratios, as illustrated in Figs 5.35–5.51, which have been shown in Annexure VII. Table 5.5 shows the pull-out load based on the model conditions.

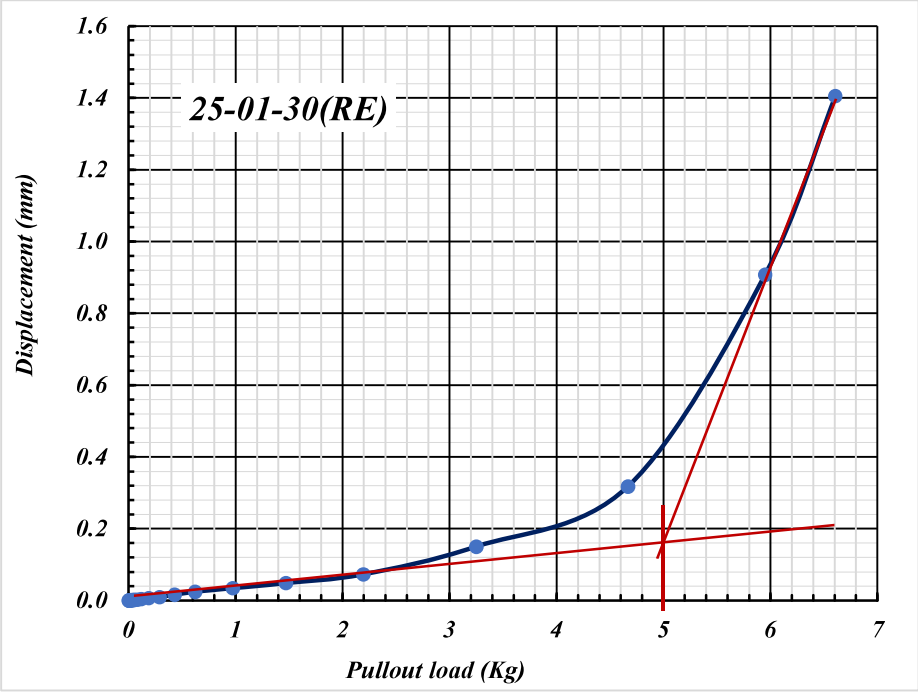

Fig. 5.34: Load vs Axial Movement for 25 mm Square Plate with (H/B =1) at 30^0 inclination

Table 5.5 has been based on the failure load obtained from load-displacement curves presented from Fig. 5.34 to 5.51, obtained by double tangent method.

Table 5.5: Model Test Results (Reinforced bed)

Sl. No.	Test Nomenclature	Ultimate Pullout Load (F)(Kg)
1	25-01-30(RE)	5
2	25-01-45(RE)	5.9
3	25-01-60(RE)	6.5
4	25-02-30(RE)	6.4
5	25-02-45(RE)	7.1
6	25-02-60(RE)	10.2
7	25-03-30(RE)	7.8
8	25-03-45(RE)	9.6
9	25-03-60(RE)	11.9
10	50-01-30(RE)	8.9
11	50-01-45(RE)	10
12	50-01-60(RE)	16
13	50-02-30(RE)	19.6
14	50-02-45(RE)	26.3
15	50-02-60(RE)	31.1
16	50-03-30(RE)	24.2
17	50-03-45(RE)	39
18	50-03-60(RE)	44.9

5.4 SUMMARY

The chapter has presented the description of the test setup and experimental procedure of model anchor tests for the inclined anchor, both in unreinforced soil bed and reinforced soil bed condition. Total 24 tests have been performed varying plate size, inclination angle and embedment depth of the inclined anchors in unreinforced soil bed, whereas for anchors in reinforced soil bed,18 tests have been performed. It has also presented the pullout-displacement graphs obtained during model tests for anchors in unreinforced and reinforced soil bed. Finally, ultimate pullout load obtained from these tests, are also furnished.

CHAPTER 6

RESPONSE OF INCLINED ANCHORS

6.1 OVERVIEW

In this chapter an attempt has been made to present a discussion based on the results obtained from both numerical and experimental studies on inclined anchors in unreinforced and reinforced bed of cohesive soil and under both static and cyclic loading. This has been done to get an insight into the effect of reinforcement, inclination angles of anchors and also frequency and amplitude of cyclic loading considered in this study. Attempt has also been made to study the effect of plate size and embedment ratio on ultimate pullout capacity to incorporate the influence of these parameters in the behaviour of inclined anchors. The discussion has been presented in different subsections with variation of bed (reinforced and unreinforced) and nature of loading (static and cyclic). At the end a regression analysis has been done with the help of machine learning to develop a predictive model of ultimate uplift capacity of inclined anchors with independent variables as plate size, inclination angle, embedment ratio, frequency and amplitude of cyclic loading. The regression analysis has been done on the basis of numerical data of this study.

6.2 INCLINED ANCHORS IN UNREINFORCED CLAY UNDER STATIC LOADING:

In this section, results obtained from numerical analysis and model tests, have been compared. The research employed several variable parameters, including plate size, embedment ratios, anchor plate inclination angles, and soil reinforcement.

6.2.1 Important Aspects of Discussion:

Based on the numerical modelling and experimental results, following aspects have been considered for discussion-

a) Load - displacement behaviour in unreinforced soft clay soil.

b) The influence of embedment ratio of anchor plate on the pull-out load in unreinforced soft clay.

c) The influence of inclination angle of anchor plate on the pull-out load in unreinforced soft clay.

d) Effect of variation of plate size on pullout capacity of anchor in unreinforced soft clay soil.

e) Breakout factor in the form of non-dimensional form of Pullout load in unreinforced soft clay soil.

f) The effect of reinforcement in numerical model test.

6.2.2 Load – Displacement Behavior:

This section comprehensively presents variation of pullout loads, due to the variations in several key design parameters (such as plate size, inclination angle, and embedment ratio) through Table 6.1 and Fig. 6.1 to 6.6, with salient observations. The corresponding load displacement curves have been plotted and the pullout load has been obtained from numerical analysis and experimental model by double tangent method for each case, which have been discussed in details in previous chapter 4 and 5. From the numerical analysis and experimental results, the deviation of pull-out capacity obtained from numerical analysis with respect to the experimental value has been calculated out for relevant cases in unreinforced soil condition as shown in the Table 6.1.

Table 6.1: Comparison of Pull-out Load between Experiment and Numerical Analysis

SL NO	PLATE SIZE (B)	EMBEDED RATIO (H/B)	INCLINATION ANGLE	PULLOUT LOAD(KG)		
				EXPERIMENT (E)	NUMERICAL (N)	DEVIATION (%) [(E-N)/E]
1	25 mm X 25 mm	1	30°	3.2	3.5	-9.37
2			45°	3.4	4	-17.65
3			60°	3.8	4.3	-13.16
4		2	30°	4.2	4.4	-4.76
5			45°	4.5	5.2	-15.56
6			60°	6.2	5.8	6.45
7		3	30°	4.7	4.7	0
8			45°	5.3	5.8	-9.43
9			60°	6.8	6.2	8.82
10	50 mm X 50 mm	1	30°	6.2	6.2	0
11			45°	6.9	7.6	-10.14
12			60°	11.6	12.2	-5.17
13		2	30°	6.8	8.8	-29.41
14			45°	10.5	10.1	3.81
15			60°	17.5	15.2	13.14
16		3	30°	10	10	0
17			45°	15	12.4	17.33
18			60°	20.5	17.6	14.15
19	75 mm X 75 mm	1	30°	17.5	17	2.86
20			45°	20.5	19.5	4.88
21			60°	23	24.5	-6.52
22		2	30°	20.8	20.5	1.44
23			45°	27	27	0
24			60°	29	30	-3.45

Among the available results presented in Table 6.1, 50 mm square plate at an embedment ratio of 3 inclined at 45° exhibits the highest deviation of 17.33% in unreinforced soft clay. It appears from the above table that, for the same parametric consideration, the pull-out loads derived from the numerical analysis and the experimental method coincides well. So, numerical analysis performed by software may be considered quite effective for further investigation of model anchors.

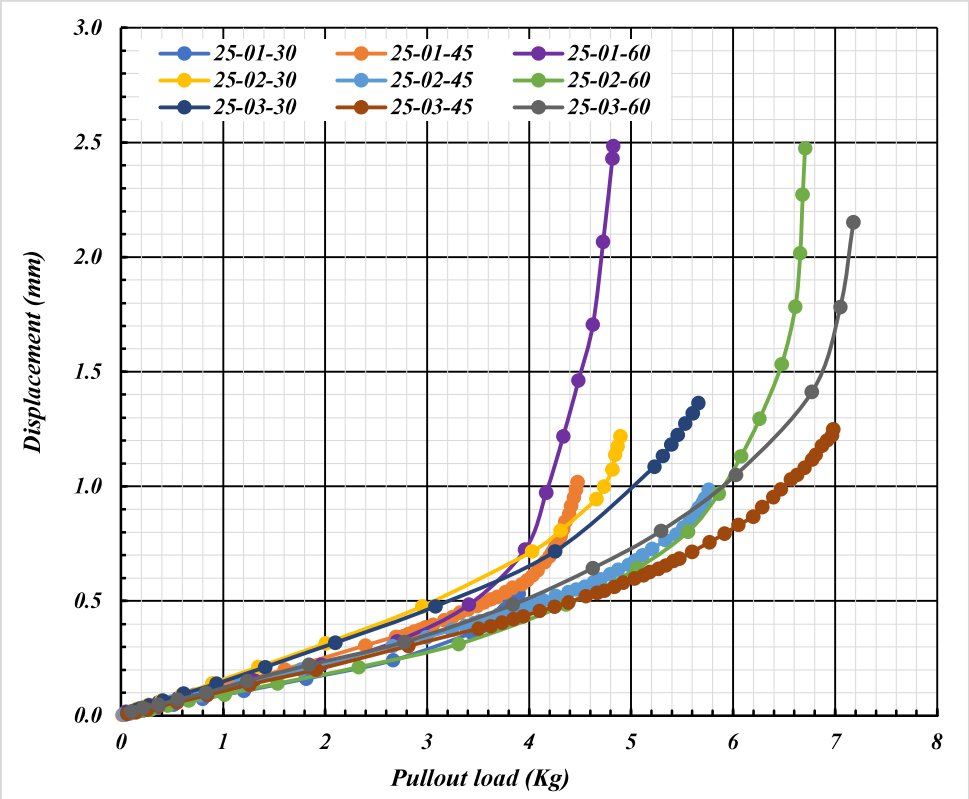

Fig. 6.1: Comparative study of pullout load vs displacement plot from numerical analysis for 25 mm square plate in unreinforced clay

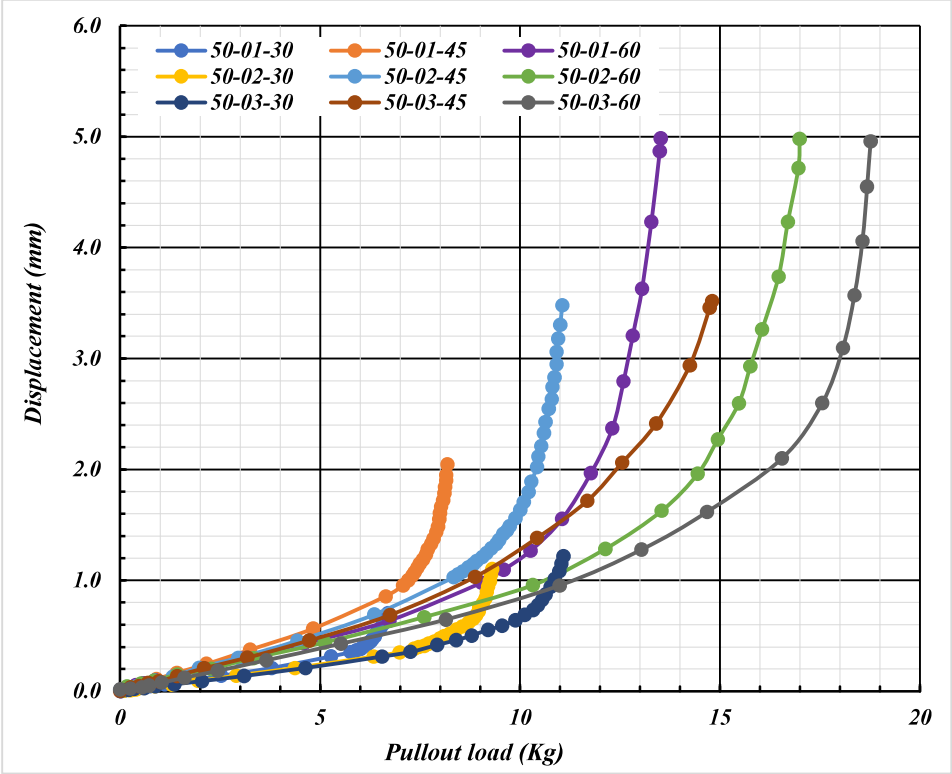

Fig. 6.2: Comparative study of load vs displacement plot from numerical analysis for 50mm square plate in unreinforced clay

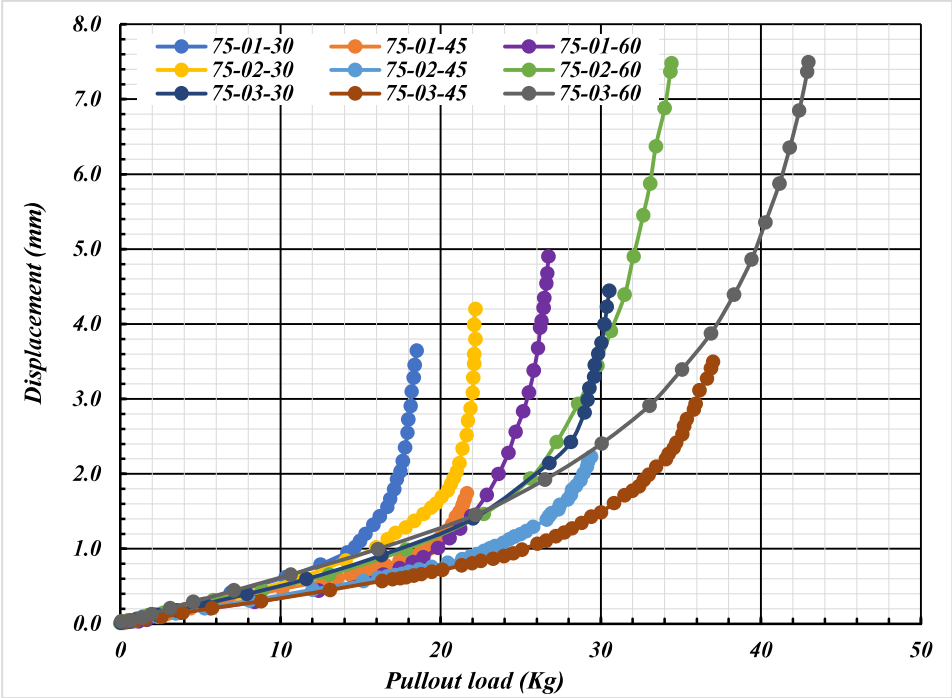

Fig. 6.3: Comparative study of load vs displacement plot from numerical analysis for 75mm square plate in unreinforced clay

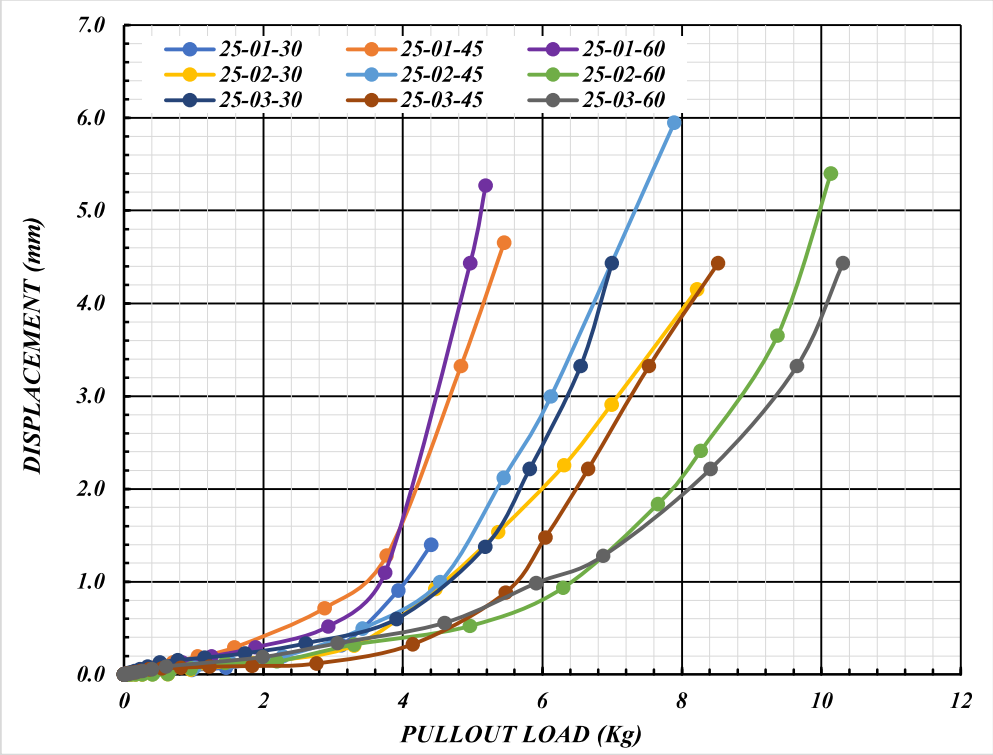

Fig. 6.4: Comparative study of load vs displacement plot from model tests for 25mm square plate in unreinforced clay

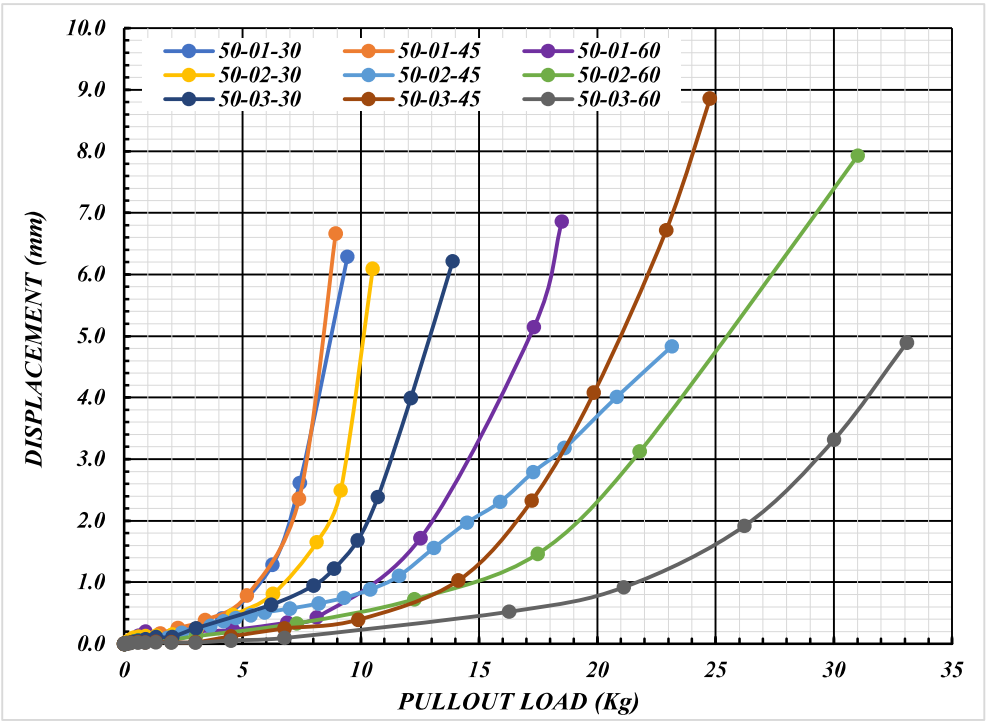

Fig. 6.5: Comparative study of load vs displacement plot from model tests for 50mm square plate in unreinforced clay

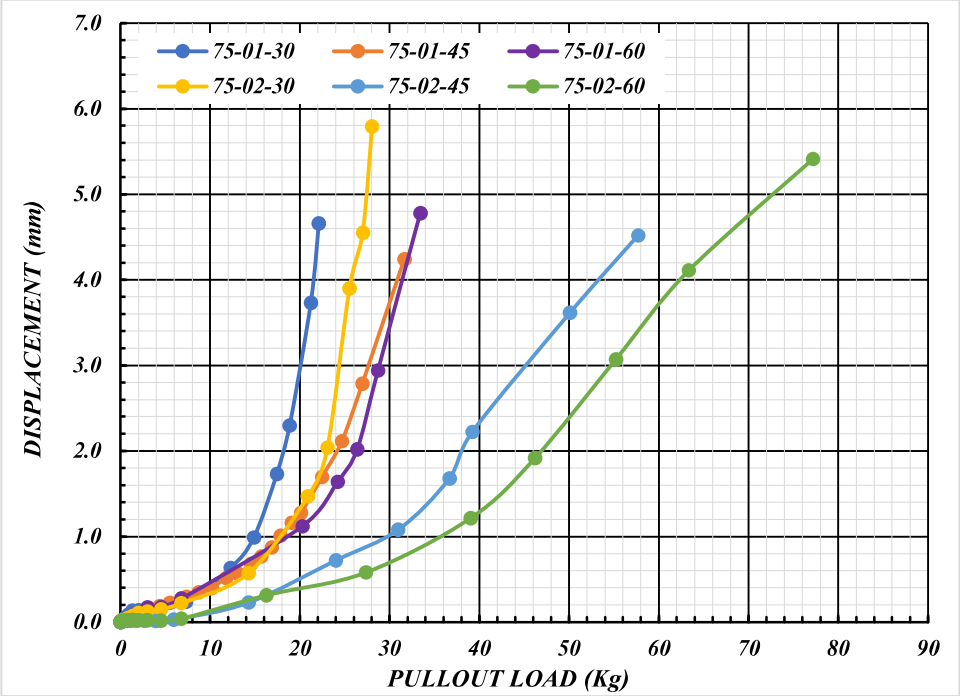

Fig. 6.6: Comparative study of load vs displacement plot from model tests for 75mm square plate in unreinforced clay

6.2.3 Effect of Embedment Ratio:

Based on the findings of the numerical analysis, Table 6.2 shows comparison of pullout capacity with embedment ratio.

Table 6.2: Comparison of Pullout Capacity with Embedment Ratio for different Plate Sizes and inclination angle in Numerical model

Sl. No	Plate size(B)	Inclination angle (degree)	Pullout capacity fordifferent embedment ratio (H/B) in (Kg)			Comparative increment of pullout capacity (%)	
			1	2	3	Change in H/B =2 from H/B=1	Change in H/B =3 from H/B=1
1	25mm X 25mm	30°	3.5	4.4	4.7	25.71	34.28
2		45°	4	5.2	5.8	30	45
3		60°	4.3	5.8	6.2	34.88	44.18
4	50mm X 50mm	30°	6.2	8.8	10	41.93	61.29
5		45°	7.6	10.1	12.4	32.89	63.15
6		60°	12.2	15.2	17.6	24.59	44.26
7	75mm X 75mm	30°	17	20.5	27.5	20.58	61.76
8		45°	19.5	27	32.5	38.46	66.66
9		60°	24.5	30	38	22.44	55.11

It is observed from Table 6.2 that pullout capacity increases with the increase in embedment ratio, when other parameters do not alter. For 75 mm plate inclined at 45° shows the maximum increase in pull capacity of 66.66% when embedment ratio increases from 1 to 3. This occurs due to the fact that with increase in embedment ratio the resisting force (due to presence of soil mass over the plate i.e., due to increase in soil volume) against the pullout load increases, leading to higher ultimate pullout load.

6.2.4 Effect of angle of Inclination:

In the current study, three inclination angles, namely 30°, 45°, and 60°, have been considered. Table 6.3 shows the change of ultimate pullout capacity with variation in angle of inclination on the basis of data furnished in Table 4.3.

Table 6.3: Comparison of Pullout Capacity with inclination angle of anchor for different Plate sizes and embedment ratio in Numerical Model

SL. NO	Plate size (B)	Embedment ratio (H/B)	Comparative increment of pullout capacity(%)				
			30°	45°	60°	For 45° w.r.t 30°	For 60° w.r.t 30°
1	25mm X 25mm	1	3.5	4	4.3	14.28	22.85
2		2	4.4	5.2	5.8	18.18	31.81
3		3	4.7	5.8	6.2	23.41	31.91
4	50mm X 50mm	1	6.2	7.6	12.2	22.58	96.77
5		2	8.8	10.1	15.2	14.77	72.72
6		3	10	12.4	17.6	24	76
7	75mm X 75mm	1	17	19.5	24.5	14.71	44.11
8		2	20.5	27	30	31.71	46.34
9		3	27.5	32.5	38	18.18	38.18

It is found from Table 6.3 that pullout capacity increases with the increase in inclination angle when other parameters do not vary. For 50 mm plate at embedment ratio 1 shows increase in pullout capacity of 96.77% when inclination angle changes from 30 to 60°. As inclination angles increase relative to vertical, so does the resisting load, thereby increasing pull-out capacity. This indicates that as inclination angles increase with respect to vertical, the involvement of soil volume (above the inclined anchor) in resisting uplift also increases,

consequently enhancing pull-out capacity. It is appropriate to mention in this regard that the same patterns of outcome have been seen in each case.

6.2.5 Effect of Plate Size:

Three square horizontal anchor plates of size 25 mm, 50 mm and 75 mm have been considered in the analysis. Fig 6.7 shows comparative study of pullout capacity with embedment ratio obtained from numerical analysis.

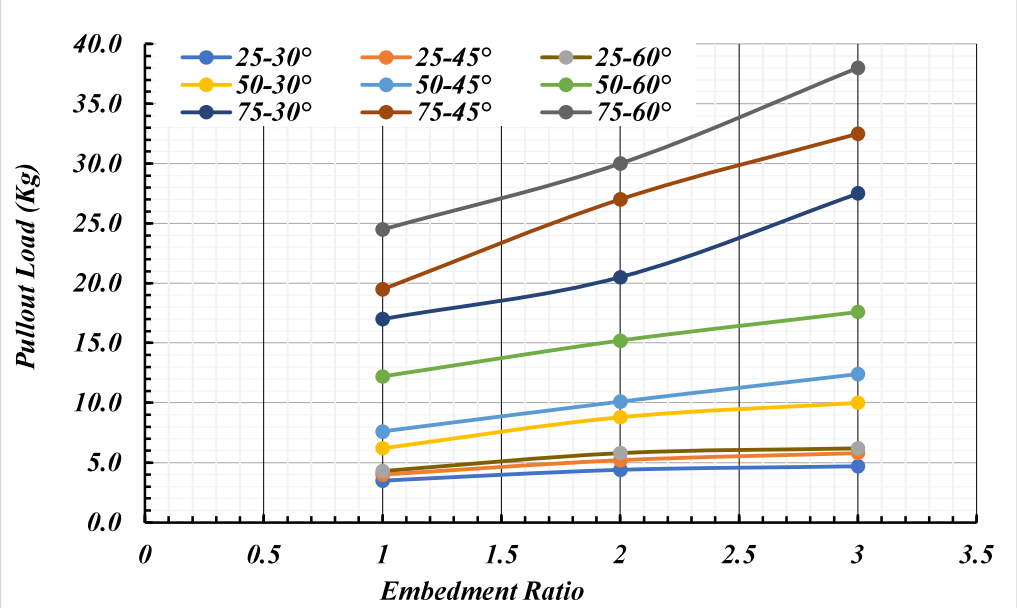

Fig. 6.7: Comparative Study of Pullout Capacity with Embedment Ratio of numerical analysis

It is observed from Fig. 6.7 that as the plate size increases, the pullout capacity also increases. For embedment ratio 3, with an inclination angle 60° pullout capacity increases maximum by 431.91% when plate size changes to 75 mm from 25 mm. The trend of variation is same for different inclined angles of the anchor plate. Effect of plate size on pullout capacity shows similar trend between numerical study and model test results. For similar depth of embedment with increase in plate size, pullout capacity increases for experimental and numerical investigations. This occurs due to the fact that with increase in plate size the volume of soil resisting axial movement of anchor also increases leading to higher pullout capacity.

6.2.6 Break Out Factor:

The ultimate anchor pullout capacity for square anchors plates in clay is usually expressed as function of the undrained shear strength as given by Das and Puri (1989)in the following Equation 6.1.

$$Q_u = A_p C_u F_c + W\cos\beta \quad \ldots\ldots (6.1)$$

Where, F_c is the Breakout Factor, Q_u is the ultimate pullout load, A_p is area of anchor plate, W is the soil weight immediately above anchor plate and $(90^o-\beta)$ is the inclination of anchor plate with the vertical. Table 6.4 and Table 6.5 show the breakout out factor value in unreinforced soil condition for model test and numerical analysis respectively.

Table 6.4: Breakout Factor of Model Test in Unreinforced soil

(Value of C_u is taken as 2500 kg/ m^2)

SL. NO	Test nomenclature	Pullout load (F) (KG)	Weight of soil (W) (Kg)	Area of the plate (A)(m^2)	Breakout factor (F-W)/(A*C_u)
1	25-01-30	3.2	0.028	0.000625	2.03
2	25-01-45	3.4	0.028	0.000625	2.16
3	25-01-60	3.8	0.028	0.000625	2.42
4	25-02-30	4.2	0.056	0.000625	2.65
5	25-02-45	4.5	0.056	0.000625	2.85
6	25-02-60	6.2	0.056	0.000625	3.95
7	25-03-30	4.7	0.084	0.000625	2.96
8	25-03-45	5.3	0.084	0.000625	3.35
9	25-03-60	6.8	0.084	0.000625	4.32
10	50-01-30	6.2	0.225	0.0025	0.96
11	50-01-45	6.9	0.225	0.0025	1.08
12	50-01-60	11.6	0.225	0.0025	1.84
13	50-02-30	8.8	0.45	0.0025	1.34
14	50-02-45	10.5	0.45	0.0025	1.63
15	50-02-60	17.5	0.45	0.0025	2.76
16	50-03-30	10	0.675	0.0025	1.50
17	50-03-45	15	0.675	0.0025	2.32
18	50-03-60	20.5	0.675	0.0025	3.22
19	75-01-30	17.5	0.76	0.005625	1.19
20	75-01-45	20.5	0.76	0.005625	1.42
21	75-01-60	23	0.76	0.005625	1.61
22	75-02-30	20.8	1.52	0.005625	1.38
23	75-02-45	27	1.52	0.005625	1.84
24	75-02-60	29	1.52	0.005625	2.00

Table 6.5: Breakout Factor of Numerical Analysis in Unreinforced soil

(Value of C_u is taken as 2500 kg/ m^2)

Sl. No	Test nomenclature	Pullout load (F) (Kg)	Weight of soil (W) (kg)	Area of the plate (A)(mm^2)	Breakout factor (F-W)/(A*C_u)
1	25-01-30	3.5	0.028	0.000625	2.22
2	25-01-45	4	0.028	0.000625	2.55
3	25-01-60	4.3	0.028	0.000625	2.74
4	25-02-30	4.4	0.056	0.000625	2.78
5	25-02-45	5.2	0.056	0.000625	3.30
6	25-02-60	5.8	0.056	0.000625	3.69
7	25-03-30	4.7	0.084	0.000625	2.96
8	25-03-45	5.8	0.084	0.000625	3.67
9	25-03-60	6.2	0.084	0.000625	3.94
10	50-01-30	6.2	0.225	0.0025	0.96
11	50-01-45	7.6	0.225	0.0025	1.19
12	50-01-60	12.2	0.225	0.0025	1.93
13	50-02-30	8.8	0.45	0.0025	1.34
14	50-02-45	10.1	0.45	0.0025	1.56
15	50-02-60	15.2	0.45	0.0025	2.39
16	50-03-30	10	0.675	0.0025	1.50
17	50-03-45	12.4	0.675	0.0025	1.90
18	50-03-60	17.6	0.675	0.0025	2.76
19	75-01-30	17	0.76	0.005625	1.16
20	75-01-45	19.5	0.76	0.005625	1.35
21	75-01-60	24.5	0.76	0.005625	1.71
22	75-02-30	20.5	1.52	0.005625	1.36
23	75-02-45	27	1.52	0.005625	1.84
24	75-02-60	30	1.52	0.005625	2.08
25	75-03-30	27.5	2.28	0.005625	1.80
26	75-03-45	32.5	2.28	0.005625	2.19
27	75-03-60	38	2.28	0.005625	2.62

Fig. 6.8 represents breakout factor vs embedment ratio curves obtained from numerical analysis of inclined anchors in unreinforced clay.

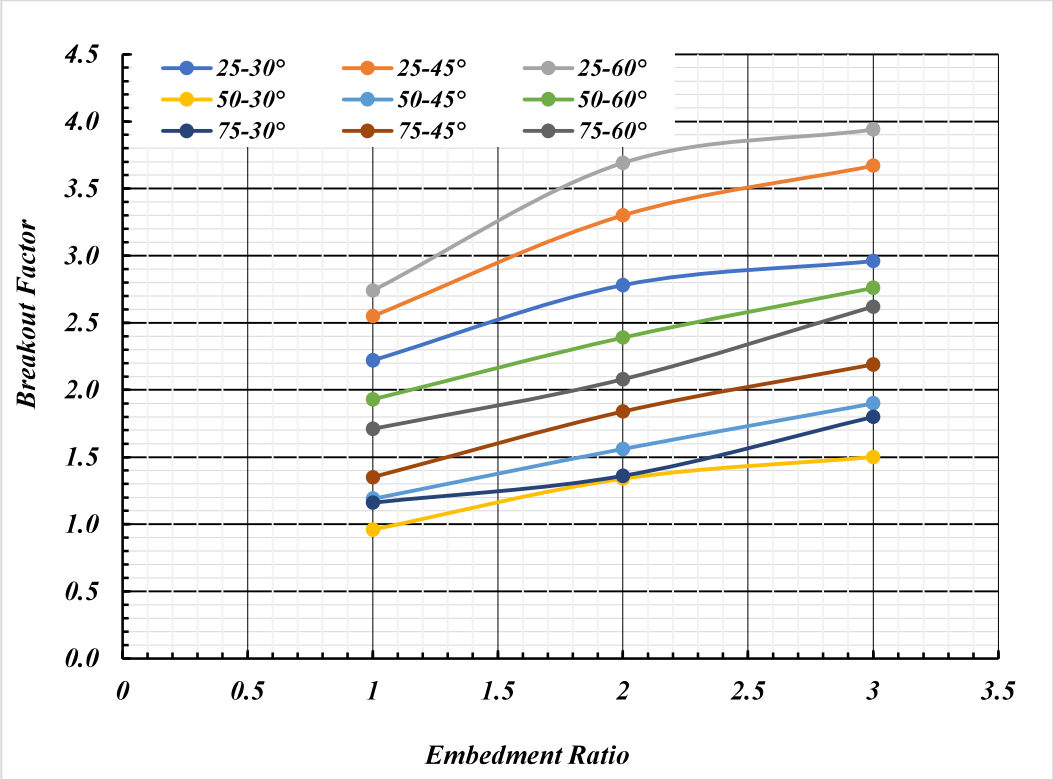

Fig. 6.8: Breakout Factor vs Embedment Ratio in Unreinforced Numerical model analysis

From the Fig 6.8 the following points have been observed:

1. Breakout factor has been increased with the increase in embedment ratio for any particular plate size.
2. Increment in inclination angle also increases the break out factor.
3. For unreinforced soil bed, maximum Breakout factor has been observed as 3.94 for 25 mm plate at an inclination angle 60° at embedment ratio 3.

Table 6.6 shows variation of breakout factor obtained in numerical analysis with respect to the experimental analysis.

Table 6.6: variation of breakout factor

Sl. No	Plate size (B)	Embedment ratio (H/B)	Inclination angle	Breakout factor		
				Numerical(N)	Experimental(E	Deviation (%) =((N-E)/E) *100
1	25mm X 25mm	1	30°	2.22	2.03	9.5%
2		1	45°	2.55	2.16	17.8%
3		1	60°	2.74	2.42	13.2%
4		2	30°	2.78	2.65	4.8%
5		2	45°	3.30	2.85	15.7%
6		2	60°	3.69	3.95	-6.5%
7		3	30°	2.96	2.96	0.0%
8		3	45°	3.67	3.35	9.5%
9		3	60°	3.94	4.32	-8.9%
10	50 mm X 50mm	1	30°	0.96	0.96	0.0%
11		1	45°	1.19	1.08	10.4%
12		1	60°	1.93	1.84	5.2%
13		2	30°	1.34	1.34	0.0%
14		2	45°	1.56	1.63	-3.9%
15		2	60°	2.39	2.76	-13.3%
16		3	30°	1.50	1.50	0.0%
17		3	45°	1.90	2.32	-17.9%
18		3	60°	2.76	3.22	-14.4%
19	75 mm X 75mm	1	30°	1.16	1.19	-3.0%
20		1	45°	1.35	1.42	-5.0%
21		1	60°	1.71	1.61	6.6%
22		2	30°	1.36	1.38	-1.5%
23		2	45°	1.84	1.84	0.0%
24		2	60°	2.08	2.00	3.5%

From the above table, it is evident that the Breakout factors attained from the numerical study have agreed well with the Breakout factors found from the experimental method for the identical parametric considerations. So, numerical analysis by the ABAQUS v6.14 may be adopted as an effective tool for further analysis of the model tests of anchors.

6.3 INCLINED ANCHORS IN REINFORCED CLAY UNDER STATIC LOADING:

6.3.1 Load – Displacement Behavior:

The pullout behaviour of inclined anchor in reinforced soil condition also has been carried out according to size of anchor plate, inclination angle of anchor plate and embedment ratio. For same sizes of plate with different embedment ratio and different inclination angle, load vs. displacement plot obtained from numerical analyses in reinforced condition. Fig. 6.9, 6.10 and 6.11 represent comparative load-displacement behaviour of different sizes of plates obtained from numerical analysis of anchor plate in reinforced soil bed. From the numerical analysis and limited number of experimental results (18 numbers), the deviation of pull-out capacity obtained from numerical analysis with respect to the experimental value has been calculated out for relevant cases in unreinforced soil condition as shown in the Table 6.7.

Table 6.7: Comparison of Pull-out Load between Experiment and Numerical Analysis

SL NO	PLATE SIZE (B)	EMBEDED RATIO (H/B)	INCLINATION ANGLE	PULLOUT LOAD(KG)		
				EXPERIMENT (E)	NUMERICAL (N)	DEVIATION (%) [(E-N)/E]
1	25 mm X 25 mm	1	30°	5	4.8	4%
2			45°	5.9	6.0	-2%
3			60°	6.5	6.4	2%
4		2	30°	6.4	5.8	9%
5			45°	7.1	7.1	0%
6			60°	10.2	8.3	19%
7		3	30°	7.8	6.8	13%
8			45°	9.6	9.1	5%
9			60°	11.9	9.4	21%
10	50 mm X 50 mm	1	30°	8.9	7.7	13%
11			45°	10	9.6	4%
12			60°	16	14.6	9%
13		2	30°	19.6	17.0	13%
14			45°	26.3	22.0	16%
15			60°	31.1	23.5	24%
16		3	30°	24.2	21.0	13%
17			45°	39	28.0	28%
18			60°	44.9	33.5	25%

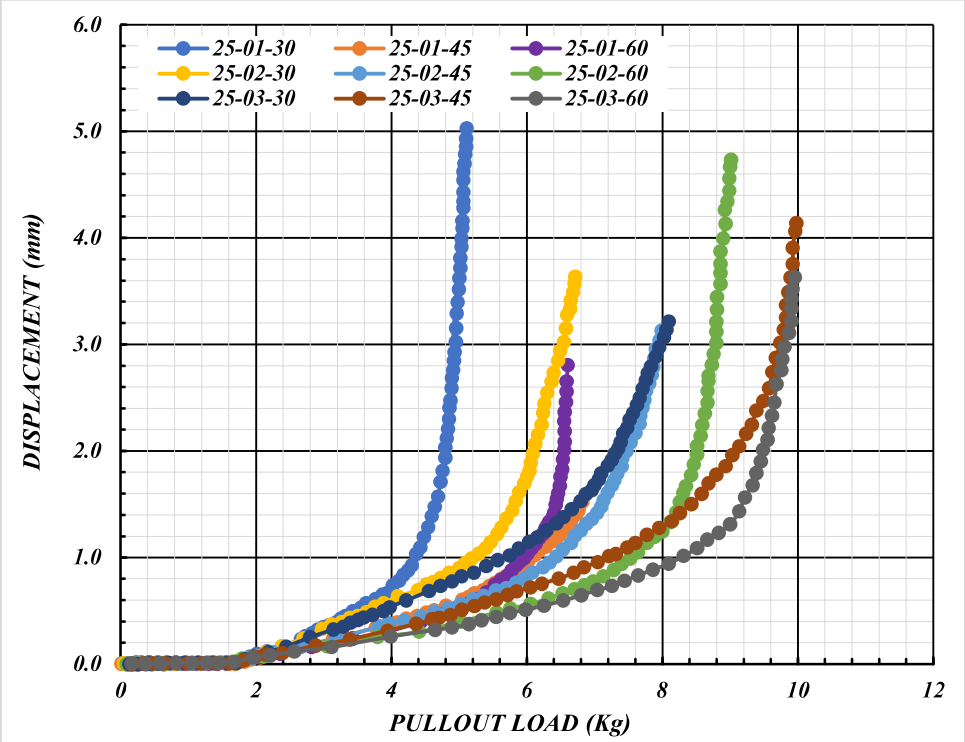

Fig. 6.9: Comparative Study of Load vs displacement plot from Numerical Analysis for 25mm square plate in reinforced soft clay

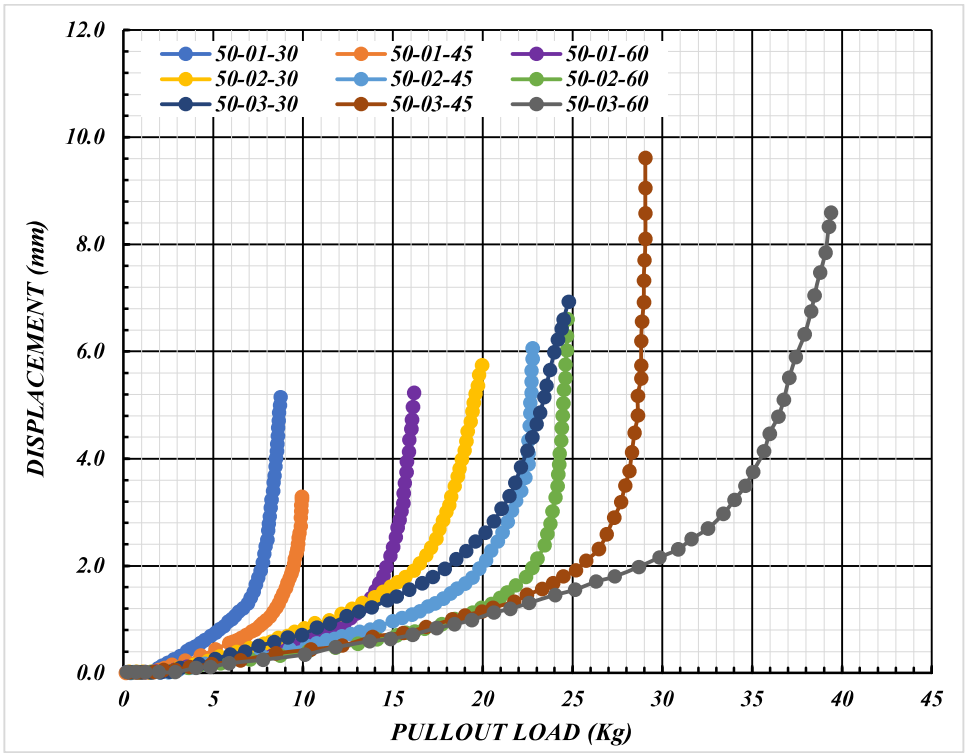

Fig. 6.10: Comparative Study of Load vs displacement plot from Numerical Analysis for 50mm square plate in reinforced soft clay

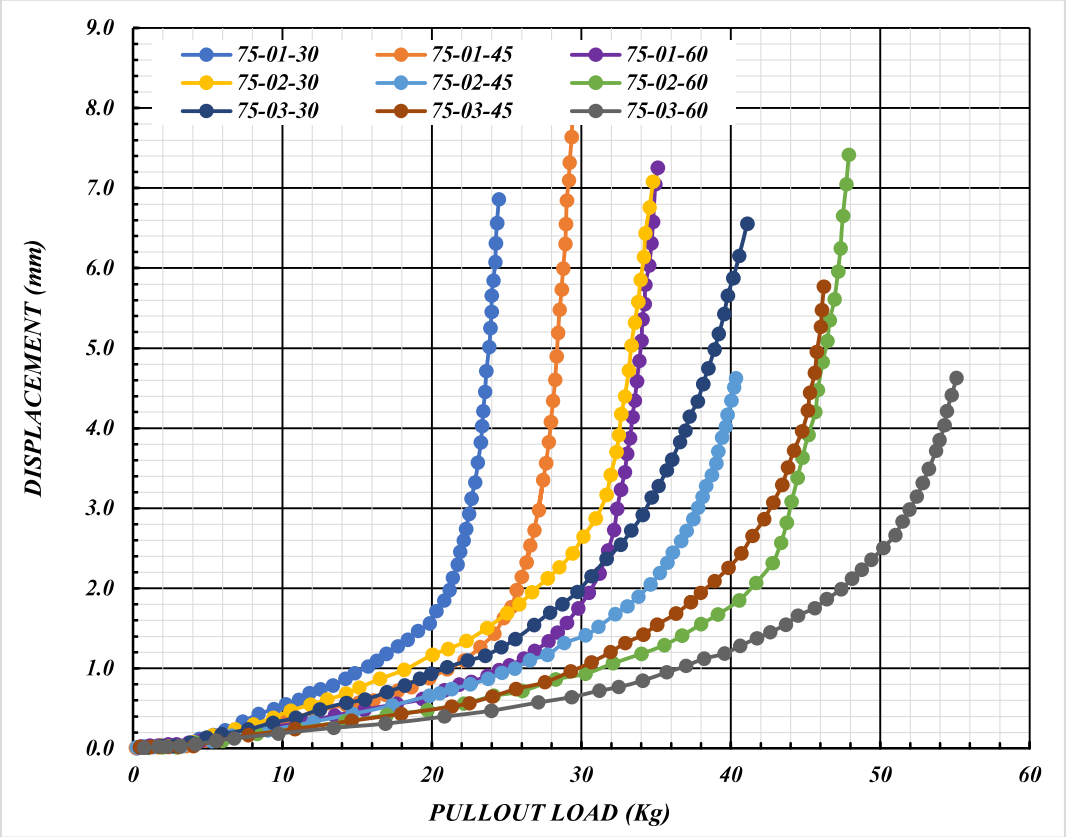

Fig. 6.11: Comparative Study of Load vs displacement plot from Numerical Analysis for 75mm square plate in reinforced soft clay

Fig. 6.9, 6.10 and 6.11 have shown that the load displacement curve is linear up to certain value of load beyond which the slope of the curve increases sharply. In this regard, it is apt to mention that same trends of results have been observed for both of unreinforced and reinforced (with geotextile) cases. It has also been noted that with the increase in embedment ratio the value of the specific magnitude of pull-out load (beyond which the displacement increases rapidly with small increase of pullout load) increases indicating that the increase in resisting soil mass will act against deformations to more extent.

6.3.2 Effect of Embedment Ratio:

Based on the findings of the numerical analysis, Table 6.8 shows comparison of pullout capacity with embedment ratio.

Table 6.8: Comparison of Pullout Capacity with Embedment Ratio for different Plate Sizes and inclination angle in Numerical model

Sl. No	Plate size (B)	Inclination angle (degree)	Pullout capacity for different embedment ratio (H/B) in (Kg)			Comparative increment of pullout capacity (%)	
			1	2	3	Change in H/B =2 from H/B=1	Change in H/B =3 from H/B=1
1	25mm X 25mm	30°	4.8	5.8	6.8	20.83%	41.67%
2		45°	6	7.1	9.1	18.33%	51.67%
3		60°	6.4	8.3	9.4	29.69%	46.88%
4	50mm X 50mm	30°	7.7	17	21	120.78%	172.73%
5		45°	9.6	22	28	129.17%	191.67%
6		60°	14.6	23.5	33.5	60.96%	129.45%
7	75mm X 75mm	30°	22.5	31	33.5	37.78%	48.89%
8		45°	27	35	43	29.63%	59.26%
9		60°	32	43	50	34.38%	56.25%

It is observed from Table 6.7 that pullout capacity increases with the increase in embedment ratio, when other parameters do not alter. For 50 mm plate inclined at 45° shows the maximum increase in pull capacity of 191.67% when embedment ratio increases from 1 to 3. The explanation behind such variation is similar to that for unreinforced bed as mentioned in section 6.2.3.

6.3.3 Effect of angle of Inclination:

In the current study, three inclination angles, namely 30°, 45°, and 60°, have been considered. Table 6.9 shows the change of ultimate pullout capacity with variation in angle of inclination.

Table 6.9: Comparison of Pullout Capacity with inclination angle of anchor for different Plate sizes and embedment ratio in Numerical Model

SL. NO	Plate size (B)	Embedment ratio (H/B)	Inclination angle with vertical			Comparative increment of pullout capacity (%)	
			30°	45°	60°	For 45° w.r.t 30°	For 60° w.r.t 30°
1	25mm X 25mm	1	4.8	6	6.4	25.00%	33.33%
2		2	5.8	7.1	8.3	22.41%	43.10%
3		3	6.8	9.1	9.4	33.82%	38.24%
4	50mm X 50mm	1	7.7	9.6	14.6	24.68%	89.61%
5		2	17	22	23.5	29.41%	38.24%
6		3	21	28	33.5	33.33%	59.52%
7	75mm X 75mm	1	22.5	27	32	20.00%	42.22%
8		2	31	35	43	12.90%	38.71%
9		3	33.5	43	50	28.36%	49.25%

It is found from Table 6.9 that pullout capacity increases with the increase in inclination angle when other parameters do not vary. For 50 mm plate at embedment ratio 1 shows increase in pullout capacity of 89.61% when inclination angle changes from 30^0 to 60°. The reason for this variance is similar to that for unreinforced beds, as discussed in section 6.2.4.

6.3.4 Effect of Plate Size:

Three square horizontal anchor plates of size 25 mm, 50 mm and 75 mm have been considered in the analysis. Fig 6.12 shows comparative study of pullout capacity with embedment ratio obtained from numerical analysis.

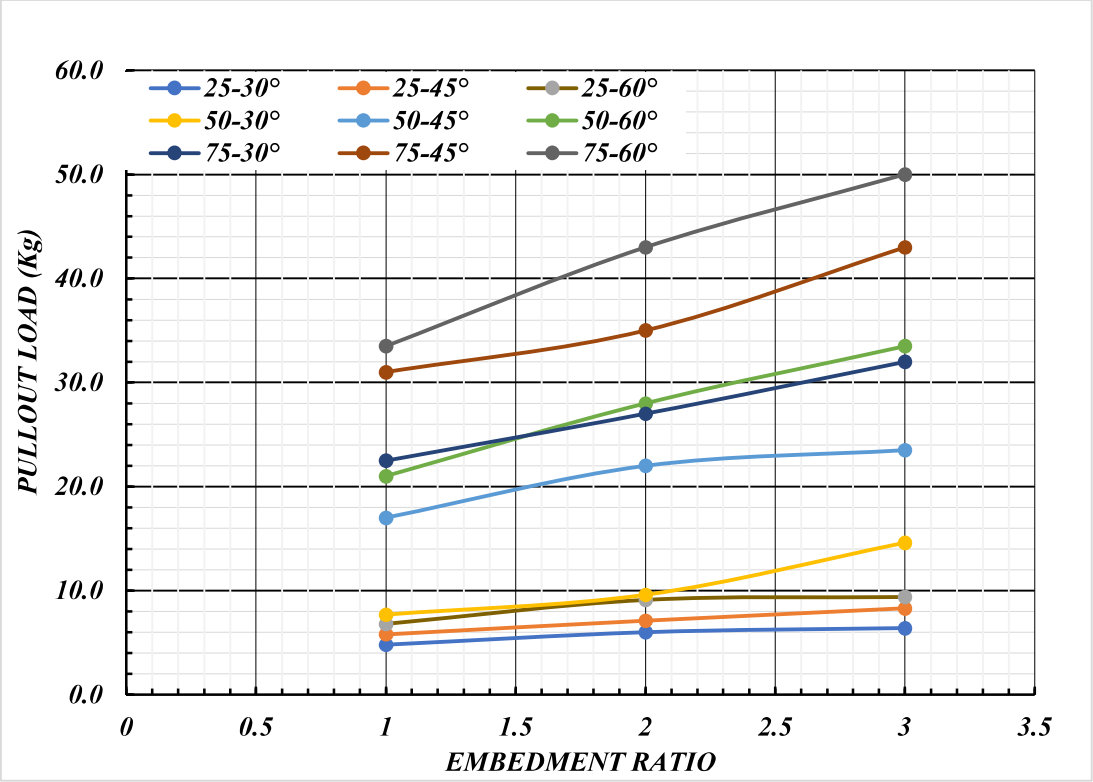

Fig. 6.12: Comparative Study of Pullout Capacity with Embedment Ratio of numerical analysis

It is observed from Fig. 6.12 that as the plate size increases, the pullout capacity also increases. The trend of variation is same for different inclined angles of the anchor plate. Effect of plate size on pullout capacity of inclined anchor shows similar trend for both unreinforced and reinforced soil bed condition. For embedment ratio 3, with an inclination angle 60° pullout capacity increases maximum by 512.9% when plate size changes to 75 mm from 25 mm.

6.3.5 Effect of Reinforcement in Numerical Cases:

From the numerical analysis of inclined anchor plate in unreinforced and reinforced soft clay, the improvement factor (Ratio of pullout capacity of anchor plate at reinforced soil to the unreinforced soil) of pull-out capacity carried out for every single case as shown in the Table 6.10.

Table 6.10: Comparison of Pull-out Load in unreinforced and reinforced soil in numerical model

Sl. No	Plate size(B)	Embedment ratio(H/B)	Inclination angle (Degree)	Pull out load (Kg)		Improvement factor (RE/UR)
				Unreinforced Condition (UR)	Reinforced Condition (RE)	
1	25mm X 25mm	1	30	3.5	4.8	1.37
2			45	4	6	1.5
3			60	4.3	6.4	1.48
4		2	30	4.4	5.8	1.31
5			45	5.2	7.1	1.36
6			60	5.8	8.3	1.43
7		3	30	4.7	6.8	1.44
8			45	5.8	9.1	1.56
9			60	6.2	9.4	1.51
10	50mm X 50mm	1	30	6.2	7.7	1.24
11			45	7.6	9.6	1.26
12			60	12.2	14.6	1.19
13		2	30	8.8	17	1.93
14			45	10.1	22	2.17
15			60	15.2	23.5	1.54
16		3	30	10	21	2.1
17			45	12.4	28	2.25
18			60	17.6	33.5	1.91
19	75mm X 75mm	1	30	17	22.5	1.32
20			45	19.5	27	1.38
21			60	24.5	32	1.31
22		2	30	20.5	31	1.51
23			45	27	35	1.29
24			60	30	43	1.43
25		3	30	27.5	33.5	1.21
26			45	32.5	43	1.32
27			60	38	50	1.31

It is found from Table 6.10 that in each case pullout capacity increases with inclusion reinforcement. This increase is due to the fact that tensile stress in geotextile is induced in the reinforcement and the force due to this, acts to resist pullout. Following observations have been made from the results obtained from Table 6.10:

1. For the plate size of 75 mm at embedment depth ratio(D/B=) 3 at inclination angle of 30 degree shows the minimum improvement factor of 1.21.
2. For the plate size of 50 mm at embedment depth ratio(D/B=) 3 at inclination angle of 45° shows the maximum improvement factor of 2.25.
3. Excluding the higher values of improvement factor (more than 1.9) the average improvement factor value for 25 mm plate is about 1.44, for 50 mm plate about 1.31 and for 75 mm plate it is about 1.2.

6.3.6 Break Out Factor:

Table 6.11 shows the obtained breakout factor from numerical analysis of inclined anchor in reinforced soil.

Table 6.11: Breakout Factor of Numerical Analysis in Reinforced soil

(Value of C_u is taken as 2500 kg/ m^2)

Sl. No	Case nomenclature	Pullout load (F_r) (Kg)	Weight of soil (W) (kg)	Area of the plate (A)(mm^2)	Breakout factor (F_r - W)/(A*C_u)
1	25-01-30-RE	4.8	0.028	0.000625	3.06
2	25-01-45-RE	6	0.028	0.000625	3.83
3	25-01-60-RE	6.4	0.028	0.000625	4.09
4	25-02-30-RE	5.8	0.056	0.000625	3.68
5	25-02-45-RE	7.1	0.056	0.000625	4.52
6	25-02-60-RE	8.3	0.056	0.000625	5.29
7	25-03-30-RE	6.8	0.084	0.000625	4.30
8	25-03-45-RE	9.1	0.084	0.000625	5.78
9	25-03-60-RE	9.4	0.084	0.000625	5.99
10	50-01-30-RE	7.7	0.225	0.0025	1.20
11	50-01-45-RE	9.6	0.225	0.0025	1.51
12	50-01-60-RE	14.6	0.225	0.0025	2.32
13	50-02-30-RE	17	0.45	0.0025	2.65
14	50-02-45-RE	22	0.45	0.0025	3.47
15	50-02-60-RE	23.5	0.45	0.0025	3.72
16	50-03-30-RE	21	0.675	0.0025	3.26
17	50-03-45-RE	28	0.675	0.0025	4.40
18	50-03-60-RE	33.5	0.675	0.0025	5.30
19	75-01-30-RE	22.5	0.76	0.005625	1.55
20	75-01-45-RE	27	0.76	0.005625	1.88
21	75-01-60-RE	32	0.76	0.005625	2.25
22	75-02-30-RE	31	1.52	0.005625	2.10
23	75-02-45-RE	35	1.52	0.005625	2.41
24	75-02-60-RE	43	1.52	0.005625	3.00
25	75-03-30-RE	33.5	2.28	0.005625	2.23
26	75-03-45-RE	43	2.28	0.005625	2.93
27	75-03-60-RE	50	2.28	0.005625	3.47

It has been observed from Table 6.11 that breakout factor increases with embedment ratio when other parameters remain same, maximum breakout factor of 5.99 has been observed for 25 mm anchor plate with inclination angle 60^0 at embedment ratio 3.

6.4 INCLINED ANCHORS IN UNREINFORCED CLAY UNDER CYCLIC LOADING:

Fig 4.122 to 4.229 in chapter 4 present the load displacement behaviour of inclined anchors in unreinforced clay under cyclic loading. Biradar et al. considered that the ultimate pullout is the peak load occurring at a displacement which is same as the maximum amplitude considered for a given frequency for the first cycle in the respective study to account for the resonance effect between soil and the applied cyclic loading. The same convention regarding the pull-out load has been adopted in the present study. The ultimate pullout load has been obtained for each of the 108 cases as furnished in Table 6.12, 6.13,6.14 and 6.15.

Table 6.12: Pull Out Load For Anchor for 0.2Hz Frequency and 2mm Amplitude cases

Case No.	Case Code	Plate Size(in mm)	Inclination Angle (in degrees)	Embedment Ratios	Pull Out Load (in N)Corresponding to amplitude	
					Cycle-1	Cycle2
Case 1	25P-1E-30A-0.2Hz-2Mm	25X25	30	1	30.1	20.85
Case 2	25P-2E-30A-0.2Hz-2Mm			2	35.91	28.6
Case 3	25P-3E-30A-0.2Hz-2Mm			3	39.13	27.27
Case 4	25P-1E-45A-0.2Hz-2Mm		45	1	32.2	25.78
Case 5	25P-2E-45A-0.2Hz-2Mm			2	35.97	32.36
Case 6	25P-3E-45A-0.2Hz-2Mm			3	39.9	33.54
Case 7	25P-1E-60A-0.2Hz-2Mm		60	1	34.88	28.53
Case 8	25P-2E-60A-0.2Hz-2Mm			2	37.66	30.05
Case 9	25P-3E-60A-0.2Hz-2Mm			3	41.98	35.87
Case 10	50P-1E-30A-0.2Hz-2Mm	50X50	30	1	37.85	30.9
Case 11	50P-2E-30A-0.2Hz-2Mm			2	41	28.22
Case 12	50P-3E-30A-0.2Hz-2Mm			3	43.15	39.19
Case 13	50P-1E-45A-0.2Hz-2Mm		45	1	39.25	28.2
Case 14	50P-2E-45A-0.2Hz-2Mm			2	42.3	35
Case 15	50P-3E-45A-0.2Hz-2Mm			3	45.94	38.85
Case 16	50P-1E-60A-0.2Hz-2Mm		60	1	49.46	44.94
Case 17	50P-2E-60A-0.2Hz-2Mm			2	52.16	45.9
Case 18	50P-3E-60A-0.2Hz-2Mm			3	55.88	48.7
Case 19	75P-1E-30A-0.2Hz-2Mm	75X75	30	1	48.58	38.87
Case 20	75P-2E-30A-0.2Hz-2Mm			2	55.24	47.97
Case 21	75P-3E-30A-0.2Hz-2Mm			3	62.19	56.8
Case 22	75P-1E-45A-0.2Hz-2Mm		45	1	51.65	34.54
Case 23	75P-2E-45A-0.2Hz-2Mm			2	57.66	49.9
Case 24	75P-3E-45A-0.2Hz-2Mm			3	66.16	56.59
Case 25	75P-1E-60A-0.2Hz-2Mm		60	1	54.32	45.45
Case 26	75P-2E-60A-0.2Hz-2Mm			2	62.86	54.59
Case 27	75P-3E-60A-0.2Hz-2Mm			3	68.95	58.98

Table 6.13: Pull Out Load For Anchor for 0.2Hz Frequency and 5mm Amplitude cases

Case No.	Case Code	Plate Size (in mm)	Inclination Angle (in degrees)	Embedment Ratios	Pull Out Load (in N)Corresponding to amplitude	
					Cycle-1	Cycle2
Case 28	25P-1E-30A-0.2Hz-5Mm	25X25	30	1	75.15	52.13
Case 29	25P-2E-30A-0.2Hz-5Mm			2	89.79	71.5
Case 30	25P-3E-30A-0.2Hz-5Mm			3	97.58	69.68
Case 31	25P-1E-45A-0.2Hz-5Mm		45	1	80.02	64.85
Case 32	25P-2E-45A-0.2Hz-5Mm			2	89.94	80.91
Case 33	25P-3E-45A-0.2Hz-5Mm			3	99.76	83.55
Case 34	25P-1E-60A-0.2Hz-5Mm		60	1	87.21	71.34
Case 35	25P-2E-60A-0.2Hz-5Mm			2	94.16	75.12
Case 36	25P-3E-60A-0.2Hz-5Mm			3	104.94	89.67
Case 37	50P-1E-30A-0.2Hz-5Mm	50X50	30	1	94.63	84.76
Case 38	50P-2E-30A-0.2Hz-5Mm			2	102.53	70.57
Case 39	50P-3E-30A-0.2Hz-5Mm			3	107.89	97.97
Case 40	50P-1E-45A-0.2Hz-5Mm		45	1	98.13	70.51
Case 41	50P-2E-45A-0.2Hz-5Mm			2	105.75	88.21
Case 42	50P-3E-45A-0.2Hz-5Mm			3	114.85	97.12
Case 43	50P-1E-60A-0.2Hz-5Mm		60	1	123.65	112.35
Case 44	50P-2E-60A-0.2Hz-5Mm			2	130.39	114.73
Case 45	50P-3E-60A-0.2Hz-5Mm			3	139.71	121.74
Case 46	75P-1E-30A-0.2Hz-5Mm	75X75	30	1	121.45	97.19
Case 47	75P-2E-30A-0.2Hz-5Mm			2	138.11	119.94
Case 48	75P-3E-30A-0.2Hz-5Mm			3	155.48	142.01
Case 49	75P-1E-45A-0.2Hz-5Mm		45	1	129.12	86.37
Case 50	75P-2E-45A-0.2Hz-5Mm			2	144.15	124.87
Case 51	75P-3E-45A-0.2Hz-5Mm			3	165.39	141.47
Case 52	75P-1E-60A-0.2Hz-5Mm		60	1	135.89	113.62
Case 53	75P-2E-60A-0.2Hz-5Mm			2	157.15	136.49
Case 54	75P-3E-60A-0.2Hz-5Mm			3	172.39	147.47

Table 6.14: Pull Out Load For Anchor for 0.5Hz Frequency and 2mm Amplitude cases

Case No.	Case Code	Plate Size (in mm)	Inclination Angle (in degrees)	Embedment Ratios	Pull Out Load (in N) Corresponding to amplitude	
					Cycle-1	Cycle2
Case 55	25P-1E-30A-0.5Hz-2Mm	25X25	30	1	26.1	18.97
Case 56	25P-2E-30A-0.5Hz-2Mm			2	31.24	26.02
Case 57	25P-3E-30A-0.5Hz-2Mm			3	33.56	25.36
Case 58	25P-1E-45A-0.5Hz-2Mm		45	1	27.84	22.42
Case 59	25P-2E-45A-0.5Hz-2Mm			2	31.3	28.15
Case 60	25P-3E-45A-0.5Hz-2Mm			3	34.71	30.52
Case 61	25P-1E-60A-0.5Hz-2Mm		60	1	30.35	25.96
Case 62	25P-2E-60A-0.5Hz-2Mm			2	32.76	27.34
Case 63	25P-3E-60A-0.5Hz-2Mm			3	36.52	33.0
Case 64	50P-1E-30A-0.5Hz-2Mm	50X50	30	1	32.93	30.85
Case 65	50P-2E-30A-0.5Hz-2Mm			2	36.85	25.98
Case 66	50P-3E-30A-0.5Hz-2Mm			3	43.15	39.19
Case 67	50P-1E-45A-0.5Hz-2Mm		45	1	34.15	25.67
Case 68	50P-2E-45A-0.5Hz-2Mm			2	37.32	30.73
Case 69	50P-3E-45A-0.5Hz-2Mm			3	45.94	38.85
Case 70	50P-1E-60A-0.5Hz-2Mm		60	1	43.1	39.9
Case 71	50P-2E-60A-0.5Hz-2Mm			2	45.37	41.76
Case 72	50P-3E-60A-0.5Hz-2Mm			3	48.61	44.31
Case 73	75P-1E-30A-0.5Hz-2Mm	75X75	30	1	42.26	34.6
Case 74	75P-2E-30A-0.5Hz-2Mm			2	48.05	43.66
Case 75	75P-3E-30A-0.5Hz-2Mm			3	54.1	51.69
Case 76	75P-1E-45A-0.5Hz-2Mm		45	1	45.45	31.09
Case 77	75P-2E-45A-0.5Hz-2Mm			2	50.74	45.95
Case 78	75P-3E-45A-0.5Hz-2Mm			3	57.55	49.23
Case 79	75P-1E-60A-0.5Hz-2Mm		60	1	47.25	35.77
Case 80	75P-2E-60A-0.5Hz-2Mm			2	57.2	50.22
Case 81	75P-3E-60A-0.5Hz-2Mm			3	59.99	53.68

Table 6.15: Pull Out Load For Anchor for 0.5Hz Frequency and 5mm Amplitude cases

Case No.	Case Code	Plate Size(in mm)	Inclination Angle (in degrees)	Embedment Ratios	Pull Out Load (in N) Corresponding to amplitude	
					Cycle-1	Cycle2
Case 82	25P-1E-30A-0.5Hz-5Mm	25X25	30	1	65.25	45.34
Case 83	25P-2E-30A-0.5Hz-5Mm			2	78.12	62.21
Case 84	25P-3E-30A-0.5Hz-5Mm			3	84.89	60.62
Case 85	25P-1E-45A-0.5Hz-5Mm		45	1	69.61	56.07
Case 86	25P-2E-45A-0.5Hz-5Mm			2	78.25	70.39
Case 87	25P-3E-45A-0.5Hz-5Mm			3	87.79	72.95
Case 88	25P-1E-60A-0.5Hz-5Mm		60	1	76.74	62.78
Case 89	25P-2E-60A-0.5Hz-5Mm			2	81.92	65.35
Case 90	25P-3E-60A-0.5Hz-5Mm			3	91.31	78.91
Case 91	50P-1E-30A-0.5Hz-5Mm	50X50	30	1	85.17	76.28
Case 92	50P-2E-30A-0.5Hz-5Mm			2	91.25	61.39
Case 93	50P-3E-30A-0.5Hz-5Mm			3	94.94	86.21
Case 94	50P-1E-45A-0.5Hz-5Mm		45	1	85.37	61.34
Case 95	50P-2E-45A-0.5Hz-5Mm			2	92	78.57
Case 96	50P-3E-45A-0.5Hz-5Mm			3	99.92	84.49
Case 97	50P-1E-60A-0.5Hz-5Mm		60	1	107.58	97.74
Case 98	50P-2E-60A-0.5Hz-5Mm			2	113.44	99.81
Case 99	50P-3E-60A-0.5Hz-5Mm			3	121.54	105.91
Case 100	75P-1E-30A-0.5Hz-5Mm	75X75	30	1	105.66	84.55
Case 101	75P-2E-30A-0.5Hz-5Mm			2	121.52	105.55
Case 102	75P-3E-30A-0.5Hz-5Mm			3	132.16	120.71
Case 103	75P-1E-45A-0.5Hz-5Mm		45	1	113.66	76
Case 104	75P-2E-45A-0.5Hz-5Mm			2	126.85	109.88
Case 105	75P-3E-45A-0.5Hz-5Mm			3	143.89	123.1
Case 106	75P-1E-60A-0.5Hz-5Mm		60	1	118.15	98.84
Case 107	75P-2E-60A-0.5Hz-5Mm			2	136.72	118.74
Case 108	75P-3E-60A-0.5Hz-5Mm			3	149.98	128.29

Note 1: Pullout load of cycle-1 has been considered as ultimate pullout capacity of the anchor as per consideration of Biradar et al.,2019

Note 2: Absolute value of displacements has only been considered (Yu et al. 2015).

Based on the results obtained from the numerical analysis for the above 108 cases shown in the Table 6.12 to 6.15, bar charts have been developed and they have been presented in Fig 6.13 to Fig 6.24.

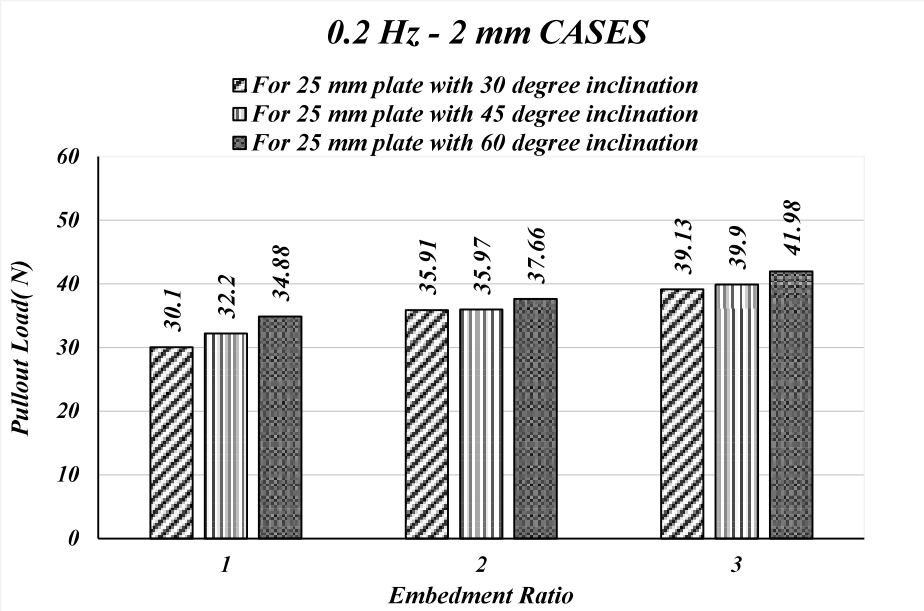

Fig. 6.13: Variation of pull-out loads for 0.2 Hz frequency and 2 mm amplitude cases for 25 mm square plate

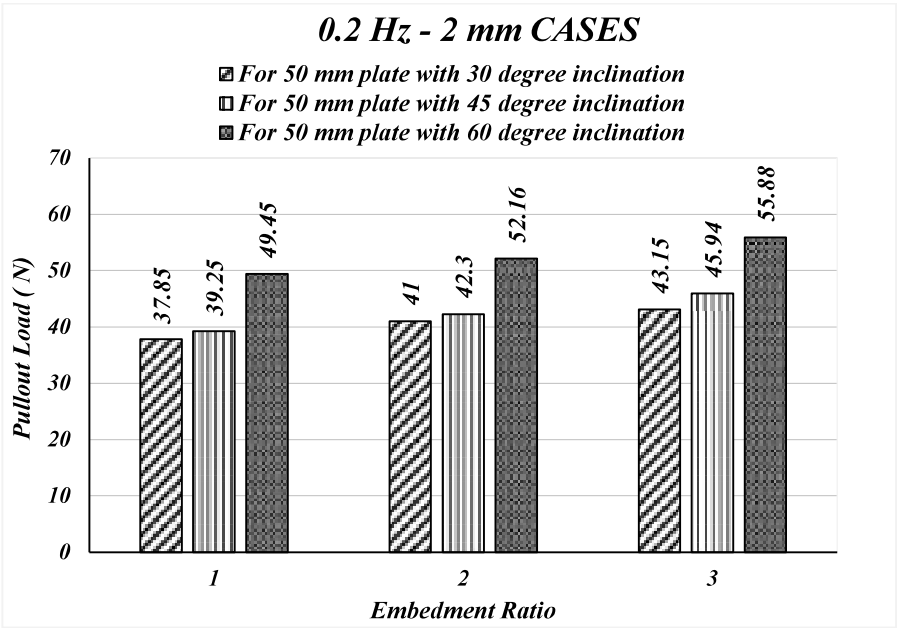

Fig. 6.14: Variation of pull-out loads for 0.2 Hz frequency and 2 mm amplitude cases for 50 mm square plate

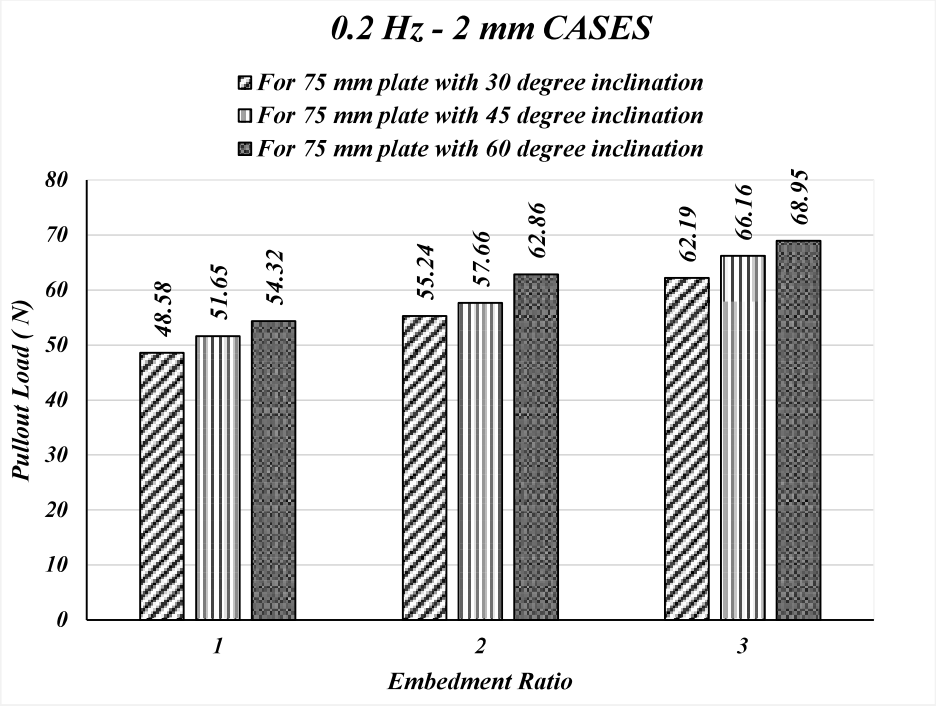

Fig. 6.15: Variation of pull-out loads for 0.2 Hz frequency and 2 mm amplitude cases for 75 mm square Plate

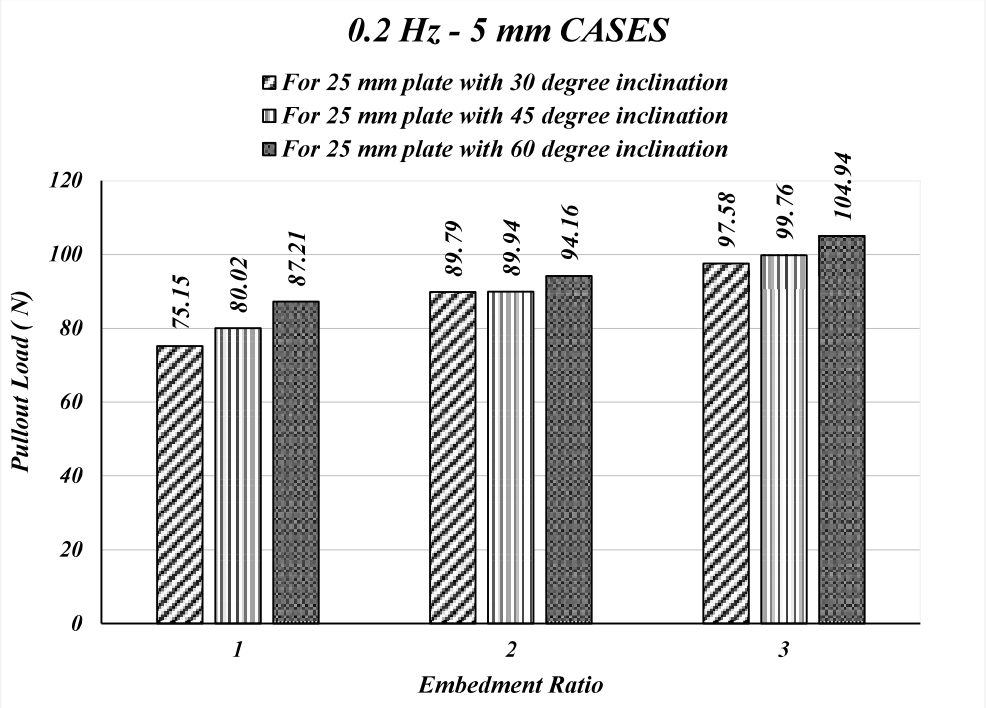

Fig. 6.16: Variation of pull-out loads for 0.2 Hz frequency and 5 mm amplitude cases for 25 mm square Plate

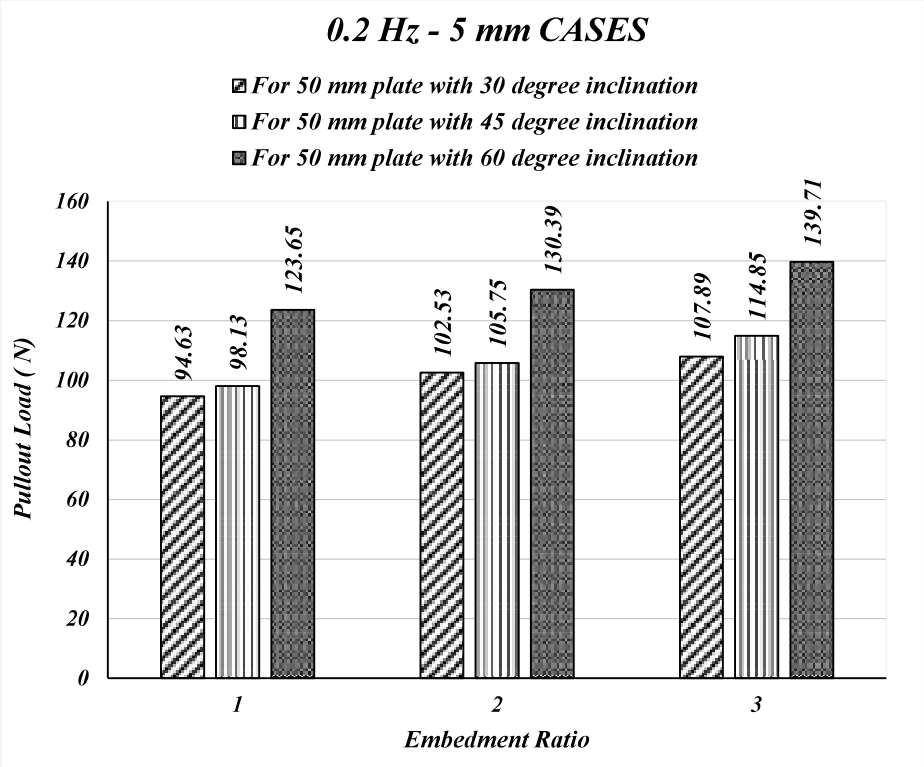

Fig. 6.17: Variation of pull-out loads for 0.2 Hz frequency and 5 mm amplitude cases for 50 mm square plate

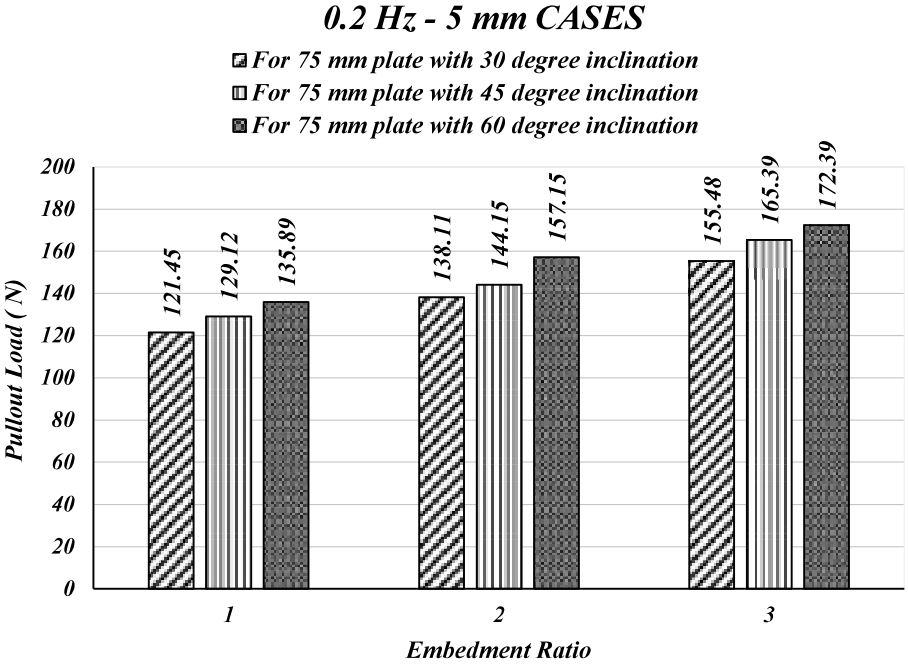

Fig. 6.18: Variation of pull-out loads for 0.2 Hz frequency and 5 mm amplitude cases for 75 mm square Plate

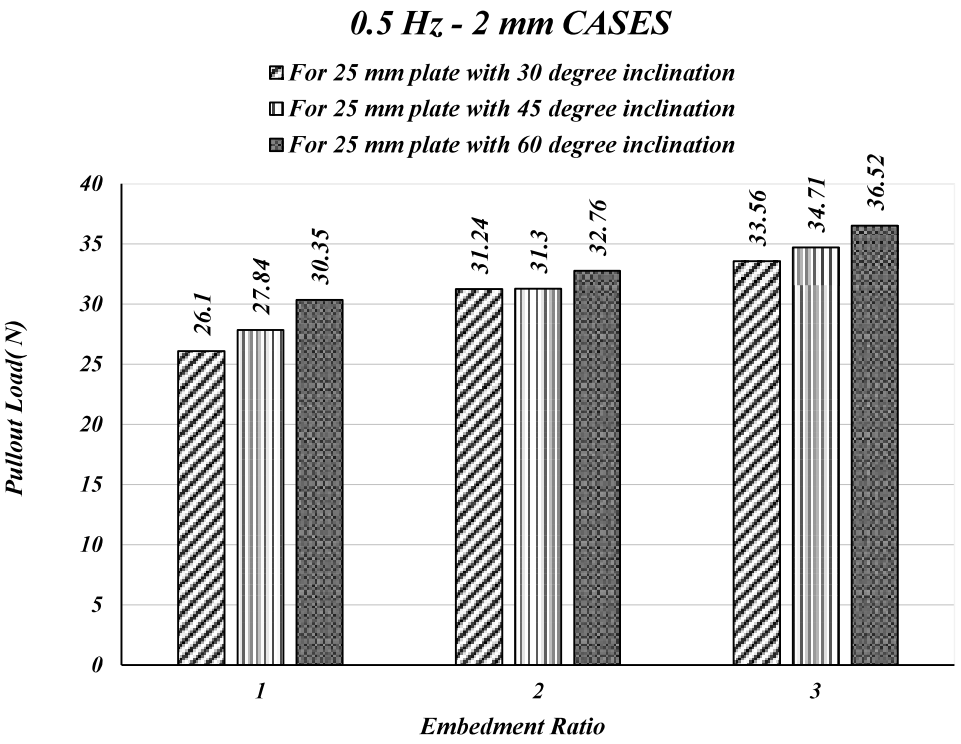

Fig. 6.19: Variation of pull-out loads for 0.5 Hz frequency and 2 mm amplitude cases for 25 mm

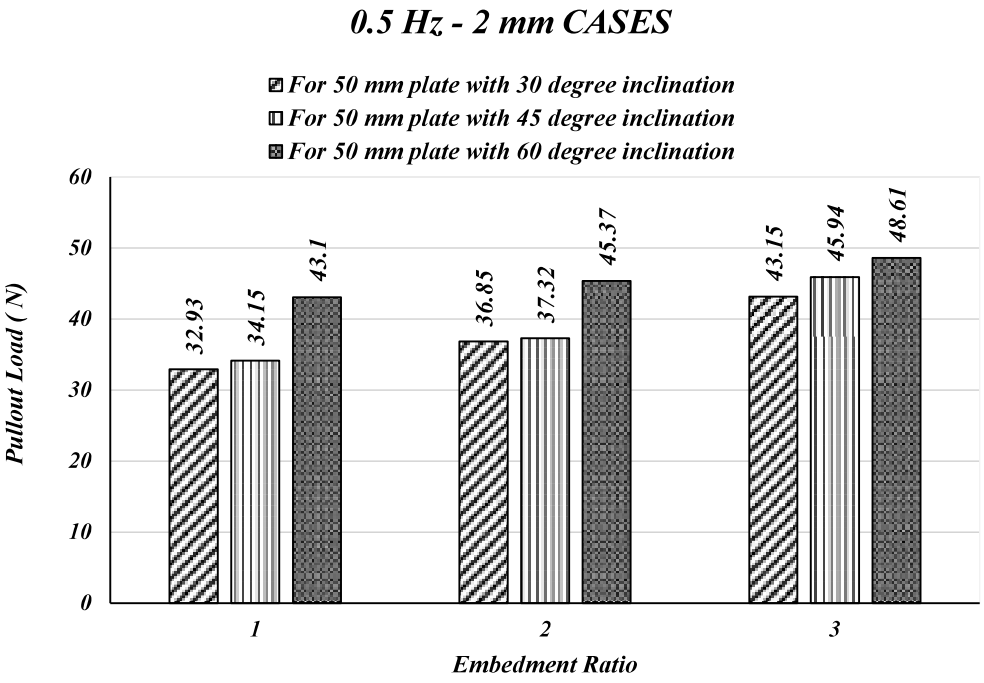

Fig. 6.20: Variation of pull-out loads for 0.5 Hz frequency and 2 mm amplitude cases for 50 mmsquare Plate

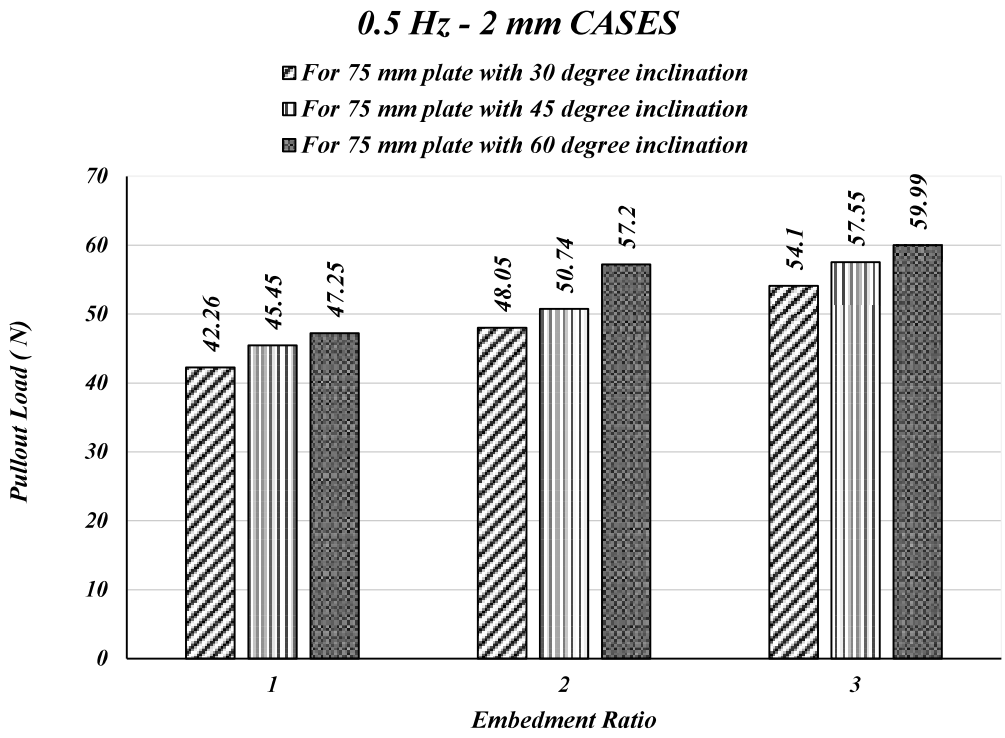

Fig. 6.21: Variation of pull-out loads for 0.5 Hz frequency and 2 mm amplitude cases for 75 mm square plate

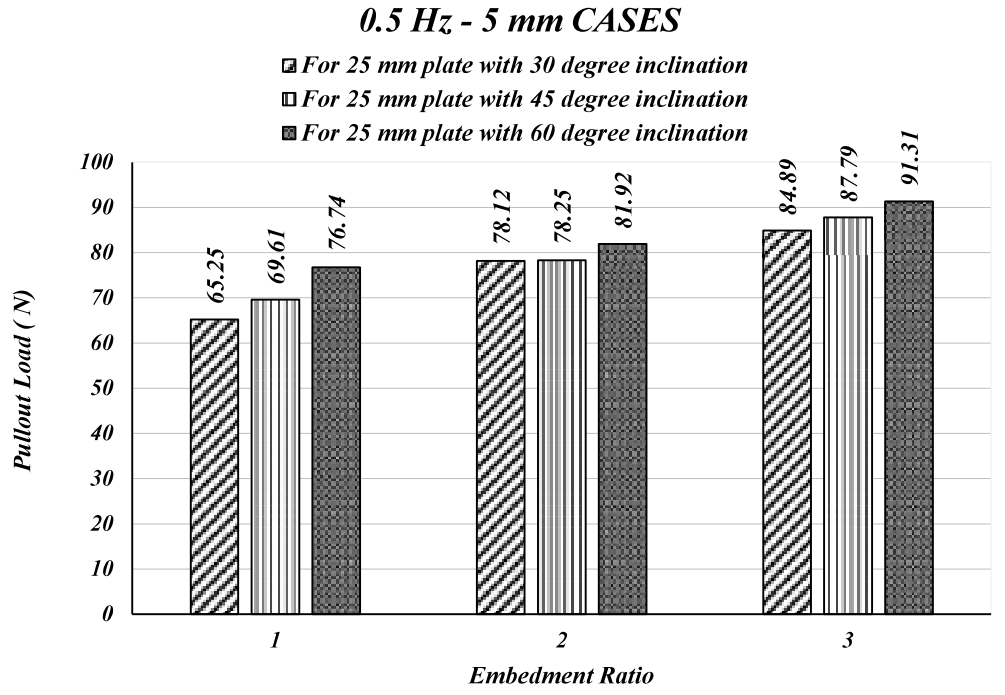

Fig. 6.22: Variation of pull-out loads for 0.5 Hz frequency and 5 mm amplitude cases for 25 mm square plate

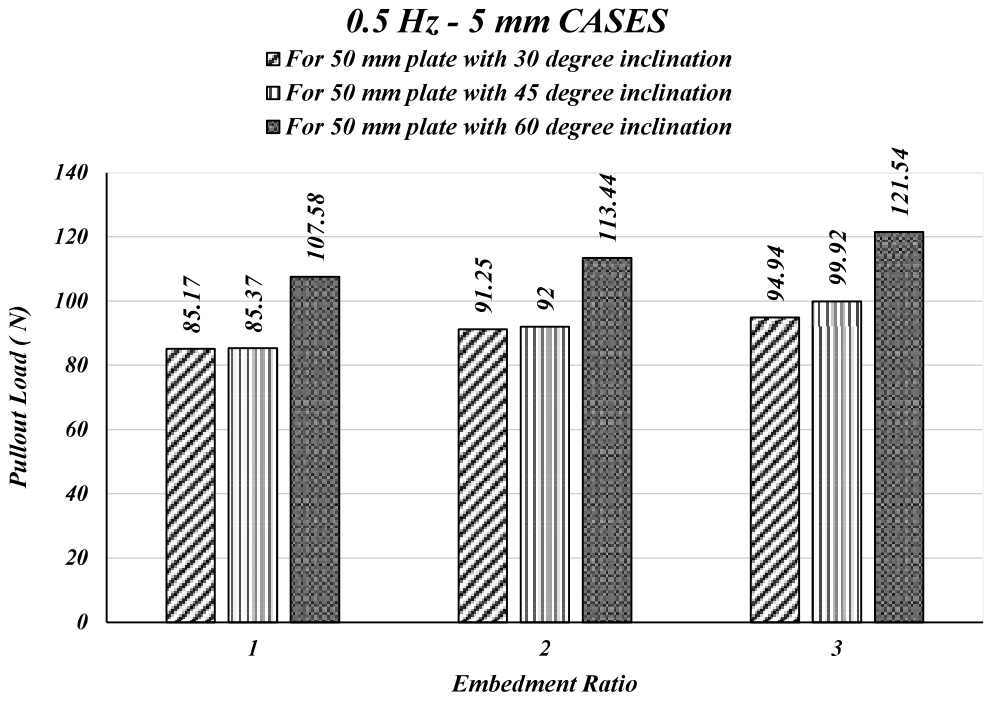

Fig. 6.23: Variation of pull-out loads for 0.5 Hz frequency and 5 mm amplitude cases for 50 mm square Plate

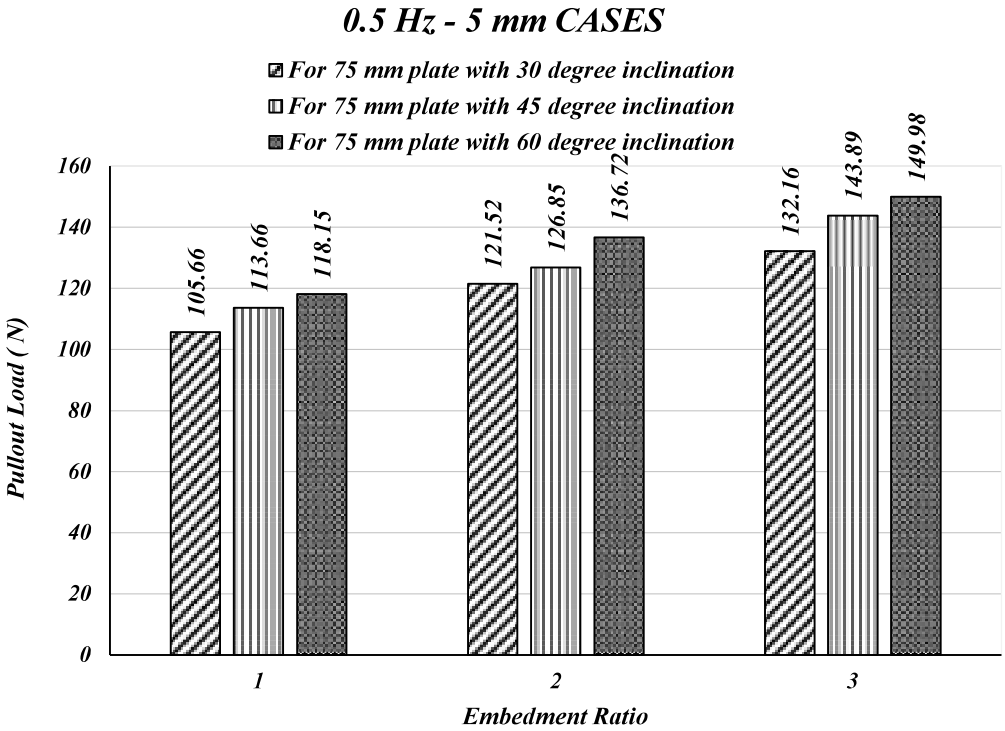

Fig. 6.24: Variation of pull-out loads for 0.5 Hz frequency and 5 mm amplitude cases for 75 mm square plate

From the above presented bar charts (Fig. 6.13 to Fig.6.24), the effect of different parameters on the increase or decrease of pull-out loads can be easily assessed, which are being elaborated and discussed in the following sections.

6.4.1 Effect of Embedment Ratio:

Table 6.16 shows load increment due to change of embedment ratio and Fig 6.25 represents typical variation of pull-out loads with respect to variation of embedment ratio for 25mm square Plate with 30° inclination under 0.2 Hz frequency and 2 mm amplitude.

Table 6.16: Load Increase in percentage for change in embedment ratio

Plate size (mm)	Inclination Angle	Embedment ratio	Pull Out Load Increase (in percentage)			
			Frequency And Amplitude			
			0.2 Hz - 2 mm	0.2 Hz - 5 mm	0.5 Hz - 2 mm	0.5 Hz - 5 mm
25X25	30°	1 to 2	19.30	19.48	19.69	19.72
		2 to 3	8.97	8.68	7.43	8.67
		1 to 3	30.00	29.85	28.58	30.10
	45°	1 to 2	11.71	12.40	12.43	12.41
		2 to 3	10.93	10.92	10.89	12.19
		1 to 3	23.91	24.67	24.68	26.12
	60°	1 to 2	7.97	7.97	7.94	6.75
		2 to 3	11.47	11.45	11.48	11.46
		1 to 3	20.36	20.33	20.33	18.99
50X50	30°	1 to 2	8.32	8.35	11.90	7.14
		2 to 3	5.24	5.23	17.10	4.04
		1 to 3	14.00	14.01	31.04	11.47
	45°	1 to 2	7.77	7.77	9.28	7.77
		2 to 3	8.61	8.61	23.10	8.61
		1 to 3	17.04	17.04	34.52	17.04
	60°	1 to 2	5.46	5.45	5.27	5.45
		2 to 3	7.13	7.15	7.14	7.14
		1 to 3	12.98	12.99	12.78	12.98
75X75	30°	1 to 2	13.71	13.72	13.70	15.01
		2 to 3	12.58	12.58	12.59	8.76
		1 to 3	28.02	28.02	28.02	25.08
	45°	1 to 2	11.64	11.64	11.64	11.60
		2 to 3	14.74	14.73	13.42	13.43
		1 to 3	28.09	28.09	26.62	26.60
	60°	1 to 2	15.72	15.65	21.06	15.72
		2 to 3	9.69	9.70	4.88	9.70
		1 to 3	26.93	26.86	26.96	26.94

From Table 6.16 and Fig 6.13 to 6.24, it has been observed that increase in embedment ratio the pull-out capacity increases when plate size and the inclination angle are fixed. For 25mm plate inclined at 45° under 0.5 Hz frequency 2mm amplitude cyclic load, shows the maximum increase in pull out capacity 34.52% when embedment ratio increases from 1 to 3 (refer Fig.6.25). This occurs due to the fact that with increase plate size the resisting force (due to presence of soil mass over the plate i.e., due to increase in soil volume) against the pull-out load increases leading to higher pull-out capacity.

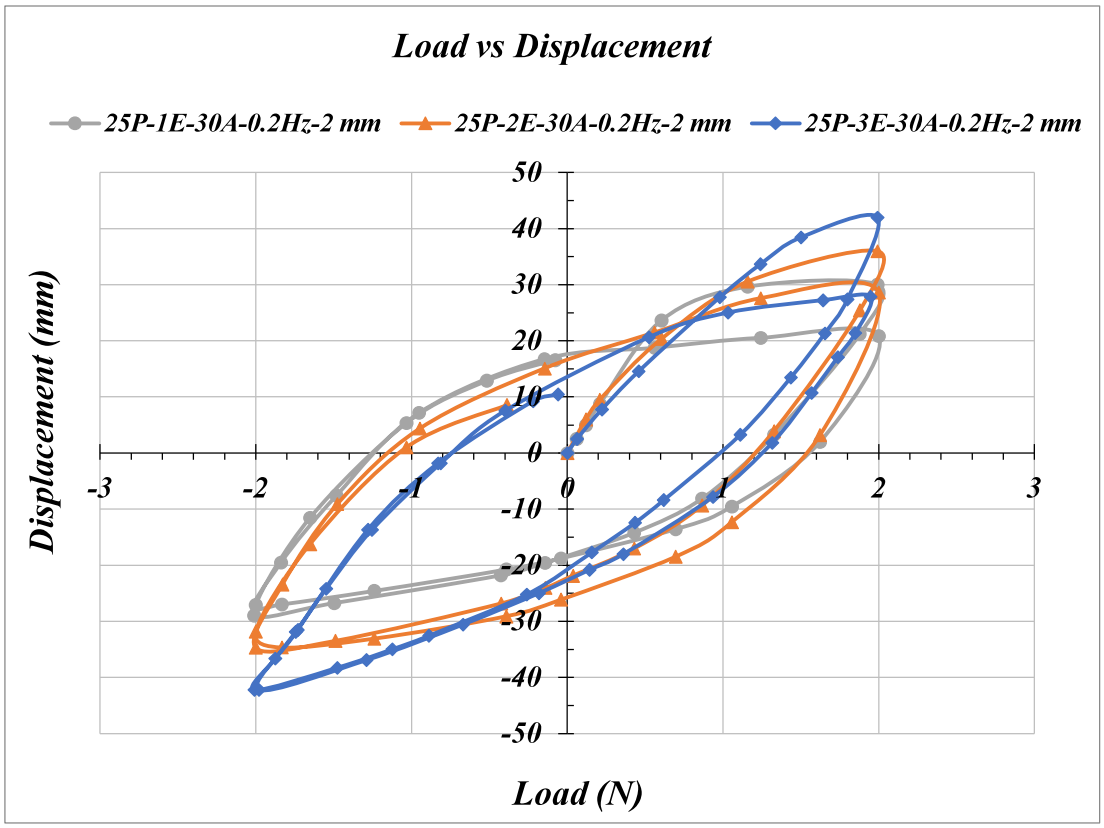

Fig. 6.25: Typical variation of pull-out loads with respect to variation of embedment ratio for 25mm square Plate with 30-degree inclination under 0.2 Hz frequency and 2 mm amplitude

6.4.2 Effect of Plate Size:

Three square horizontal anchor plates of size 25 mm, 50 mm and 75 mm considered in the analysis. Table 6.17 shows load increment due to change of plate size and Fig 6.26 represents typical variation of pull-out loads with respect to variation of plate sizes for embedment ratio 2 with 30-degree inclination under 0.5 Hz frequency and 2 mm amplitude.

Table 6.17: Load Increase in percentage for change in Plate Size

Embedment Ratio	Inclination Angle	Plate size (mm)	Pull Out Load Increase (in percentage)			
			Frequency And Amplitude			
			0.2 Hz	0.2 Hz	0.5 Hz	0.5 Hz
			- 2 mm	- 5 mm	- 2 mm	- 5 mm
1	30	25 to 50	25.75	25.92	26.17	30.53
		50 to 75	28.35	28.34	28.33	24.06
		25 to 75	61.40	61.61	61.92	61.93
	45	25 to 50	21.89	22.63	22.67	22.64
		50 to 75	31.59	31.58	33.09	33.14
		25 to 75	53.83	53.81	53.81	55.56
	60	25 to 50	41.80	41.78	42.01	40.19
		50 to 75	9.83	9.90	9.63	9.83
		25 to 75	58.93	59.34	61.20	55.68
2	30	25 to 50	14.17	14.19	17.96	16.81
		50 to 75	34.73	34.70	30.39	33.17
		25 to 75	60.40	61.36	63.25	63.28
	45	25 to 50	17.60	17.58	19.23	17.57
		50 to 75	36.31	36.31	35.96	37.88
		25 to 75	60.30	60.27	62.11	62.11
	60	25 to 50	38.50	38.48	38.49	38.48
		50 to 75	20.51	20.52	26.07	20.52
		25 to 75	65.81	65.79	65.80	63.90
3	30	25 to 50	10.27	10.57	28.58	11.84
		50 to 75	44.13	44.11	25.38	39.20
		25 to 75	55.73	55.82	55.68	53.96
	45	25 to 50	15.14	15.13	32.35	13.82
		50 to 75	44.01	44.01	25.27	44.01
		25 to 75	66.91	66.90	74.60	66.89
	60	25 to 50	33.11	33.13	33.11	33.11
		50 to 75	23.39	23.39	23.41	23.40
		25 to 75	64.24	64.27	64.27	64.25

It is observed from Table 6.17, as the plate size increases the pull-out capacity also increases. The patterns are same for different inclined angles of anchor plate. It has been noted that from current investigations that for same depth of embedment, pull-out capacity increases with increase in plate size. Thus, for a specific embedment depth, with increase in plate size pull-out capacity is observed to increase. This occurs due to the fact that with increase in plate size the volume of soil resisting axial movement of anchor also increases. This phenomenon is the reason behind such higher pull-out capacity. For embedment ratio 3, with inclination angle 45° under 0.5 Hz frequency 2 mm amplitude cyclic load, shows the maximum increase in pull capacity of 74.6% when plate size increases 25mm to 75mm (refer Fig. 6.26)

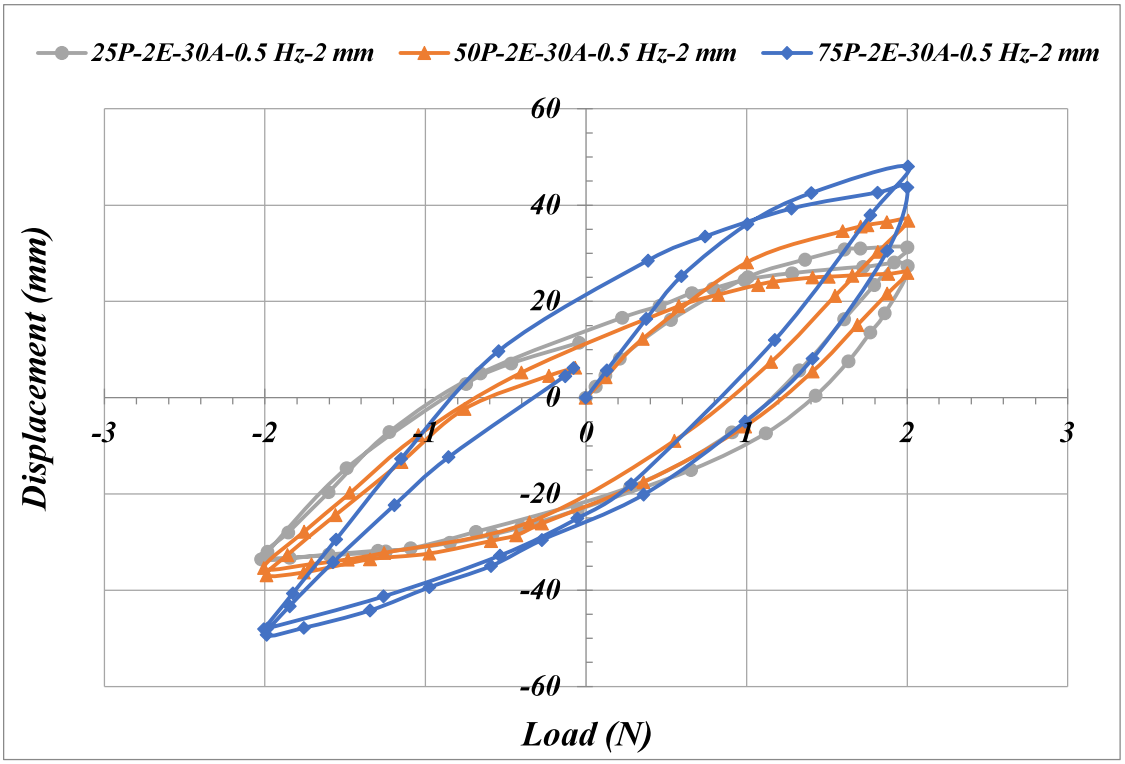

Fig. 6.26: Typical variation of pull-out loads with respect to variation of plate sizes for embedment ratio 2 with 30-degree inclination under 0.5 Hz frequency and 2 mm amplitude

6.4.3 Effect of Inclination angle:

Table 6.18 shows load increment due to change in inclination angle and Fig. 6.27 represents typical variation of pull-out loads with respect to variation of inclination angle for 50 mm plate with embedment ratio 1 under 0.2 Hz frequency and 2 mm amplitude.

Table 6.18: Load Increase in percentage for change in Inclination Angle

Plate size	Inclination Angle	Embedment Ratio	Pull Out Load Increase (in percentage)			
			Frequency And Amplitude			
			0.2 Hz	0.2 Hz	0.5 Hz	0.5 Hz
			- 2 mm	- 5 mm	- 2 mm	- 5 mm
25X25	30 to 45	1	6.98	6.48	6.67	6.68
		2	0.17	0.17	0.19	0.17
		3	1.97	2.23	3.43	3.42
	45 to 60	1	8.32	8.99	9.02	10.24
		2	4.70	4.69	4.66	4.69
		3	5.21	5.19	5.21	4.01
	30 to 60	1	15.88	16.05	16.28	17.61
		2	4.87	4.87	4.87	4.86
		3	7.28	7.54	8.82	7.56
50X50	30 to 45	1	3.70	3.70	3.70	0.23
		2	3.17	3.14	1.28	0.82
		3	6.47	6.45	6.47	5.25
	45 to 60	1	26.01	26.01	26.21	26.02
		2	23.31	23.30	21.57	23.30
		3	21.64	21.65	5.81	21.64
	30 to 60	1	30.67	30.67	30.88	26.31
		2	27.22	27.17	23.12	24.32
		3	29.50	29.49	12.65	28.02
75X75	30 to 45	1	6.32	6.32	7.55	7.57
		2	4.38	4.37	5.60	4.39
		3	6.38	6.37	6.38	8.88
	45 to 60	1	5.17	5.24	3.96	3.95
		2	9.02	9.02	12.73	7.78
		3	4.22	4.23	4.24	4.23
	30 to 60	1	11.82	11.89	11.81	11.82
		2	13.79	13.79	19.04	12.51
		3	10.87	10.88	10.89	13.48

From Table 6.18, it is being noted that with the increase in inclined angles (with respect to vertical level), the pullout capacity increases. For 50 mm plate at embedment ratio 1 shows

increase in pull out capacity of 30.88% when inclination angle (with respect to vertical level) changes from 30 to 60° under 0.5Hz frequency and 2 mm amplitude cyclic load (refer Fig.6.27). This occurs due to the fact that with increase in inclined angles with respect to vertical, the vertical component of the load decreases leading to higher pull-out capacity. In this regard, it is apt to mention that same trends of results as have been observed for all the cases.

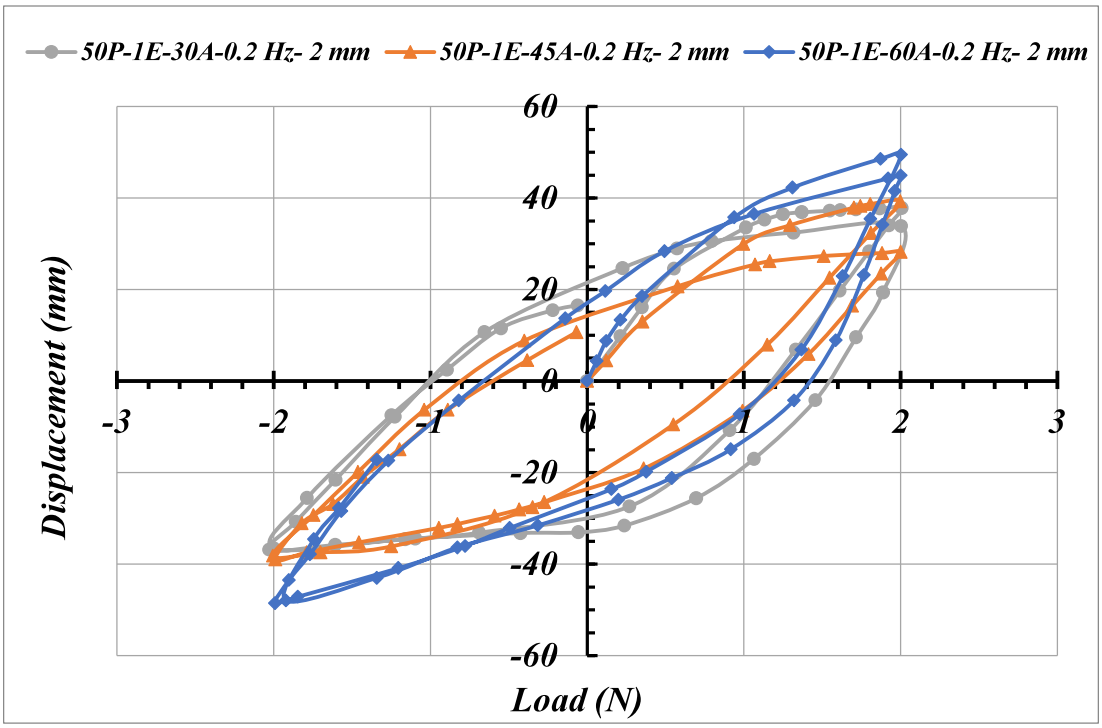

Fig. 6.27: Typical variation of pull-out loads with respect to variation of inclination angle for 50 mm plate with embedment ratio 1 under 0.2 Hz frequency and 2 mm amplitude

6.4.4 Effect of Cyclic loading with change in amplitude and frequency:

Following Table 6.19 shows the load vs. displacement behaviour of all the anchor plates with all the embedment ratios. Fig. 6.28 and Fig 6.29 represent typical variation of pull-out loads with respect to variation of frequency for 25 mm plate with embedment ratio 1 and inclination angle 30° when amplitude is 2 mm and 5 mm respectively.

Table 6.19: Comparison for change in frequency and amplitude

Plate Size	Inclination Angle	Embedment Ratio	Pull Out Load Increase (in percentage)			
			Change in frequency (from 0.5 Hz to 0.2 Hz)		Change in Amplitude(from 2 mm to 5 mm)	
			Magnitude of Amplitude		Magnitude of Frequency	
			2 mm	5 mm	0.2 Hz	0.5 Hz
25X25	30	1	15.3257	15.1724	149.6678	150.0000
		2	14.9488	14.9386	150.0418	150.0640
		3	16.5971	14.9488	149.3739	152.9499
	45	1	15.6609	14.9547	148.5093	150.0359
		2	14.9201	14.9393	150.0417	150.0000
		3	14.9525	13.6348	150.0251	152.9242
	60	1	14.9259	13.6435	150.0287	152.8501
		2	14.9573	14.9414	150.0266	150.0611
		3	14.9507	14.9272	149.9762	150.0274
50X50	30	1	14.9408	11.1072	150.0132	158.6395
		2	11.2619	12.3616	150.0732	147.6255
		3	4.5900	13.6402	150.0348	120.0232
	45	1	14.9341	14.9467	150.0127	149.9854
		2	13.3441	14.9457	150.0000	146.5166
		3	5.4900	14.9420	150.0000	117.5011
	60	1	14.7564	14.9377	150.0000	149.6056
		2	14.9658	14.9418	149.9808	150.0331
		3	14.9558	14.9498	150.0179	150.0309
75X75	30	1	14.9550	14.9442	150.0000	150.0237
		2	14.9636	13.6521	150.0181	152.9032
		3	14.9538	17.6453	150.0080	144.2884
	45	1	13.6414	13.6020	149.9903	150.0770
		2	13.6382	13.6382	150.0000	150.0000
		3	14.9609	14.9420	149.9849	150.0261
	60	1	14.9630	15.0148	150.1657	150.0529
		2	9.8951	14.9429	150.0000	139.0210
		3	14.9358	14.9420	150.0218	150.0083

The increase in the pull-out load is generally less in higher amplitude when frequency changes from 0.5 Hz to 0.2 Hz. For 25mm square plate, with 30° inclination and embedment ratio 3, when cyclic load frequency decreases from 0.5 Hz to 0.2 Hz at 2mm amplitude, pull out load increases 16.59% (refer Fig.6.28). On the other hand, it can be observed that the increase in the pull-out load is generally more in higher frequency when amplitude changes from 2 to 5mm. For 25mm square plate, with 30°s inclination and embedment ratio 3, when cyclic load

amplitude increases from 2mm to 5mm at 0.5 Hz frequency, pull out load increases 152.924% (refer Fig.6.29).

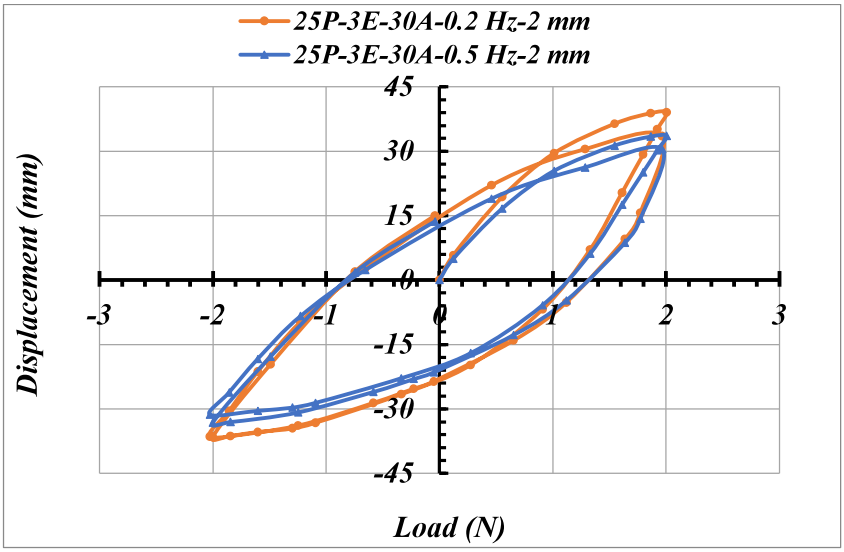

Fig. 6.28: Typical variation of pull-out loads with respect to variation of frequency when amplitude is 2mm for 25 mm plate with embedment ratio 3 and inclination angle 30°

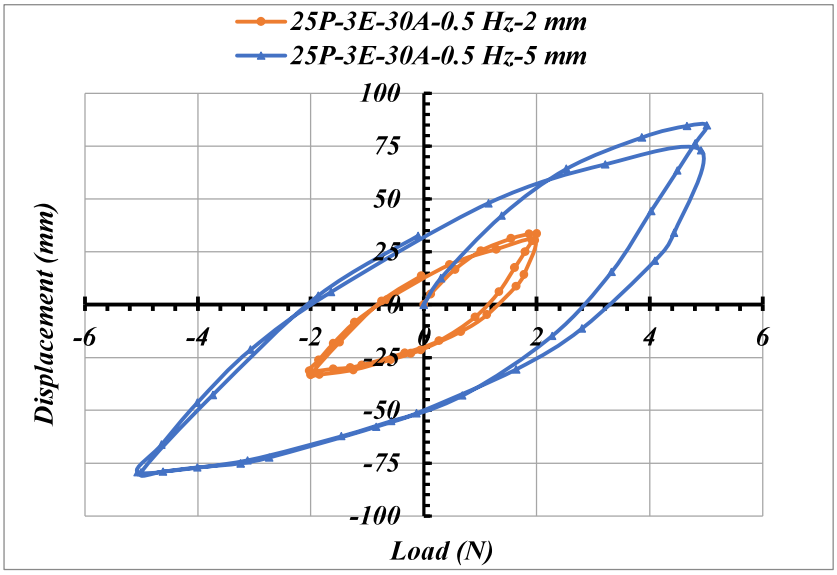

Fig. 6.29: Typical variation of pull-out loads with respect to variation of amplitude when frequency is 0.5Hz for 25 mm plate with embedment ratio 3 and inclination angle 30°

6.4.5 Break Out Factor in Unreinforced Clay:

Biradar et al. (2019) has been normalized the maximum load using breakout factor as,

$$N_c = (F/AC_u) \quad \text{..... (6.2)}$$

where F is the maximum load (pullout load), A is the cross-section area of the square anchor plate and Cu is the undrained cohesion of the clay. The same consideration has been

followed here in the current study. Fig 6.30 to Fig 6.33 and Table 6.20 and 6.21 show the variation of the breakout factors with the embedment ratio as considered here.

Table 6.20: Change in Breakout Factor when frequency is 0.2 Hz Value of Cu (used to calculate the N_C for all the cases in this table) = 22000 N/ m^2

Plate size(in m) and related Area (in m^2)	Inclination Angle	Embedment Ratio	Frequency And Amplitude			
			0.2 Hz - 2 mm	0.2 Hz - 5 mm	0.2 Hz - 2 mm	0.2 Hz - 5 mm
			Corresponding Load for the Breakoutfactor		Value in Breakout Factor N_C = (F/ACu)	
			Load (N)	Load (N)	(F/ACu)	(F/AC_u)
25 mm square plate with area of 0.000625 m^2	30	1	30.1	75.15	2.1891	5.4655
		2	35.91	89.79	2.6116	6.5302
		3	39.13	97.58	2.8458	7.0967
	45	1	32.2	80.02	2.3418	5.8196
		2	35.97	89.94	2.6160	6.5411
		3	39.9	99.76	2.9018	7.2553
	60	1	34.88	87.21	2.5367	6.3425
		2	37.66	94.16	2.7389	6.8480
		3	41.98	104.94	3.0531	7.6320
50 mm square plate with area of 0.0025 m^2	30	1	37.85	94.63	0.6882	1.7205
		2	41	102.53	0.7455	1.8642
		3	43.15	107.89	0.7845	1.9616
	45	1	39.25	98.13	0.7136	1.7842
		2	42.3	105.75	0.7691	1.9227
		3	45.94	114.85	0.8353	2.0882
	60	1	49.46	123.65	0.8993	2.2482
		2	52.16	130.39	0.9484	2.3707
		3	55.88	139.71	1.0160	2.5402
75 mm square plate with areaof 0.005625 m^2	30	1	48.58	121.45	0.3926	0.9814
		2	55.24	138.11	0.4464	1.1160
		3	62.19	155.48	0.5025	1.2564
	45	1	51.65	129.12	0.4174	1.0434
		2	57.66	144.15	0.4659	1.1648
		3	66.16	165.39	0.5346	1.3365
	60	1	54.32	135.89	0.4389	1.0981
		2	62.86	157.15	0.5080	1.2699
		3	68.95	172.39	0.5572	1.3931

Table 6.21: Change in Breakout Factor when frequency is 0.5 Hz Value of C_u (used to calculate the N_c for all the cases in this table) = 22000 N/ m^2

Plate size (in m) and related Area (in m^2)	Inclination Angle	Embedment Ratio	Frequency And Amplitude			
			0.5 Hz - 2 mm	0.5 Hz - 5 mm	0.5 Hz - 2 mm	0.5 Hz - 5 mm
			Corresponding Load for the Breakout factor		Value in Breakout Factor $N_c = (F/AC_u)$	
			Load (N)	Load (N)	(F/ACu)	(F/AC_u)
25 mm square plate with area of 0.000625 m2	30	1	26.1	65.25	1.8982	4.7455
		2	31.24	78.12	2.272	5.6815
		3	33.56	84.89	2.4407	6.1738
	45	1	27.84	69.61	2.0247	5.0625
		2	31.3	78.25	2.2764	5.6909
		3	34.71	87.79	2.5244	6.3847
	60	1	30.35	76.74	2.2073	5.5811
		2	32.76	81.92	2.3825	5.9578
		3	36.52	91.31	2.656	6.6407
50 mm square plate with area of 0.0025 m2	30	1	32.93	85.17	0.5987	1.5485
		2	36.85	91.25	0.67	1.6591
		3	43.15	94.94	0.7845	1.7262
	45	1	34.15	85.37	0.6209	1.5522
		2	37.32	92	0.6785	1.6727
		3	45.94	99.92	0.8353	1.8167
	60	1	43.1	107.58	0.7836	1.956
		2	45.37	113.44	0.8249	2.0625
		3	48.61	121.54	0.8838	2.2098
75 mm square plate with area of 0.005625 m2	30	1	42.26	105.66	0.3415	0.8538
		2	48.05	121.52	0.3883	0.982
		3	54.1	132.16	0.4372	1.068
	45	1	45.45	113.66	0.3673	0.9185
		2	50.74	126.85	0.41	1.0251
		3	57.55	143.89	0.4651	1.1627
	60	1	47.25	118.15	0.3818	0.9547
		2	57.2	136.72	0.4622	1.1048
		3	59.99	149.98	0.4848	1.212

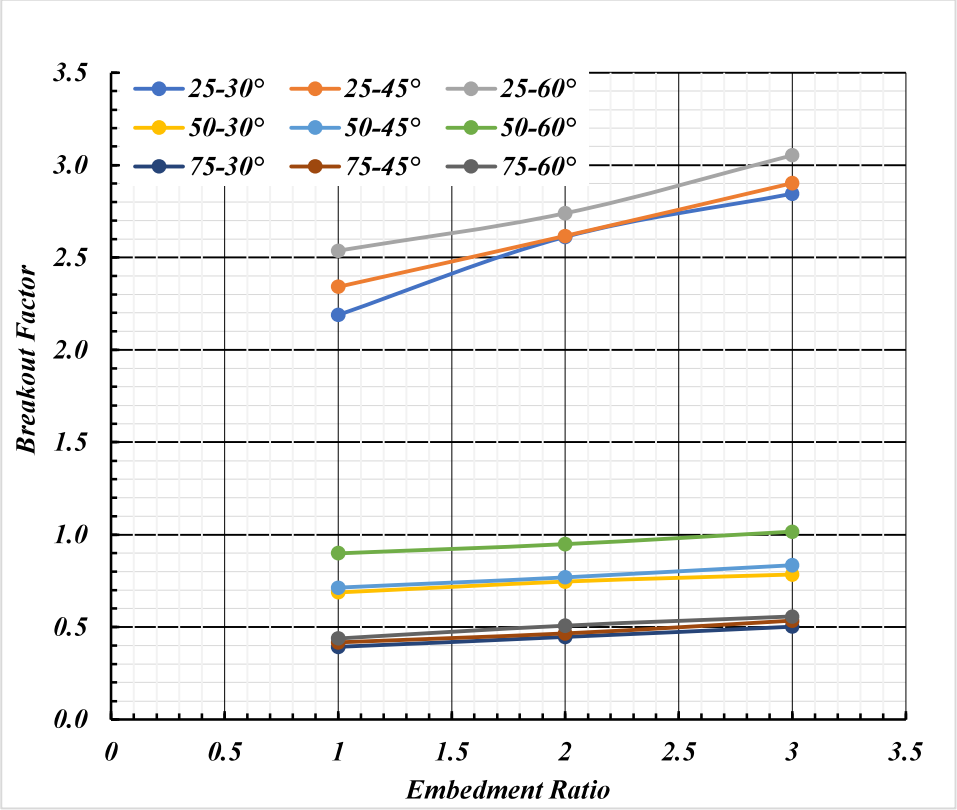

Fig. 6.30: Breakout Factor vs Embedment Ratio for 0.2Hz frequency and 2mm amplitude

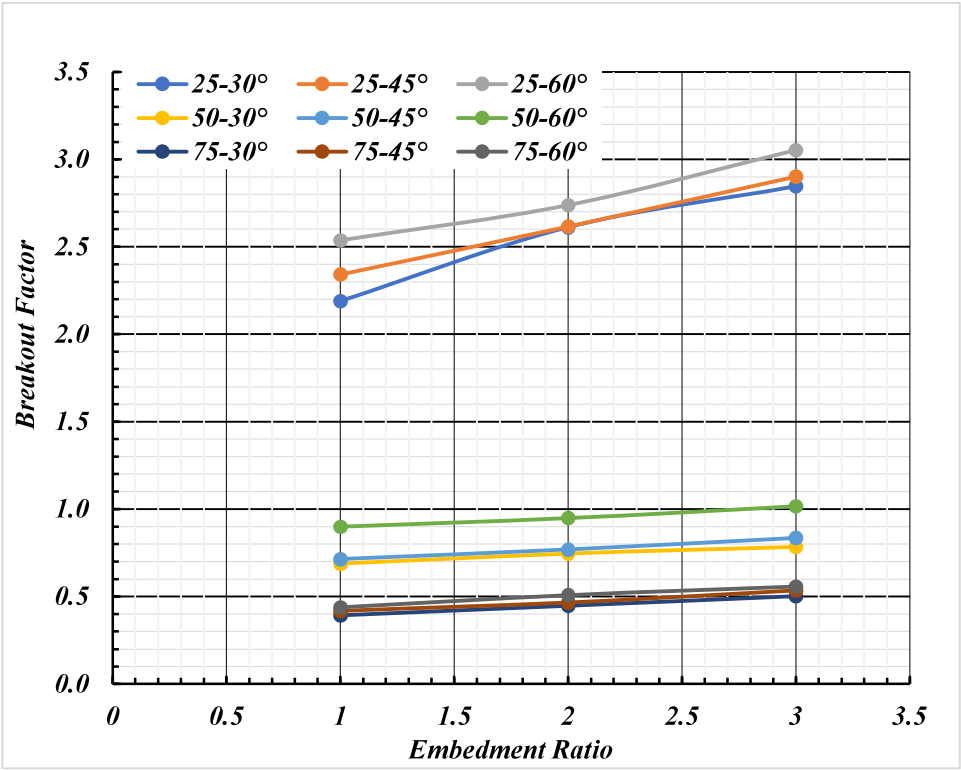

Fig. 6.31: Breakout Factor vs Embedment Ratio for 0.2Hz frequency and 5mm amplitude

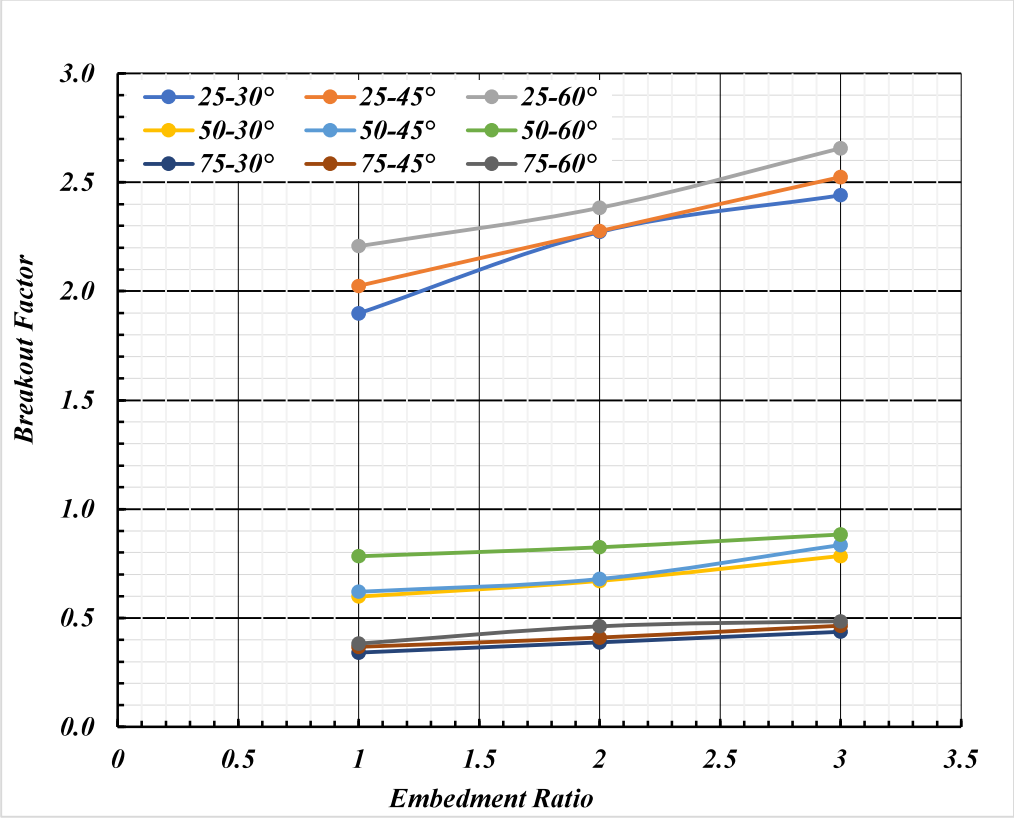

Fig. 6.32: Breakout Factor vs Embedment Ratio for 0.5 Hz frequency and 2 mm amplitude

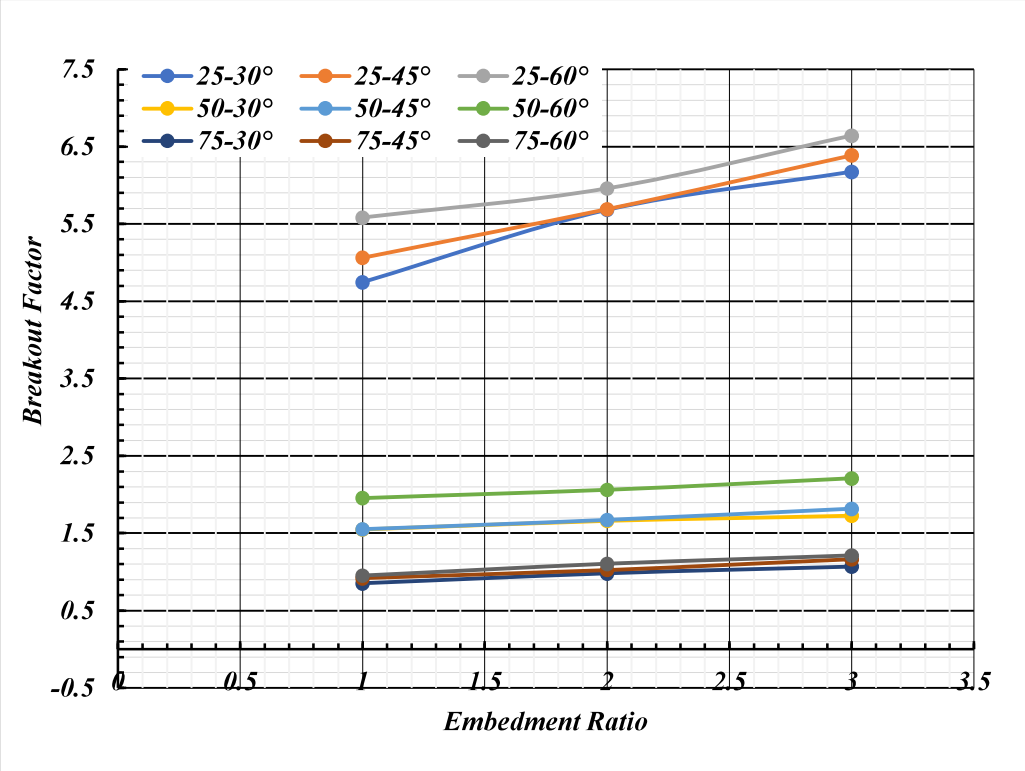

Fig. 6.33: Breakout Factor vs Embedment Ratio for 0.5 Hz frequency and 5 mm amplitude

It is to be noted that the increase in percentage breakout factor for change in embedment ratio is totally same with respect to pull out load increase in percentage for change in embedment ratio, as breakout factor is non-dimensional form of the pull-out load. The same observation is also true for increase in percentage in the breakout factor for change in Inclination Angle. From the Fig. 6.26 to Fig. 6.29 and from the Table 6.20 and 6.21, the following points have been observed for inclined anchor in soft clay soil:

1.Breakout Factor has been found to increase with the increase in embedment ratio for anyparticular plate size for any particular inclination.

2.Increment in inclination angle also increases the break out factor.

6.5 INCLINED ANCHORS IN REINFORCED SOIL UNDER CYCLIC LOADING:

Here, an attempt has been made to interpret the results obtained from the numerical modelling (done by the ABAQUS software; Version 6.14). Load-displacement curves generated from the output of the numerical modelling which have been plotted together in the previous Chapter. Here pull-out loads for anchor plates are being presented from Table 6.22 to 6.29.

Table 6.22: Pull Out Load For Anchor for 0.2Hz Frequency and 2mm Amplitude cases

Case No.	Case Code	Plate Size (in mm)	Inclination Angle (in degrees)	Embedment Ratios	Pull Out Load (in N) Corresponding to amplitude	
					Cycle-1	Cycle 2
Case 1	25P-1E-30A-0.2Hz-2Mm	25X25	30	1	32.448	22.540
Case 2	25P-2E-30A-0.2Hz-2Mm			2	39.103	32.061
Case 3	25P-3E-30A-0.2Hz-2Mm			3	42.735	28.370
Case 4	25P-1E-45A-0.2Hz-2Mm		45	1	35.369	28.486
Case 5	25P-2E-45A-0.2Hz-2Mm			2	40.675	37.687
Case 6	25P-3E-45A-0.2Hz-2Mm			3	43.724	40.324
Case 7	25P-1E-60A-0.2Hz-2Mm		60	1	39.176	32.040
Case 8	25P-2E-60A-0.2Hz-2Mm			2	41.904	34.029
Case 9	25P-3E-60A-0.2Hz-2Mm			3	45.131	42.052
Case 10	50P-1E-30A-0.2Hz-2Mm	50X50	30	1	41.939	37.563
Case 11	50P-2E-30A-0.2Hz-2Mm			2	47.092	39.462
Case 12	50P-3E-30A-0.2Hz-2Mm			3	48.285	43.844
Case 13	50P-1E-45A-0.2Hz-2Mm		45	1	44.431	38.924
Case 14	50P-2E-45A-0.2Hz-2Mm			2	48.497	39.883
Case 15	50P-3E-45A-0.2Hz-2Mm			3	52.718	44.579
Case 16	50P-1E-60A-0.2Hz-2Mm		60	1	56.901	50.937
Case 17	50P-2E-60A-0.2Hz-2Mm			2	60.504	53.235
Case 18	50P-3E-60A-0.2Hz-2Mm			3	65.367	56.961
Case 19	75P-1E-30A-0.2Hz-2Mm	75X75	30	1	55.105	44.099
Case 20	75P-2E-30A-0.2Hz-2Mm			2	62.963	54.686
Case 21	75P-3E-30A-0.2Hz-2Mm			3	70.07	65.065
Case 22	75P-1E-45A-0.2Hz-2Mm		45	1	59.858	39.812
Case 23	75P-2E-45A-0.2Hz-2Mm			2	67.279	58.281
Case 24	75P-3E-45A-0.2Hz-2Mm			3	76.268	66.494
Case 25	75P-1E-60A-.2Hz-2Mm		60	1	63.977	53.529
Case 26	75P-2E-60A-0.2Hz-2Mm			2	74.678	64.860
Case 27	75P-3E-60A-0.2Hz-2Mm			3	80.917	70.548

Table 6.23: Pull Out Load For Anchor for 0.2Hz Frequency and 5mm Amplitude cases

Case No.	Case Code	Plate Size (in mm)	Inclination Angle (in degrees)	Embedment Ratios	Pull Out Load (in N) Corresponding to amplitude	
					Cycle-1	Cycle-2
Case 28	25P-1E-30A-0.2Hz-5Mm	25X25	30	1	81.12	56.373
Case 29	25P-2E-30A-0.2Hz-5Mm			2	97.592	81.774
Case 30	25P-3E-30A-0.2Hz-5Mm			3	106.572	95.856
Case 31	25P-1E-45A-0.2Hz-5Mm		45	1	88.424	75.216
Case 32	25P-2E-45A-0.2Hz-5Mm			2	100.072	79.557
Case 33	25P-3E-45A-0.2Hz-5Mm			3	111.754	100.452
Case 34	25P-1E-60A-0.2Hz-5Mm		60	1	97.941	80.132
Case 35	25P-2E-60A-0.2Hz-5Mm			2	106.63	95.911
Case 36	25P-3E-60A-0.2Hz-5Mm			3	119.853	104.566
Case 37	50P-1E-30A-0.2Hz-5Mm	50X50	30	1	104.849	93.908
Case 38	50P-2E-30A-0.2Hz-5Mm			2	114.154	98.287
Case 39	50P-3E-30A-0.2Hz-5Mm			3	120.708	109.606
Case 40	50P-1E-45A-0.2Hz-5Mm		45	1	112.359	80.732
Case 41	50P-2E-45A-0.2Hz-5Mm			2	120.523	80.429
Case 42	50P-3E-45A-0.2Hz-5Mm			3	132.422	111.981
Case 43	50P-1E-60A-0.2Hz-5Mm		60	1	143.058	129.98
Case 44	50P-2E-60A-0.2Hz-5Mm			2	151.514	133.312
Case 45	50P-3E-60A-0.2Hz-5Mm			3	163.6	142.561
Case 46	75P-1E-30A-0.2Hz-5Mm	75X75	30	1	138.611	110.926
Case 47	75P-2E-30A-0.2Hz-5Mm			2	157.749	137.01
Case 48	75P-3E-30A-0.2Hz-5Mm			3	175.345	162.827
Case 49	75P-1E-45A-0.2Hz-5Mm		45	1	150.038	99.789
Case 50	75P-2E-45A-0.2Hz-5Mm			2	173.123	145.703
Case 51	75P-3E-45A-0.2Hz-5Mm			3	191.438	166.905
Case 52	75P-1E-60A-0.2Hz-5Mm		60	1	159.943	133.824
Case 53	75P-2E-60A-0.2Hz-5Mm			2	187.134	162.533
Case 54	75P-3E-60A-0.2Hz-5Mm			3	202.645	176.675

Table 6.24: Pull Out Load For Anchor for 0.5Hz Frequency and 2mm Amplitude cases

Case No.	Case Code	Plate Size (in mm)	Inclination Angle (in degrees)	Embedment Ratios	Pull Out Load (in N) Corresponding to amplitude	
					Cycle-1	Cycle-2
Case 55	25P-1E-30A-0.5Hz-2Mm	25X 25	30	1	30.101	22.112
Case 56	25P-2E-30A-0.5Hz-2Mm			2	33.512	30.522
Case 57	25P-3E-30A-0.5Hz-2Mm			3	39.135	32.971
Case 58	25P-1E-45A-0.5Hz-2Mm		45	1	32.292	25.781
Case 59	25P-2E-45A-0.5Hz-2Mm			2	35.977	30.111
Case 60	25P-3E-45A-0.5Hz-2Mm			3	39.922	36.966
Case 61	25P-1E-60A-0.5Hz-2Mm		60	1	34.882	30.000
Case 62	25P-2E-60A-0.5Hz-2Mm			2	37.662	34.372
Case 63	25P-3E-60A-0.5Hz-2Mm			3	41.742	28.96
Case 64	50P-1E-30A-0.5Hz-2Mm	50X 50	30	1	37.851	36.887
Case 65	50P-2E-30A-0.5Hz-2Mm			2	41.421	28.849
Case 66	50P-3E-30A-0.5Hz-2Mm			3	46.734	42.435
Case 67	50P-1E-45A-0.5Hz-2Mm		45	1	39.252	29.051
Case 68	50P-2E-45A-0.5Hz-2Mm			2	42.313	34.698
Case 69	50P-3E-45A-0.5Hz-2Mm			3	51.138	45.295
Case 70	50P-1E-60A-0.5Hz-2Mm		60	1	49.462	50.919
Case 71	50P-2E-60A-0.5Hz-2Mm			2	52.161	48.444
Case 72	50P-3E-60A-0.5Hz-2Mm			3	55.880	52.111
Case 73	75P-1E-30A-0.5Hz-2Mm	75X 75	30	1	48..307	39.247
Case 74	75P-2E-30A-0.5Hz-2Mm			2	54.777	49.764
Case 75	75P-3E-30A-0.5Hz-2Mm			3	60.976	58.781
Case 76	75P-1E-45A-0.5Hz-2Mm		45	1	51.771	35.831
Case 77	75P-2E-45A-0.5Hz-2Mm			2	64.742	53.621
Case 78	75P-3E-45A-0.5Hz-2Mm			3	66.873	57.852
Case 79	75P-1E-60A-0.5Hz-2Mm		60	1	56.661	48.712
Case 80	75P-2E-60A-0.5Hz-2Mm			2	68.216	59.671
Case 81	75P-3E-60A-0.5Hz-2Mm			3	70.626	64.199

Table 6.25: Pull Out Load For Anchor for 0.5Hz Frequency and 5mm Amplitude cases

Case No.	Case Code	Plate Size (in mm)	Inclination Angle (in degrees)	Embedment Ratios	Pull Out Load (in N) Corresponding to amplitude	
					Cycle-1	Cycle-2
Case 82	25P-1E-30A-0.5Hz-5Mm	25X25	30	1	75.151	51.239
Case 83	25P-2E-30A-0.5Hz-5Mm			2	85.852	76.363
Case 84	25P-3E-30A-0.5Hz-5Mm			3	97.581	83.388
Case 85	25P-1E-45A-0.5Hz-5Mm		45	1	80.024	64.958
Case 86	25P-2E-45A-0.5Hz-5Mm			2	89.990	72.211
Case 87	25P-3E-45A-0.5Hz-5Mm			3	99.760	87.759
Case 88	25P-1E-60A-0.5Hz-5Mm		60	1	87.213	70.505
Case 89	25P-2E-60A-0.5Hz-5Mm			2	94.245	81.289
Case 90	25P-3E-60A-0.5Hz-5Mm			3	104.943	69.231
Case 91	50P-1E-30A-0.5Hz-5Mm	50X50	30	1	94.631	94.373
Case 92	50P-2E-30A-0.5Hz-5Mm			2	102.532	87.475
Case 93	50P-3E-30A-0.5Hz-5Mm			3	107.895	96.456
Case 94	50P-1E-45A-0.5Hz-5Mm		45	1	98.346	69.442
Case 95	50P-2E-45A-0.5Hz-5Mm			2	105.750	69.973
Case 96	50P-3E-45A-0.5Hz-5Mm			3	114.857	96.961
Case 97	50P-1E-60A-0.5Hz-5Mm		60	1	123.654	112.431
Case 98	50P-2E-60A-0.5Hz-5Mm			2	130.912	115.786
Case 99	50P-3E-60A-0.5Hz-5Mm			3	140.135	123.920
Case 100	75P-1E-30A-0.5Hz-5Mm	75X75	30	1	120.970	95.914
Case 101	75P-2E-30A-0.5Hz-5Mm			2	139.02	120.308
Case 102	75P-3E-30A-0.5Hz-5Mm			3	149.525	138.263
Case 103	75P-1E-45A-0.5Hz-5Mm		45	1	132.482	87.536
Case 104	75P-2E-45A-0.5Hz-5Mm			2	155.227	128.218
Case 105	75P-3E-45A-0.5Hz-5Mm			3	169.075	144.625
Case 106	75P-1E-60A-0.5Hz-5Mm		60	1	139.151	116.469
Case 107	75P-2E-60A-0.5Hz-5Mm			2	163.421	141.072
Case 108	75P-3E-60A-0.5Hz-5Mm			3	179.377	154.440

Table 6.26: Comparison of Pullout Loads for Anchor for 0.2Hz Frequency and 2mm Amplitude cases

Case No.	Case Code	Plate Size (in mm)	Inclination Angle (in degrees)	Embedment Ratios	Pull Out Load (in N) Corresponding to amplitude		
					Cycle-1 With Geotextile	Cycle-1 Without Geotextile	% Increase
Case 1	25P-1E-30A-0.2Hz-2Mm	25X25	30	1	32.448	30.1	7.80
Case 2	25P-2E-30A-0.2Hz-2Mm			2	39.103	35.91	8.89
Case 3	25P-3E-30A-0.2Hz-2Mm			3	42.735	39.13	9.21
Case 4	25P-1E-45A-0.2Hz-2Mm		45	1	35.369	32.2	9.84
Case 5	25P-2E-45A-0.2Hz-2Mm			2	40.675	35.97	13.08
Case 6	25P-3E-45A-0.2Hz-2Mm			3	43.724	39.9	9.58
Case 7	25P-1E-60A-0.2Hz-2Mm		60	1	39.176	34.88	12.32
Case 8	25P-2E-60A-0.2Hz-2Mm			2	41.904	37.66	11.27
Case 9	25P-3E-60A-0.2Hz-2Mm			3	45.131	41.98	7.51
Case 10	50P-1E-30A-0.2Hz-2Mm	50X50	30	1	41.939	37.85	10.80
Case 11	50P-2E-30A-0.2Hz-2Mm			2	47.092	41	14.86
Case 12	50P-3E-30A-0.2Hz-2Mm			3	48.285	43.15	11.90
Case 13	50P-1E-45A-0.2Hz-2Mm		45	1	44.431	39.25	13.20
Case 14	50P-2E-45A-0.2Hz-2Mm			2	48.497	42.3	14.65
Case 15	50P-3E-45A-0.2Hz-2Mm			3	52.718	45.94	14.75
Case 16	50P-1E-60A-0.2Hz-2Mm		60	1	56.901	49.46	15.04
Case 17	50P-2E-60A-0.2Hz-2Mm			2	60.504	52.16	16.00
Case 18	50P-3E-60A-0.2Hz-2Mm			3	65.367	55.88	16.98
Case 19	75P-1E-30A-0.2Hz-2Mm	75X75	30	1	55.105	48.58	13.43
Case 20	75P-2E-30A-0.2Hz-2Mm			2	62.963	55.24	13.98
Case 21	75P-3E-30A-0.2Hz-2Mm			3	70.07	62.19	12.67
Case 22	75P-1E-45A-0.2Hz-2Mm		45	1	59.858	51.65	15.89
Case 23	75P-2E-45A-0.2Hz-2Mm			2	67.279	57.66	16.68
Case 24	75P-3E-45A-0.2Hz-2Mm			3	76.268	66.16	15.28
Case 25	75P-1E-60A-0.2Hz-2Mm		60	1	63.977	54.32	17.78
Case 26	75P-2E-60A-0.2Hz-2Mm			2	74.678	62.86	18.80
Case 27	75P-3E-60A-0.2Hz-2Mm			3	80.917	68.95	17.36

Table 6.27: Comparison of Pullout Loads for Anchor for 0.2Hz Frequency and 5 mm Amplitude cases

Case No.	Case Code	Plate Size (in mm)	Angle Inclination (in degrees)	Embedment Ratios	Pull Out Load (in N) Corresponding to amplitude		
					Cycle-1 With Geotextile	Cycle-1 Without Geotextile	% Increase
Case 28	25P-1E-30A-0.2Hz-5Mm	25X25	30	1	81.12	75.15	7.94
Case 29	25P-2E-30A-0.2Hz-5Mm			2	97.592	89.79	8.69
Case 30	25P-3E-30A-0.2Hz-5Mm			3	106.572	97.58	9.22
Case 31	25P-1E-45A-0.2Hz-5Mm		45	1	88.424	80.02	10.50
Case 32	25P-2E-45A-0.2Hz-5Mm			2	100.072	89.94	11.27
Case 33	25P-3E-45A-0.2Hz-5Mm			3	111.754	99.76	12.02
Case 34	25P-1E-60A-0.2Hz-5Mm		60	1	97.941	87.21	12.30
Case 35	25P-2E-60A-0.2Hz-5Mm			2	106.630	94.16	13.24
Case 36	25P-3E-60A-0.2Hz-5Mm			3	119.853	104.94	14.21
Case 37	50P-1E-30A-0.2Hz-5Mm	50X50	30	1	104.849	94.63	11.20
Case 38	50P-2E-30A-0.2Hz-5Mm			2	114.154	102.53	11.34
Case 39	50P-3E-30A-0.2Hz-5Mm			3	120.708	107.89	11.88
Case 40	50P-1E-45A-0.2Hz-5Mm		45	1	112.359	98.13	14.51
Case 41	50P-2E-45A-0.2Hz-5Mm			2	120.523	105.75	13.97
Case 42	50P-3E-45A-0.2Hz-5Mm			3	132.422	114.85	15.3
Case 43	50P-1E-60A-0.2Hz-5Mm		60	1	143.058	123.65	15.7
Case 44	50P-2E-60A-0.2Hz-5Mm			2	151.514	130.39	16.2
Case 45	50P-3E-60A-0.2Hz-5Mm			3	163.600	139.71	17.1
Case 46	75P-1E-30A-0.2Hz-5Mm	75X75	30	1	138.611	121.45	14.13
Case 47	75P-2E-30A-0.2Hz-5Mm			2	157.749	138.11	14.22
Case 48	75P-3E-30A-0.2Hz-5Mm			3	175.345	155.48	12.78
Case 49	75P-1E-45A-0.2Hz-5Mm		45	1	150.038	129.12	16.2
Case 50	75P-2E-45A-0.2Hz-5Mm			2	173.123	144.15	20.10
Case 51	75P-3E-45A-0.2Hz-5Mm			3	191.438	165.39	15.75
Case 52	75P-1E-60A-0.2Hz-5Mm		60	1	159.943	135.89	17.70
Case 53	75P-2E-60A-0.2Hz-5Mm			2	187.134	157.15	19.08
Case 54	75P-3E-60A-0.2Hz-5Mm			3	202.645	172.39	17.55

Table 6.28: Comparison Pullout Loads for Anchor for 0.5Hz Frequency and 2mm Amplitude cases

Case No.	Case Code	Plate Size (in mm)	Inclination Angle (in degrees)	Embedment Ratios	Pull Out Load (in N) Corresponding to amplitude		
					Cycle-1 With Geotextile	Cycle-1 Without Geotextile	% Increase
Case 55	25P-1E-30A-0.5Hz-2Mm	25X25	30	1	30.101	26.1	15.33
Case 56	25P-2E-30A-0.5Hz-2Mm			2	33.512	31.24	7.27
Case 57	25P-3E-30A-0.5Hz-2Mm			3	39.135	33.56	16.61
Case 58	25P-1E-45A-0.5Hz-2Mm		45	1	32.292	27.84	15.99
Case 59	25P-2E-45A-0.5Hz-2Mm			2	35.977	31.3	14.94
Case 60	25P-3E-45A-0.5Hz-2Mm			3	39.922	34.71	15.02
Case 61	25P-1E-60A-0.5Hz-2Mm		60	1	34.882	30.35	14.93
Case 62	25P-2E-60A-0.5Hz-2Mm			2	37.662	32.76	14.96
Case 63	25P-3E-60A-0.5Hz-2Mm			3	41.742	36.52	14.30
Case 64	50P-1E-30A-0.5Hz-2Mm	50X50	30	1	37.851	32.93	14.94
Case 65	50P-2E-30A-0.5Hz-2Mm			2	41.421	36.85	12.40
Case 66	50P-3E-30A-0.5Hz-2Mm			3	46.734	43.15	8.31
Case 67	50P-1E-45A-0.5Hz-2Mm		45	1	39.252	34.15	14.94
Case 68	50P-2E-45A-0.5Hz-2Mm			2	42.313	37.32	13.38
Case 69	50P-3E-45A-0.5Hz-2Mm			3	51.138	45.94	11.31
Case 70	50P-1E-60A-0.5Hz-2Mm		60	1	49.462	43.1	14.76
Case 71	50P-2E-60A-0.5Hz-2Mm			2	52.161	45.37	14.97
Case 72	50P-3E-60A-0.5Hz-2Mm			3	55.880	48.61	14.96
Case 73	75P-1E-30A-0.5Hz-2Mm	75X75	30	1	48..307	42.26	14.31
Case 74	75P-2E-30A-0.5Hz-2Mm			2	54.777	48.05	14.00
Case 75	75P-3E-30A-0.5Hz-2Mm			3	60.976	54.1	12.71
Case 76	75P-1E-45A-0.5Hz-2Mm		45	1	51.771	45.45	13.91
Case 77	75P-2E-45A-0.5Hz-2Mm			2	64.742	50.74	27.60
Case 78	75P-3E-45A-0.5Hz-2Mm			3	66.873	57.55	16.2
Case 79	75P-1E-60A-0.5Hz-2Mm		60	1	56.661	47.25	19.92
Case 80	75P-2E-60A-0.5Hz-2Mm			2	68.216	57.2	19.26
Case 81	75P-3E-60A-0.5Hz-2Mm			3	70.626	59.99	17.73

Table 6.29: Comparison of Pullout Loads for Anchor for 0.5Hz Frequency and 5mm Amplitude cases

Case No.	Case Code	Plate Size (in mm)	Inclination Angle (in degrees)	Embedment Ratios	Pull Out Load (in N) Corresponding to amplitude		
					Cycle-1 With Geotextile	Cycle-1 Without Geotextile	% Increase
Case 82	25P-1E-30A-0.5Hz-5Mm	25 X25	30	1	75.151	65.25	15.17
Case 83	25P-2E-30A-0.5Hz-5Mm			2	85.852	78.12	9.9
Case 84	25P-3E-30A-0.5Hz-5Mm			3	97.581	84.89	14.45
Case 85	25P-1E-45A-0.5Hz-5Mm		45	1	80.024	69.61	12.35
Case 86	25P-2E-45A-0.5Hz-5Mm			2	89.990	78.25	12.69
Case 87	25P-3E-45A-0.5Hz-5Mm			3	99.760	87.79	13.63
Case 88	25P-1E-60A-0.5Hz-5Mm		60	1	87.213	76.74	13.65
Case 89	25P-2E-60A-0.5Hz-5Mm			2	94.245	81.92	14.94
Case 90	25P-3E-60A-0.5Hz-5Mm			3	104.943	91.31	15.23
Case 91	50P-1E-30A-0.5Hz-5Mm	50 X50	30	1	94.631	85.17	11.11
Case 92	50P-2E-30A-0.5Hz-5Mm			2	102.532	91.25	12.36
Case 93	50P-3E-30A-0.5Hz-5Mm			3	107.895	94.94	13.65
Case 94	50P-1E-45A-0.5Hz-5Mm		45	1	98.346	85.37	12.6
Case 95	50P-2E-45A-0.5Hz-5Mm			2	105.750	92	13.89
Case 96	50P-3E-45A-0.5Hz-5Mm			3	114.857	99.92	14.95
Case 97	50P-1E-60A-0.5Hz-5Mm		60	1	123.654	107.58	13.2
Case 98	50P-2E-60A-0.5Hz-5Mm			2	130.912	113.44	14.65
Case 99	50P-3E-60A-0.5Hz-5Mm			3	140.135	121.54	15.86
Case 100	75P-1E-30A-0.5Hz-5Mm	75 X75	30	1	120.970	105.66	13.43
Case 101	75P-2E-30A-0.5Hz-5Mm			2	139.02	121.52	13.99
Case 102	75P-3E-30A-0.5Hz-5Mm			3	149.525	132.16	14.65
Case 103	75P-1E-45A-0.5Hz-5Mm		45	1	132.482	113.66	15.86
Case 104	75P-2E-45A-0.5Hz-5Mm			2	155.227	126.85	17.89
Case 105	75P-3E-45A-0.5Hz-5Mm			3	169.075	143.89	17.5
Case 106	75P-1E-60A-0.5Hz-5Mm		60	1	139.151	118.15	17.77
Case 107	75P-2E-60A-0.5Hz-5Mm			2	163.421	136.72	18.8
Case 108	75P-3E-60A-0.5Hz-5Mm			3	179.377	149.98	19.6

Based on the results obtained from the numerical analysis (as shown in the Table 6.22 to 6.29) for the above 108 cases, bar charts have been developed and presented from Fig 6.34 to Fig 6.45 as follows:

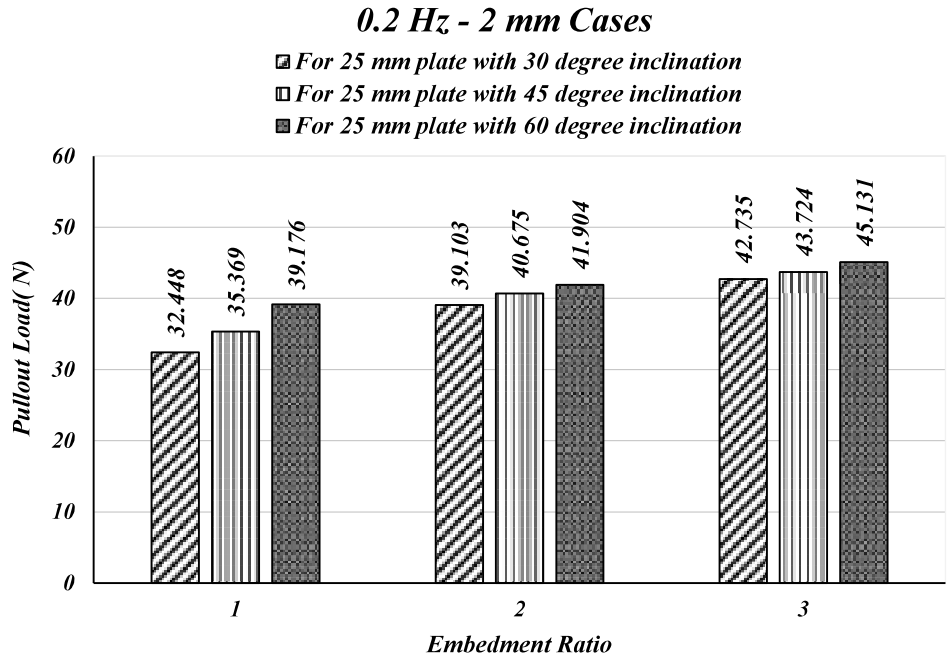

Fig. 6.34: Variation of pull-out loads for 0.2 Hz frequency and 2 mm amplitude cases for 25 mm square Plate

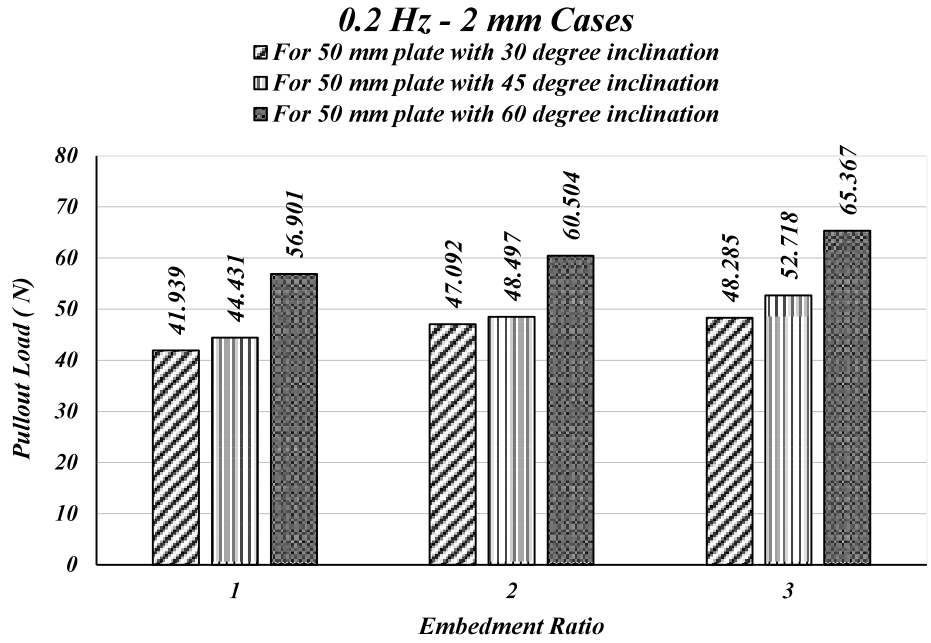

Fig. 6.35: Variation of pull-out loads for 0.2 Hz frequency and 2 mm amplitude cases for 50 mm square Plate

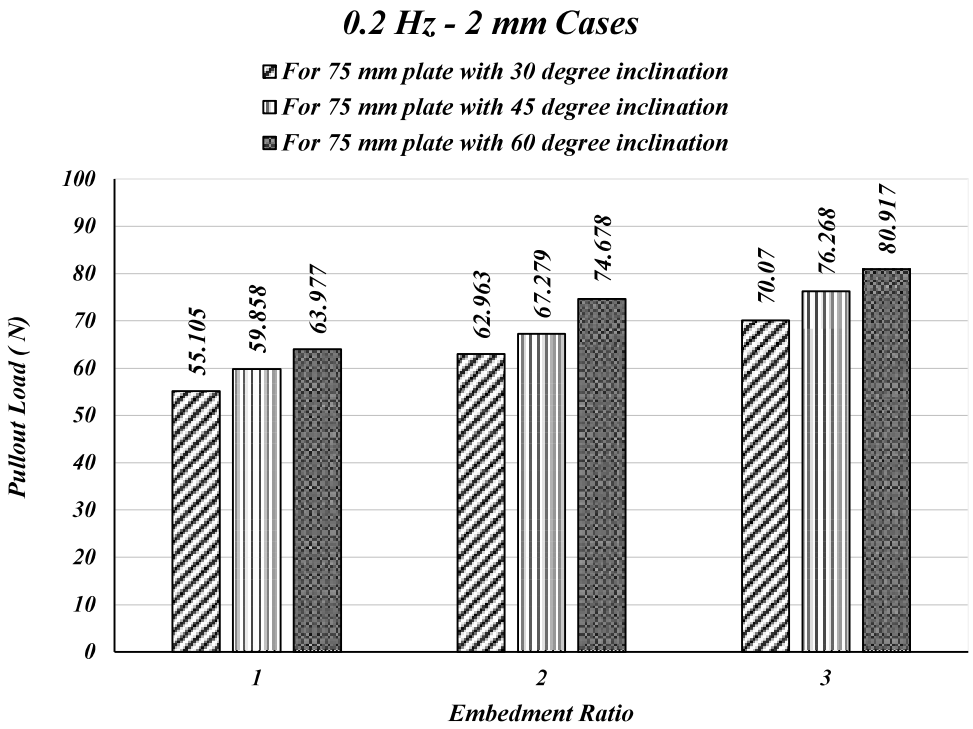

Fig. 6.36: Variation of pull-out loads for 0.2 Hz frequency and 2 mm amplitude cases for 75 mm square Plate

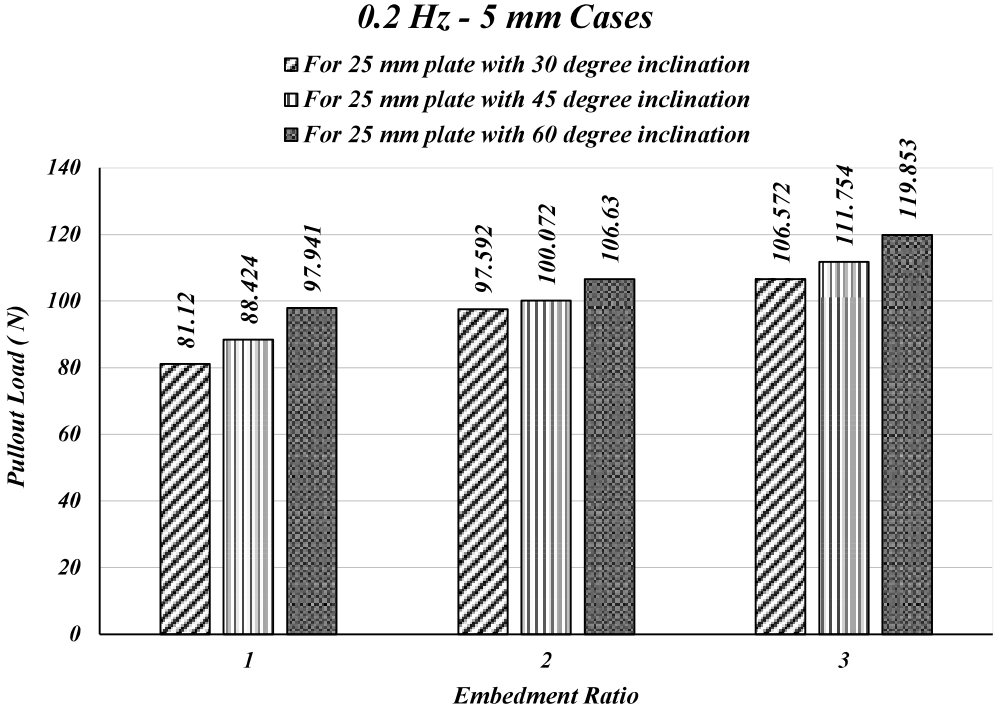

Fig. 6.37: Variation of pull-out loads for 0.2 Hz frequency and 5 mm amplitude cases for 25 mm square Plate

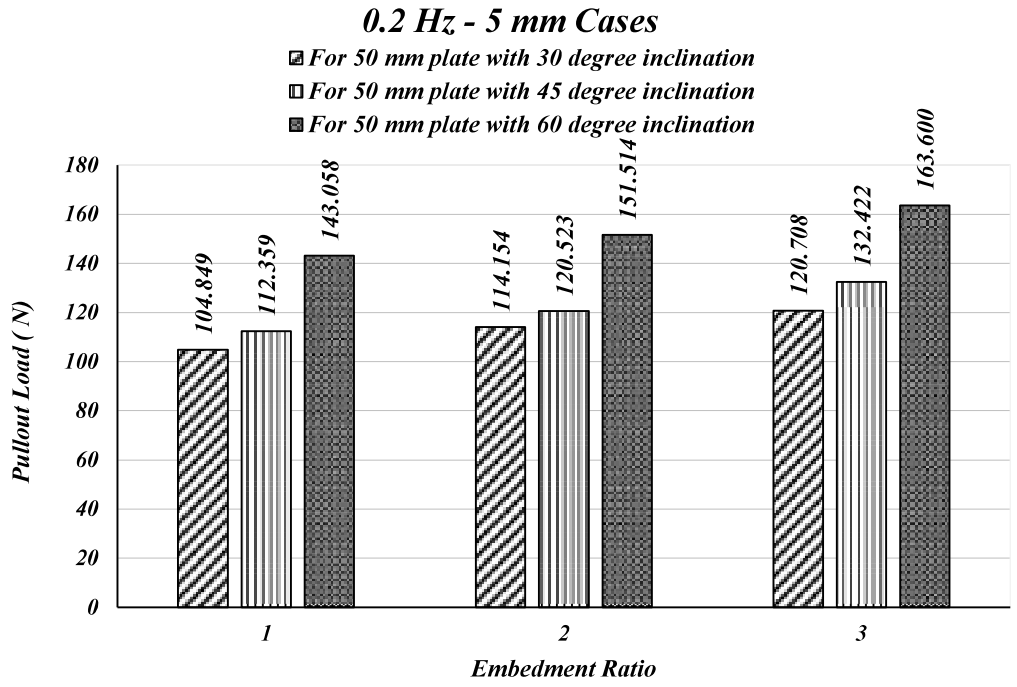

Fig. 6.38: Variation of pull-out loads for 0.2 Hz frequency and 5 mm amplitude cases for 50 mm square Plate

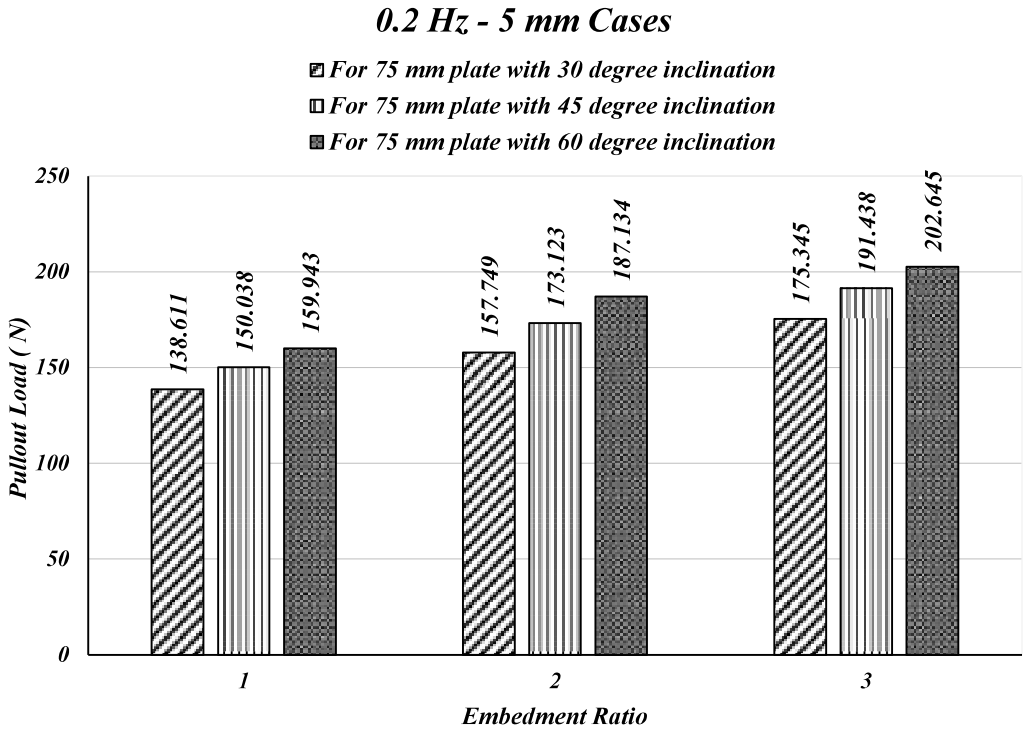

Fig. 6.39: Variation of pull-out loads for 0.2 Hz frequency and 5 mm amplitude cases for 75 mm square Plate

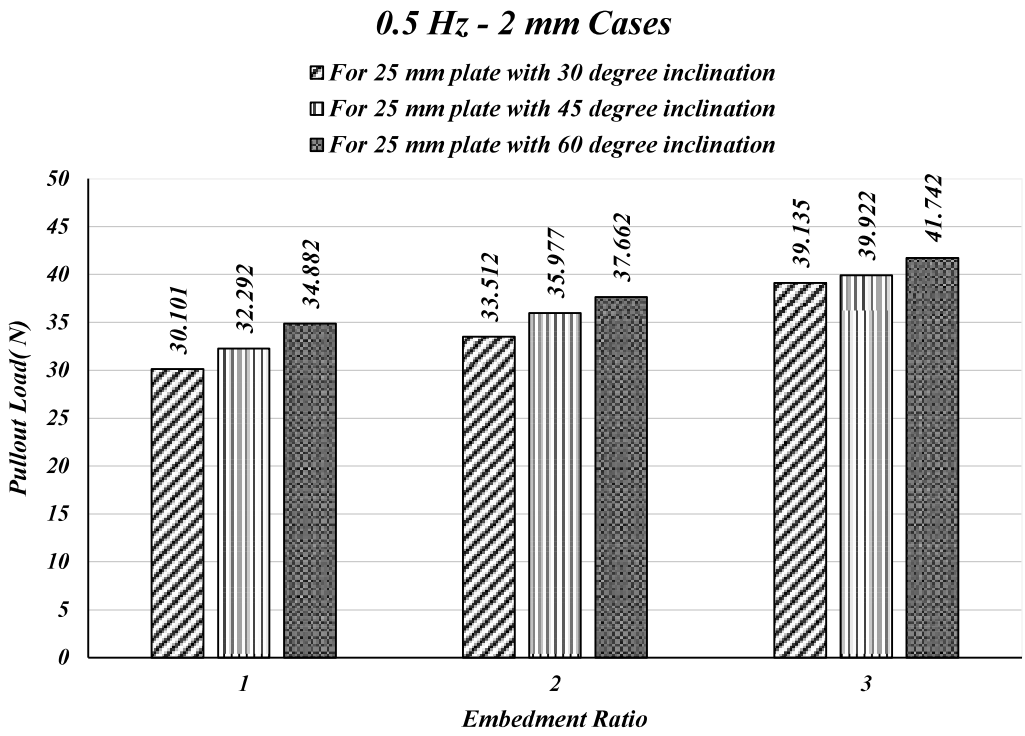

Fig. 6.40: Variation of pull-out loads for 0.5 Hz frequency and 2 mm amplitude cases for 25 mm square Plate

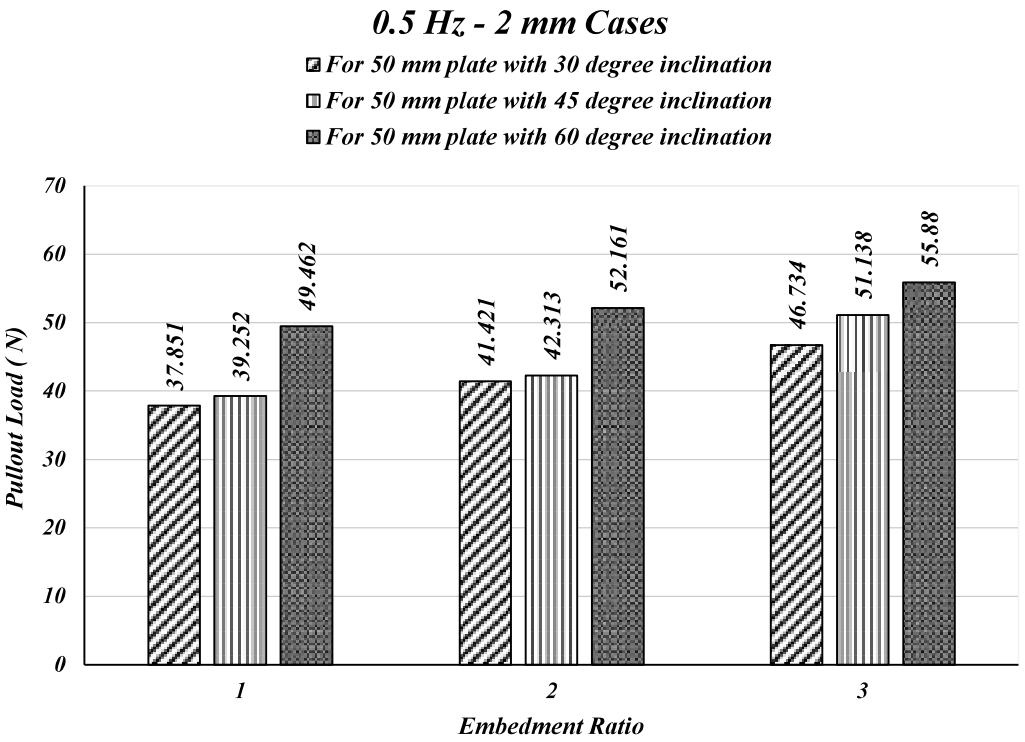

Fig. 6.41: Variation of pull-out loads for 0.5 Hz frequency and 2 mm amplitude cases for 50 mm square Plate

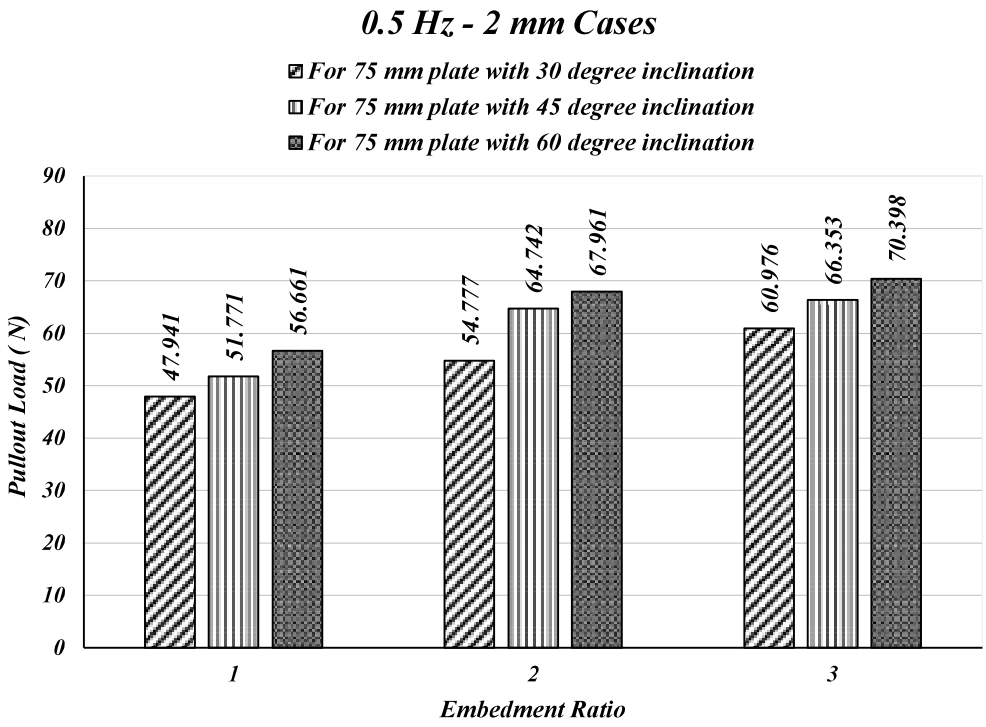

Fig. 6.42: Variation of pull-out loads for 0.5 Hz frequency and 2 mm amplitude cases for 75 mm square Plate

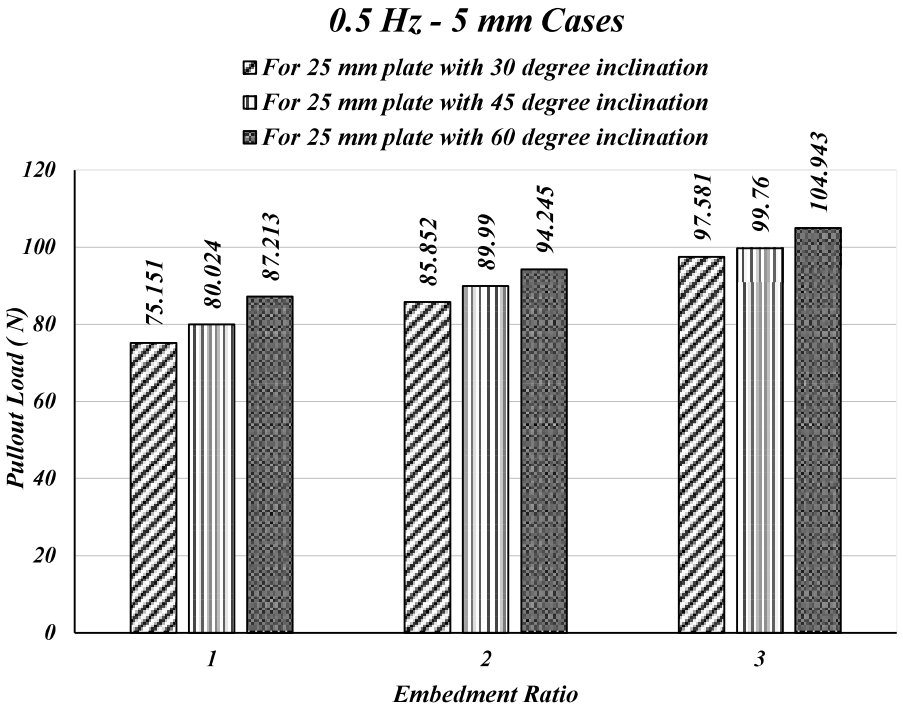

Fig. 6.43: Variation of pull-out loads for 0.5 Hz frequency and 5 mm amplitude cases for 25 mm square Plate

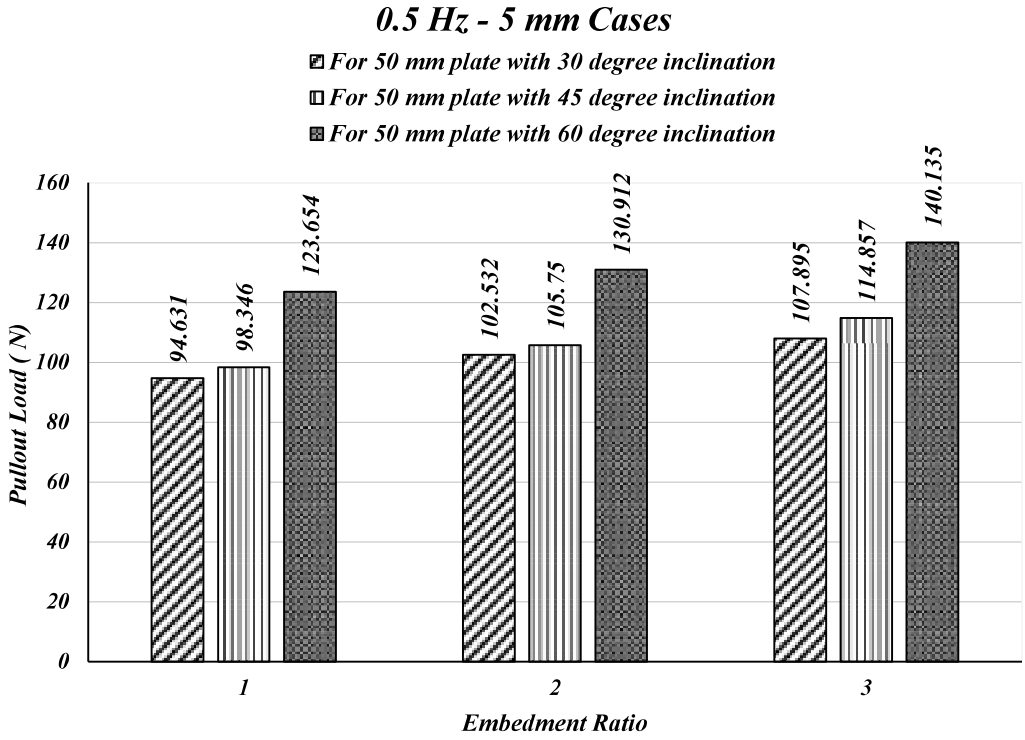

Fig. 6.44: Variation of pull-out loads for 0.5 Hz frequency and 5 mm amplitude cases for 50 mm square Plate

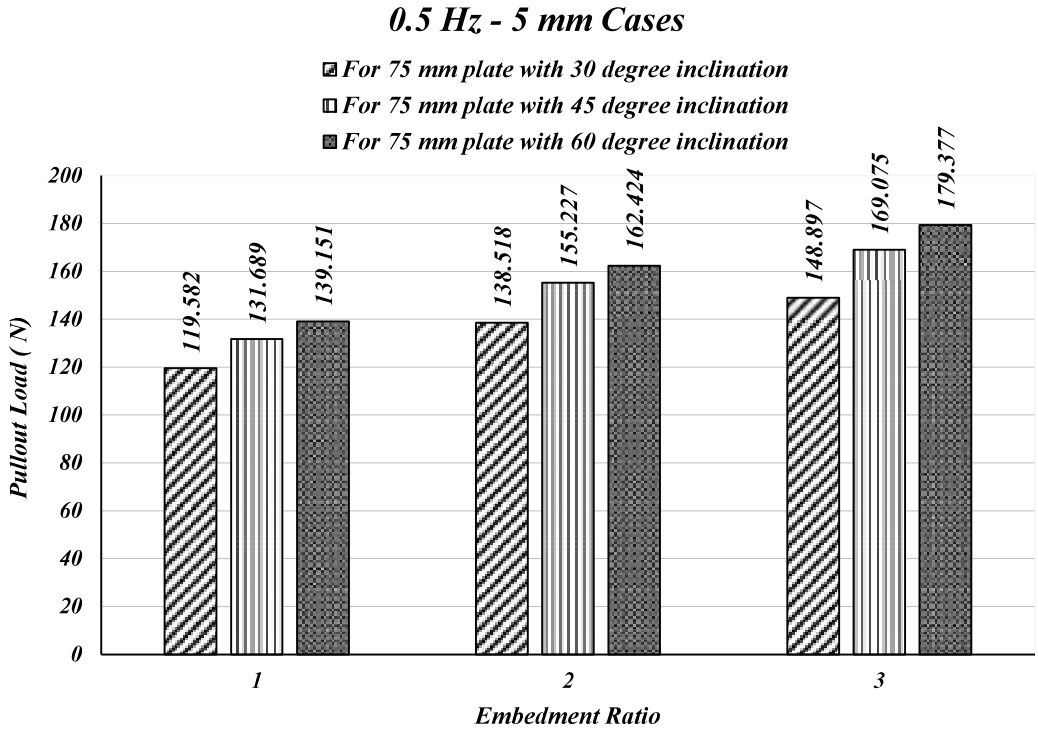

Fig. 6.45: Variation of pull-out loads for 0.5 Hz frequency and 5 mm amplitude cases for 75 mm square Plate

From the above presented bar chart from Fig.6.34 to Fig. 6.45, the effect of different parameters on the increase or decrease of pull-out loads can be easily assessed, which are being elaborated and discussed in the following sections of this chapter.

6.5.1 Effect of Embedment Ratio:

Table 6.30 has been developed on the basis of Fig. 6.30 to 6.41 and it presents the value of increase of ultimate pullout load in percentage for change in embedment ratio.

Table 6.30: Load Increase in percentage for change in embedment ratio

Plate size	Inclination Angle	Embedment ratio	Pull Out Load Increase (in percentage)			
			Frequency And Amplitude			
			0.2 Hz - 2 mm	0.2 Hz - 5 mm	0.5 Hz - 2 mm	0.5 Hz - 5 mm
25X25	30	1 to 2	20.510	20.306	11.332	14.239
		2 to 3	9.288	9.202	16.779	13.662
		1 to 3	31.703	31.376	30.012	29.847
	45	1 to 2	15.002	13.173	11.411	12.454
		2 to 3	7.496	11.674	10.965	10.857
		1 to 3	23.622	26.384	23.628	24.663
	60	1 to 2	6.963	8.872	7.970	8.063
		2 to 3	7.701	12.401	10.833	11.351
		1 to 3	15.201	22.373	19.666	20.330
50X50	30	1 to 2	9.139	8.875	9.432	8.349
		2 to 3	5.490	5.741	12.827	5.231
		1 to 3	15.132	15.126	23.468	14.017
	45	1 to 2	9.151	7.266	7.798	7.529
		2 to 3	8.704	9.873	20.856	8.612
		1 to 3	18.651	17.856	30.281	16.789
	60	1 to 2	6.332	5.911	5.457	5.870
		2 to 3	8.037	7.977	7.130	7.045
		1 to 3	14.878	14.359	12.976	13.328
75X75	30	1 to 2	14.260	13.807	13.394	14.921
		2 to 3	11.288	11.154	11.317	7.556
		1 to 3	27.157	26.502	26.226	23.605
	45	1 to 2	12.398	15.386	25.055	17.168
		2 to 3	13.361	10.579	3.292	8.921
		1 to 3	27.415	27.593	29.171	27.621
	60	1 to 2	16.726	17.000	20.393	17.441
		2 to 3	8.355	8.289	3.533	9.764
		1 to 3	26.478	26.698	24.647	28.908

It is being observed from Table 6.29 that for increase in embedment ratio the pull-out capacity increases when plate size and the inclination angle are fixed. For 25mm plate inclined at 30° under 0.2Hz frequency 2mm amplitude cyclic load, shows the maximum increase in pullout

capacity of 31.703% when embedment ratio increases from 1 to 3. This occurs due to the fact that with increase plate size the resisting force (due to presence of soil mass over the plate i.e., due to increase in soil volume) against the pull-out load increases leading to higher pull-out capacity.

6.5.2 Effect of Plate Size

Three square horizontal anchor plates of size 25 mm, 50 mm and 75 mm considered in the analysis. Table 6.31 has been developed on the basis of Fig. 6.30 to 6.41 and it presents the value of increase of ultimate pullout load in percentage for change in plate size.

Table 6.31: Load Increase in percentage for change in Plate Size

Embedment ratio	Inclination Angle	Plate size (mm)	Pull Out Load Increase (in percentage)			
			Frequency And Amplitude			
			0.2 Hz - 2 mm	0.2 Hz - 5 mm	0.5 Hz - 2 mm	0.5 Hz - 5 mm
Embedment ratio 1	30	25 to 50	29.250	29.252	25.747	25.921
		50 to 75	31.393	32.201	27.624	27.833
		25 to 75	69.826	70.872	60.483	60.969
	45	25 to 50	25.621	27.068	21.553	22.896
		50 to 75	34.721	33.534	31.894	34.710
		25 to 75	69.239	69.680	60.321	65.553
	60	25 to 50	45.245	46.065	41.798	41.784
		50 to 75	12.436	11.803	14.555	12.533
		25 to 75	63.307	63.305	62.436	59.553
Embedment ratio 2	30	25 to 50	17.055	16.971	23.601	19.429
		50 to 75	37.558	38.190	32.245	35.587
		25 to 75	61.018	61.641	63.455	61.930
	45	25 to 50	19.230	20.436	17.611	17.513
		50 to 75	38.728	43.643	53.007	46.787
		25 to 75	65.406	72.998	79.954	72.494
	60	25 to 50	44.387	42.093	38.498	38.906
		50 to 75	23.427	23.509	30.780	24.833
		25 to 75	78.212	75.498	81.127	73.400
Embedment ratio 3	30	25 to 50	12.987	13.264	19.417	10.570
		50 to 75	45.118	45.264	30.475	38.584
		25 to 75	63.964	64.532	55.809	53.232
	45	25 to 50	20.570	18.494	28.095	15.133
		50 to 75	44.672	44.567	30.770	47.205
		25 to 75	74.431	71.303	67.509	69.482
	60	25 to 50	44.838	36.501	33.870	33.534
		50 to 75	23.789	23.866	26.389	28.003
		25 to 75	79.294	69.078	69.196	70.928

It is observed from Table 6.30 that with increase of plate size increases the pull-out capacity. The trend of variation is same for different inclined angles of anchor plate and for same embedment depth. This occurs due to the fact that with increase in plate size the volume of soil resisting axial movement of anchor also increases. This phenomenon is the reason behind

such increase in pull-out capacity. For embedment ratio 2, with inclination angle 60° under 0.5Hz frequency 2mm amplitude cyclic load, shows the maximum increase in pull capacity of 81.127 % when plate size increases 25mm to 75mm.

6.5.3 Effect of Inclination angle:

Table 6.32 represents load increase in percentage for change in inclination angle.

Table 6.32: Load Increase in percentage for change in Inclination Angle

Plate size (mm)	Inclination Angle	Embedment ratio	Pull Out Load Increase (in percentage)			
			Frequency And Amplitude			
			0.2 Hz - 2 mm	0.2 Hz - 5 mm	0.5 Hz - 2 mm	0.5 Hz - 5 mm
25X25	30 to 45	1	9.002	9.004	7.279	6.484
		2	4.020	2.541	7.356	4.820
		3	2.314	4.862	2.011	2.233
	45 to 60	1	10.764	10.763	8.021	8.984
		2	3.022	6.553	4.684	4.728
		3	3.218	7.247	4.559	5.195
	30 to 60	1	20.735	20.736	15.883	16.050
		2	7.163	9.261	12.384	9.776
		3	5.607	12.462	6.662	7.545
50X50	30 to 45	1	5.942	7.163	3.701	3.926
		2	5.953	5.579	2.153	3.139
		3	9.181	9.704	9.424	6.453
	45 to 60	1	28.066	27.322	26.011	25.734
		2	24.758	25.714	23.274	23.794
		3	23.994	23.544	9.273	22.008
	30 to 60	1	35.676	36.442	30.676	30.670
		2	32.186	32.728	25.929	27.679
		3	35.377	35.534	19.570	29.881
75X75	30 to 45	1	8.625	8.244	7.171	9.516
		2	6.855	9.746	18.192	11.658
		3	8.845	9.178	9.671	13.075
	45 to 60	1	6.881	6.602	9.445	5.034
		2	10.997	8.093	5.366	5.279
		3	6.096	5.854	5.612	6.093
	30 to 60	1	16.100	15.390	17.294	15.029
		2	18.606	18.628	24.534	17.552
		3	15.480	15.569	15.826	19.965

From Table 6.32 it is being noted that with the increase in inclined angles (with respect to vertical level), the pullout capacity increases. For 50 mm plate at embedment ratio 1 shows maximum increase in pull out capacity of 36.442% when inclination angle (with respect to vertical) changes from 30° to 60° under 0.2 Hz frequency and 5 mm amplitude cyclic load.

The explanation behind such variation is similar to that for unreinforced bed as mentioned in section 6.4.3.

6.5.4 Effect of Cyclic loading with change in amplitude and frequency:

Table 6.33 shows the load vs. displacement behaviour of all the anchor plates with all the embedment ratios.

Table 6.33: Comparison for change in frequency and amplitude (plate size and embedment ratio are same)

Plate Size (mm)	Inclination Angle	Embedment Ratio	Pull Out Load Increase (in percentage)			
			Change in frequency (from 0.5 Hz to 0.2 Hz)		Change in Amplitude (from 2 mm to 5 mm)	
			Magnitude of Amplitude		Magnitude of Frequency	
			2 mm	5 mm	0.2 Hz	0.5 Hz
25X25	30	1	7.797	7.943	150.000	149.663
		2	16.684	13.675	149.577	156.183
		3	9.199	9.214	149.379	149.345
	45	1	9.529	10.497	150.004	147.814
		2	13.058	11.203	146.028	150.132
		3	9.524	12.023	155.590	149.887
	60	1	12.310	12.301	150.003	150.023
		2	11.263	13.141	154.463	150.239
		3	8.119	14.208	165.567	151.409
50X50	30	1	10.800	10.798	150.004	150.009
		2	10.504	11.335	149.397	147.536
		3	3.319	11.875	149.991	130.870
	45	1	13.194	14.249	152.884	150.550
		2	14.615	13.970	148.516	149.923
		3	3.090	15.293	151.189	124.602
	60	1	15.040	15.692	151.416	149.998
		2	15.995	15.737	150.420	150.977
		3	16.977	16.745	150.279	150.778
75X75	30	1	14.072	14.583	151.540	150.419
		2	14.944	13.472	150.542	153.793
		3	14.914	17.268	150.243	145.219
	45	1	15.621	13.252	150.657	155.900
		2	3.919	11.529	157.321	139.762
		3	14.049	13.227	151.007	152.830
	60	1	12.912	14.942	150.001	145.585
		2	9.473	14.510	150.588	139.564
		3	14.571	12.972	150.436	153.982

From Table 6.33, It has been found that increase in pull out load is generally more for same amplitude when frequency changes from 0.5 Hz to 0.2 Hz. This may be attributed to more impact of cyclic force with decreasing frequency when other parameters remain the same. For a 75 mm square plate, with 30° inclination and embedment ratio 3, when cyclic load

frequency decreases from 0.5 Hz to 0.2 Hz at 2 mm amplitude, pull-out load increases maximum about 17.27 %. On the other hand, it is observed that the increase in pull out load is generally more for same frequency when amplitude changes from 2 mm to 5 mm. This is attributed to the fact that, with increase in amplitude higher pullout load is required to displace the plate, other variables being unaltered. For a 25 mm square plate, with a 60° inclination angle and embedment ratio of 3, when cyclic load amplitude increases from 2 mm to 5 mm at 0.2 Hz frequency, maximum pull-out load increases about 165.567%.

6.5.5 Break Out Factor in Reinforced Clay:

Table 6.34 and 6.35 show the variation of the breakout factors with the embedment ratio.

Table 6.34: Change in Breakout Factor when frequency is 0.2 Hz Value of Cu (used to calculate the Nc for all the cases in this table) = 22000 N/ m^2

Plate size (in m) and related Area (in m^2)	Inclination Angle	Embedment Ratio	Frequency And Amplitude			
			0.2 Hz - 2 mm	0.2 Hz - 5 mm	0.2 Hz - 2 mm	0.2 Hz - 5 mm
			Corresponding Load for the Breakout factor		Value in Breakout Factor N_c = (F_r/AC_u)	
			Load (N)	Load (N)	(F_r/AC_u)	(F_r/AC_u)
25 mm square plate with area of 0.000625 m^2	30	1	32.448	81.12	2.360	5.900
		2	39.103	97.592	2.844	7.098
		3	42.735	106.572	3.108	7.751
	45	1	35.369	88.424	2.572	6.431
		2	40.675	100.072	2.958	7.278
		3	43.724	111.754	3.180	8.128
	60	1	39.176	97.941	2.849	7.123
		2	41.904	106.63	3.048	7.755
		3	45.131	119.853	3.282	8.717
50 mm square plate with area of 0.0025 m^2	30	1	41.939	104.849	0.763	1.906
		2	45.772	114.154	0.832	2.076
		3	48.285	120.708	0.878	2.195
	45	1	44.431	111.081	0.808	2.043
		2	48.497	120.523	0.882	2.191
		3	52.718	131.795	0.959	2.408
	60	1	56.901	142.261	1.035	2.601
		2	60.504	151.264	1.100	2.755
		3	65.367	163.419	1.188	2.975
75 mm square plate with area of 0.005625 m^2	30	1	55.105	137.761	0.445	1.120
		2	62.963	157.407	0.509	1.275
		3	70.07	175.173	0.566	1.417
	45	1	59.858	149.646	0.484	1.212
		2	67.279	173.123	0.544	1.399
		3	76.268	190.67	0.616	1.547
	60	1	63.977	159.943	0.517	1.292
		2	74.678	186.695	0.603	1.512
		3	80.917	202.293	0.654	1.638

Table 6.35: Change in Breakout Factor when frequency is 0.5 Hz Value of C_u (used to calculate the N_c for all the cases in this table) = 22000 N/ m^2

Plate size (in m) and related Area (in m^2)	**Inclination Angle**	**Embedment Ratio**	**Frequency And Amplitude**			
			0.5 Hz - 2 mm	**0.5 Hz - 5 mm**	**0.5 Hz - 2 mm**	**0.5 Hz - 5 mm**
			Corresponding Load for the Breakout factor		**Value in Breakout Factor N_c = (F_r /AC_u)**	
			Load (N)	**Load (N)**	**F_r /AC_u**	**F_r /AC_u**
25 mm square plate with area of 0.000625 m^2	30	1	30.101	75.151	2.189	5.466
		2	33.512	85.852	2.437	6.244
		3	39.135	97.581	2.846	7.097
	45	1	32.292	80.024	2.349	5.820
		2	35.977	89.942	2.617	6.545
		3	39.922	99.76	2.903	7.255
	60	1	34.882	87.213	2.537	6.343
		2	37.662	94.161	2.739	6.854
		3	41.983	104.943	3.036	7.632
50 mm square plate with area of 0.0025 m^2	30	1	37.851	94.631	0.688	1.721
		2	41.421	102.532	0.753	1.864
		3	43.155	107.895	0.850	1.962
	45	1	39.252	98.131	0.714	1.788
		2	42.313	105.75	0.769	1.923
		3	45.942	114.857	0.930	2.088
	60	1	49.462	123.654	0.899	2.248
		2	52.161	130.395	0.948	2.380
		3	55.88	139.711	1.016	2.548
75 mm square plate with area of 0.005625 m^2	30	1	47.941	119.852	0.390	0.978
		2	54.777	138.518	0.443	1.123
		3	60.976	148.897	0.493	1.208
	45	1	51.771	131.689	0.418	1.071
		2	64.742	155.227	0.523	1.254
		3	66.353	169.075	0.540	1.366
	60	1	56.661	139.151	0.458	1.124
		2	67.961	162.424	0.551	1.321
		3	70.398	179.377	0.571	1.450

Fig 6.46 to 6.49 have been developed on the basis of Table 6.34 and 6.35, which represent the variation of breakout factor with embedment ration for different frequency and amplitude of cyclic load.

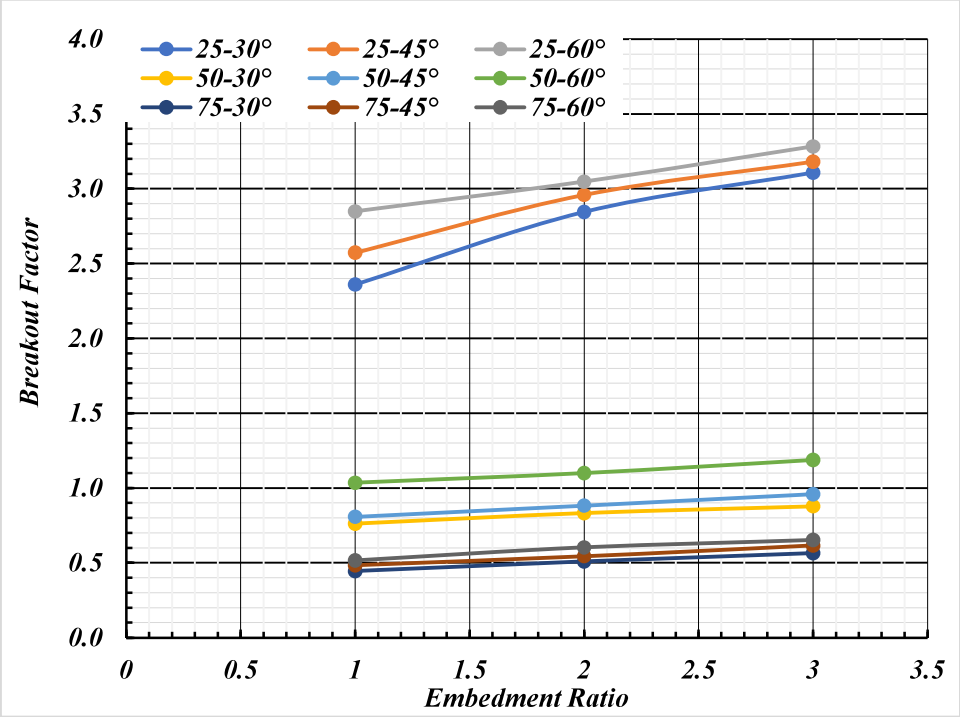

Fig. 6.46: Breakout Factor vs Embedment Ratio for 0.2 Hz frequency and 2 mm amplitude

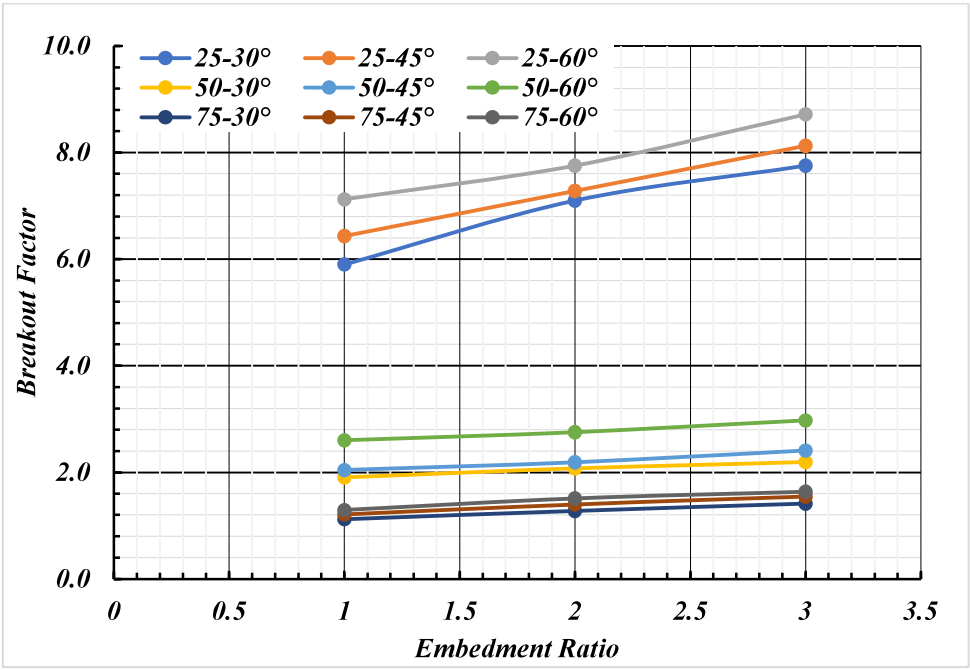

Fig. 6.47: Breakout Factor vs Embedment Ratio for 0.2 Hz frequency and 5 mm amplitude

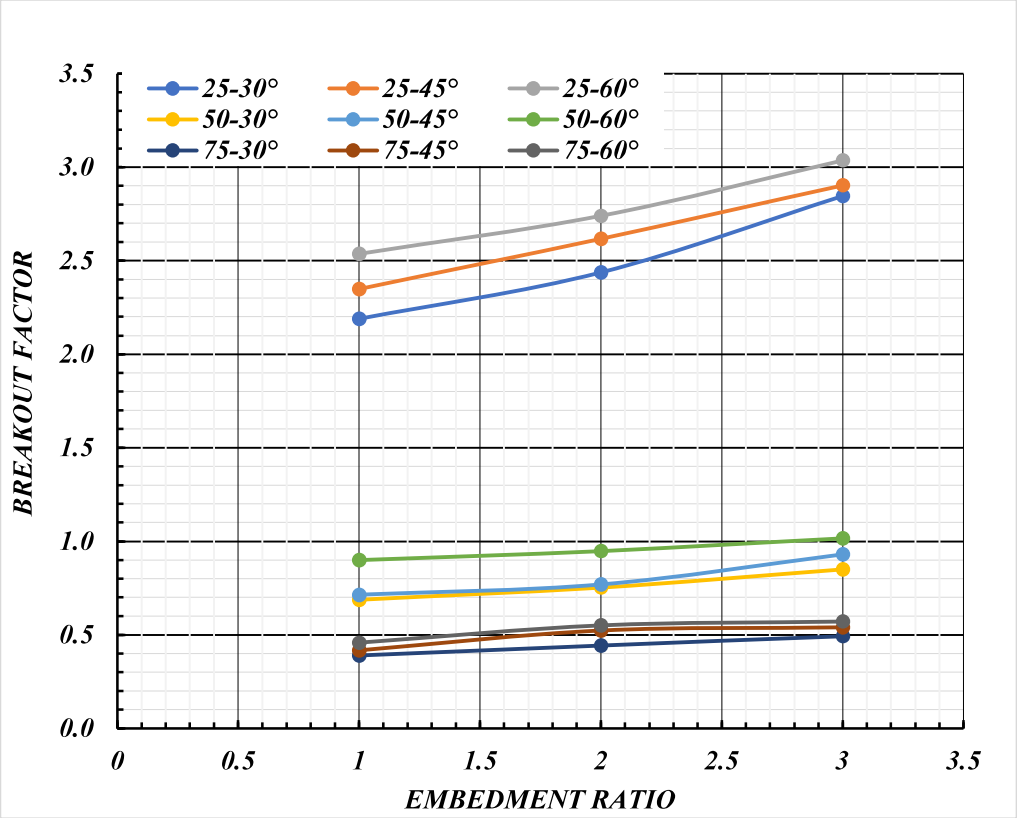

Fig. 6.48: Breakout Factor vs Embedment Ratio for 0.5 Hz frequency and 2 mm amplitude

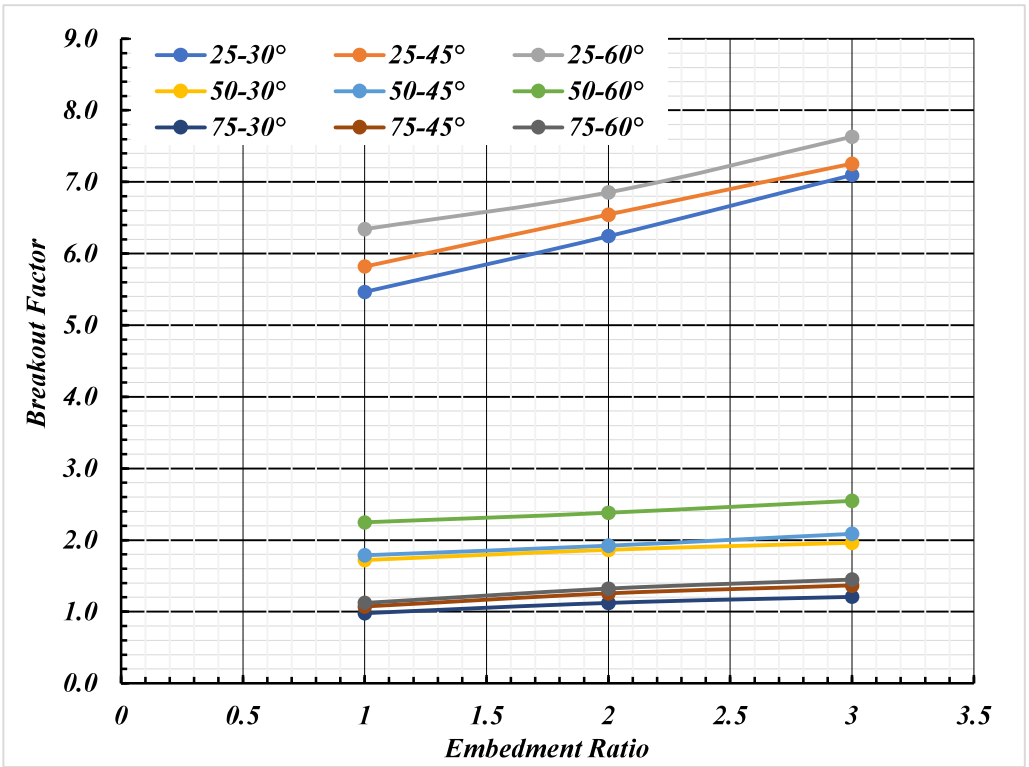

Fig. 6.49: Breakout Factor vs Embedment Ratio for 0.5 Hz frequency and 5 mm amplitude

From the Fig. 6.46 to Fig. 6.49 and from the Table. 6.35,6.36 the following points have been observed for inclined anchor in soft clay soil:

1) Breakout Factor has been found to increase with the increase in embedment ratio for any particular plate size for any particular inclination.
2) Increment in inclination angle also increases the break out factor.

6.6 COMPARISION BETWEEN THE RESULTS OF REINFORCED AND THE UNREINFORCED BED UNDER CYCLIC LOADING:

Based on the results obtained from the numerical analysis, as shown in the Table 6.30 to 6.33, presented earlier in this chapter for the 108 cases, bar charts have been developed for comparing the reinforced cases with the unreinforced cases and presented from Fig. 6.50 to Fig. 6.61 as follows:

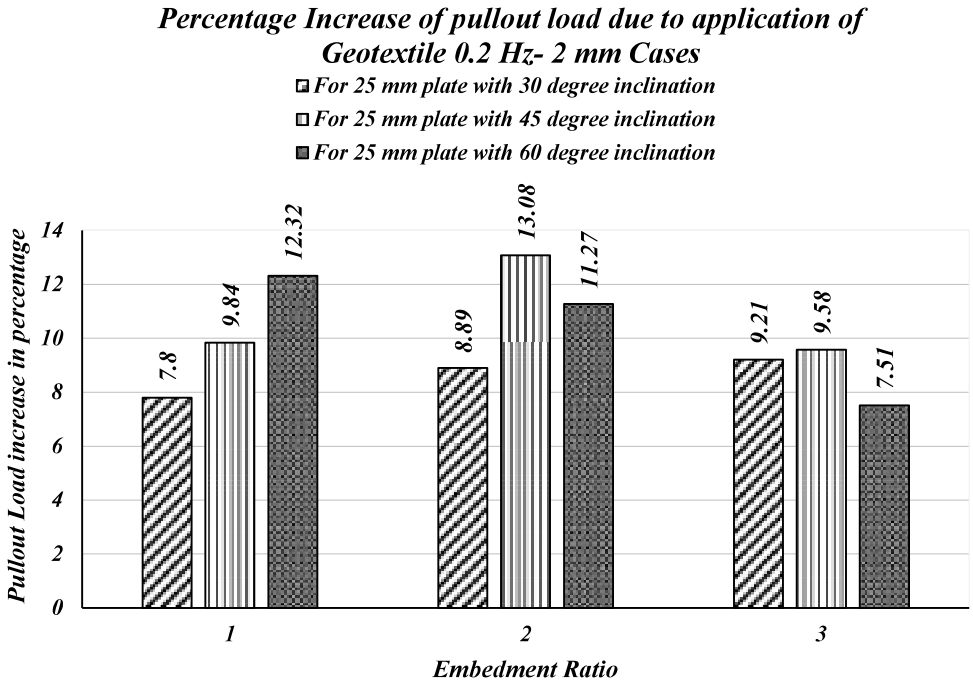

Fig. 6.50: Percentage increase of pull-out loads due to application of geotextile for 0.2 Hz frequency and 2 mm amplitude cases for 25 mm square Plate

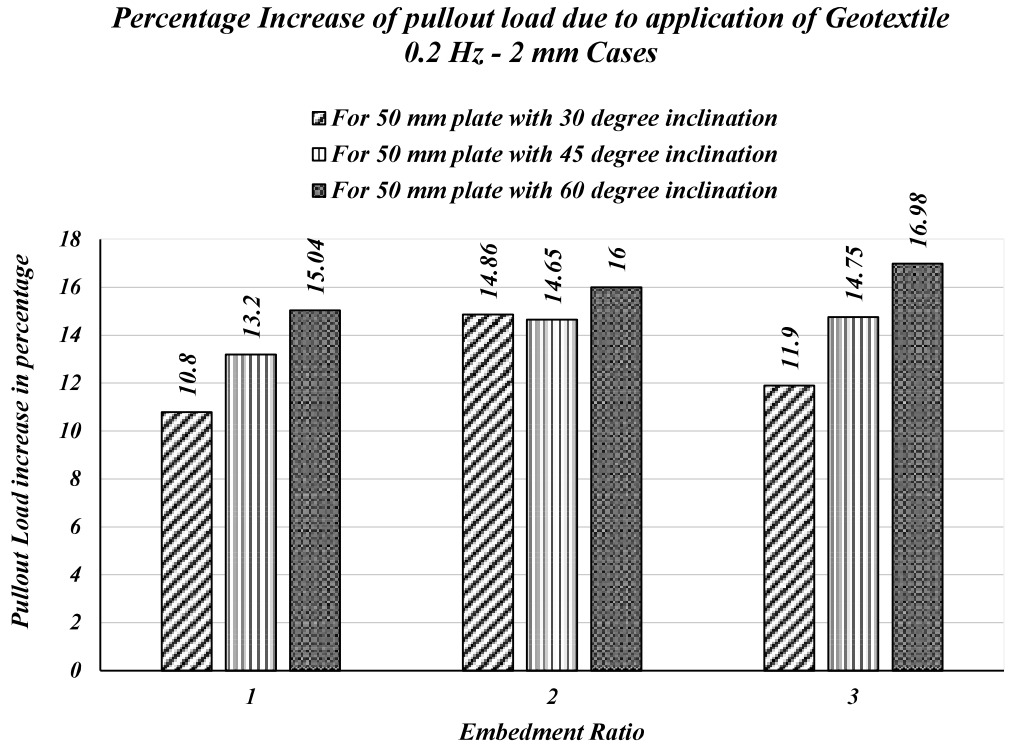

Fig. 6.51: Percentage increase of pull-out loads due to application of geotextile for 0.2 Hz frequency and 2 mm amplitude cases for 50 mm square Plate

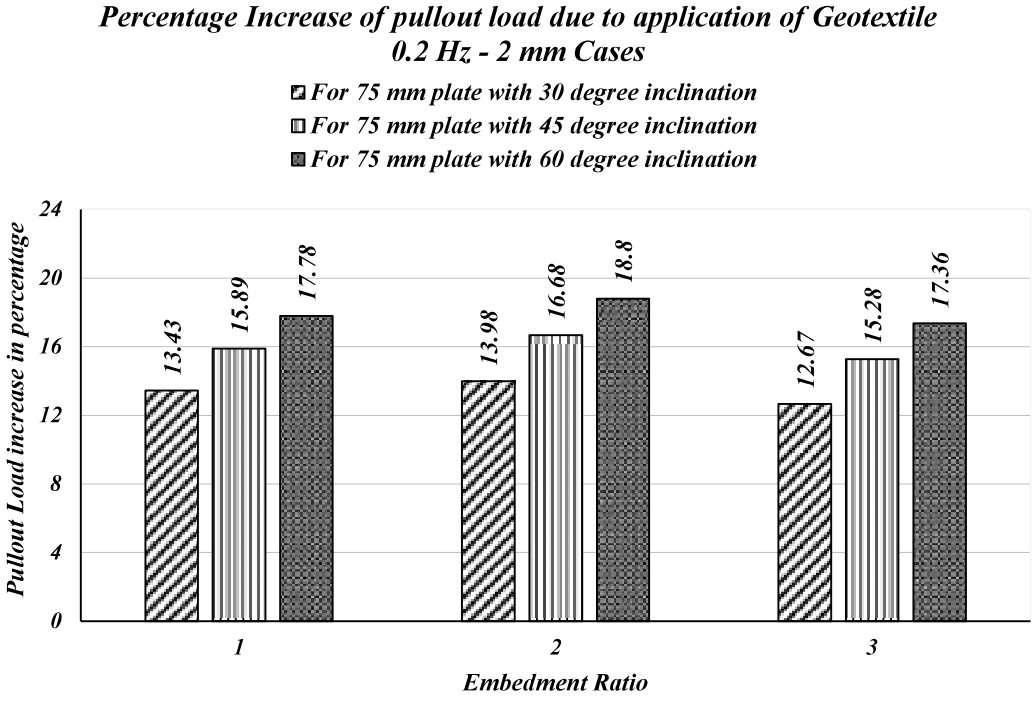

Fig. 6.52: Percentage increase of pull-out loads due to application of geotextile for 0.2 Hz frequency and 2 mm amplitude cases for 75 mm square Plate

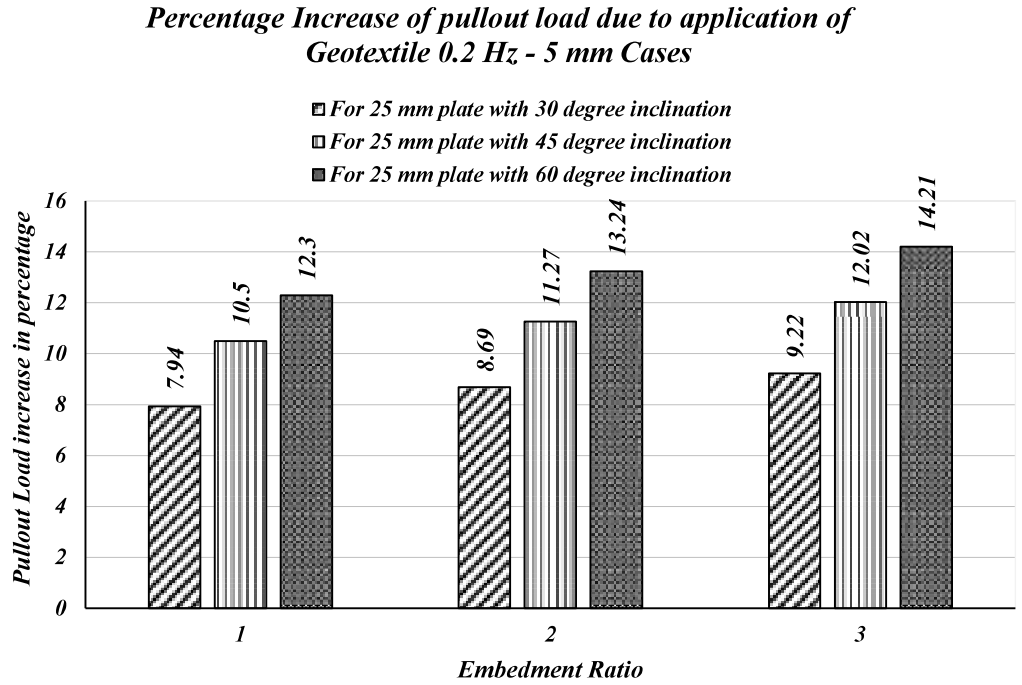

Fig. 6.53: Percentage increase of pull-out loads due to application of geotextile for 0.2 Hz frequency and 5 mm amplitude cases for 25 mm square Plate

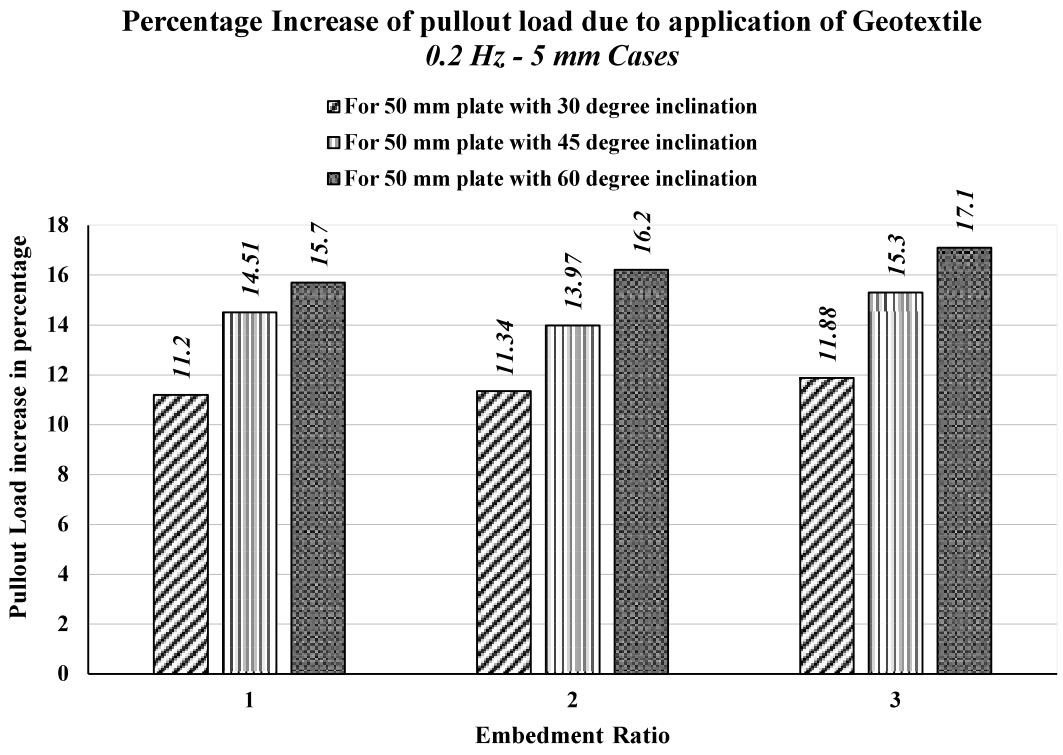

Fig. 6.54: Percentage increase of pull-out loads due to application of geotextile for 0.2 Hz frequency and 5 mm amplitude cases for 50 mm square Plate

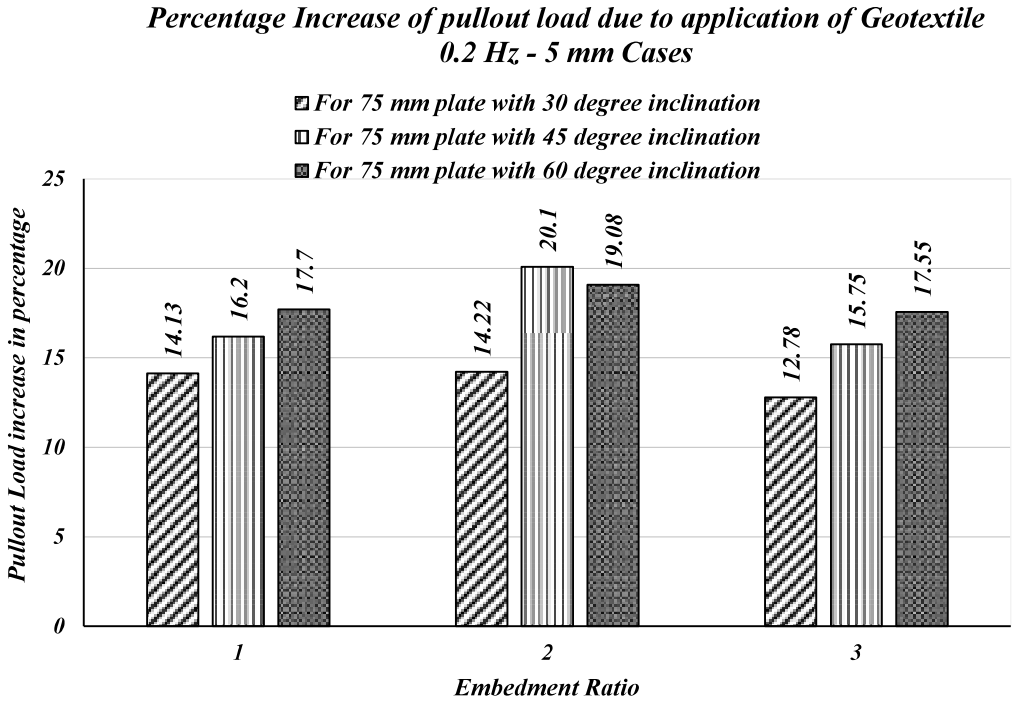

Fig. 6.55: Percentage increase of pull-out loads due to application of geotextile for 0.2 Hz frequency and 5 mm amplitude cases for 75 mm square Plate

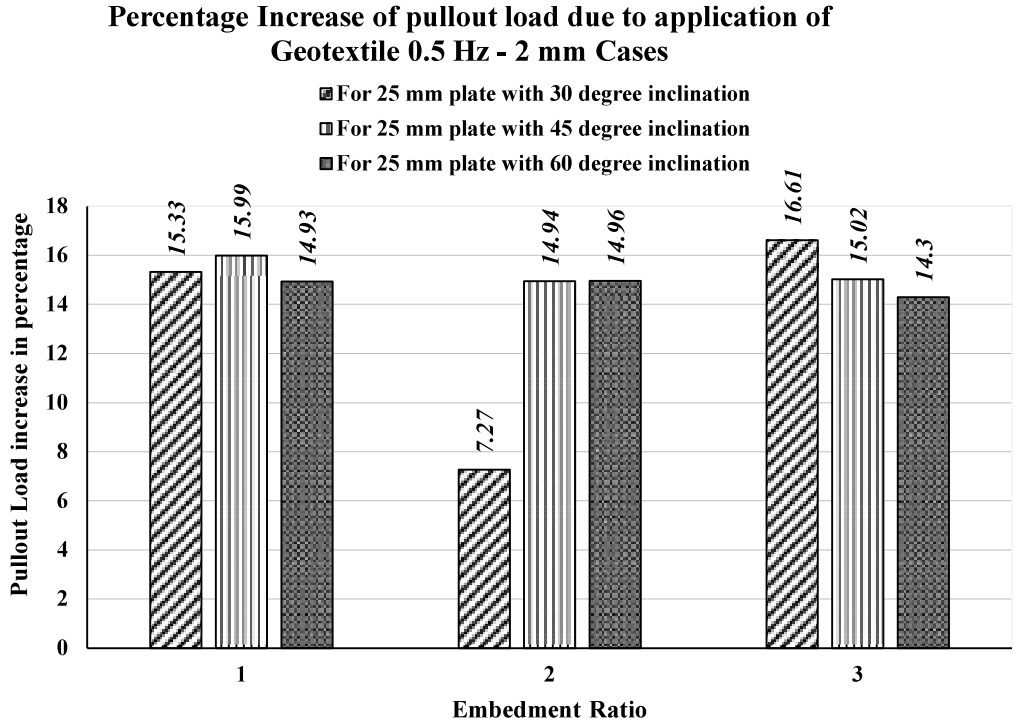

Fig. 6.56: Percentage increase of pull-out loads due to application of geotextile for 0.5 Hz frequency and 2 mm amplitude cases for 25 mm square Plate

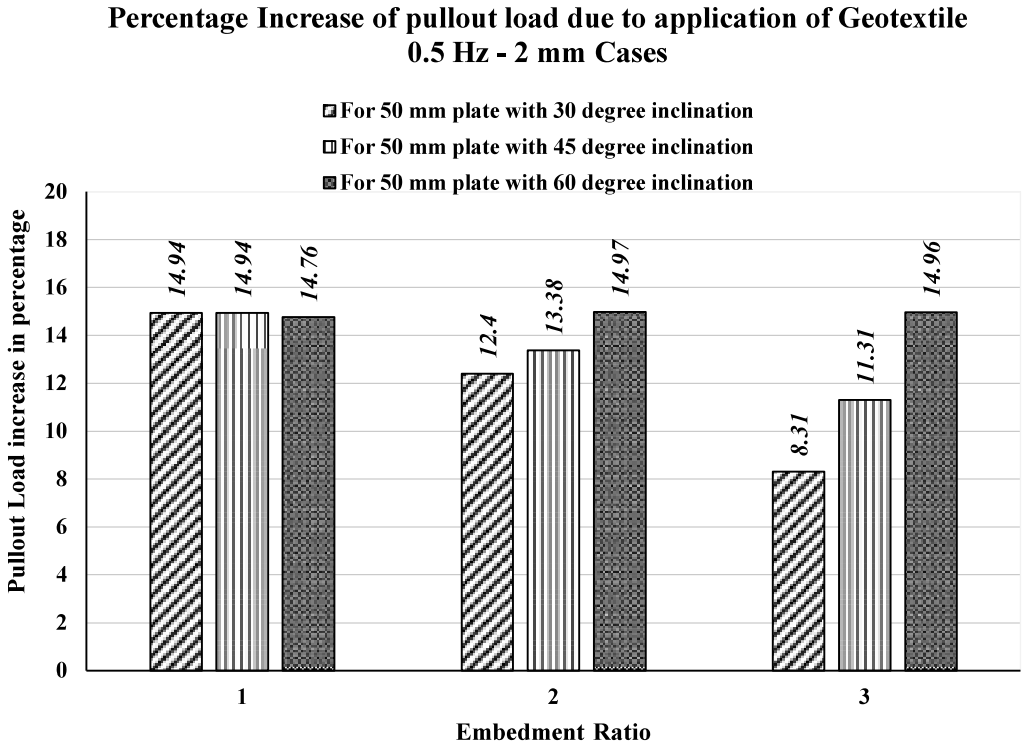

Fig. 6.57: Percentage increase of pull-out loads due to application of geotextile for 0.5 Hz frequency and 2 mm amplitude cases for 50 mm square Plate

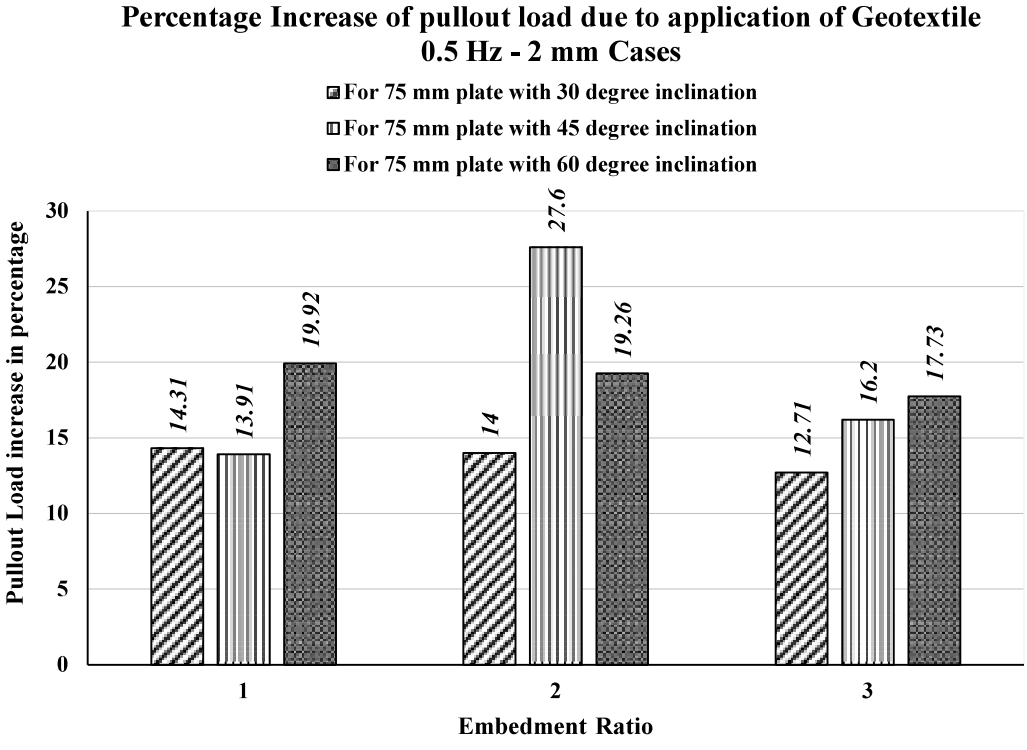

Fig. 6.58: Percentage increase of pull-out loads due to application of geotextile for 0.5 Hz frequency and 2 mm amplitude cases for 75 mm square Plate

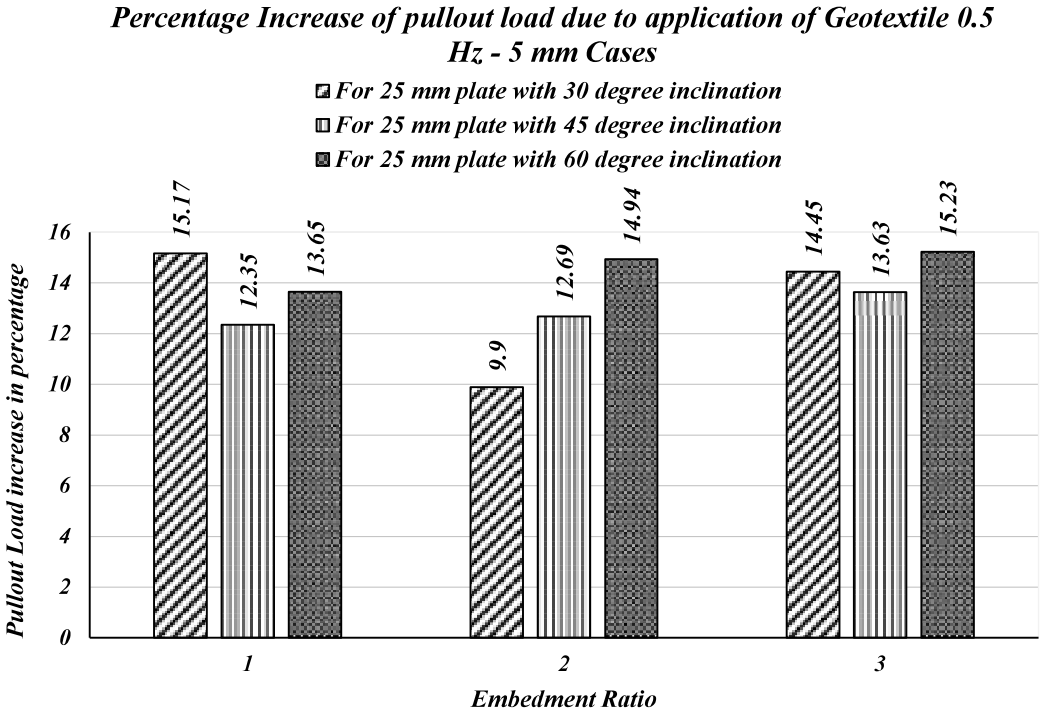

Fig. 6.59: Percentage increase of pull-out loads due to application of geotextile for 0.5 Hz frequency and 5 mm amplitude cases for 25 mm square Plate

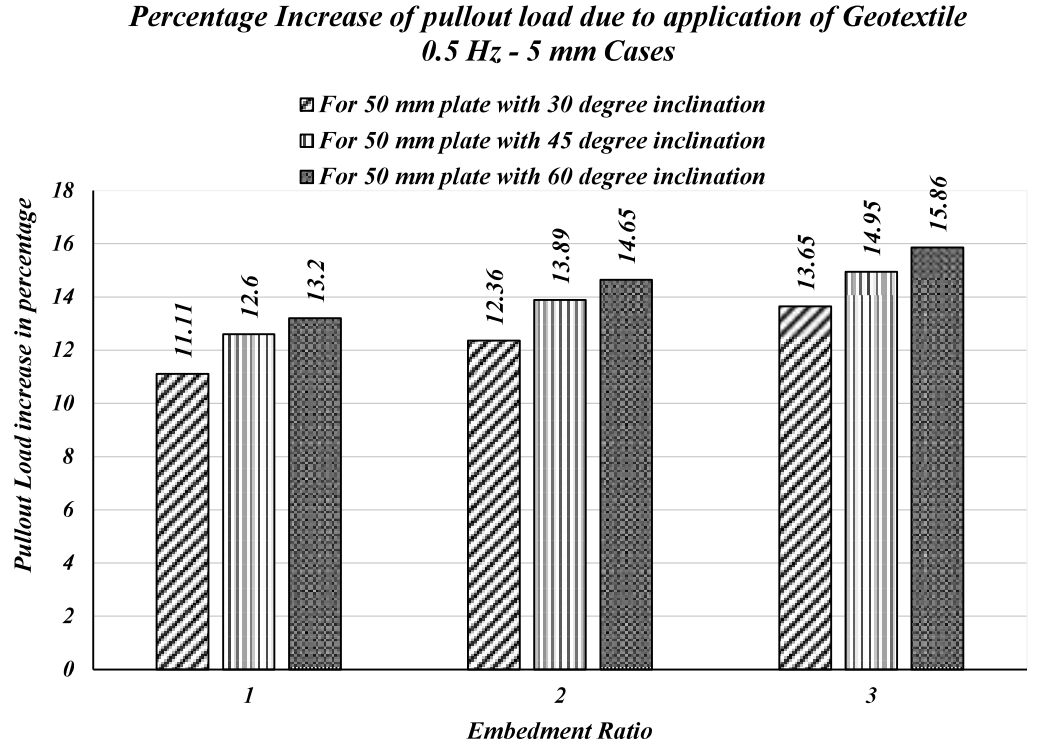

Fig. 6.60: Percentage increase of pull-out loads due to application of geotextile for 0.5 Hz frequency and 5 mm amplitude cases for 50 mm square Plate

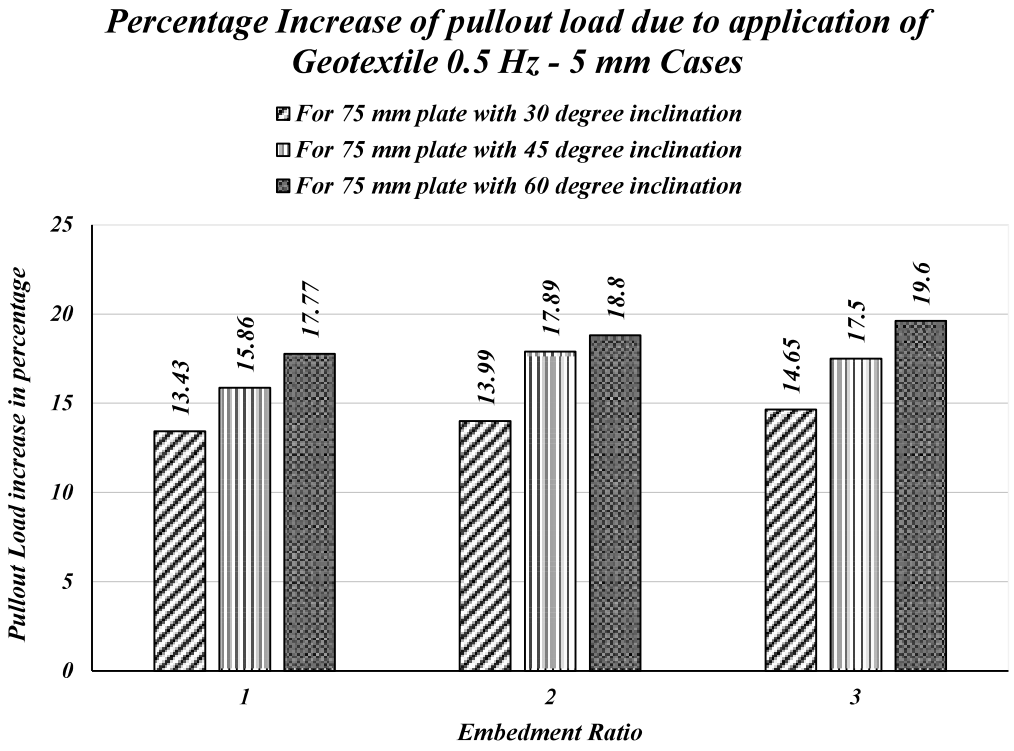

Fig. 6.61: Percentage increase of pull-out loads due to application of geotextile for 0.5 Hz frequency and 5 mm amplitude cases for 75 mm square Plate

From the Fig. 6.50 to Fig. 6.61 and from the Table 6.26 to 6.29, it has been observed for inclined anchor in reinforced soft clay soil that Pullout load capacity increases with the application of geotextile in soft clay soil for any particular plate size for any particular inclination. This increase is due to the fact that tensile stress in geotextile is induced in the reinforcement and the force due to this, acts to resist pullout. Maximum increase in pull capacity of 27.2% has been observed from the bar charts due to the inclusion of reinforcement for 75 mm square plate with a 45° inclination angle and embedment ratio of 32 when cycling loading frequency and amplitude are 0.5 Hz and 2 mm respectively. Furthermore, the general trend observed is an increase in the percentage improvement of pullout capacity with increasing embedment depth and inclination angle. However, at certain points, this percentage may drop due to a decrease in rate of increase in pullout capacity. Overall, the percentage increase in pullout load tends to increase with greater embedment depth. However, beyond a certain optimum embedment depth, the rate of increase in pullout capacity may level off or even decrease, indicating that the benefits of further increasing depth or inclination angle may diminish beyond this point.

6.7 COMPARISION OF PULLOUT CAPACITY BETWEEN STATIC AND CYCLIC LOADING

Table 6.36 and Table 6.37 represent comparison of pullout capacity of the anchor under static and cyclic loading both in unreinforced and reinforced soil condition.

Table 6.36: Comparison of pullout capacity of the anchor under static and cyclic loading in unreinforced condition

TEST NAME	STATIC PULLOUT CAPACITY (KG)	PULLOUT CAPACITY (N)				
		STATIC	CYCLIC			
			0.2 HZ-2MM	0.2 HZ- 5 MM	0.5HZ-2 MM	0.5HZ-5MM
25-01-30	3.5	34.335	30.1	75.15	26.1	65.25
25-01-45	4	39.24	35.91	89.79	31.24	78.12
25-01-60	4.3	42.183	39.13	97.58	33.56	84.89
25-02-30	4.4	43.164	32.2	80.02	27.84	69.61
25-02-45	5.2	51.012	35.97	89.94	31.3	78.25
25-02-60	5.8	56.898	39.9	99.76	34.71	87.79
25-03-30	4.7	46.107	34.88	87.21	30.35	76.74
25-03-45	5.8	56.898	37.66	94.16	32.76	81.92
25-03-60	6.2	60.822	41.98	104.94	36.52	91.31
50-01-30	6.2	60.822	37.85	94.63	32.93	85.17
50-01-45	7.6	74.556	41	102.53	36.85	91.25
50-01-60	12.2	119.682	43.15	107.89	43.15	94.94
50-02-30	8.8	86.328	39.25	98.13	34.15	85.37
50-02-45	10.1	99.081	42.3	105.75	37.32	92
50-02-60	15.2	149.112	45.94	114.85	45.94	99.92
50-03-30	10	98.1	49.46	123.65	43.1	107.58
50-03-45	12.4	121.644	52.16	130.39	45.37	113.44
50-03-60	17.6	172.656	55.88	139.71	48.61	121.54
75-01-30	17	166.77	48.58	121.45	42.26	105.66
75-01-45	19.5	191.295	55.24	138.11	48.05	121.52
75-01-60	24.5	240.345	62.19	155.48	54.1	132.16
75-02-30	20.5	201.105	51.65	129.12	45.45	113.66
75-02-45	27	264.87	57.66	144.15	50.74	126.85
75-02-60	30	294.3	66.16	165.39	57.55	143.89
75-03-30	27.5	269.775	54.32	135.89	47.25	118.15
75-03-45	32.5	318.825	62.86	157.15	57.2	136.72
75-03-60	38	372.78	68.95	172.39	59.99	149.98

Table 6.37: Comparison of pullout capacity of the anchor under static and cyclic loading in reinforced condition

TEST NAME	STATIC PULLOUT CAPACITY (KG)	PULLOUT CAPACITY (N)				
		STATIC	CYCLIC			
			0.2 HZ-2MM	0.2 HZ- 5 MM	0.5HZ-2 MM	0.5HZ-5MM
25-01-30	4.8	47.088	32.448	81.12	30.101	75.151
25-01-45	6	58.86	39.103	97.592	33.512	85.852
25-01-60	6.4	62.784	42.735	106.572	39.135	97.581
25-02-30	5.8	56.898	35.369	88.424	32.292	80.024
25-02-45	7.1	69.651	40.675	100.072	35.977	89.99
25-02-60	8.3	81.423	43.724	111.754	39.922	99.76
25-03-30	6.8	66.708	39.176	97.941	34.882	87.213
25-03-45	9.1	89.271	41.904	106.63	37.662	94.245
25-03-60	9.4	92.214	45.131	119.853	41.742	104.943
50-01-30	7.7	75.537	41.939	104.849	37.851	94.631
50-01-45	9.6	94.176	47.092	114.154	41.421	102.532
50-01-60	14.6	143.226	48.285	120.708	46.734	107.895
50-02-30	17	166.77	44.431	112.359	39.252	98.346
50-02-45	22	215.82	48.497	120.523	42.313	105.75
50-02-60	23.5	230.535	52.718	132.422	51.138	114.857
50-03-30	21	206.01	56.901	143.058	49.462	123.654
50-03-45	28	274.68	60.504	151.514	52.161	130.912
50-03-60	33.5	328.635	65.367	163.6	55.88	140.135
75-01-30	22.5	220.725	55.105	138.611	48..307	120.97
75-01-45	27	264.87	62.963	157.749	54.777	139.02
75-01-60	32	313.92	70.07	175.345	60.976	149.525
75-02-30	31	304.11	59.858	150.038	51.771	132.482
75-02-45	35	343.35	67.279	173.123	64.742	155.227
75-02-60	43	421.83	76.268	191.438	66.873	169.075
75-03-30	33.5	328.635	63.977	159.943	56.661	139.151
75-03-45	43	421.83	74.678	187.134	68.216	163.421
75-03-60	50	490.5	80.917	202.645	70.626	179.377

The comparison between static and cyclic loading reveals a consistent reduction in pullout capacity under cyclic conditions, especially with increased frequency and displacement. For example, in the unreinforced case at an embedment of 50-03-45, the static pullout capacity is 12.4 kg (121.64 N), which drops to 52.16 N under cyclic loading at 0.2 Hz and 2 mm displacement—a decrease to about 43% of the static value. In reinforced conditions, the reduction is somewhat mitigated but still significant. For instance, at 75-03-60, the static

pullout capacity is 50 kg (490.5 N), which decreases to 179.38 N at 0.5 Hz and 5 mm displacement, a reduction of nearly 63%. In certain instances, the pullout capacity under cyclic loading at 0.2 Hz with a 5 mm displacement is observed to be higher than the static pullout capacity, which may appear counterintuitive. This trend suggests that specific cyclic loading conditions can mobilize additional soil resistance that is not fully engaged during static loading. At lower frequencies, like 0.2 Hz, combined with a larger displacement amplitude of 5 mm, the cyclic motion may enhance soil-anchor interaction, allowing the anchor to "lock" into a more stable position and thereby increasing the pullout capacity. This can be seen in cases such as 25-01-30 (unreinforced), where the static capacity is 34.34 N, but it increases to 75.15 N under cyclic loading, and in 25-01-45 (reinforced), where the static capacity of 58.86 N rises to 97.59 N under the same cyclic conditions.

In some cases, the pullout load increases from static loading. The increased pullout capacity in these situations could be attributed to the densification of the surrounding soil caused by repeated cyclic movements, especially if the soil is initially loose or partially compacted. Additionally, cyclic loading might reorient soil particles or improve interlock between the soil and the anchor, thus enhancing load-bearing performance temporarily. However, in case of cyclic loading several factors like inertia etc come into play, for which it is difficult to predict, which loading condition-static or cyclic, will yield higher value of pullout capacity.

6.8 REGRESSION ANALYSIS OF PULLOUT CAPACITY OF INCLINED ANCHORS BY MACHINE LEARNING (ML):

Numerical results for anchor plates in different unreinforced and reinforced soil condition indicated that the anchor pate behavior is significantly influenced by the plate size, inclination angle, embedment ratio, frequency and amplitude of the cyclic load. Hence, a predictive model of ultimate pullout capacity in the form of a function of plate size, inclination angle, embedment ratio, soil type, frequency and amplitude of the cyclic load, has been attempted by regression analysis based on the numerical data and presented in this section. This has been done with the help of machine learning.

6.8.1 Glossary:

Machine learning has been adopted here as a tool for data analysis. This enables machines to learn without being explicitly programmed. A computer program is said to have learned from experience E related to a class of tasks T when its performance on tasks in that class, as measured by a performance measure P, improves with experience E. Machine learning is a broad term for a programme that uses data analysis and data exploration to manage a variety

of tasks. Regression analysis is a type of machine learning which is used to establish relationship among a set of dependent and independent variables. The significance and accuracy of a regression model can be accessed through different indices and performance metrics, such as coefficient of determination (R^2), MAE (mean absolute error), MSE (mean squared error), ME (max error) and MAPE (mean absolute percentage error). Which have been used in this study.

a) Coefficient of determination (R^2): The correlation between the observed and the predicted values and effectiveness of the model can be assessed by R^2, which is defined as below

$$R^2 = 1 - \frac{SSres}{SStot} \quad \text{..... (6.3)}$$

Where, the value of R^2 lies between 0 to 1. The closeness of R^2 to 1 signifies the betterment of the fit, and R^2 =0 implies the absolute mismatch among the variables.

b) Mean absolute error (MAE): It is a performance metric used for regression models. It measures accuracy of a model on a test data set by averaging the absolute differences between the predicted and actual values for all instances in the test set. Essentially, each prediction error is calculated as the difference between the predicted value and the actual value. MAE is one of several metrics used to evaluate and summarize the performance of a machine learning model.

$$MAE(y, x) = \left(\frac{1}{n_{samples}}\right) \sum_{i=0}^{n_{samples}-1} |y_i - x_i| \quad \text{..... (6.4)}$$

Where y_i represents the actual values, x_i represents the expected values.

c) Mean squared error (MSE): This is another widely used metric for assessing the performance of regression models. It calculates the average of the squared differences between the predicted and actual values of the target variable.

In other words, it quantifies the average squared "error" between the predicted values and the actual values, giving more weight to larger errors. The formula for the calculating the MSE is as follows:

$$MSE = \frac{1}{n}\sum_{i=1}^{n}(y_i - \hat{y}_i)^2 \quad \text{..... (6.5)}$$

Where,

n is the number of data points.

y_i is the actual target value for the i^{th} data point.

$\hat{y}_i$ is the predicted value for the i^{th} data point.

d) Max Error (ME): The worst-case error between the expected and actual numbers is represented by the function max error, which calculates the greatest standard error. The maximum error in a completely fitted single-output regression analysis would be zero on the test set, which is extremely improbable in real-world scenarios. This measure shows how much error the model shows when used with actual data.

$$\mathbf{MaxError(y, x) = max(|y_i - x_i|)} \quad \textbf{(6.6)}$$

Where y_i describes the actual values, x_i describes the expected values.

e) Mean absolute percentage error (MAPE): It is a metric that expresses the percentage difference between the expected and actual values as a means of assessing the forecasting or precision of regression model. It is especially helpful when attempting to determine the relative magnitude between the actual and predicted values of a given variable.

The formula for calculating MAPE is given below:

$$\text{MAPE} = \frac{1}{n}\sum_{i=1}^{n}\frac{|y_i - \hat{y}_i|}{y_i} \cdot 100\% \quad \textbf{(6.7)}$$

where,

y_i is the actual target value for the i^{th} data point.

$\hat{y}_i$ is the predicted value for the i^{th} data point.

6.8.2 Regression Models:

The pull-out capacity of anchor plate in different soil condition, such as reinforced and unreinforced bed has been considered as the dependent variable for the regression analysis. The influencing parameters, as per the test configurations, such as the plate size, inclination angle, embedment ratio, soil type, frequency and amplitude of the cyclic load have been considered as the independent variables. The regression analysis was performed using four machine learning techniques (such as Linear Regression, Random Forest Regression, SGD Regression and XGBoost Regression) with Python language (version 3.10.6) in Jupyter Notebook (version 6.4.12).

The data set has been used in the regression analysis were obtained from the numerical investigations. Because of lack of enough experimental results, in each regression model 80%

of data has been used to train the model and generate the regression coefficients and the remaining data has been used for the testing purpose.

Then, hyperparameter tunning has been done for each model. Hyperparameter tuning is a crucial step in the process of developing machine learning models. Hyperparameters are settings that are not learned directly from the data during the training process, but rather are set by the user before training begins. They have a substantial impact on the performance of the model and generalization capabilities. The goal of hyperparameter optimization is to determine the global optimal value x^* of the objective function f(x), which can be evaluated for any arbitrary x $\boldsymbol{x}\in\boldsymbol{X}$, x^*=arg min $\boldsymbol{x}\in\boldsymbol{X}$ $f(xx)$ and X represents the hyperparameter space containing categorical, discrete, and continuous variables. Effective hyperparameter optimization techniques streamline the process of identifying the best hyperparameters for constructing various machine learning models. This method includes four main components: first, an estimator, which could be a regressor or classifier with one or more objective functions; second, a search space; third, an optimization method to find the best combinations; and fourth, a function to compare the effectiveness of different hyperparameter configurations. Common hyperparameter optimization techniques used in this study include Grid Search, Random Search, and Bayesian Optimization.

The evaluation of the four models has been done with the performance metrics and the results obtained from all the models (with different hyperparameter tunning process also) are presented in the Table 6.38.

Table 6.38: Model summary

SCORE	LINEAR REGRESSION	RANDOM FOREST REGRESSION				SGD REGRESSION				XGBOOST REGRESSION			
		Default HP	Bayesian optimization Technique	Random Search Technique	Grid Search CV Technique	Default HP	Bayesian optimization Technique	Random Search Technique	Grid Search CV Technique	Default HP	Bayesian optimization Technique	Random Search Technique	Grid Search CV Technique
R2 Score	0.923	0.976	0.977	0.977	0.971	0.923	0.923	0.923	0.923	0.989	0.997	0.997	0.996
Mean Absolute Error (MAE)	8.099	4.371	3.429	4.295	4.947	8.098	8.097	8.098	8.099	2.743	1.639	1.638	1.816
Mean Squared Error (MSE)	127.720	40.253	31.914	37.969	48.575	127.653	127.726	127.817	127.704	18.889	4.851	4.682	8.478
Maximum Error (ME)	42.773	18.592	21.430	19.103	19.479	42.803	42.822	42.872	42.780	17.583	7.638	5.371	7.688
Mean Absolute Percentage Error (MAPE)	0.117	0.048	0.0379	0.048	0.054	0.117	0.117	0.117	0.118	0.029	0.019	0.021	0.025

The results showed that the XGBoost model performed consistently well in respect of all criteria. It performed better than the other machine learning models, having the lowest error metrics and high accuracy. Specifically, it achieved R^2 score of 0.997, MAE of 1.638, MSE

of 4.602, ME of5.731 and MAPE of 0.021% respectively, indicating superior accuracy and precision in predicting pullout capacity. These findings lead to the conclusion that the XGBoost model performs very well while utilizing data with few input variables, as it estimates the uplift capacity of anchors. Based on these results, this may be inferred that the XGBoost model is highly effective at accurately predicting uplift capacity of inclined anchors using the data with minimal input features, based on the parameters considered in this study as independent and dependent variables.

Fig. 6.62 illustrates the correlation of actual uplift load and predicted uplift load using the XGBoost Regression model, which results in ±10% error indicated by red lines. The green line show deviation between actual values from predicted ones.

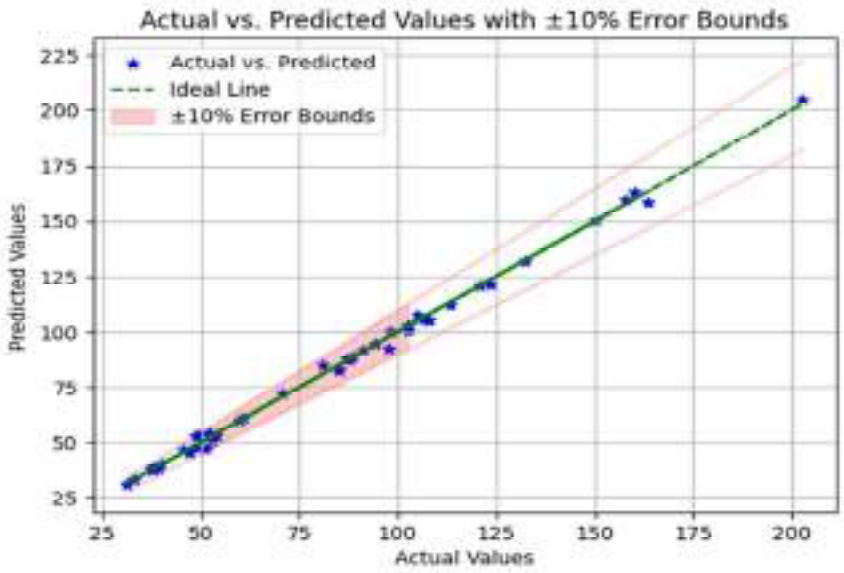

Fig. 6.62: Scatter plot illustrating the correlation between actual vs predicted values (XGBoost Regression)

The model is developed based on a limited number of datasets, which may have limitations in terms of robustness.

Incorporating additional experimental and field data across different soil conditions, anchor types, and loading scenarios may enhance the accuracy and robustness of the model. Using a more comprehensive dataset would improve its predictive capabilities. Additionally, varying the dependent parameters used in the regression analysis could generate more data points, thereby refining the prediction model and increasing its accuracy

6.9 SUMMARY

This chapter has provided an evaluation of response of inclined anchors under both static and cyclic loading, based on findings from numerical and experimental research conducted in cohesive soil beds under both reinforced and unreinforced conditions. It has also included the effects of the plate size, inclination angle and embedment ratio on ultimate pullout capacity. The response of the inclined anchor has also been found due to inclusion of reinforcement for both static and cyclic loading. Finally, a regression analysis has been carried out using machine learning to create a predictive model of the ultimate uplift capacity of inclined anchors, comprising of independent factors, such as, plate size, inclination angle, embedment ratio, along with frequency and amplitude of cyclic loading.

CHAPTER 7

SUMMARY, CONCLUSIONS, LIMITATION AND FUTURE SCOPE OF STUDY

7.1 SUMMARY

In order to study the behaviour of inclined plate anchors numerical analysis has been done by ABAQUS software. In the analysis the following parameters have been varied:

a) Plate anchor Size: 25 mm × 25 mm, 50 mm × 50 mm, and 75 mm × 75 mm
b) Embedment ratio: 1, 2 and 3.
c) Inclination angle: 30°, 45°, and 60° with vertical

The soil has been modelled considering material nonlinearity and Mohr Columb criteria.

The anchor has been modelled as 2-D wire elements. Interaction at the soil-anchor interface has been considered with soil as slave surface and anchor as master surface.

The study has been done with both unreinforced and reinforced soil bed with geotextile reinforcement with its width having four times that of the plate width and placed at a distance of 0.25 times the depth of embedment above the bottom surface of the plate.

Soil, anchor material and geotextile have been tested to determine their respective properties.

The numerical studies have been performed with static and cyclic loading.

The cyclic load has been considered to be applied with the following parameters

i. Frequency: 0.2 Hz, 0.5 Hz
ii. Amplitude: 2 mm and 5 mm

Further an attempt has been made to supplement this numerical study by conducting limited number of laboratory model tests. The tests have been done under similar conditions, considered in the numerical study. Total 42 experiments have been conducted varying the parameters as follows:

In general, the numerical results have been found to agree with experimental ones. The study has been done to emphasis on the behaviour of inclined anchors in reinforced clay bed under cyclic loading.

7.2 CONCLUSIONS:

The following conclusions may be drawn from the present study:

A. For unreinforced and reinforced bed under static loading:

i) As the embedment ratio becomes higher, the pullout capacity also becomes higher for both reinforced and unreinforced soil bed when the plate size, the inclination angle, frequency, and amplitude of the cyclic loading remain unchanged.

   a) When 75 mm plate is placed in unreinforced soil bed with anchor inclined at 45°with vertical, the maximum increase in pullout capacity of 66.66% has been obtained, when embedment ratio increases from 1 to 3.

   b) For 50 mm plate, placed in reinforced soil bed with anchor inclined at 45° shows the maximum increase in pullout capacity of 191.67% when embedment ratio increases from 1 to 3.

ii) The pullout capacity increases for both cases with increasing inclination angles (with respect to the vertical), while other factors remain constant.

   a) For 50 mm plate, placed in unreinforced soil bed at embedment ratio 1 shows maximum increase in pullout capacity of 96.77% when inclination angle changes from 30^0 to 60°.

   b) When 50 mm plate is placed at embedment ratio 1 shows maximum increase in pullout capacity of 89.61% when inclination angle changes from 30^0 to 60°, in reinforced soil bed.

iii) While the embedment ratio, inclination angle, frequency, and amplitude of the cyclic loading are constant, the pullout capacity of both reinforced and unreinforced beds increases as the plate size increases.

   a) In unreinforced soil bed, for inclined anchor at embedment ratio 3, with an inclination angle 60° pullout capacity increases maximum by 431.91% when plate size changes to 75 mm from 25 mm.

   b) In reinforced soil bed, for embedment ratio 3, with an inclination angle 60° pullout capacity increases maximum by 512.9% when plate size changes to 75 mm from 25 mm

iv) Breakout factor has increased with the increase in embedment ratio for any particular plate size for both cases.

a) For inclined anchor plate in unreinforced soil bed, maximum Breakout factor has been observed as 3.94 for 25 mm plate at an inclination angle 60° at embedment ratio 3.

b) For inclined anchor plate in reinforced soil bed, maximum breakout factor of 5.99 has been observed for 25 mm anchor plate with inclination angle 60^0 at embedment ratio 3.

v) Maximum pullout load improvement factor of 2.25 has been observed when the plate size of 50 mm at embedment depth ratio 3 at inclination angle of 45° has been placed in reinforced soil bed from unreinforced soil bed.

B. For unreinforced and reinforced soil bed under cyclic loading

i) As the plate dimension becomes higher, the pullout capacity also becomes higher for both reinforced and unreinforced bed when the embedment ratio, the inclination angle, frequency, and amplitude of the cyclic loading do not vary.

a) For unreinforced bed, when embedment ratio 3, with inclination angle 45° under 0.5 Hz frequency 2 mm amplitude cyclic load, anchor plate shows the maximum increase in pull capacity of 74.6% when plate size increases 25 mm to 75mm.

b) For reinforced bed, the maximum pullout capacity improves by approximately 81.127% when the plate size increases from 25 mm to 75 mm at an inclination angle of 60°, embedment ratio of 2, and 2 .m amplitude under 0.5 Hz frequency for reinforced bed.

ii) When the plate size, inclination angle, frequency, and amplitude of cyclic loading remain constant, the embedment ratio increases, as does the pullout capacity for both reinforced and unreinforced soil beds.

a) When inclined anchor plate is placed in unreinforced soil bed, for 25mm plate inclined at 45° under 0.5 Hz frequency 2 mm amplitude cyclic load, shows the maximum increase in pull out capacity of 34.52% when embedment ratio increases from 1 to 3.

b) In reinforced soil bed, for 25mm plate inclined at 30° under 0.2Hz frequency 2mm amplitude cyclic load, shows the maximum increase in pull capacity of 31.703% when embedment ratio increases from 1 to 3.

iii) With the increase in inclination angles (with respect to the vertical plane), the pullout capacity also becomes higher, other variables being unchanged.

a) When the inclination angle changes from 30° to 60°, at a fixed embedment ratio of 3, for 0.050 m plate in unreinforced soil bed under 0.2 Hz frequency and 5 mm amplitude, the pullout capacity increases by about 30.88%, as obtained from numerical analysis.

b) For 50 mm plate, placed in reinforced soil bed at embedment ratio 1 shows maximum increase in pull out capacity of 36.442% when inclination angle (with respect to vertical) changes from 30 to 60° under 0.2 Hz frequency and 5 mm amplitude cyclic load

iv) Increase in pullout load is generally more for cyclic load with equal frequency when amplitude changes from 2 to 5 mm. In other words, with increase in amplitude, higher pullout load is required to displace the plate when other parameters remain the same.

a) When cyclic load amplitude increases from 2 mm to 5 mm at 0.5 Hz frequency, pull out load increases 152.924% for 25mm square plate in unreinforced soil bed, with 30° inclination and embedment ratio 3.

b) When cyclic load amplitude increases from 2 mm to 5 mm at 0.2 Hz frequency, maximum pull-out load increases by. almost 165.567% for 25 mm square plate in reinforced soil bed, with a 60° inclination angle and embedment ratio of 3,

v) Increase in pullout load is generally more for cyclic load with same amplitude when frequency changes from 0.5 to 0.2 Hz. This may be attributed to mor impact of dynamic force with decrease in frequency when other parameters remain the same.

a) 25mm square plate in unreinforced soil bed, with 30° inclination and embedment ratio 3, shows maximum pull-out load increases 16.59% when cyclic load frequency decreases from 0.5 Hz to 0.2 Hz at 2mm amplitude.

b) For a 75 mm square plate, with 30° inclination and embedment ratio 3, when cyclic load frequency decreases from 0.5 Hz to 0.2 Hz at 2 mm amplitude, pull-out load increases maximum about 17.27 %.

vi) Maximum increase in pull capacity of 27.2% has been observed for 75 mm square plate with a 45° inclination angle and embedment ratio of 2 when cycling loading frequency and amplitude are 0.5 Hz and 2 mm respectively.

C. Prediction Model:

From regression analysis it has been found that the XGBoost model has achieved R^2 score of 0.997, MAE of 1.638, MSE of 4.602, ME of 5.731 and MAPE of 0.021% respectively. The values demonstrate its overall superior performance and high accuracy in predicting pullout load, even when trained with minimal input features. Therefore, due to its outstanding performance among various metrics, the XGBoost model may be considered as a software package for easy and precise prediction of anchor pullout load.

7.3 DESIGN RECOMMENDATIONS FOR INCLINED ANCHORS IN REINFORCED COHESIVE SOIL UNDER STATIC AND CYCLIC LOADING CONDITION:

With the help of regression analysis, the pullout capacity of inclined anchors in reinforced cohesive soil under both static and cyclic loading conditions can be accurately predicted. These predictive models can then be utilized to develop practical design recommendations. By using regression-based equations, engineers can estimate the pullout capacity for various anchor inclinations, reinforcement configurations, and loading scenarios, thereby optimizing anchor design for enhanced stability and performance. From the study it has found that the XGBoost model performed consistently well in respect of all criteria. It performed better than the other machine learning models, having the lowest error metrics and high accuracy. Specifically, it achieved R2 score of 0.997, MAE of 1.638, MSE of 4.602, ME of5.731 and MAPE of 0.021% respectively, indicating superior accuracy and precision in predicting pullout capacity. These findings lead to the conclusion that the XGBoost model performs very well while utilizing data with few input variables, as it estimates the uplift capacity of anchors. Based on these results, this may be inferred that the XGBoost model is highly effective at accurately predicting uplift capacity of inclined anchors using the data with minimal input features, based on the parameters considered in this study as independent and dependent variables, which may be utilised as design purpose

7.4 LIMITATIONS:

The limitations of the study are:

1. The study has been conducted only with 30^o, 45^o and 60^o inclination angles.
2. The study has been conducted only with square plate sizes of 25 mm × 25 mm, 50 mm × 50 mm and 75 mm × 75 mm dimensions.
3. The variation considered in embedment ratios are only three viz. 1, 2, and 3.

4. In this study homogeneous soft clay with particular specific properties has been considered.
5. The regression analysis relied solely on the numerical analysis data for training ML models and the dataset has limited input features.

7.5 FUTURE SCOPE OF STUDY:

The key findings of the study have been summarized as quantitative variations, which have been addressed in detail throughout the conclusion chapter. However, there is scope to expand the future work section by incorporating more specific research questions or hypotheses that can be explored further in the following manner:

a) The Study may be extended for different shapes of anchors (like- circular and strip anchor) by which effect of shape factor may be studied.

b) The study may be extended for more angles of inclination of anchors which may range from 10-85 degree.

c) The study may be extended for different types of soil (sand or clay) with different soil properties as well as layered soil. In layered soil, the thickness of the layers and order of the layers may be varied to extend the study.

d) Anchor test should be done in the field as well as the model anchors in lab and simulation should be done by appropriate numerical method. This will generate large number of datasets for prediction model.

REFERENCES

Andreadis, A., Burley, E., & Harvey, R. C. (1981). Embedded anchor response to uplift loading. Journal of the Geotechnical Engineering Division, 107(1), 59-78.

Balla, A. (1961). "The resistance to breaking out of mushroom foundations for pylons". Proc. 5th Intl. Conf. on Soil Mechanics and Foundation Engineering, Paris, France: pp.569-576.

Banerjee, S., Nagaraju, M. (2017). Pullout behaviour of square anchor plates in reinforced soft clay. International Journal of Geosynthetics and Ground Engineering, 3(3).

Bhattacharya, P., Bhowmik, D., Mukherjee, S. P., & Chattopadhyay, B. C. (2008). Pullout Behaviour of Square Anchors in Reinforced Clay.

Bhattacharya, P., & Kumar, J. (2016). Uplift Capacity of Anchors in Layered Sand Using Finite-Element Limit Analysis: Formulation and Results. International Journal of Geomechanics, 16(3).

Biradar, J., Banerjee, S., Shankar, R., Ghosh, P., Mukherjee, S., Fatahi, B. (2019). Response of square anchor plates embedded in reinforced soft clay subjected to cyclic loading. Geomechanics and Engineering, 17(2), 165-173.

Chattopadhyay, B. C., & Pise, P. J. (1986). Breakout resistance of horizontal anchors in sand. Soils and Foundations, 26(4), 16–22.

Das, B. M., Puri, V. K. (1989). Holding capacity of inclined square plate anchors in clay. Soils and Foundations, 29(3), 138–144.

Das, B. M., Tarquin, A. J., & Moreno, R. (1985). Model tests for pullout resistance of vertical anchors in clay. Civil Eng. for Practicing and Design Engineers, 4(2), 191-209.

Dickin, E. A., & Leung, C. F. (1983). Centrifuge model tests on vertical anchor plates. J. Geotech. Engg., 1503–1525.

Ghaly, M. Ashraf. (1997). Load-Displacement Prediction for Horizontally Loaded Vertical Plates. Journal of Geotechnical and Geoenvironmental Engineering, 123(1), 74–76.

Ghaly, M. Ashraf, & Clemence, P. Samuel. (1998). Pullout Performance of Inclined Helical Screw Anchors in Sand. Journal of Geotechnical and Geoenvironmental Engineering, 124(7), 617–627.

Ghaly. A, Hanna. A, Hanna. M, (1991), "Uplift Behavior of Screw Anchors in Sand". I: Dry Sand, International Journal of Rock Mechanics & Mining Sciences & Geomechanics Abstracts 117(5).

Goel, S., Shalini, & Patra,N. R. (2006). Break out resistance of inclined anchors in sand. Geotechnical & Geological Engineering, 24(6), 1511–1525.

Hanna, A. M., Das, B. M. and Foriero, A. (1988): Behavior of shallow inclined plate anchor in sand. In Special Topics in Foundations, ASCE Geotech. Special Publication, 16, pp. 54-7.

Harvey, R. C., & Burley, E. (1973). Behavior of shallow inclined anchorages in cohesionless sand. Ground Engineering, 6(5).

Ilamparuthi, K., Dickin, E. A., & Muthukrisnaiah, K. (2002). Experimental investigation of the uplift behaviour of circular plate anchors embedded in sand. Canadian Geotechnical Journal, 39(3), 648–664.

Khatri, V. N., & Kumar, J. (2009). Vertical uplift resistance of circular plate anchors in clays under undrained condition. Computers and Geotechnics, 36(8), 1352–1359.

Mariupol'skii, L. G. (1965). The bearing capacity of anchor foundations. Soil Mechanics and Foundation Engineering, 2(1), 26-32.

Mendoza C.E., Colmenares J.E. & Merchán V.E. (2005). Stiffness of unsaturated compacted clayey soils at very small strains, Proc. Int. Symp. on Advanced Experimental Unsaturated Soil Mechanics, Trento, Italy, June 27 – 29. 2005: 199-204.

Merifield, R. S., Lyamin, A. V., Sloan, S. W., & Yu, H. S. (2003). Three-Dimensional Lower Bound Solutions for Stability of Plate Anchors in Clay. Journal of Geotechnical and Geoenvironmental Engineering, 129, 243–253.

Merifield, R. S., Lyamin, A. V., & Sloan, S. W. (2005). Stability of Inclined Strip Anchors in Purely Cohesive Soil. Journal of Geotechnical and Geoenvironmental Engineering, 131(6), 792–799.

Merifield, R. S., Sloan, S. W., & Yu, H. S. (2001). Stability of plate anchors in undrained clay. Geotechnique, 51(2), 141–153.

Meyerhof, G. G. and Adams, J. I. (1968). The ultimate uplift capacity of foundations. Canadian Geotechnical Journal, 5(4), 225-244.

Mistri, B., & Singh, B. (2011). Pullout Behavior of Plate Anchors in Cohesive Soils. Electronic Journal of Geotechnical Engineering, 16.

Moghaddas Tafreshi, S. N., Rahimi, M., Dawson, A. R., & Leshchinsky, B. (2019). Cyclic and post-cycling anchor response in geocell-reinforced sand. Canadian Geotechnical Journal, 56(11), 1700-1718.

Murray, E. J., & Geddes, J. D. (1989). Resistance of passive inclined anchors in cohesionless medium.

Nene, A. S., & Garg, S. (1991). Behaviour of shallow plate anchors in reinforced cohesive soils. Indian Geotechnical Journal, 21(4), 327-336.

Niroumand, H., Kassim, K. A., & Nazir, R. (2010). Analytical and numerical studies of vertical anchor plates in cohesionless soils. Electronic Journal of Geotechnical Engineering, 15.

Niroumand, Hamed & Kassim, Khairul & Nazir, Ramli. (2012). The Role of Soil Anchors in Construction Projects. Archives Des Sciences Journal. 65. 1661-464.

Niroumand, H., Kassim, K. A., & Nazir, R. (2013). The influence of soil reinforcement on the uplift response of symmetrical anchor plate embedded in sand. Measurement, 46(8), 2608-2629.

Nouri, H., Biscontin, G., & Aubeny, C. P. (2017). Numerical prediction of undrained response of plate anchors under combined translation and torsion. Computers and Geotechnics, 81, 39-48.

O'Beirne, C., O'Loughlin, C. D., & Gaudin, C. (2017). Assessing the penetration resistance acting on a dynamically installed anchor in normally consolidated and over consolidated clay. Canadian Geotechnical Journal, 54(1), 1-17.

Oh, W. T., & Vanapalli, S. K. (2011). Relationship between Poisson's ratio and soil suction for unsaturated soils. In Proc., 5th Asia-Pacific Conf. on Unsaturated Soils (pp. 239-245). Bangkok, Thailand: Kasetsart Univ.

Rao, K. S. S., & Kumar, J. (1994). Vertical uplift capacity of horizontal anchors. Journal of Geotechnical Engineering, 120(7), 1134-1147.

Ravichandran, P. T., Ilamparuthi, K., & Toufeeq, M. M. (2008, October). Study on uplift behaviour of plate anchors under monotonic and cyclic loading in geo-grid reinforced sand bed. In Proceedings of the 12th International Conference of International Association for Computer Methods and Advances in Geomechanics (IACMAG) (pp. 1-6).

Ravishankar, S., Banerjee, S., & Sarvesh, et al. (2022). Static, Cyclic, and Post-cyclic Pullout Response of Horizontal Plate Anchors in Reinforced Soft Clay. International Journal of Geosynthetics and Ground Engineering, 8, 37.

Rowe, R. K., & Davis, E. H. (1982). The behaviour of anchor plates in sand. Geotechnique, 32(1), 25-41.

Saran, S., Ranjan, G. and Nene, A. S. (1986): Soil anchors and constitutive laws. Journal of Geotechnical Engineering, 112(12), pp. 1084-1100.

Sengupta, A., Mukherjee, S., & Ghosh, A. (2017). Improvement of Bearing Ratio of Clayey Subgrade Using Compacted Flyash Layer. Geotech Geol Eng, 35, 1885–1894.

Singh, B., & Mistri, B. (2011). A study on load capacity of horizontal and inclined plate anchors in sandy soils. International Journal of Engineering Science and Technology, 3(9), 6914–6922.

Singh, S. P., & Ramaswamy, S. V. (2008). Influence of frequency on the behaviour of plate anchors subjected to cyclic loading. Marine Geo resources and Geotechnology, 26(1), 36-50.

Subramaniam, P., & Banerjee, S. (2013). Shear modulus degradation model for cohesive soils. Soil Dynamics and Earthquake Engineering, 53, 210-216.

Subramaniam, P., & Banerjee, S. (2014). Factors affecting shear modulus degradation of cement treated clay. Soil Dynamics and Earthquake Engineering, 65, 181-188.

Tagaya, K., Scott, R. F., & Aboshi, H. (1988). Pullout resistance of buried anchor in sand. Soils and Foundations, 28(3), 114–130.

Thorne, C. P., Wang, C. X., & Carter, J. P. (2004). Uplift capacity of rapidly loaded strip anchors in uniform strength clay. Geotechnique, 54(8), 507-517..

Vesić, A. S. (1971). Breakout resistance of objects embedded in ocean bottom. Journal of the Soil Mechanics and Foundations Division, 97(9), 1183-1205.

Wang, D., Hu, Y., & Randolph, M. F. (2010). Three-Dimensional Large Deformation Finite-Element Analysis of Plate Anchors in Uniform Clay. Journal of Geotechnical and Geoenvironmental Engineering, 136(2), 355–365.

Yu, L., Liu, J., Kong, X. J., & Hu, Y. (2011). Numerical study on plate anchor stability in clay. Geotechnique, 61(3), 235–246.

Yu, L., Zhou, Q., & Liu, J. (2015). Experimental study on the stability of plate anchors in clay under cyclic loading. Theoretical and Applied Mechanics Letters, 5(2), 93-96.

https://www.williamsform.com/concrete/cast-in-place-concrete-anchors.

ANNEXURE -I

DEGREE OF SATURATION AND POISSON'S RATIO DETERMINATION

Average water content during testing (w) = 18%

Unit wt. of compacted soil during testing (γ) = 19.38 kN/m^3

Specific Gravity of soil (G) = 2.67

Dry Density of soil $\gamma_d = \frac{\gamma}{1+w} = \frac{19.38}{1+0.18} = 16.42$ kN/m^3

Degree of Saturation determination:

$$\frac{G(1+w)\gamma_w}{1+\frac{wG}{S_r}} = \gamma$$

Using the values of $\gamma_w, w \text{ and } G$, Degree of saturation ($S_r$) has been determined to be 0.768. (Approximately 77%).

Poisson's ratio of the clay is taken 0.33 from the reference of Oh et al, (2011).

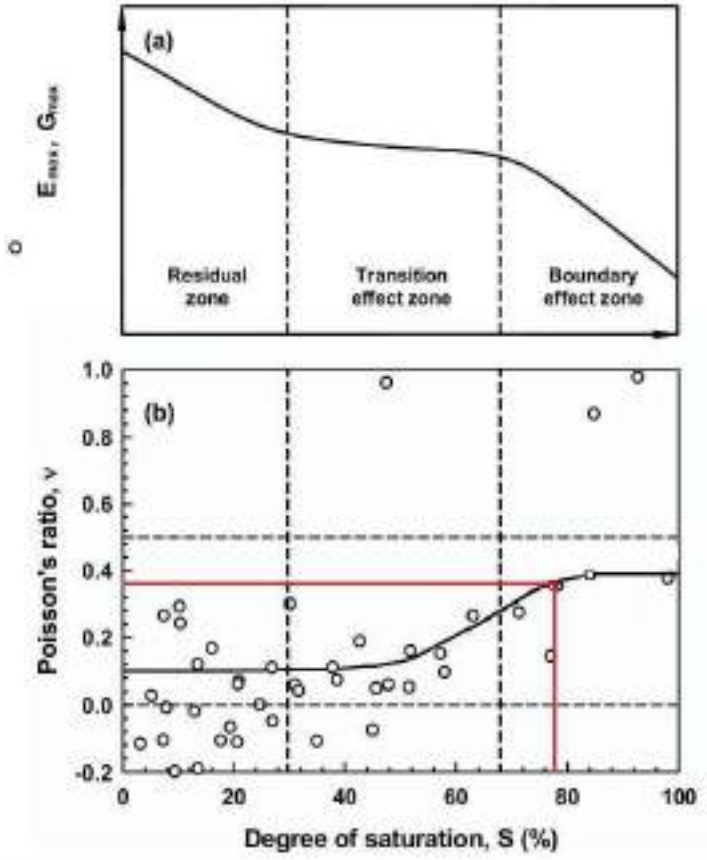

Degree of saturation, back calculated Poisson's ratio, with respect to degree of saturation, S (analyzing data from Mendoza et al. 2005).

ANNEXURE -II

PRESENTATION OF RESULTS OF NUMERICAL ANALYSIS (STATIC UNREINFORCED)

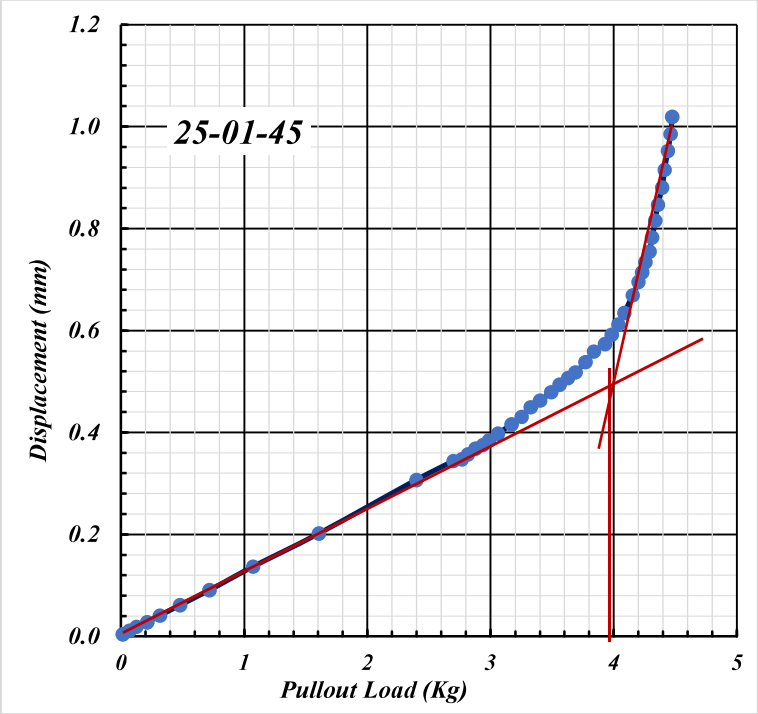

Fig. 4.5: Load vs Axial movement for 25mm Square Plate with (H/B=1) inclined at 45° with Vertical in unreinforced soil

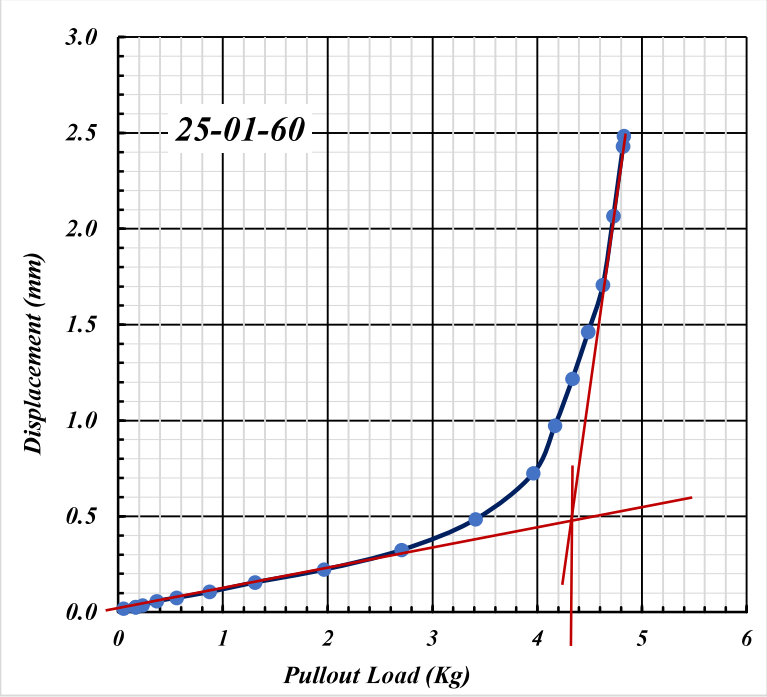

Fig. 4.6: Load vs Axial movement for 25mm Square Plate with (H/B=1) inclined at 60° with vertical in unreinforced soil

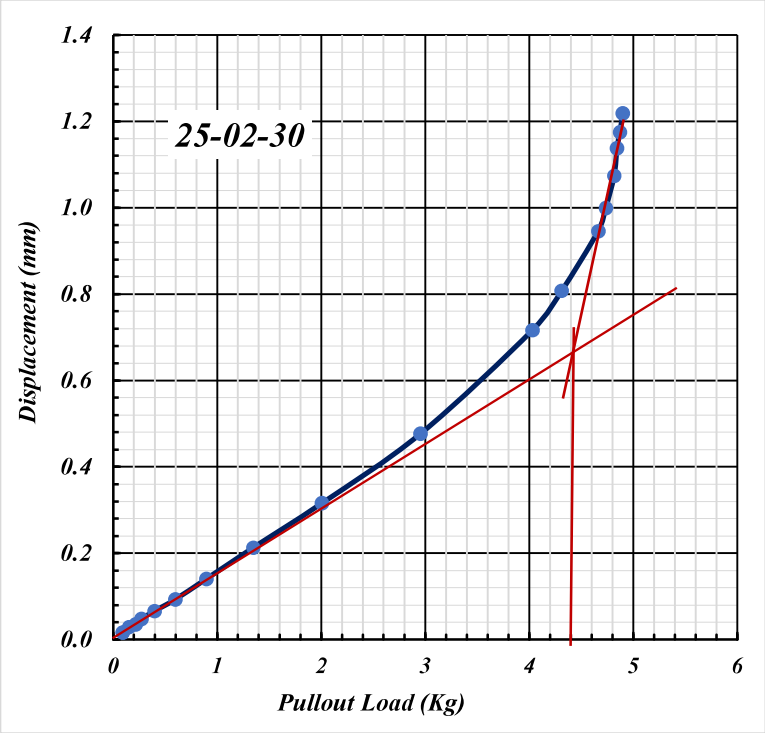

Fig. 4.7: Load vs Axial movement for 25mm Square Plate with (H/B=2) inclined at 30° with vertical in unreinforced soil

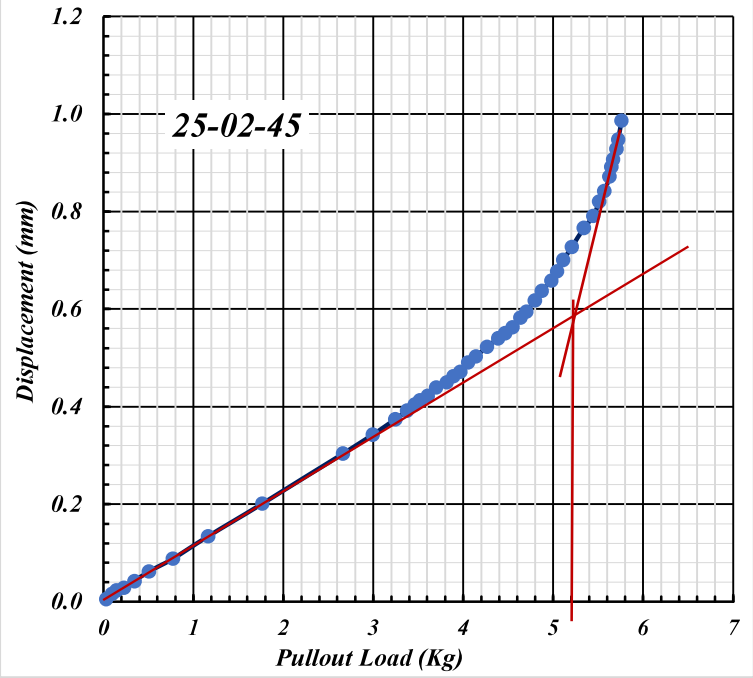

Fig. 4.8: Load vs Axial movement for 25mm Square Plate with (H/B=2) inclined at 45° with vertical in unreinforced soil

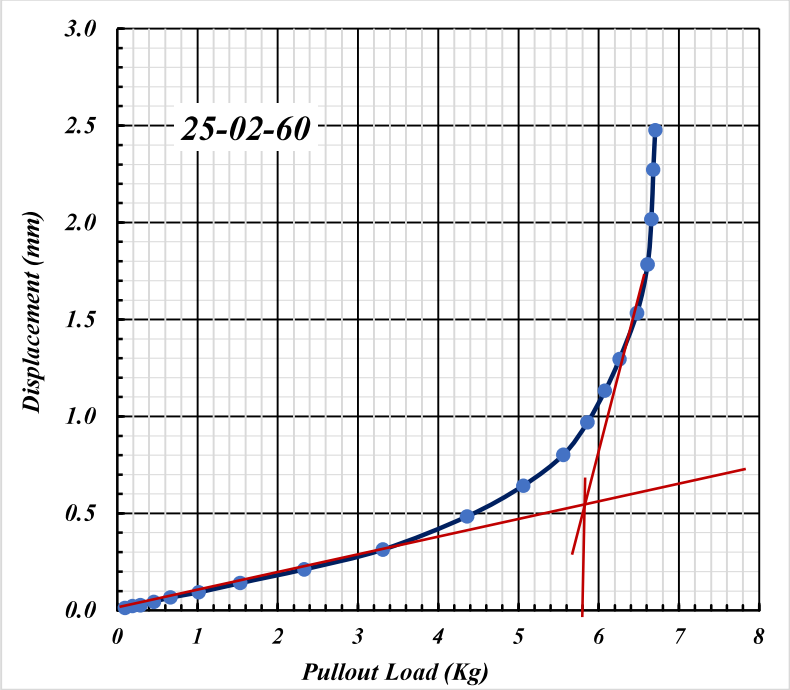

Fig. 4.9: Load vs Axial movement for 25mm Square Plate with (H/B=2) inclined at 60° with vertical in unreinforced soil

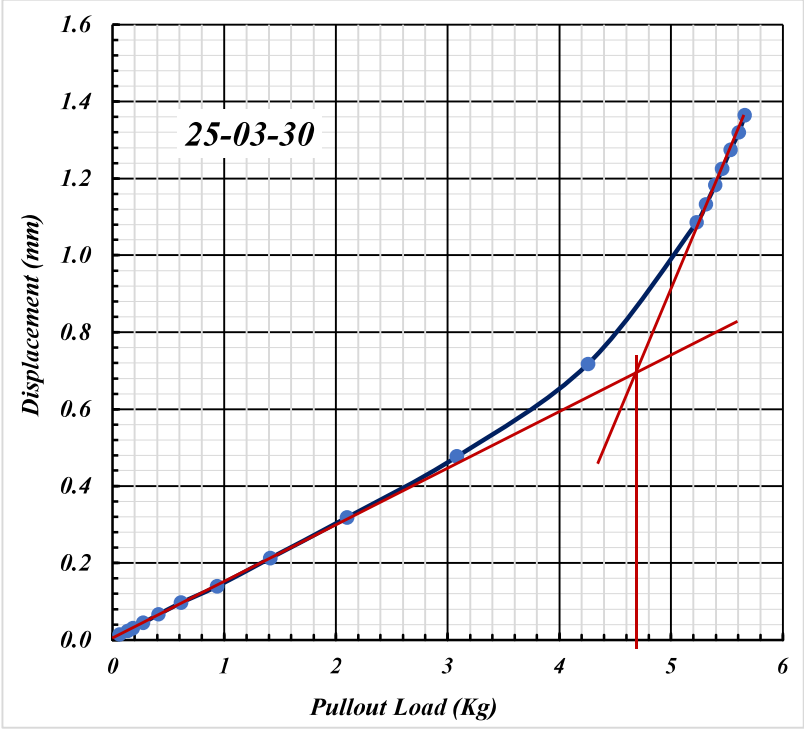

Fig. 4.10: Load vs Axial movement for 25mm Square Plate with (H/B=3) inclined at 30° with vertical in unreinforced soil

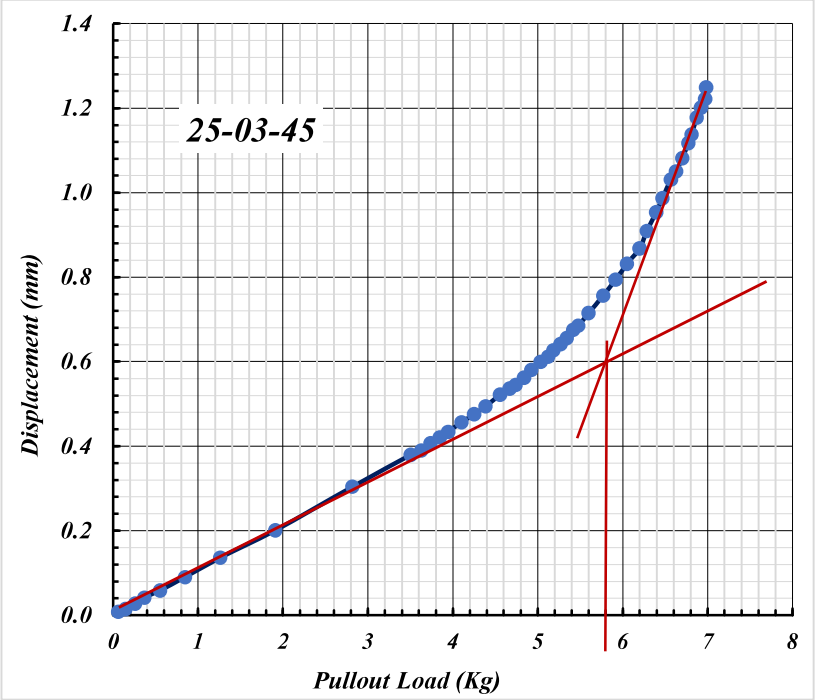

Fig. 4.11: Load vs Axial movement for 25mm Square Plate with (H/B=3) inclined at 45° with vertical in unreinforced soil

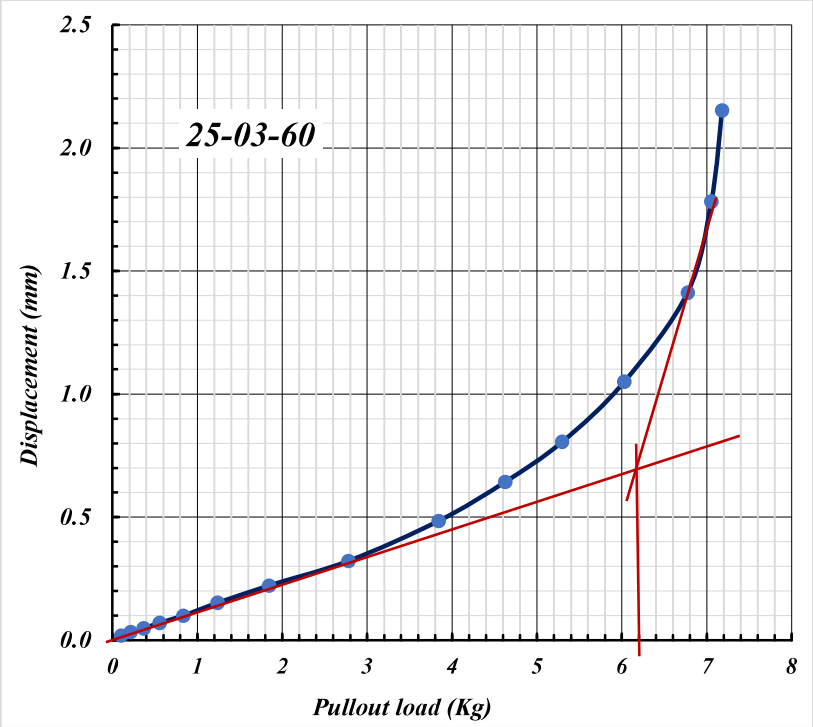

Fig. 4.12: Load vs Axial movement for 25mm Square Plate with (H/B=3) inclined at 60° with vertical in unreinforced soil

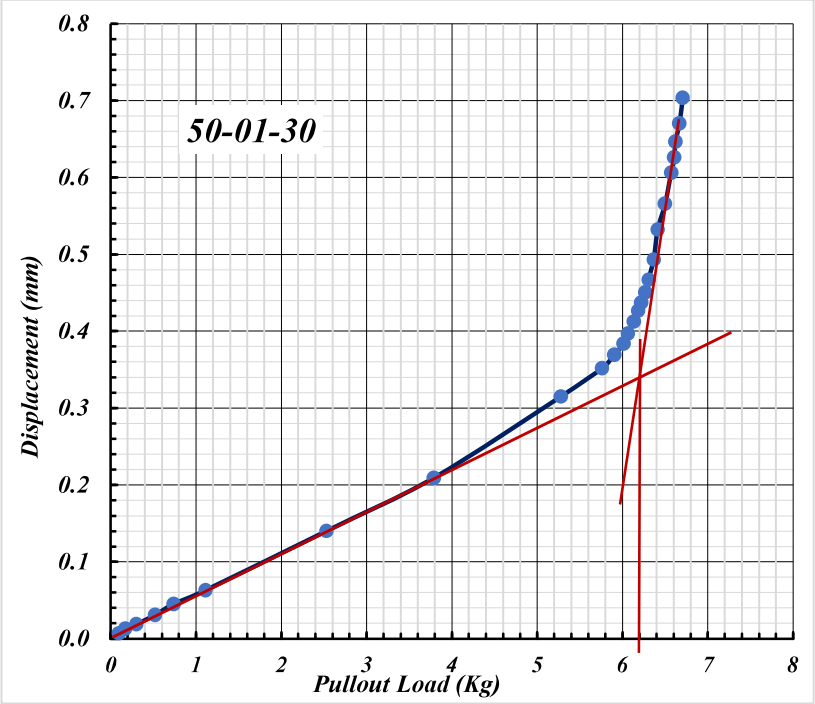

Fig. 4.13: Load vs Axial movement for 50mm Square Plate with (H/B=1) inclined at 30° with vertical in unreinforced soil

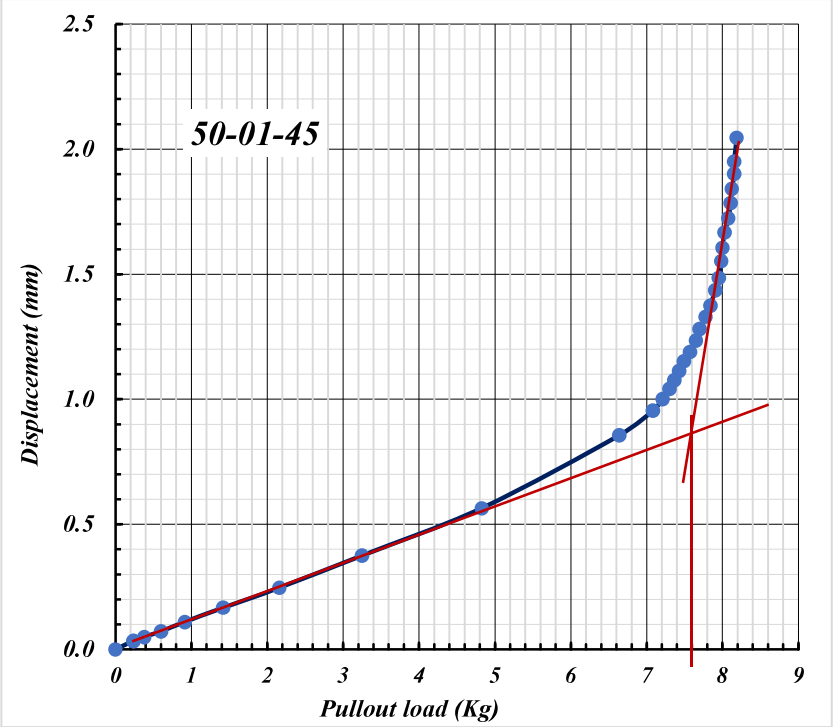

Fig. 4.14: Load vs Axial movement for 50mm Square Plate with (H/B=1) inclined at 45° with vertical in unreinforced soil

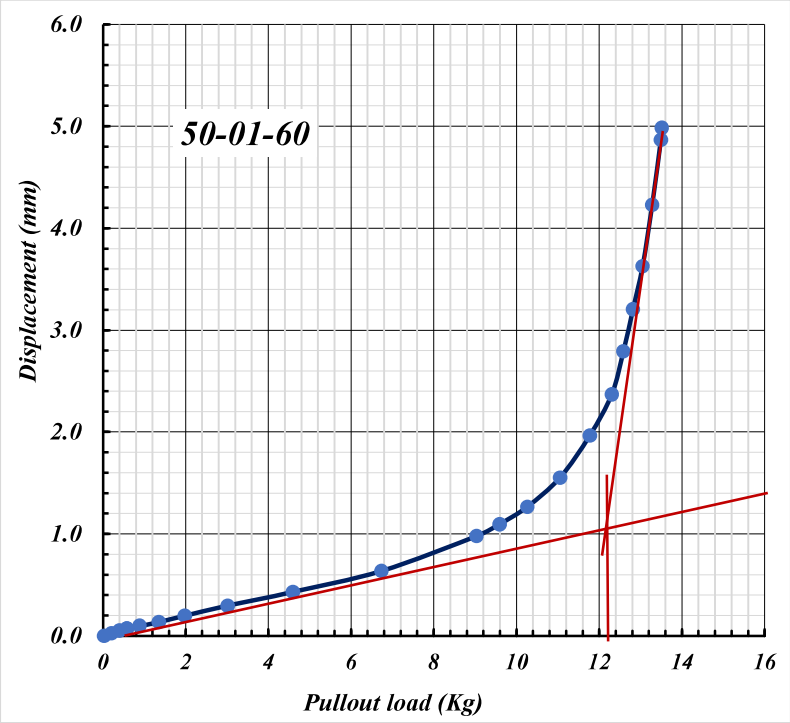

Fig. 4.15: Load vs Axial movement for 50mm Square Plate with (H/B=1) inclined at 60° with vertical in unreinforced soil

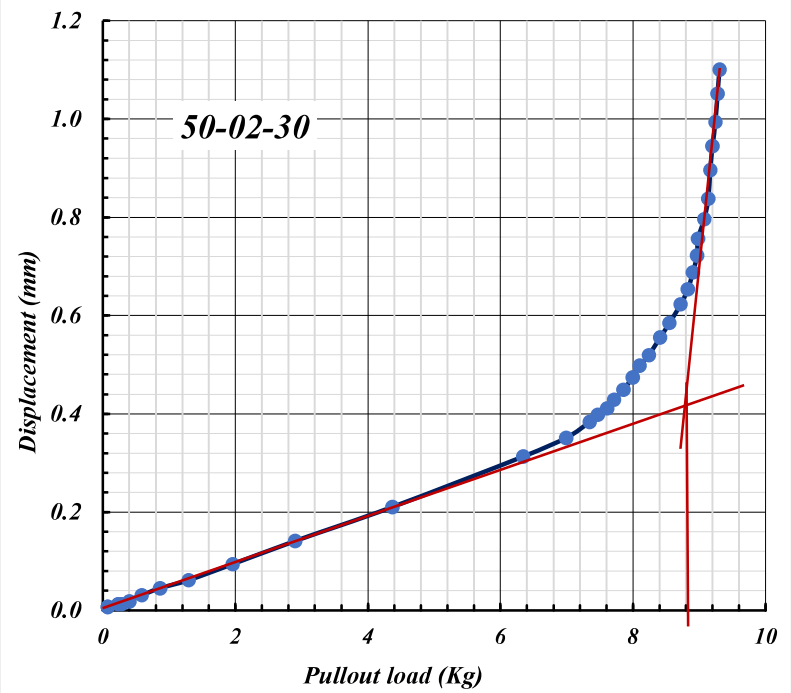

Fig. 4.16: Load vs Axial movement for 50mm Square Plate with (H/B=2) inclined at 30° with vertical in unreinforced soil

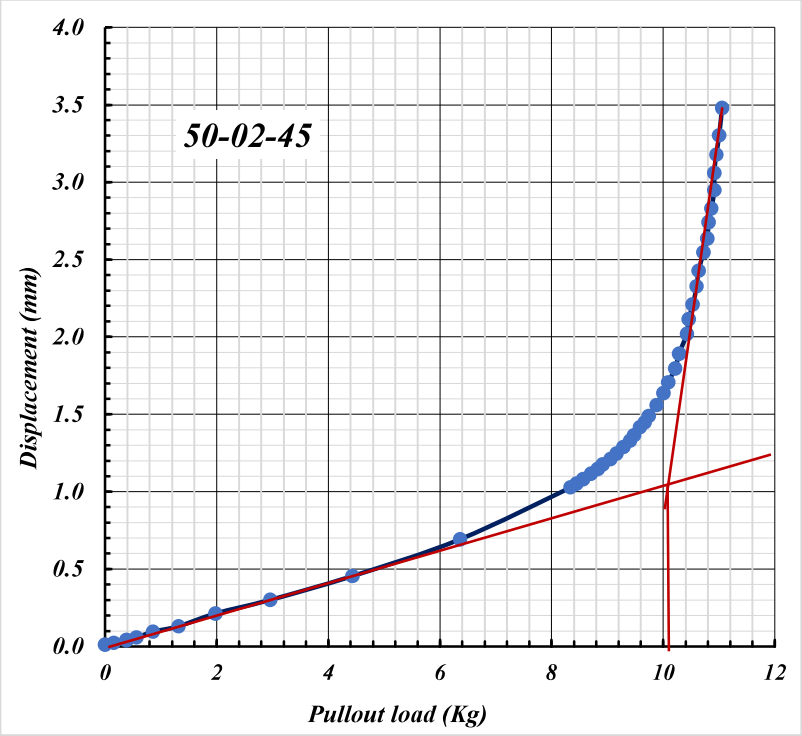

Fig. 4.17: Load vs Axial movement for 50mm Square Plate with (H/B=2) inclined at 45° with vertical in unreinforced soil

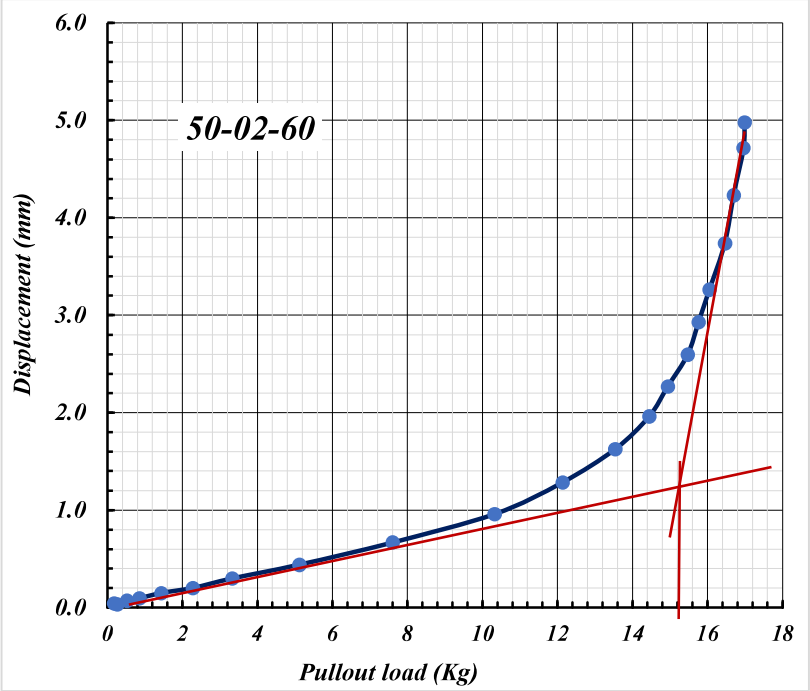

Fig. 4.18: Load vs Axial movement for 50mm Square Plate with (H/B=2) inclined at 60° with vertical in unreinforced soil

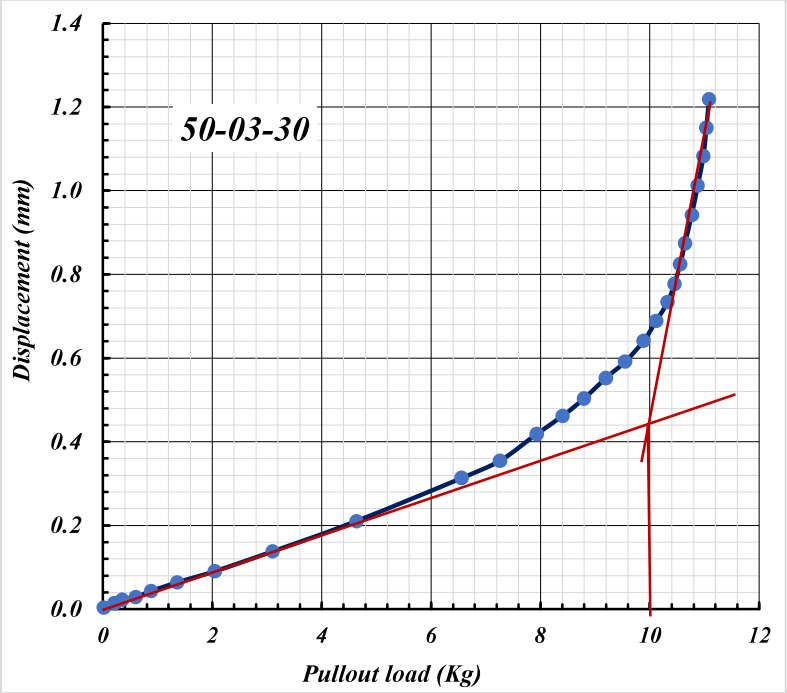

Fig. 4.19: Load vs Axial movement for 50mm Square Plate with (H/B=3) inclined at 30° with vertical in unreinforced soil

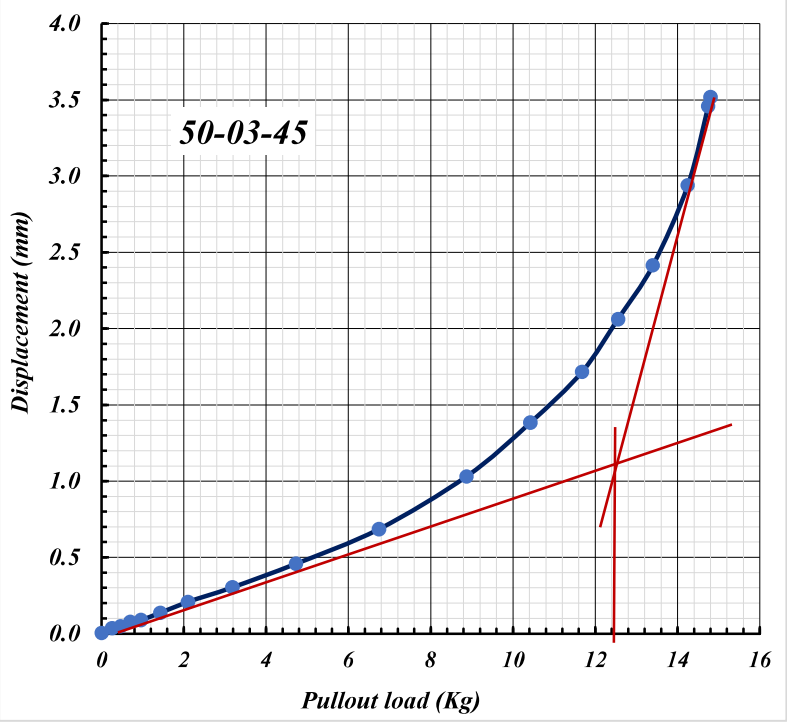

Fig. 4.20: Load vs Axial movement for 50mm Square Plate with (H/B=3) inclined at 45° with vertical in unreinforced soil

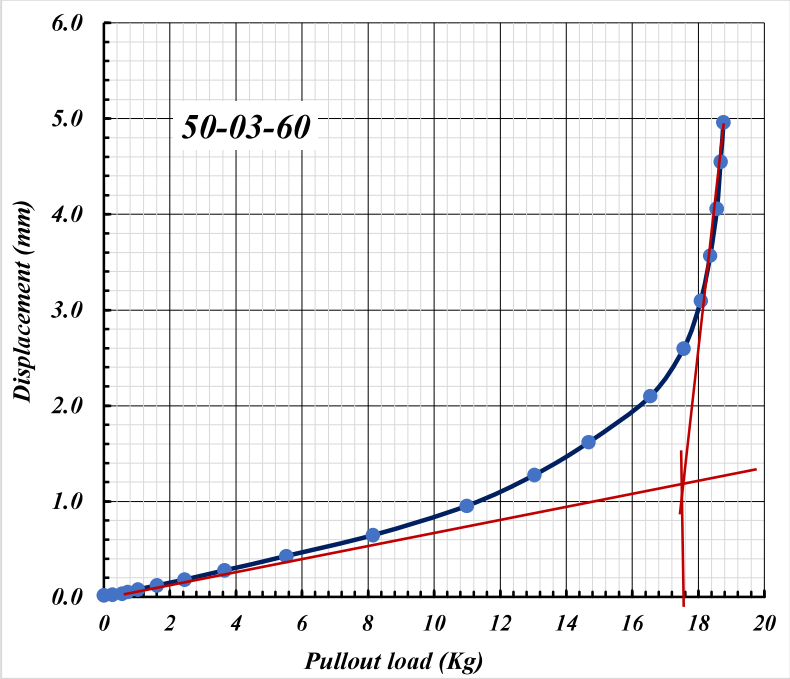

Fig. 4.21: Load vs Axial movement for 50mm Square Plate with (H/B=3) inclined at 60° with vertical in unreinforced soil

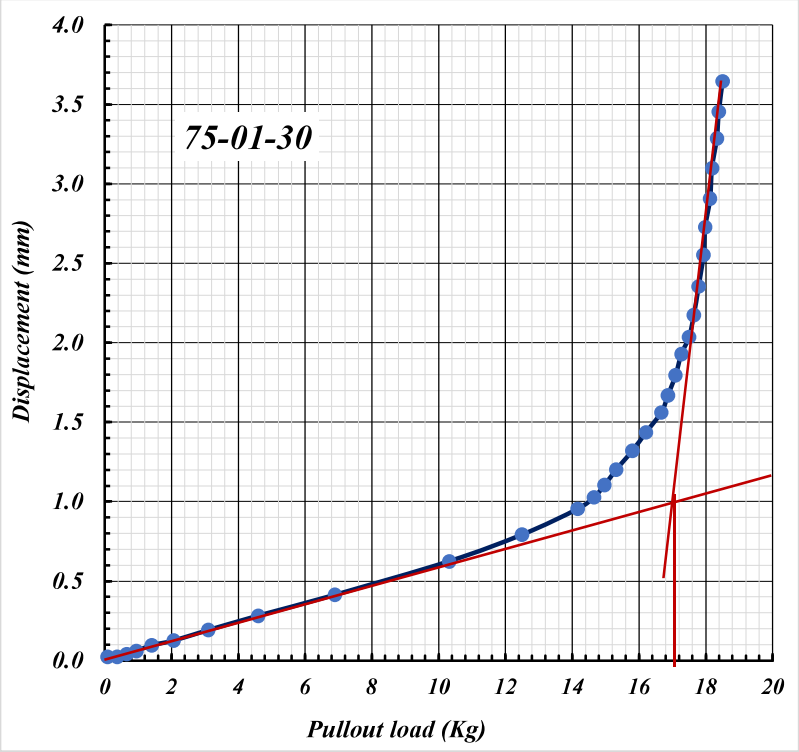

Fig. 4.22: Load vs Axial movement for 75mm Square Plate with (H/B=1) inclined at 30° with vertical in unreinforced soil

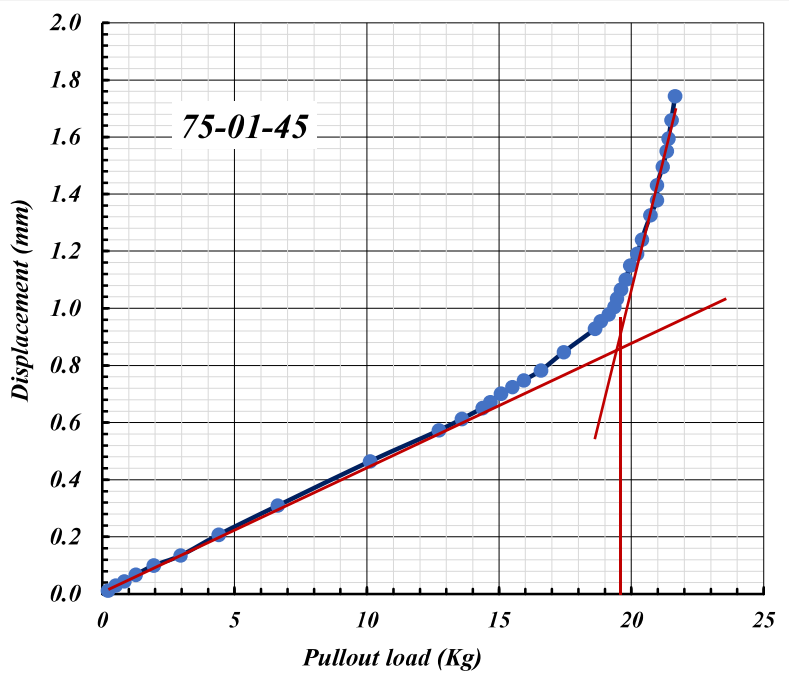

Fig. 4.23: Load vs Axial movement for 75 mm Square Plate with (H/B=1) inclined at 45° with vertical in unreinforced soil

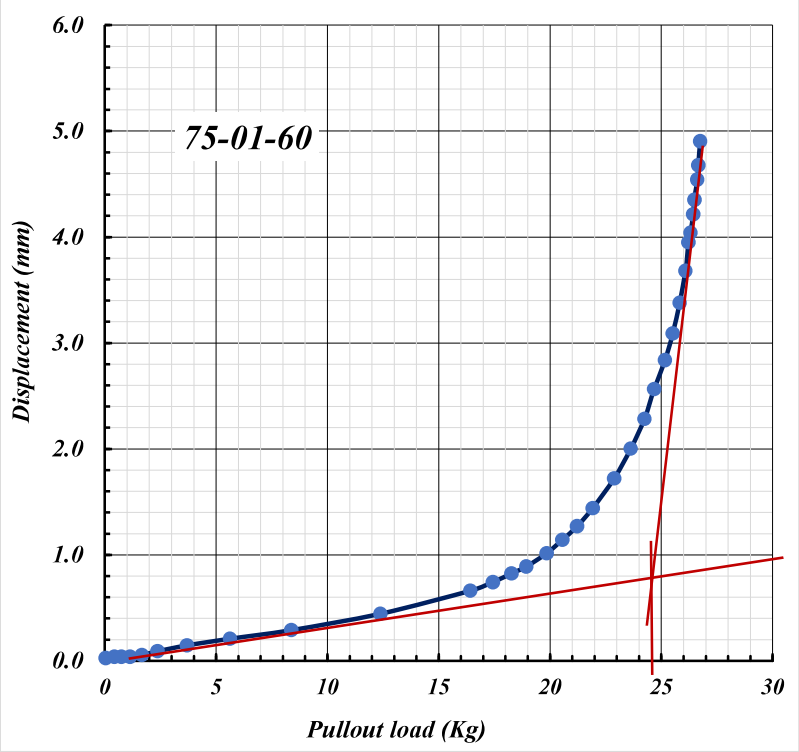

Fig. 4.24: Load vs Axial movement for 75mm Square Plate with (H/B=1) inclined at 60° with vertical in unreinforced soil

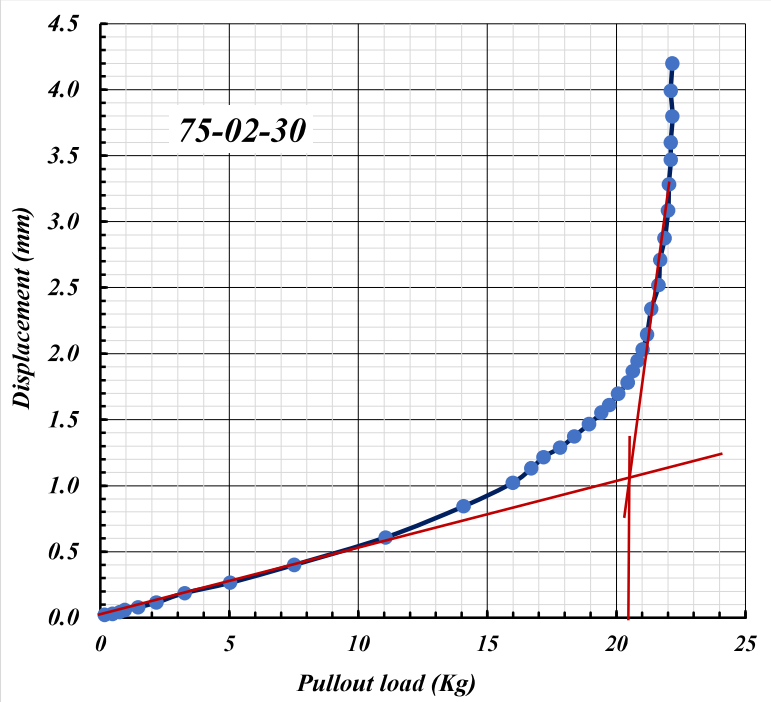

Fig. 4.25: Load vs Axial movement for 75mm Square Plate with (H/B=2) inclined at 30° with vertical in unreinforced soil

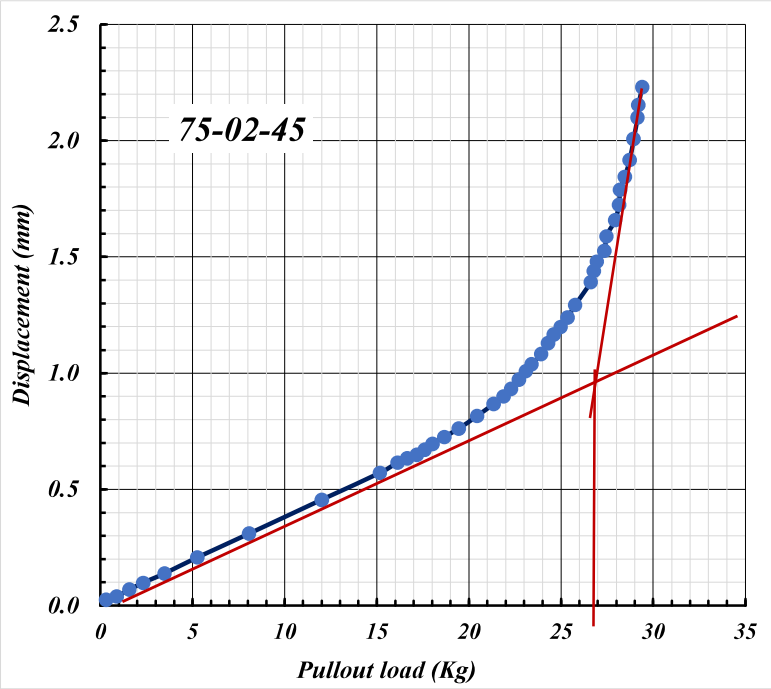

Fig. 4.26: Load vs Axial movement for 75mm Square Plate with (H/B=2) inclined at 45° with vertical in unreinforced soil

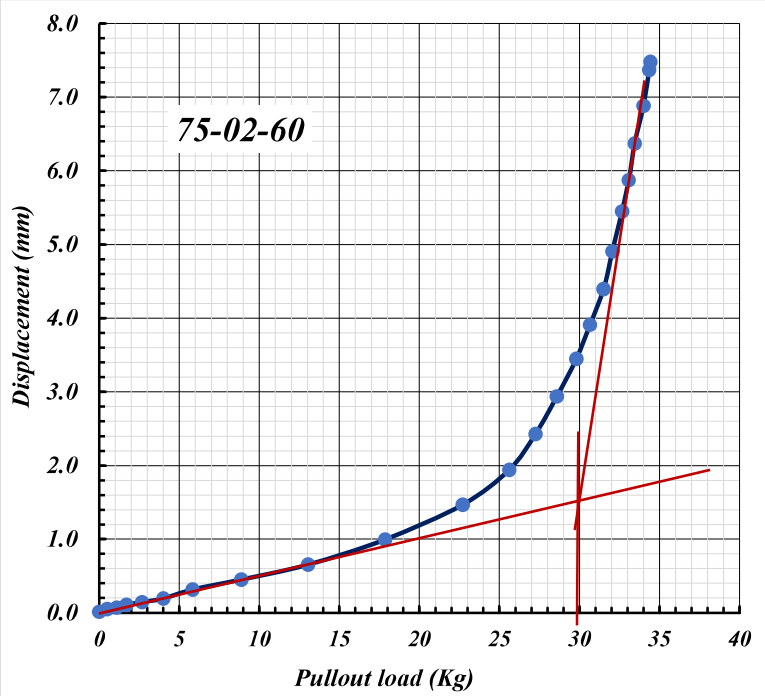

Fig. 4.27: Load vs Axial movement for 75mm Square Plate with (H/B=2) inclined at 60° with vertical in unreinforced soil

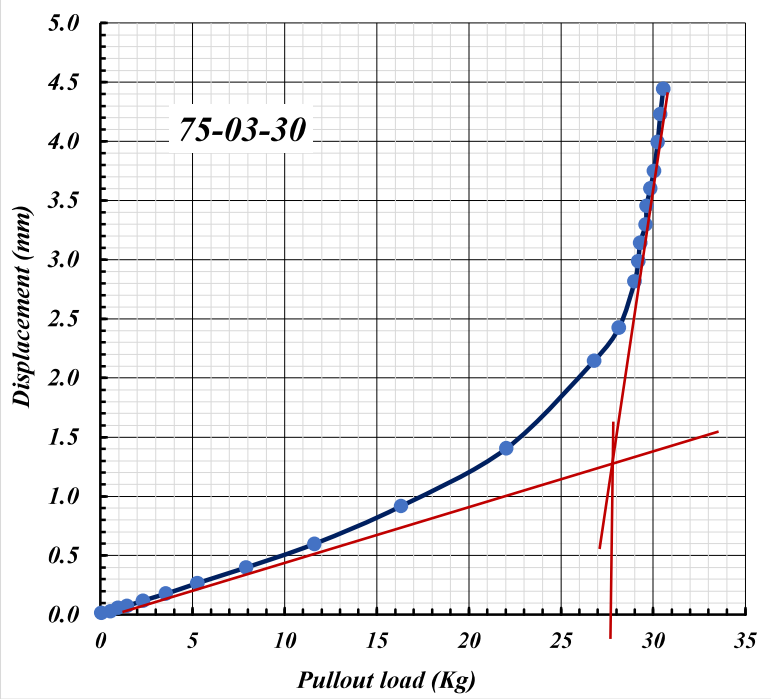

Fig. 4.28: Load vs Axial movement for 75mm Square Plate with (H/B=3) inclined at 30° with vertical in unreinforced soil

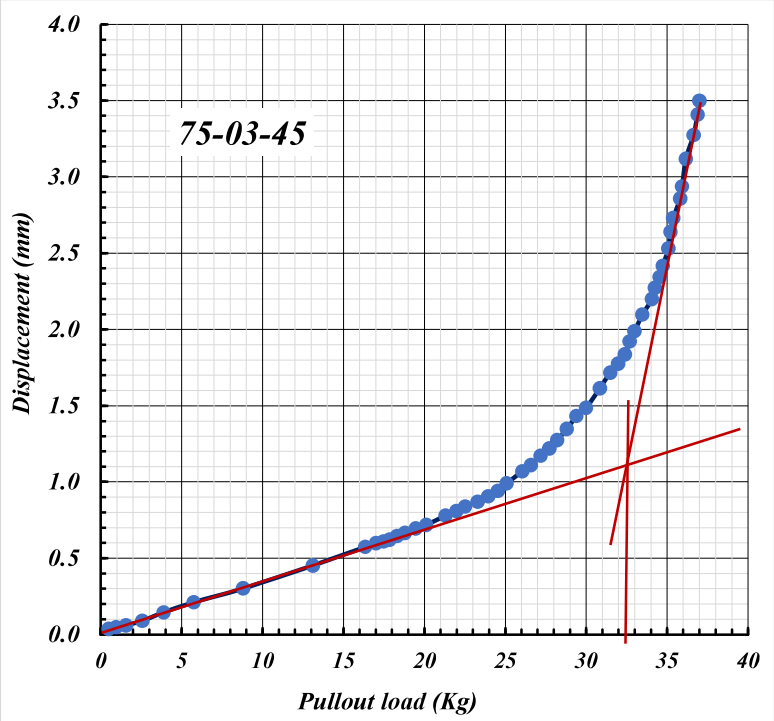

Fig. 4.29: Load vs Axial movement for 75mm Square Plate with (H/B=3) inclined at 45° with vertical in unreinforced soil

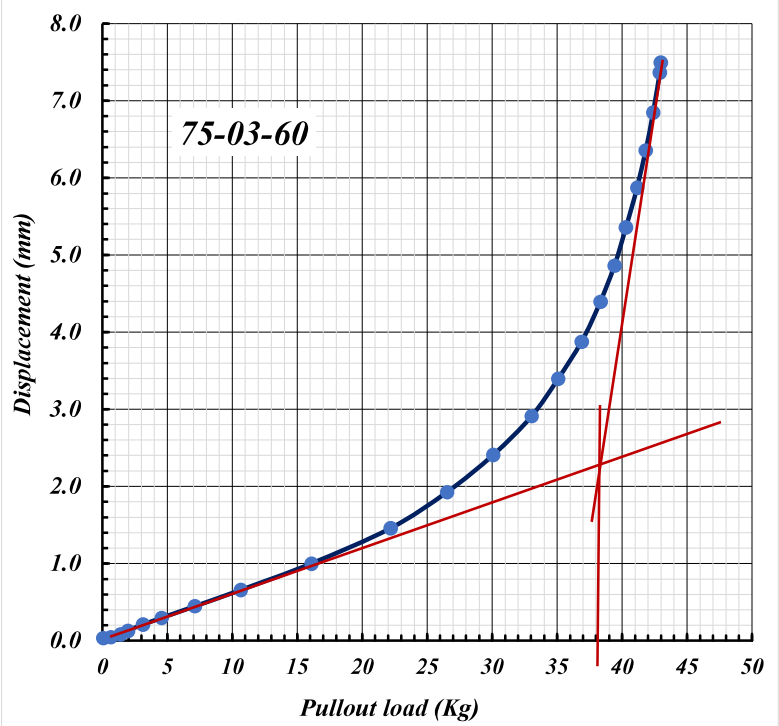

Fig. 4.30: Load vs Axial movement for 75mm Square Plate with (H/B=3) inclined at 60° with vertical in unreinforced soil

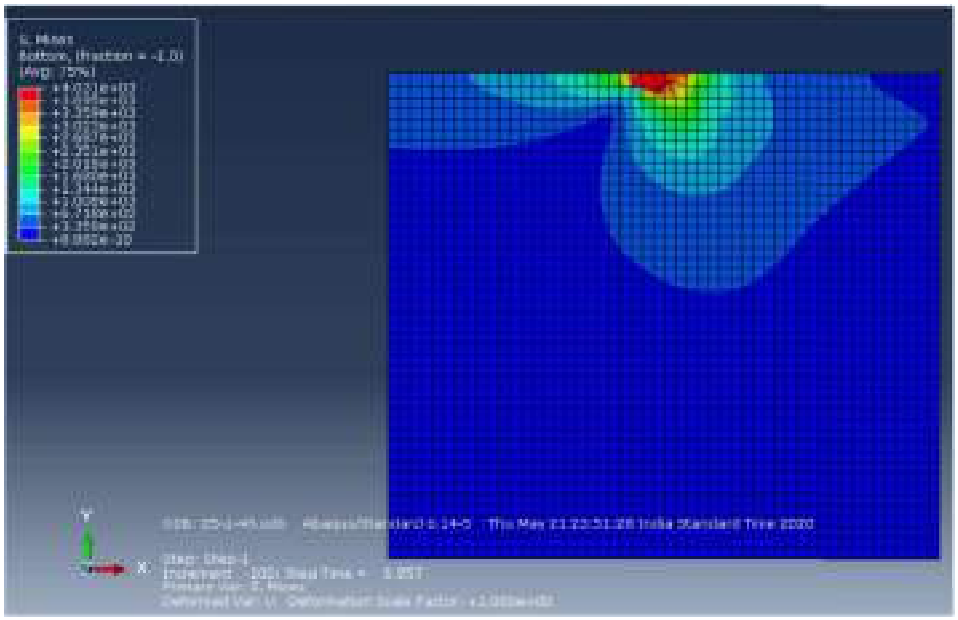

Fig. 4.32: Stress Contour for 25mm Square Anchor Plate with (H/B =1) inclined at 45° with vertical in unreinforced soil

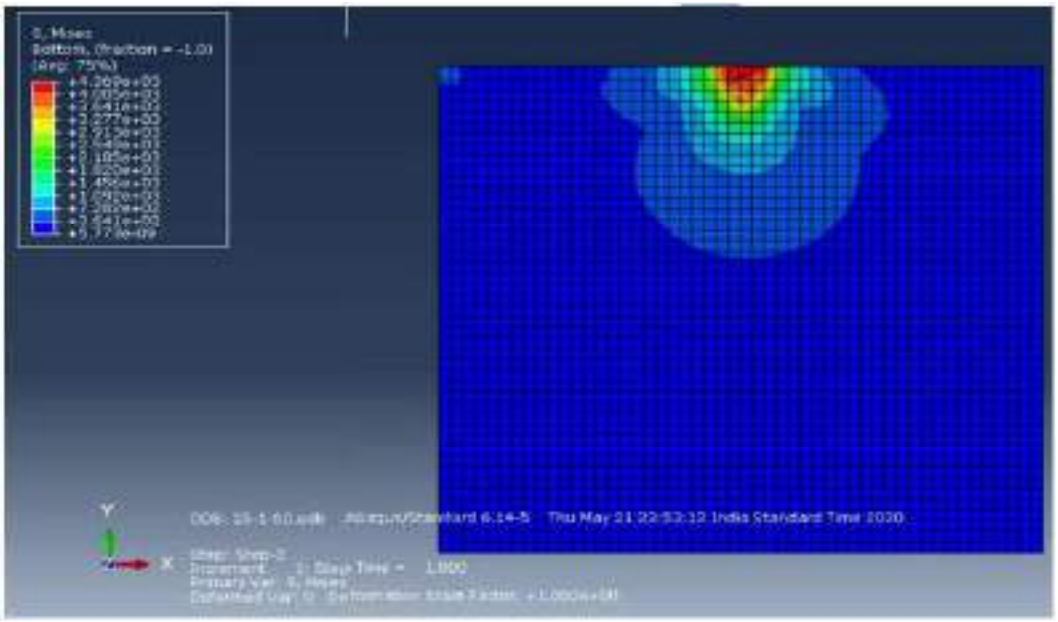

Fig. 4.33: Stress Contour for 25 mm Square Anchor Plate with (H/B =1) inclined at 60° with Vertical in unreinforced soil

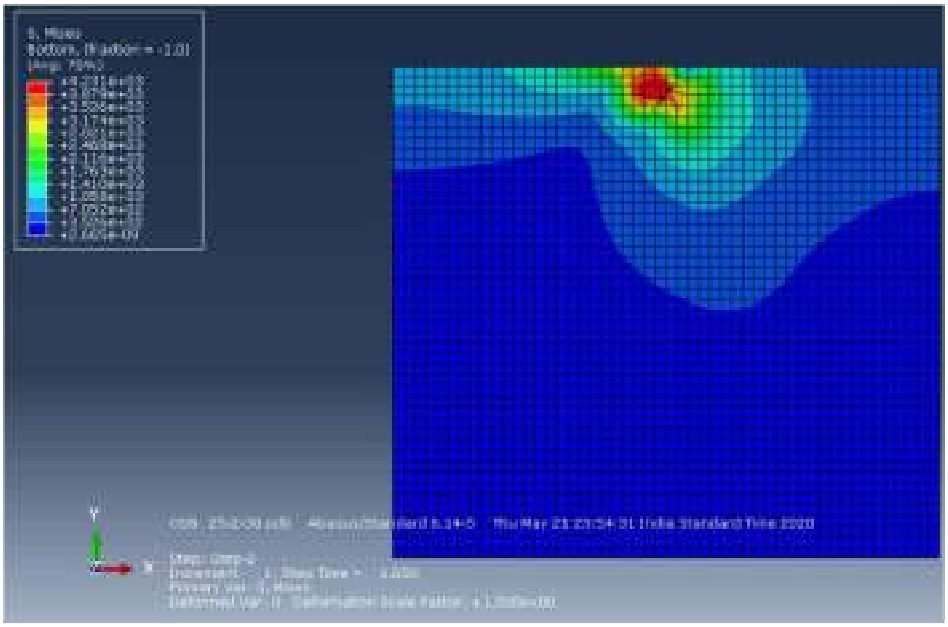

Fig. 4.34: Stress Contour for 25mm Square Anchor Plate with (H/B =2) inclined at 30° with Vertical in unreinforced soil

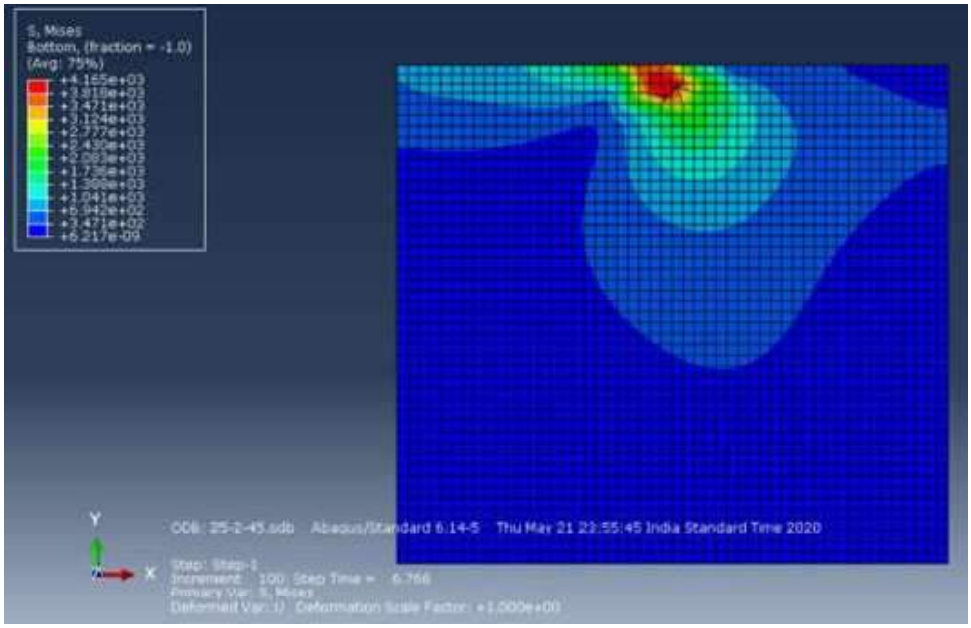

Fig. 4.35: Stress Contour for 25mm Square Anchor Plate with (H/B =2) inclined at 45° with Vertical in unreinforced soil

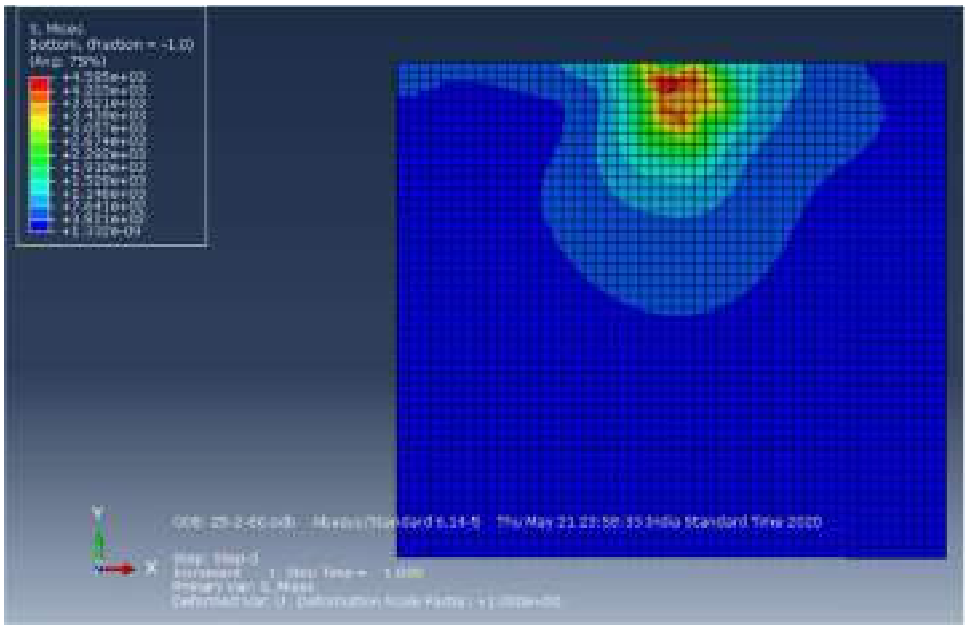

Fig. 4.36: Stress Contour for 25mm Square Anchor Plate with (H/B =2) inclined at 60° with Vertical in unreinforced soil

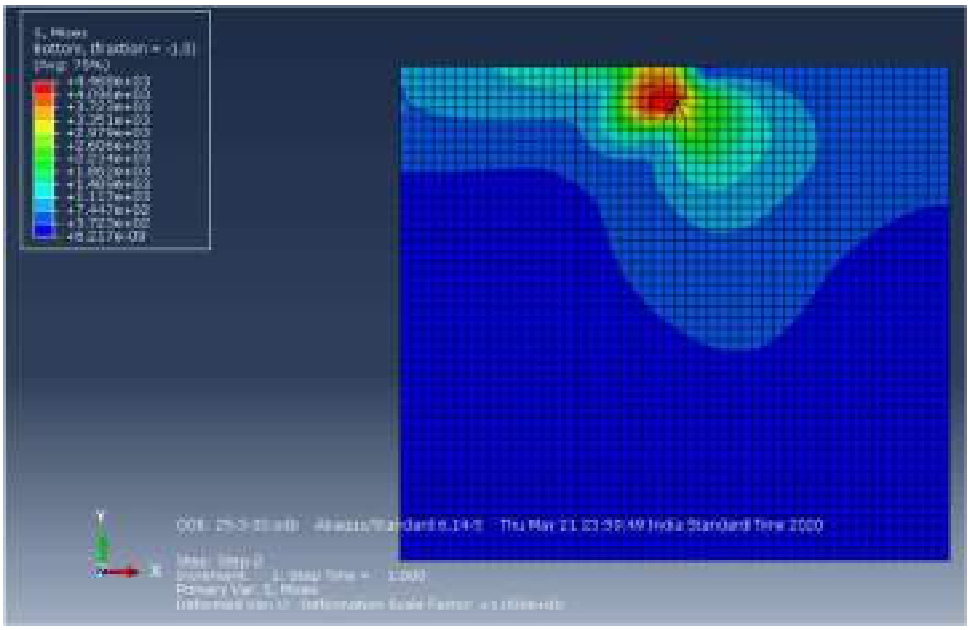

Fig. 4.37: Stress Contour for 25mm Square Anchor Plate with (H/B =3) inclined at 30° with Vertical in unreinforced soil

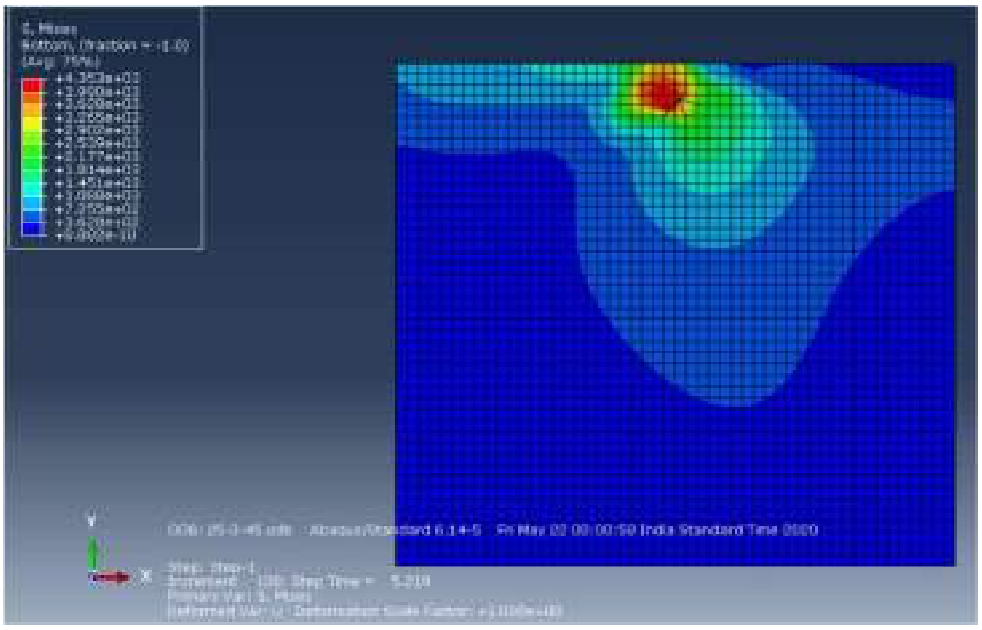

Fig. 4.38: Stress Contour for 25mm Square Anchor Plate with (H/B =3) inclined at 45° with Vertical in unreinforced soil

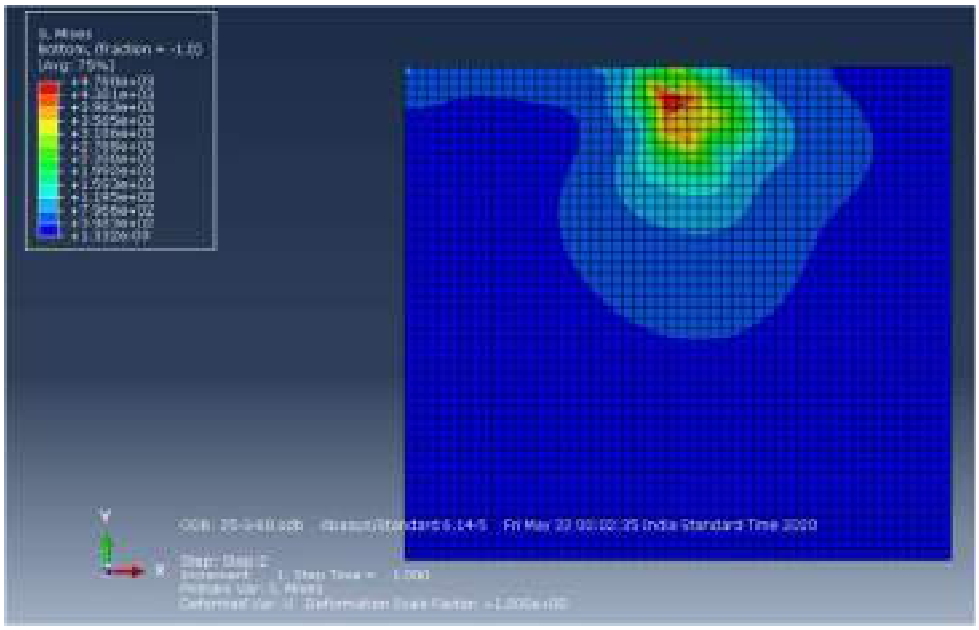

Fig. 4.39: Stress Contour for 25mm Square Anchor Plate with (H/B =3) inclined at 60° with vertical in unreinforced soil

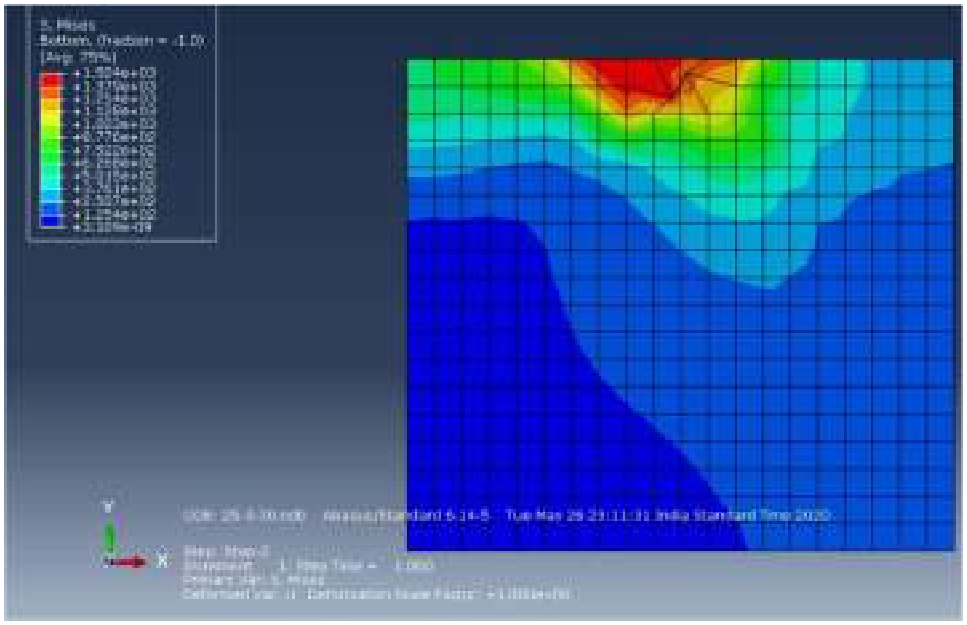

Fig. 4.40: Stress Contour for 50mm Square Anchor Plate with (H/B =1) inclined at 30° with vertical in unreinforced soil

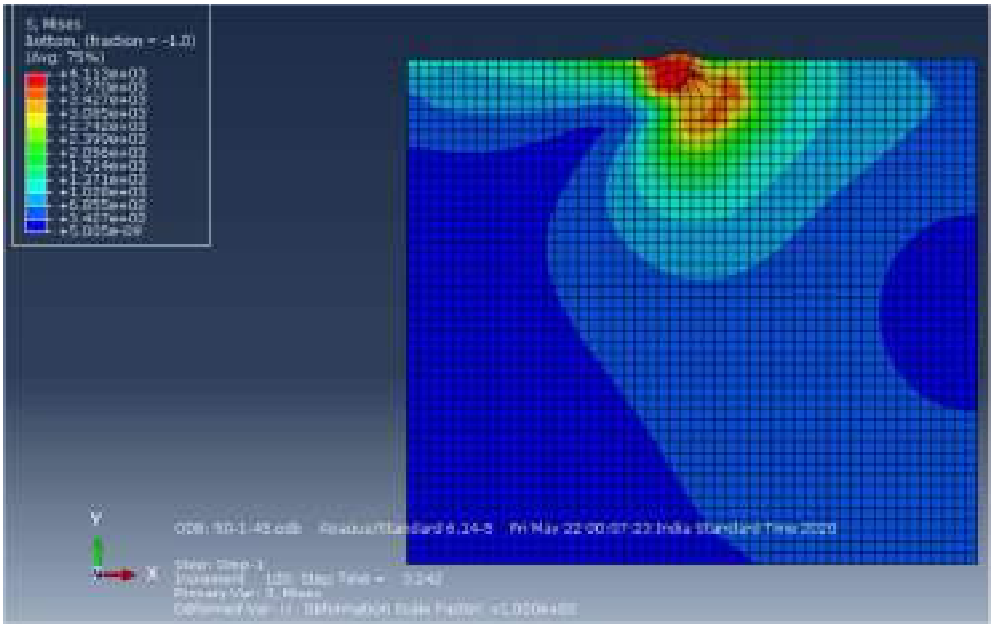

Fig. 4.41: Stress Contour for 50mm Square Anchor Plate with (H/B =1) inclined at 45° with vertical in unreinforced soil

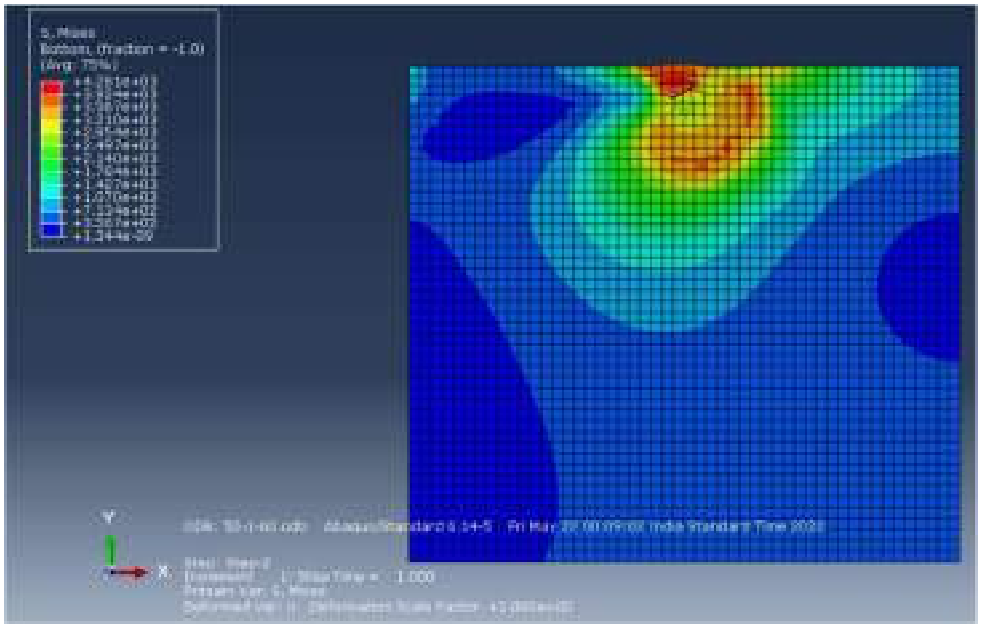

Fig. 4.42: Stress Contour for 50mm Square Anchor Plate with (H/B =1) inclined at 60° with vertical in unreinforced soil

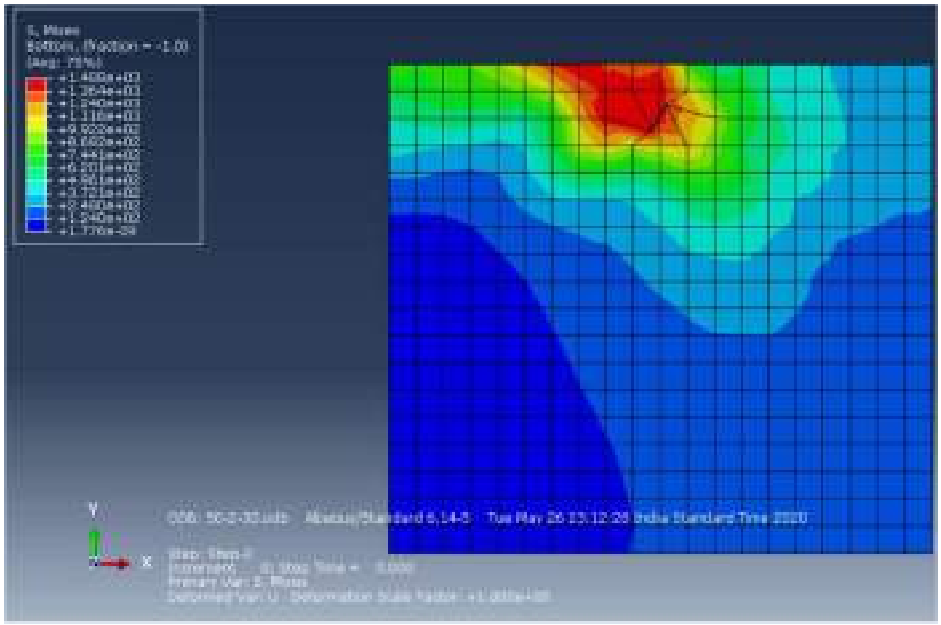

Fig. 4.43: Stress Contour for 50mm Square Anchor Plate with (H/B =2) inclined at 30° with vertical in unreinforced soil

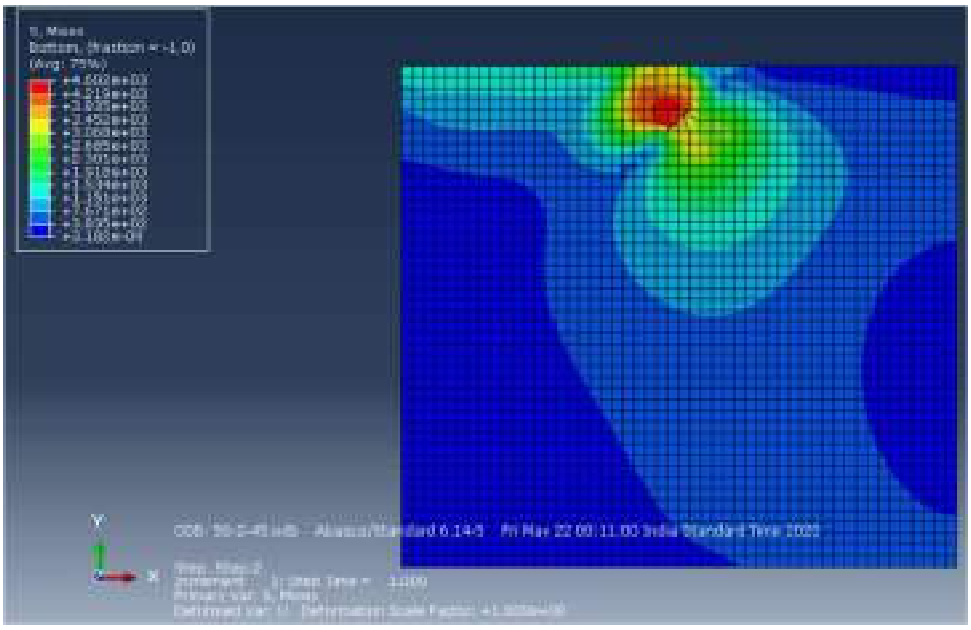

Fig. 4.44: Stress Contour for 50mm Square Anchor Plate with (H/B =2) inclined at 45° with vertical in unreinforced soil

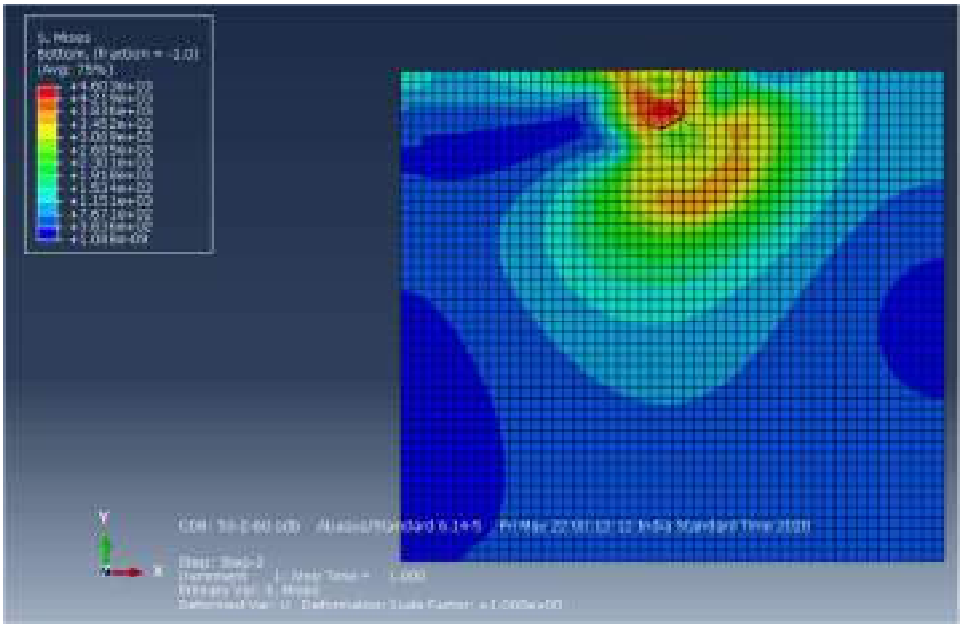

Fig. 4.45: Stress Contour for 50mm Square Anchor Plate with (H/B =2) inclined at 60° with vertical in unreinforced soil

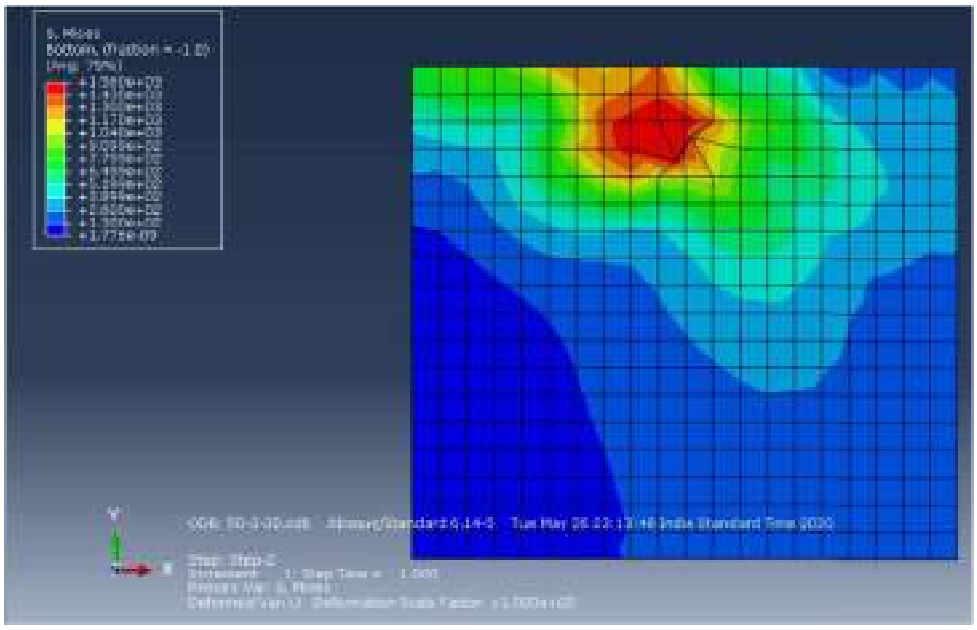

Fig. 4.46: Stress Contour for 50mm Square Anchor Plate with (H/B =3) inclined at 30° with vertical in unreinforced soil

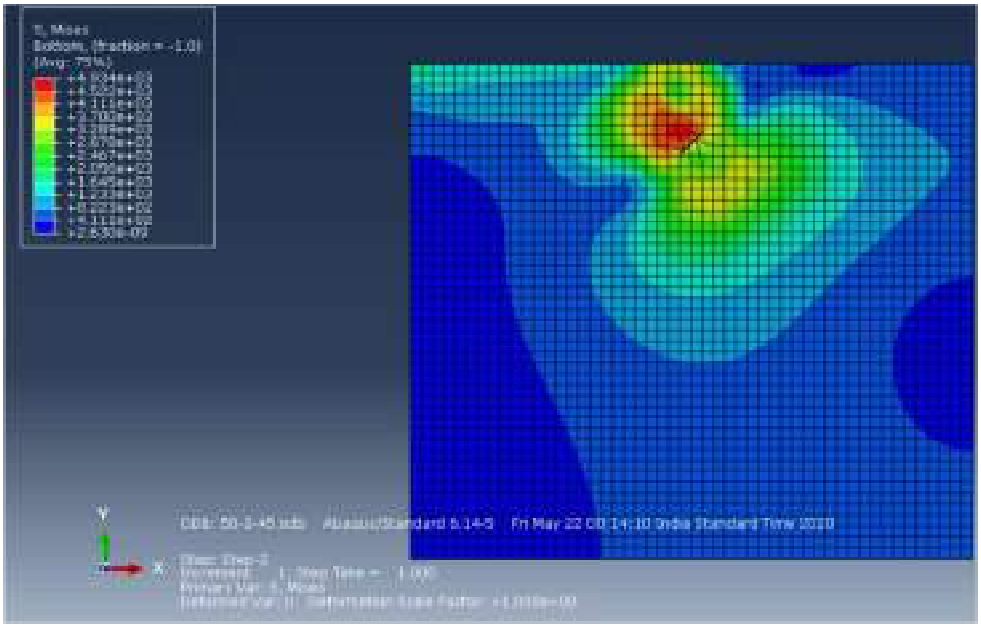

Fig. 4.47: Stress Contour for 50mm Square Anchor Plate with (H/B =3) inclined at 45° with vertical in unreinforced soil

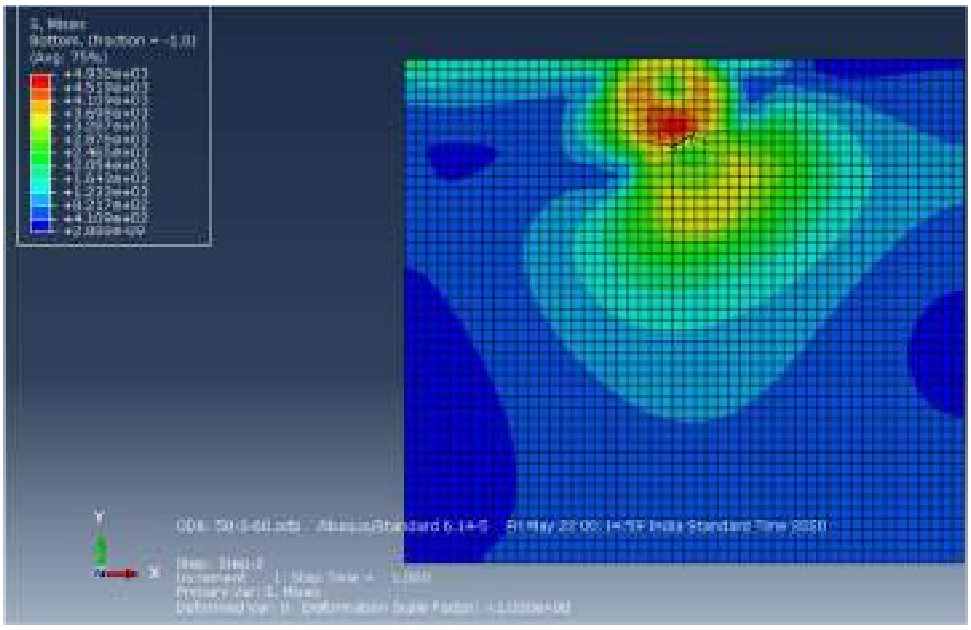

Fig. 4.48: Stress Contour for 50mm Square Anchor Plate with (H/B =3) inclined at 60° with vertical in unreinforced soil

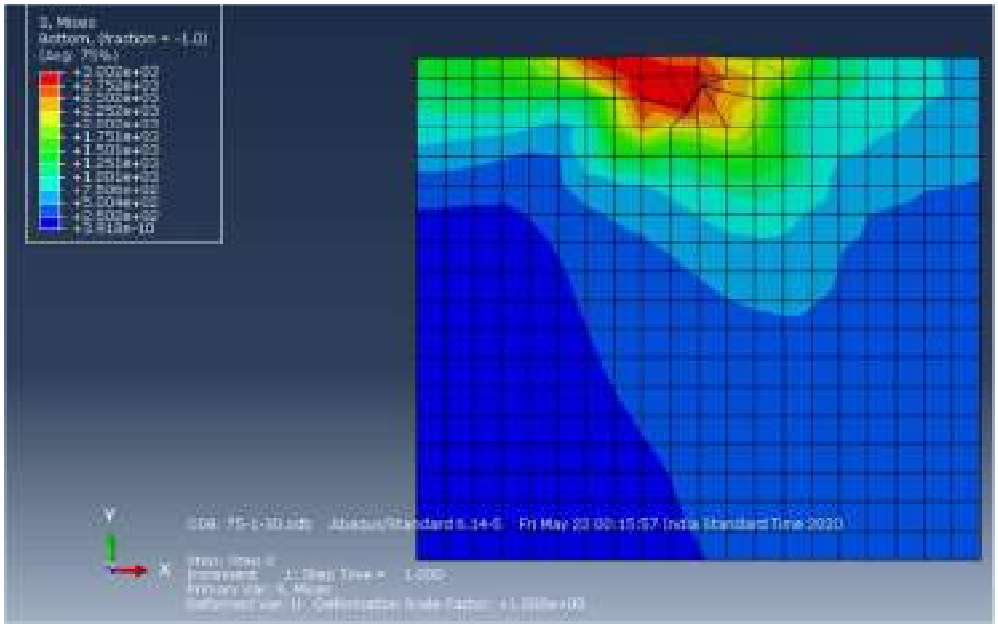

Fig. 4.49: Stress Contour for 75mm Square Anchor Plate with (H/B =1) inclined at 30° with vertical in unreinforced soil

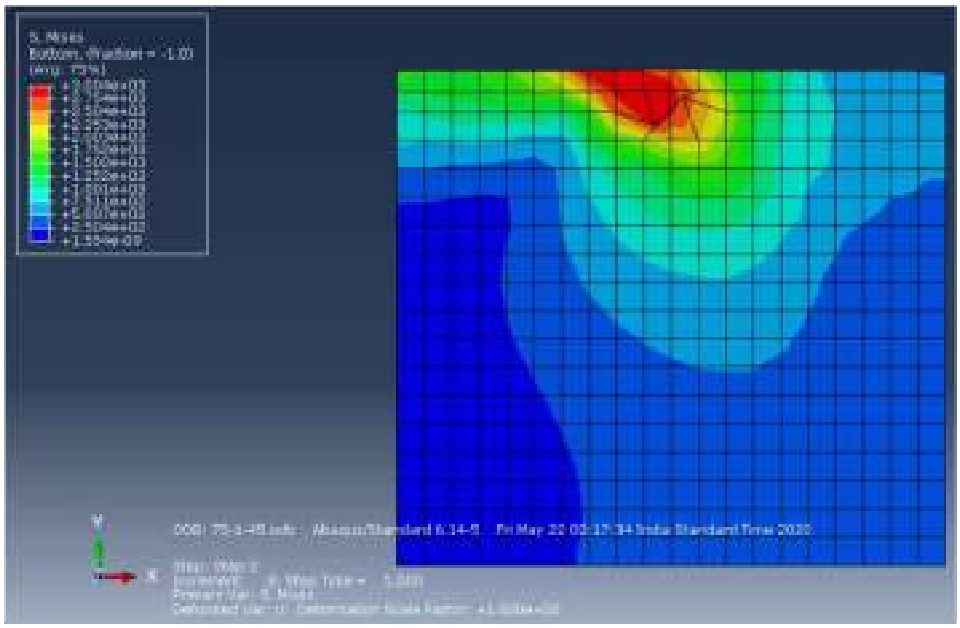

Fig. 4.50: Stress Contour for 75mm Square Anchor Plate with (H/B =1) inclined at 45° with vertical in unreinforced soil

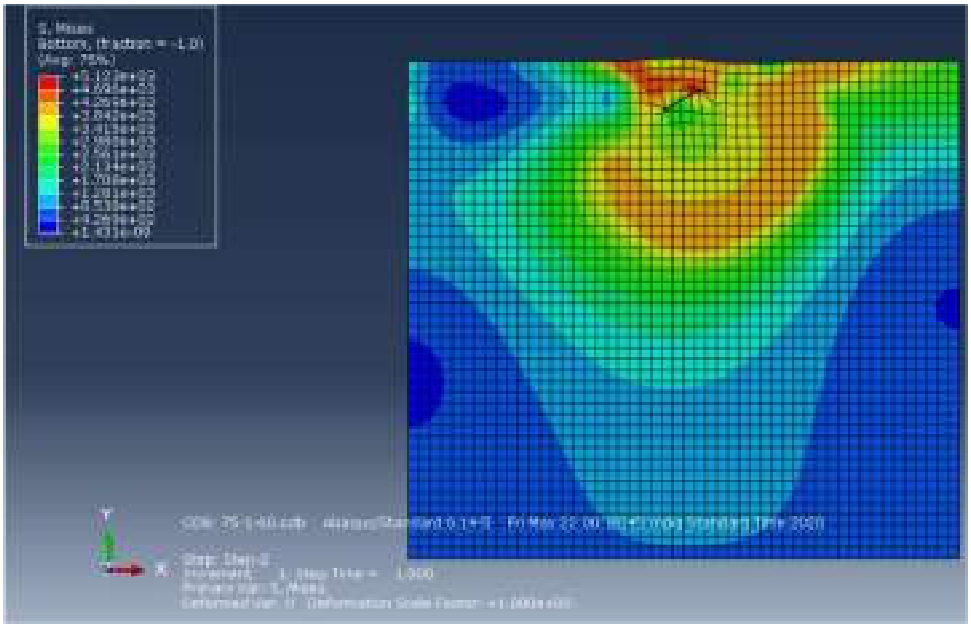

Fig. 4.51: Stress Contour for 75mm Square Anchor Plate with (H/B =1) inclined at 60° with vertical in unreinforced soil

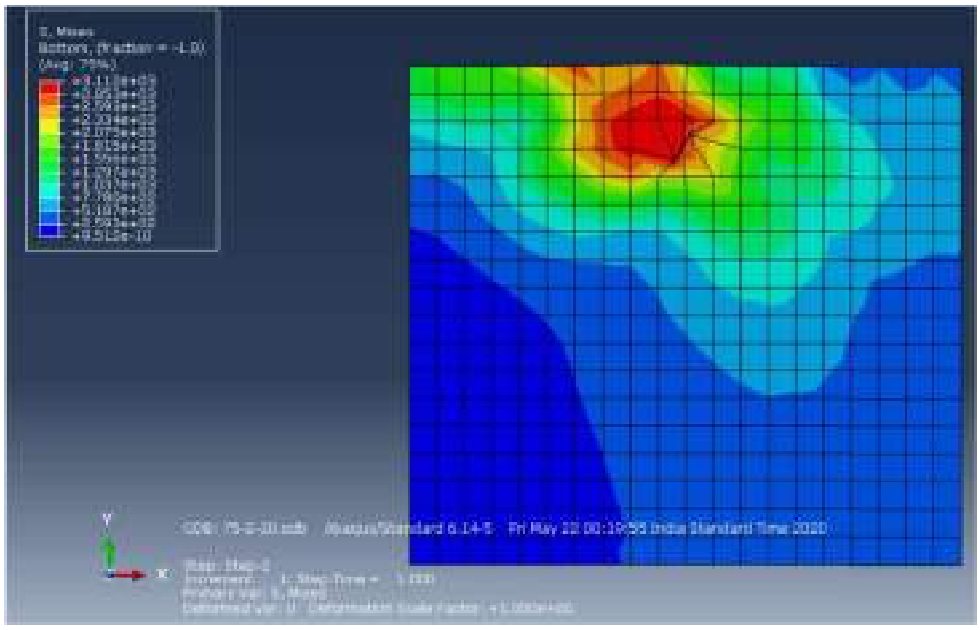

Fig. 4.52: Stress Contour for 75mm Square Anchor Plate with (H/B =2) inclined at 30° with vertical in unreinforced soil

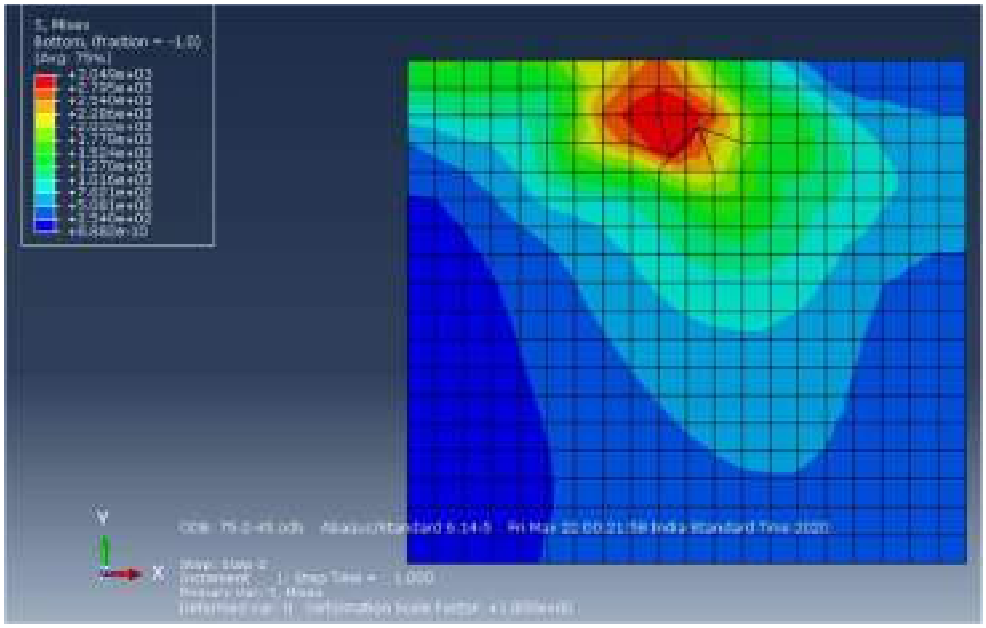

Fig. 4.53: Stress Contour for 75mm Square Anchor Plate with (H/B =2) inclined at 45° with vertical in unreinforced soil

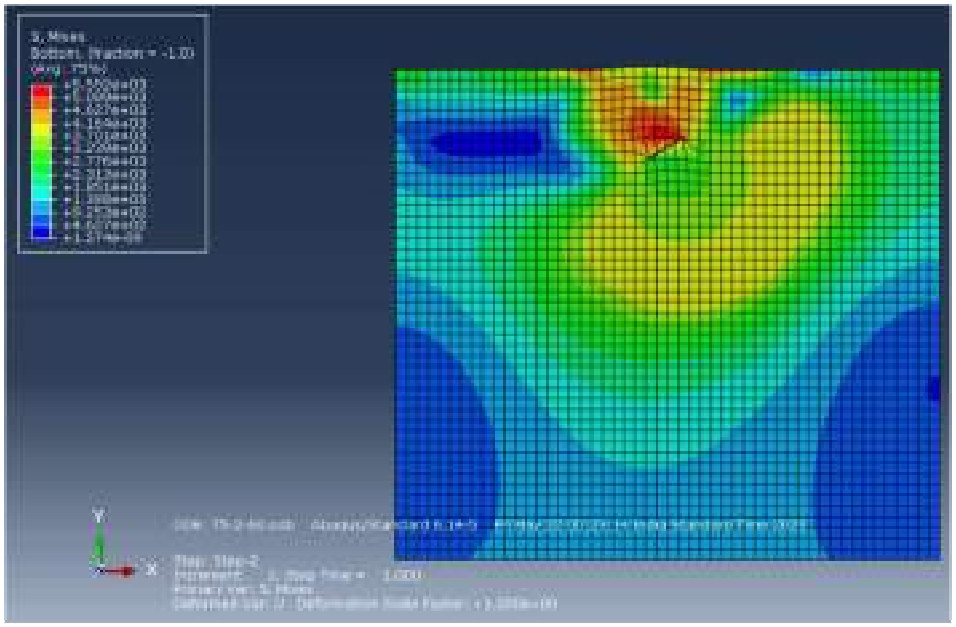

Fig. 4.54: Stress Contour for 75mm Square Anchor Plate with (H/B =2) inclined at 60° with vertical in unreinforced soil

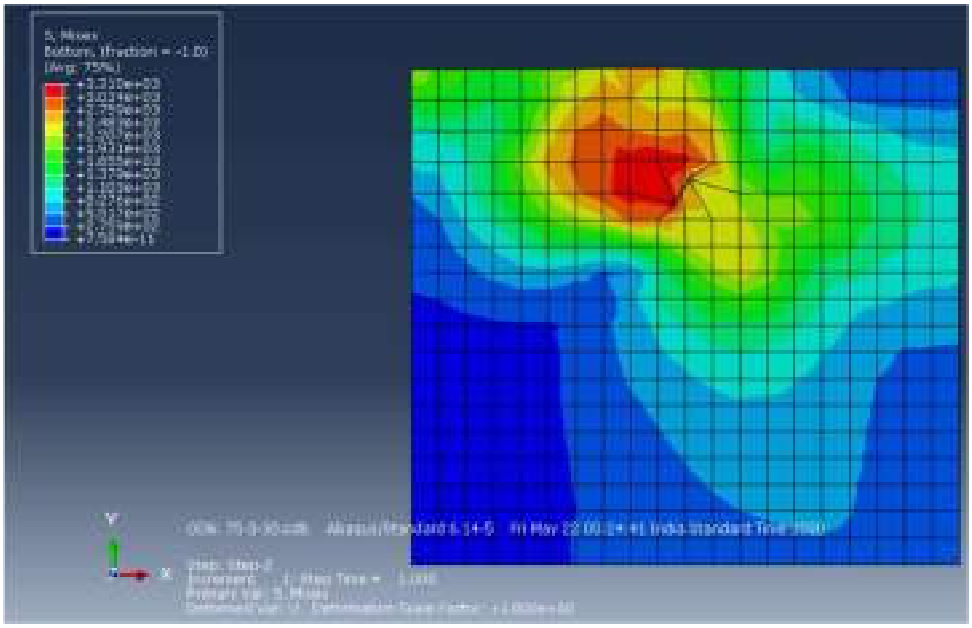

Fig. 4.55: Stress Contour for 75mm Square Anchor Plate with (H/B =3) inclined at 30° with vertical in unreinforced soil

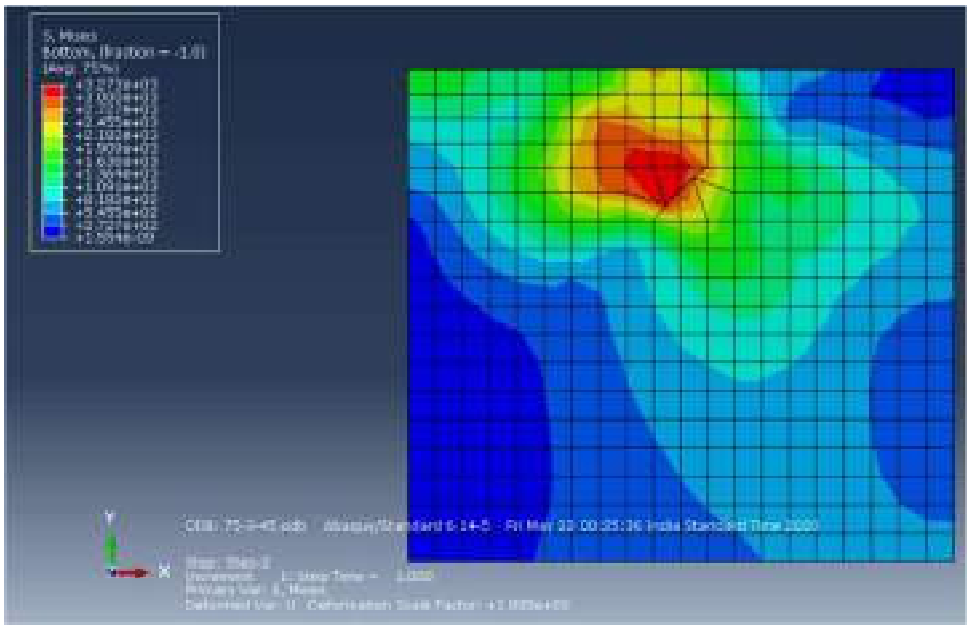

Fig. 4.56: Stress Contour for 75mm Square Anchor Plate with (H/B =3) inclined at 45° with vertical in unreinforced soil

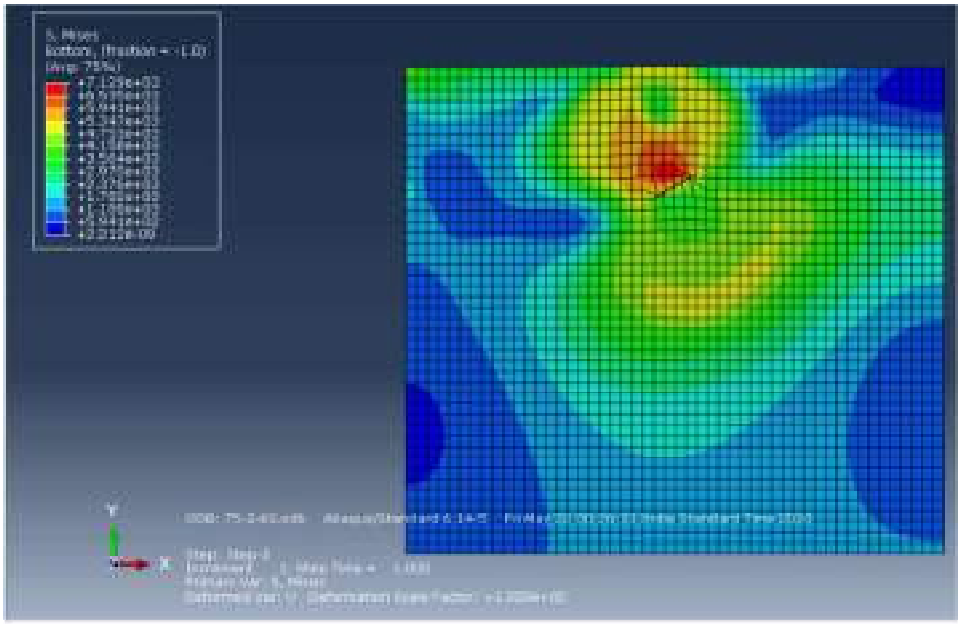

Fig. 4.57: Stress Contour for 75mm Square Anchor Plate with (H/B =3) inclined at 60° with vertical in unreinforced soil

ANNEXURE -III

PRESENTATION OF RESULTS OF NUMERICAL ANALYSIS (STATIC REINFORCED)

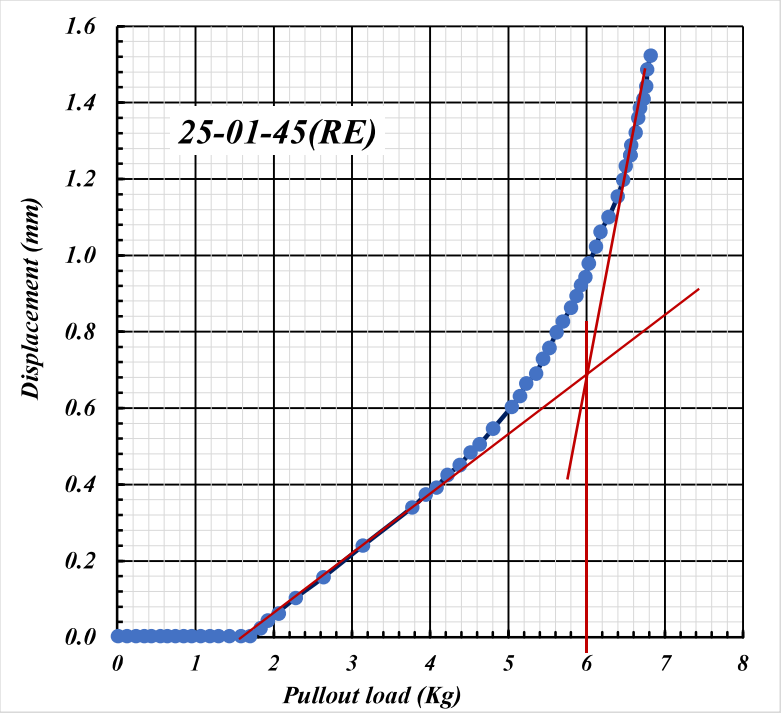

Fig. 4.61: Load vs Axial Movement for 25mm Square Plate with (H/B=1) inclined at 45° with vertical in reinforced condition

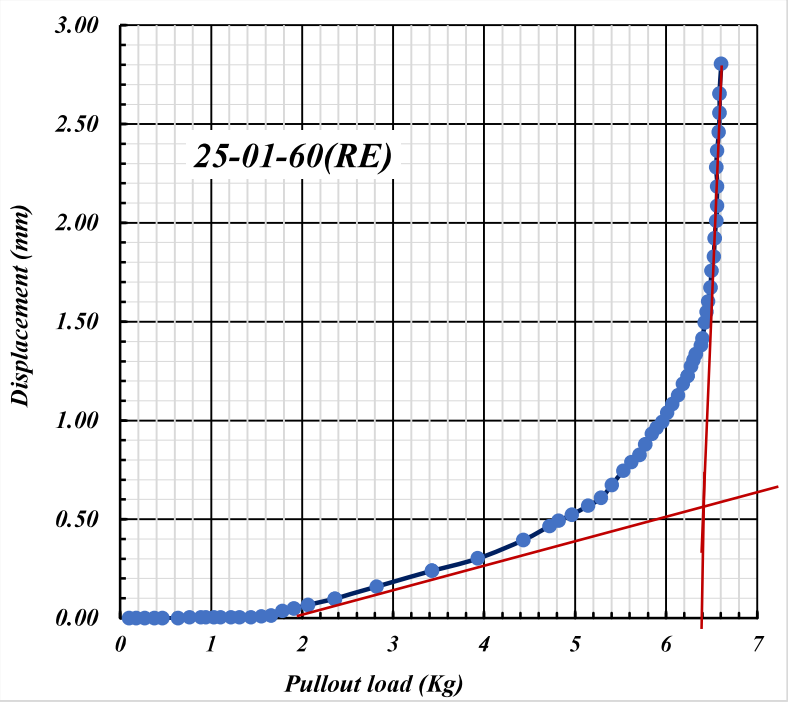

Fig. 4.62: Load vs Axial Movement for 25mm Square Plate with (H/B=1) inclined at 60° with vertical in reinforced condition

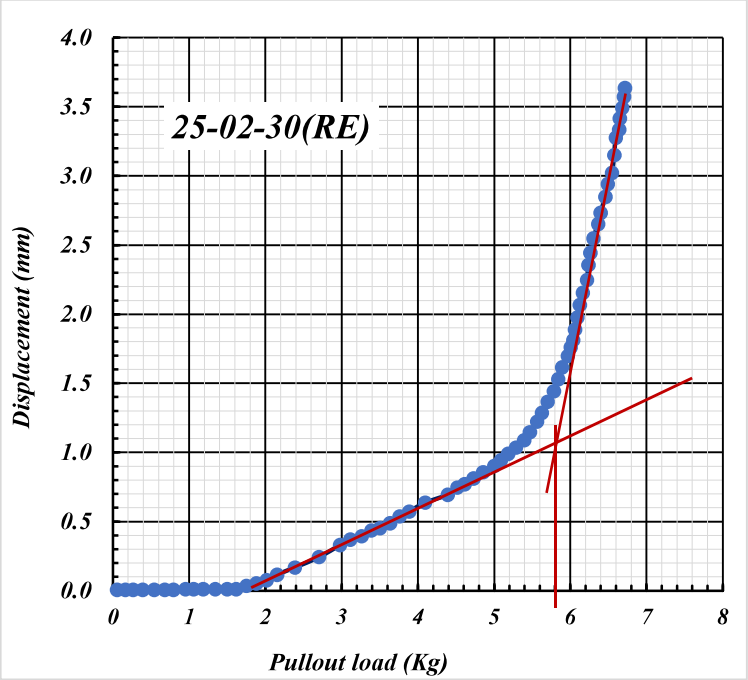

Fig. 4.63: Load vs Axial Movement for 25mm Square Plate with (H/B=2) inclined at 30° with vertical in reinforced condition

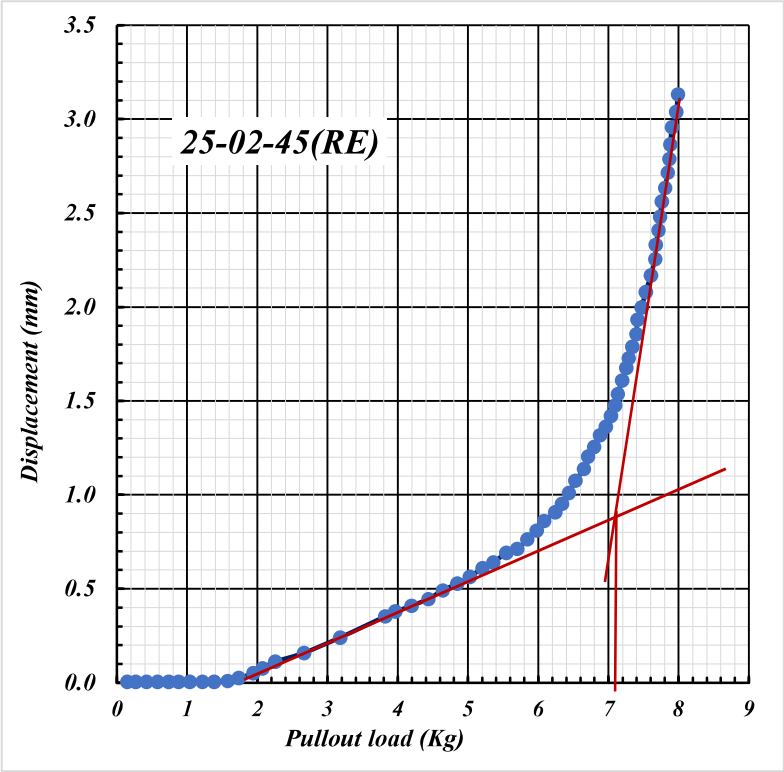

Fig. 4.64: Load vs Axial Movement for 25mm Square Plate with (H/B=2) inclined at 45° with vertical in reinforced condition

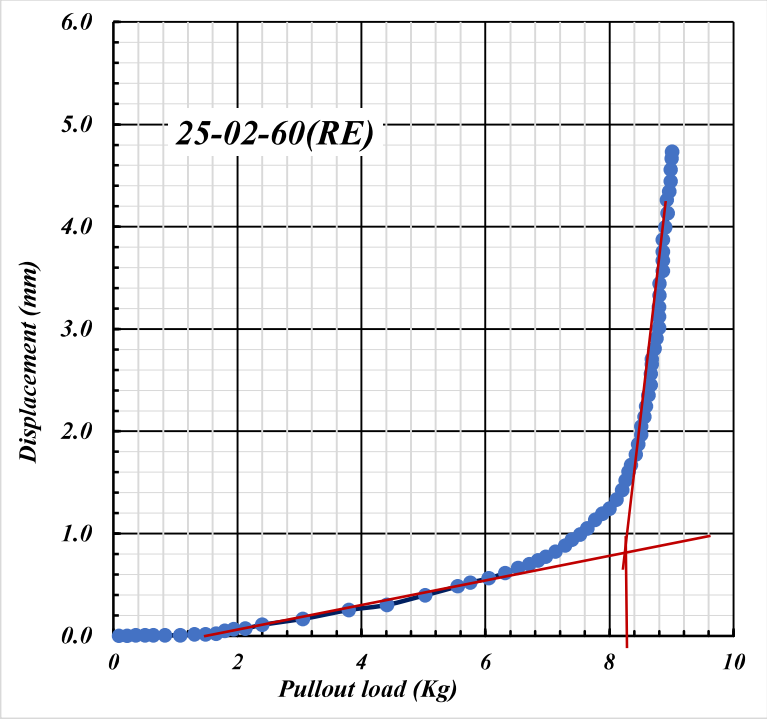

Fig. 4.65: Load vs Axial Movement for 25mm Square Plate with (H/B=2) inclined at 60° with vertical in reinforced condition

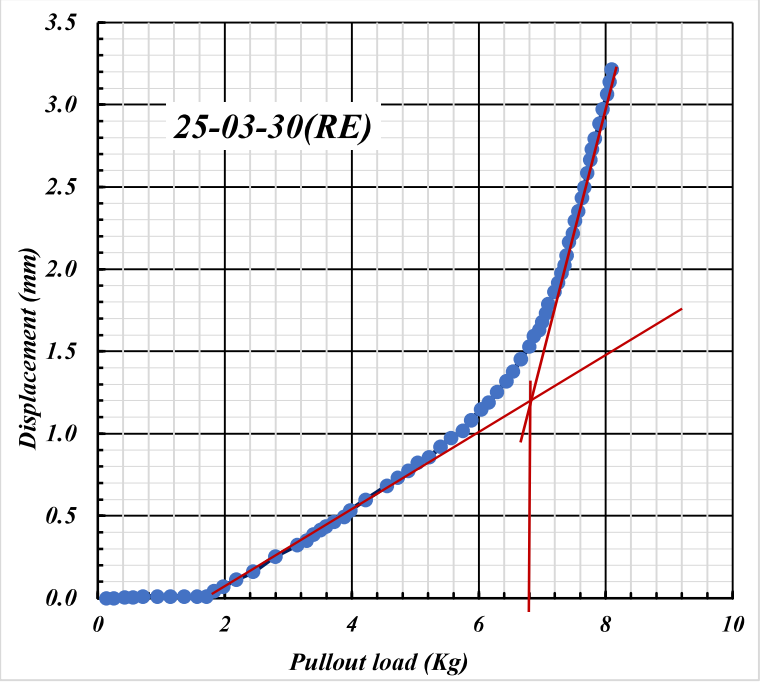

Fig. 4.66: Load vs Axial Movement for 25mm Square Plate with (H/B=3) inclined at 30° with vertical in reinforced condition

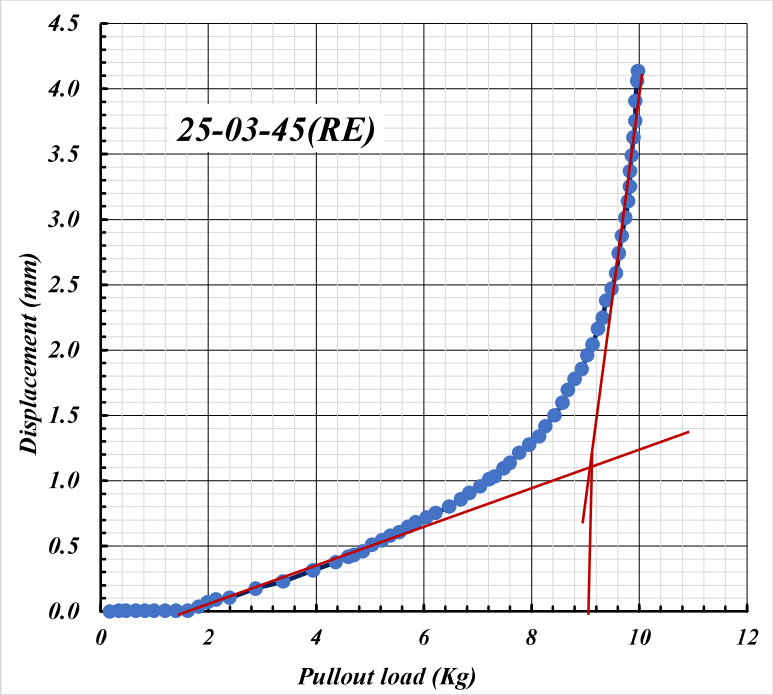

Fig. 4.67: Load vs Axial Movement for 25mm Square Plate with (H/B=3) inclined at 45° with vertical in reinforced condition

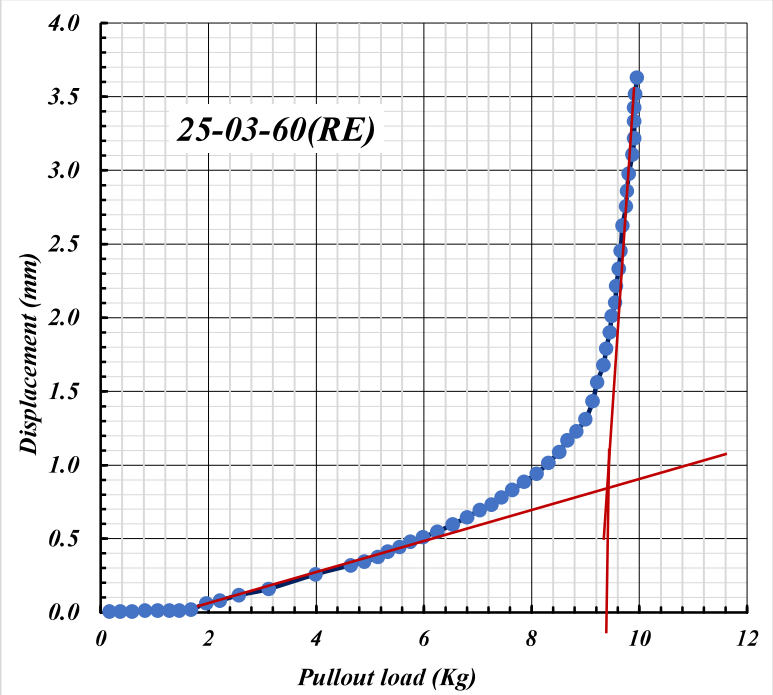

Fig. 4.68: Load vs Axial Movement for 25mm Square Plate with (H/B=3) inclined at 60° with vertical in reinforced condition

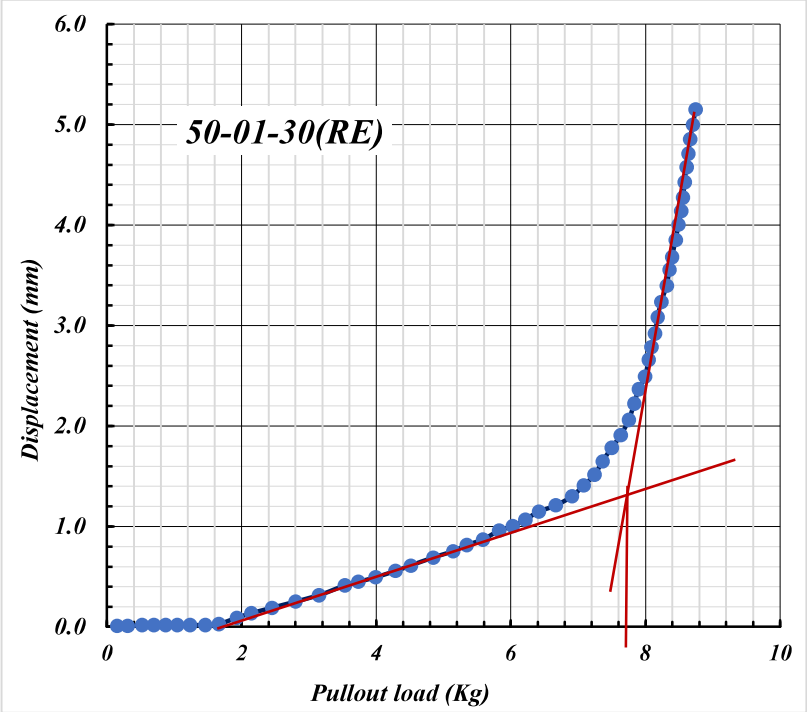

Fig. 4.69: Load vs Axial Movement for 50mm Square Plate with (H/B=1) inclined at 30° with vertical in reinforced condition

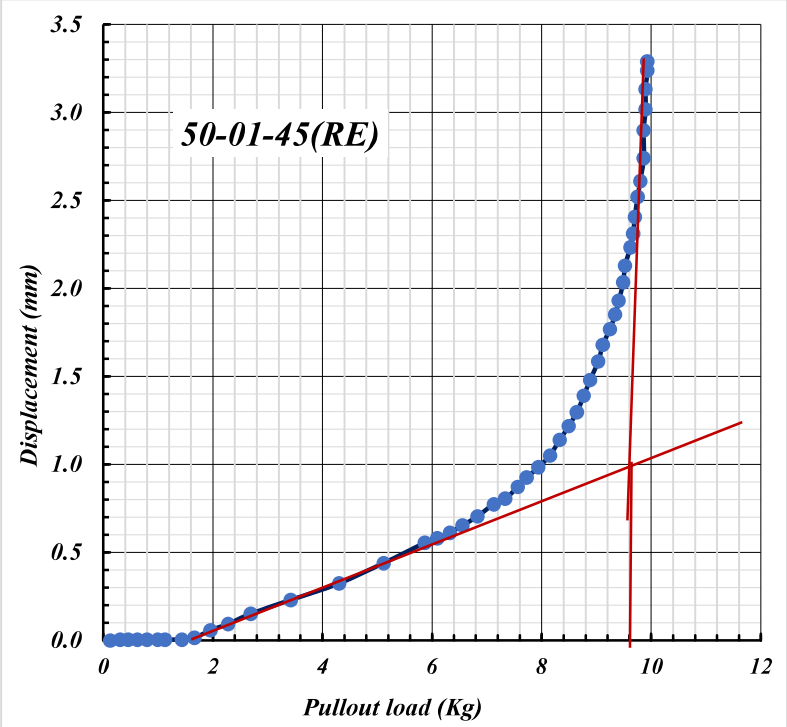

Fig. 4.70: Load vs Axial Movement for 50mm Square Plate with (H/B=1) inclined at 45° with vertical in reinforced condition

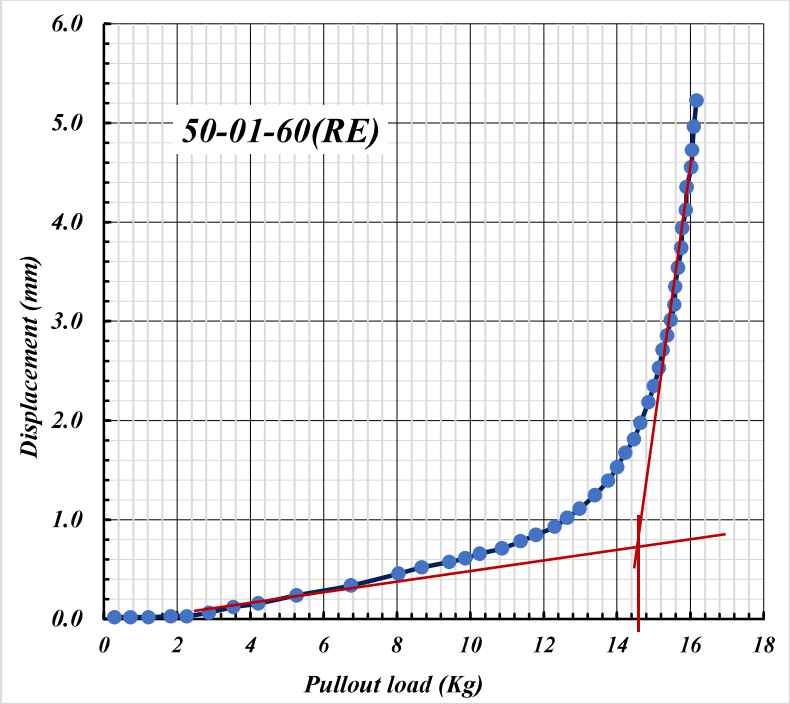

Fig. 4.71: Load vs Axial Movement for 50mm Square Plate with (H/B=1) inclined at 60° with vertical in reinforced condition

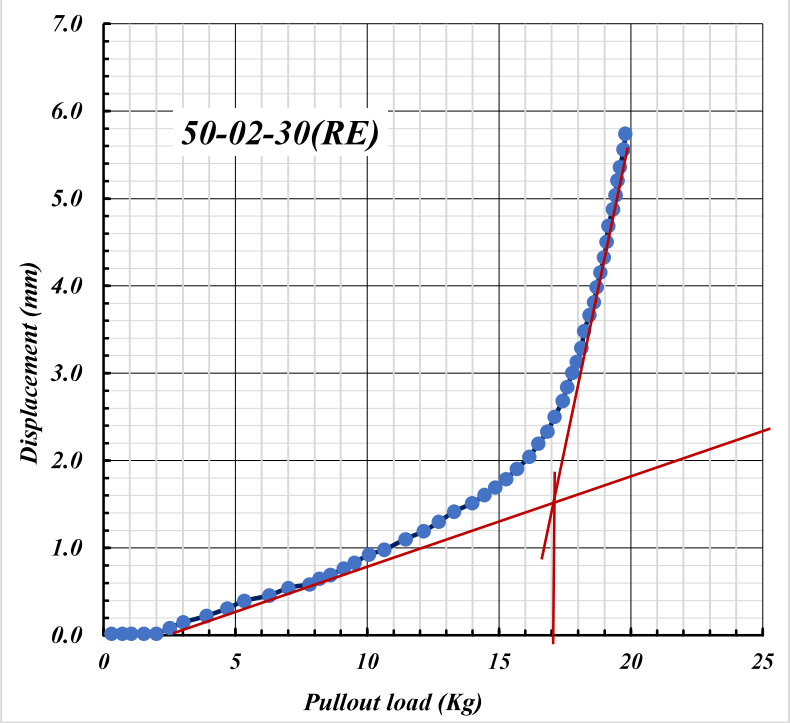

Fig. 4.72: Load vs Axial Movement for 50mm Square Plate with (H/B=2) inclined at 30° with vertical in reinforced condition

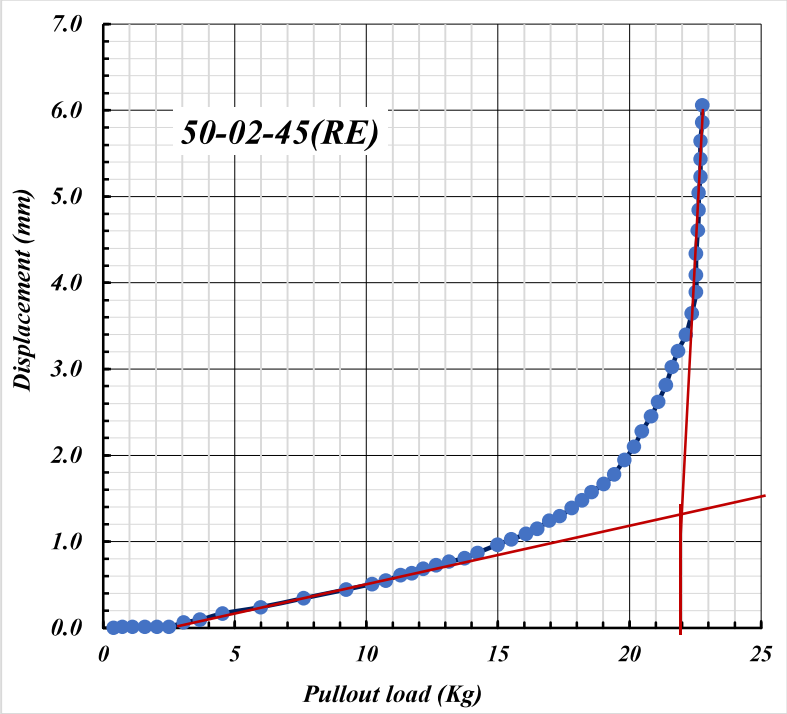

Fig. 4.73: Load vs Axial Movement for 50mm Square Plate with (H/B=2) inclined at 45° with vertical in reinforced condition

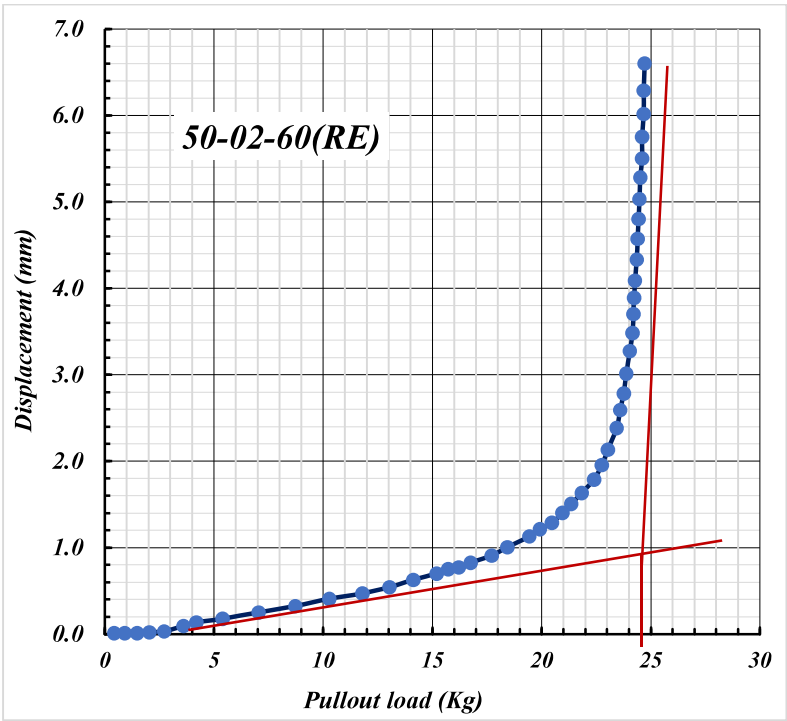

Fig. 4.74: Load vs Axial Movement for 50mm Square Plate with (H/B=2) inclined at 60° with vertical in reinforced condition

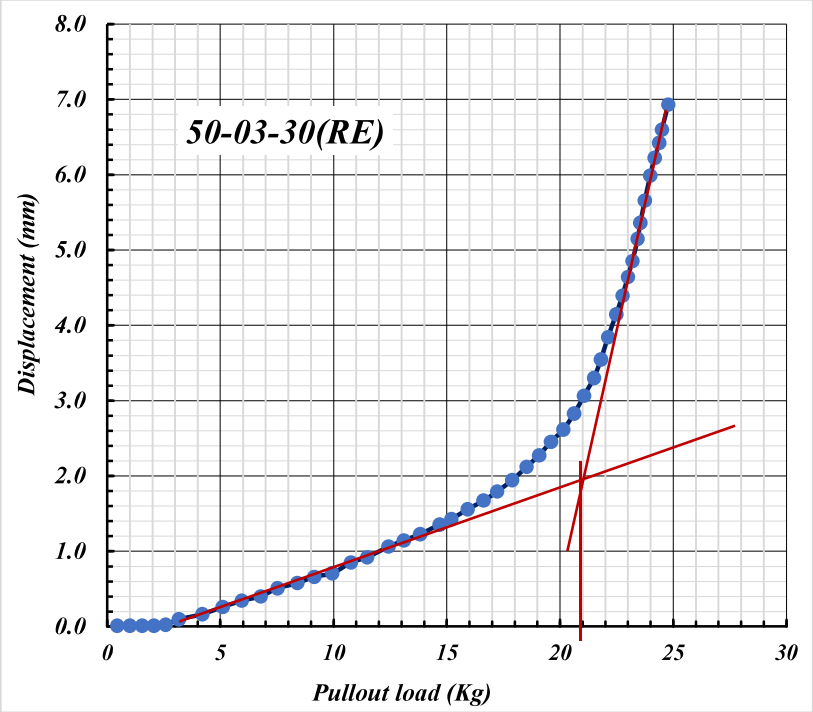

Fig. 4.75: Load vs Axial Movement for 50mm Square Plate with (H/B=3) inclined at 30° with vertical in reinforced condition

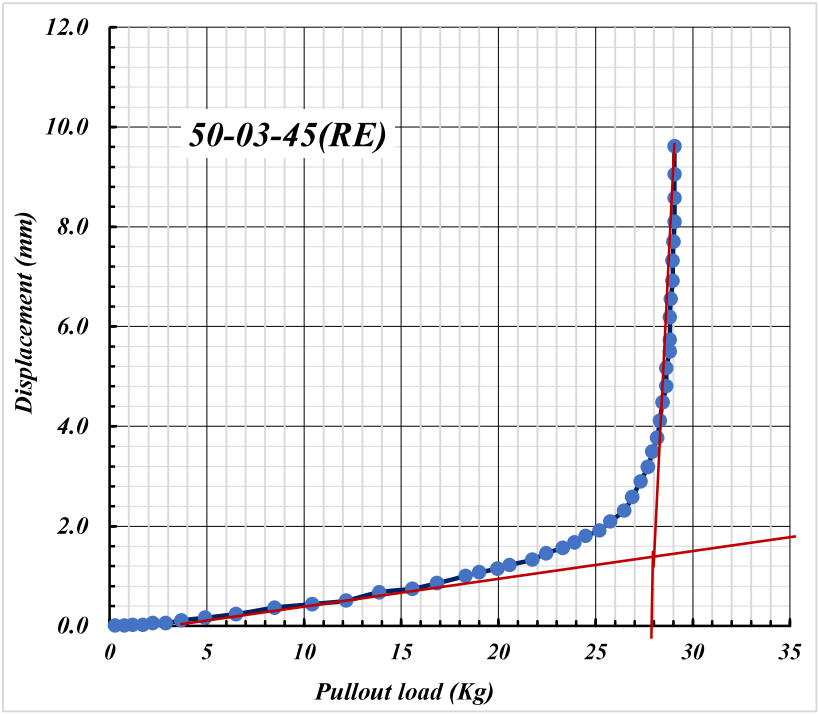

Fig. 4.76: Load vs Axial Movement for 50mm Square Plate with (H/B=3) inclined at 45° with vertical in reinforced condition

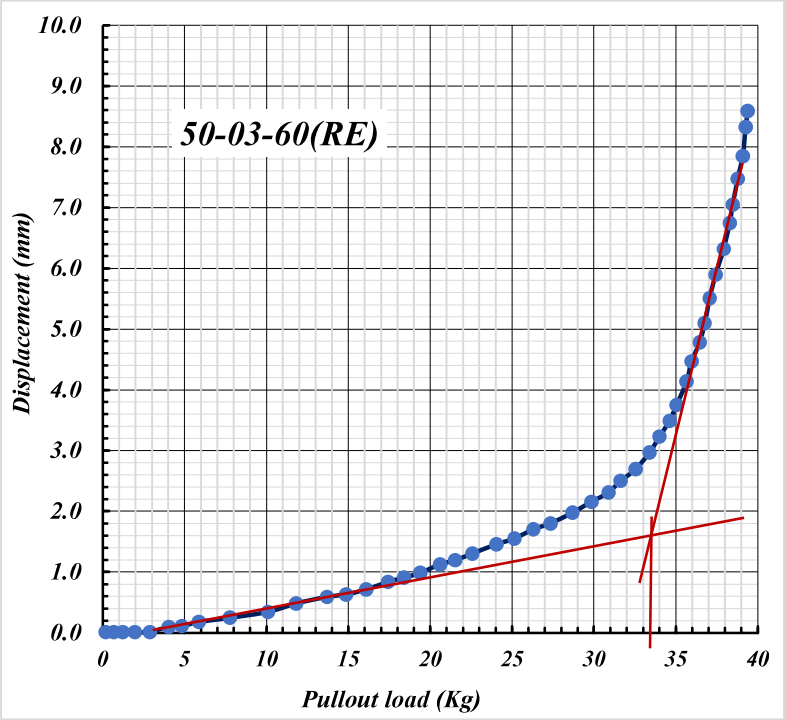

Fig. 4.77: Load vs Axial Movement for 50mm Square Plate with (H/B=3) inclined at 60° with vertical in reinforced condition

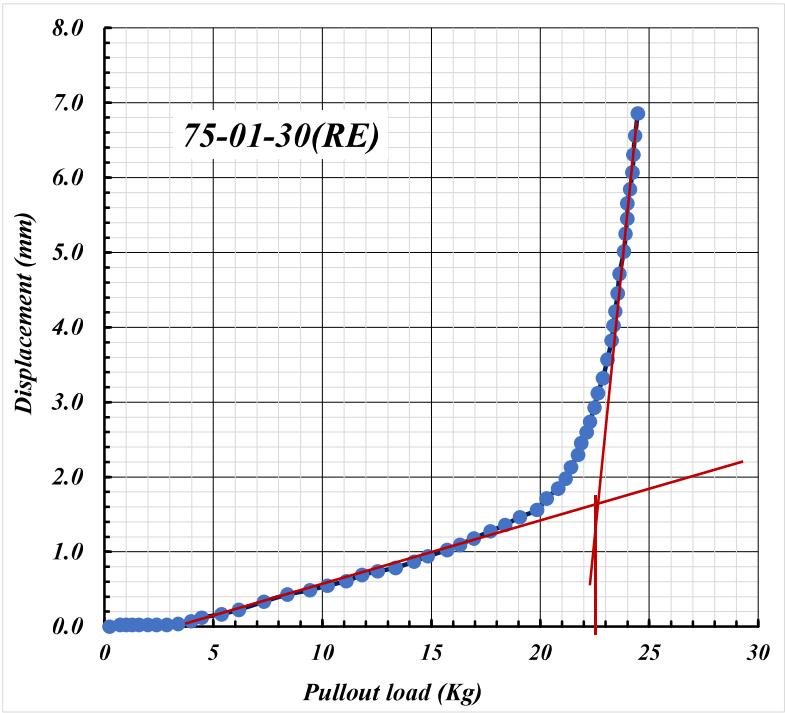

Fig. 4.78: Load vs Axial Movement for 75mm Square Plate with (H/B=1) inclined at 30° with vertical in reinforced condition

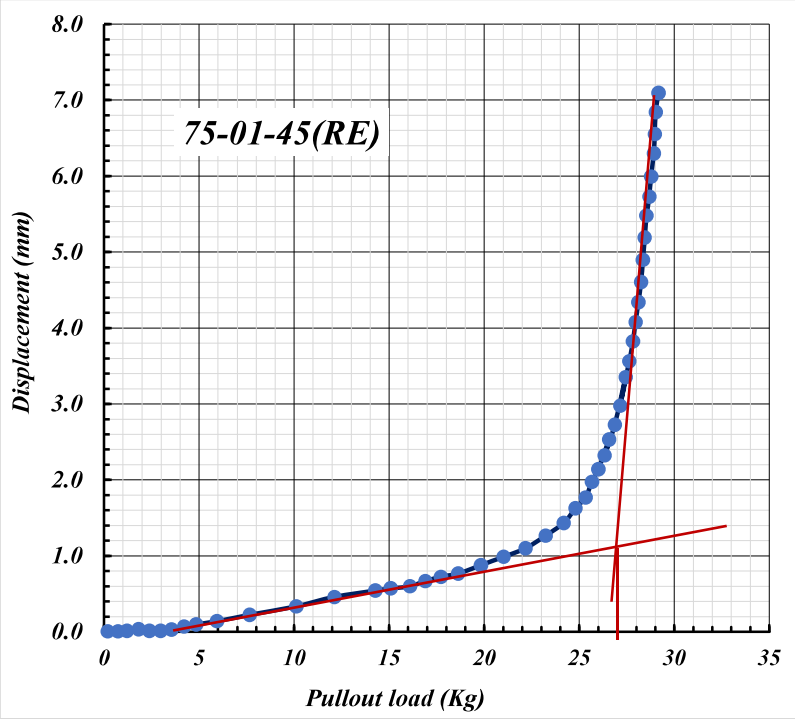

Fig. 4.79: Load vs Axial Movement for 75mm Square Plate with (H/B=1) inclined at 45° with vertical in reinforced condition

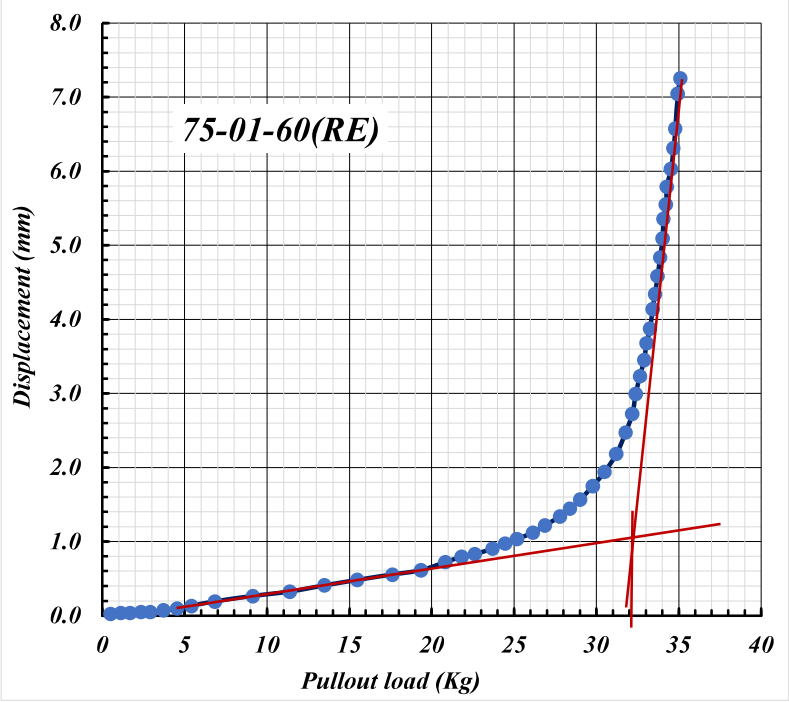

Fig. 4.80: Load vs Axial Movement for 75mm Square Plate with (H/B=1) inclined at 60° with vertical in reinforced condition

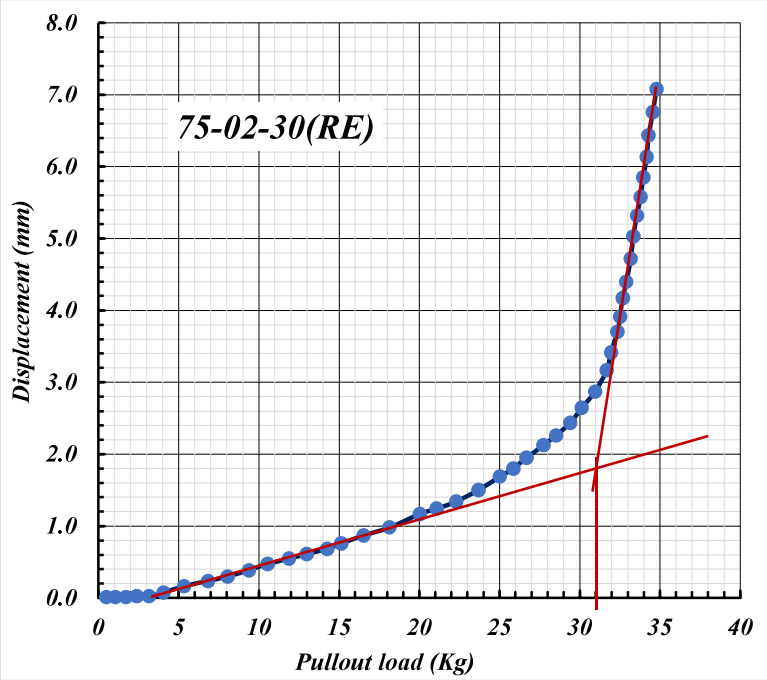

Fig. 4.81: Load vs Axial Movement for 75mm Square Plate with (H/B=2) inclined at 30° with vertical in reinforced condition

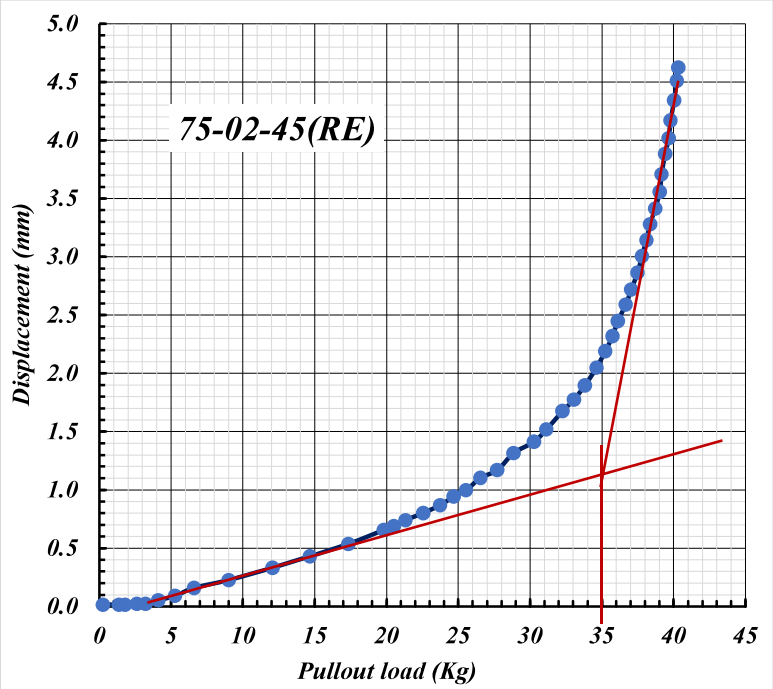

Fig. 4.82: Load vs Axial Movement for 75mm Square Plate with (H/B=2) inclined at 45° with vertical in reinforced condition

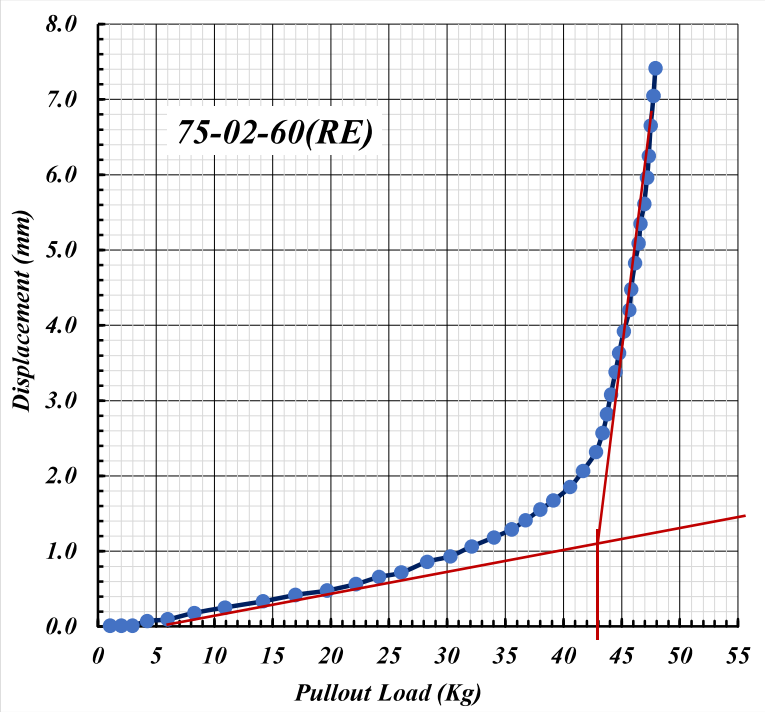

Fig. 4.83: Load vs Axial Movement for 75mm Square Plate with (H/B=2) inclined at 60° with vertical in reinforced condition

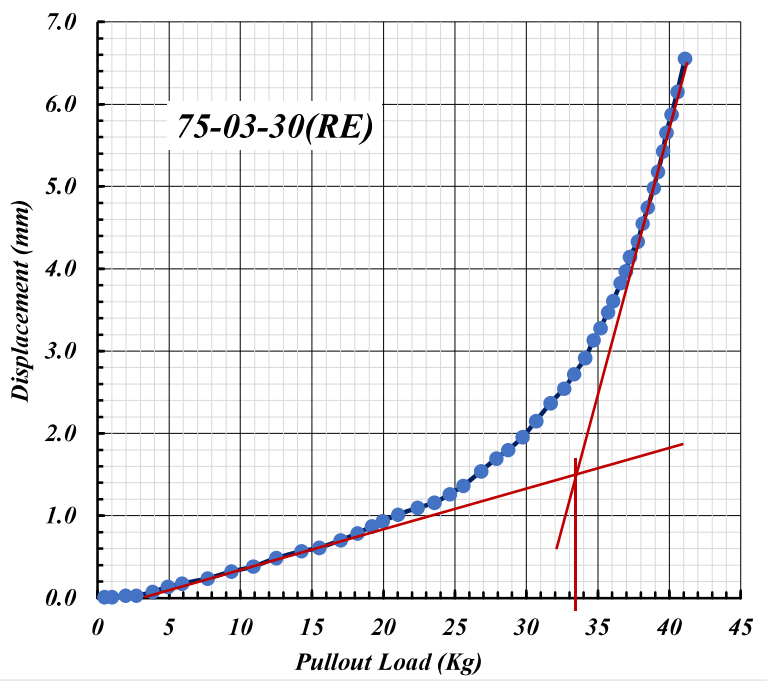

Fig. 4.84: Load vs Axial Movement for 75mm Square Plate with (H/B=3) inclined at 30° with vertical in reinforced condition

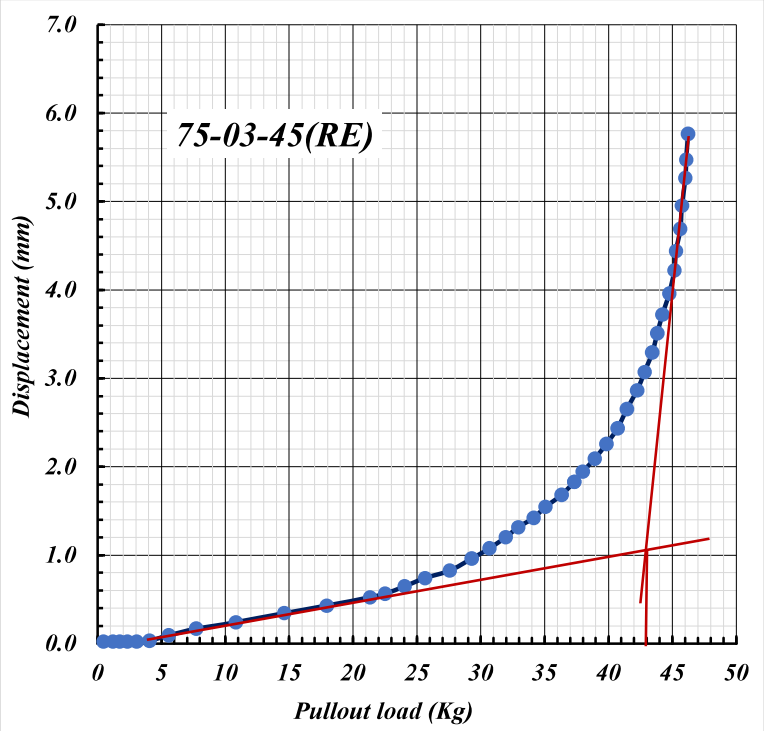

Fig. 4.85: Load vs Axial Movement for 75mm Square Plate with (H/B=3) inclined at 45° with vertical in reinforced condition

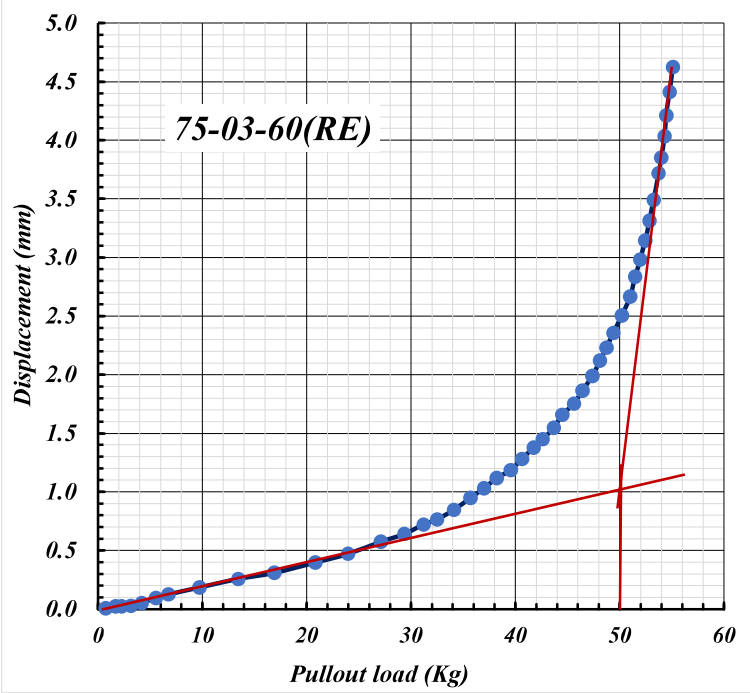

Fig. 4.86: Load vs Axial Movement for 75mm Square Plate with (H/B=3) inclined at 60° with vertical in reinforced condition

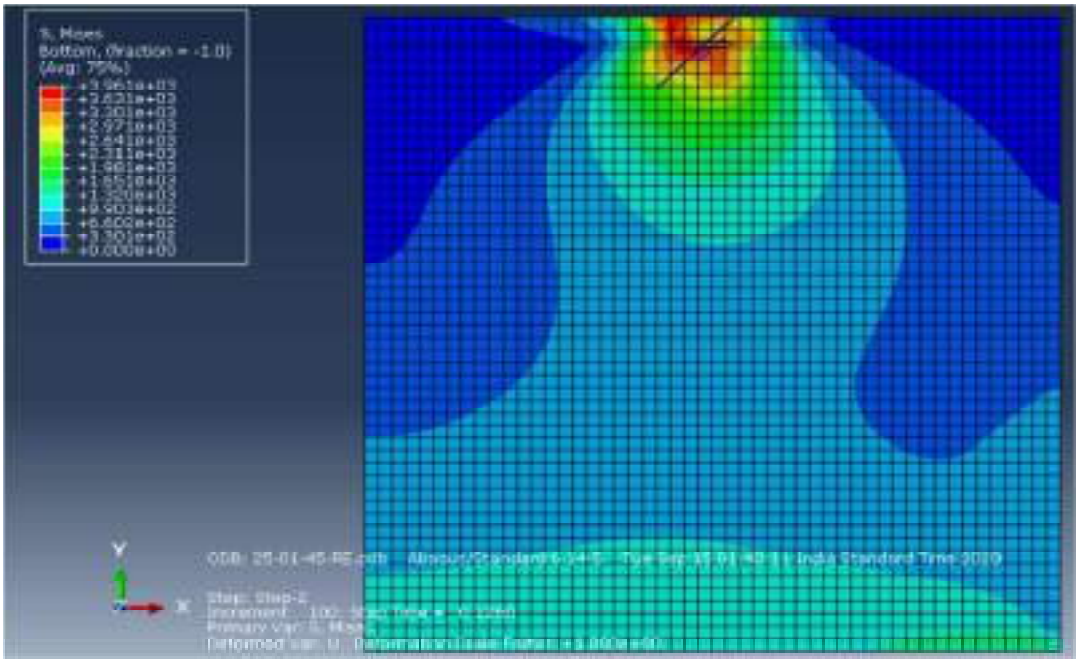

Fig. 4.88: Stress contour for 25mm Square Anchor Plate with (H/B=1) inclined at 45° with vertical in reinforced soil

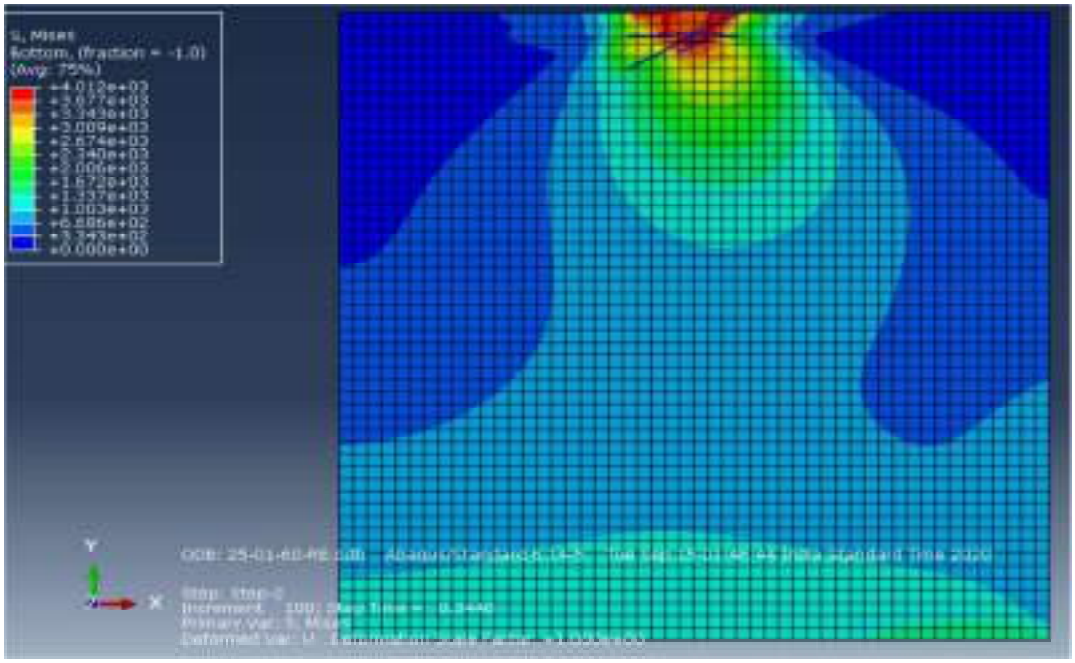

Fig. 4.89: Stress contour for 25mm Square Anchor Plate with (H/B=1) inclined at 60° with vertical in reinforced soil

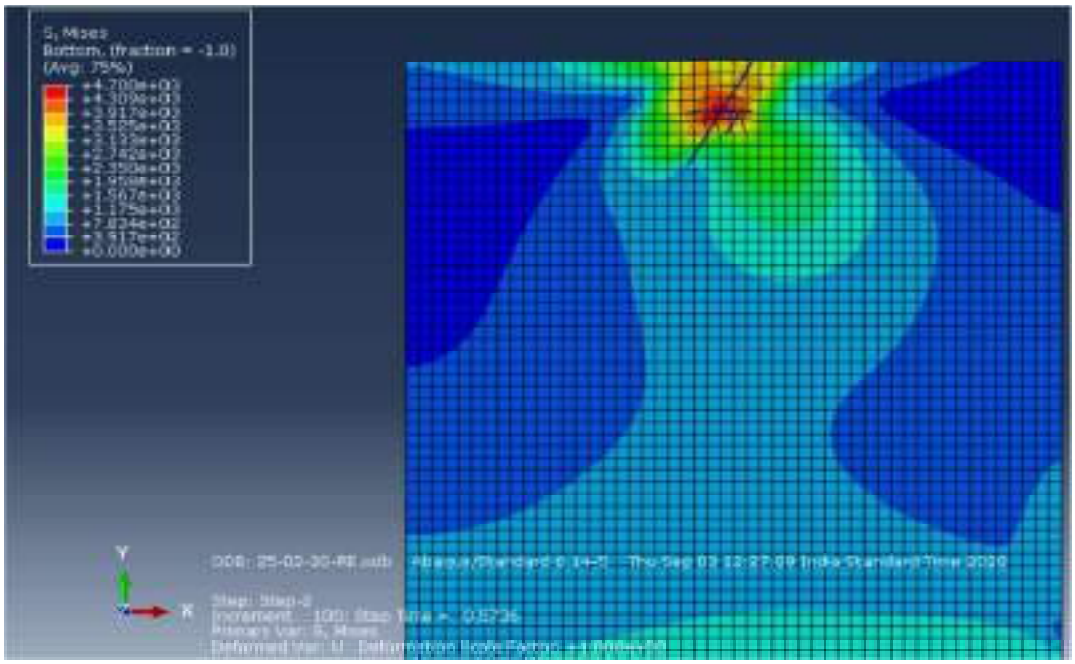

Fig. 4.90: Stress contour for 25mm Square Anchor Plate with (H/B=2) inclined at 30° with vertical in reinforced soil

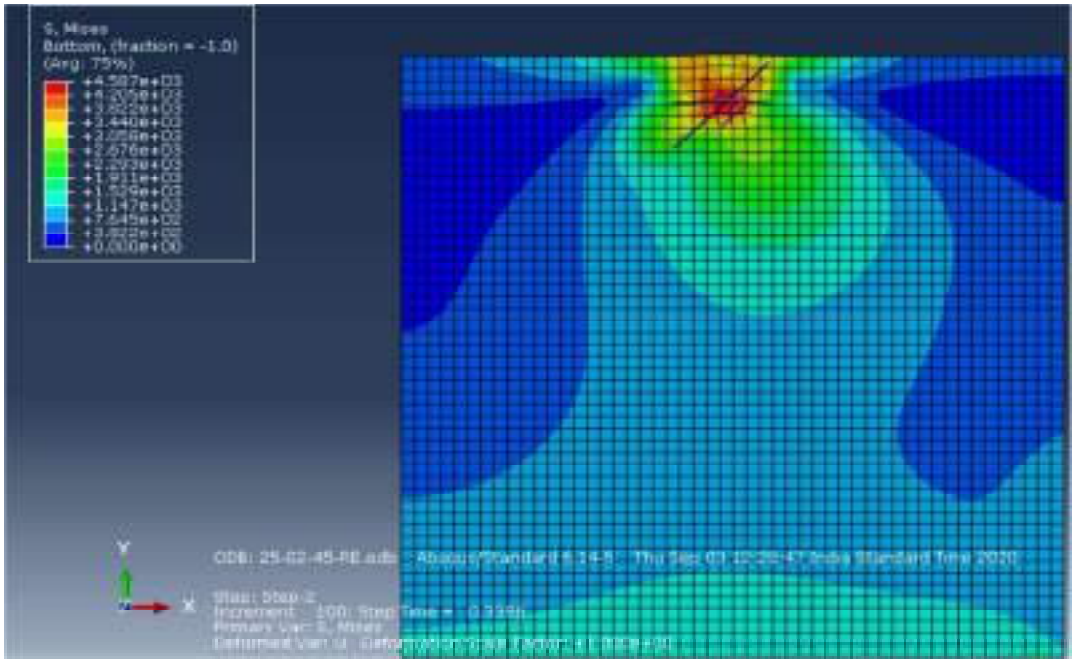

Fig. 4.91: Stress contour for 25mm Square Anchor Plate with (H/B=2) inclined at 45° with vertical in reinforced soil

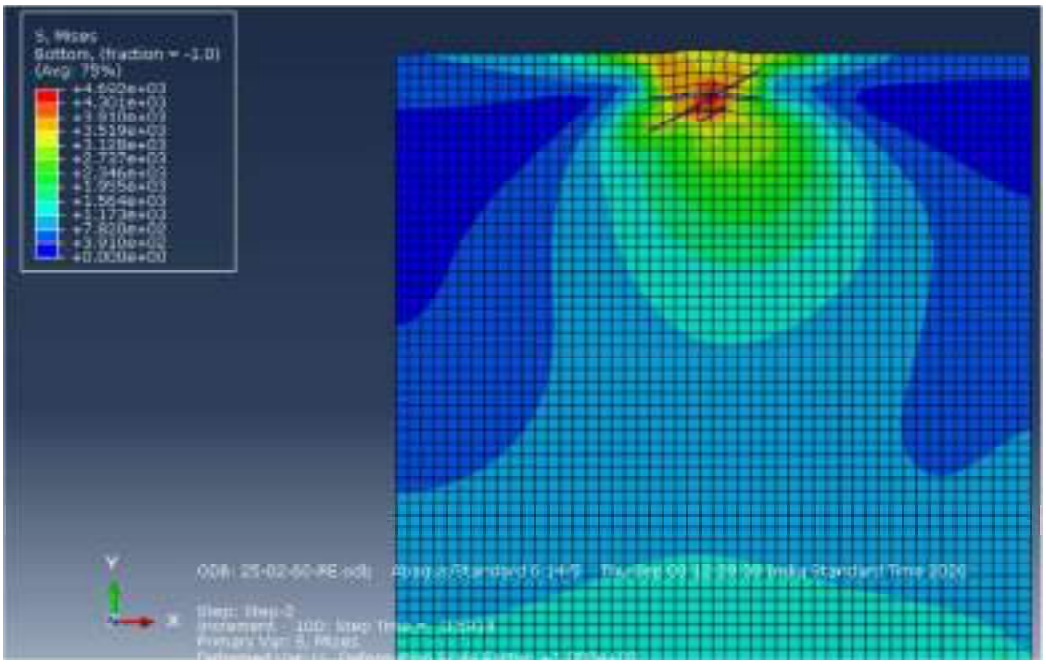

Fig. 4.92: Stress contour for 25mm Square Anchor Plate with (H/B=2) inclined at 60° with vertical in reinforced soil

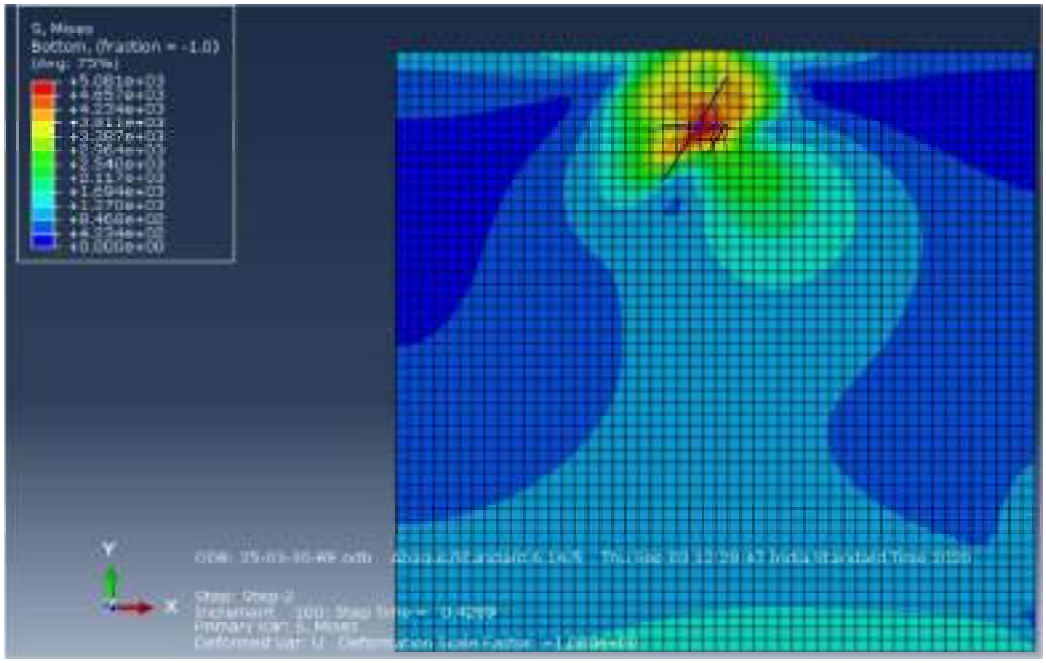

Fig. 4.93: Stress contour for 25mm Square Anchor Plate with (H/B=3) inclined at 30° with vertical in reinforced soil

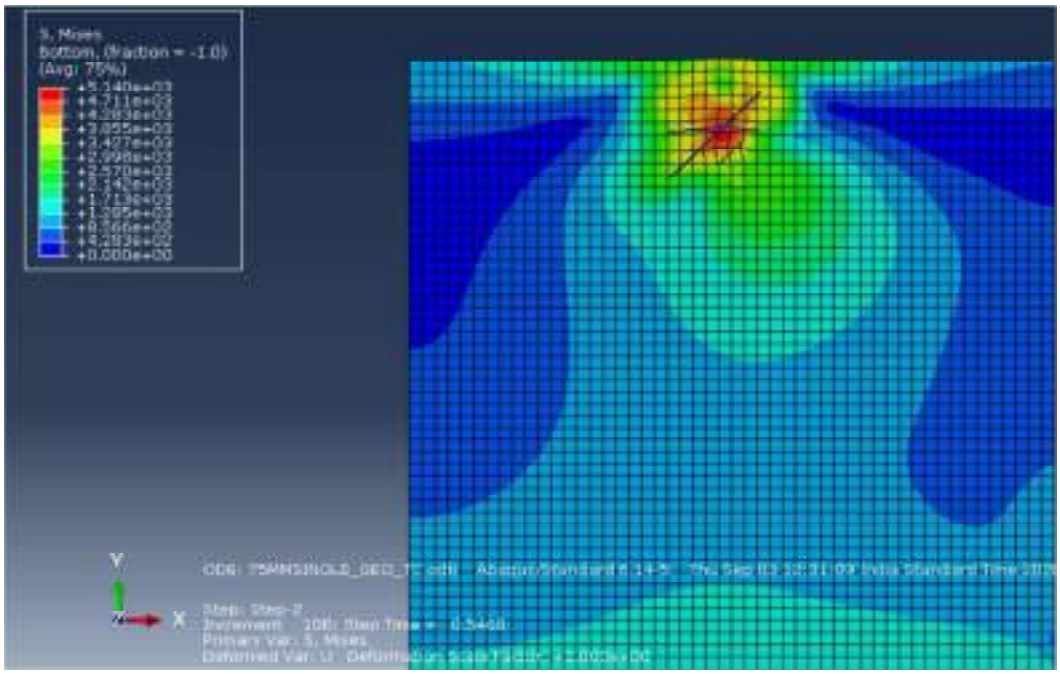

Fig. 4.94: Stress contour for 25mm Square Anchor Plate with (H/B=3) inclined at 45° with vertical in reinforced soil

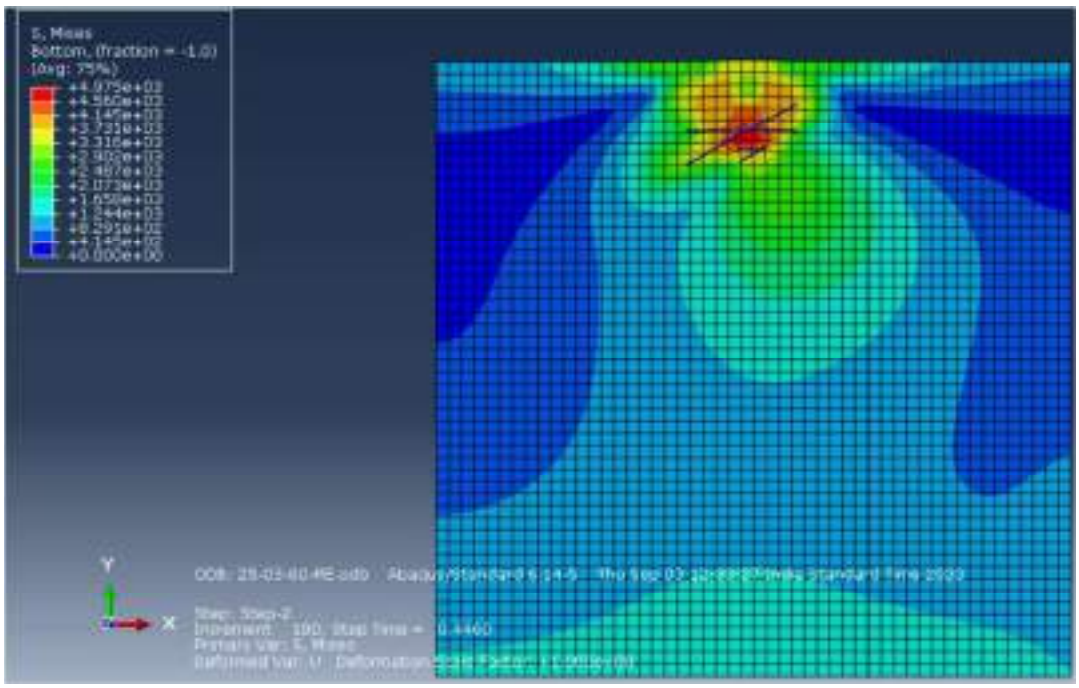

Fig. 4.95: Stress contour for 25mm Square Anchor Plate with (H/B=3) inclined at 60° with vertical in reinforced soil

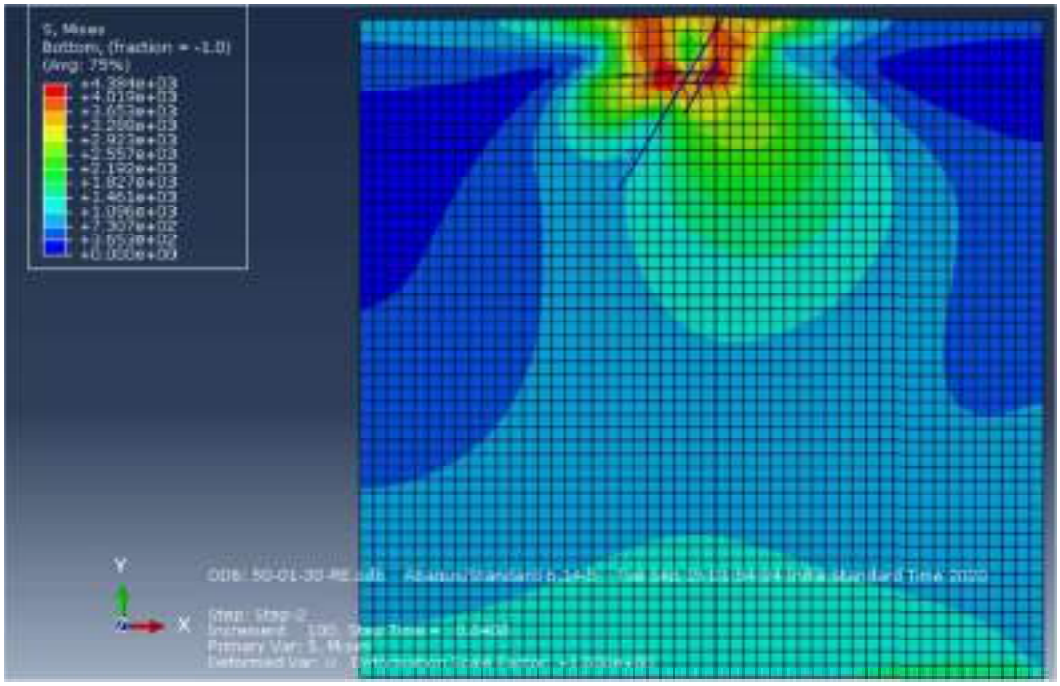

Fig. 4.96: Stress contour for 50mm Square Anchor Plate with (H/B=1) inclined at 30° with vertical in reinforced soil

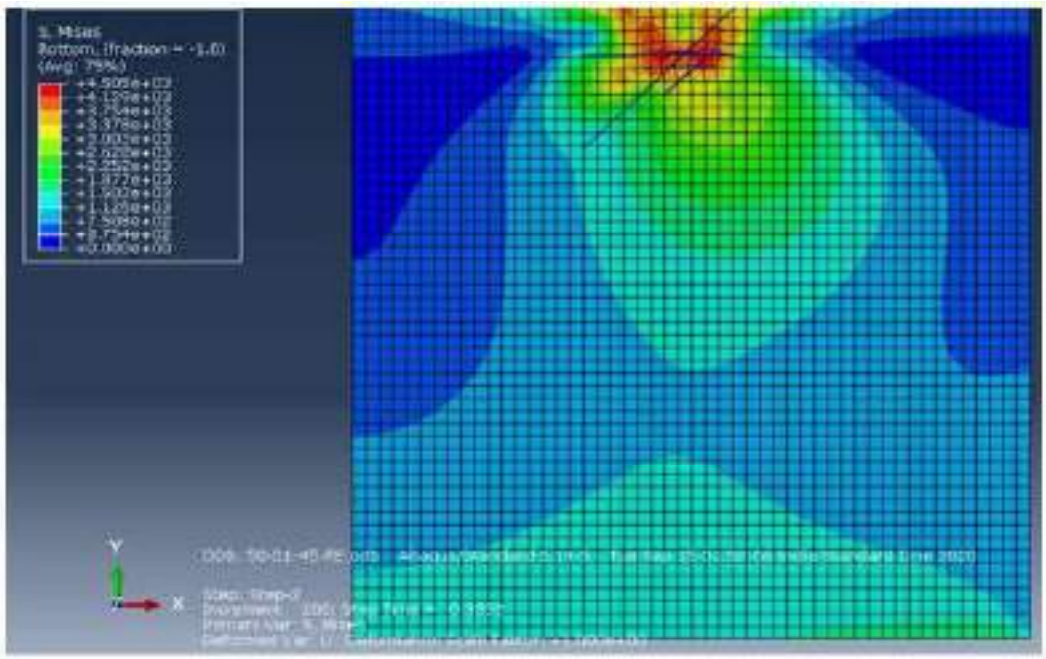

Fig. 4.97: Stress contour for 50mm Square Anchor Plate with (H/B=1) inclined at 45° with vertical in reinforced soil

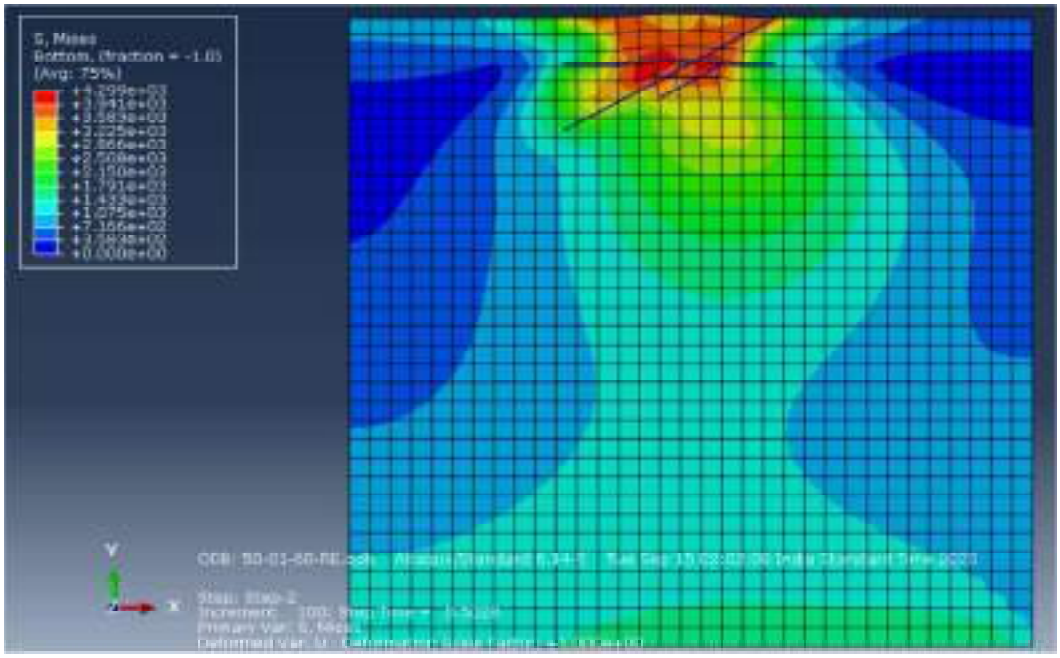

Fig. 4.98: Stress contour for 50mm Square Anchor Plate with (H/B=1) inclined at 60° with vertical in reinforced soil

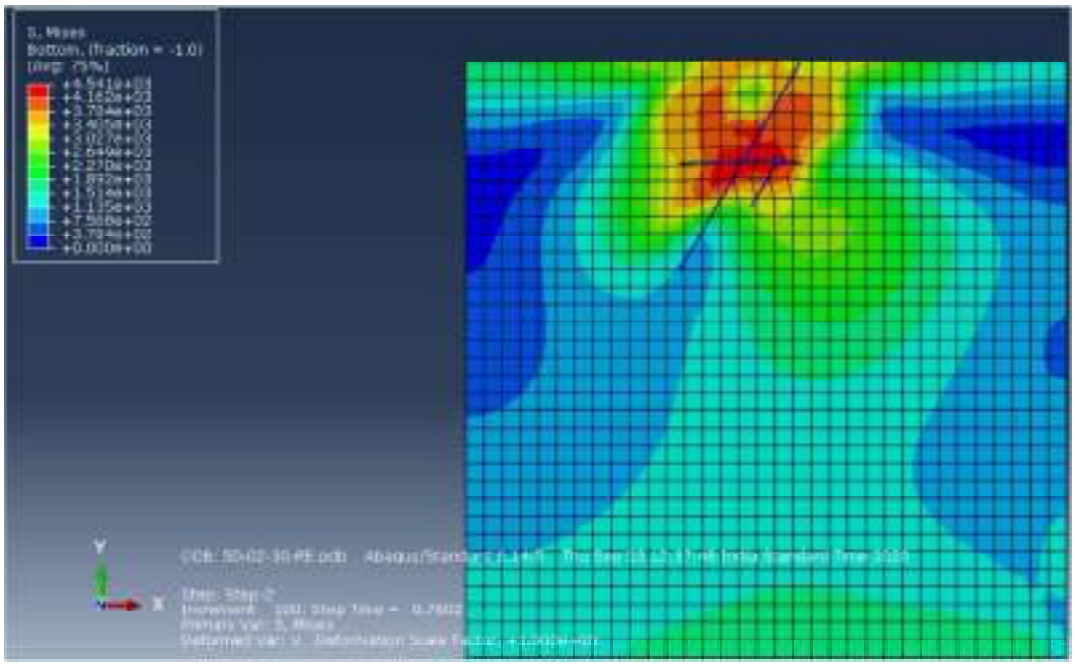

Fig. 4.99: Stress contour for 50mm Square Anchor Plate with (H/B=2) inclined at 30° with vertical in reinforced soil

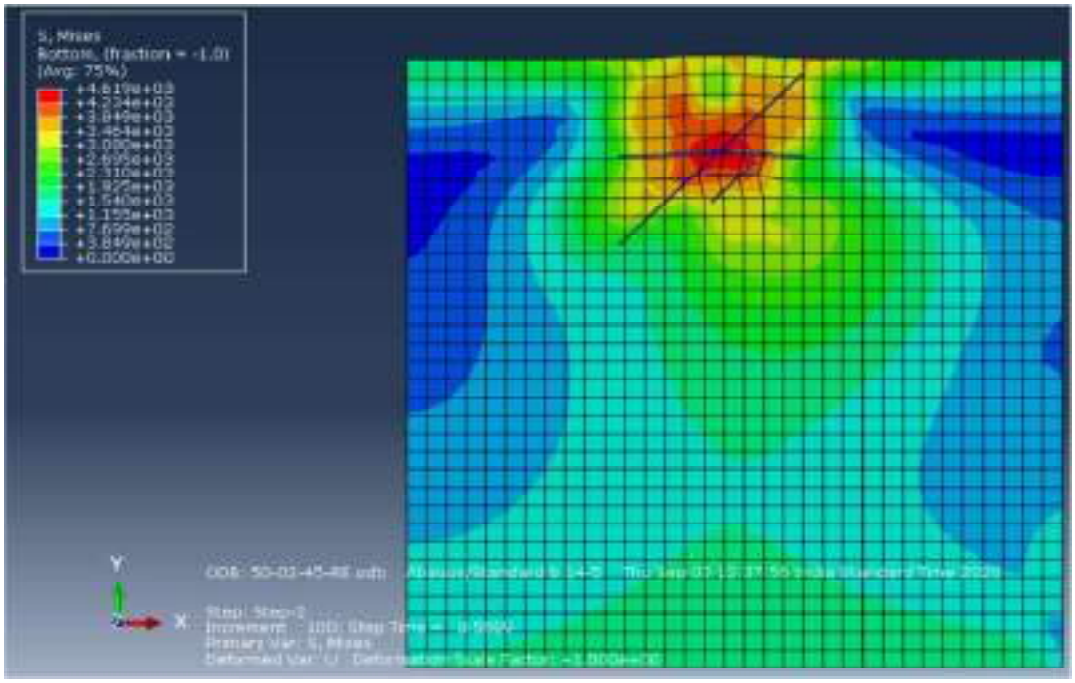

Fig. 4.100: Stress contour for 50mm Square Anchor Plate with (H/B=2) inclined at 45° with vertical in reinforced soil

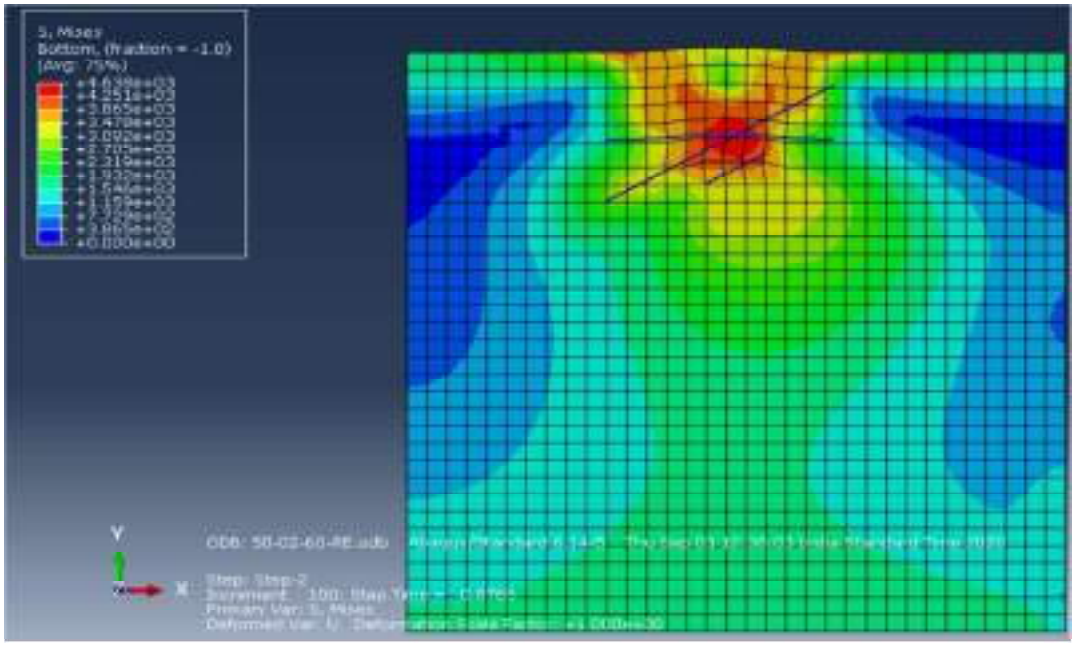

Fig. 4.101: Stress contour for 50mm Square Anchor Plate with (H/B=2) inclined at 60° with vertical in reinforced soil

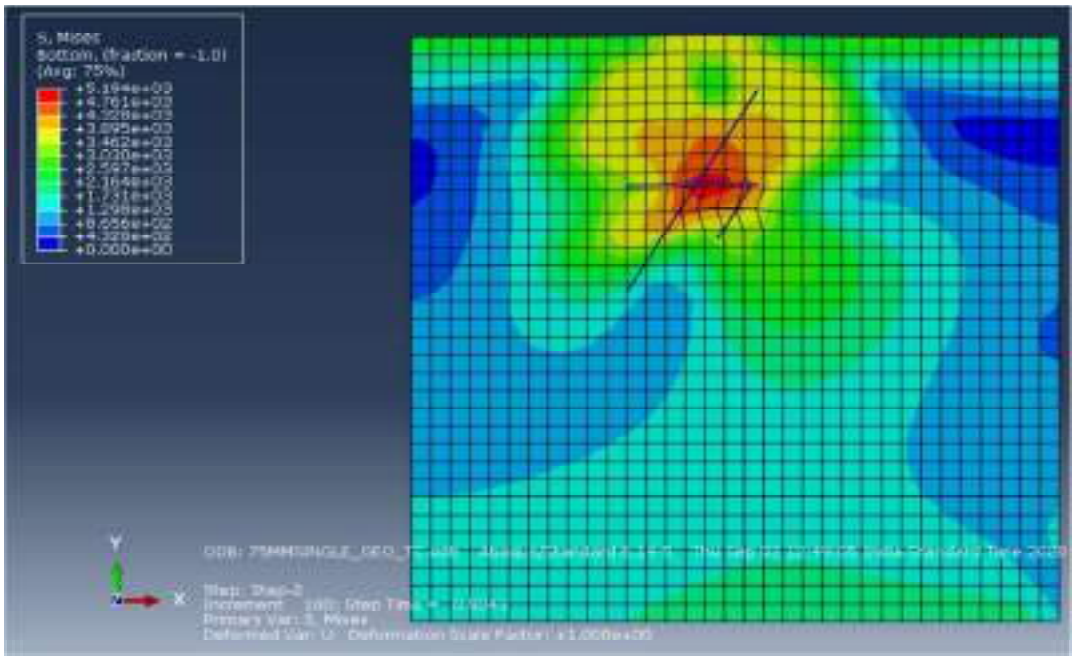

Fig. 4.102: Stress contour for 50mm Square Anchor Plate with (H/B=3) inclined at 30° with vertical in reinforced soil

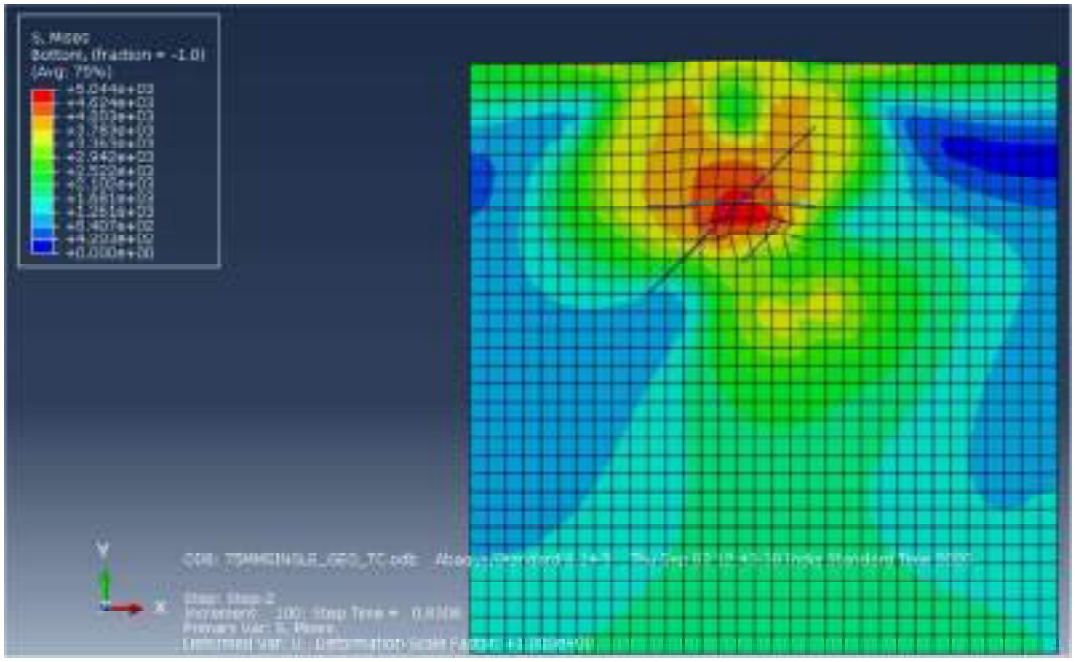

Fig. 4.103: Stress contour for 50mm Square Anchor Plate with (H/B=3) inclined at 45° with vertical in reinforced soil

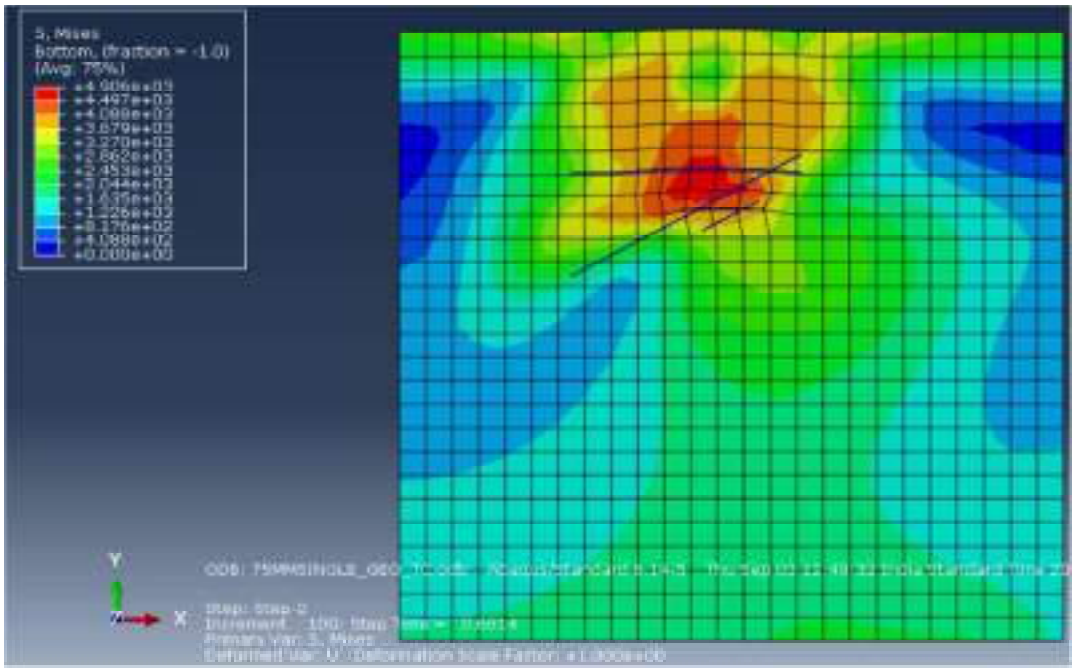

Fig. 4.104: Stress contour for 50mm Square Anchor Plate with (H/B=3) inclined at 60° with vertical in reinforced soil

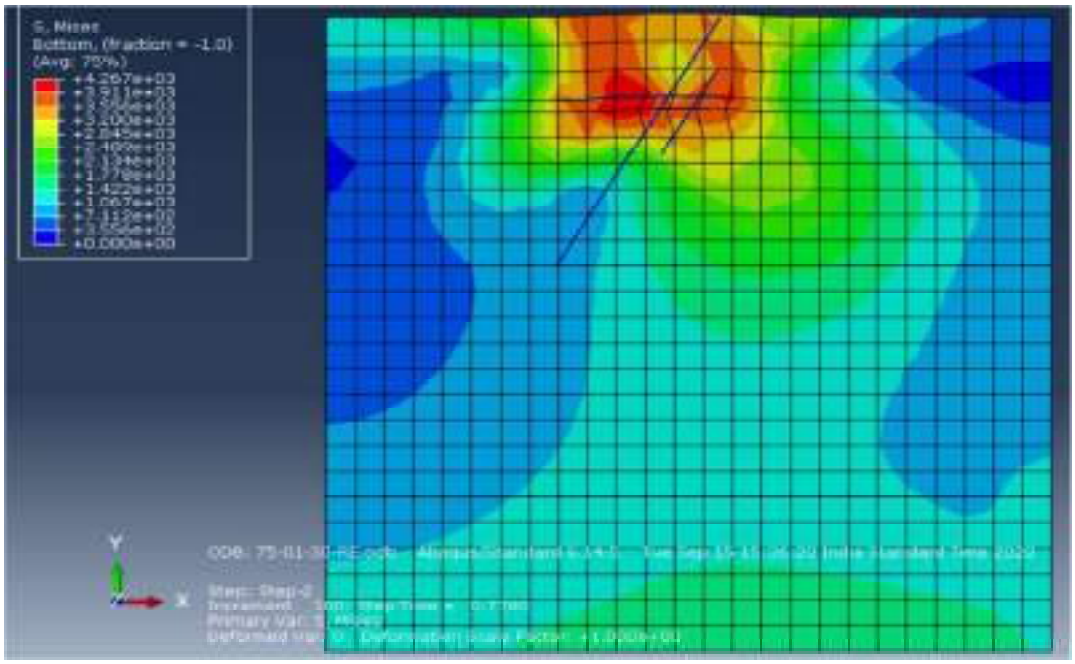

Fig. 4.105: Stress contour for 75mm Square Anchor Plate with (H/B=1) inclined at 30° with vertical in reinforced soil

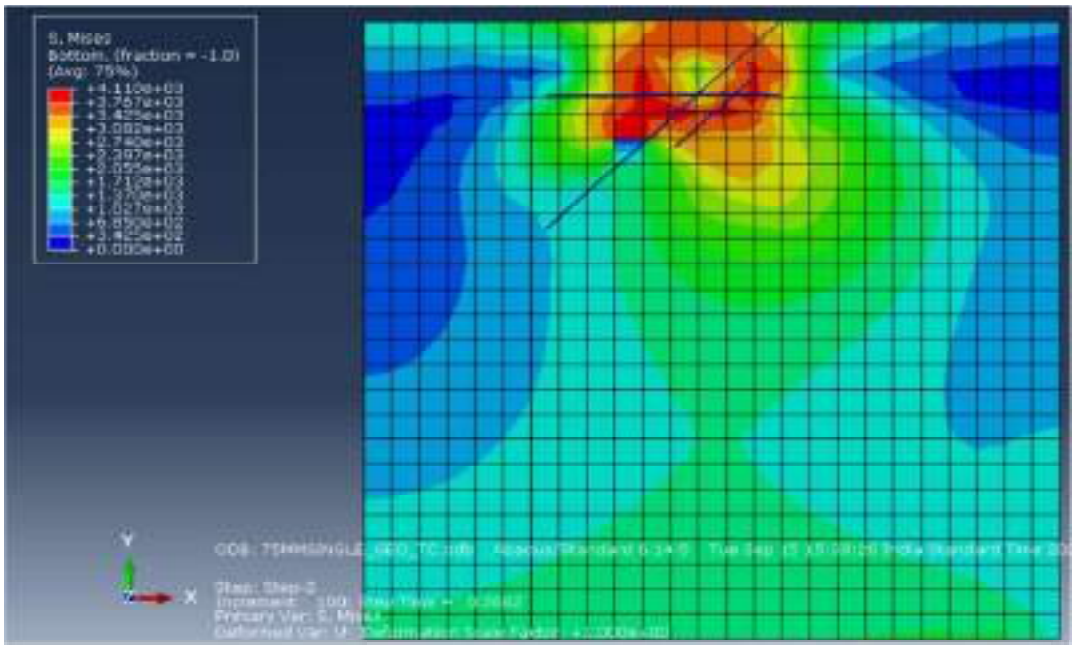

Fig. 4.106: Stress contour for 75mm Square Anchor Plate with (H/B=1) inclined at 45° with vertical in reinforced soil

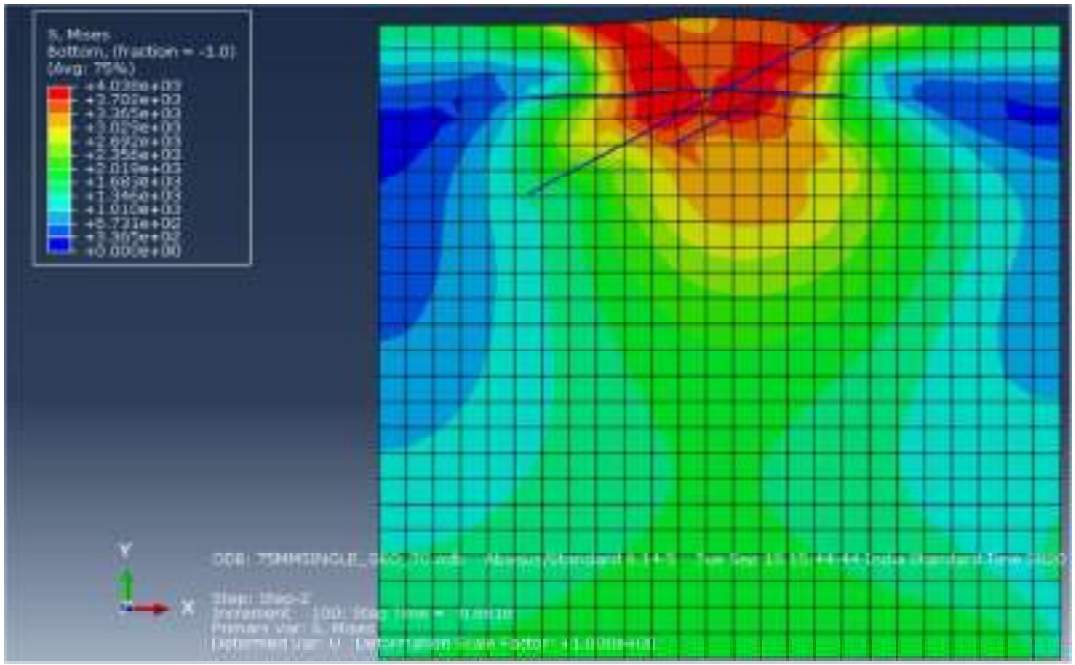

Fig. 4.107: Stress contour for 75mm Square Anchor Plate with (H/B=1) inclined at 60° with vertical in reinforced soil

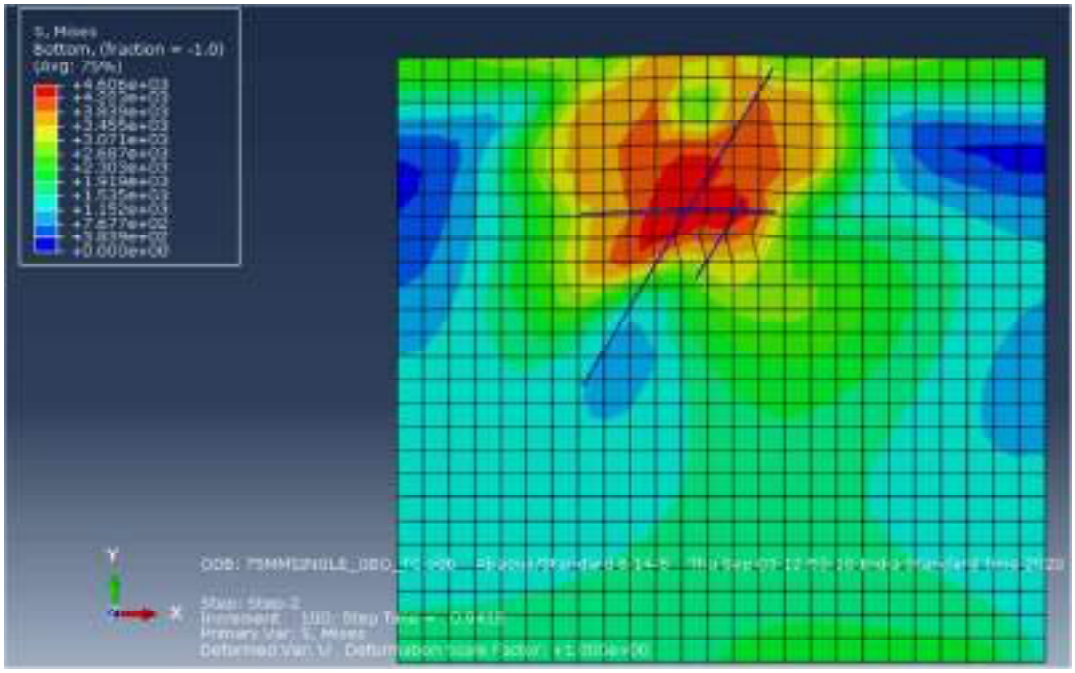

Fig. 4.108: Stress contour for 75mm Square Anchor Plate with (H/B=2) inclined at 30° with vertical in reinforced soil

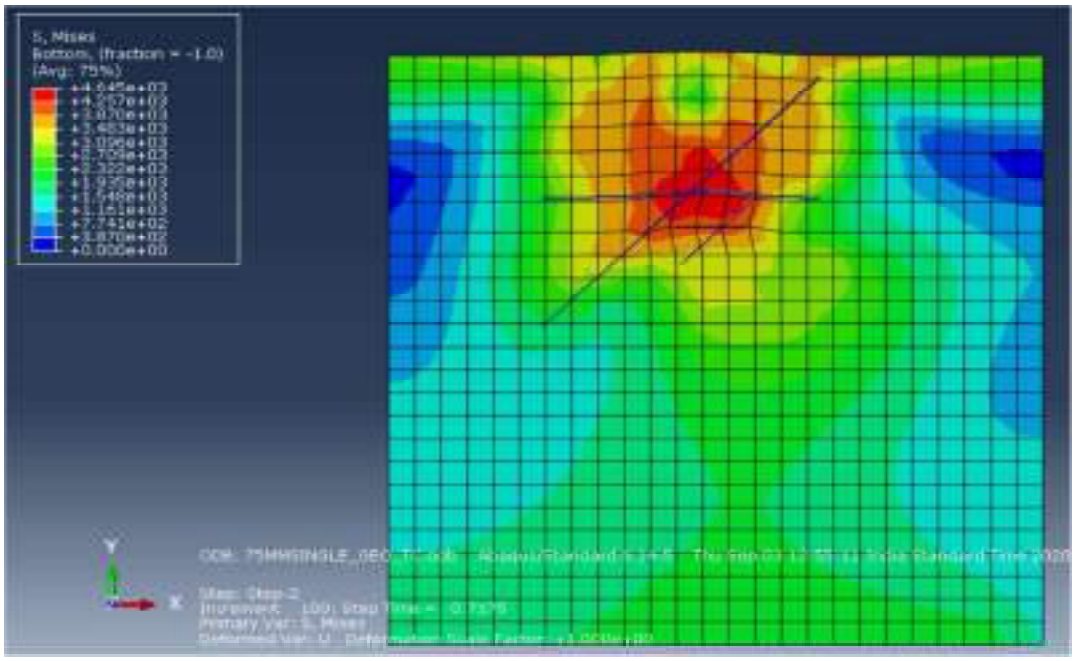

Fig. 4.109: Stress contour for 75mm Square Anchor Plate with (H/B=2) inclined at 45° with vertical in reinforced soil

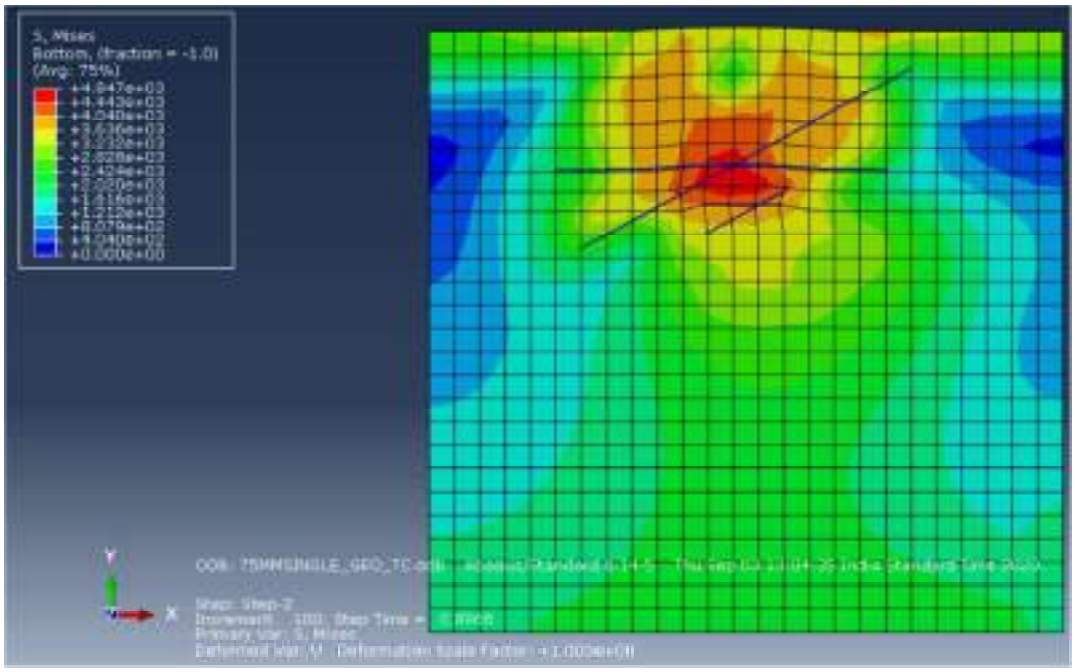

Fig. 4.110: Stress contour for 75mm Square Anchor Plate with (H/B=2) inclined at 60° with vertical in reinforced soil

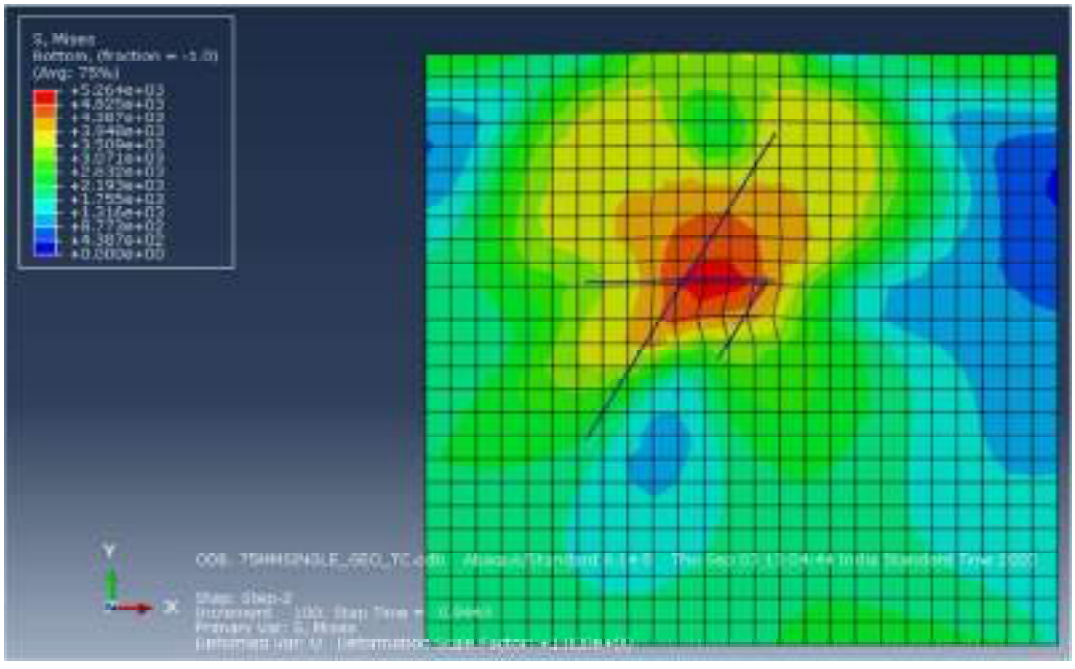

Fig. 4.111: Stress contour for 75mm Square Anchor Plate with (H/B=3) inclined at 30° with vertical in reinforced soil

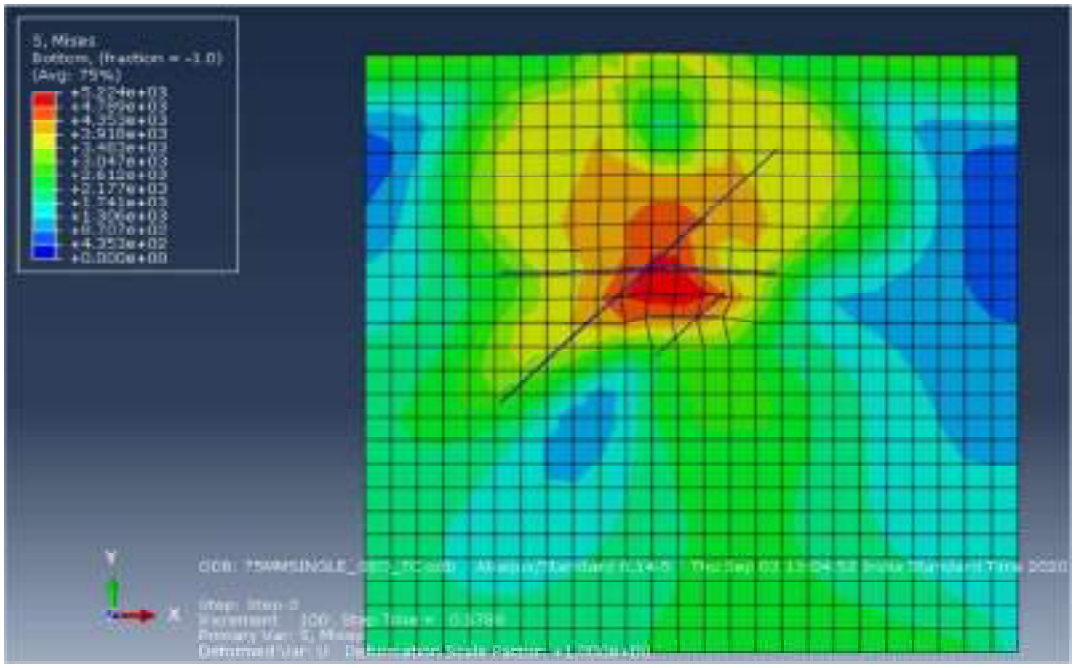

Fig. 4.112: Stress contour for 75mm Square Anchor Plate with (H/B=3) inclined at 45° with vertical in reinforced soil

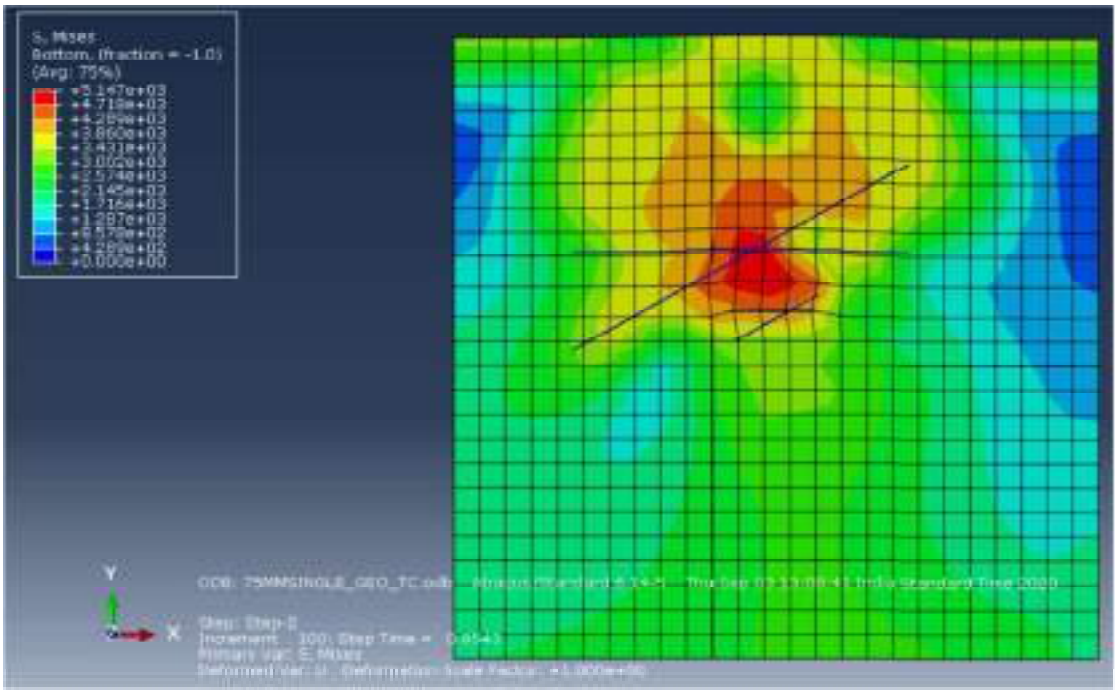

Fig. 4.113: Stress contour for 75mm Square Anchor Plate with (H/B=3) inclined at 60° with vertical in reinforced soil

ANNEXURE -IV

PRESENTATION OF RESULTS OF NUMERICAL ANALYSIS (CYCLIC REINFORCED)

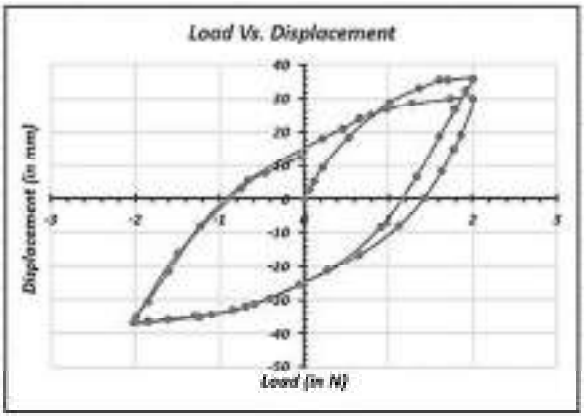

Fig. 4.123: Load vs. Displacement for 25 mm Square Plate with (H/B =2) at 30° inclination under 0.2 Hz frequency and 2mm amplitude

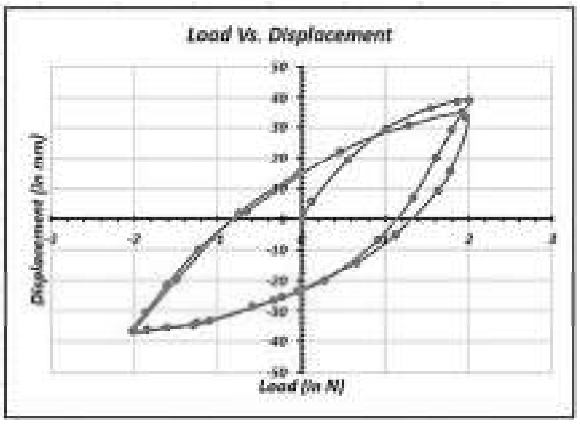

Fig. 4.124: Load vs. Displacement for 25 mm Square Plate with (H/B =3) at 30° inclination under 0.2 Hz frequency and 2mm amplitude

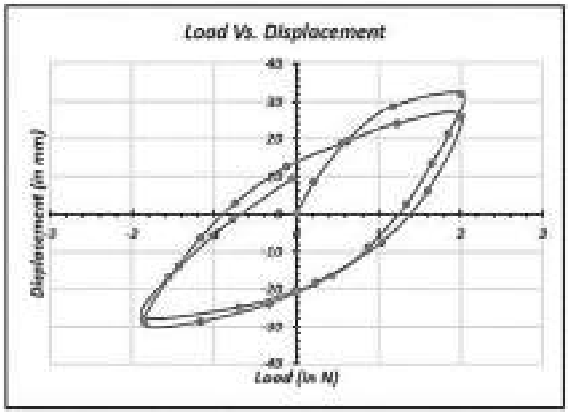

Fig. 4.125: Load vs. Displacement for 25 mm Square Plate with (H/B =1) at 45° inclination under 0.2 Hz frequency and 2mm amplitude

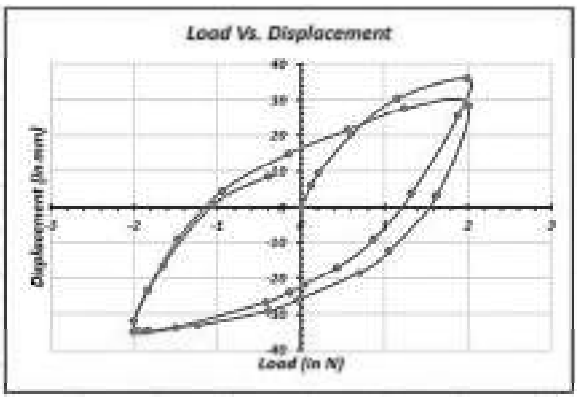

Fig. 4.126: Load vs. Displacement for 25 mm Square Plate with (H/B =2) at 45° inclination under 0.2 Hz frequency and 2mm amplitude

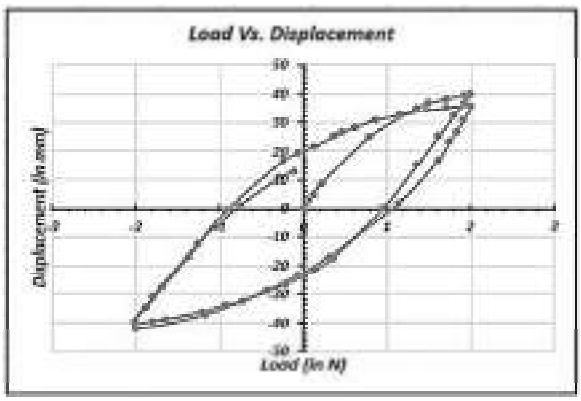

Fig. 4.127: Load vs. Displacement for 25 mm Square Plate with (H/B =3) at 45° inclination under 0.2 Hz frequency and 2mm amplitude

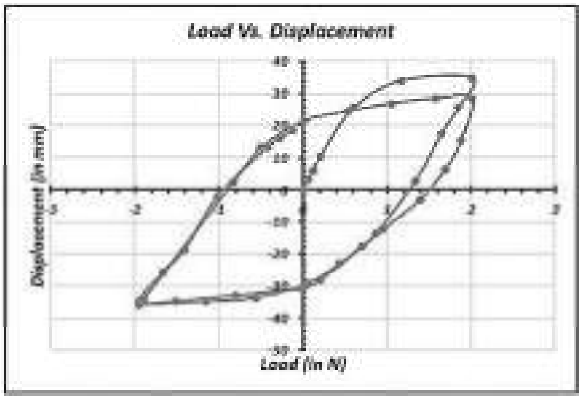

Fig. 4.128: Load vs. Displacement for 25 mm Square Plate with (H/B =1) at 60° inclination under 0.2 Hz frequency and 2mm amplitude

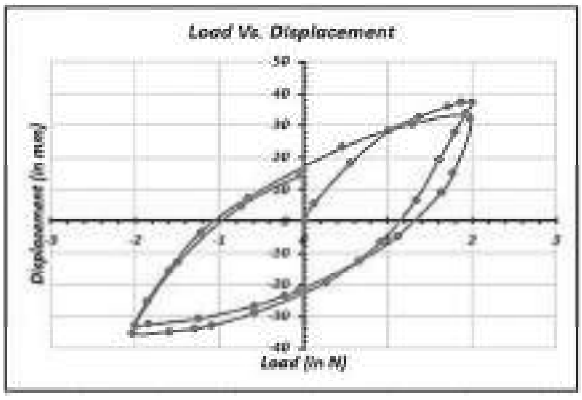

Fig. 4.129: Load vs. Displacement for 25 mm Square Plate with (H/B =2) at 60° inclination under 0.2 Hz frequency and 2mm amplitude

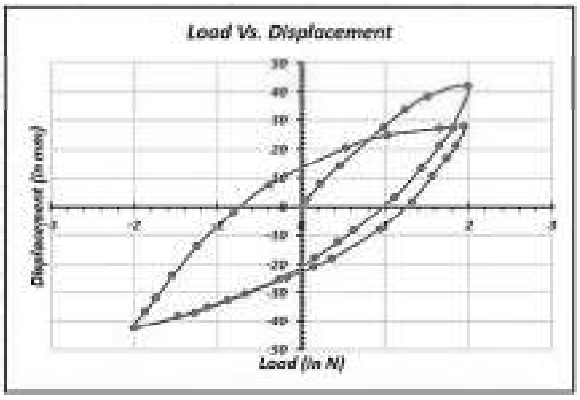

Fig. 4.130: Load vs. Displacement for 25 mm Square Plate with (H/B =3) at 60° inclination under 0.2 Hz frequency and 2mm amplitude

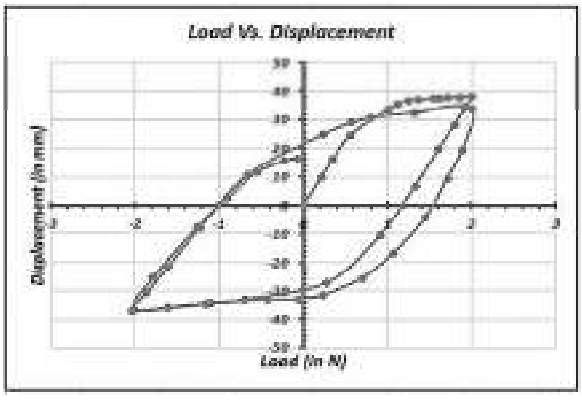

Fig. 4.131: Load vs. Displacement for 50 mm Square Plate with (H/B =1) at 30° inclination under 0.2 Hz frequency and 2mm amplitude

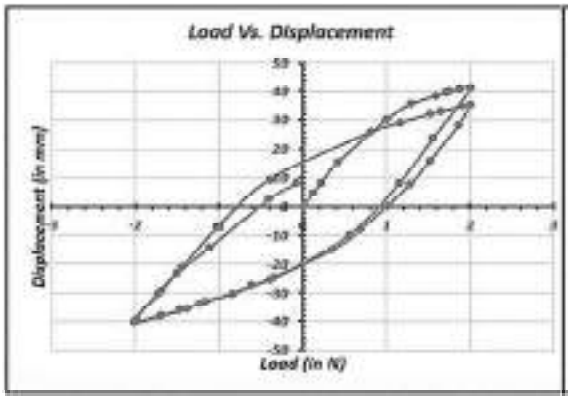

Fig. 4.132: Load vs. Displacement for 50 mm Square Plate with (H/B =2) at 30° inclination under 0.2 Hz frequency and 2mm amplitude

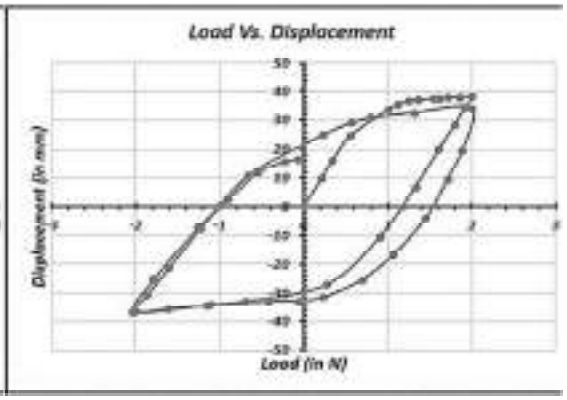

Fig. 4.133: Load vs. Displacement for 50 mm Square Plate with (H/B =3) at 30° inclination under 0.2 Hz frequency and 2mm amplitude

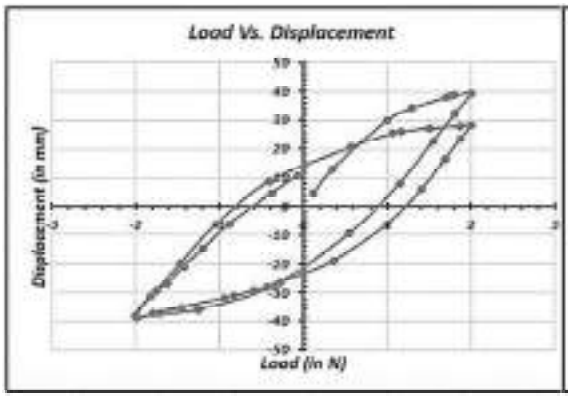

Fig. 4.134: Load vs. Displacement for 50 mm Square Plate with (H/B =1) at 45° inclination under 0.2 Hz frequency and 2mm amplitude

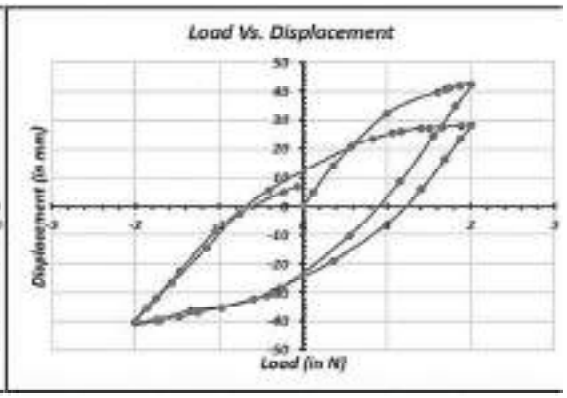

Fig. 4.135: Load vs. Displacement for 50 mm Square Plate with (H/B =2) at 45° inclination under 0.2 Hz frequency and 2mm amplitude

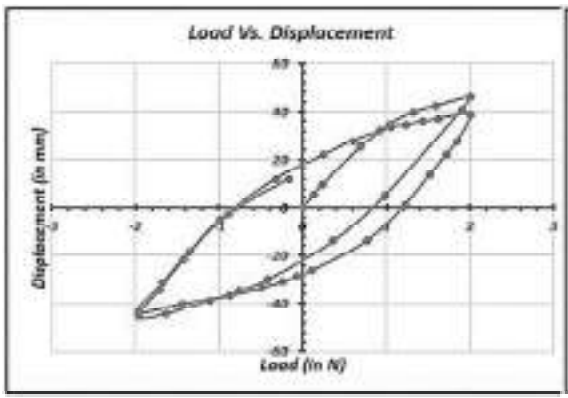

Fig. 4.136: Load vs. Displacement for 50 mm Square Plate with (H/B =3) at 45° inclination under 0.2 Hz frequency and 2mm amplitude

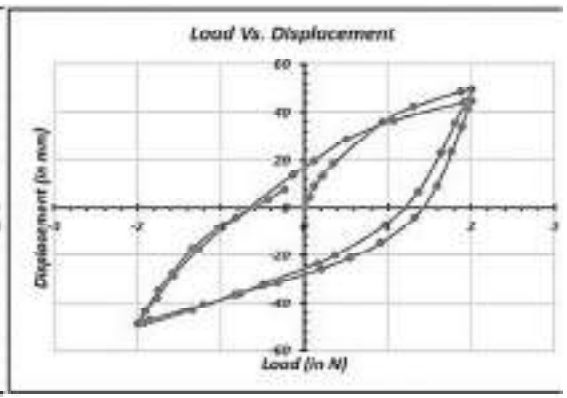

Fig. 4.137: Load vs. Displacement for 50 mm Square Plate with (H/B =1) at 60° inclination under 0.2 Hz frequency and 2mm amplitude

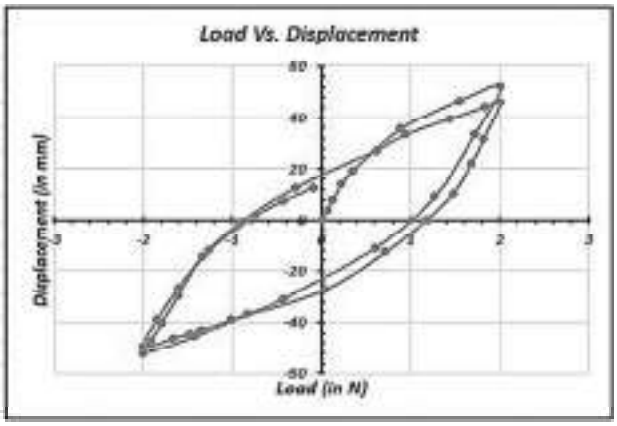

Fig. 4.138: Load vs. Displacement for 50 mm Square Plate with (H/B =2) at 60° inclination under 0.2 Hz frequency and 2mm amplitude

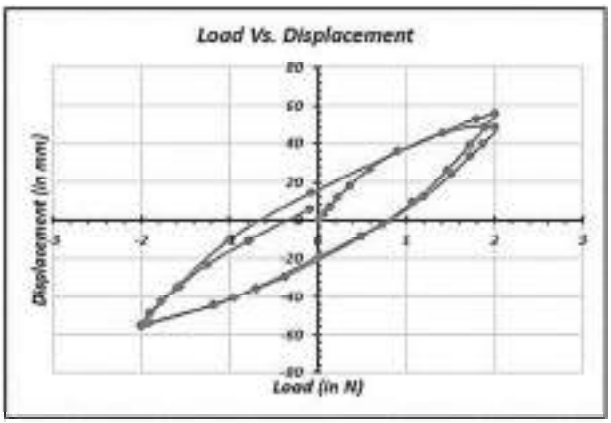

Fig. 4.139: Load vs. Displacement for 50 mm Square Plate with (H/B =3) at 60° inclination under 0.2 Hz frequency and 2mm amplitude

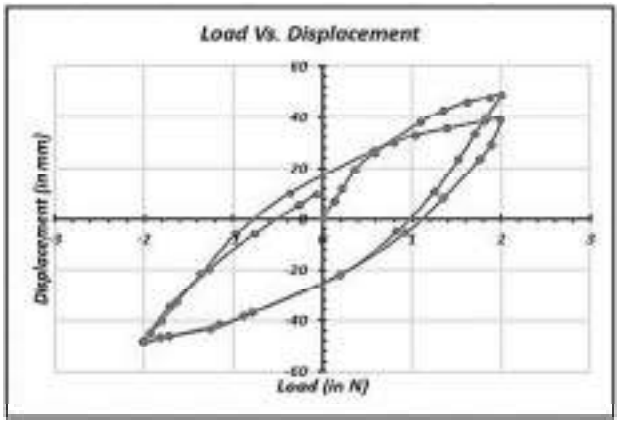

Fig. 4.140: Load vs. Displacement for 75 mm Square Plate with (H/B =1) at 30° inclination under 0.2 Hz frequency and 2mm amplitude

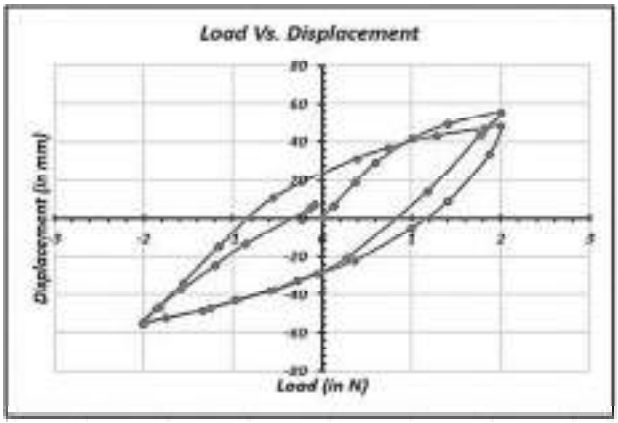

Fig. 4.141: Load vs. Displacement for 75 mm Square Plate with (H/B =2) at 30° inclination under 0.2 Hz frequency and 2mm amplitude

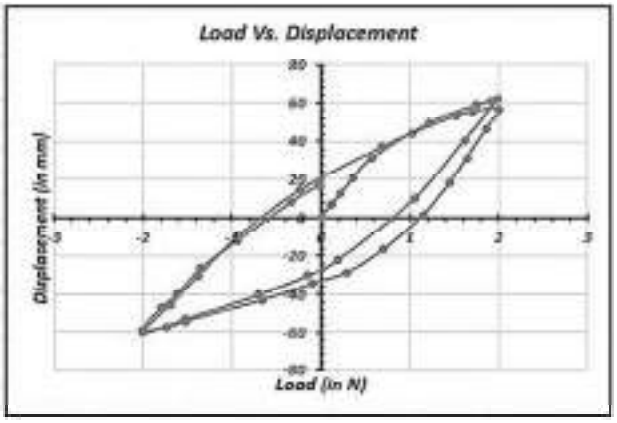

Fig. 4.142: Load vs. Displacement for 75 mm Square Plate with (H/B =3) at 30° inclination under 0.2 Hz frequency and 2mm amplitude

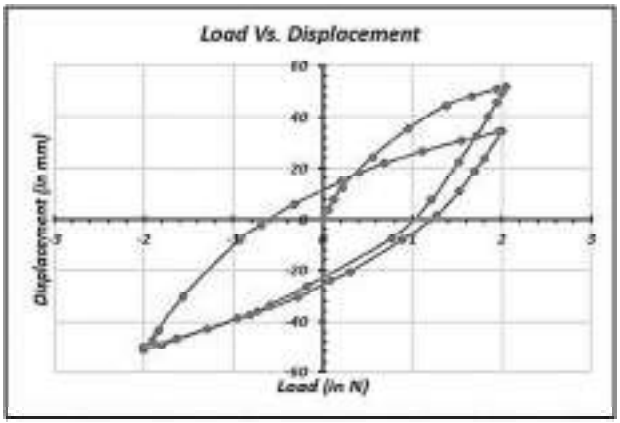

Fig. 4.143: Load vs. Displacement for 75 mm Square Plate with (H/B =1) at 45° inclination under 0.2 Hz frequency and 2mm amplitude

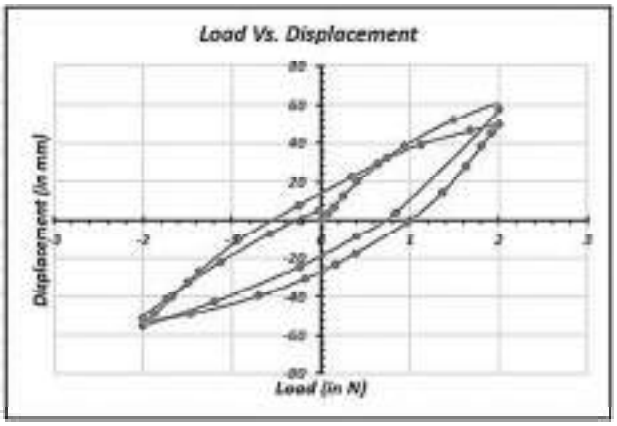

Fig. 4.144: Load vs. Displacement for 75 mm Square Plate with (H/B =2) at 45° inclination under 0.2 Hz frequency and 2mm amplitude

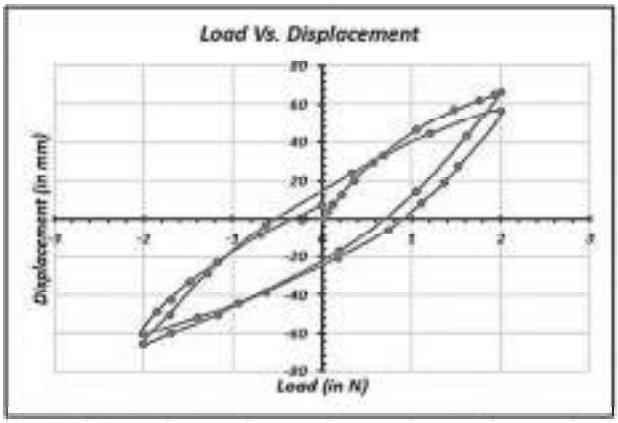

Fig. 4.145: Load vs. Displacement for 75 mm Square Plate with (H/B =3) at 45° inclination under 0.2 Hz frequency and 2mm amplitude

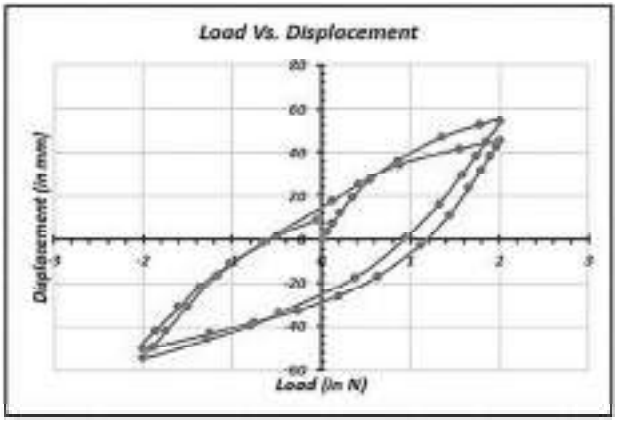

Fig. 4.146: Load vs. Displacement for 75 mm Square Plate with (H/B =1) at 60° inclination under 0.2 Hz frequency and 2mm amplitude

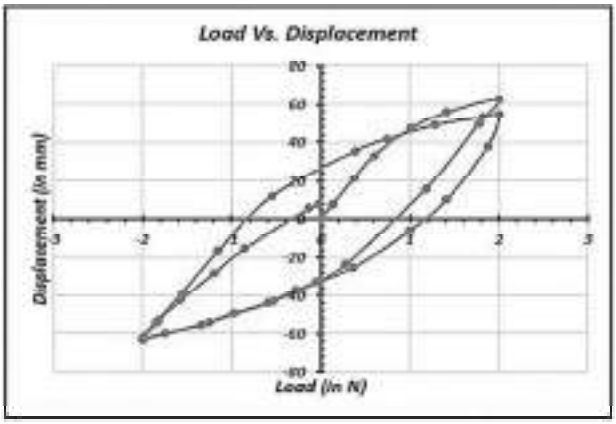

Fig. 4.147: Load vs. Displacement for 75 mm Square Plate with (H/B =2) at 60° inclination under 0.2 Hz frequency and 2mm amplitude

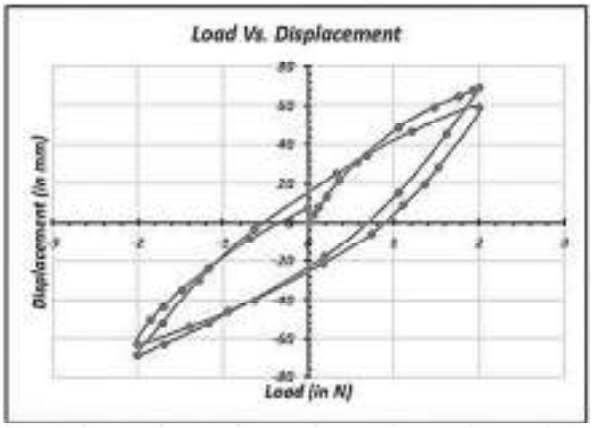

Fig. 4.148: Load vs. Displacement for 75 mm Square Plate with (H/B =3) at 60° inclination under 0.2 Hz frequency and 2mm amplitude

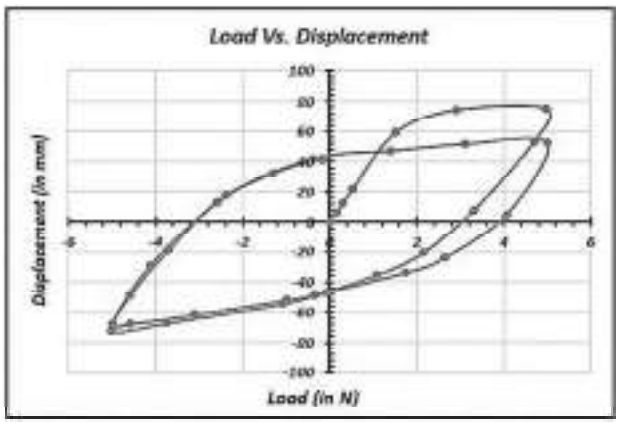

Fig. 4.149: Load vs. Displacement for 25 mm Square Plate with (H/B =1) at 30° inclination under 0.2 Hz frequency and 5mm amplitude

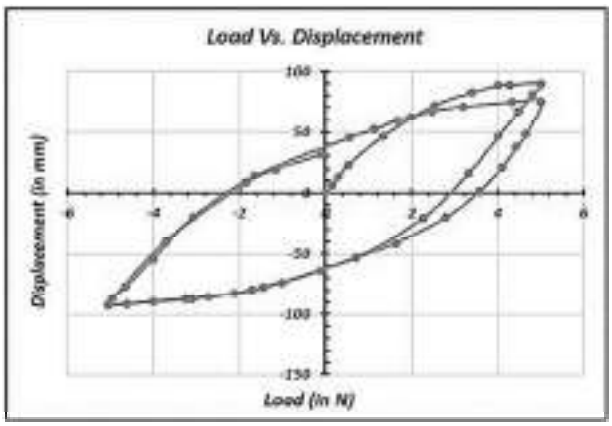

Fig. 4.150: Load vs. Displacement for 25 mm Square Plate with (H/B =2) at 30° inclination under 0.2 Hz frequency and 5mm amplitude

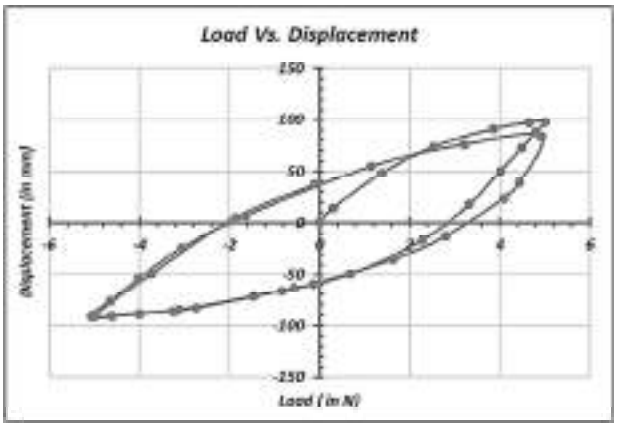

Fig. 4.151: Load vs. Displacement for 25 mm Square Plate with (H/B =3) at 30° inclination under 0.2 Hz frequency and 5mm amplitude

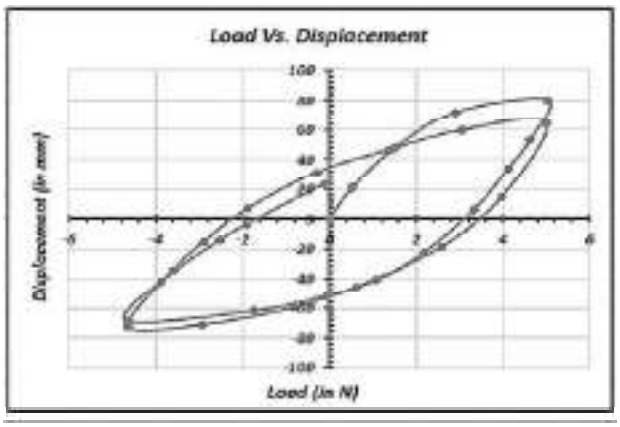

Fig. 4.152: Load vs. Displacement for 25 mm Square Plate with (H/B =1) at 45° inclination under 0.2 Hz frequency and 5mm amplitude

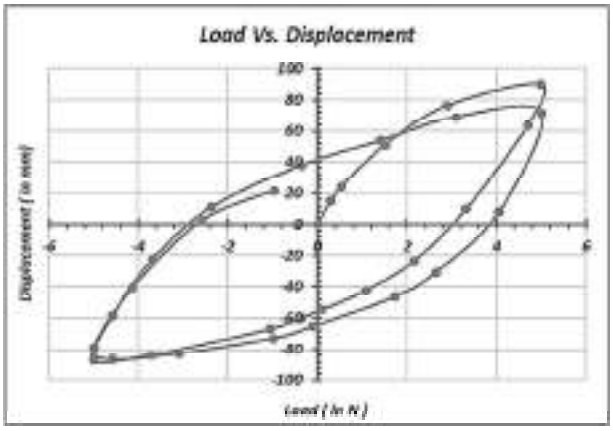

Fig. 4.153: Load vs. Displacement for 25 mm Square Plate with (H/B =2) at 45° inclination under 0.2 Hz frequency and 5mm amplitude

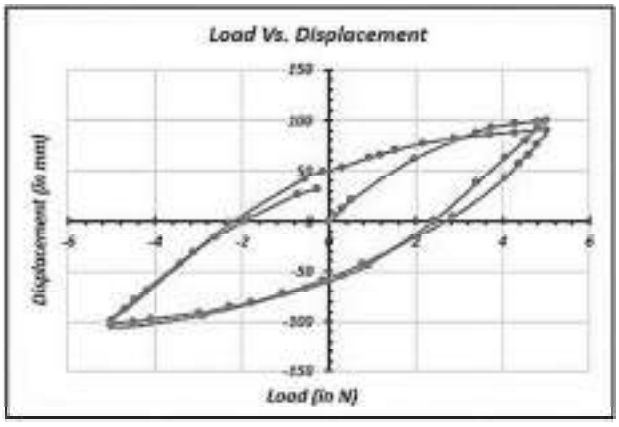

Fig. 4.154: Load vs. Displacement for 25 mm Square Plate with (H/B =3) at 45° inclination under 0.2 Hz frequency and 5mm amplitude

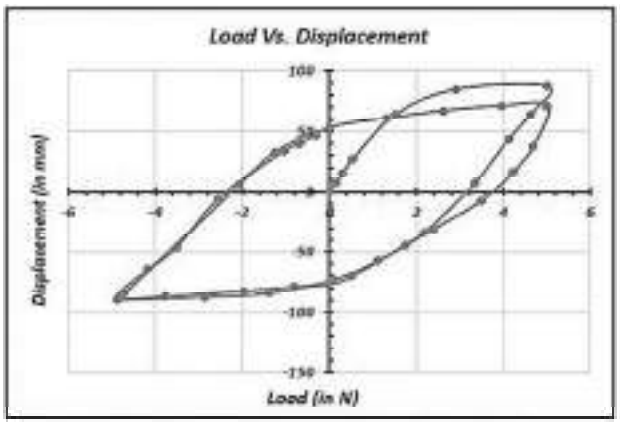

Fig. 4.155: Load vs. Displacement for 25 mm Square Plate with (H/B =1) at 60° inclination under 0.2 Hz frequency and 5mm amplitude

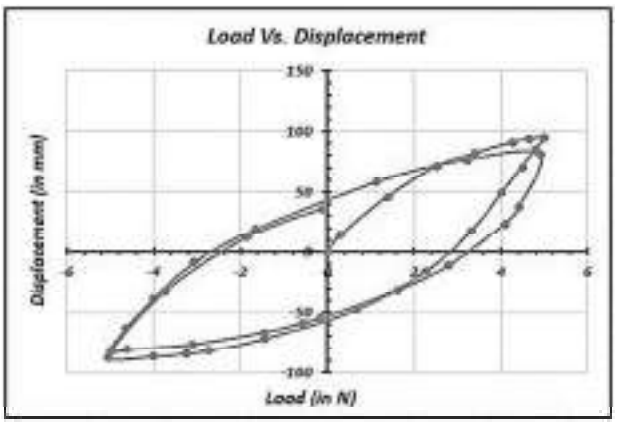

Fig. 4.156: Load vs. Displacement for 25 mm Square Plate with (H/B =2) at 60° inclination under 0.2 Hz frequency and 5mm amplitude

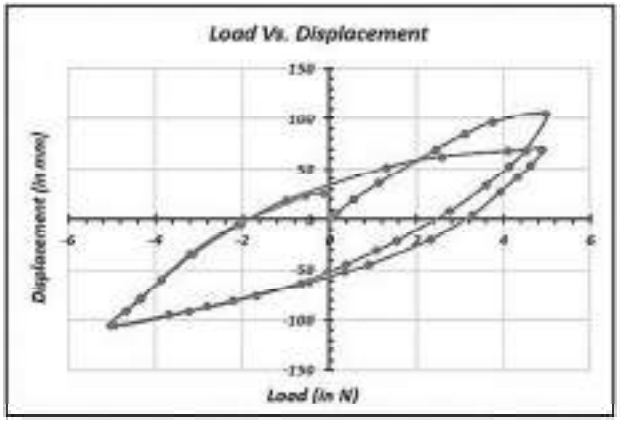

Fig. 4.157: Load vs. Displacement for 25 mm Square Plate with (H/B =3) at 60° inclination under 0.2 Hz frequency and 5mm amplitude

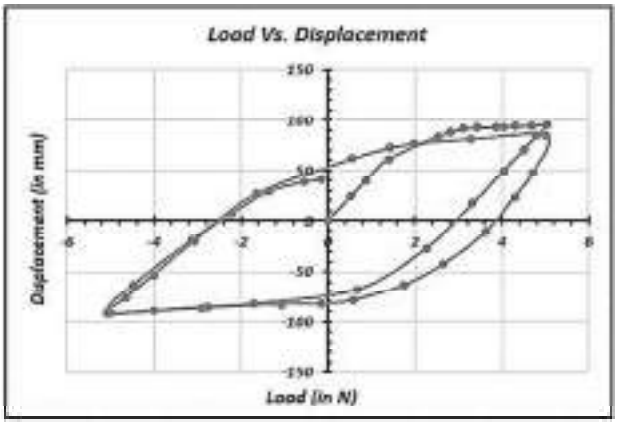

Fig. 4.158: Load vs. Displacement for 50 mm Square Plate with (H/B =1) at 30° inclination under 0.2 Hz frequency and 5mm amplitude

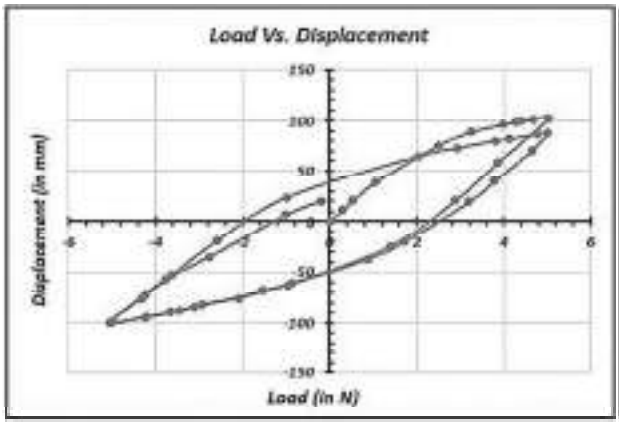

Fig. 4.159: Load vs. Displacement for 50 mm Square Plate with (H/B =2) at 30° inclination under 0.2 Hz frequency and 5mm amplitude

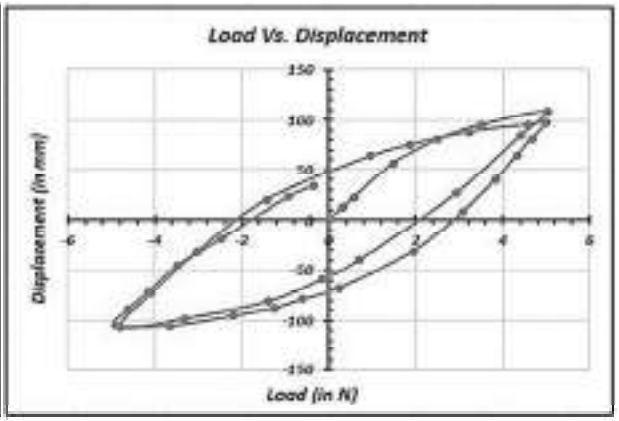

Fig. 4.160: Load vs. Displacement for 50 mm Square Plate with (H/B =3) at 30° inclination under 0.2 Hz frequency and 5mm amplitude

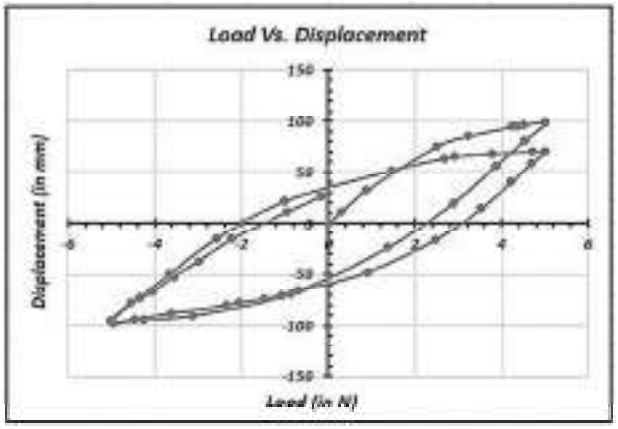

Fig. 4.161: Load vs. Displacement for 50 mm Square Plate with (H/B =1) at 45° inclination under 0.2 Hz frequency and 5mm amplitude

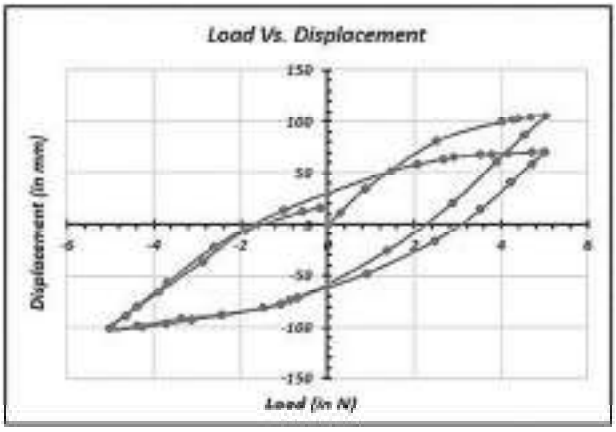

Fig. 4.162: Load vs. Displacement for 50 mm Square Plate with (H/B =2) at 45° inclination under 0.2 Hz frequency and 5mm amplitude

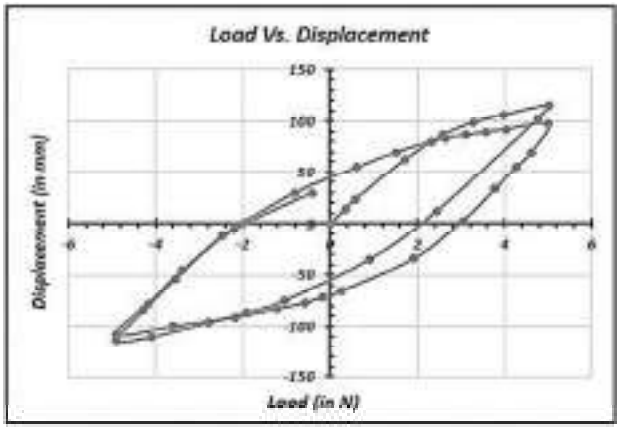

Fig. 4.163: Load vs. Displacement for 50 mm Square Plate with (H/B =3) at 45° inclination under 0.2 Hz frequency and 5mm amplitude

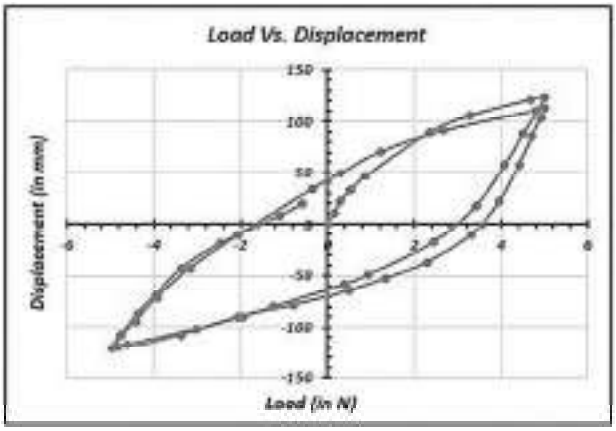

Fig. 4.164: Load vs. Displacement for 50 mm Square Plate with (H/B =1) at 60° inclination under 0.2 Hz frequency and 5mm amplitude

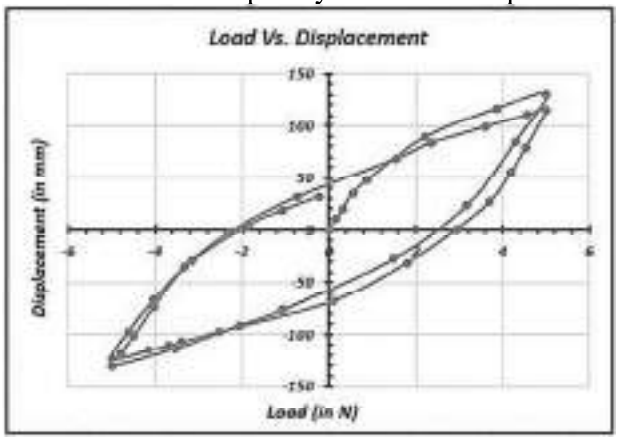

Fig. 4.165: Load vs. Displacement for 50 mm Square Plate with (H/B =2) at 60° inclination under 0.2 Hz frequency and 5mm amplitude

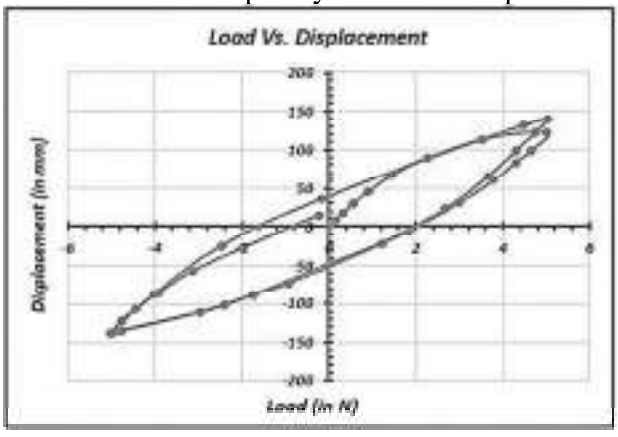

Fig. 4.166: Load vs. Displacement for 50 mm Square Plate with (H/B =3) at 60° inclination under 0.2 Hz frequency and 5mm amplitude

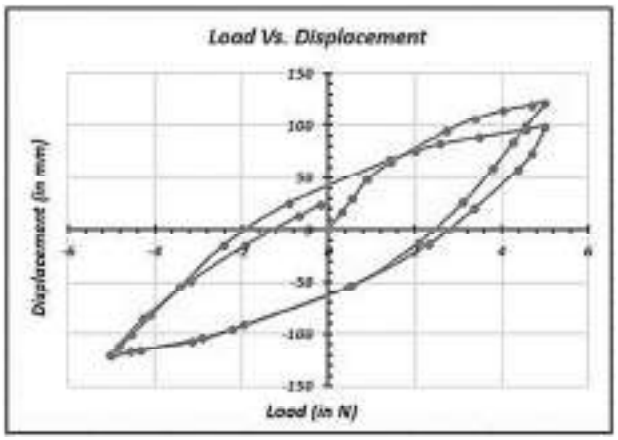

Fig. 4.167: Load vs. Displacement for 75 mm Square Plate with (H/B =1) at 30° inclination under 0.2 Hz frequency and 5mm amplitude

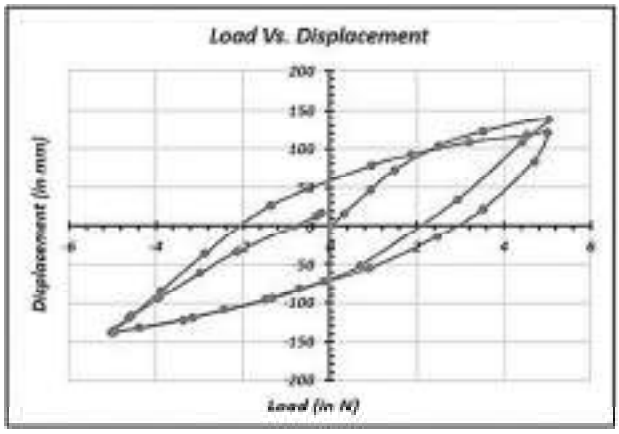

Fig. 4.168: Load vs. Displacement for 75 mm Square Plate with (H/B =2) at 30° inclination under 0.2 Hz frequency and 5mm amplitude

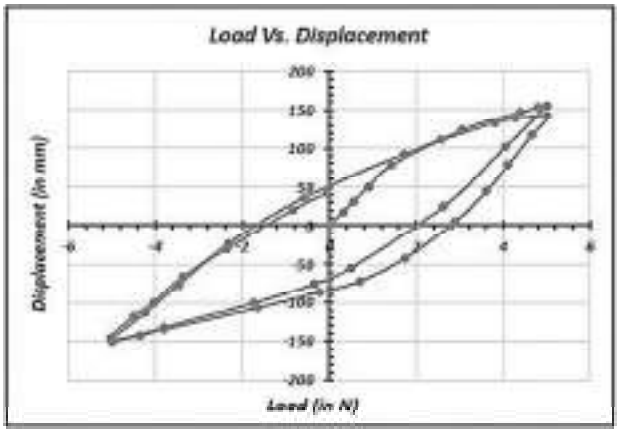

Fig. 4.169: Load vs. Displacement for 75 mm Square Plate with (H/B =3) at 30° inclination under 0.2 Hz frequency and 5mm amplitude

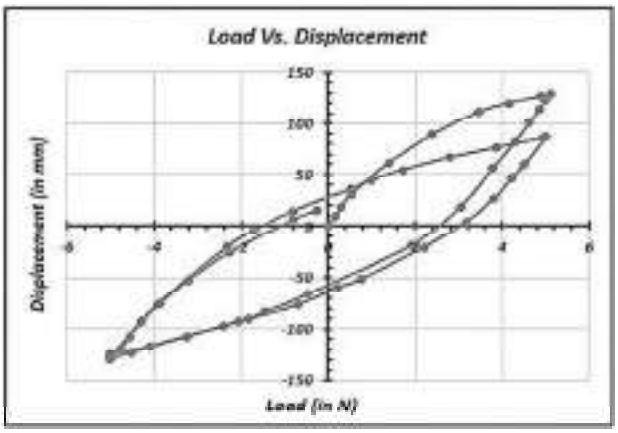

Fig. 4.170: Load vs. Displacement for 75 mm Square Plate with (H/B =1) at 45° inclination under 0.2 Hz frequency and 5mm amplitude

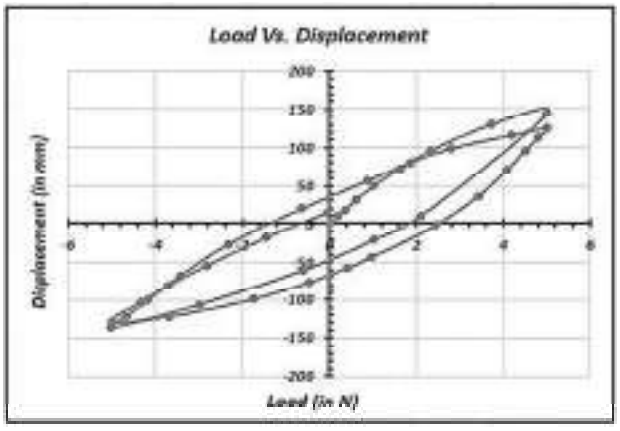

Fig. 4.171: Load vs. Displacement for 75 mm Square Plate with (H/B =2) at 45° inclination under 0.2 Hz frequency and 5mm amplitude

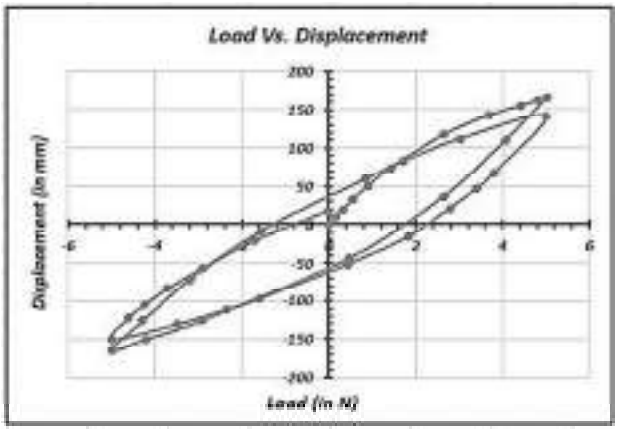

Fig. 4.172: Load vs. Displacement for 75 mm Square Plate with (H/B =3) at 45° inclination under 0.2 Hz frequency and 5mm amplitude

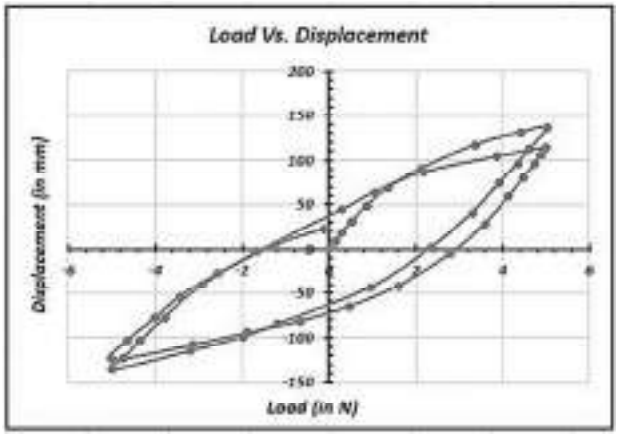

Fig. 4.173: Load vs. Displacement for 75 mm Square Plate with (H/B =1) at 60° inclination under 0.2 Hz frequency and 5mm amplitude

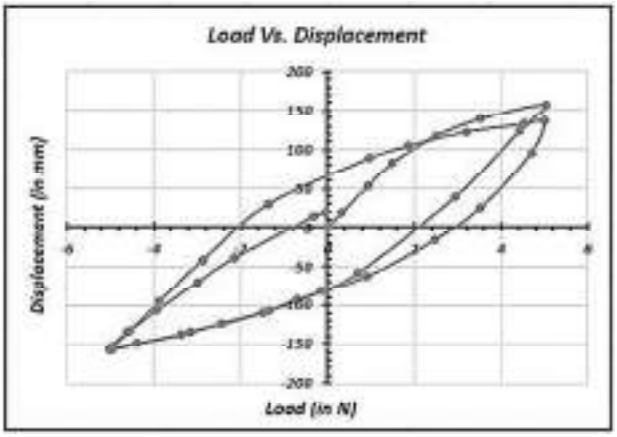

Fig. 4.174: Load vs. Displacement for 75 mm Square Plate with (H/B =2) at 60° inclination under 0.2 Hz frequency and 5mm amplitude

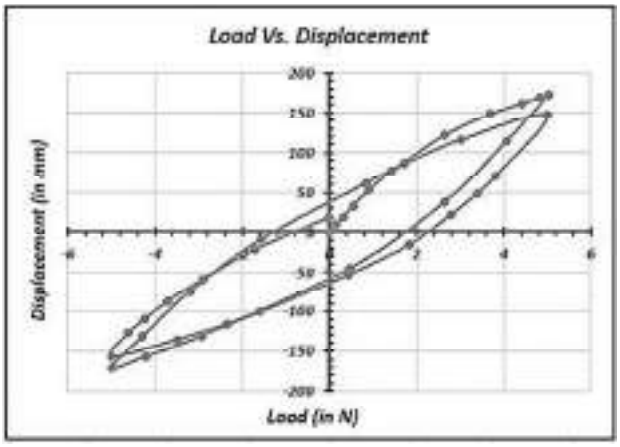

Fig. 4.175: Load vs. Displacement for 75 mm Square Plate with (H/B =3) at 60° inclination under 0.2 Hz frequency and 5mm amplitude

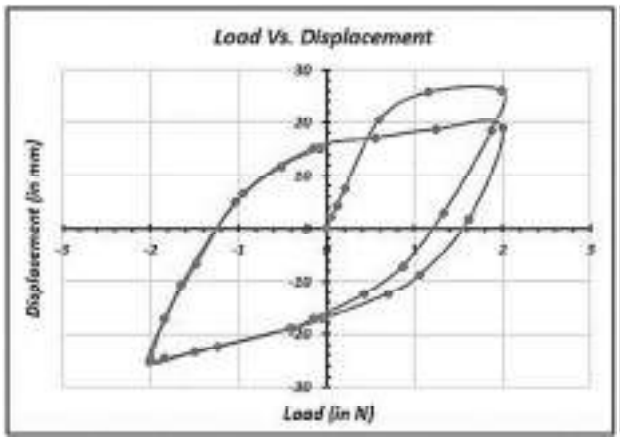

Fig. 4.176: Load vs. Displacement for 25 mm Square Plate with (H/B =1) at 30° inclination under 0.5 Hz frequency and 2mm amplitude

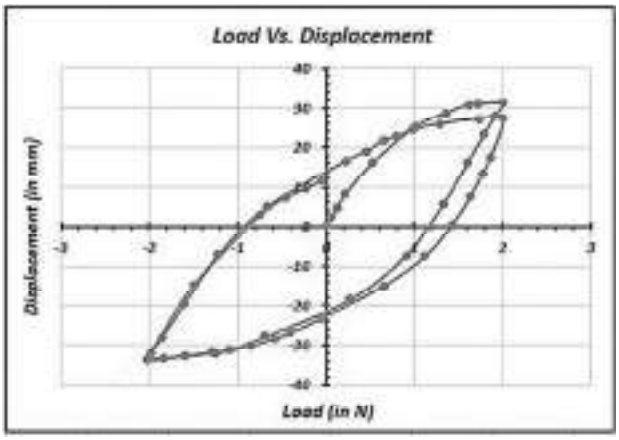

Fig. 4.177: Load vs. Displacement for 25 mm Square Plate with (H/B =2) at 30° inclination under 0.5 Hz frequency and 2mm amplitude

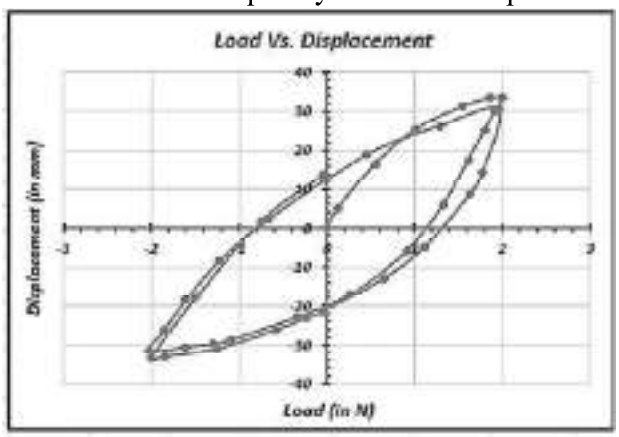

Fig. 4.178: Load vs. Displacement for 25 mm Square Plate with (H/B =3) at 30° inclination under 0.5 Hz frequency and 2mm amplitude

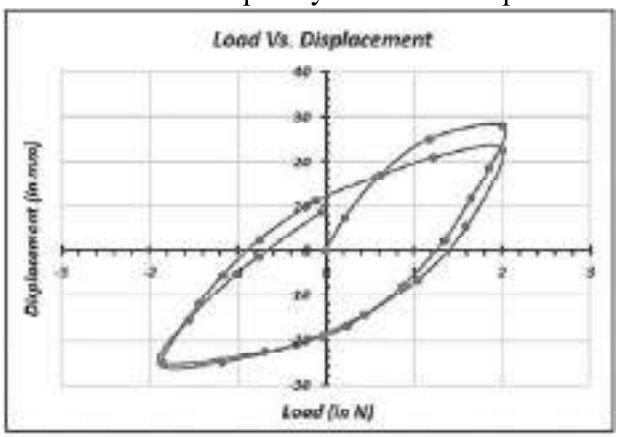

Fig. 4.179: Load vs. Displacement for 25 mm Square Plate with (H/B =1) at 45° inclination under 0.5 Hz frequency and 2mm amplitude

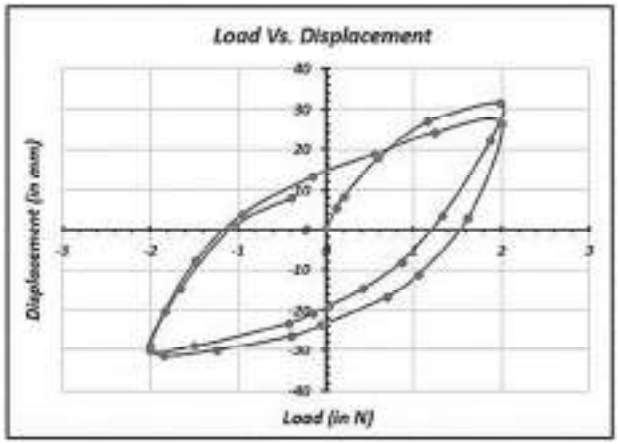

Fig. 4.180: Load vs. Displacement for 25 mm Square Plate with (H/B =2) at 45° inclination under 0.5 Hz frequency and 2mm amplitude

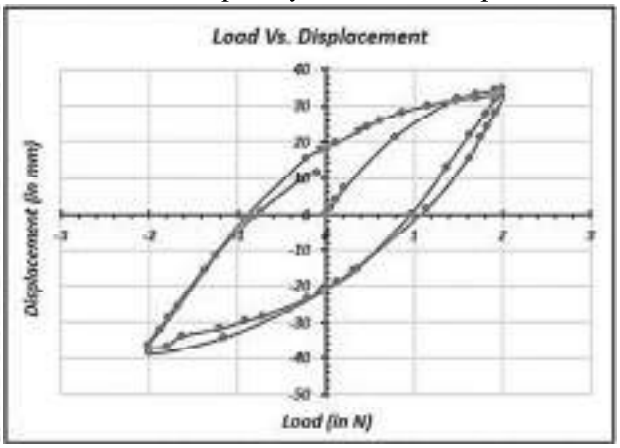

Fig. 4.181: Load vs. Displacement for 25 mm Square Plate with (H/B =3) at 45° inclination under 0.5 Hz frequency and 2mm amplitude

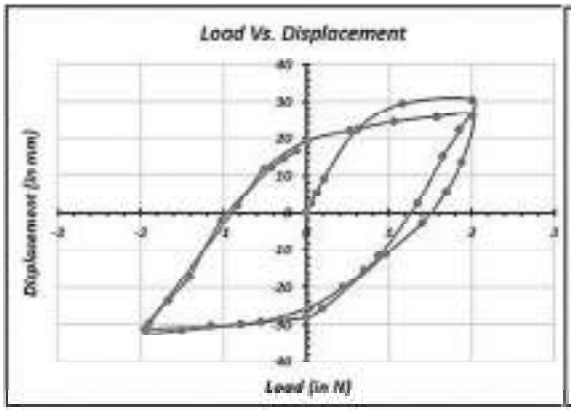

Fig. 4.182: Load vs. Displacement for 25 mm Square Plate with (H/B =1) at 60° inclination under 0.5 Hz frequency and 2mm amplitude

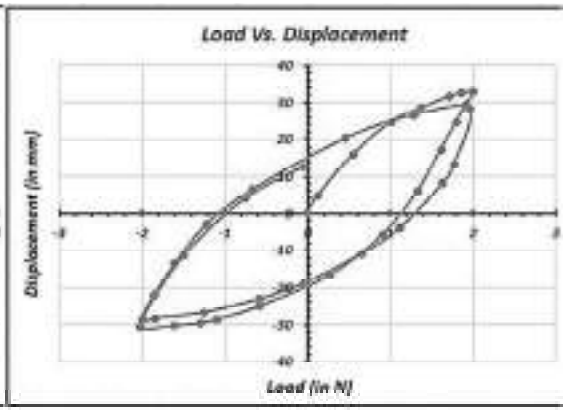

Fig. 4.183: Load vs. Displacement for 25 mm Square Plate with (H/B =2) at 60° inclination under 0.5 Hz frequency and 2mm amplitude

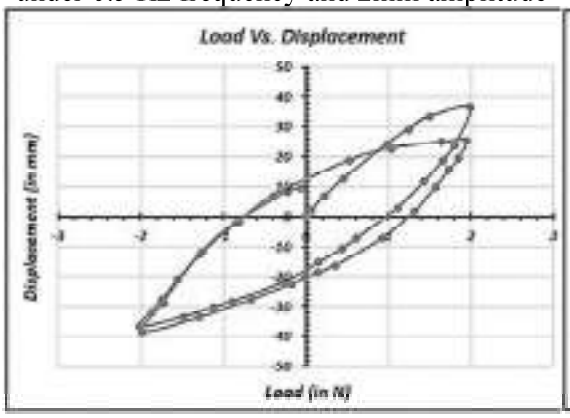

Fig. 4.184: Load vs. Displacement for 25 mm Square Plate with (H/B =3) at 60° inclination under 0.5 Hz frequency and 2mm amplitude

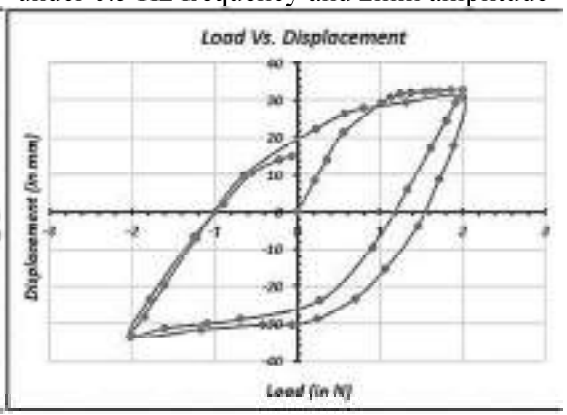

Fig. 4.185: Load vs. Displacement for 50 mm Square Plate with (H/B =1) at 30° inclination under 0.5 Hz frequency and 2mm amplitude

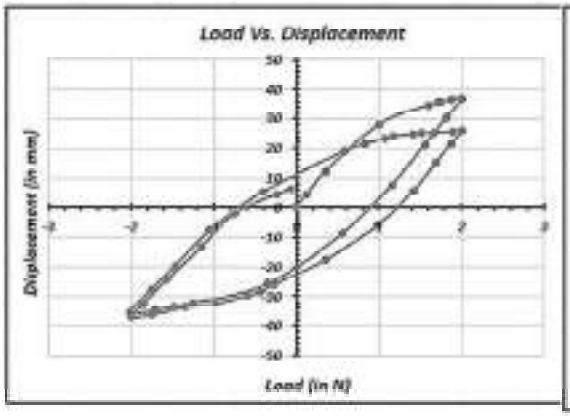

Fig. 4.186: Load vs. Displacement for 50 mm Square Plate with (H/B =2) at 30° inclination under 0.5 Hz frequency and 2mm amplitude

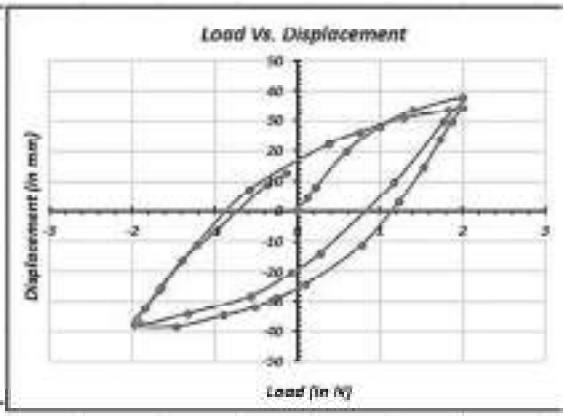

Fig. 4.187: Load vs. Displacement for 50 mm Square Plate with (H/B =3) at 30° inclination under 0.5 Hz frequency and 2mm amplitude

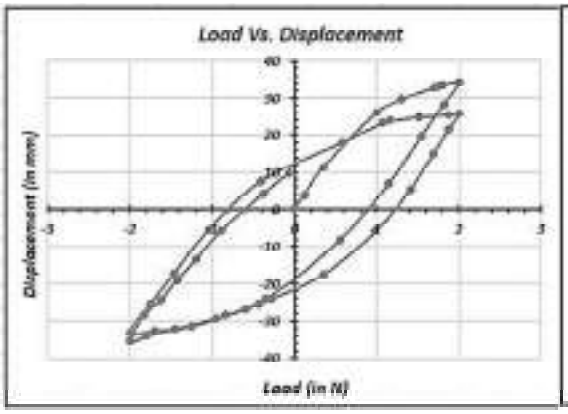

Fig. 4.188: Load vs. Displacement for 50 mm Square Plate with (H/B =1) at 45° inclination under 0.5 Hz frequency and 2mm amplitude

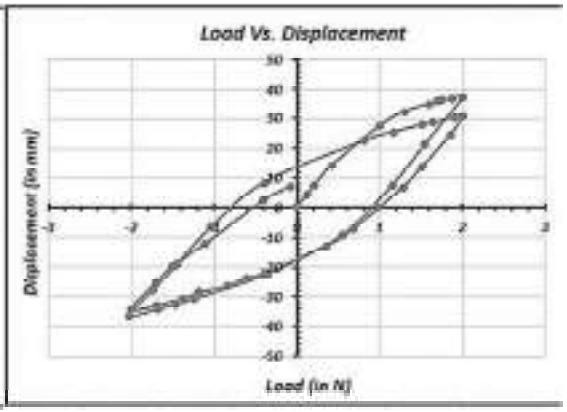

Fig. 4.189: Load vs. Displacement for 50 mm Square Plate with (H/B =2) at 45° inclination under 0.5 Hz frequency and 2mm amplitude

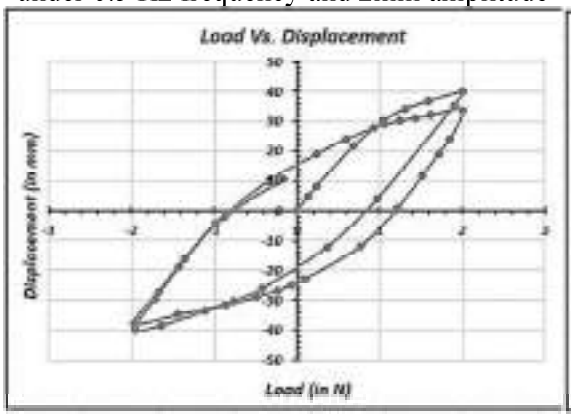

Fig. 4.190: Load vs. Displacement for 50 mm Square Plate with (H/B =3) at 45° inclination under 0.5 Hz frequency and 2mm amplitude

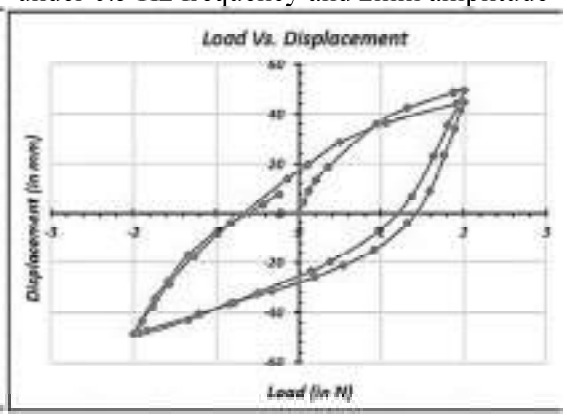

Fig. 4.191: Load vs. Displacement for 50 mm Square Plate with (H/B =1) at 60° inclination under 0.5 Hz frequency and 2mm amplitude

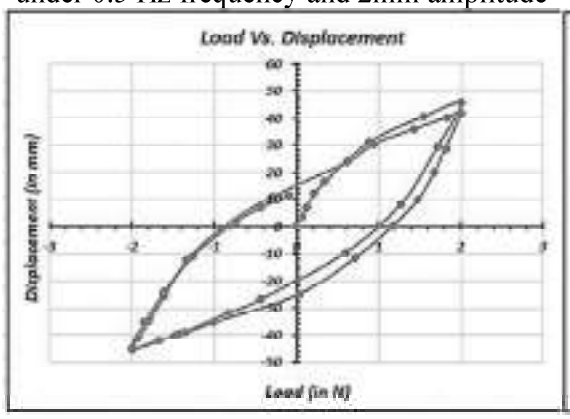

Fig. 4.192: Load vs. Displacement for 50 mm Square Plate with (H/B =2) at 60° inclination under 0.5 Hz frequency and 2mm amplitude

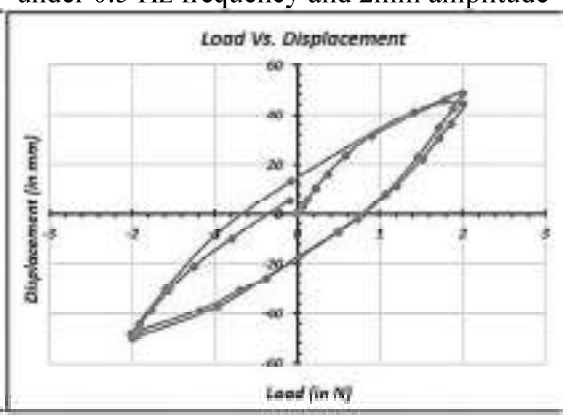

Fig. 4.193: Load vs. Displacement for 50 mm Square Plate with (H/B =3) at 60° inclination under 0.5 Hz frequency and 2mm amplitude

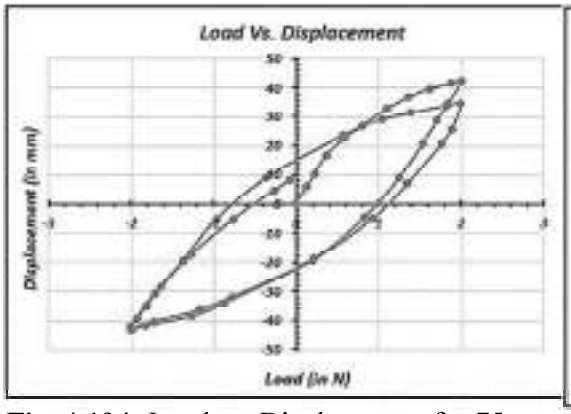

Fig. 4.194: Load vs. Displacement for 75 mm Square Plate with (H/B =1) at 30° inclination under 0.5 Hz frequency and 2mm amplitude

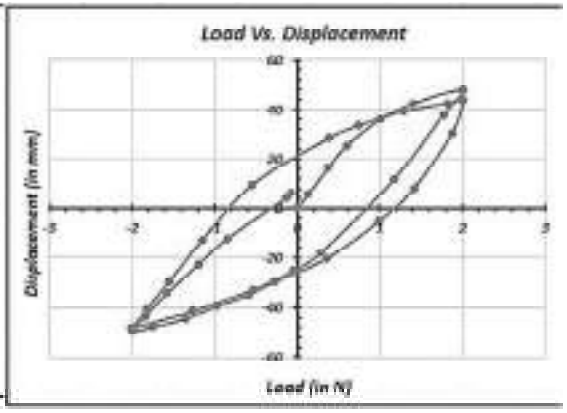

Fig. 4.195: Load vs. Displacement for 75 mm Square Plate with (H/B =2) at 30° inclination under 0.5 Hz frequency and 2mm amplitude

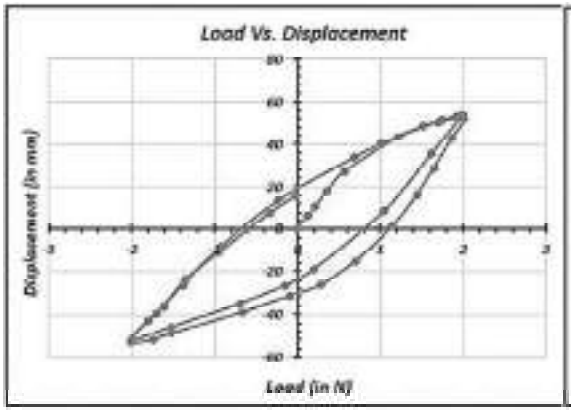

Fig. 4.196: Load vs. Displacement for 75 mm Square Plate with (H/B =3) at 30° inclination under 0.5 Hz frequency and 2mm amplitude

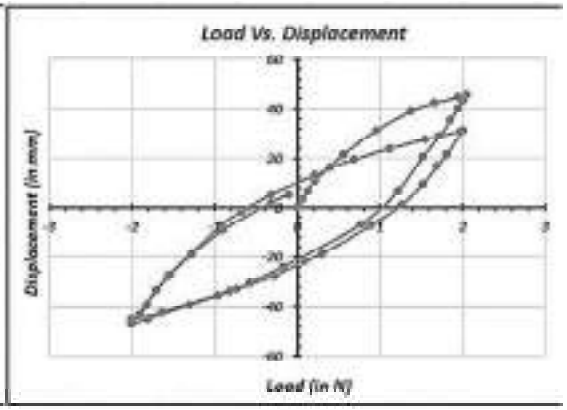

Fig. 4.197: Load vs. Displacement for 75 mm Square Plate with (H/B =1) at 45° inclination under 0.5 Hz frequency and 2mm amplitude

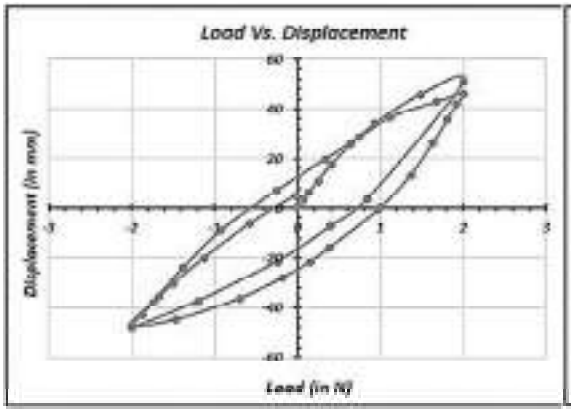

Fig. 4.198: Load vs. Displacement for 75 mm Square Plate with (H/B =2) at 45° inclination under 0.5 Hz frequency and 2mm amplitude

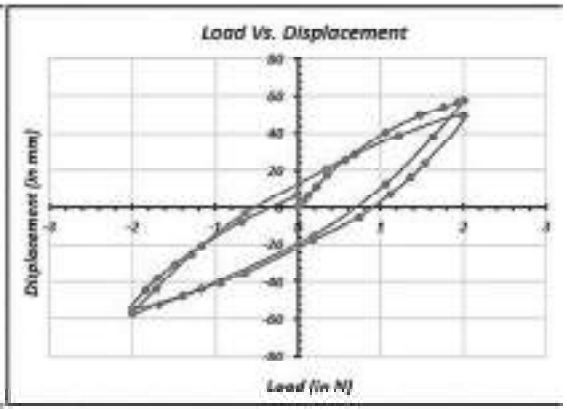

Fig. 4.199: Load vs. Displacement for 75 mm Square Plate with (H/B =3) at 45° inclination under 0.5 Hz frequency and 2mm amplitude

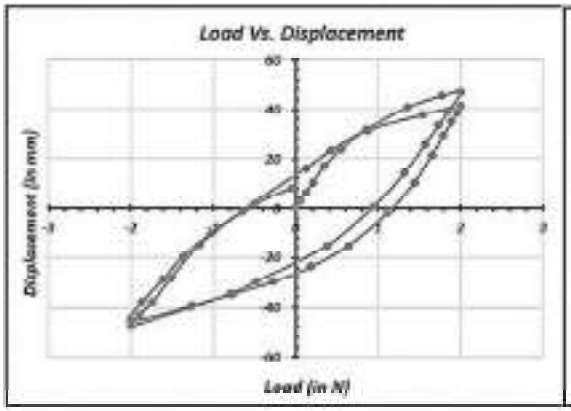

Fig. 4.200: Load vs. Displacement for 75 mm Square Plate with (H/B =1) at 60° inclination under 0.5 Hz frequency and 2mm amplitude

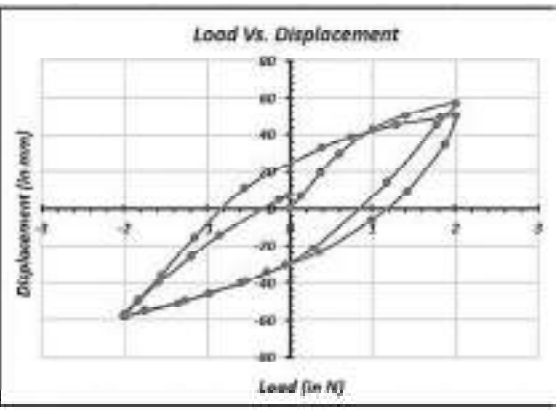

Fig. 4.201: Load vs. Displacement for 75 mm Square Plate with (H/B =2) at 60° inclination under 0.5 Hz frequency and 2mm amplitude

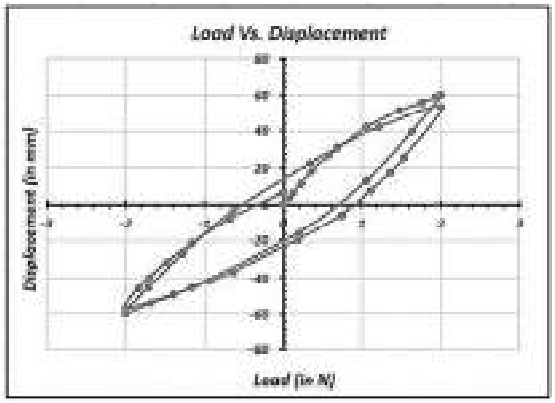

Fig. 4.202: Load vs. Displacement for 75 mm Square Plate with (H/B =3) at 60° inclination under 0.5 Hz frequency and 2mm amplitude

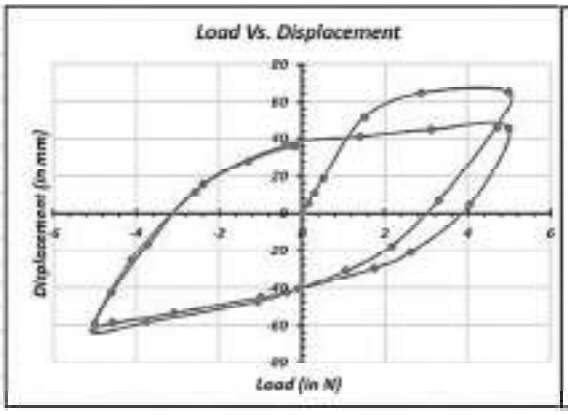

Fig. 4.203: Load vs. Displacement for 25 mm Square Plate with (H/B =1) at 30° inclination under 0.5 Hz frequency and 5mm amplitude

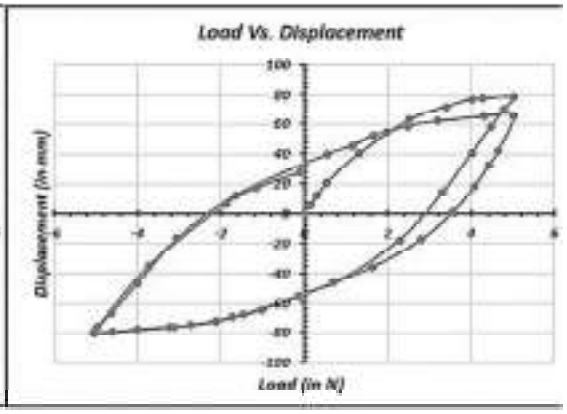

Fig. 4.204: Load vs. Displacement for 25 mm Square Plate with (H/B =2) at 30° inclination under 0.5 Hz frequency and 5mm amplitude

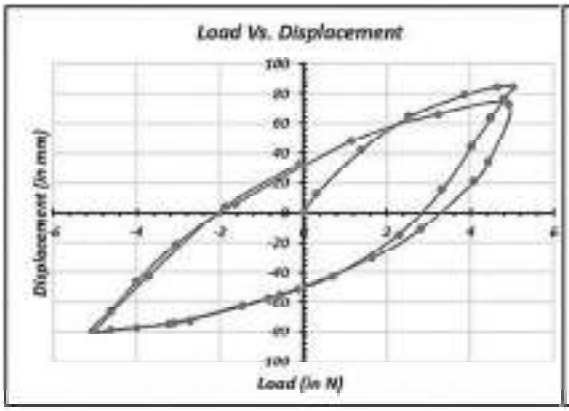

Fig. 4.205: Load vs. Displacement for 25 mm Square Plate with (H/B =3) at 30° inclination under 0.5 Hz frequency and 5mm amplitude

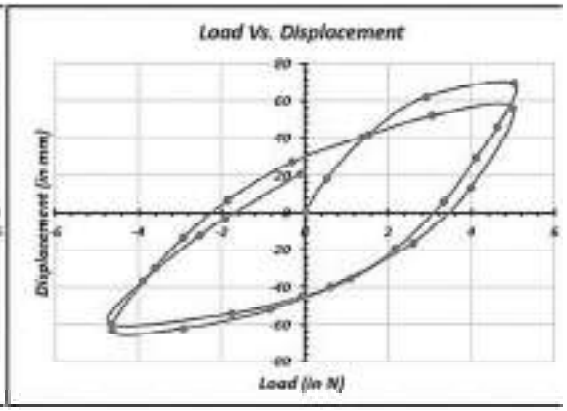

Fig. 4.206: Load vs. Displacement for 25 mm Square Plate with (H/B =1) at 45° inclination under 0.5 Hz frequency and 5mm amplitude

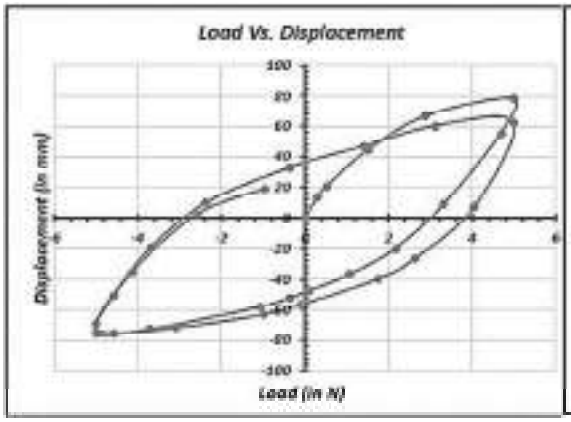

Fig. 4.207: Load vs. Displacement for 25 mm Square Plate with (H/B =2) at 45° inclination under 0.5 Hz frequency and 5mm amplitude

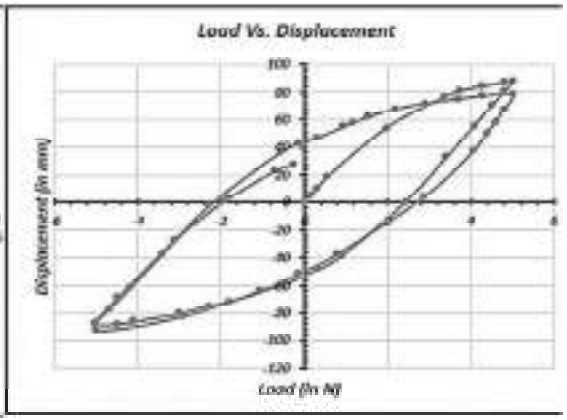

Fig. 4.208: Load vs. Displacement for 25 mm Square Plate with (H/B =3) at 45° inclination under 0.5 Hz frequency and 5mm amplitude

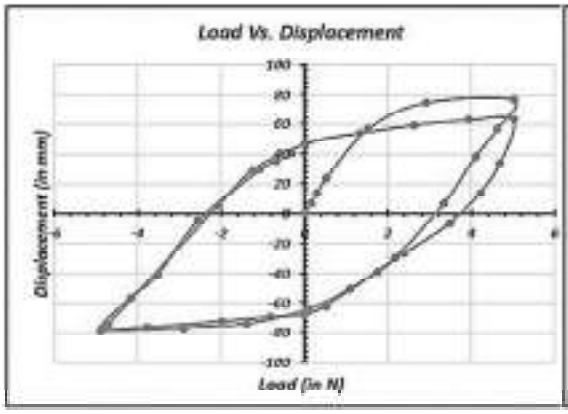

Fig. 4.209: Load vs. Displacement for 25 mm Square Plate with (H/B =1) at 60° inclination under 0.5 Hz frequency and 5mm amplitude

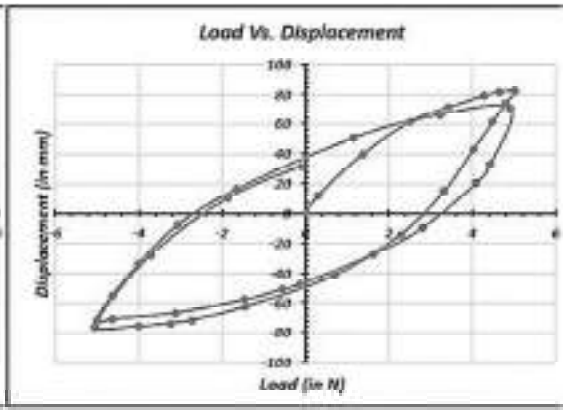

Fig. 4.210: Load vs. Displacement for 25 mm Square Plate with (H/B =2) at 60° inclination under 0.5 Hz frequency and 5mm amplitude

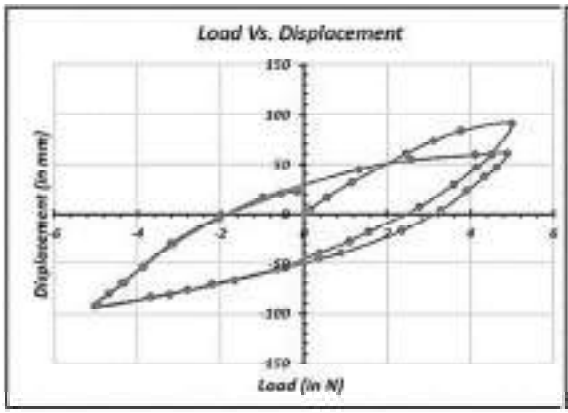

Fig. 4.211: Load vs. Displacement for 25 mm Square Plate with (H/B =3) at 60° inclination under 0.5 Hz frequency and 5mm amplitude

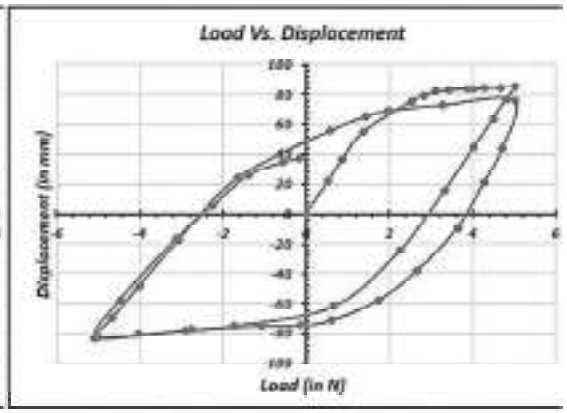

Fig. 4.212: Load vs. Displacement for 50 mm Square Plate with (H/B =1) at 30° inclination under 0.5 Hz frequency and 5mm amplitude

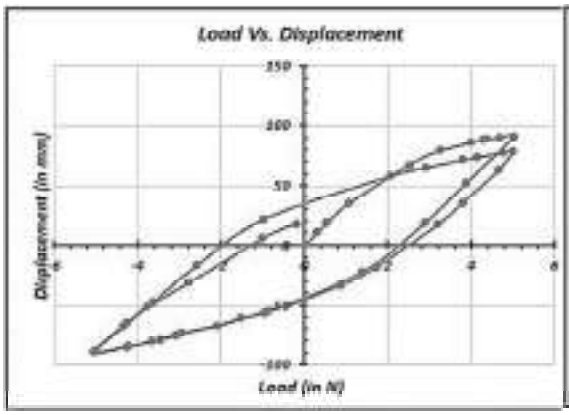

Fig. 4.213: Load vs. Displacement for 50 mm Square Plate with (H/B =2) at 30° inclination under 0.5 Hz frequency and 5mm amplitude

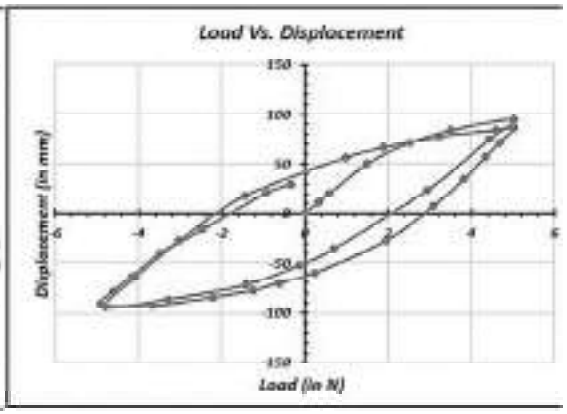

Fig. 4.214: Load vs. Displacement for 50 mm Square Plate with (H/B =3) at 30° inclination under 0.5 Hz frequency and 5mm amplitude

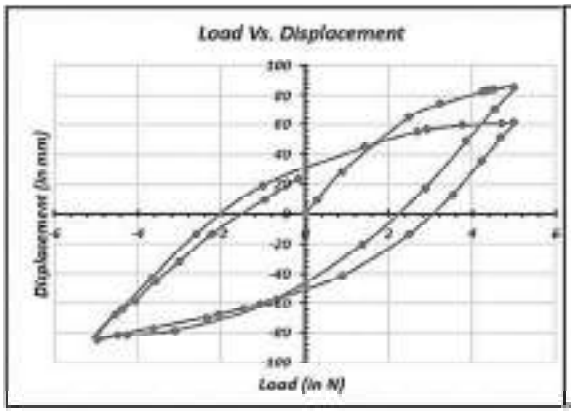

Fig. 4.215: Load vs. Displacement for 50 mm Square Plate with (H/B =1) at 45° inclination under 0.5 Hz frequency and 5mm amplitude

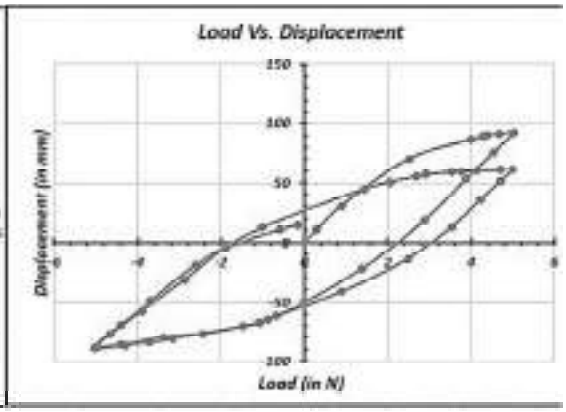

Fig. 4.216: Load vs. Displacement for 50 mm Square Plate with (H/B =2) at 45° inclination under 0.5 Hz frequency and 5mm amplitude

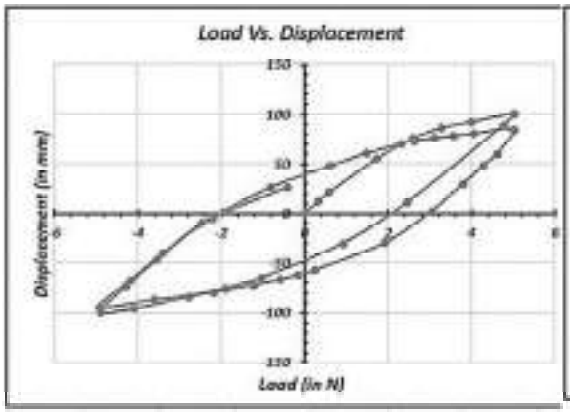

Fig. 4.217: Load vs. Displacement for 50 mm Square Plate with (H/B =3) at 45° inclination under 0.5 Hz frequency and 5mm amplitude

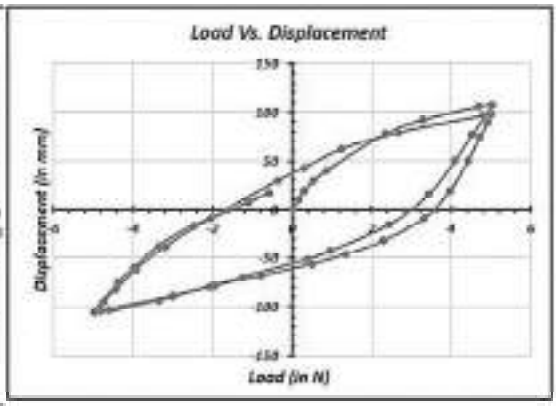

Fig. 4.218: Load vs. Displacement for 50 mm Square Plate with (H/B =1) at 60° inclination under 0.5 Hz frequency and 5mm amplitude

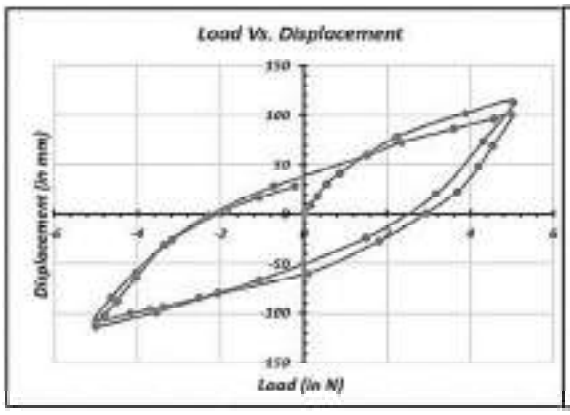

Fig. 4.219: Load vs. Displacement for 50 mm Square Plate with (H/B =2) at 60° inclination under 0.5 Hz frequency and 5mm amplitude

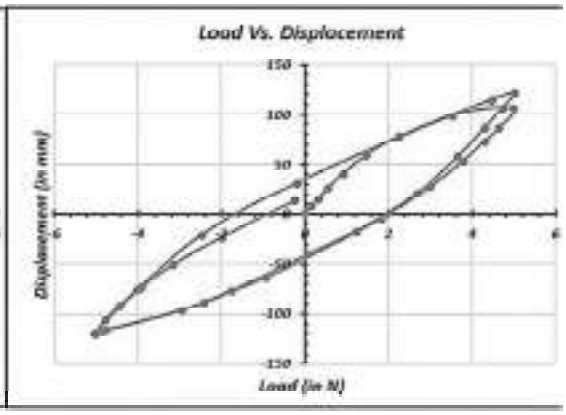

Fig. 4.220: Load vs. Displacement for 50 mm Square Plate with (H/B =3) at 60° inclination under 0.5 Hz frequency and 5mm amplitude

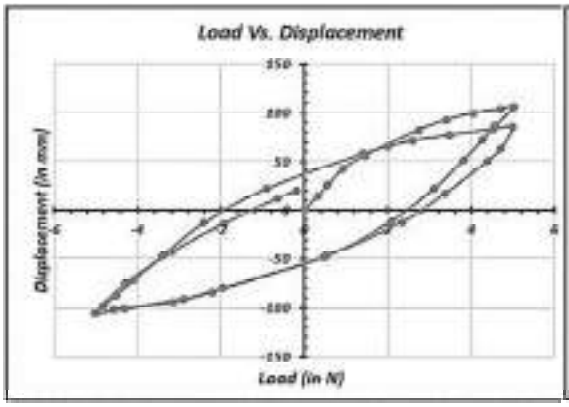

Fig. 4.221: Load vs. Displacement for 75 mm Square Plate with (H/B =1) at 30° inclination under 0.5 Hz frequency and 5mm amplitude

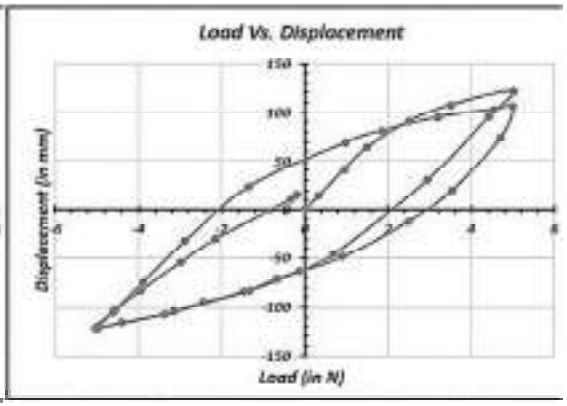

Fig. 4.222: Load vs. Displacement for 75 mm Square Plate with (H/B =2) at 30° inclination under 0.5 Hz frequency and 5mm amplitude

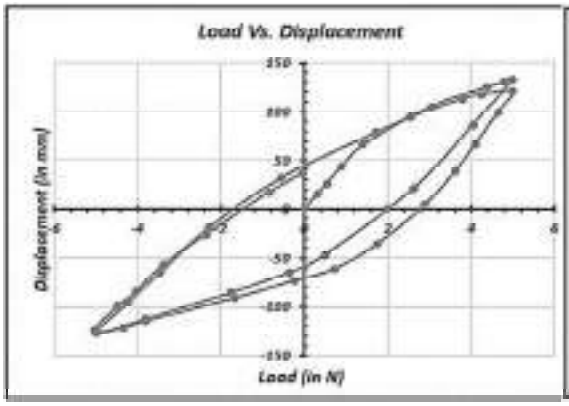

Fig. 4.223: Load vs. Displacement for 75 mm Square Plate with (H/B =3) at 30° inclination under 0.5 Hz frequency and 5mm amplitude

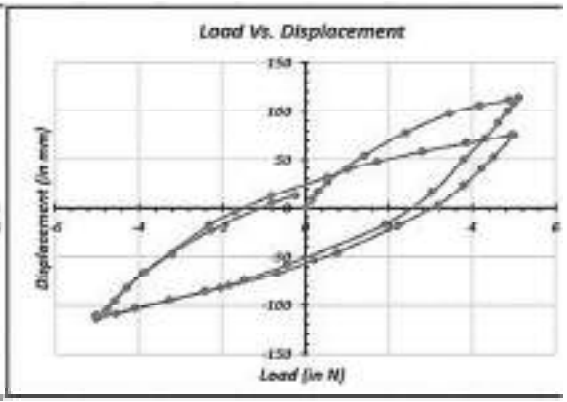

Fig. 4.224: Load vs. Displacement for 75 mm Square Plate with (H/B =1) at 45° inclination under 0.5 Hz frequency and 5mm amplitude

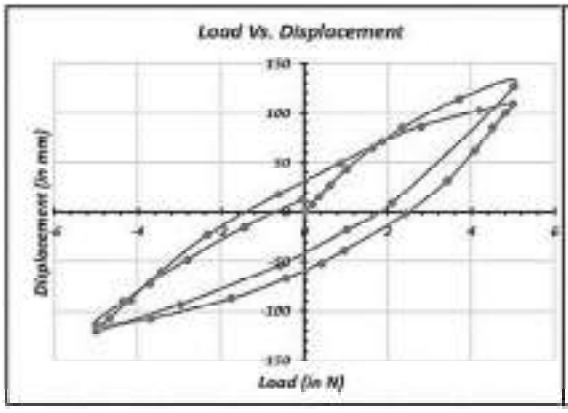

Fig. 4.225: Load vs. Displacement for 75 mm Square Plate with (H/B =2) at 45° inclination under 0.5 Hz frequency and 5mm amplitude

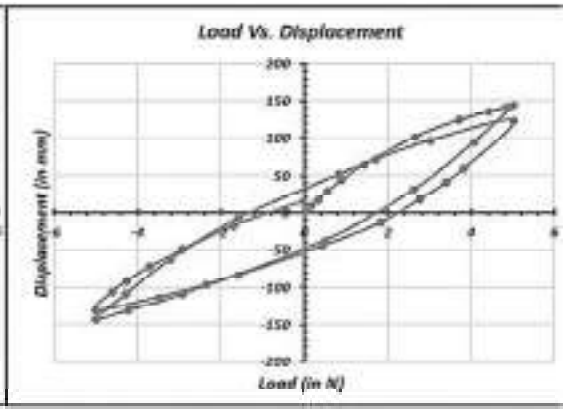

Fig. 4.226: Load vs. Displacement for 75 mm Square Plate with (H/B =3) at 45° inclination under 0.5 Hz frequency and 5mm amplitude

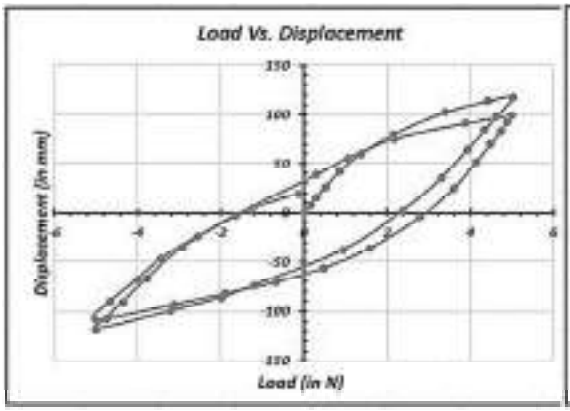

Fig. 4.227: Load vs. Displacement for 75 mm Square Plate with (H/B =1) at 60° inclination under 0.5 Hz frequency and 5mm amplitude

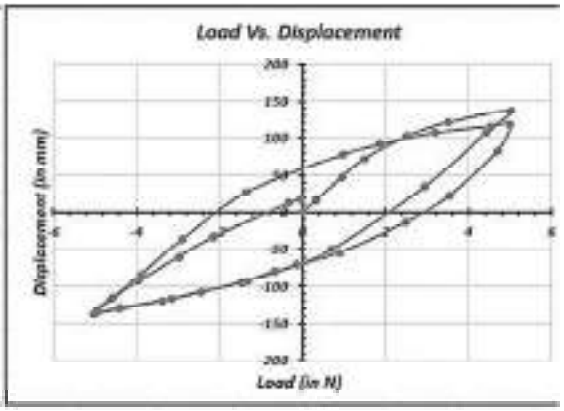

Fig. 4.228: Load vs. Displacement for 75 mm Square Plate with (H/B =2) at 60° inclination under 0.5 Hz frequency and 5mm amplitude

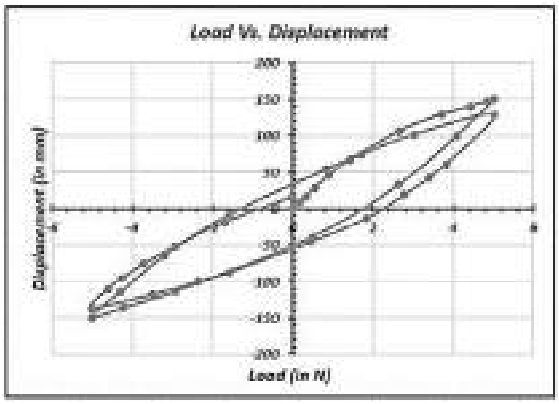

Fig. 4.229: Load vs. Displacement for 75 mm Square Plate with (H/B =3) at 60° inclination under 0.5 Hz frequency and 5mm amplitude

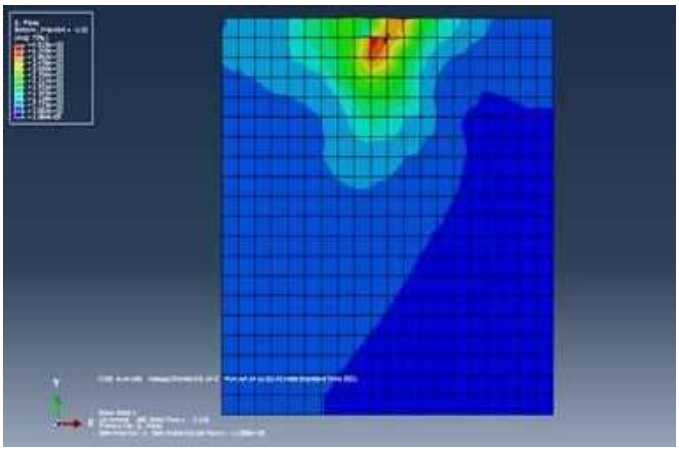

Fig. 4.231: Stress Contour for 25 mm Square Plate with (H/B =2) at 30° inclination under 0.2 Hz frequency and 2mm amplitude

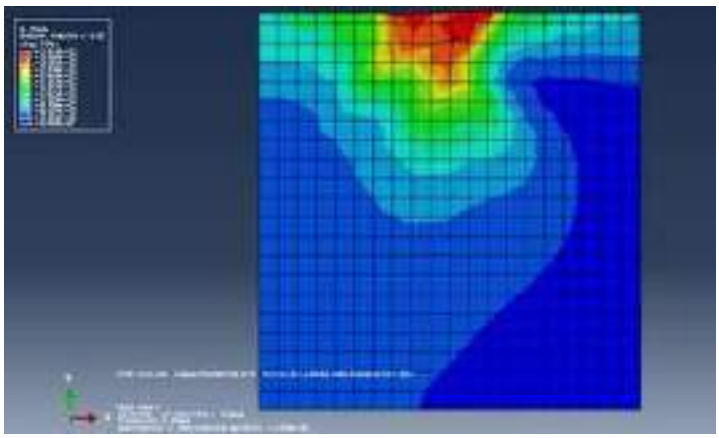

Fig. 4.232: Stress Contour for 25 mm Square Plate with (H/B =3) at 30° inclination under 0.2 Hz frequency and 2mm amplitude

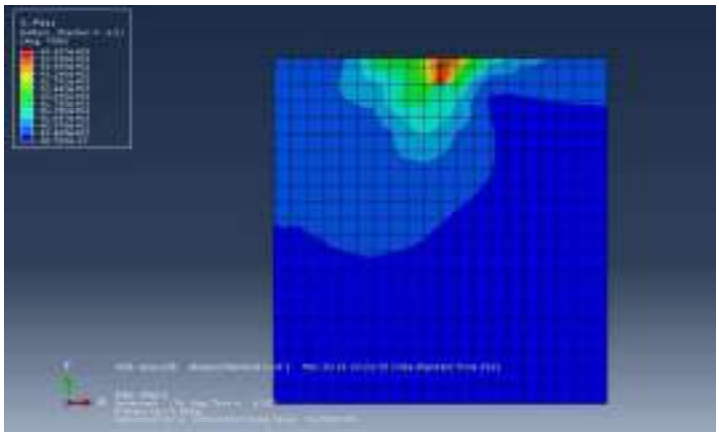

Fig. 4.233: Stress Contour for 25 mm Square Plate with (H/B =1) at 45° inclination under 0.2 Hz frequency and 2mm amplitude

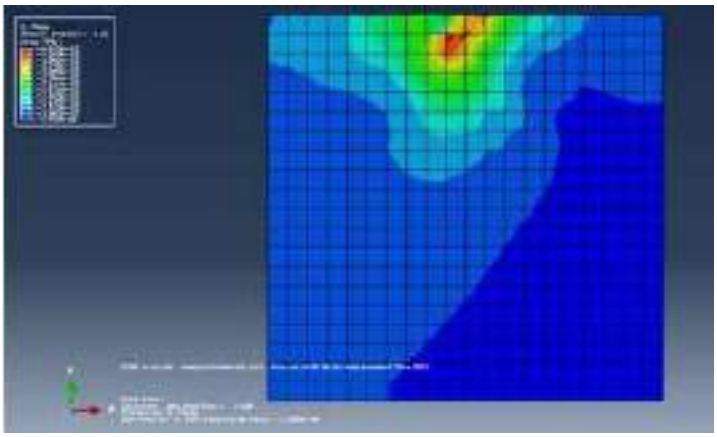

Fig. 4.234: Stress Contour for 25 mm Square Plate with (H/B =2) at 45° inclination under 0.2 Hz frequency and 2mm amplitude

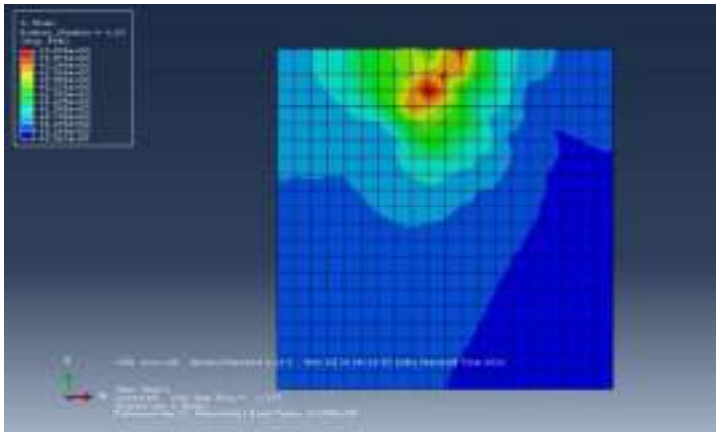

Fig. 4.235: Stress Contour for 25 mm Square Plate with (H/B =3) at 45° inclination under 0.2 Hz frequency and 2mm amplitude

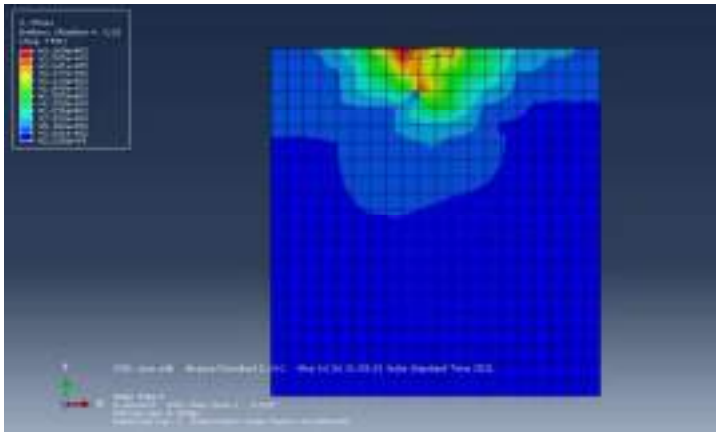

Fig. 4.236: Stress Contour for 25 mm Square Plate with (H/B =1) at 60° inclination under 0.2 Hz frequency and 2mm amplitude

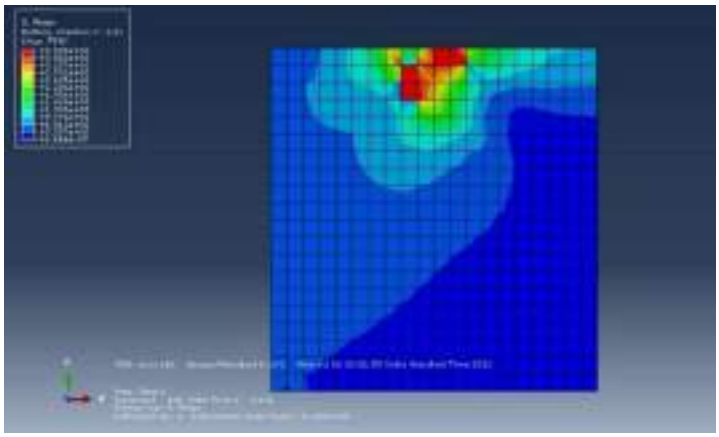

Fig. 4.237: Stress Contour for 25 mm Square Plate with (H/B =2) at 60° inclination under 0.2 Hz frequency and 2 mm amplitude

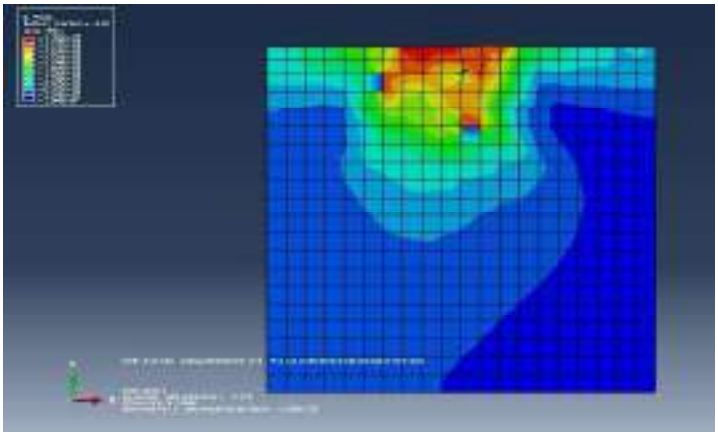

Fig. 4.238: Stress Contour for 25 mm Square Plate with (H/B =3) at 60° inclination under 0.2 Hz frequency and 2mm amplitude

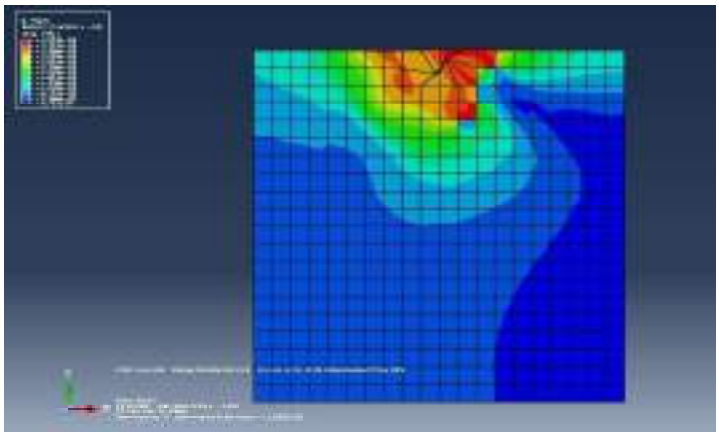

Fig. 4.239: Stress Contour for 50 mm Square Plate with (H/B =1) at 30° inclination under 0.2 Hz frequency and 2mm amplitude

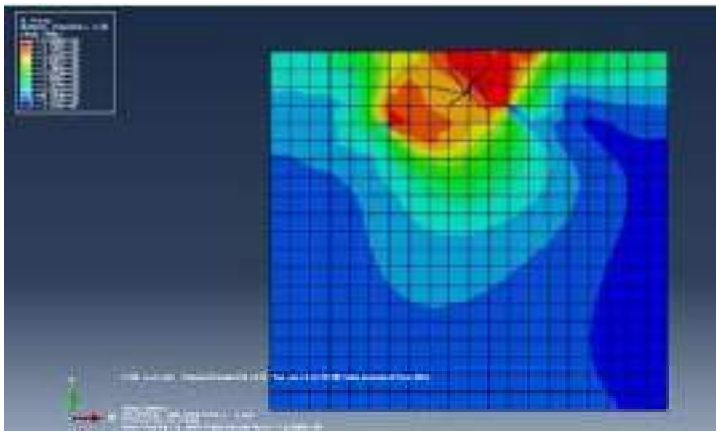

Fig. 4.240: Stress Contour for 50 mm Square Plate with (H/B =2) at 30° inclination under 0.2 Hz frequency and 2mm amplitude

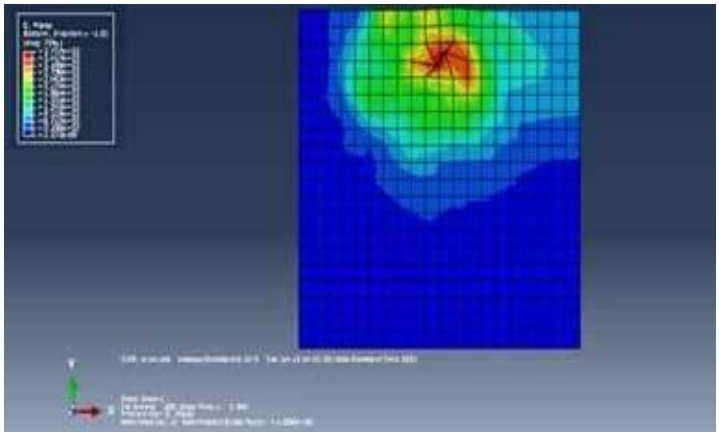

Fig. 4.241: Stress Contour for 50 mm Square Plate with (H/B =3) at 30° inclination under 0.2 Hz frequency and 2mm amplitude

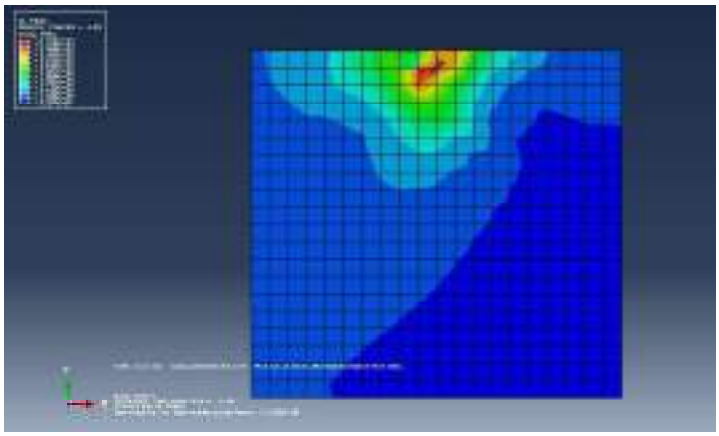

Fig. 4.242: Stress Contour for 50 mm Square Plate with (H/B =1) at 45° inclination under 0.2 Hz frequency and 2mm amplitude

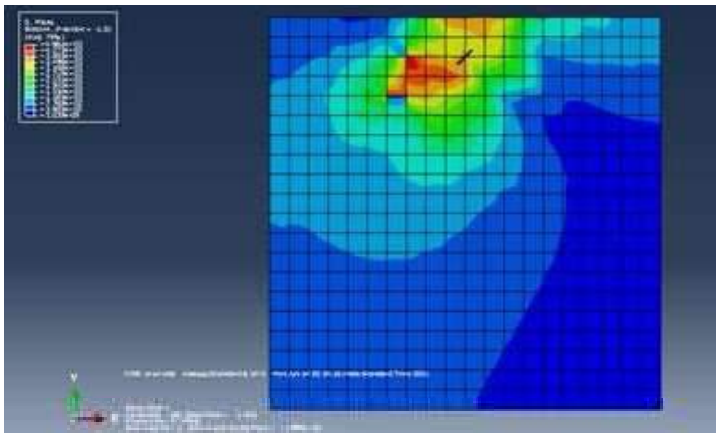

Fig. 4.243: Stress Contour for 50 mm Square Plate with (H/B =2) at 45° inclination under 0.2 Hz frequency and 2mm amplitude

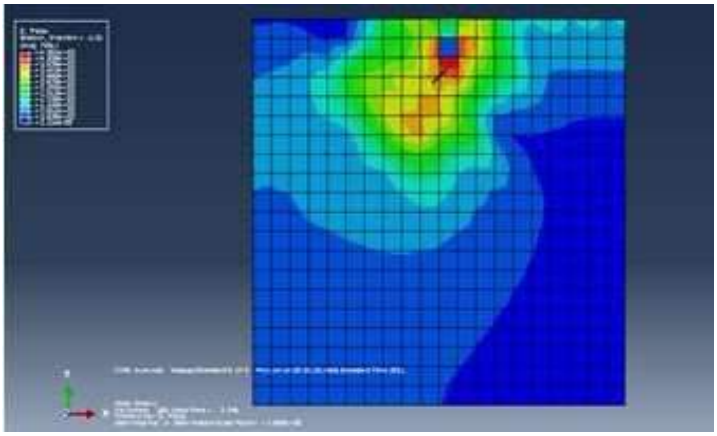

Fig. 4.244: Stress Contour for 50 mm Square Plate with (H/B =3) at 45° inclination under 0.2 Hz frequency and 2mm amplitude

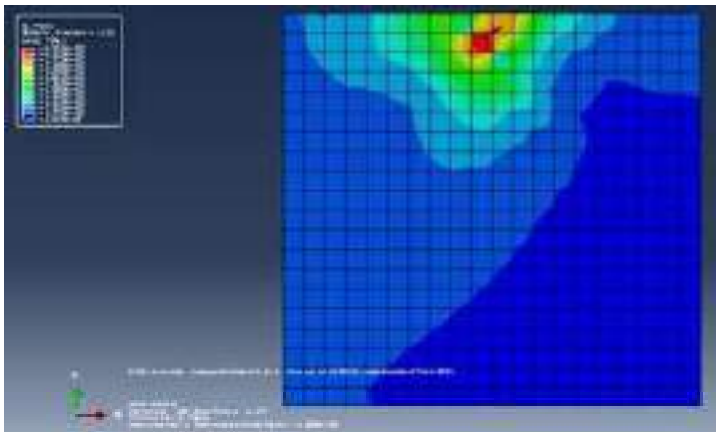

Fig. 4.245: Stress Contour for 50 mm Square Plate with (H/B =1) at 60° inclination under 0.2 Hz frequency and 2mm amplitude

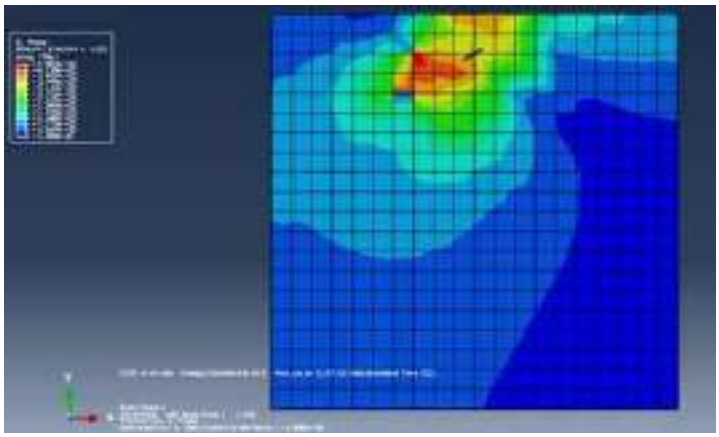

Fig. 4.246: Stress Contour for 50 mm Square Plate with (H/B =2) at 60° inclination under 0.2 Hz frequency and 2mm amplitude

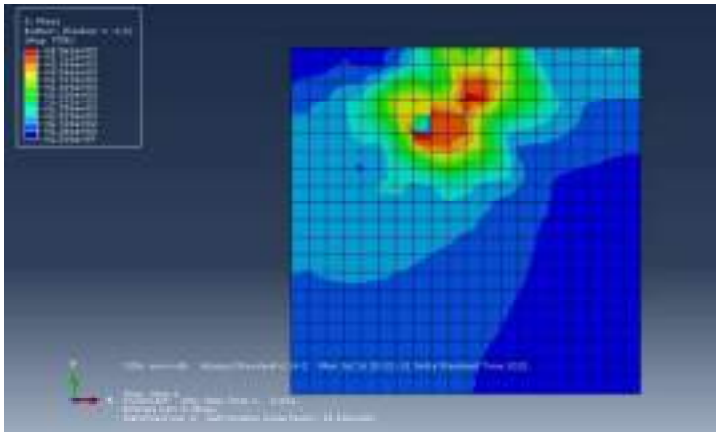

Fig. 4.247: Stress Contour for 50 mm Square Plate with (H/B =3) at 60° inclination under 0.2 Hz frequency and 2mm amplitude

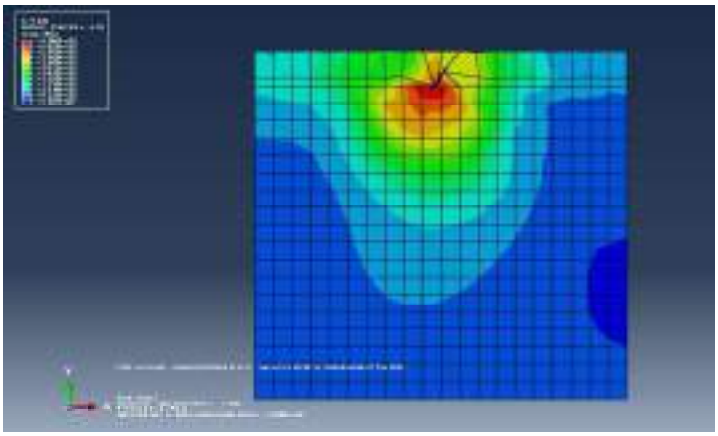

Fig. 4.248: Stress Contour for 75 mm Square Plate with (H/B =1) at 30° inclination under 0.2 Hz frequency and 2mm amplitude

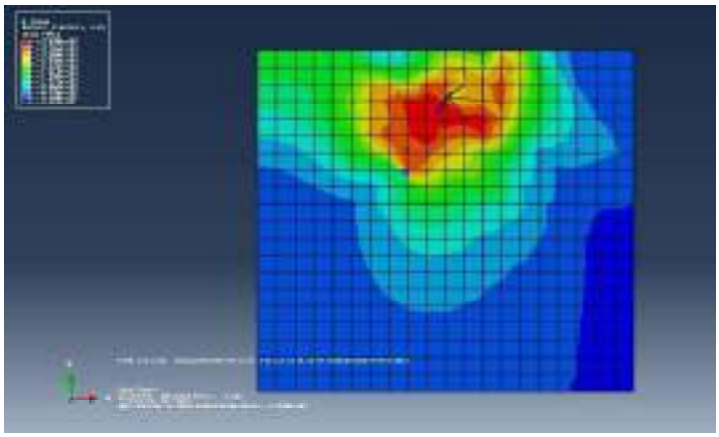

Fig. 4.249: Stress Contour for 75 mm Square Plate with (H/B =2) at 30° inclination under 0.2 Hz frequency and 2mm amplitude

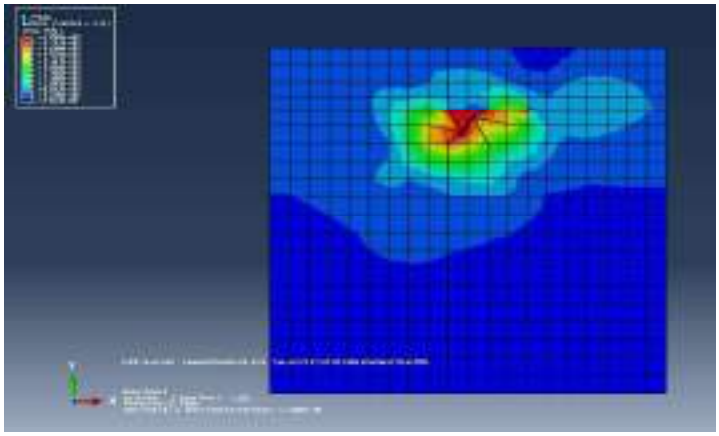

Fig. 4.250: Stress Contour for 75 mm Square Plate with (H/B =3) at 30° inclination under 0.2 Hz frequency and 2mm amplitude

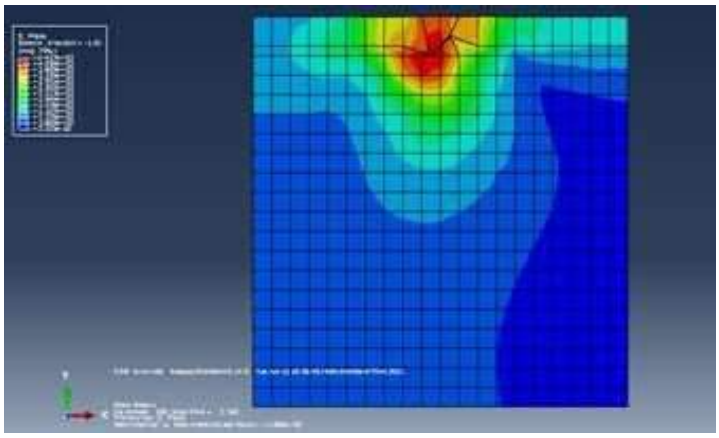

Fig. 4.251: Stress Contour for 75 mm Square Plate with (H/B =1) at 45° inclination under 0.2 Hz frequency and 2mm amplitude

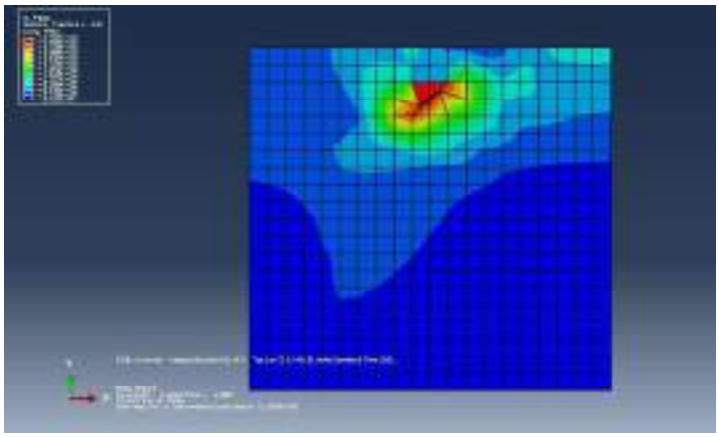

Fig. 4.252: Stress Contour for 75 mm Square Plate with (H/B =2) at 45° inclination under 0.2 Hz frequency and 2mm amplitude

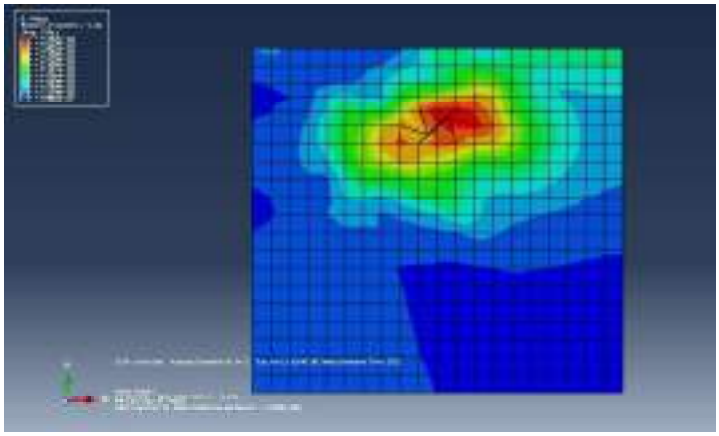

Fig. 4.253: Stress Contour for 75 mm Square Plate with (H/B =3) at 45° inclination under 0.2 Hz frequency and 2mm amplitude

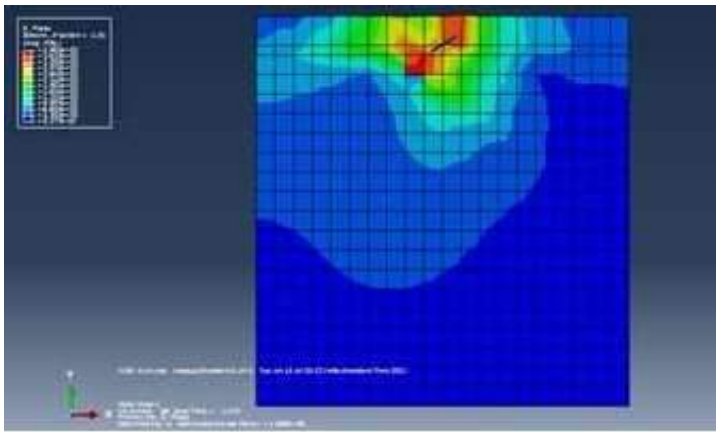

Fig. 4.254: Stress Contour for 75 mm Square Plate with (H/B =1) at 60° inclination under 0.2 Hz frequency and 2mm amplitude

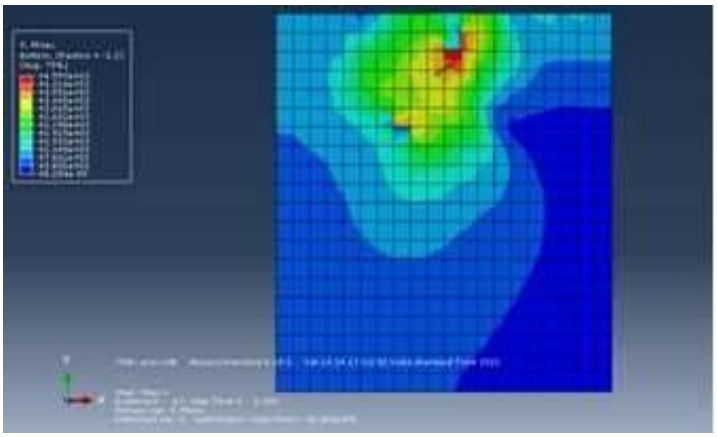

Fig. 4.255: Stress Contour for 75 mm Square Plate with (H/B =2) at 60° inclination under 0.2 Hz frequency and 2mm amplitude

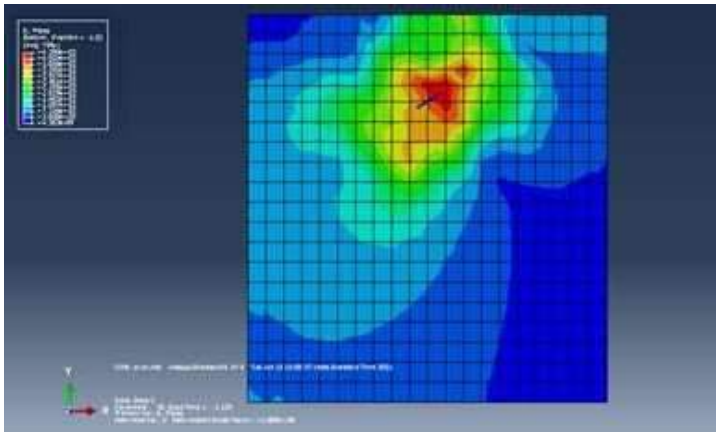

Fig. 4.256: Stress Contour for 75 mm Square Plate with (H/B =3) at 60° inclination under 0.2 Hz frequency and 2mm amplitude

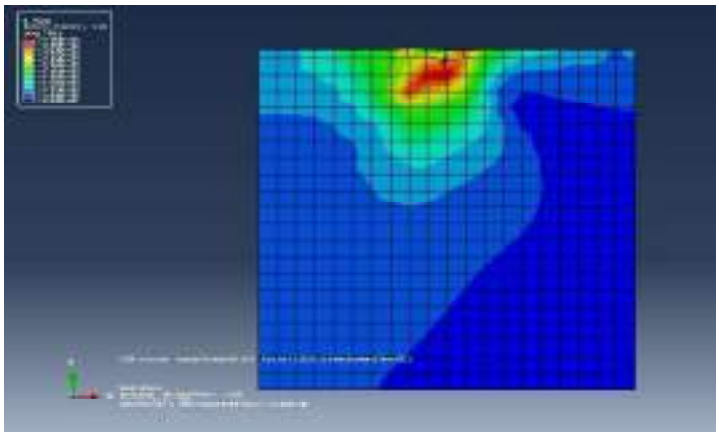

Fig. 4.257: Stress Contour for 25 mm Square Plate with (H/B =1) at 30° inclination under 0.2 Hz frequency and 5mm amplitude

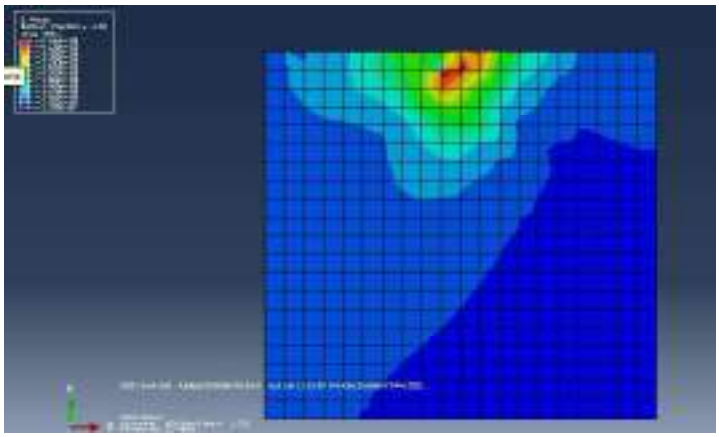

Fig. 4.258: Stress Contour for 25 mm Square Plate with (H/B =2) at 30° inclination under 0.2 Hz frequency and 5mm amplitude

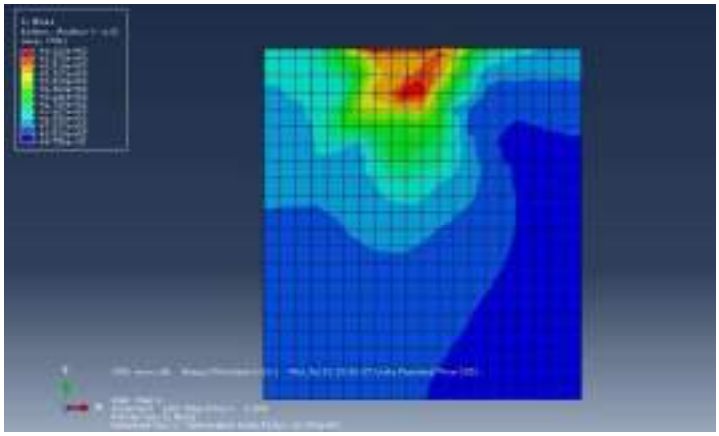

Fig. 4.259: Stress Contour for 25 mm Square Plate with (H/B =3) at 30° inclination under 0.2 Hz frequency and 5mm amplitude

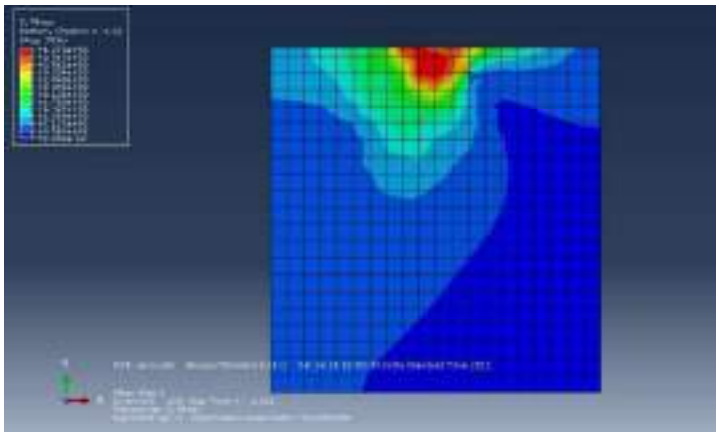

Fig. 4.260: Stress Contour for 25 mm Square Plate with (H/B =1) at 45° inclination under 0.2 Hz frequency and 5mm amplitude

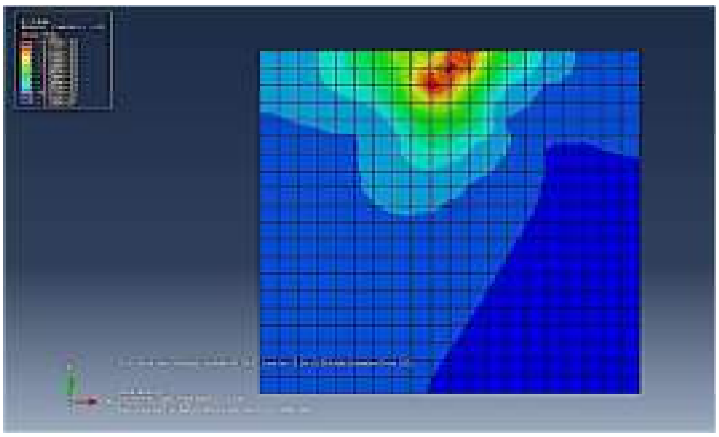

Fig. 4.261: Stress Contour for 25 mm Square Plate with (H/B =2) at 45° inclination under 0.2 Hz frequency and 5mm amplitude

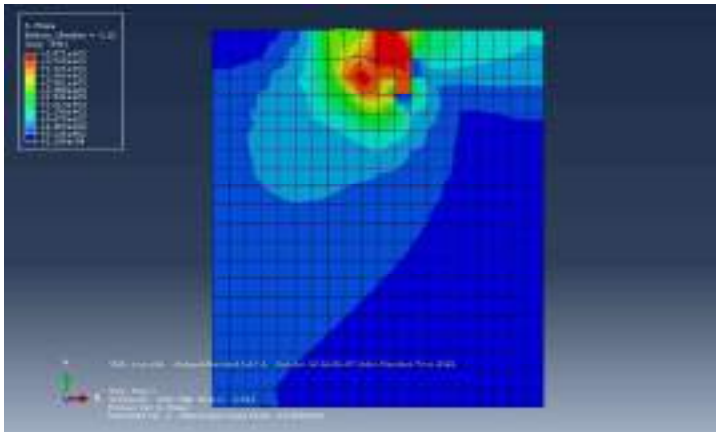

Fig. 4.262: Stress Contour for 25 mm Square Plate with (H/B =3) at 45° inclination under 0.2 Hz frequency and 5mm amplitude

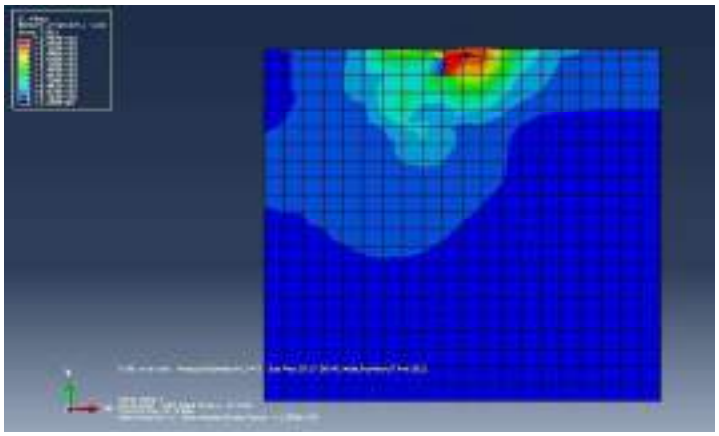

Fig. 4.263: Stress Contour for 25 mm Square Plate with (H/B =1) at 60° inclination under 0.2 Hz frequency and 5mm amplitude

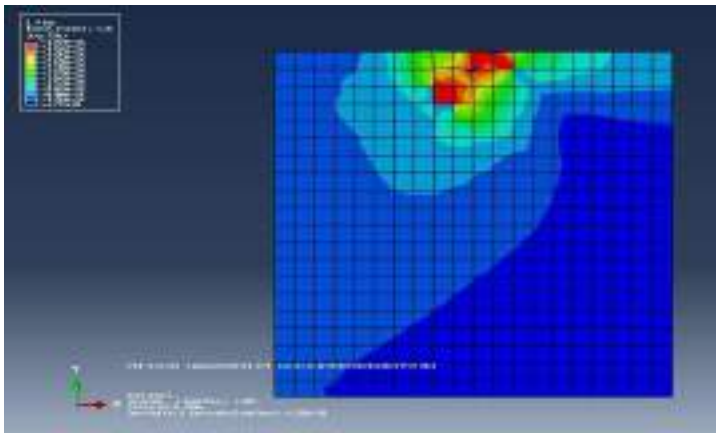

Fig. 4.264: Stress Contour for 25 mm Square Plate with (H/B =2) at 60° inclination under 0.2 Hz frequency and 5mm amplitude

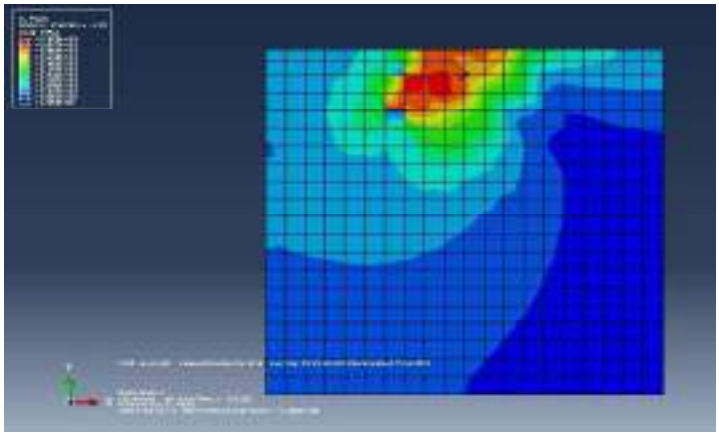

Fig. 4.265: Stress Contour for 25 mm Square Plate with (H/B =3) at 60° inclination under 0.2 Hz frequency and 5mm amplitude

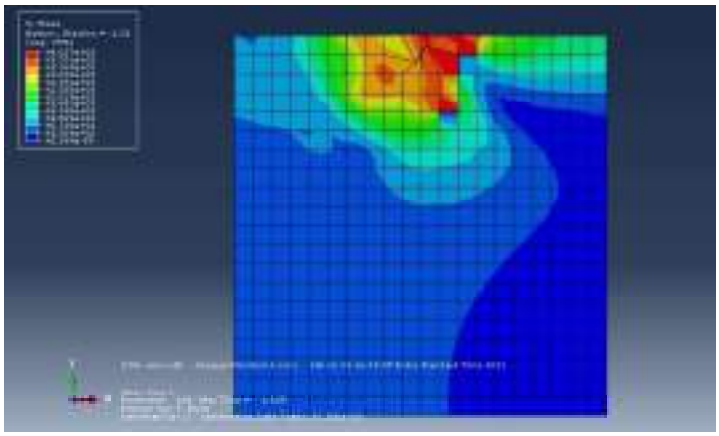

Fig. 4.266: Stress Contour for 50 mm Square Plate with (H/B =1) at 30° inclination under 0.2 Hz frequency and 5mm amplitude

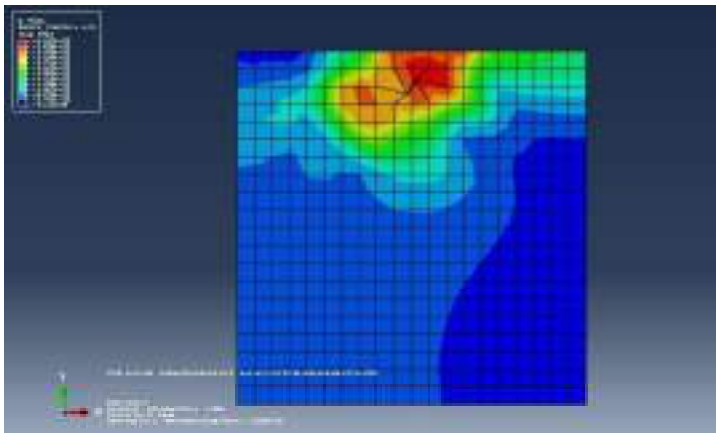

Fig. 4.267: Stress Contour for 50 mm Square Plate with (H/B =2) at 30° inclination under 0.2 Hz frequency and 5mm amplitude

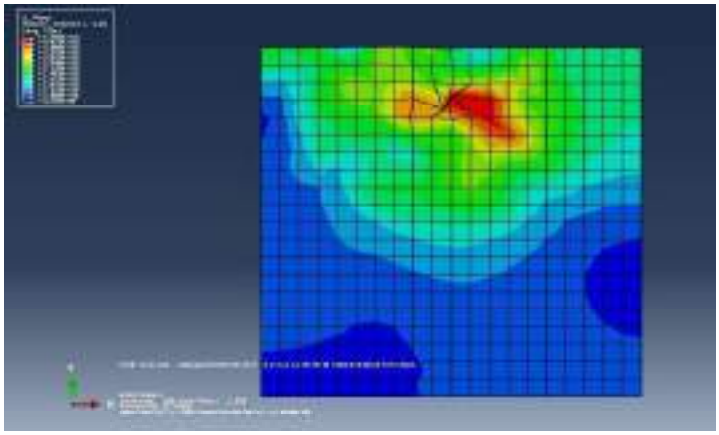

Fig. 4.268: Stress Contour for 50 mm Square Plate with (H/B =3) at 30° inclination under 0.2 Hz frequency and 5mm amplitude

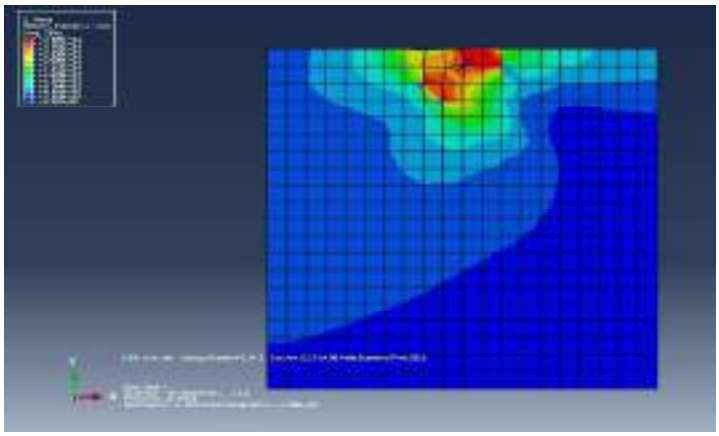

Fig. 4.269: Stress Contour for 50 mm Square Plate with (H/B =1) at 45° inclination under 0.2 Hz frequency and 5mm amplitude

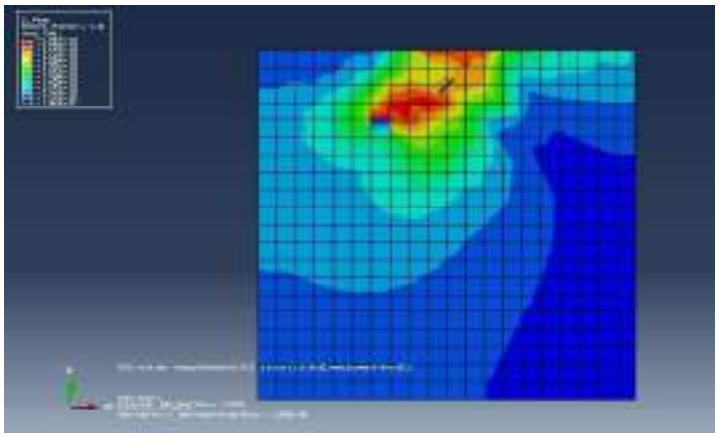

Fig. 4.270: Stress Contour for 50 mm Square Plate with (H/B =2) at 45° inclination under 0.2 Hz frequency and 5mm amplitude

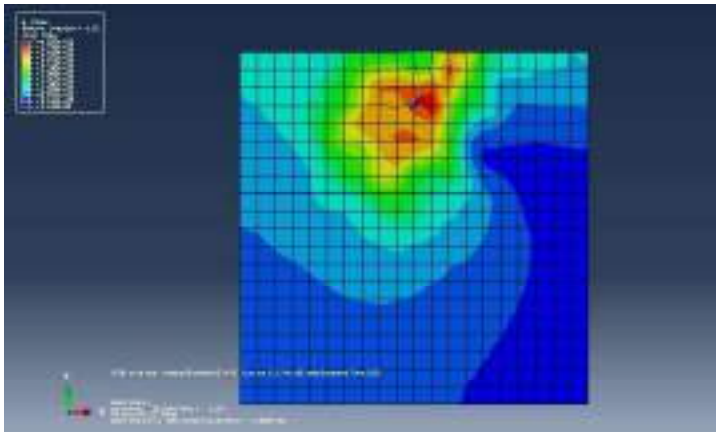

Fig. 4.271: Stress Contour for 50 mm Square Plate with (H/B =3) at 45° inclination under 0.2 Hz frequency and 5mm amplitude

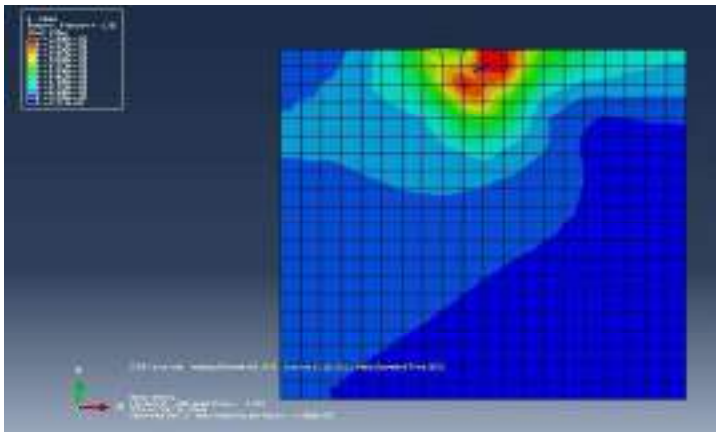

Fig. 4.272: Stress Contour for 50 mm Square Plate with (H/B =1) at 60° inclination under 0.2 Hz frequency and 5mm amplitude

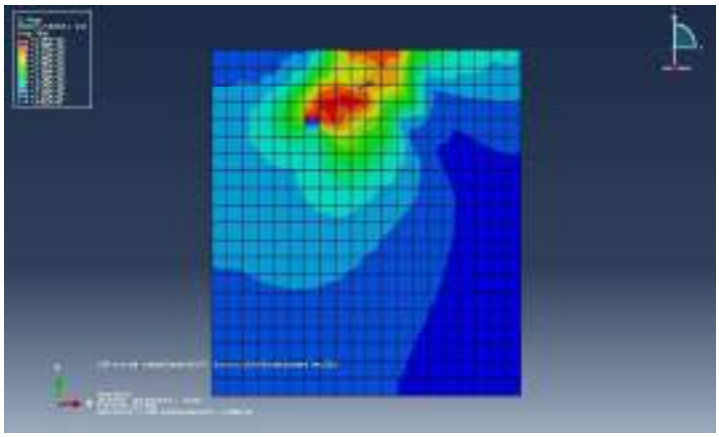

Fig. 4.273: Stress Contour for 50 mm Square Plate with (H/B =2) at 60° inclination under 0.2 Hz frequency and 5mm amplitude

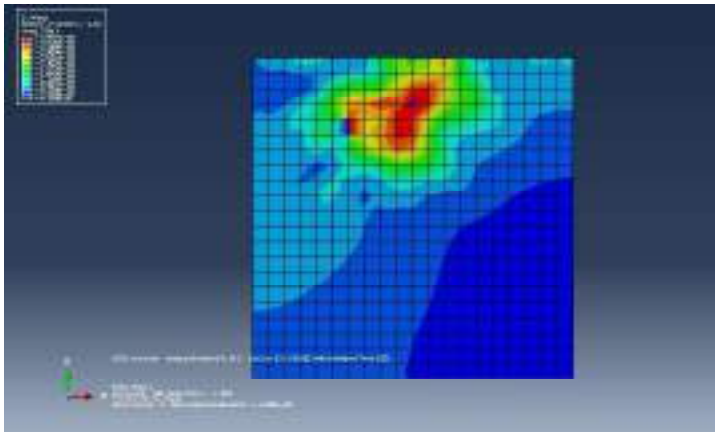

Fig. 4.274: Stress Contour for 50 mm Square Plate with (H/B =3) at 60° inclination under 0.2 Hz frequency and 5mm amplitude

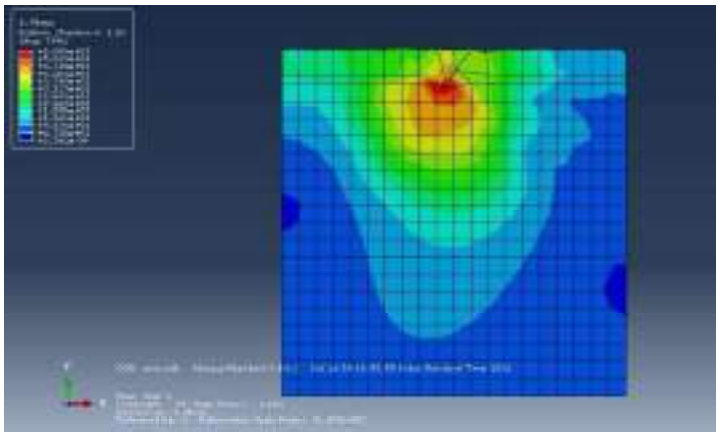

Fig. 4.275: Stress Contour for 75mm Square Plate with (H/B =1) at 30° inclination under 0.2 Hz frequency and 5mm amplitude

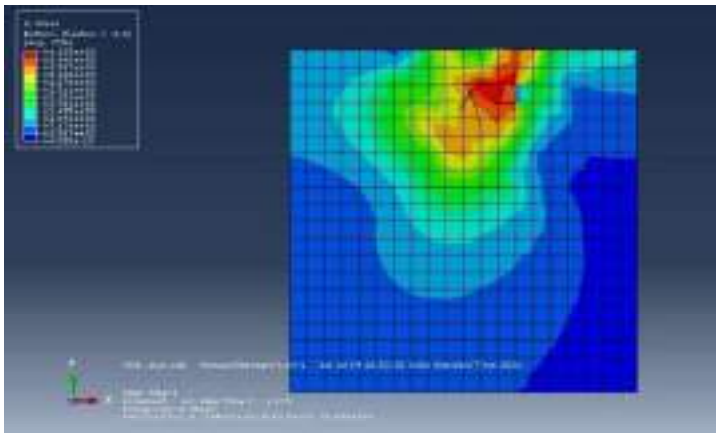

Fig. 4.276: Stress Contour for 75mm Square Plate with (H/B =2) at 30° inclination under 0.2 Hz frequency and 5mm amplitude

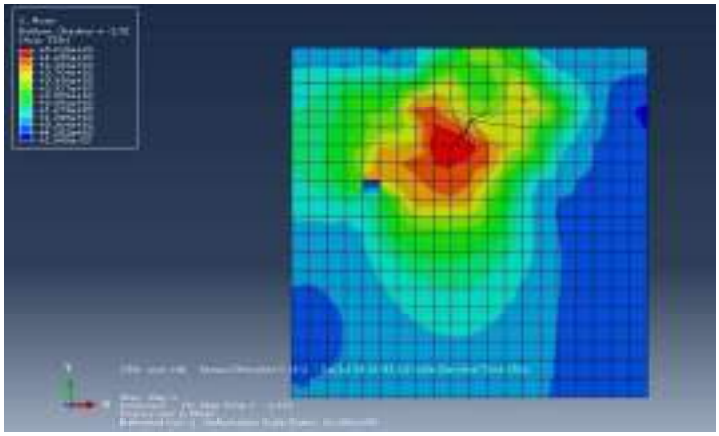

Fig. 4.277: Stress Contour for 75mm Square Plate with (H/B =3) at 30° inclination under 0.2 Hz frequency and 5mm amplitude

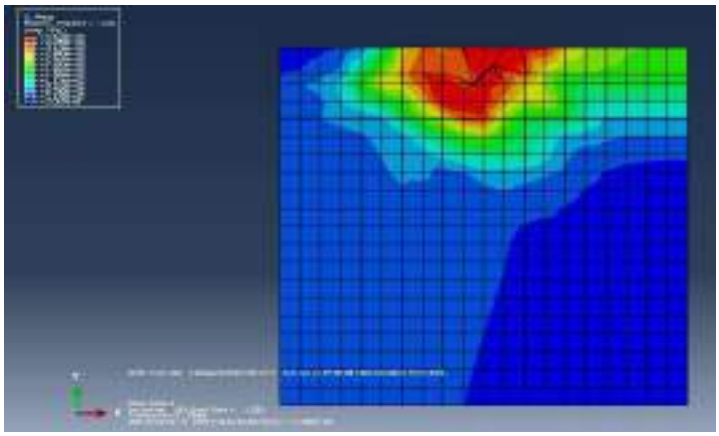

Fig. 4.278: Stress Contour for 75mm Square Plate with (H/B =1) at 45° inclination under 0.2 Hz frequency and 5mm amplitude

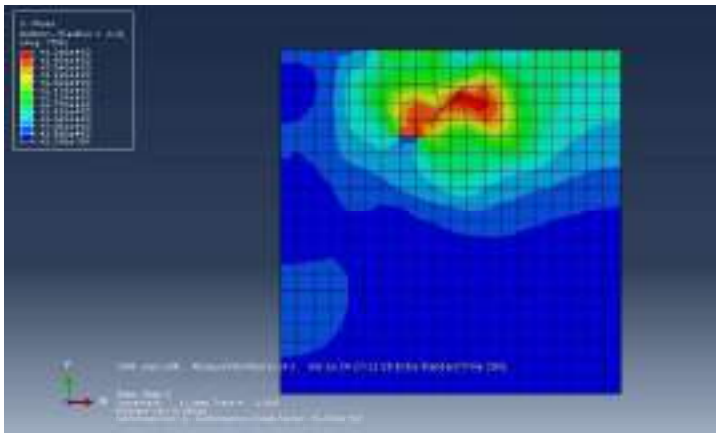

Fig. 4.279: Stress Contour for 75mm Square Plate with (H/B =2) at 45° inclination under 0.2 Hz frequency and 5mm amplitude

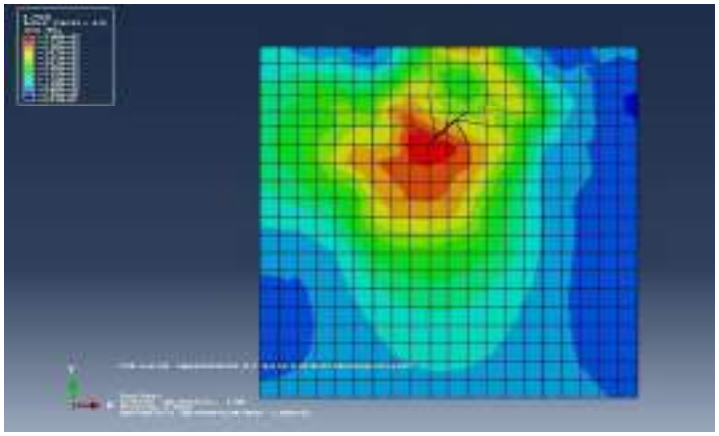

Fig. 4.280: Stress Contour for 75mm Square Plate with (H/B =3) at 45° inclination under 0.2 Hz frequency and 5mm amplitude

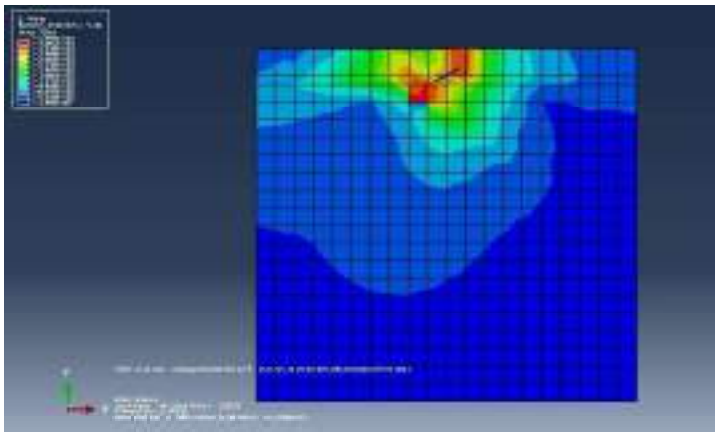

Fig. 4.281: Stress Contour for 75mm Square Plate with (H/B =1) at 60° inclination under 0.2 Hz frequency and 5mm amplitude

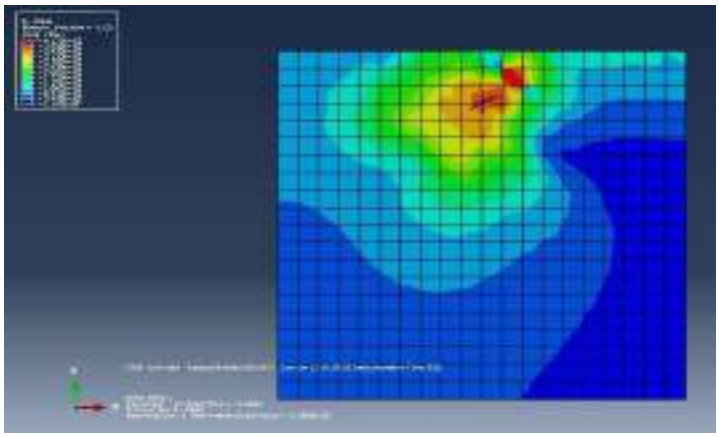

Fig. 4.282: Stress Contour for 75mm Square Plate with (H/B =2) at 60° inclination under 0.2 Hz frequency and 5mm amplitude

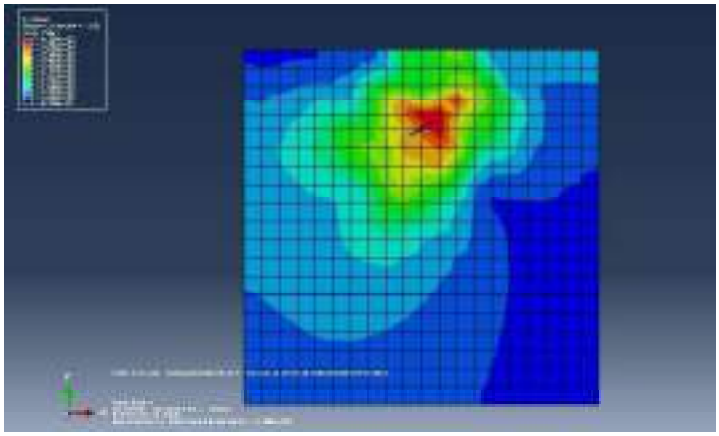

Fig. 4.283: Stress Contour for 75mm Square Plate with (H/B =3) at 60° inclination under 0.2 Hz frequency and 5mm amplitude

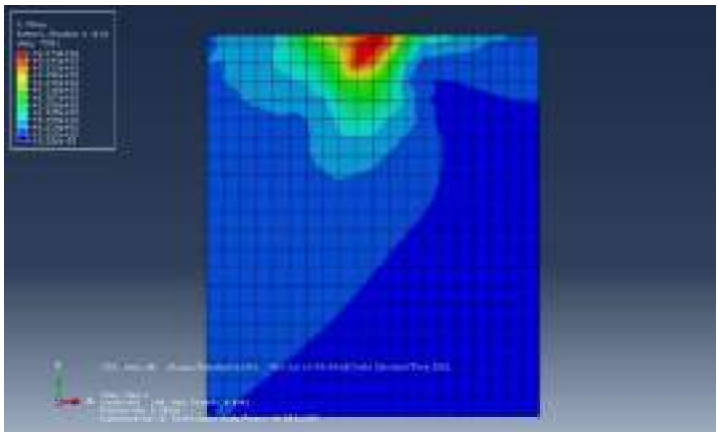

Fig. 4.284: Stress Contour for 25mm Square Plate with (H/B =1) at 30° inclination under 0.5 Hz frequency and 2mm amplitude

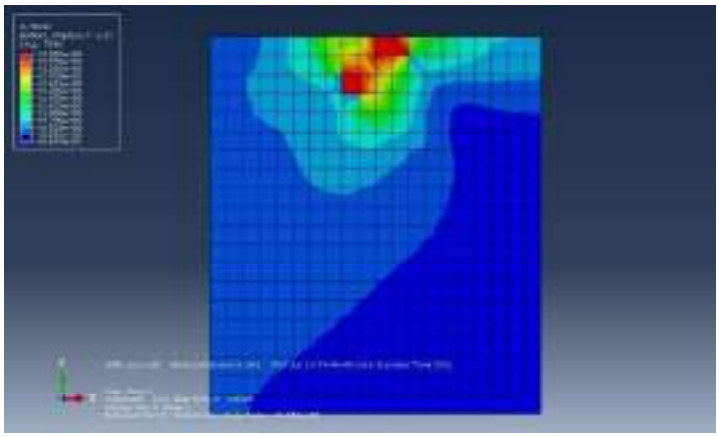

Fig. 4.285: Stress Contour for 25mm Square Plate with (H/B =2) at 30° inclination under 0.5 Hz frequency and 2mm amplitude

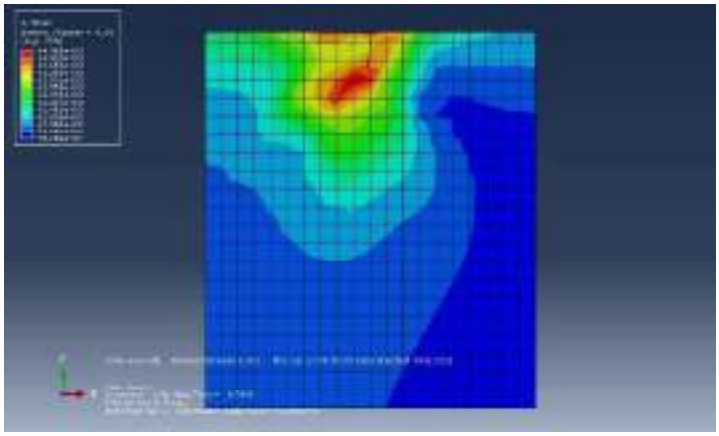

Fig. 4.286: Stress Contour for 25mm Square Plate with (H/B =3) at 30° inclination under 0.5 Hz frequency and 2mm amplitude

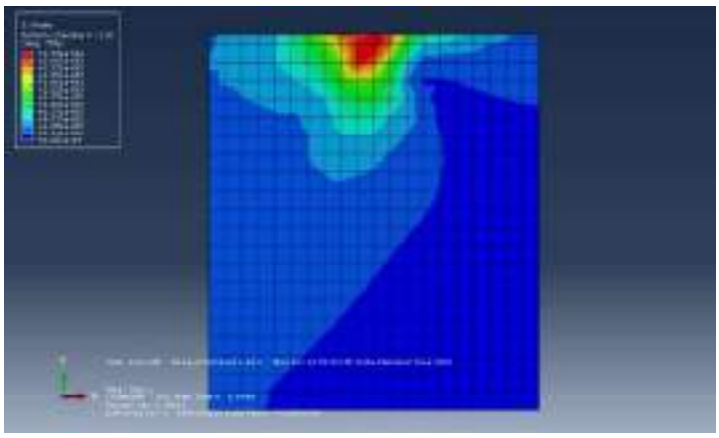

Fig. 4.287: Stress Contour for 25mm Square Plate with (H/B =1) at 45° inclination under 0.5 Hz frequency and 2mm amplitude

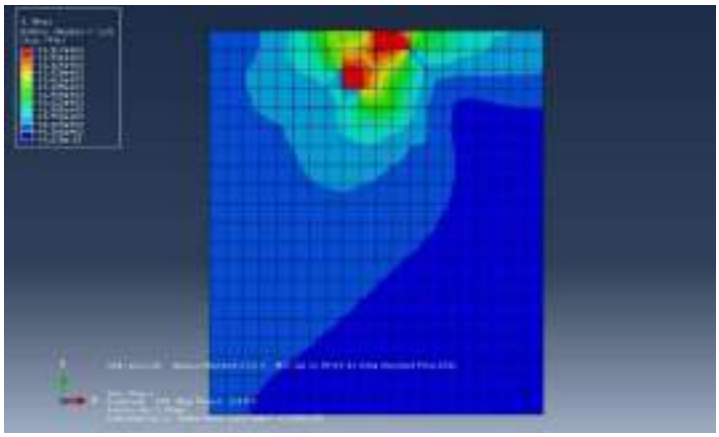

Fig. 4.288: Stress Contour for 25mm Square Plate with (H/B =2) at 45° inclination under 0.5 Hz frequency and 2mm amplitude

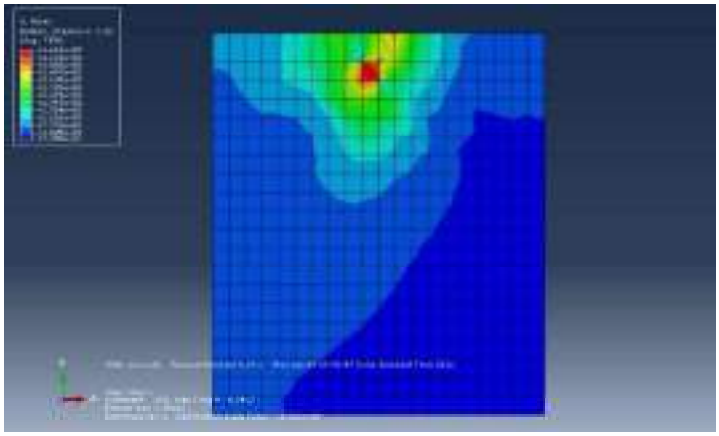

Fig. 4.289: Stress Contour for 25mm Square Plate with (H/B =3) at 45° inclination under 0.5 Hz frequency and 2mm amplitude

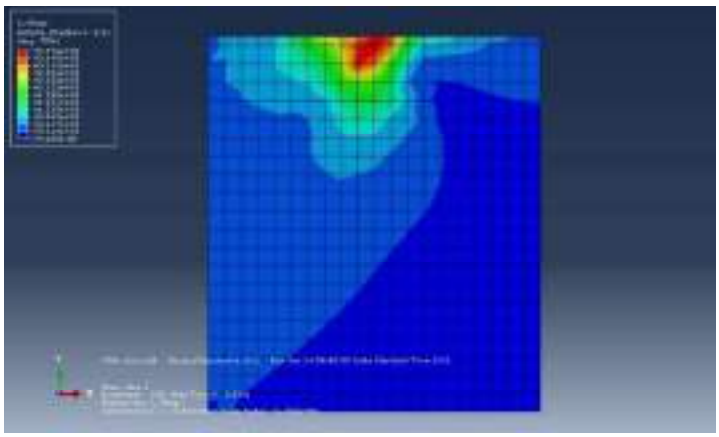

Fig. 4.290: Stress Contour for 25mm Square Plate with (H/B =1) at 60° inclination under 0.5 Hz frequency and 2mm amplitude

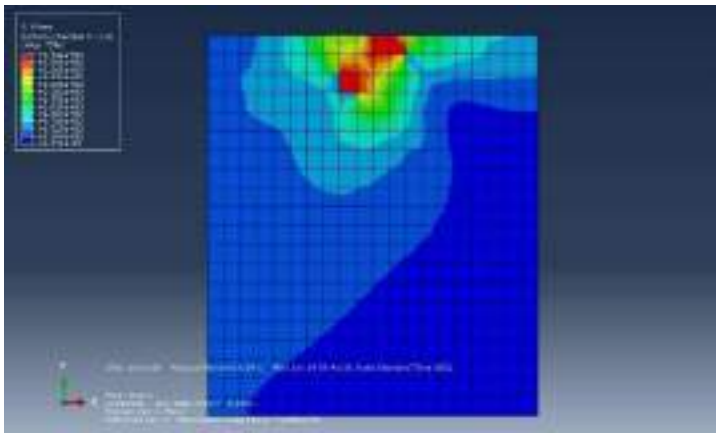

Fig. 4.291: Stress Contour for 25mm Square Plate with (H/B =2) at 60° inclination under 0.5 Hz frequency and 2mm amplitude

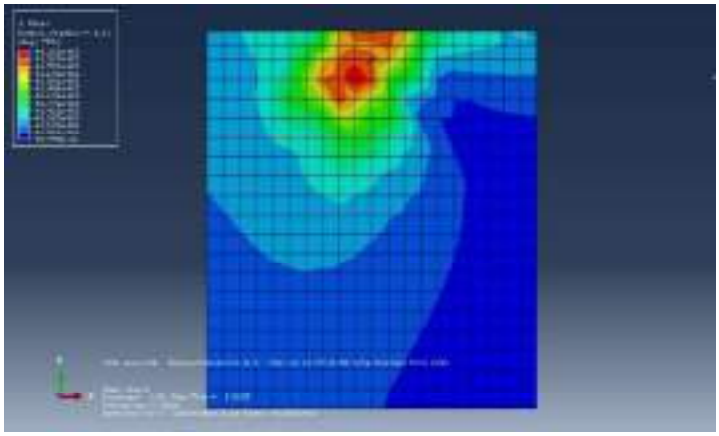

Fig. 4.292: Stress Contour for 25mm Square Plate with (H/B =3) at 60° inclination under 0.5 Hz frequency and 2mm amplitude

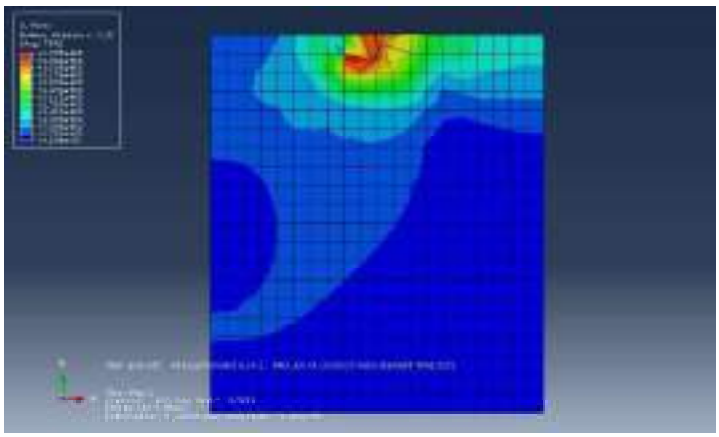

Fig. 4.293: Stress Contour for 50mm Square Plate with (H/B =1) at 30° inclination under 0.5 Hz frequency and 2mm amplitude

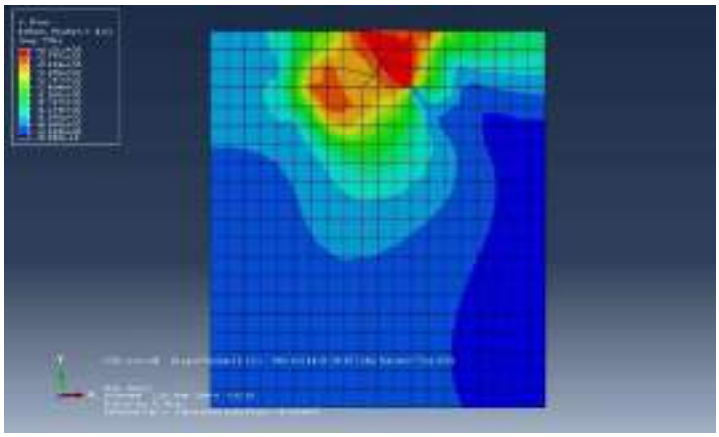

Fig. 4.294: Stress Contour for 50mm Square Plate with (H/B =2) at 30° inclination under 0.5 Hz frequency and 2mm amplitude

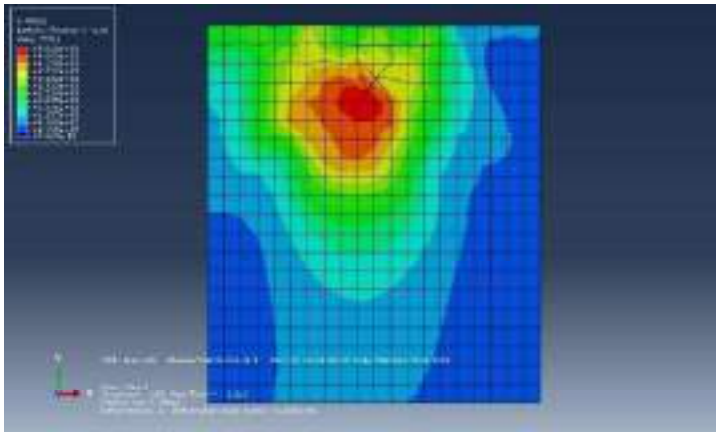

Fig. 4.295: Stress Contour for 50mm Square Plate with (H/B =3) at 30° inclination under 0.5 Hz frequency and 2mm amplitude

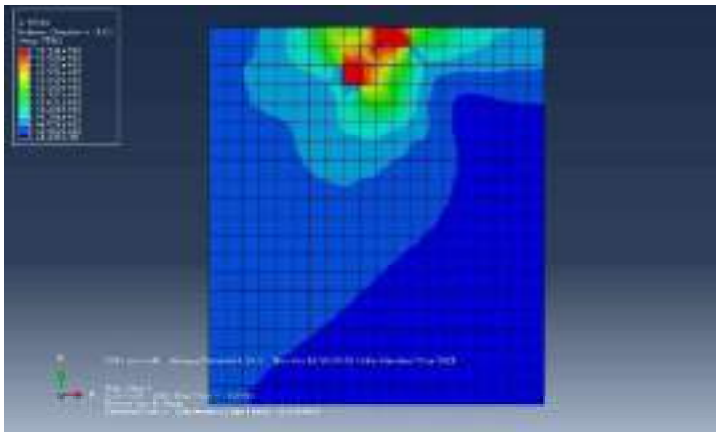

Fig. 4.296: Stress Contour for 50mm Square Plate with (H/B =1) at 45° inclination under 0.5 Hz frequency and 2mm amplitude

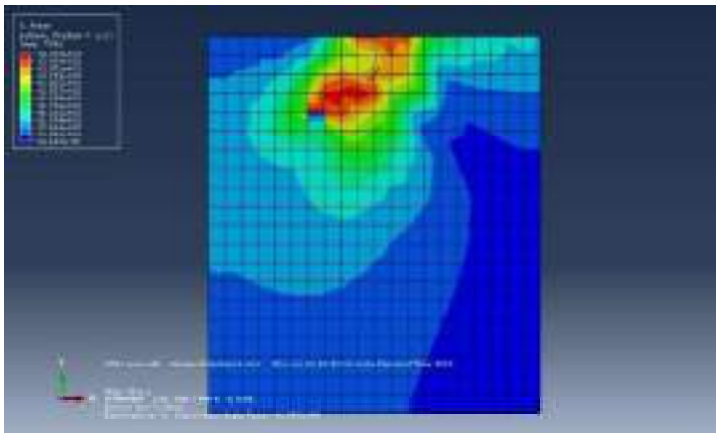

Fig. 4.297: Stress Contour for 50mm Square Plate with (H/B =2) at 45° inclination under 0.5 Hz frequency and 2mm amplitude

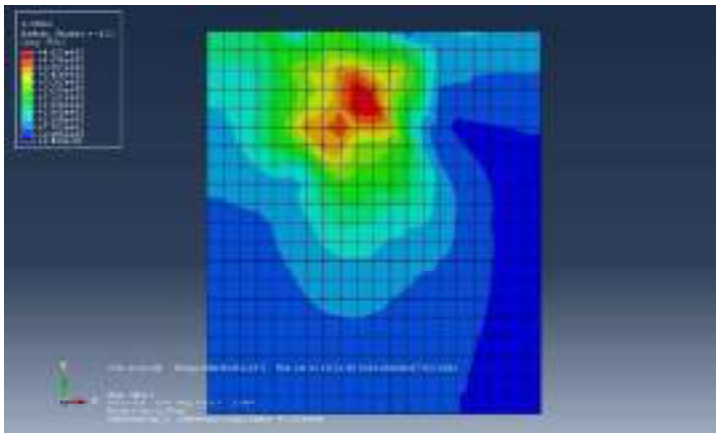

Fig. 4.298: Stress Contour for 50mm Square Plate with (H/B =3) at 45° inclination under 0.5 Hz frequency and 2mm amplitude

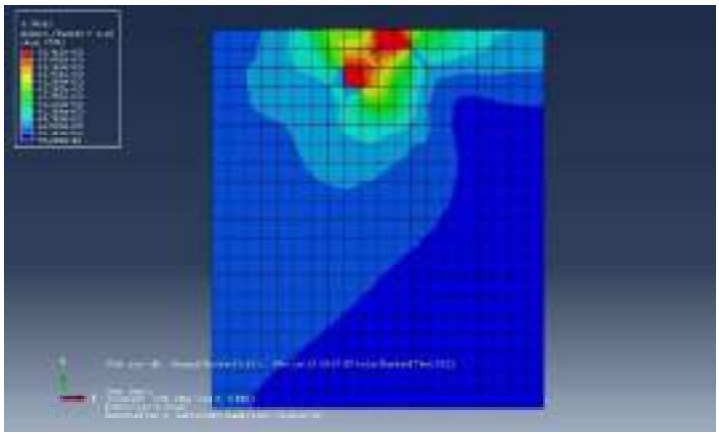

Fig. 4.299: Stress Contour for 50mm Square Plate with (H/B =1) at 60° inclination under 0.5 Hz frequency and 2mm amplitude

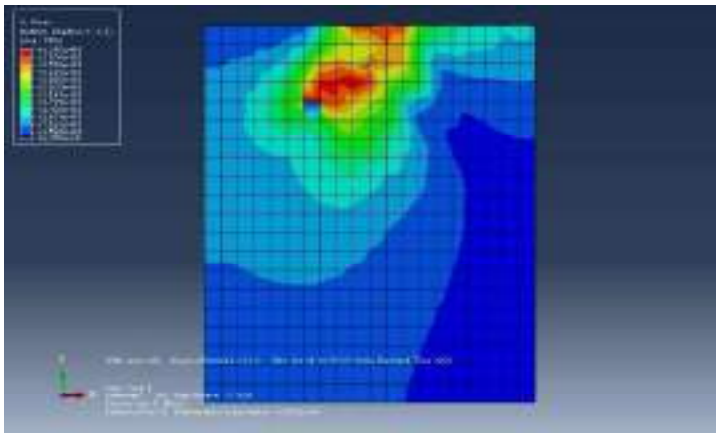

Fig. 4.300: Stress Contour for 50mm Square Plate with (H/B =2) at 60° inclination under 0.5 Hz frequency and 2mm amplitude

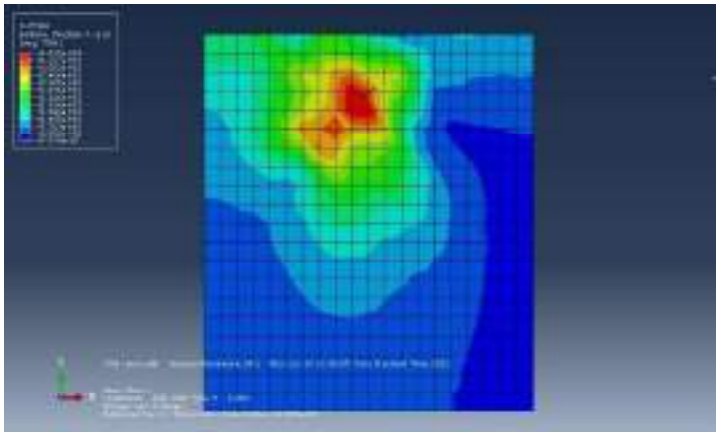

Fig. 4.301: Stress Contour for 50mm Square Plate with (H/B =3) at 60° inclination under 0.5 Hz frequency and 2mm amplitude

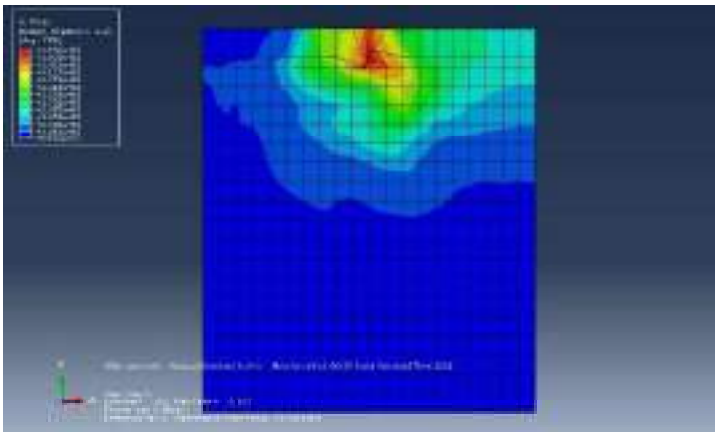

Fig. 4.302: Stress Contour for 75mm Square Plate with (H/B =1) at 30° inclination under 0.5 Hz frequency and 2mm amplitude

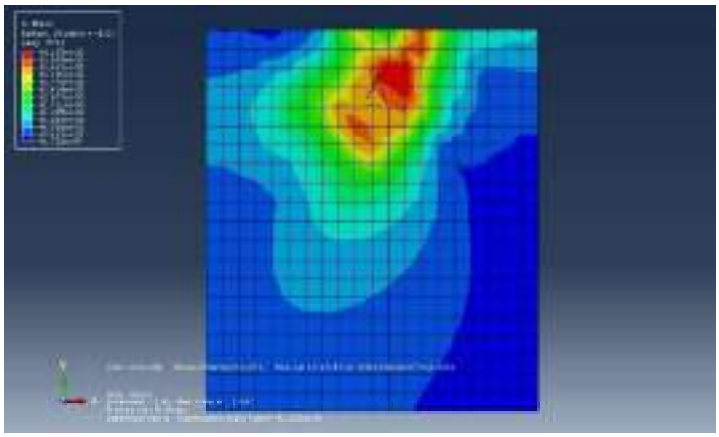

Fig. 4.303: Stress Contour for 75mm Square Plate with (H/B =2) at 30° inclination under 0.5 Hz frequency and 2mm amplitude

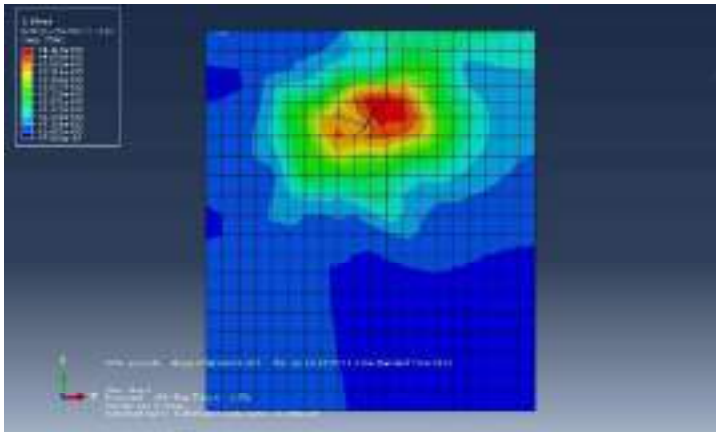

Fig. 4.304: Stress Contour for 75mm Square Plate with (H/B =3) at 30° inclination under 0.5 Hz frequency and 2mm amplitude

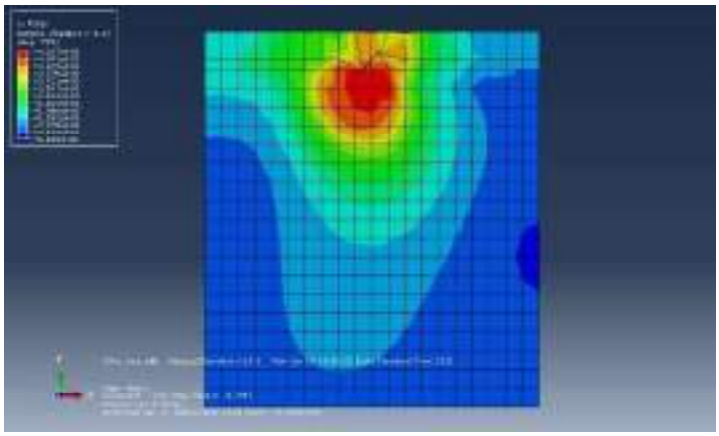

Fig. 4.305: Stress Contour for 75mm Square Plate with (H/B =1) at 45° inclination under 0.5 Hz frequency and 2mm amplitude

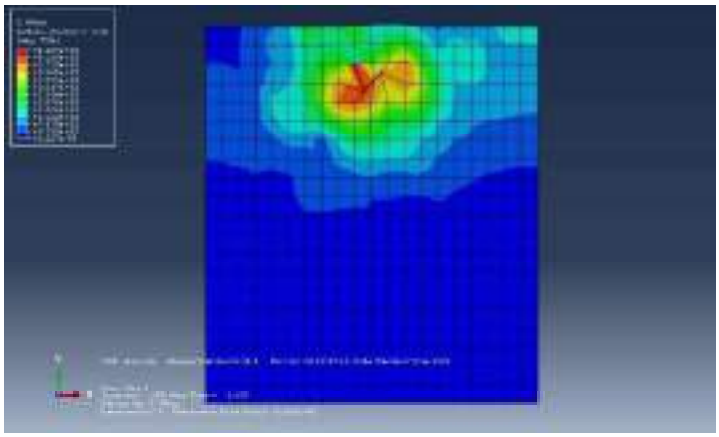

Fig. 4.306: Stress Contour for 75mm Square Plate with (H/B =2) at 45° inclination under 0.5 Hz frequency and 2mm amplitude

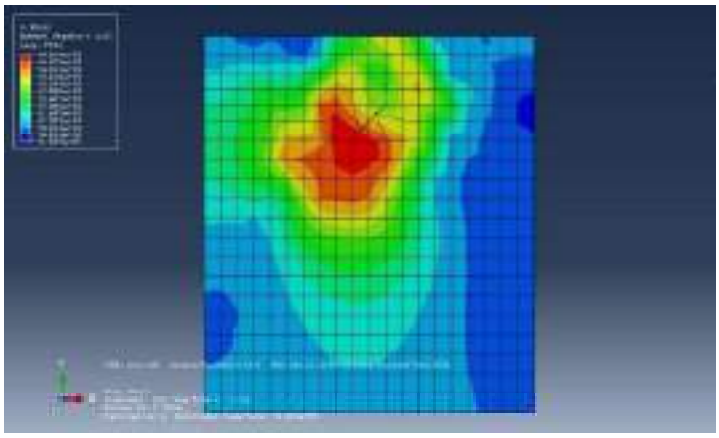

Fig. 4.307: Stress Contour for 75mm Square Plate with (H/B =3) at 45° inclination under 0.5 Hz frequency and 2mm amplitude

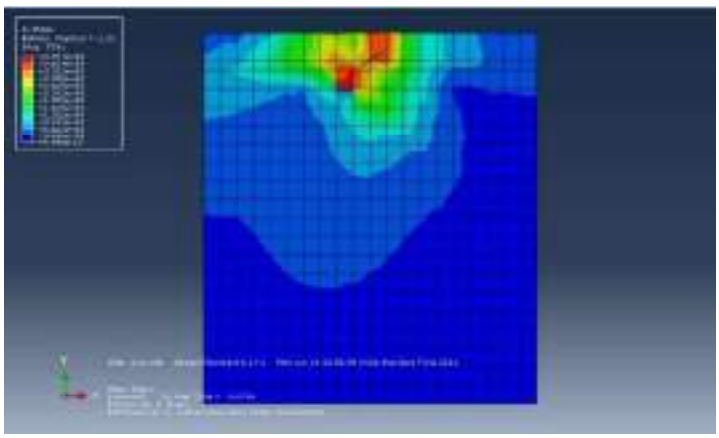

Fig. 4.308: Stress Contour for 75mm Square Plate with (H/B =1) at 60° inclination under 0.5 Hz frequency and 2mm amplitude

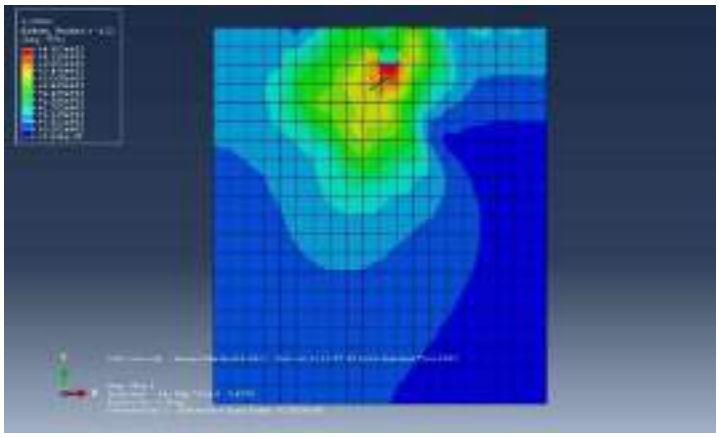

Fig. 4.309: Stress Contour for 75mm Square Plate with (H/B =2) at 60° inclination under 0.5 Hz frequency and 2mm amplitude

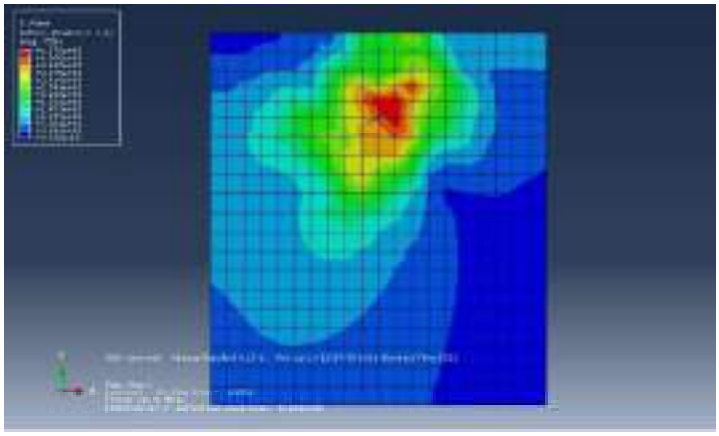

Fig. 4.310: Stress Contour for 75mm Square Plate with (H/B =3) at 60° inclination under 0.5 Hz frequency and 2mm amplitude

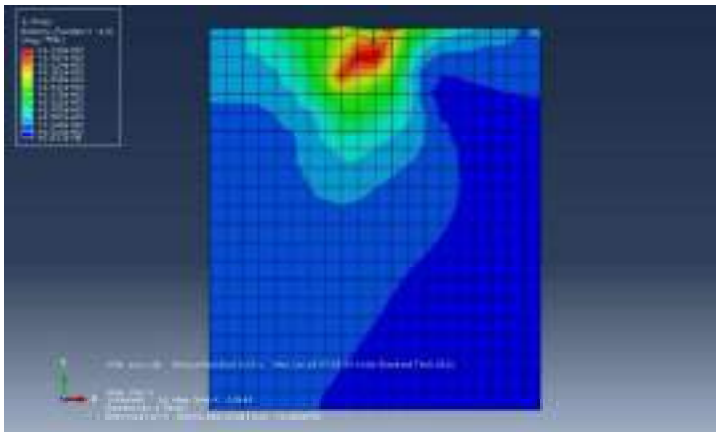

Fig. 4.311: Stress Contour for 25mm Square Plate with (H/B =1) at 30° inclination under 0.5 Hz frequency and 5mm amplitude

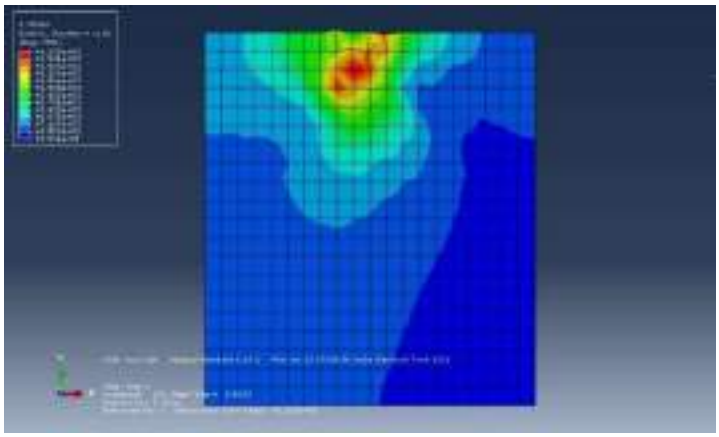

Fig. 4.312: Stress Contour for 25mm Square Plate with (H/B =2) at 30° inclination under 0.5 Hz frequency and 5mm amplitude

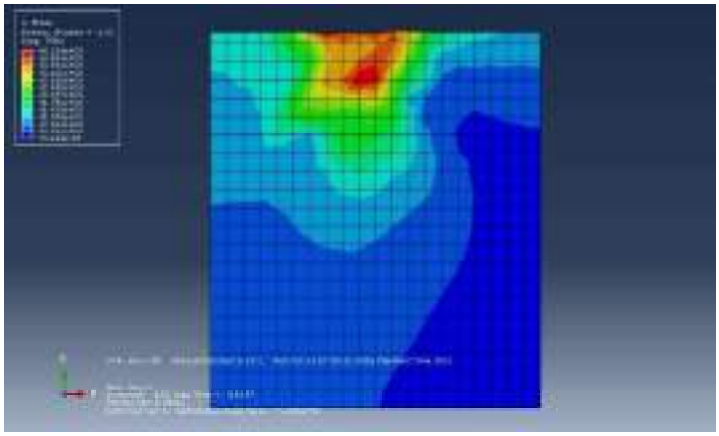

Fig. 4.313: Stress Contour for 25mm Square Plate with (H/B =3) at 30° inclination under 0.5 Hz frequency and 5mm amplitude

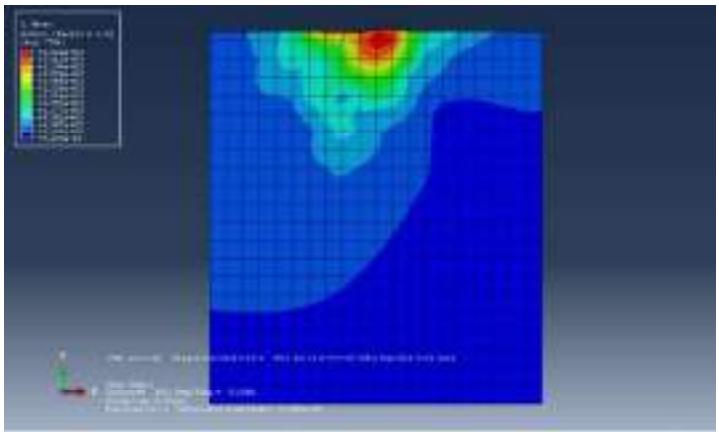

Fig. 4.314: Stress Contour for 25mm Square Plate with (H/B =1) at 45° inclination under 0.5 Hz frequency and 5mm amplitude

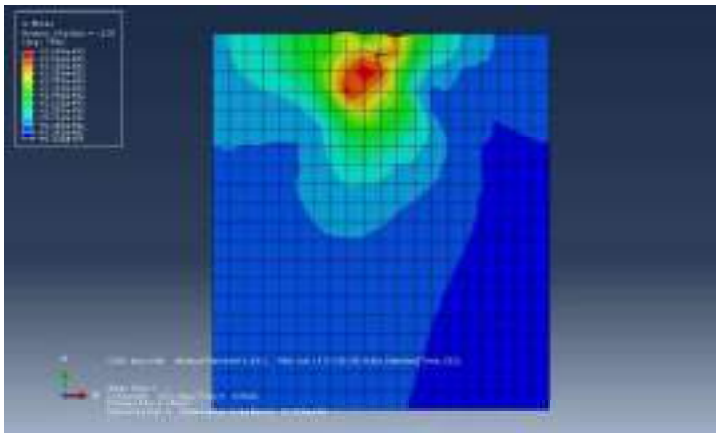

Fig. 4.315: Stress Contour for 25mm Square Plate with (H/B =2) at 45° inclination under 0.5 Hz frequency and 5mm amplitude

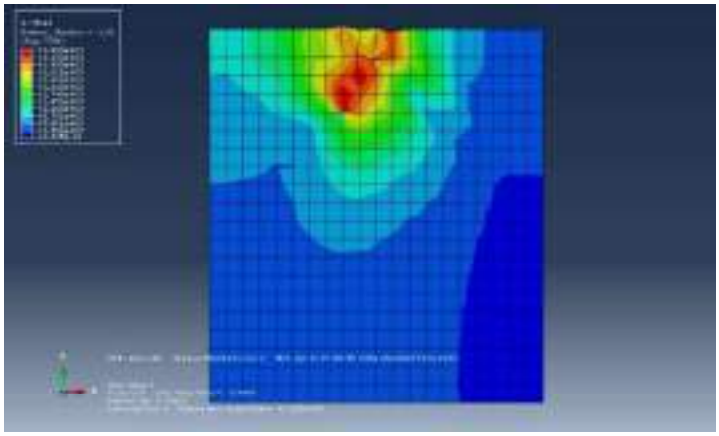

Fig. 4.316: Stress Contour for 25mm Square Plate with (H/B =3) at 45° inclination under 0.5 Hz frequency and 5mm amplitude

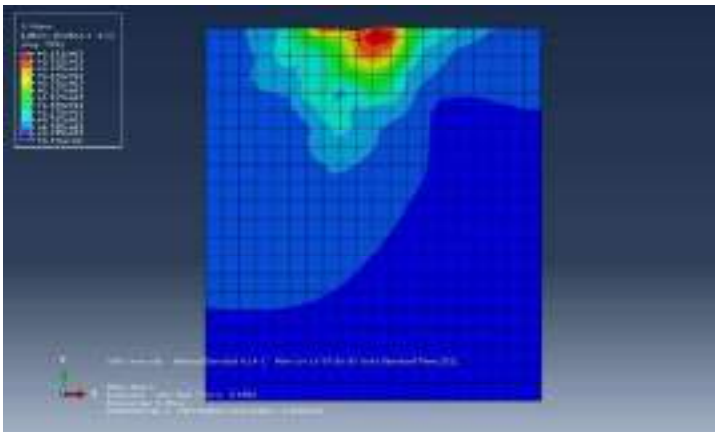

Fig. 4.317: Stress Contour for 25mm Square Plate with (H/B =1) at 60° inclination under 0.5 Hz frequency and 5mm amplitude

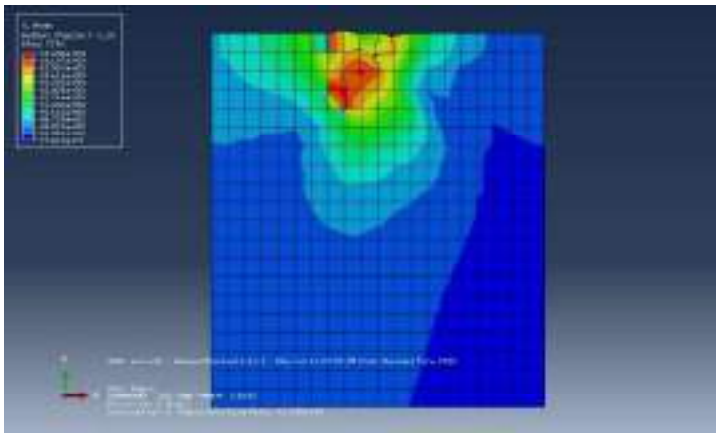

Fig. 4.318: Stress Contour for 25mm Square Plate with (H/B =2) at 60° inclination under 0.5 Hz frequency and 5mm amplitude

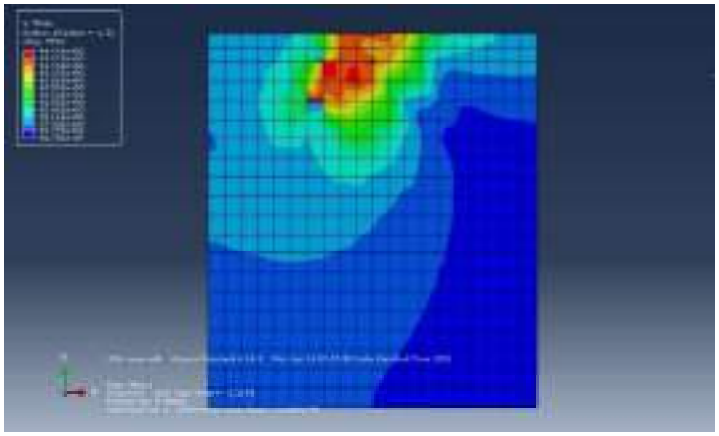

Fig. 4.319: Stress Contour for 25mm Square Plate with (H/B =3) at 60° inclination under 0.5 Hz frequency and 5mm amplitude

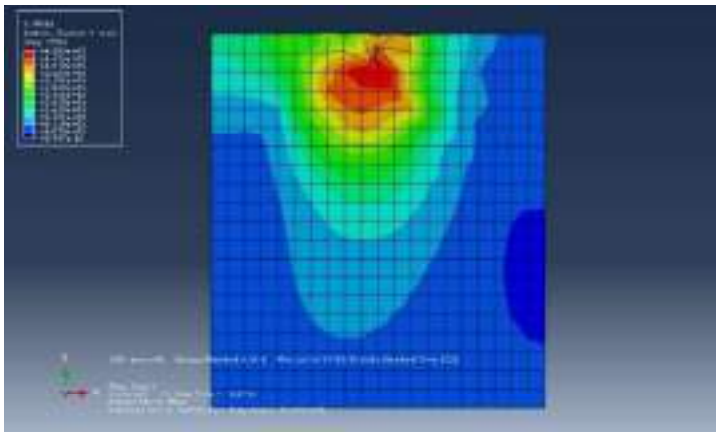

Fig. 4.320: Stress Contour for 50mm Square Plate with (H/B =1) at 30° inclination under 0.5 Hz frequency and 5mm amplitude

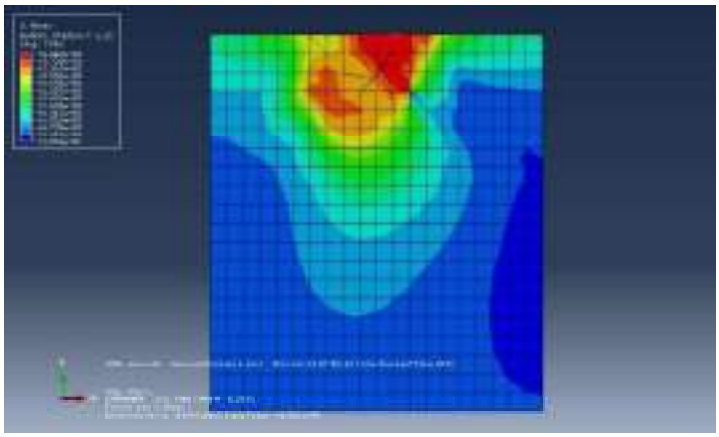

Fig. 4.321: Stress Contour for 50mm Square Plate with (H/B =2) at 30° inclination under 0.5 Hz frequency and 5mm amplitude

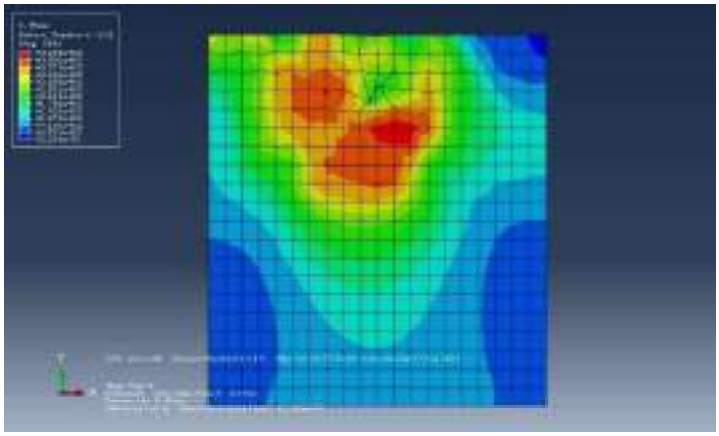

Fig. 4.322: Stress Contour for 50mm Square Plate with (H/B =3) at 30° inclination under 0.5 Hz frequency and 5mm amplitude

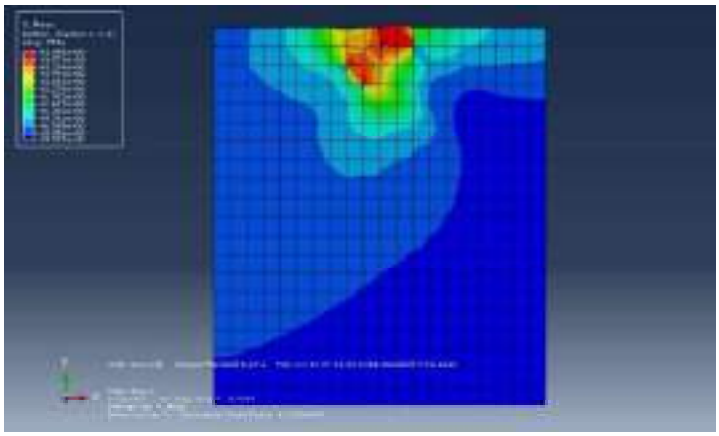

Fig. 4.323: Stress Contour for 50mm Square Plate with (H/B =1) at 45° inclination under 0.5 Hz frequency and 5mm amplitude

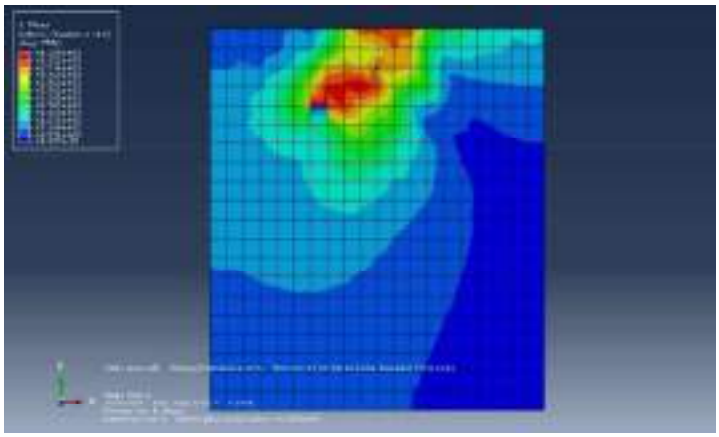

Fig. 4.324: Stress Contour for 50mm Square Plate with (H/B =2) at 45° inclination under 0.5 Hz frequency and 5mm amplitude

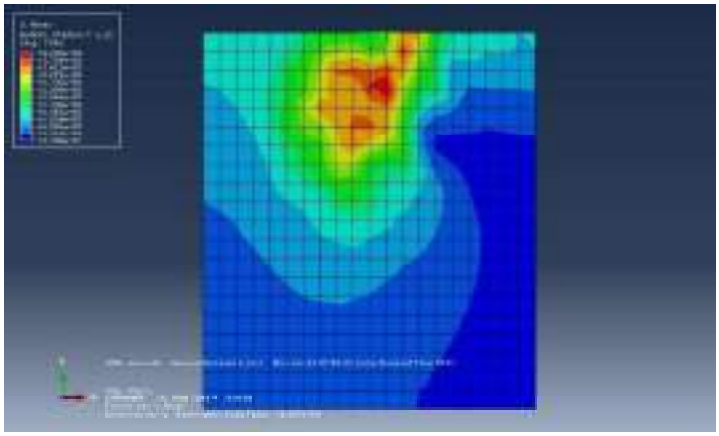

Fig. 4.325: Stress Contour for 50mm Square Plate with (H/B =3) at 45° inclination under 0.5 Hz frequency and 5mm amplitude

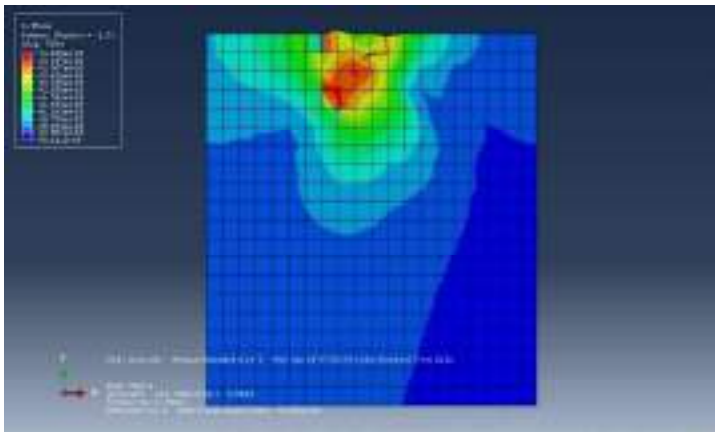

Fig. 4.326: Stress Contour for 50mm Square Plate with (H/B =1) at 60° inclination under 0.5 Hz frequency and 5mm amplitude

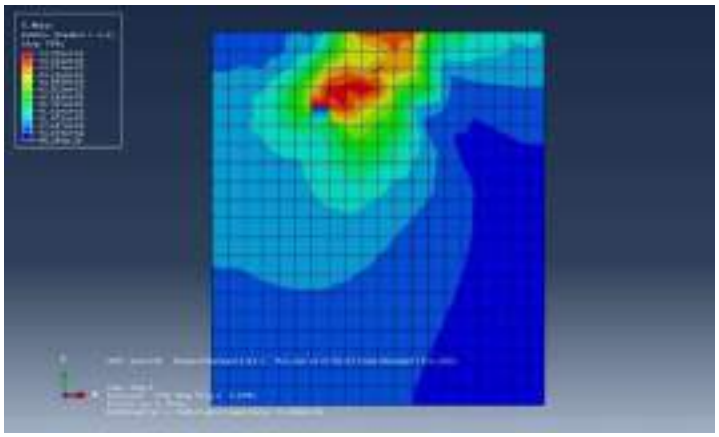

Fig. 4.327: Stress Contour for 50mm Square Plate with (H/B =2) at 60° inclination under 0.5 Hz frequency and 5mm amplitude

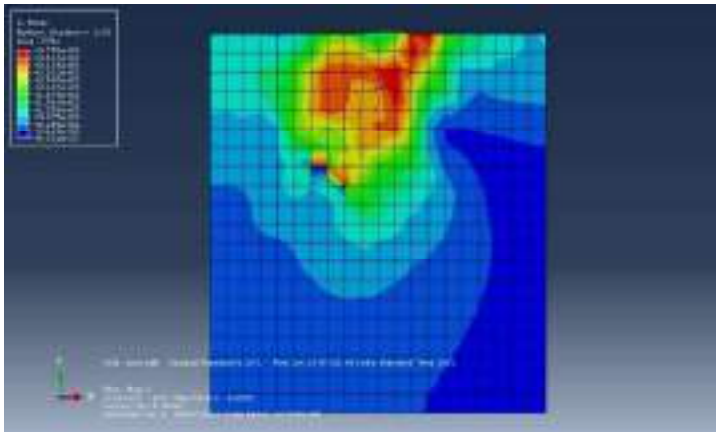

Fig. 4.328: Stress Contour for 50mm Square Plate with (H/B =3) at 60° inclination under 0.5 Hz frequency and 5mm amplitude

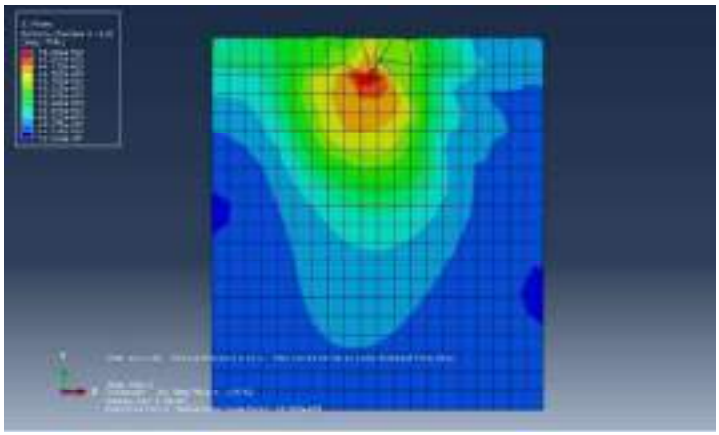

Fig. 4.329: Stress Contour for 75mm Square Plate with (H/B =1) at 30° inclination under 0.5 Hz frequency and 5mm amplitude

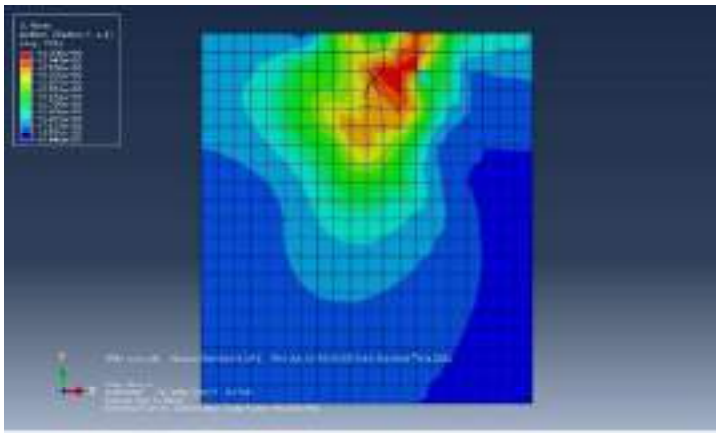

Fig. 4.330: Stress Contour for 75mm Square Plate with (H/B =2) at 30° inclination under 0.5 Hz frequency and 5mm amplitude

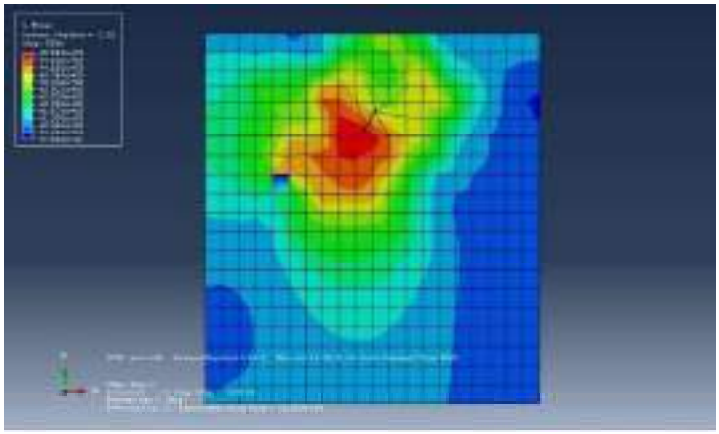

Fig. 4.331: Stress Contour for 75mm Square Plate with (H/B =3) at 30° inclination under 0.5 Hz frequency and 5mm amplitude

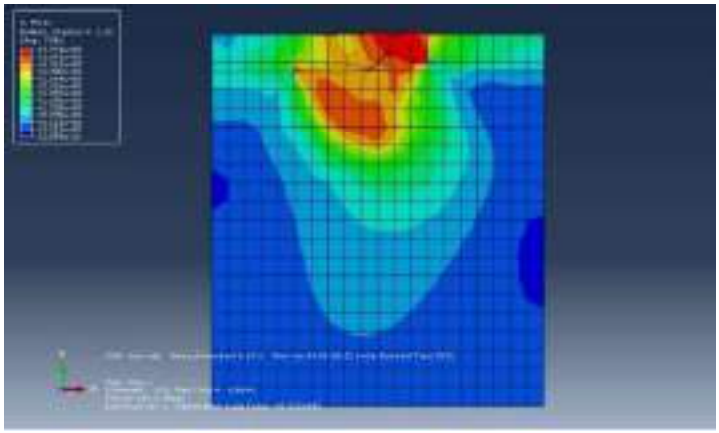

Fig. 4.332: Stress Contour for 75mm Square Plate with (H/B =1) at 45° inclination under 0.5 Hz frequency and 5mm amplitude

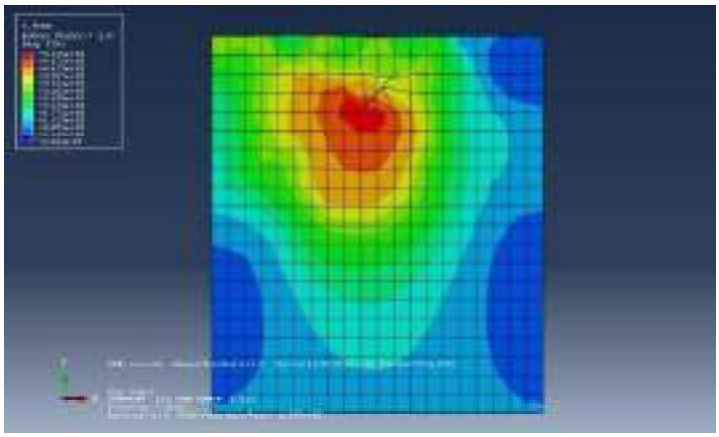

Fig. 4.333: Stress Contour for 75mm Square Plate with (H/B =2) at 45° inclination under 0.5 Hz frequency and 5mm amplitude

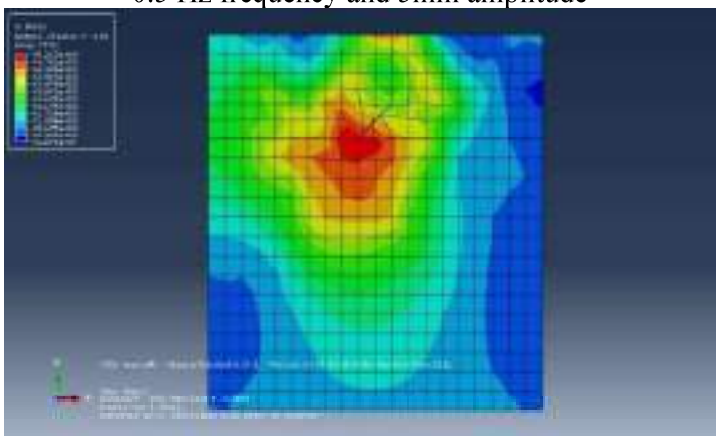

Fig. 4.334: Stress Contour for 75mm Square Plate with (H/B =3) at 45° inclination under 0.5 Hz frequency and 5mm amplitude

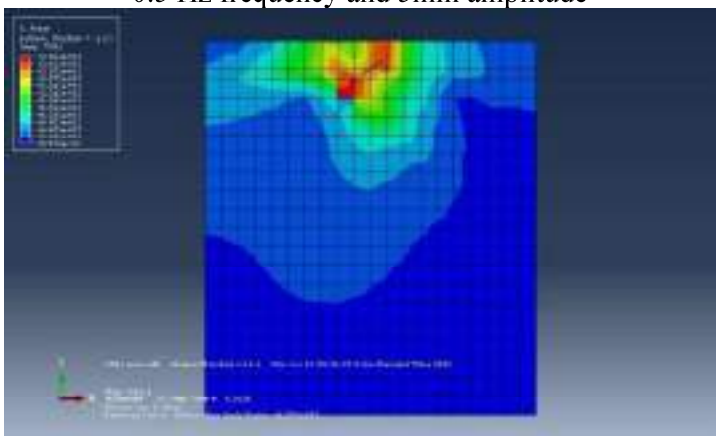

Fig. 4.335: Stress Contour for 75mm Square Plate with (H/B =1) at 60° inclination under 0.5 Hz frequency and 5mm amplitude

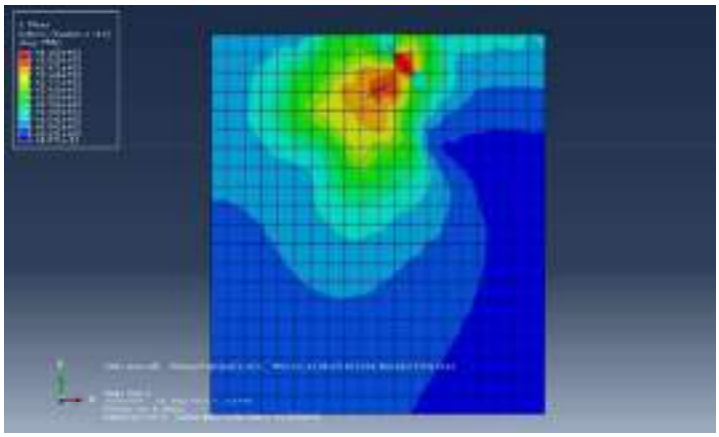

Fig. 4.336: Stress Contour for 75mm Square Plate with (H/B =2) at 60° inclination under 0.5 Hz frequency and 5mm amplitude

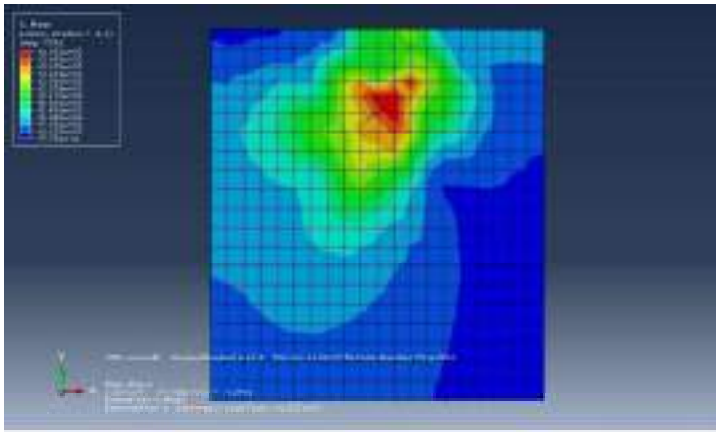

Fig. 4.337: Stress Contour for 75mm Square Plate with (H/B =3) at 60° inclination under 0.5 Hz frequency and 5mm amplitude

ANNEXURE -V

PRESENTATION OF RESULTS OF NUMERICAL ANALYSIS (CYCLIC UNREINFORCED)

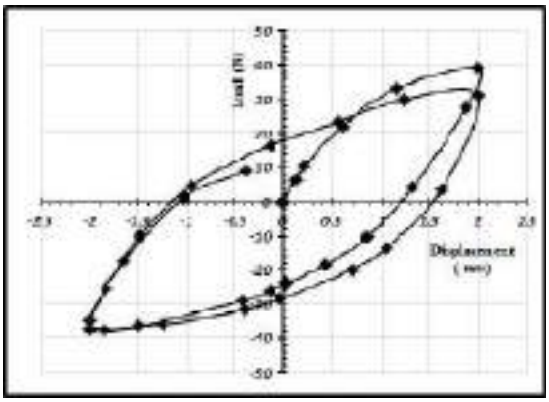

Fig. 4.343: Load vs. Displacement for 25 mm Square Plate with (H/B =2) at 30° inclination under 0.2 Hz frequency and 2mm amplitude

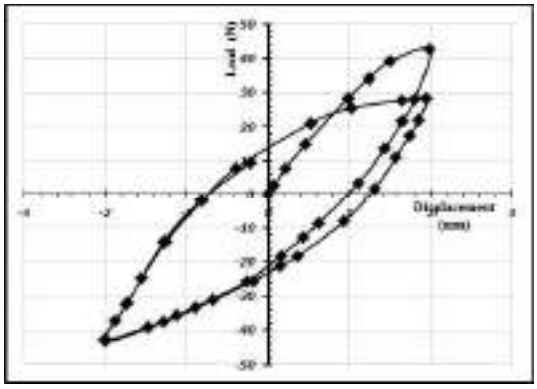

Fig. 4.344: Load vs. Displacement for 25 mm Square Plate with (H/B =3) at 30° inclination under 0.2 Hz frequency and 2mm amplitude

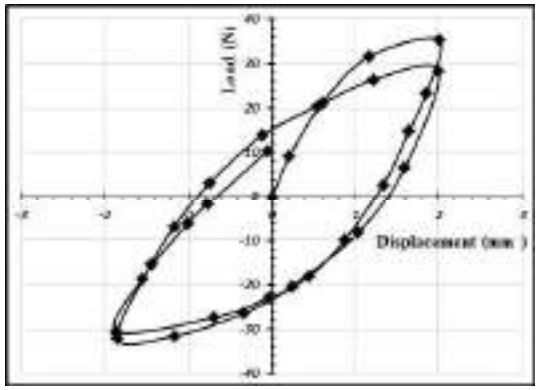

Fig. 4.345: Load vs. Displacement for 25 mm Square Plate with (H/B =1) at 45° inclination under 0.2 Hz frequency and 2mm amplitude

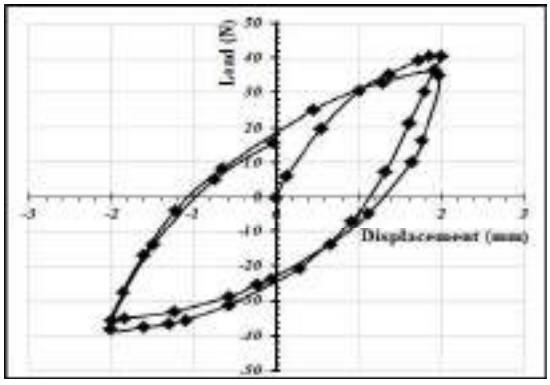

Fig. 4.346: Load vs. Displacement for 25 mm Square Plate with (H/B =2) at 45° inclination under 0.2 Hz frequency and 2mm amplitude

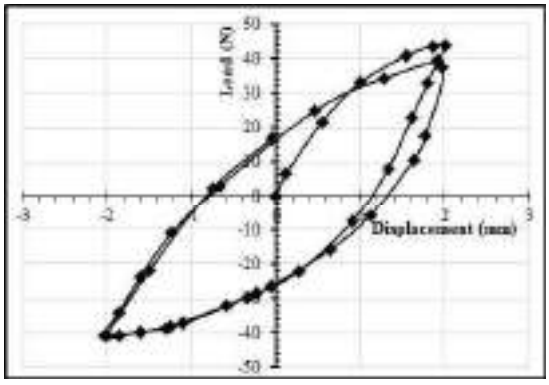

Fig. 4.347: Load vs. Displacement for 25 mm Square Plate with (H/B =3) at 45° inclination under 0.2 Hz frequency and 2mm amplitude

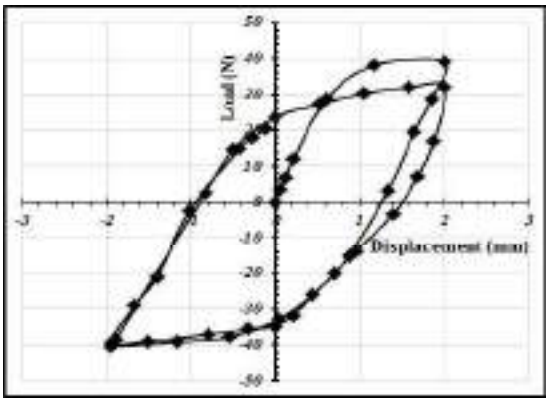

Fig. 4.348: Load vs. Displacement for 25 mm Square Plate with (H/B =1) at 60° inclination under 0.2 Hz frequency and 2mm amplitude

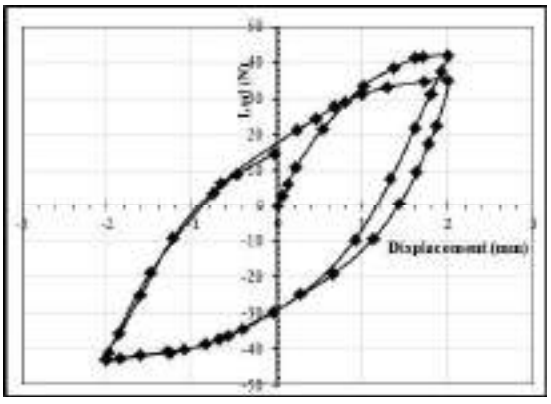

Fig. 4.349: Load vs. Displacement for 25 mm Square Plate with (H/B =2) at 60° inclination under 0.2 Hz frequency and 2mm amplitude

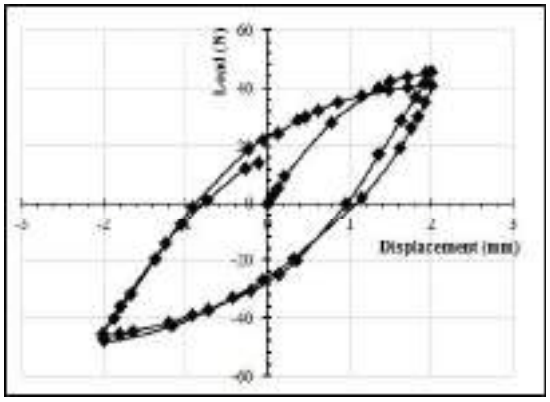

Fig. 4.350: Load vs. Displacement for 25 mm Square Plate with (H/B =3) at 60° inclination under 0.2 Hz frequency and 2mm amplitude

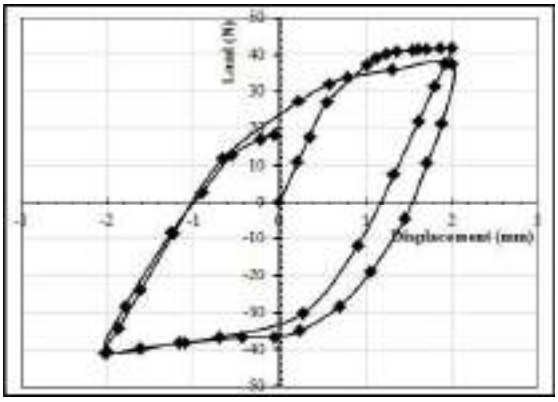

Fig. 4.351: Load vs. Displacement for 50 mm Square Plate with (H/B =1) at 30° inclination under 0.2 Hz frequency and 2mm amplitude

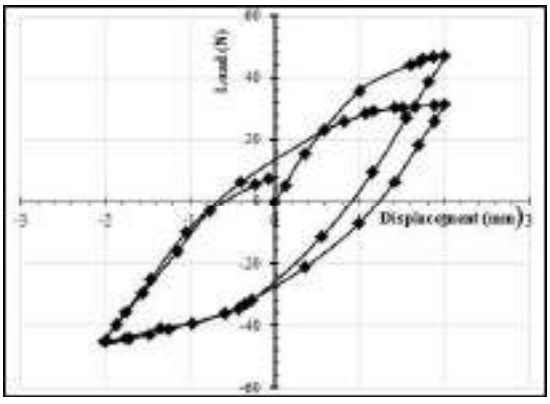

Fig. 4.352: Load vs. Displacement for 50 mm Square Plate with (H/B =2) at 30° inclination under 0.2 Hz frequency and 2mm amplitude

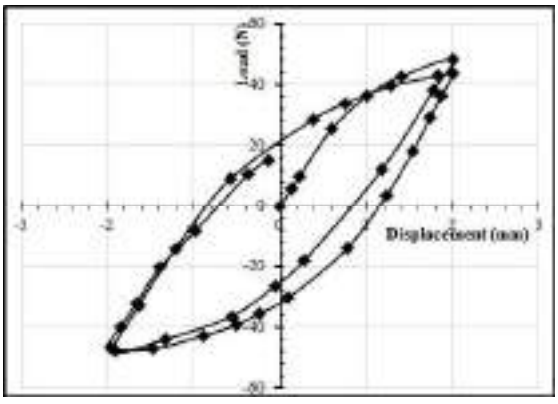

Fig. 4.353: Load vs. Displacement for 50 mm Square Plate with (H/B =3) at 30° inclination under 0.2 Hz frequency and 2mm amplitude

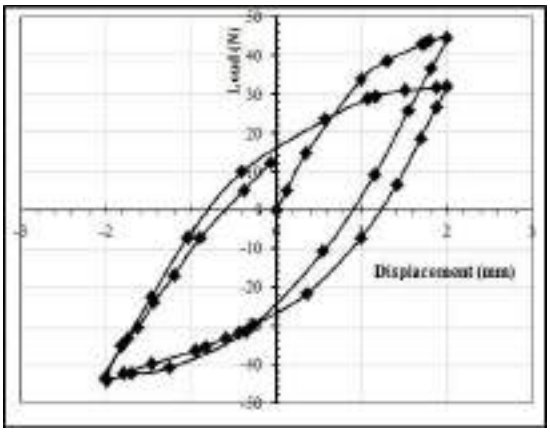

Fig. 4.354: Load vs. Displacement for 50 mm Square Plate with (H/B =1) at 45° inclination under 0.2 Hz frequency and 2mm amplitude

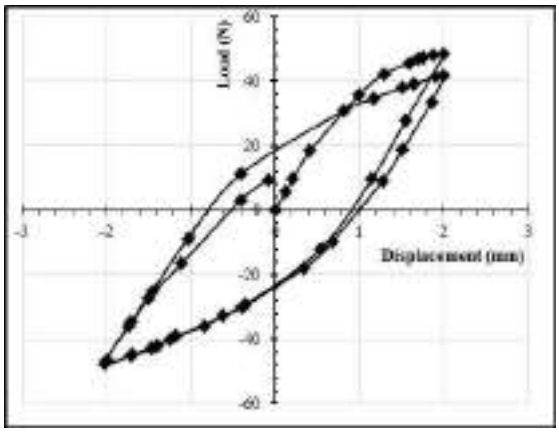

Fig. 4.355: Load vs. Displacement for 50 mm Square Plate with (H/B =2) at 45° inclination under 0.2 Hz frequency and 2mm amplitude

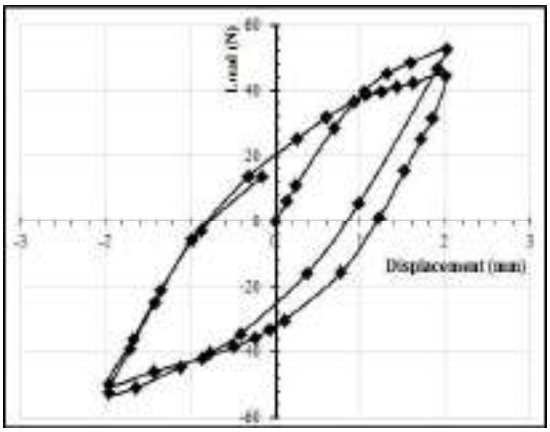

Fig. 4.356: Load vs. Displacement for 50 mm Square Plate with (H/B =3) at 45° inclination under 0.2 Hz frequency and 2mm amplitude

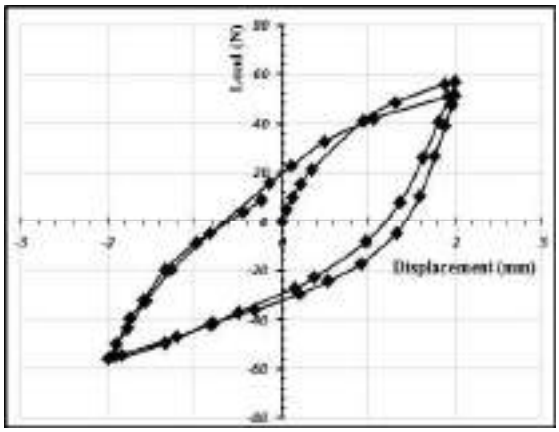

Fig. 4.357: Load vs. Displacement for 50 mm Square Plate with (H/B =1) at 60° inclination under 0.2 Hz frequency and 2mm amplitude

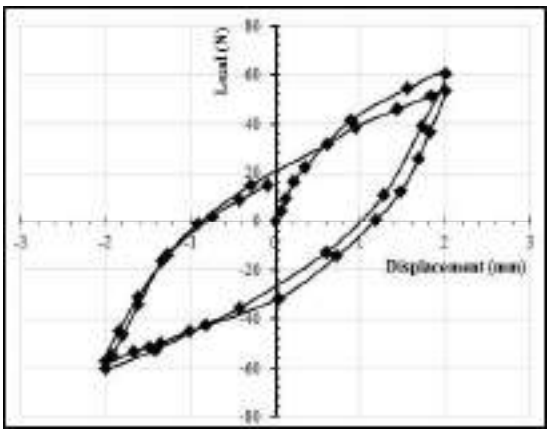

Fig. 4.358: Load vs. Displacement for 50 mm Square Plate with (H/B =2) at 60° inclination under 0.2 Hz frequency and 2mm amplitude

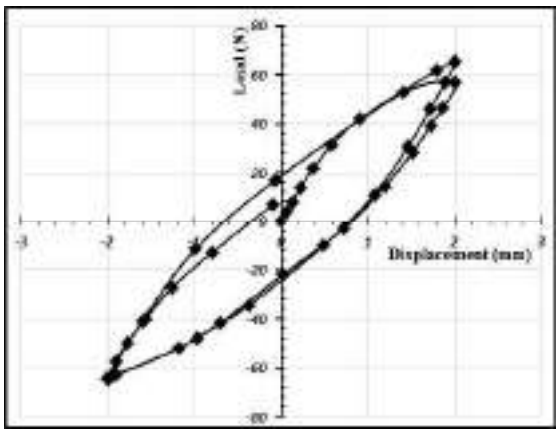

Fig. 4.359: Load vs. Displacement for 50 mm Square Plate with (H/B =3) at 60° inclination under 0.2 Hz frequency and 2mm amplitude

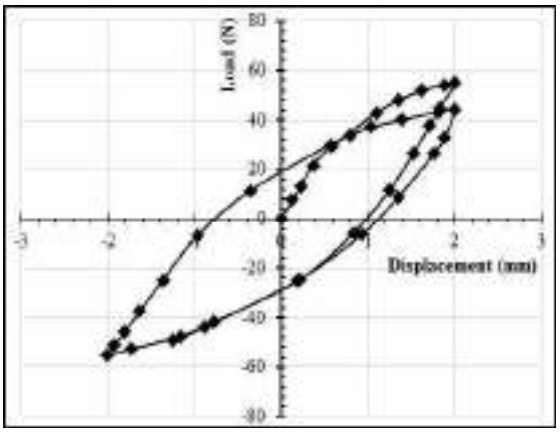

Fig. 4.360: Load vs. Displacement for 75 mm Square Plate with (H/B =1) at 30° inclination under 0.2 Hz frequency and 2mm amplitude

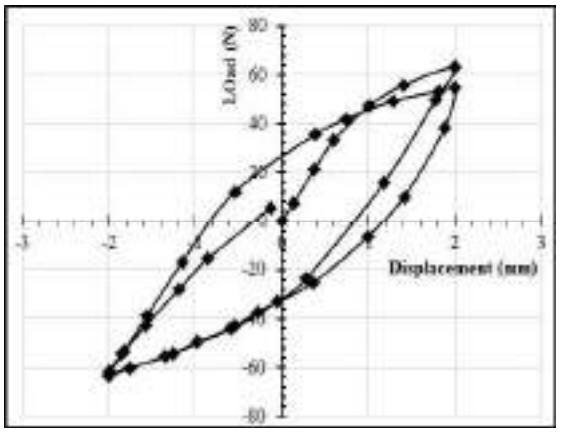

Fig. 4.361: Load vs. Displacement for 75 mm Square Plate with (H/B =2) at 30° inclination under 0.2 Hz frequency and 2mm amplitude

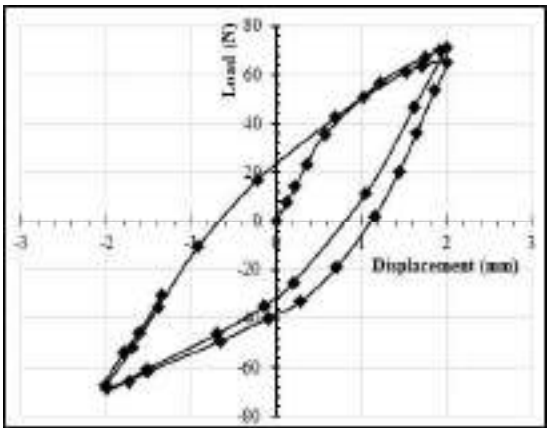

Fig. 4.362: Load vs. Displacement for 75 mm Square Plate with (H/B =3) at 30° inclination under 0.2 Hz frequency and 2mm amplitude

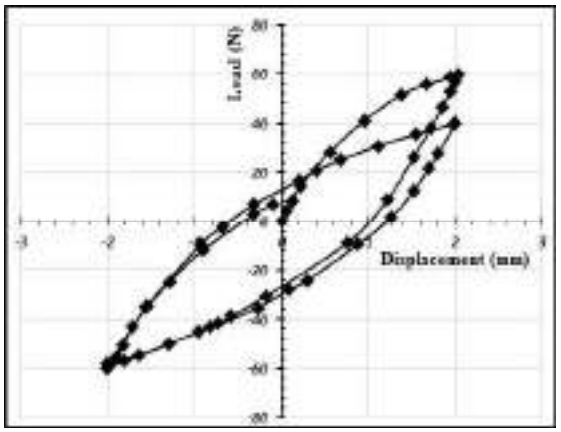

Fig. 4.363: Load vs. Displacement for 75 mm Square Plate with (H/B =1) at 45° inclination under 0.2 Hz frequency and 2mm amplitude

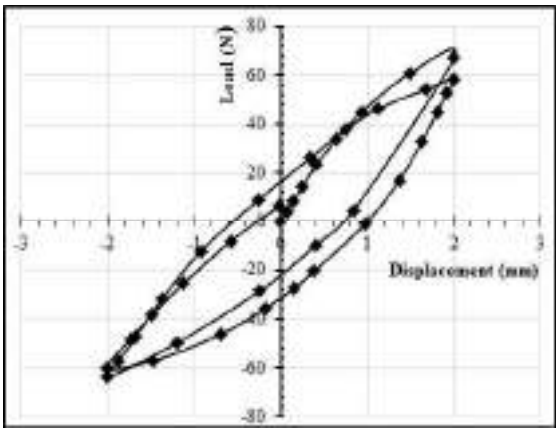

Fig. 4.364: Load vs. Displacement for 75 mm Square Plate with (H/B =2) at 45° inclination under 0.2 Hz frequency and 2mm amplitude

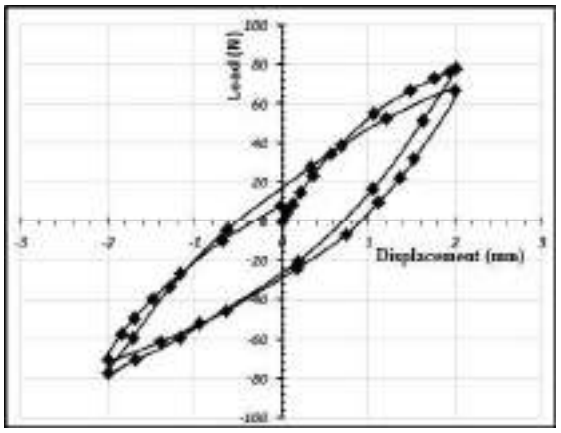

Fig. 4.365: Load vs. Displacement for 75 mm Square Plate with (H/B =3) at 45° inclination under 0.2 Hz frequency and 2mm amplitude

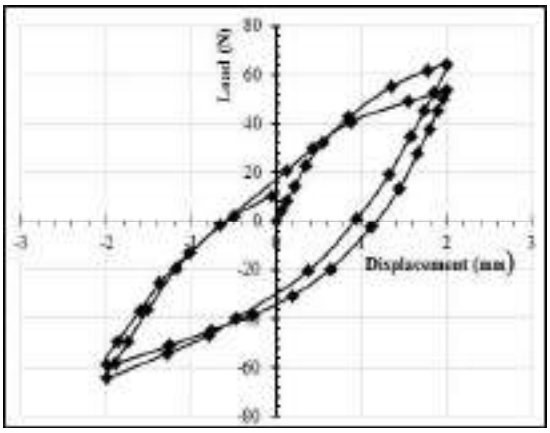

Fig. 4.366: Load vs. Displacement for 75 mm Square Plate with (H/B =1) at 60° inclination under 0.2 Hz frequency and 2mm amplitude

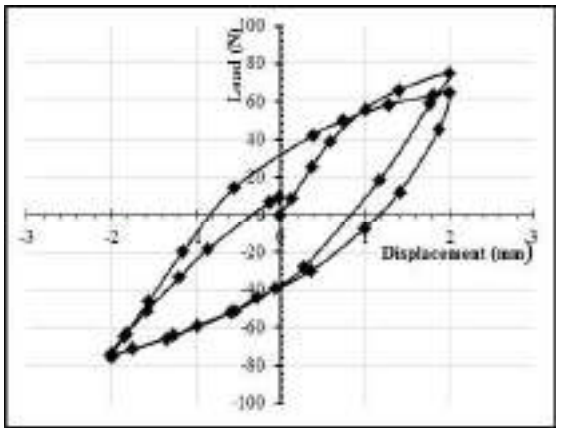

Fig. 4.367: Load vs. Displacement for 75 mm Square Plate with (H/B =2) at 60° inclination under 0.2 Hz frequency and 2mm amplitude

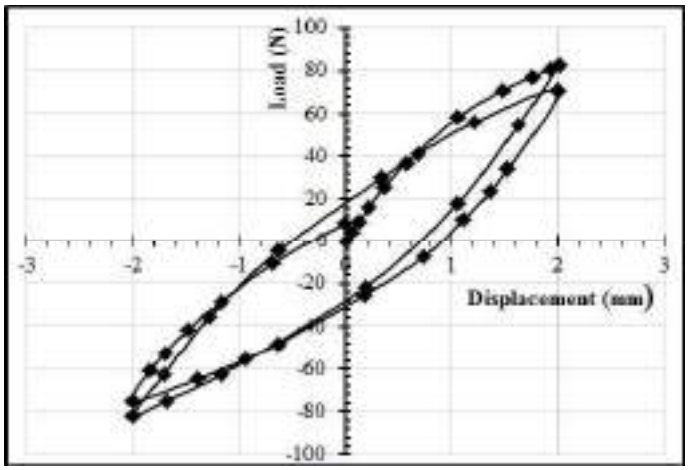

Fig. 4.368: Load vs. Displacement for 75 mm Square Plate with (H/B =3) at 60° inclination under 0.2 Hz frequency and 2mm amplitude

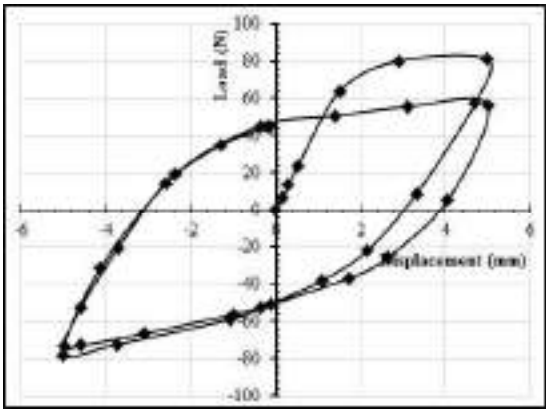

Fig. 4.369: Load vs. Displacement for 25 mm Square Plate with (H/B =1) at 30° inclination under 0.2 Hz frequency and 5mm amplitude

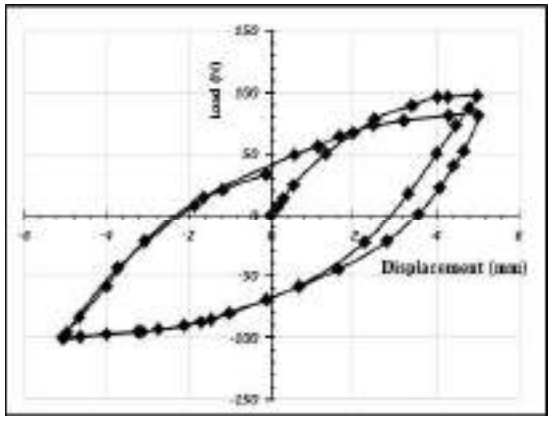

Fig. 4.370: Load vs. Displacement for 25 mm Square Plate with (H/B =2) at 30° inclination under 0.2 Hz frequency and 5mm amplitude

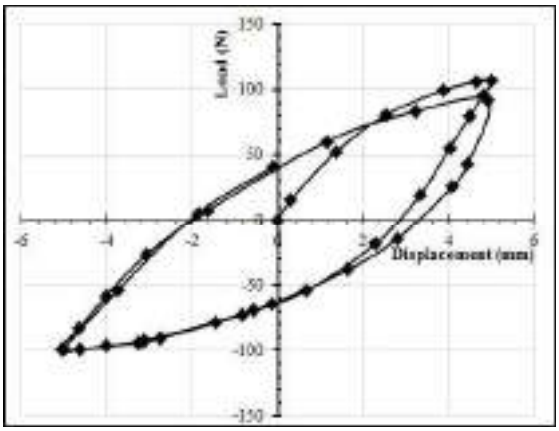

Fig. 4.371: Load vs. Displacement for 25 mm Square Plate with (H/B =3) at 30° inclination under 0.2 Hz frequency and 5mm amplitude

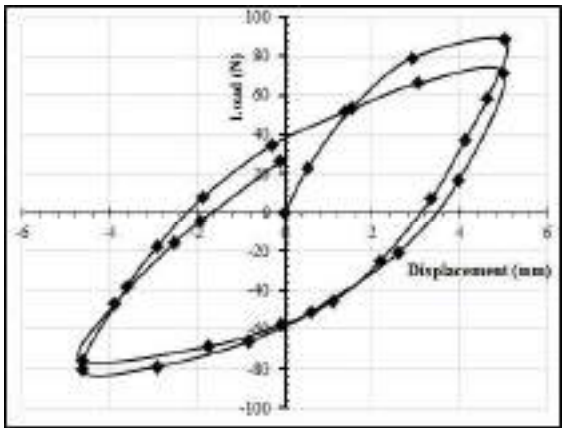

Fig. 4.372: Load vs. Displacement for 25 mm Square Plate with (H/B =1) at 45° inclination under 0.2 Hz frequency and 5mm amplitude

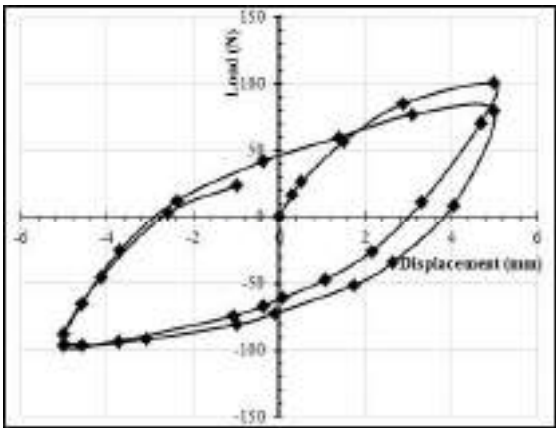

Fig. 4.373: Load vs. Displacement for 25 mm Square Plate with (H/B =2) at 45° inclination under 0.2 Hz frequency and 5mm amplitude

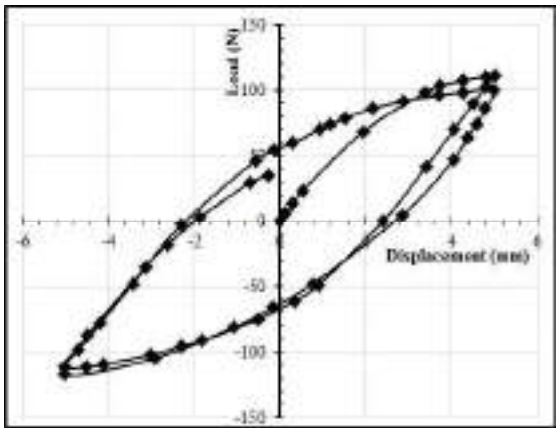

Fig. 4.374: Load vs. Displacement for 25 mm Square Plate with (H/B =3) at 45° inclination under 0.2 Hz frequency and 5mm amplitude

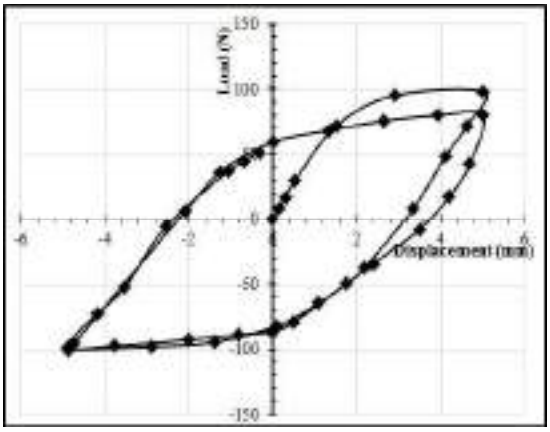

Fig. 4.375: Load vs. Displacement for 25 mm Square Plate with (H/B =1) at 60° inclination under 0.2 Hz frequency and 5mm amplitude

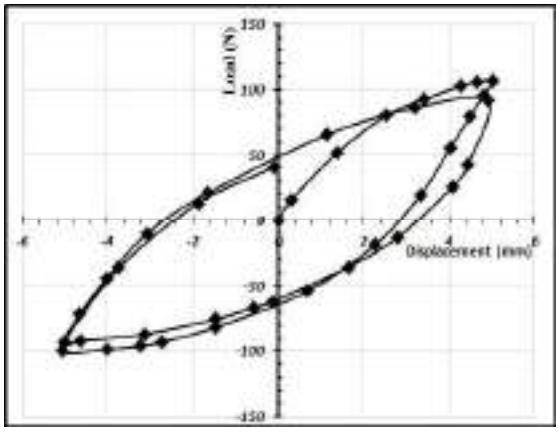

Fig. 4.376: Load vs. Displacement for 25 mm Square Plate with (H/B =2) at 60° inclination under 0.2 Hz frequency and 5mm amplitude

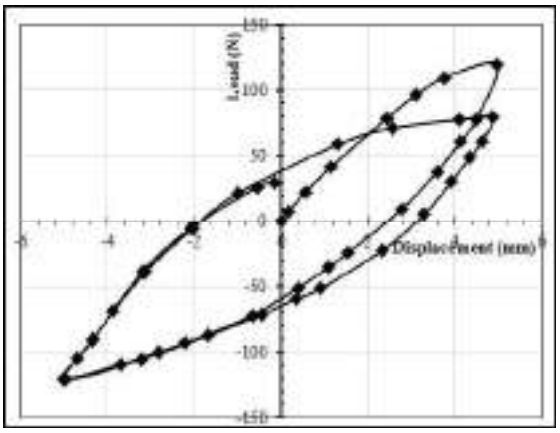

Fig. 4.377: Load vs. Displacement for 25 mm Square Plate with (H/B =3) at 60° inclination under 0.2 Hz frequency and 5mm amplitude

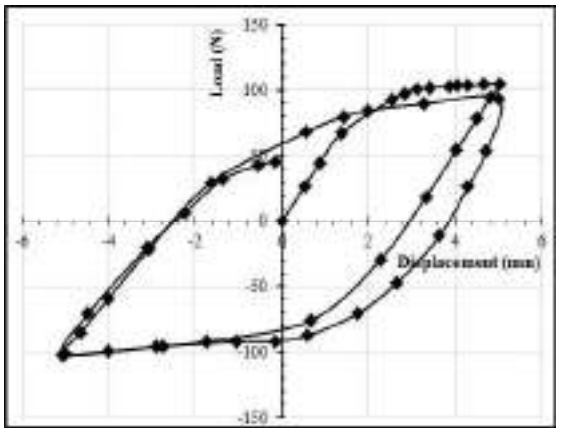

Fig. 4.378: Load vs. Displacement for 50 mm Square Plate with (H/B =1) at 30° inclination under 0.2 Hz frequency and 5mm amplitude

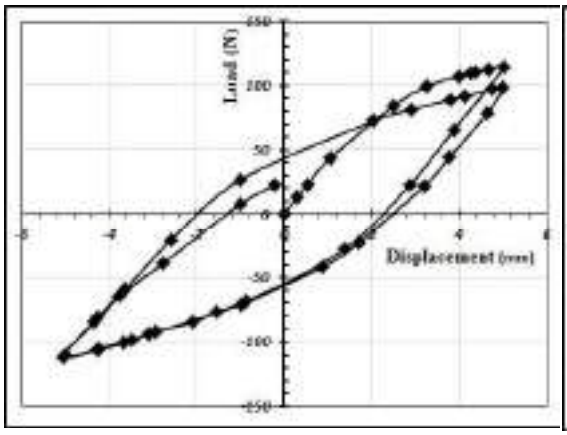

Fig. 4.379: Load vs. Displacement for 50 mm Square Plate with (H/B =2) at 30° inclination under 0.2 Hz frequency and 5mm amplitude

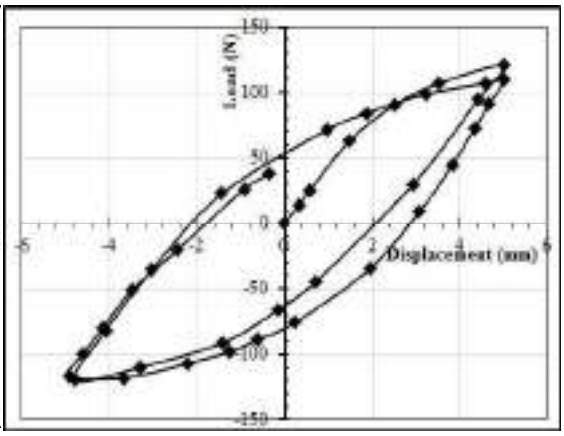

Fig. 4.380: Load vs. Displacement for 50 mm Square Plate with (H/B =3) at 30° inclination under 0.2 Hz frequency and 5mm amplitude

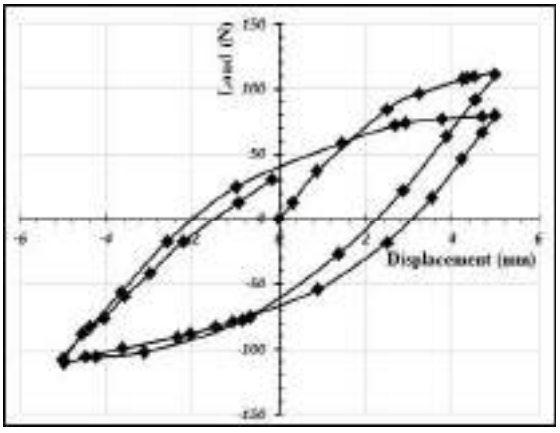

Fig. 4.381: Load vs. Displacement for 50 mm Square Plate with (H/B =1) at 45° inclination under 0.2 Hz frequency and 5mm amplitude

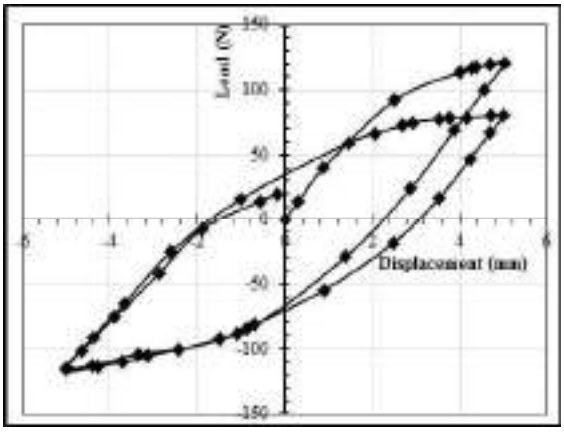

Fig. 4.382: Load vs. Displacement for 50 mm Square Plate with (H/B =2) at 45° inclination under 0.2 Hz frequency and 5mm amplitude

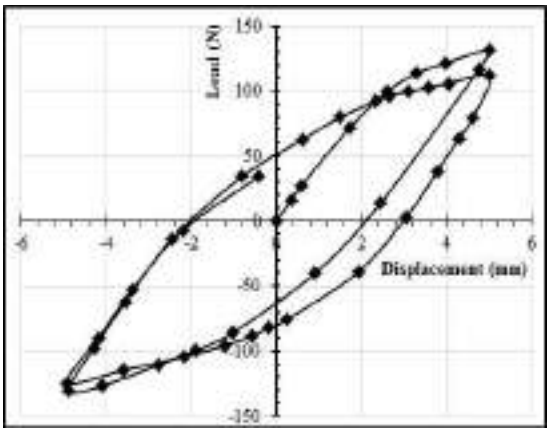

Fig. 4.383: Load vs. Displacement for 50 mm Square Plate with (H/B =3) at 45° inclination under 0.2 Hz frequency and 5mm amplitude

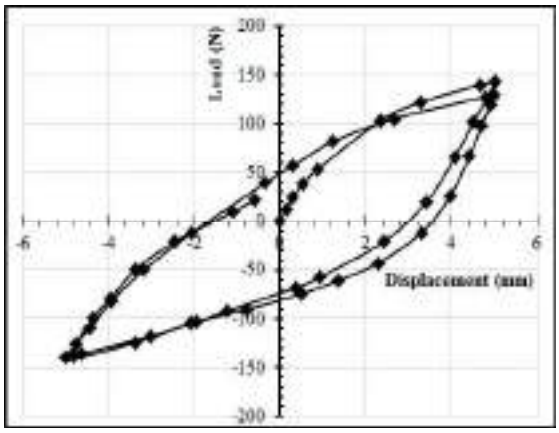

Fig. 4.384: Load vs. Displacement for 50 mm Square Plate with (H/B =1) at 60° inclination under 0.2 Hz frequency and 5mm amplitude

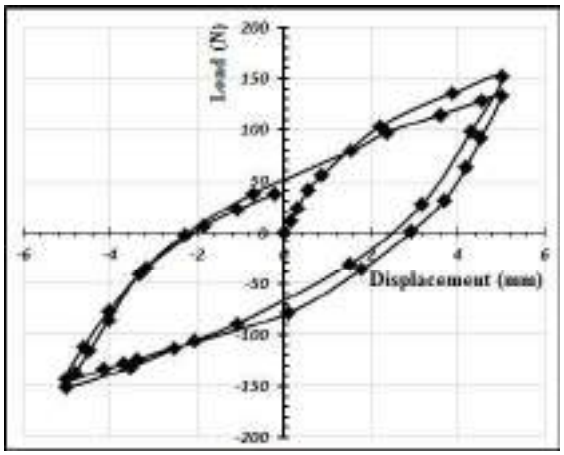

Fig. 4.385: Load vs. Displacement for 50 mm Square Plate with (H/B =2) at 60° inclination under 0.2 Hz frequency and 5mm amplitude

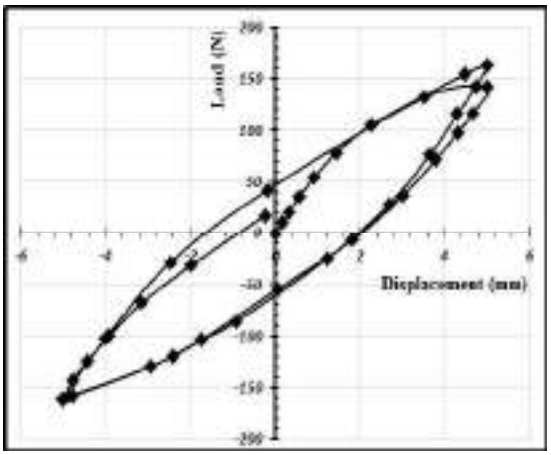

Fig. 4.386: Load vs. Displacement for 50 mm Square Plate with (H/B =3) at 60° inclination under 0.2 Hz frequency and 5mm amplitude

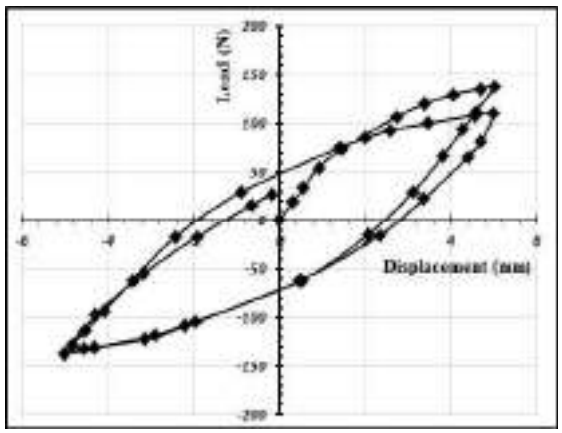

Fig. 4.387: Load vs. Displacement for 75 mm Square Plate with (H/B =1) at 30° inclination under 0.2 Hz frequency and 5mm amplitude

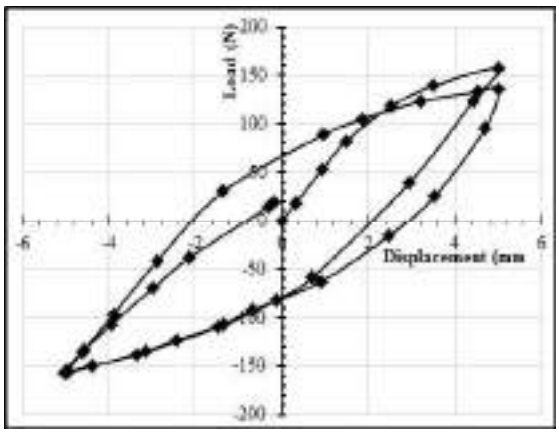

Fig. 4.388: Load vs. Displacement for 75 mm Square Plate with (H/B =2) at 30° inclination under 0.2 Hz frequency and 5mm amplitude

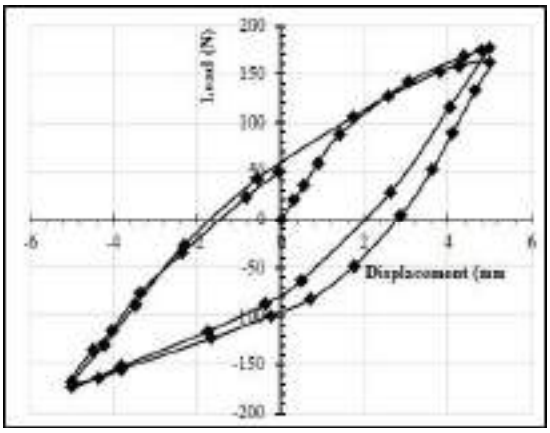

Fig. 4.389: Load vs. Displacement for 75 mm Square Plate with (H/B =3) at 30° inclination under 0.2 Hz frequency and 5mm amplitude

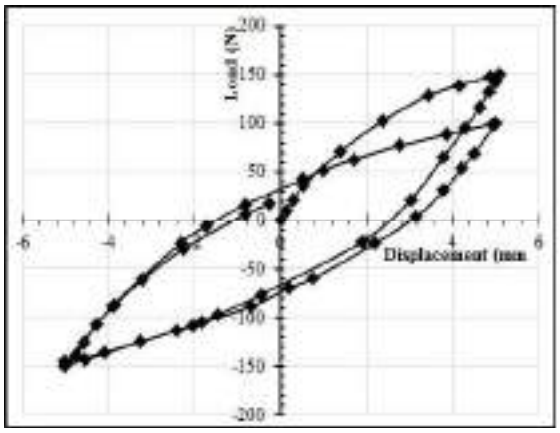

Fig. 4.390: Load vs. Displacement for 75 mm Square Plate with (H/B =1) at 45° inclination under 0.2 Hz frequency and 5mm amplitude

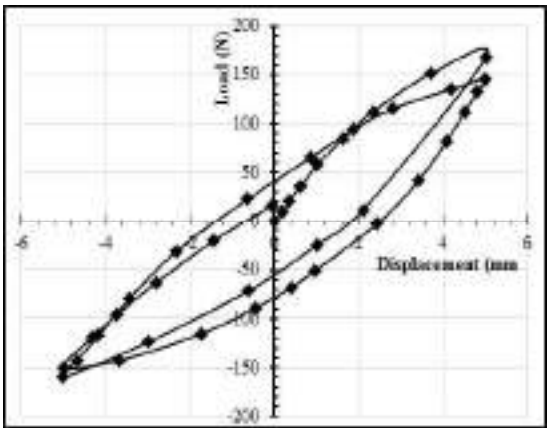

Fig. 4.391: Load vs. Displacement for 75 mm Square Plate with (H/B =2) at 45° inclination under 0.2 Hz frequency and 5mm amplitude

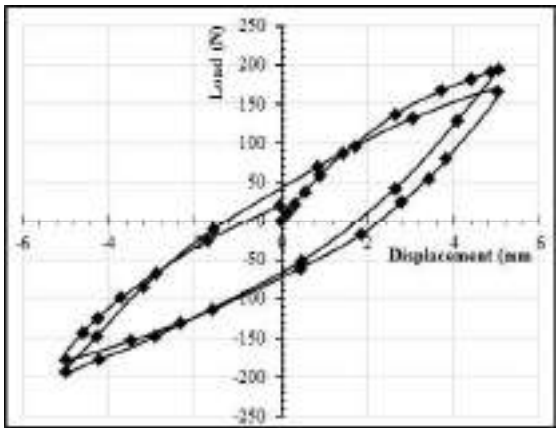

Fig. 4.392: Load vs. Displacement for 75 mm Square Plate with (H/B =3) at 45° inclination under 0.2 Hz frequency and 5mm amplitude

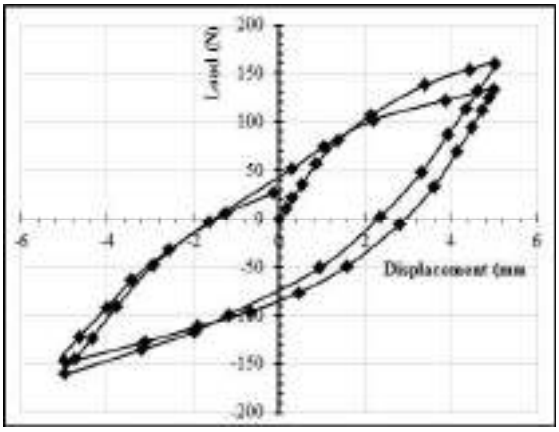

Fig. 4.393: Load vs. Displacement for 75 mm Square Plate with (H/B =1) at 60° inclination under 0.2 Hz frequency and 5mm amplitude

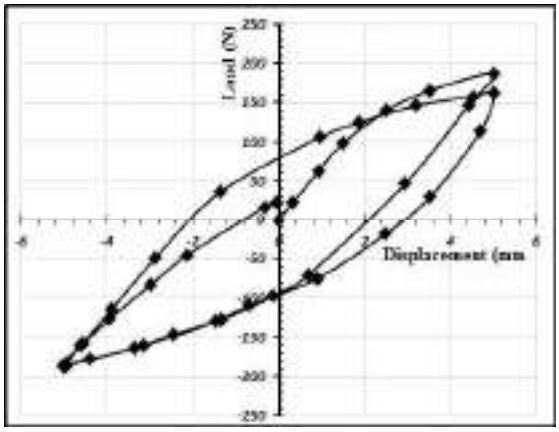

Fig. 4.394: Load vs. Displacement for 75 mm Square Plate with (H/B =2) at 60° inclination under 0.2 Hz frequency and 5mm amplitude

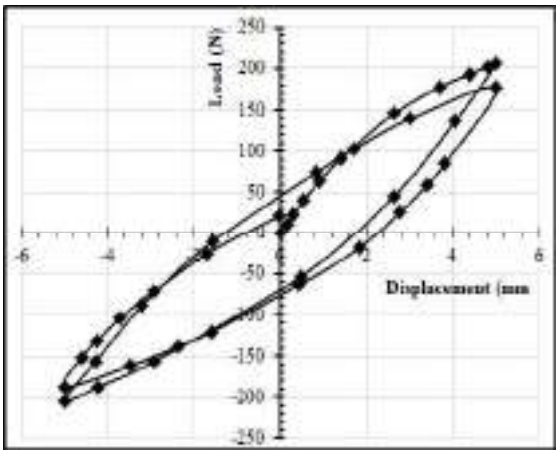

Fig. 4.395: Load vs. Displacement for 75 mm Square Plate with (H/B =3) at 60° inclination under 0.2 Hz frequency and 5mm amplitude

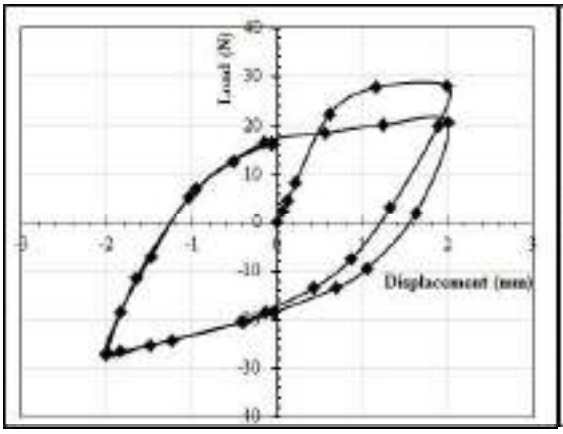

Fig. 4.396: Load vs. Displacement for 25 mm Square Plate with (H/B =1) at 30° inclination under 0.5 Hz frequency and 2mm amplitude

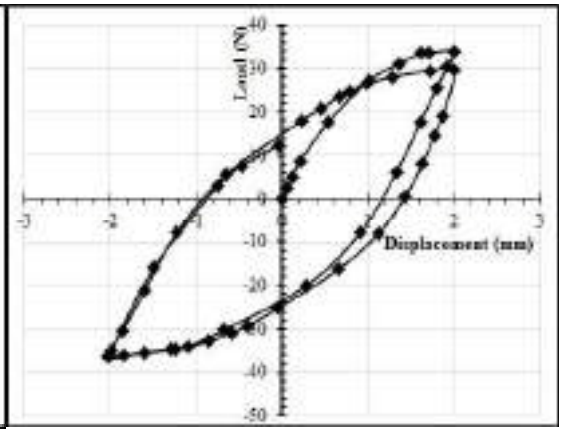

Fig. 4.397: Load vs. Displacement for 25 mm Square Plate with (H/B =2) at 30° inclination under 0.5 Hz frequency and 2mm amplitude

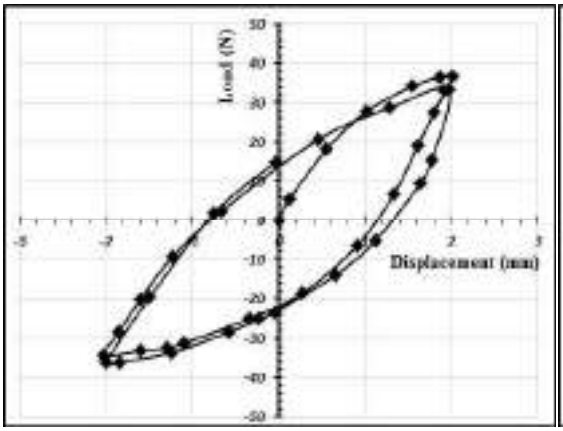

Fig. 4.398: Load vs. Displacement for 25 mm Square Plate with (H/B =3) at 30° inclination under 0.5 Hz frequency and 2mm amplitude

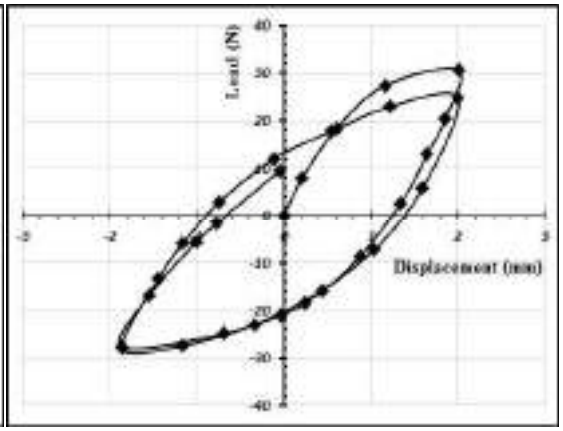

Fig. 4.399: Load vs. Displacement for 25 mm Square Plate with (H/B =1) at 45° inclination under 0.5 Hz frequency and 2mm amplitude

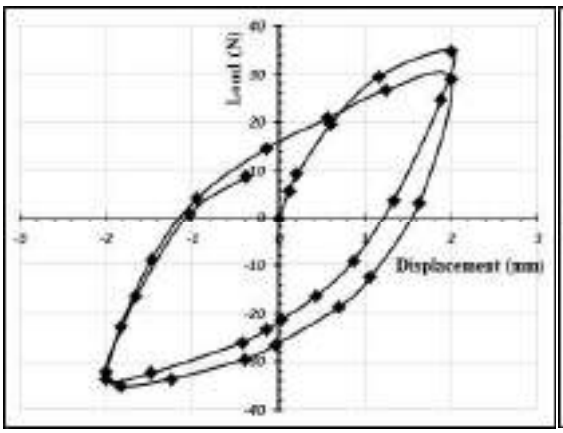

Fig. 4.400: Load vs. Displacement for 25 mm Square Plate with (H/B =2) at 45° inclination under 0.5 Hz frequency and 2mm amplitude

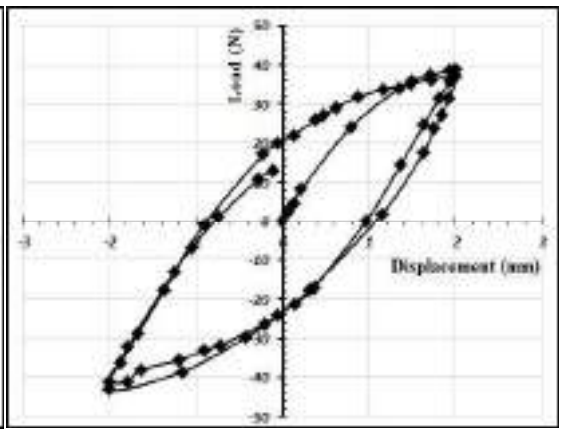

Fig. 4.401: Load vs. Displacement for 25 mm Square Plate with (H/B =2) at 45° inclination under 0.5 Hz frequency and 2mm amplitude

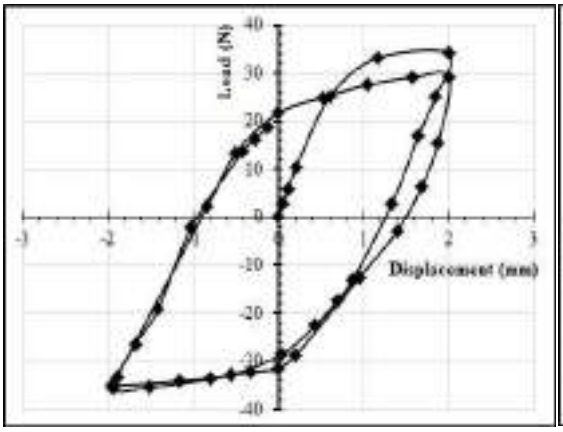

Fig. 4.402: Load vs. Displacement for 25 mm Square Plate with (H/B =1) at 60° inclination under 0.5 Hz frequency and 2mm amplitude

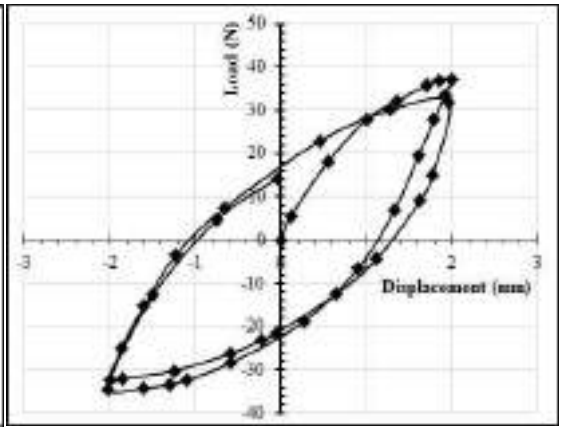

Fig. 4.403: Load vs. Displacement for 25 mm Square Plate with (H/B =2) at 60° inclination under 0.5 Hz frequency and 2mm amplitude

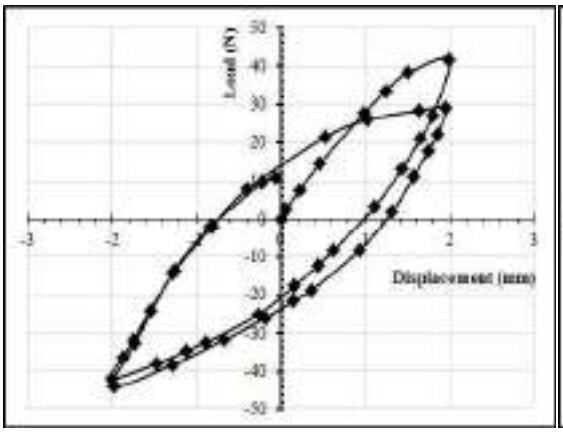

Fig. 4.404: Load vs. Displacement for 25 mm Square Plate with (H/B =3) at 60° inclination under 0.5 Hz frequency and 2mm amplitude

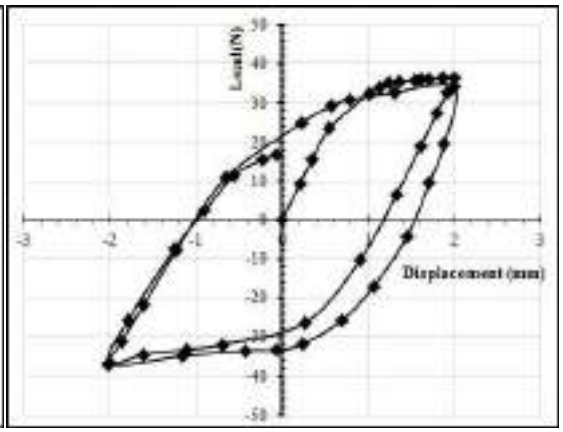

Fig. 4.405: Load vs. Displacement for 50mm Square Plate with (H/B =1) at 30° inclination under 0.5 Hz frequency and 2mm amplitude

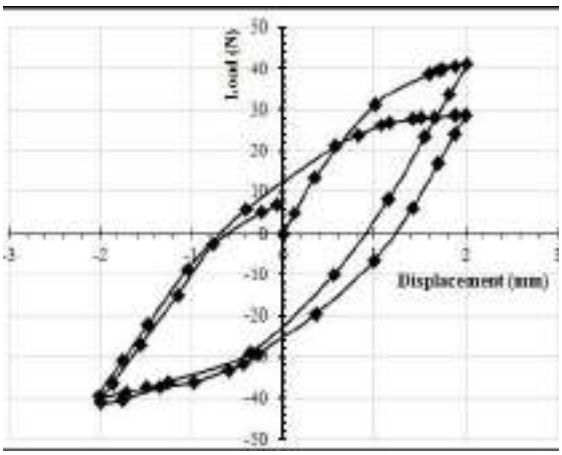

Fig. 4.406: Load vs. Displacement for 50mm Square Plate with (H/B =2) at 30° inclination under 0.5 Hz frequency and 2mm amplitude

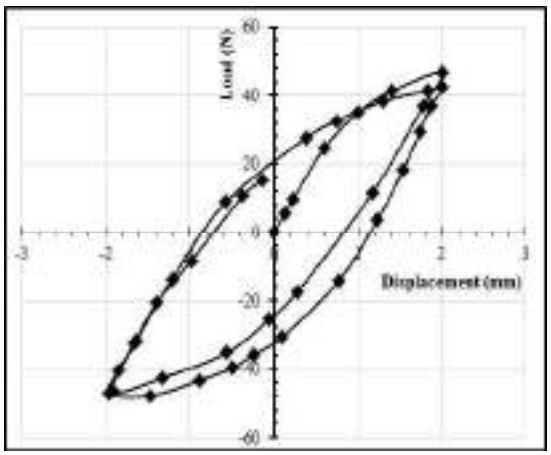

Fig. 4.407: Load vs. Displacement for 50mm Square Plate with (H/B =3) at 30° inclination under 0.5 Hz frequency and 2mm amplitude

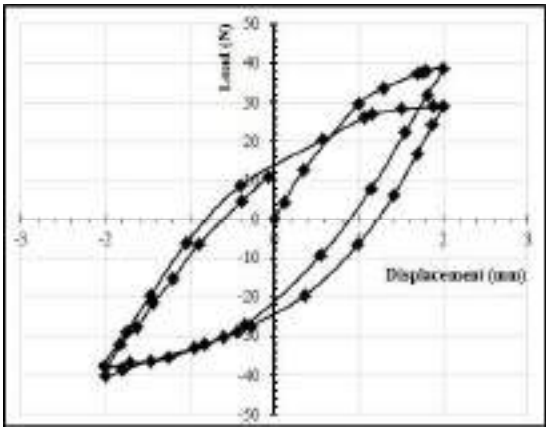

Fig. 4.408: Load vs. Displacement for 50mm Square Plate with (H/B =1) at 45° inclination under 0.5 Hz frequency and 2mm amplitude

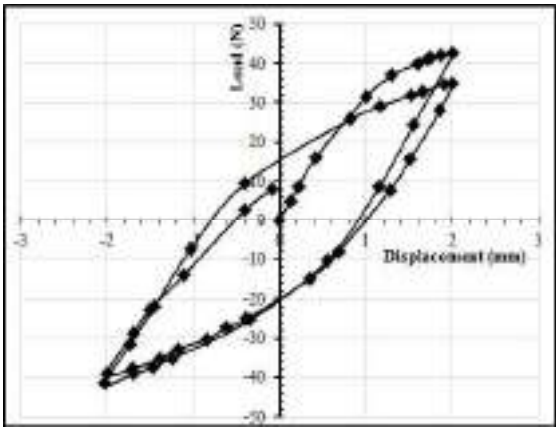

Fig. 4.409: Load vs. Displacement for 50mm Square Plate with (H/B =2) at 45° inclination under 0.5 Hz frequency and 2mm amplitude

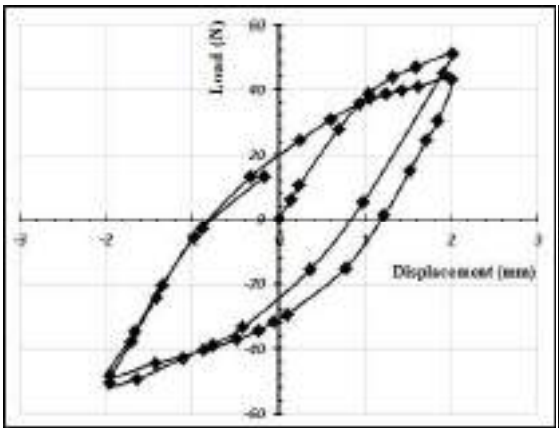

Fig. 4.410: Load vs. Displacement for 50mm Square Plate with (H/B =3) at 45° inclination under 0.5 Hz frequency and 2mm amplitude

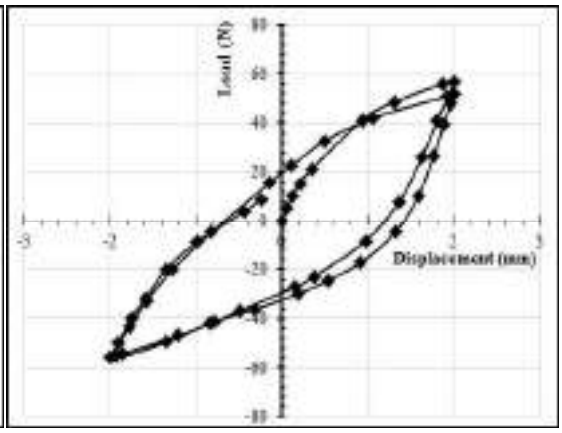

Fig. 4.411: Load vs. Displacement for 50mm Square Plate with (H/B =1) at 60° inclination under 0.5 Hz frequency and 2mm amplitude

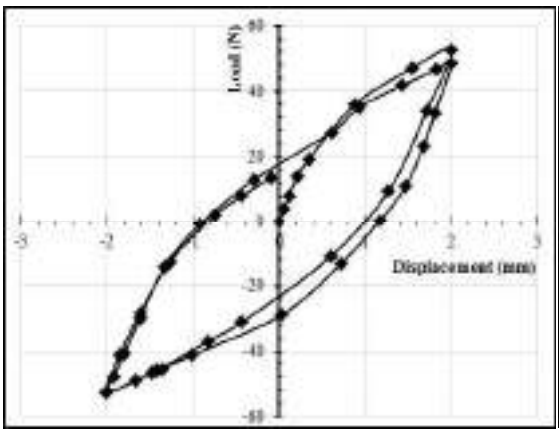

Fig. 4.412: Load vs. Displacement for 50mm Square Plate with (H/B =2) at 60° inclination under 0.5 Hz frequency and 2mm amplitude

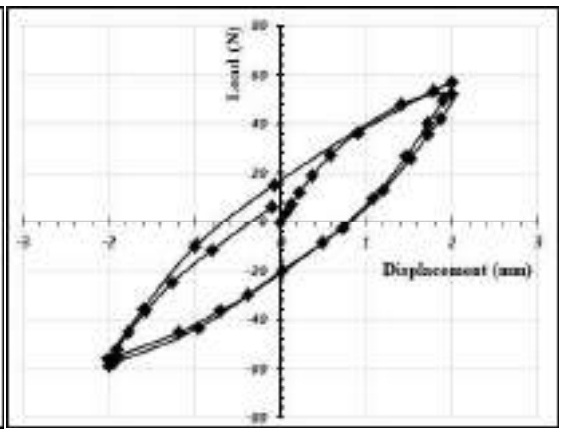

Fig. 4.413: Load vs. Displacement for 50mm Square Plate with (H/B =3) at 60° inclination under 0.5 Hz frequency and 2mm amplitude

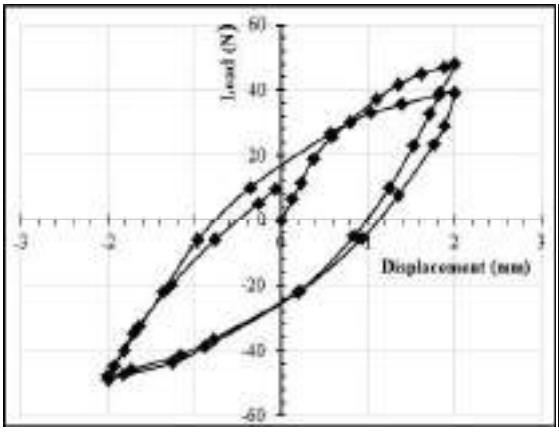

Fig. 4.414: Load vs. Displacement for 75mm Square Plate with (H/B =1) at 30° inclination under 0.5 Hz frequency and 2mm amplitude

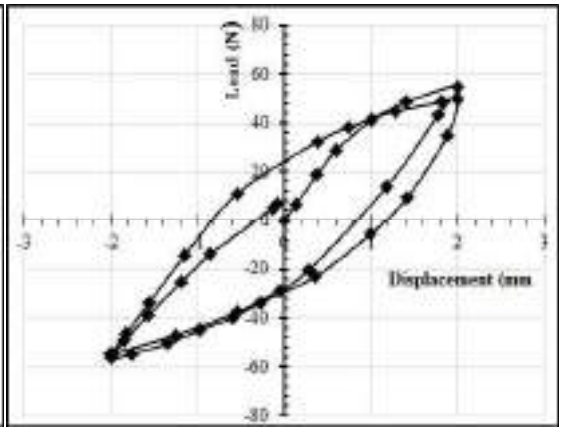

Fig. 4.415: Load vs. Displacement for 75mm Square Plate with (H/B =2) at 30° inclination under 0.5 Hz frequency and 2mm amplitude

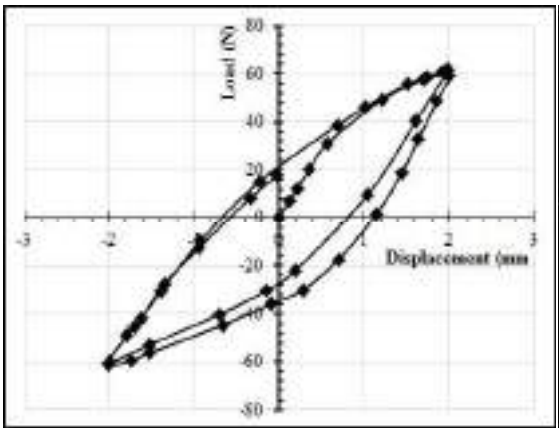

Fig. 4.416: Load vs. Displacement for 75mm Square Plate with (H/B =3) at 30° inclination under 0.5 Hz frequency and 2mm amplitude

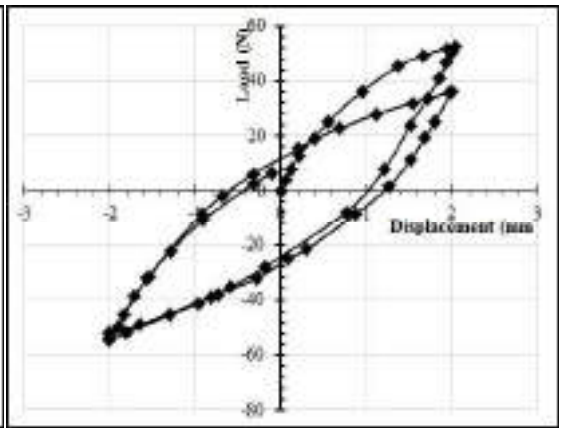

Fig. 4.417: Load vs. Displacement for 75mm Square Plate with (H/B =1) at 45° inclination under 0.5 Hz frequency and 2mm amplitude

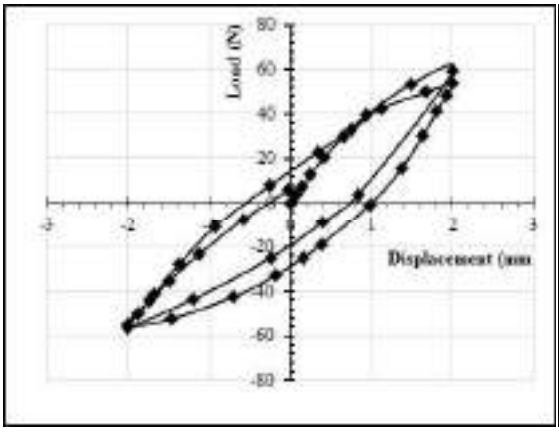

Fig. 4.418: Load vs. Displacement for 75mm Square Plate with (H/B =2) at 45° inclination under 0.5 Hz frequency and 2mm amplitude

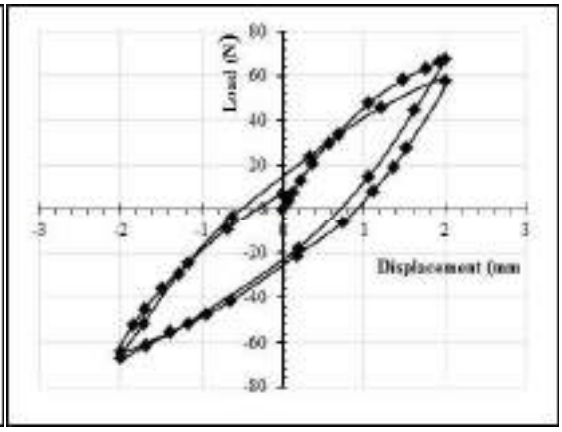

Fig. 4.419: Load vs. Displacement for 75mm Square Plate with (H/B =3) at 45° inclination under 0.5 Hz frequency and 2mm amplitude

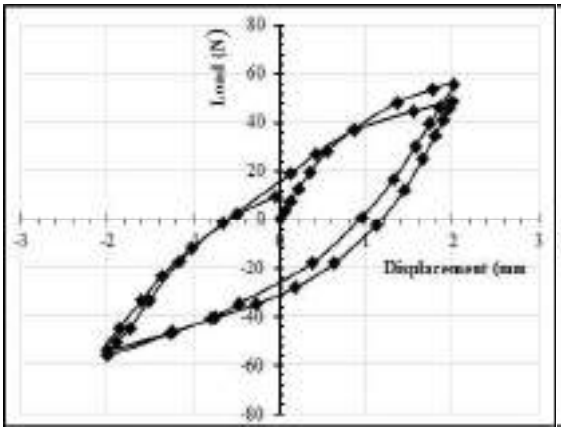

Fig. 4.420: Load vs. Displacement for 75mm Square Plate with (H/B =1) at 60° inclination under 0.5 Hz frequency and 2mm amplitude

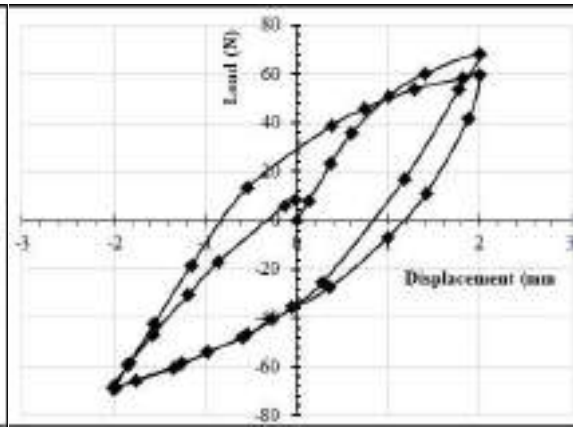

Fig. 4.421 Load vs. Displacement for 75mm Square Plate with (H/B =2) at 60° inclination under 0.5 Hz frequency and 2mm amplitude

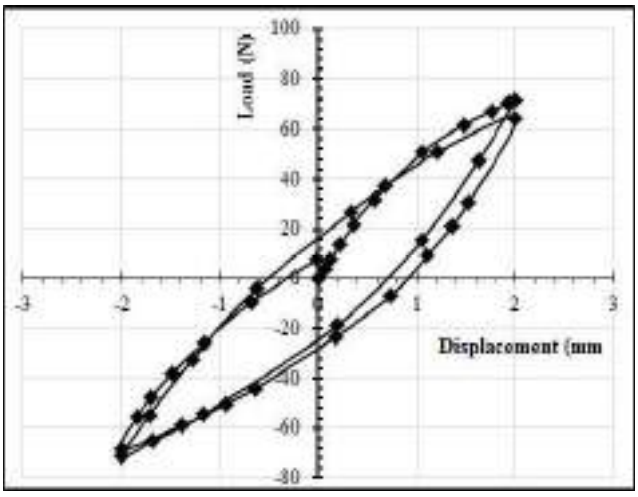

Fig. 4.422: Load vs. Displacement for 75mm Square Plate with (H/B =3) at 60° inclination under 0.5 Hz frequency and 2mm amplitude

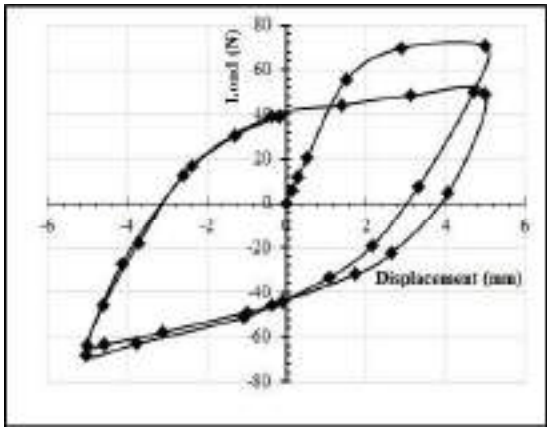

Fig. 4.423: Load vs. Displacement for 25 mm Square Plate with (H/B =1) at 30° inclination under 0.5 Hz frequency and 5mm amplitude

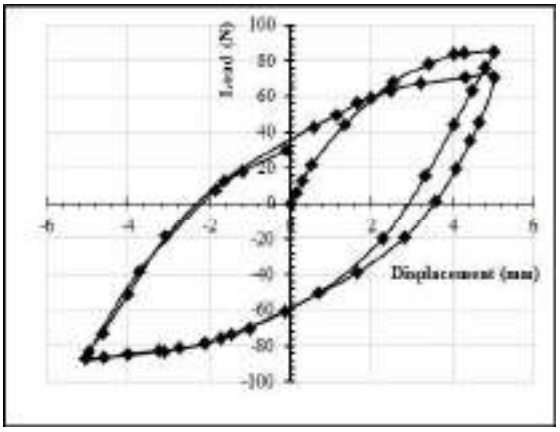

Fig. 4.424: Load vs. Displacement for 25 mm Square Plate with (H/B =2) at 30° inclination under 0.5 Hz frequency and 5mm amplitude

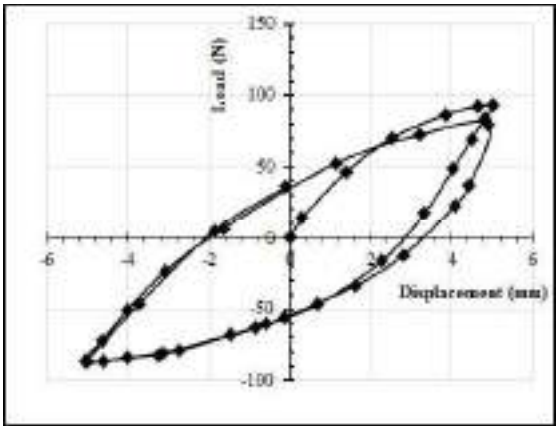

Fig. 4.425: Load vs. Displacement for 25 mm Square Plate with (H/B =3) at 30° inclination under 0.5 Hz frequency and 5mm amplitude

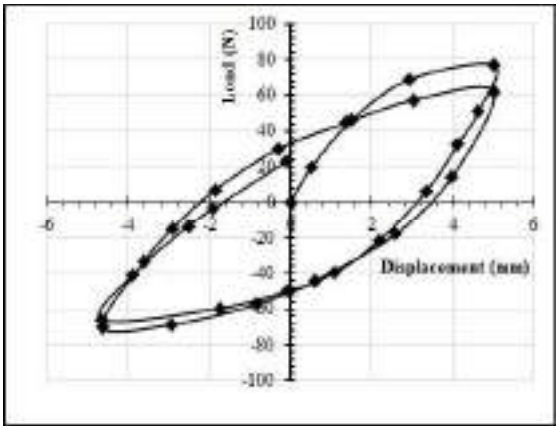

Fig. 4.426: Load vs. Displacement for 25 mm Square Plate with (H/B =1) at 45° inclination under 0.5 Hz frequency and 5mm amplitude

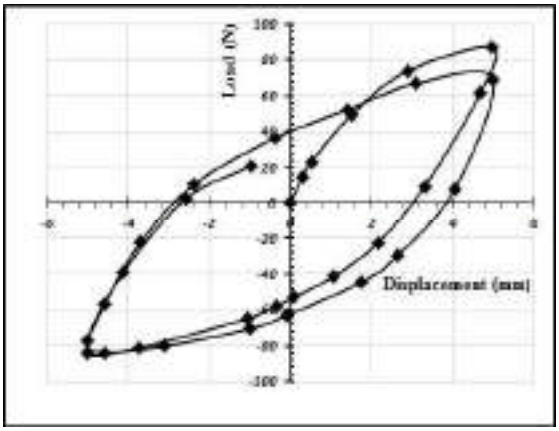

Fig. 4.427: Load vs. Displacement for 25 mm Square Plate with (H/B =2) at 45° inclination under 0.5 Hz frequency and 5mm amplitude

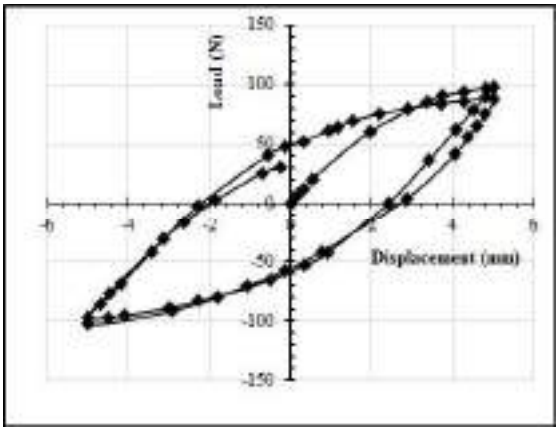

Fig. 4.428: Load vs. Displacement for 25 mm Square Plate with (H/B =3) at 45° inclination under 0.5 Hz frequency and 5mm amplitude

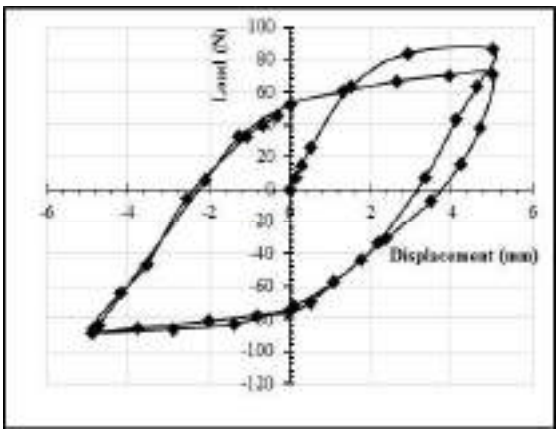

Fig. 4.429: Load vs. Displacement for 25 mm Square Plate with (H/B =1) at 60° inclination under 0.5 Hz frequency and 5mm amplitude

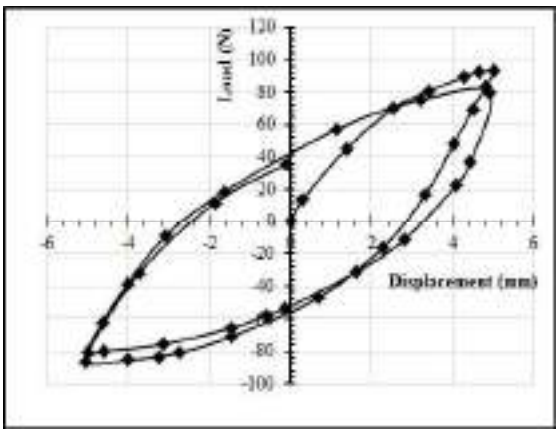

Fig. 4.430: Load vs. Displacement for 25 mm Square Plate with (H/B =2) at 60° inclination under 0.5 Hz frequency and 5mm amplitude

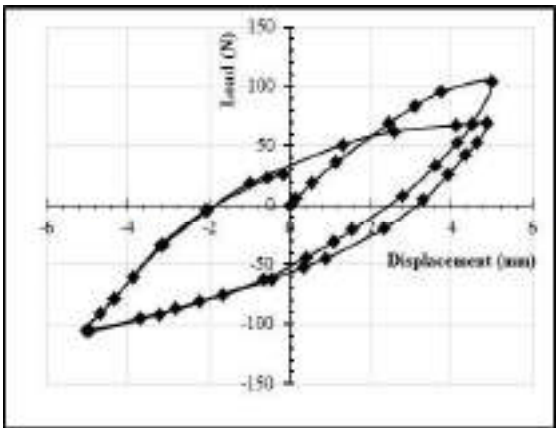

Fig. 4.431: Load vs. Displacement for 25 mm Square Plate with (H/B =3) at 60° inclination under 0.5 Hz frequency and 5mm amplitude

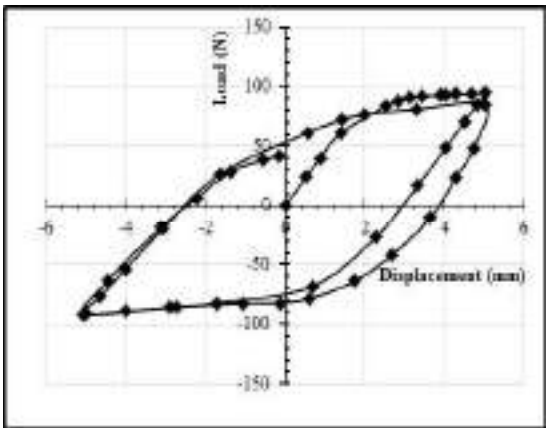

Fig. 4.432: Load vs. Displacement for 50mm Square Plate with (H/B =1) at 30° inclination under 0.5 Hz frequency and 5mm amplitude

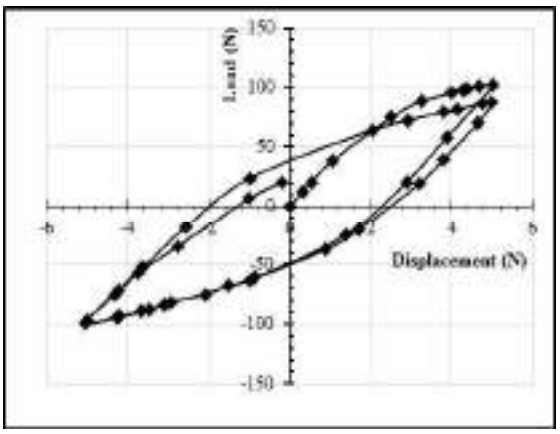

Fig. 4.433: Load vs. Displacement for 50mm Square Plate with (H/B =2) at 30° inclination under 0.5 Hz frequency and 5mm amplitude

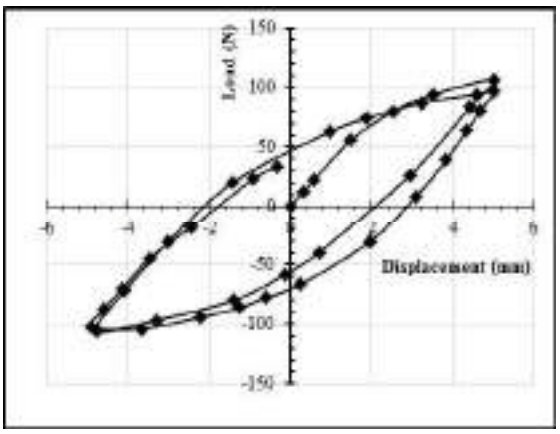

Fig. 4.434: Load vs. Displacement for 50mm Square Plate with (H/B =3) at 30° inclination under 0.5 Hz frequency and 5mm amplitude

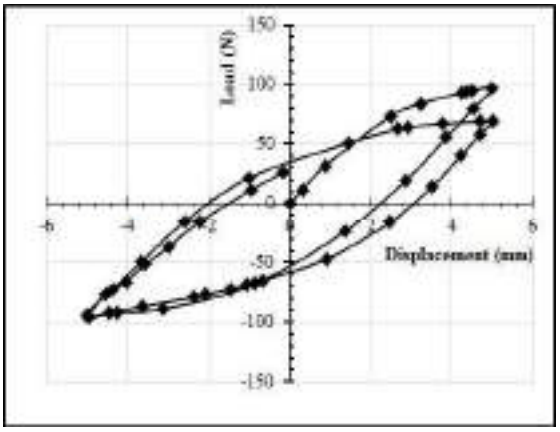

Fig. 4.435: Load vs. Displacement for 50mm Square Plate with (H/B =1) at 45° inclination under 0.5 Hz frequency and 5mm amplitude

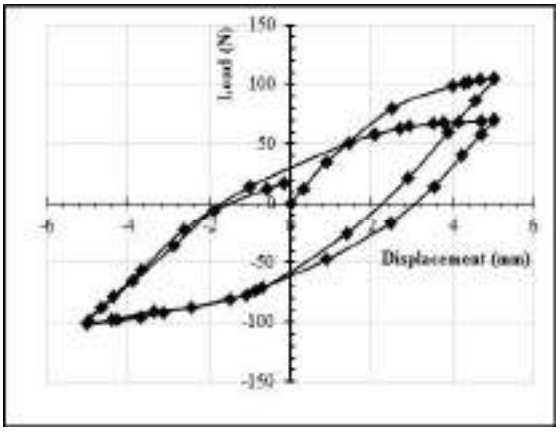

Fig. 4.436: Load vs. Displacement for 50mm Square Plate with (H/B =2) at 45° inclination under 0.5 Hz frequency and 5mm amplitude

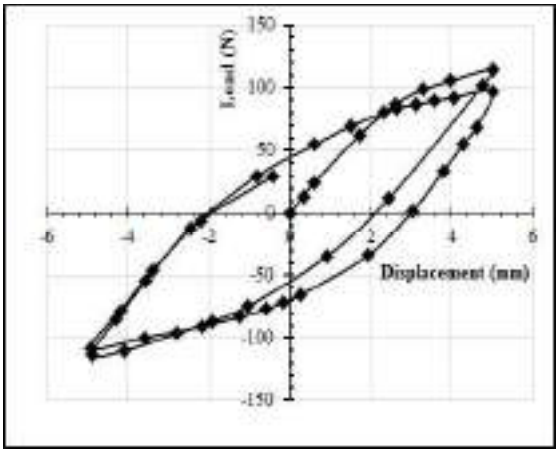

Fig. 4.437: Load vs. Displacement 50mm Square Plate with (H/B =3) at 45° inclination under 0.5 Hz frequency and 5mm amplitude

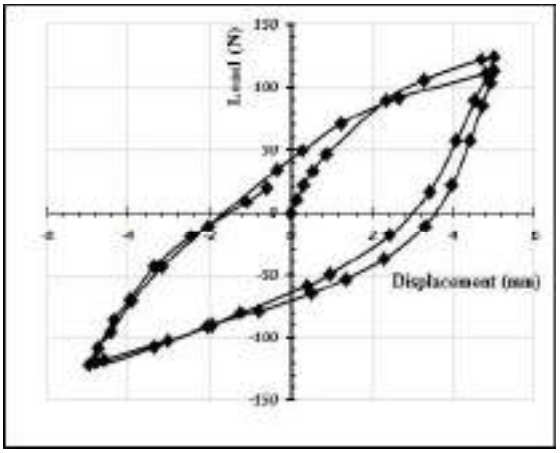

Fig. 4.438: Load vs. Displacement for 50mm Square Plate with (H/B =1) at 60° inclination under 0.5 Hz frequency and 5mm amplitude

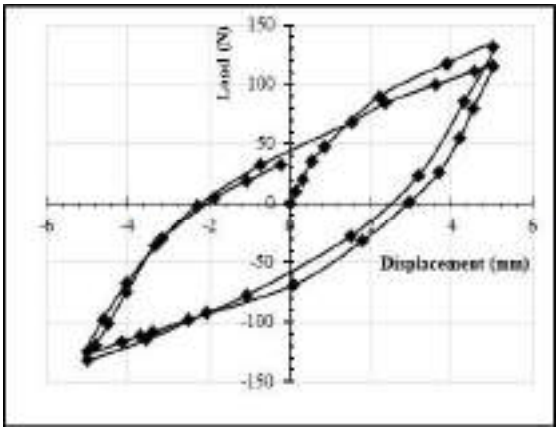

Fig. 4.439: Load vs. Displacement for 50mm Square Plate with (H/B =2) at 60° inclination under 0.5 Hz frequency and 5mm amplitude

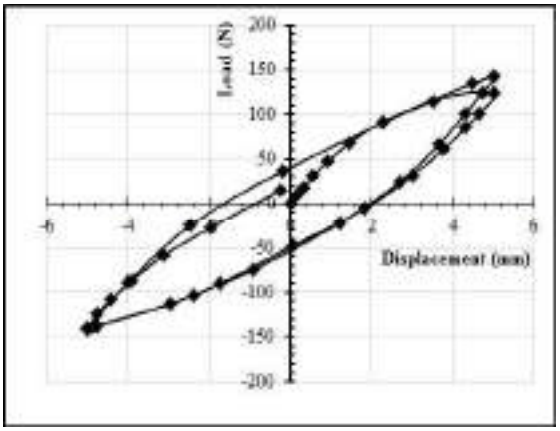

Fig. 4.440: Load vs. Displacement for 50mm Square Plate with (H/B =3) at 60° inclination under 0.5 Hz frequency and 5mm amplitude

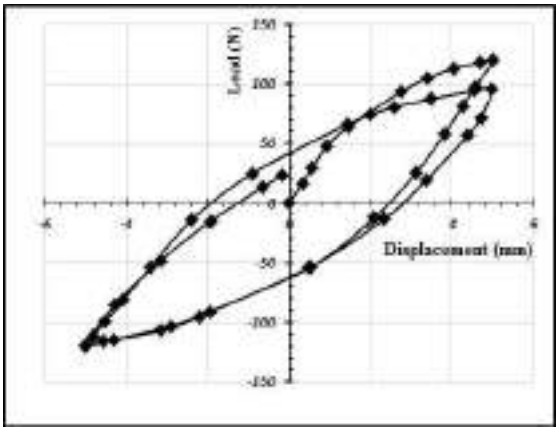

Fig. 4.441: Load vs. Displacement for 75mm Square Plate with (H/B =1) at 30° inclination under 0.5 Hz frequency and 5mm amplitude

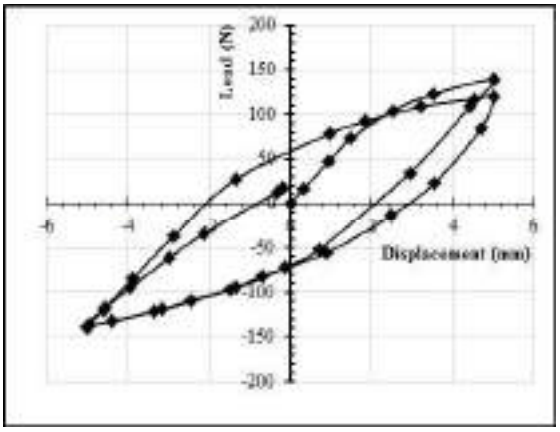

Fig. 4.442: Load vs. Displacement for 75mm Square Plate with (H/B =2) at 30° inclination under 0.5 Hz frequency and 5mm amplitude

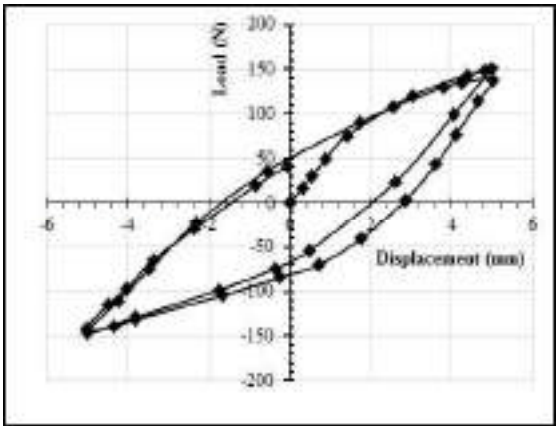

Fig. 4.443: Load vs. Displacement for 75mm Square Plate with (H/B =3) at 30° inclination under 0.5 Hz frequency and 5mm amplitude

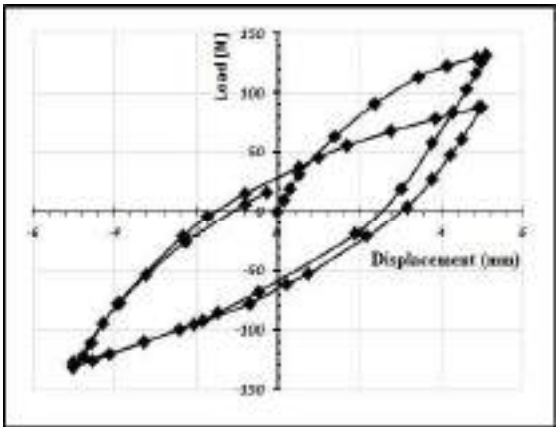

Fig. 4.444: Load vs. Displacement for 75mm Square Plate with (H/B =1) at 45° inclination under 0.5 Hz frequency and 5mm amplitude

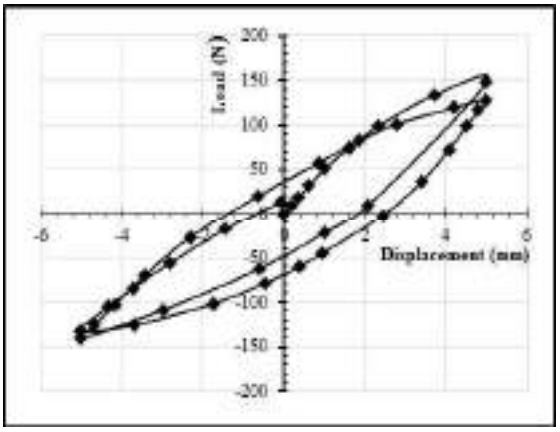

Fig. 4.445: Load vs. Displacement for 75mm Square Plate with (H/B =2) at 45° inclination under 0.5 Hz frequency and 5mm amplitude

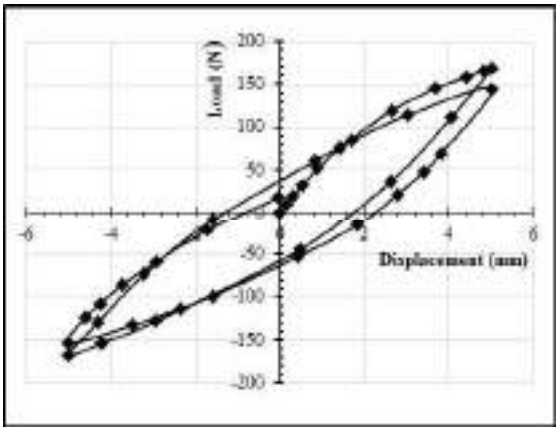

Fig. 4.446: Load vs. Displacement for 75mm Square Plate with (H/B =3) at 45° inclination under 0.5 Hz frequency and 5mm amplitude

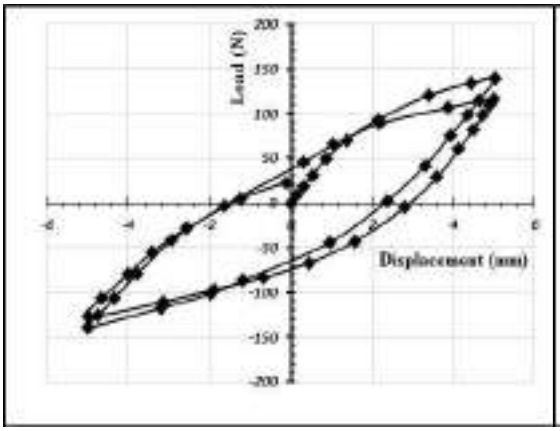

Fig. 4.447: Load vs. Displacement for 75mm Square Plate with (H/B =1) at 60° inclination under 0.5 Hz frequency and 5mm amplitude

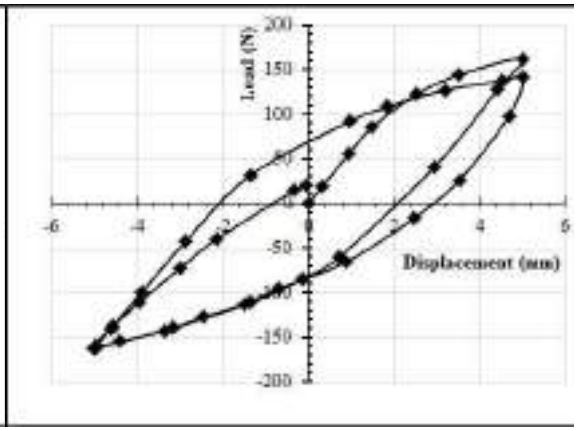

Fig. 4.448: Load vs. Displacement for 75mm Square Plate with (H/B =2) at 60° inclination under 0.5 Hz frequency and 5mm amplitude

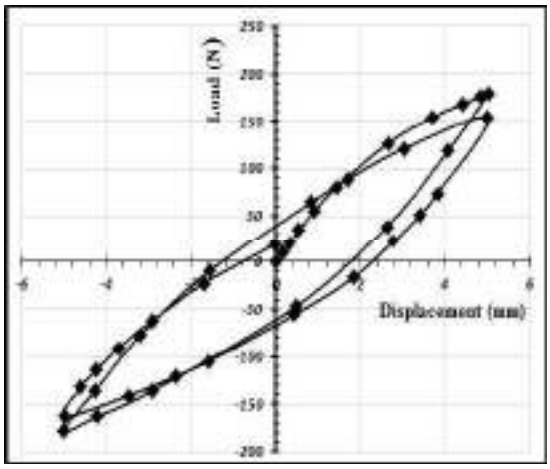

Fig. 4.449: Load vs. Displacement for 75mm Square Plate with (H/B =3) at 60° inclination under 0.5 Hz frequency and 5mm amplitude

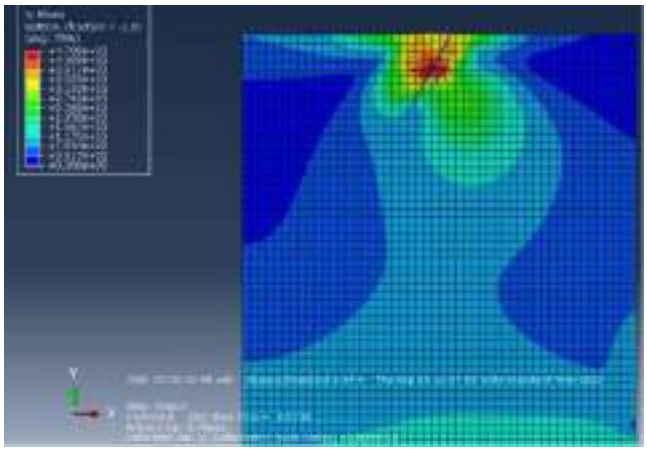

Fig. 4.451: Stress Contour for 25 mm Square Plate with (H/B =2) at 30° inclination under 0.2 Hz frequency and 2mm amplitude

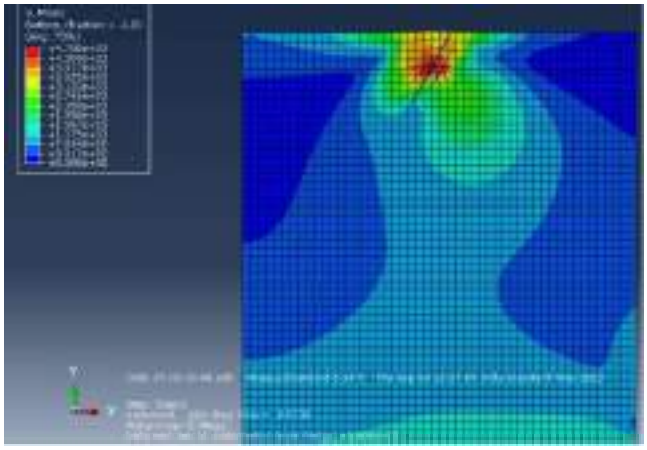

Fig. 4.452: Stress Contour for 25 mm Square Plate with (H/B =3) at 30° inclination under 0.2 Hz frequency and 2mm amplitude

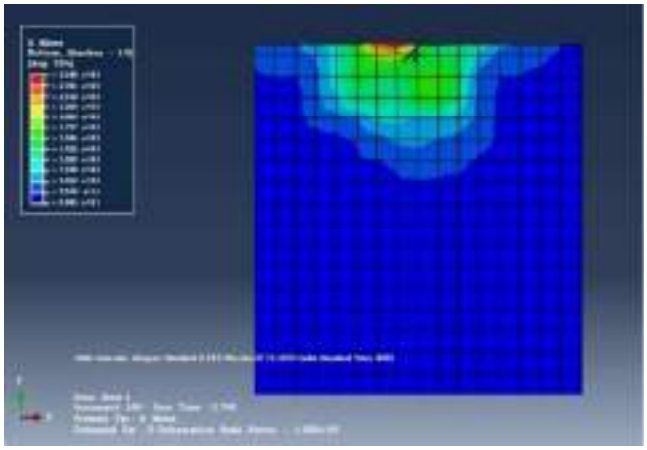

Fig. 4.453: Stress Contour for 25 mm Square Plate with (H/B =1) at 45° inclination under 0.2 Hz frequency and 2mm amplitude

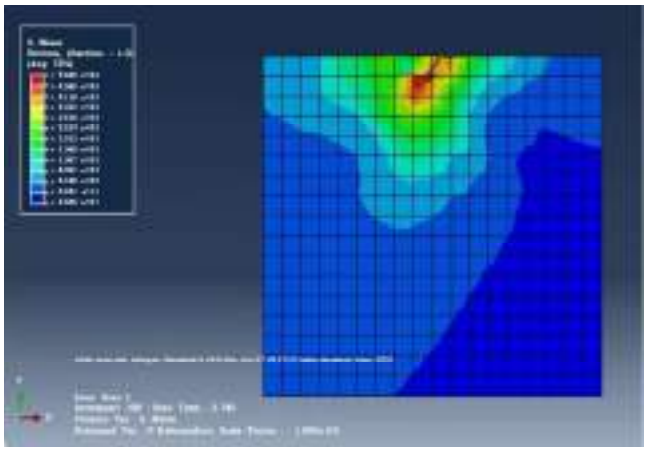

Fig. 4.454: Stress Contour for 25 mm Square Plate with (H/B =2) at 45° inclination under 0.2 Hz frequency and 2mm amplitude

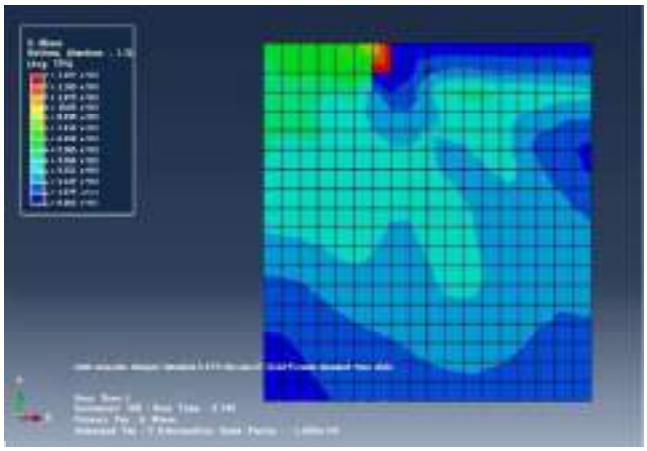

Fig. 4.455: Stress Contour for 25 mm Square Plate with (H/B =3) at 45° inclination under 0.2 Hz frequency and 2mm amplitude

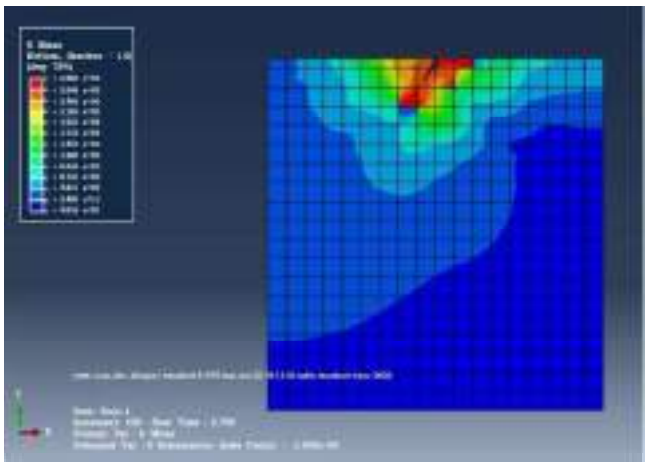

Fig. 4.456: Stress Contour for 25 mm Square Plate with (H/B =1) at 60° inclination under 0.2 Hz frequency and 2mm amplitude

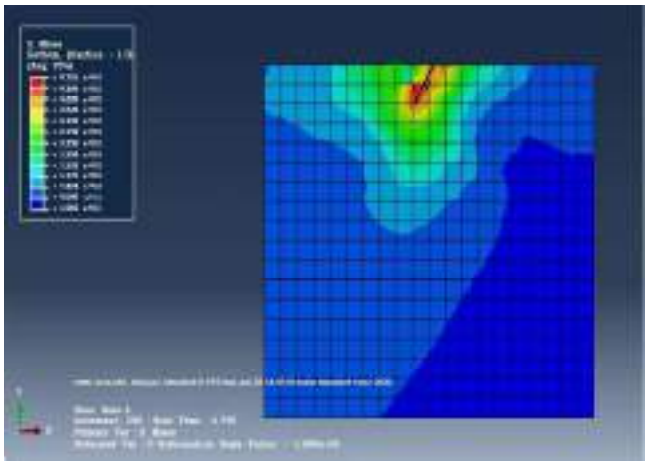

Fig. 4.457: Stress Contour for 25 mm Square Plate with (H/B =2) at 60° inclination under 0.2 Hz frequency and 2mm amplitude

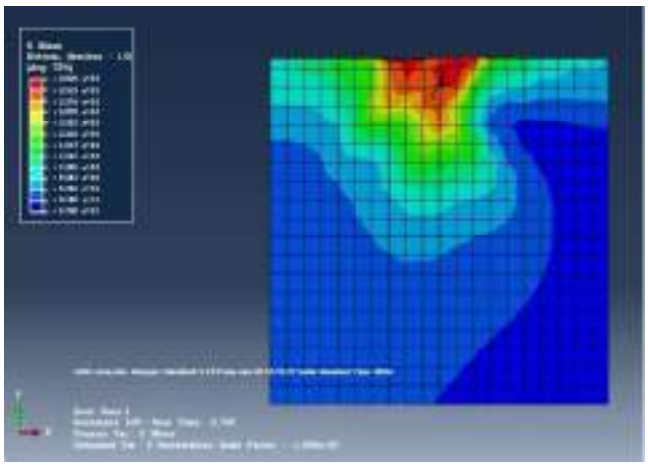

Fig. 4.458: Stress Contour for 25 mm Square Plate with (H/B =3) at 60° inclination under 0.2 Hz frequency and 2mm amplitude

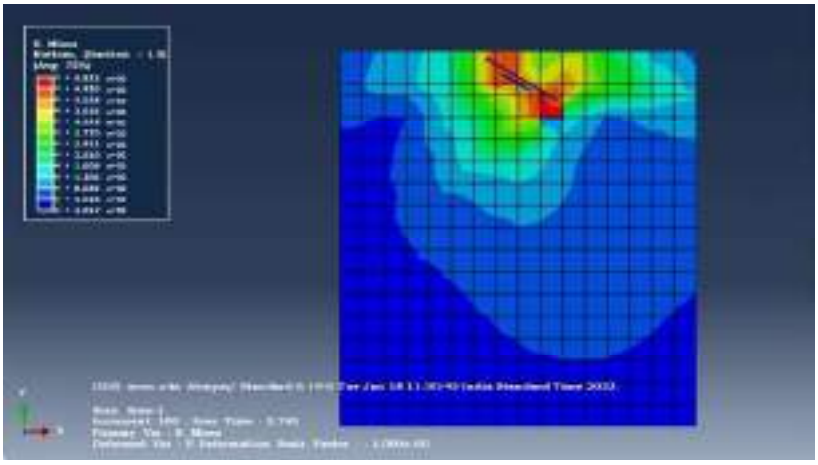

Fig. 4.459: Stress Contour for 50mm Square Plate with (H/B =1) at 30° inclination under 0.2 Hz frequency and 2mm amplitude

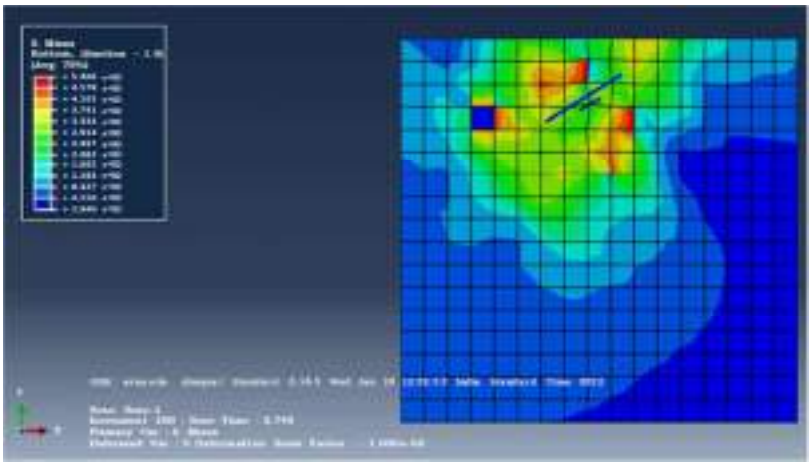

Fig. 4.460: Stress Contour for 50mmSquare Plate with (H/B =2) at 30° inclination under 0.2 Hz frequency and 2mm amplitude

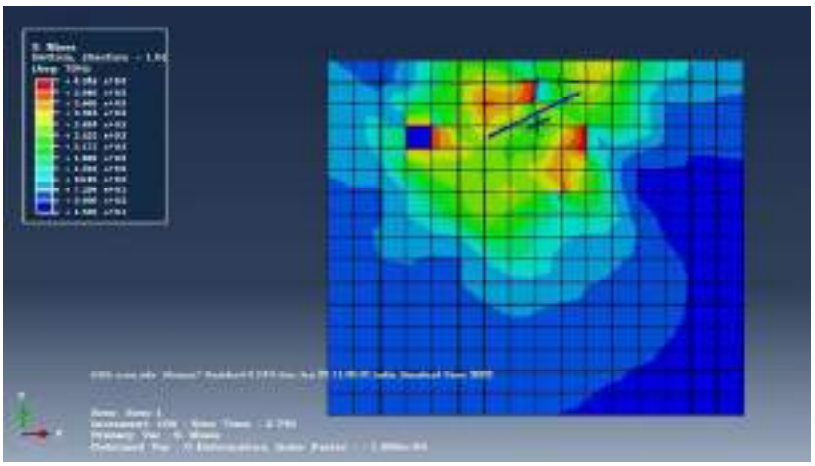

Fig. 4.461: Stress Contour for 50mm Square Plate with (H/B =3) at 30° inclination under 0.2 Hz frequency and 2mm amplitude

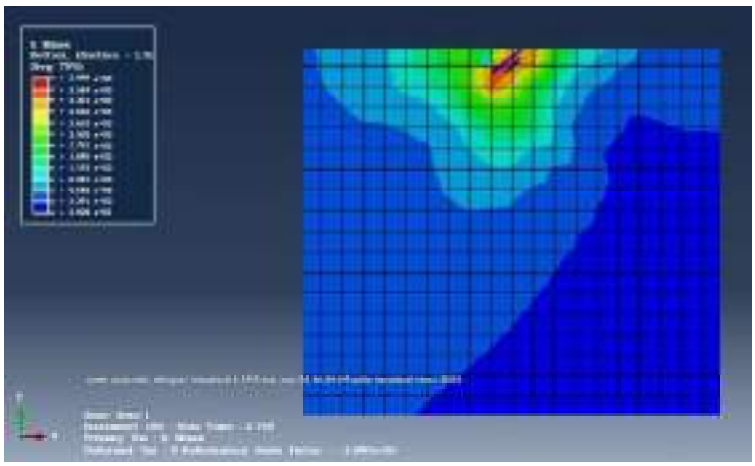

Fig. 4.462: Stress Contour for 50mm Square Plate with (H/B =1) at 45° inclination under 0.2 Hz frequency and 2mm amplitude

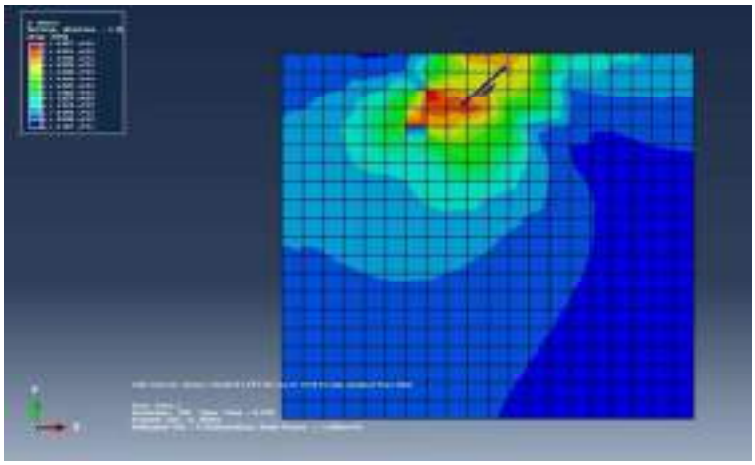

Fig. 4.463: Stress Contour for 50mmSquare Plate with (H/B =2) at 45° inclination under 0.2 Hz frequency and 2mm amplitude

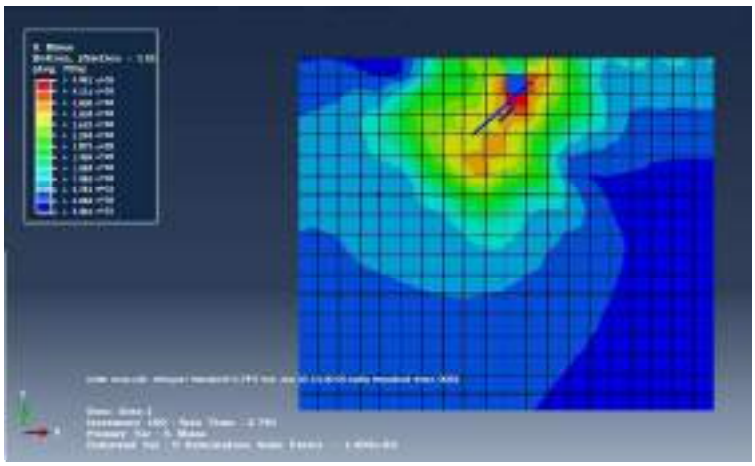

Fig. 4.464: Stress Contour for 50mm Square Plate with (H/B =3) at 45° inclination under 0.2 Hz frequency and 2mm amplitude

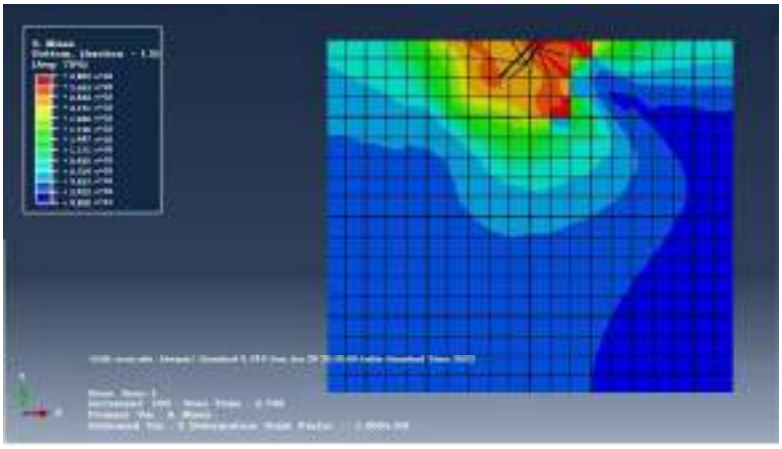

Fig. 4.465: Stress Contour for 50mm Square Plate with (H/B =1) at 60° inclination under 0.2 Hz frequency and 2mm amplitude

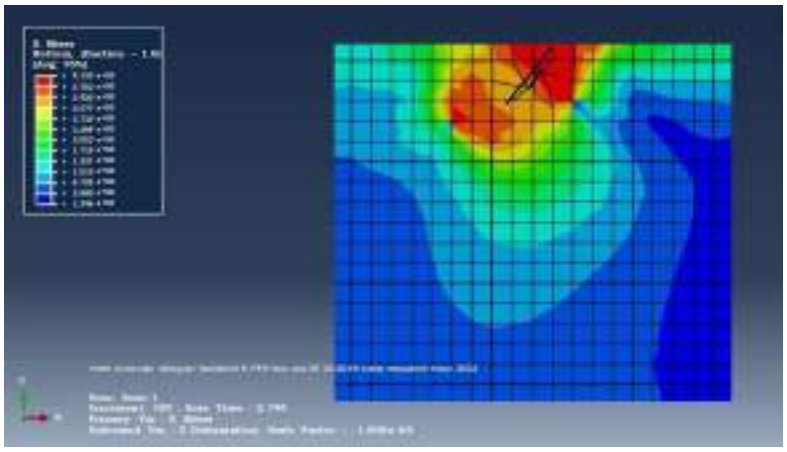

Fig. 4.466: Stress Contour for 50mm Square Plate with (H/B =2) at 60° inclination under 0.2 Hz frequency and 2mm amplitude

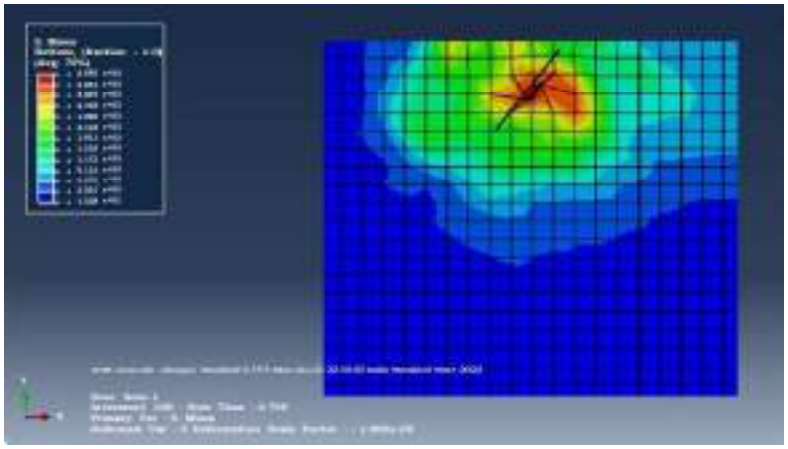

Fig. 4.467: Stress Contour for 50mm Square Plate with (H/B =3) at 60° inclination under 0.2 Hz frequency and 2mm amplitude

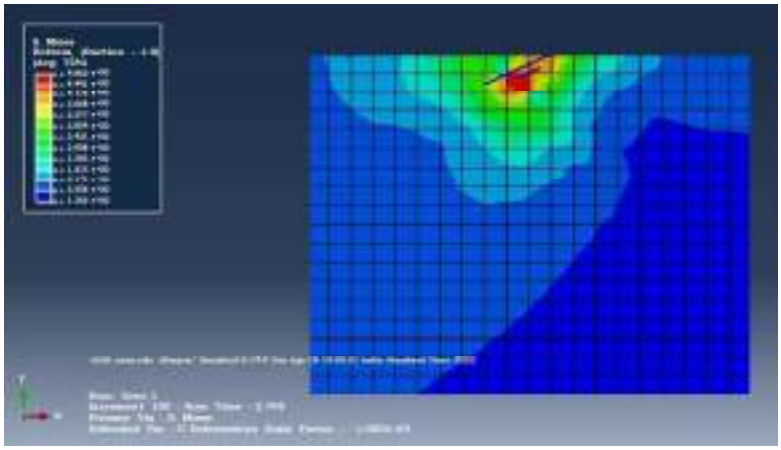

Fig. 4.468: Stress Contour for 75mm Square Plate with (H/B =1) at 30° inclination under 0.2 Hz frequency and 2mm amplitude

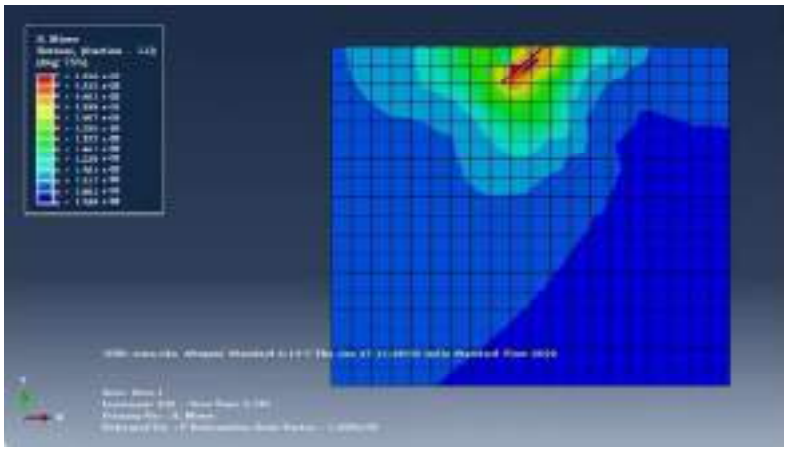

Fig. 4.469: Stress Contour for 75mmSquare Plate with (H/B =2) at 30° inclination under 0.2 Hz frequency and 2mm amplitude

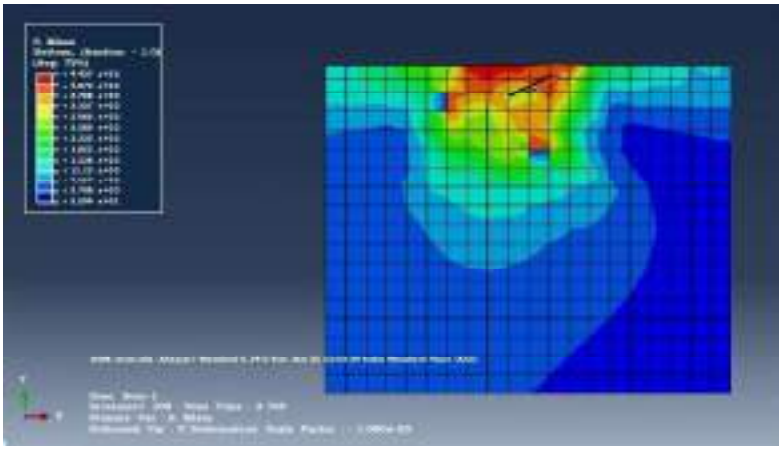

Fig. 4.470: Stress Contour for 75mmSquare Plate with (H/B =3) at 30° inclination under 0.2 Hz frequency and 2mm amplitude

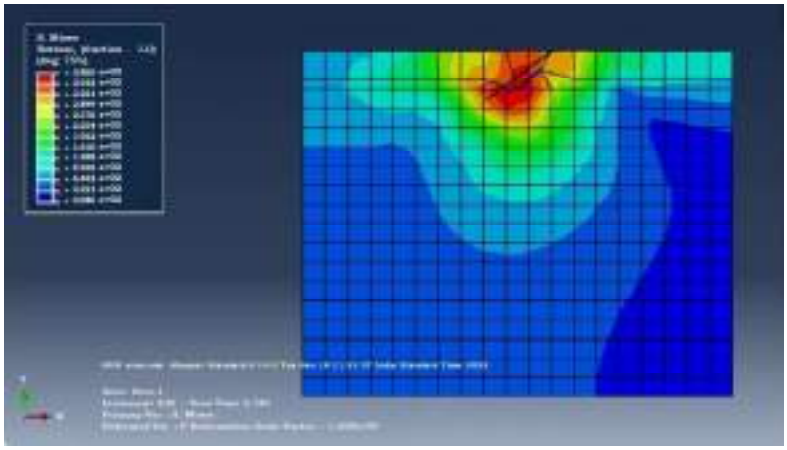

Fig. 4.471: Stress Contour for 75mm Square Plate with (H/B =1) at 45° inclination under 0.2 Hz frequency and 2mm amplitude

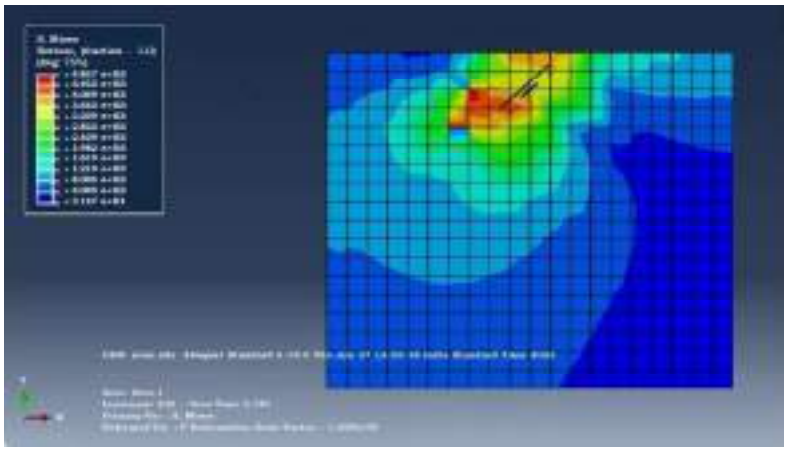

Fig. 4.472: Stress Contour for 75mm Square Plate with (H/B =2) at 45° inclination under 0.2 Hz frequency and 2mm amplitude

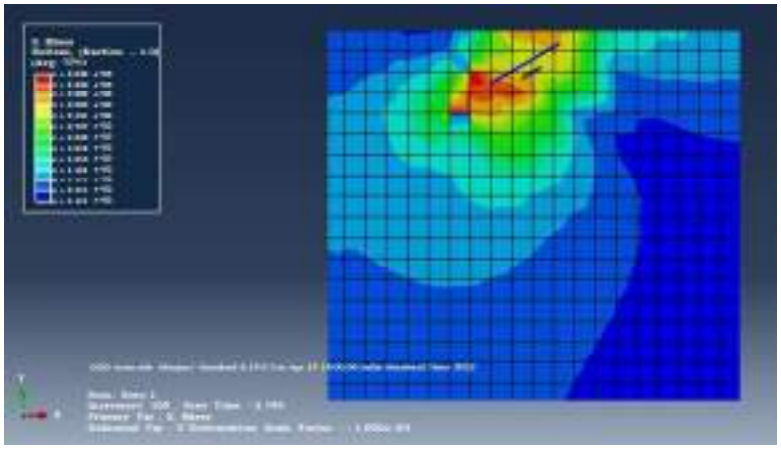

Fig. 4.473: Stress Contour for 75mm Square Plate with (H/B =3) at 45° inclination under 0.2 Hz frequency and 2mm amplitude

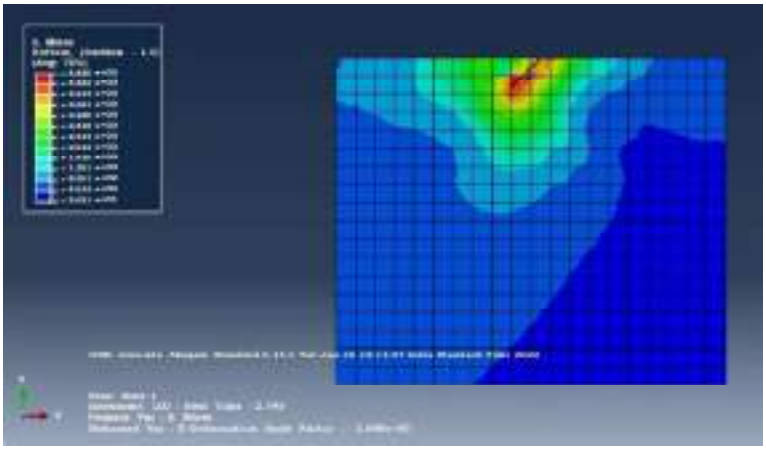

Fig. 4.474: Stress Contour for 75mm Square Plate with (H/B =1) at 60° inclination under 0.2 Hz frequency and 2mm amplitude

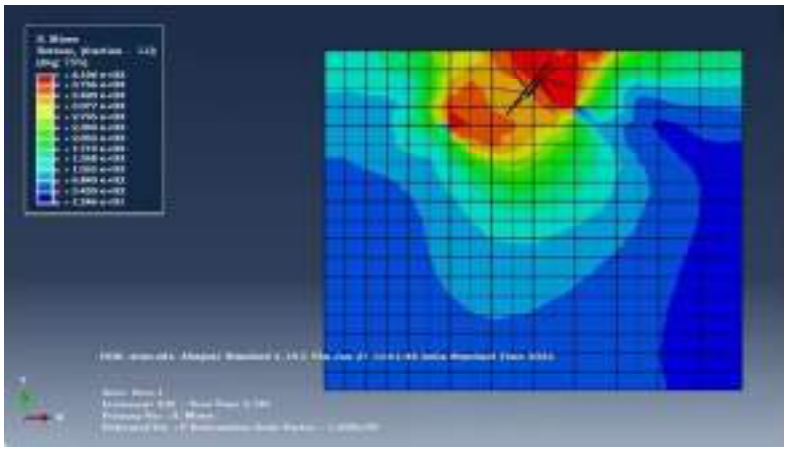

Fig. 4.475: Stress Contour for 75mm Square Plate with (H/B =2) at 60° inclination under 0.2 Hz frequency and 2mm amplitude

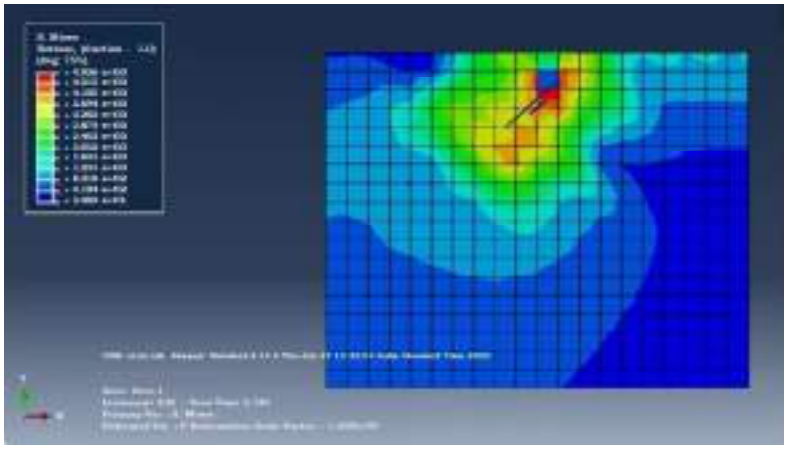

Fig. 4.476: Stress Contour for 75mm Square Plate with (H/B =3) at 60° inclination under 0.2 Hz frequency and 2mm amplitude

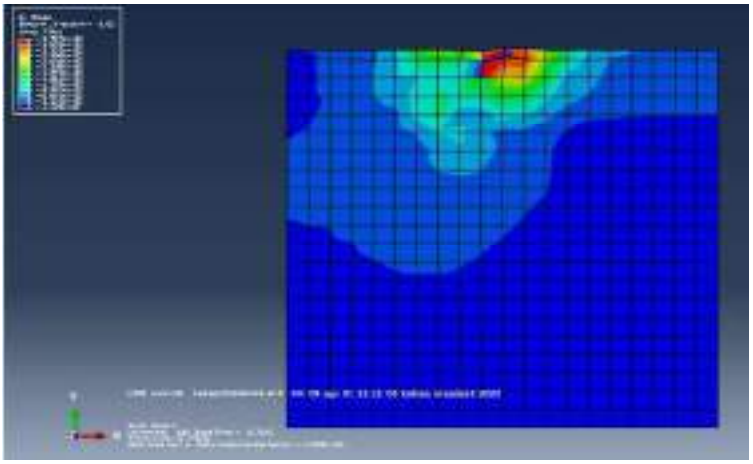

Fig. 4.477: Stress Contour for 25mm Square Plate with (H/B =1) at 30° inclination under 0.2 Hz frequency and 5mm amplitude

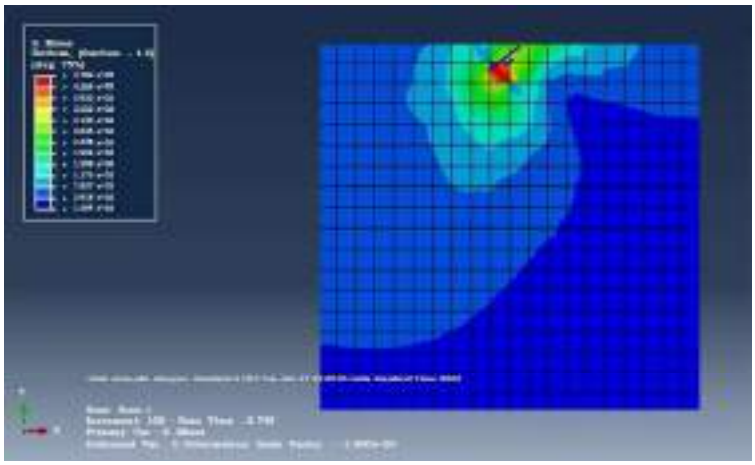

Fig. 4.478: Stress Contour for 25mm Square Plate with (H/B =2) at 30° inclination under 0.2 Hz frequency and 5mm amplitude

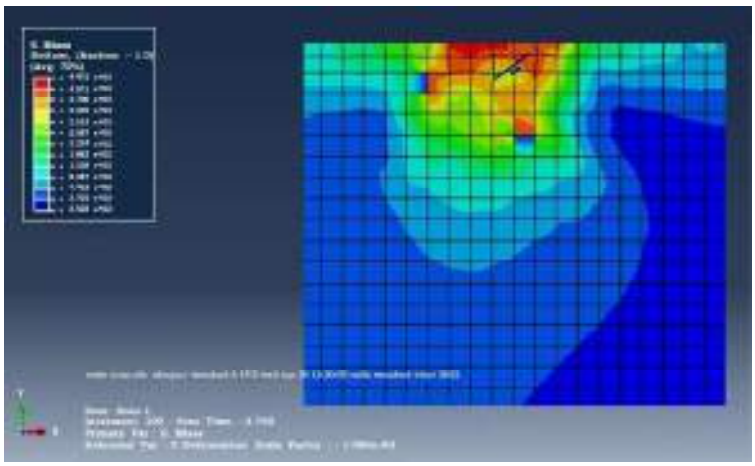

Fig. 4.479: Stress Contour for 25mm Square Plate with (H/B =3) at 30° inclination under 0.2 Hz frequency and 5mm amplitude

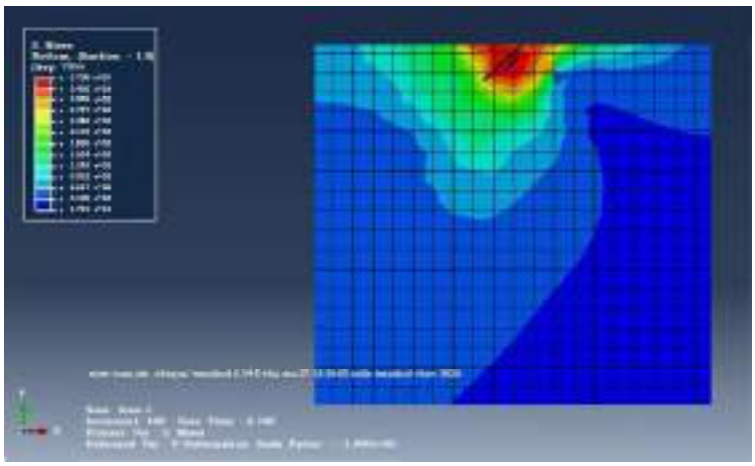

Fig. 4.480: Stress Contour for 25mm Square Plate with (H/B =1) at 45° inclination under 0.2 Hz frequency and 5mm amplitude

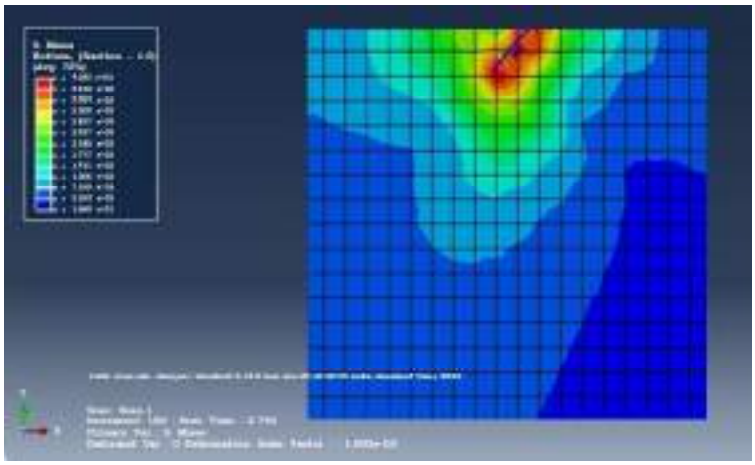

Fig. 4.481: Stress Contour for 25mm Square Plate with (H/B =2) at 45° inclination under 0.2 Hz frequency and 5mm amplitude

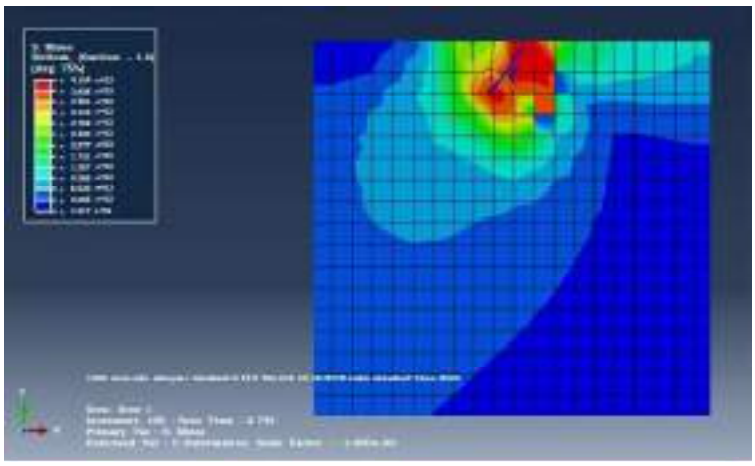

Fig. 4.482: Stress Contour for 25mm Square Plate with (H/B =3) at 45° inclination under 0.2 Hz frequency and 5mm amplitude

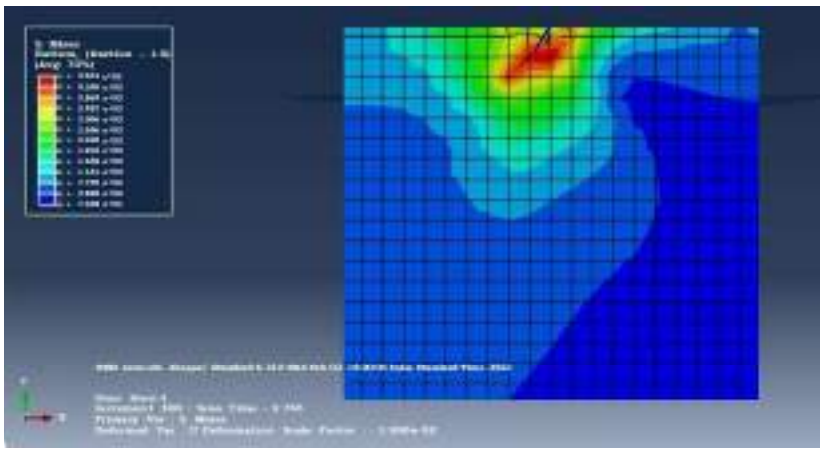

Fig. 4.483: Stress Contour for 25mm Square Plate with (H/B =1) at 60° inclination under 0.2 Hz frequency and 5mm amplitude

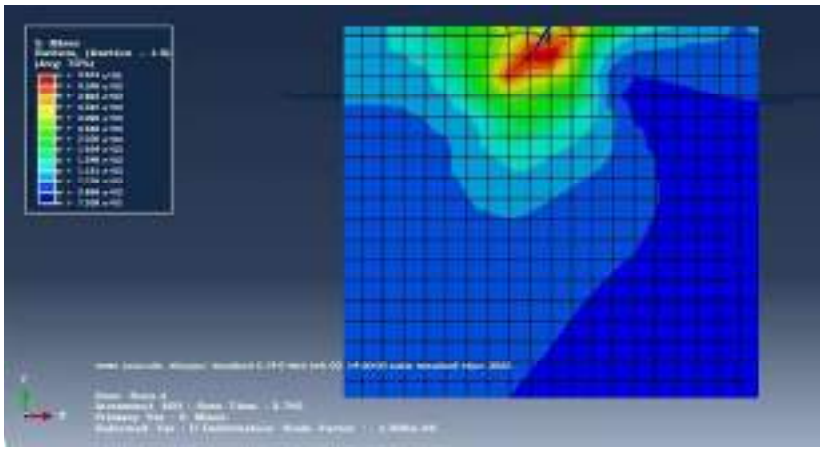

Fig. 4.484: Stress Contour for 25mm Square Plate with (H/B =2) at 60° inclination under 0.2 Hz frequency and 5mm amplitude

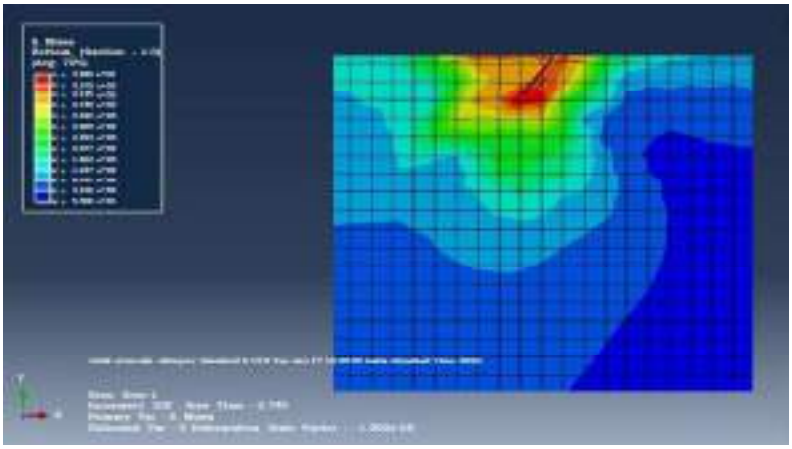

Fig. 4.485: Stress Contour for 25mm Square Plate with (H/B =3) at 60° inclination under 0.2 Hz frequency and 5mm amplitude

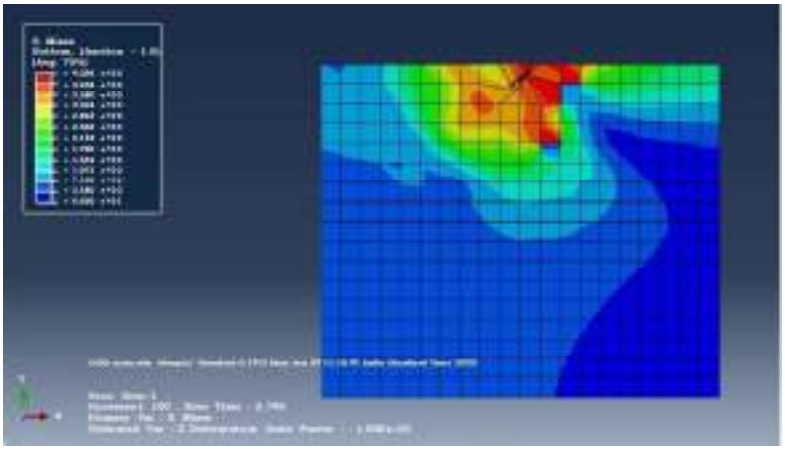

Fig. 4.486: Stress Contour for 50mm Square Plate with (H/B =1) at 30° inclination under 0.2 Hz frequency and 5mm amplitude

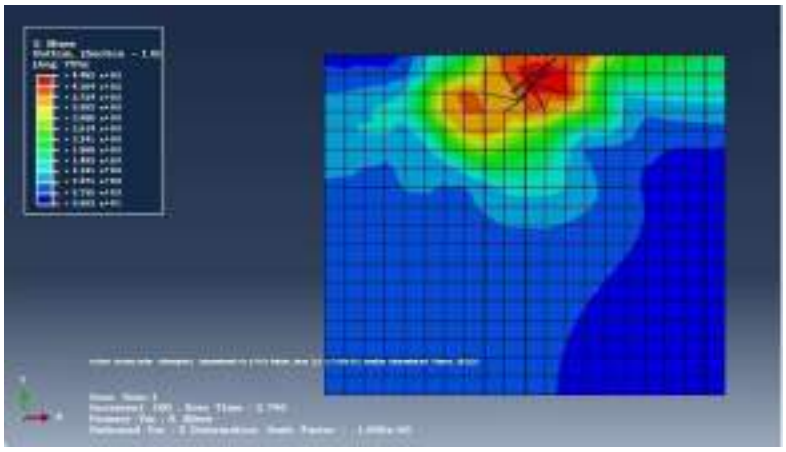

Fig. 4.487: Stress Contour for 50mm Square Plate with (H/B =2) at 30° inclination under 0.2 Hz frequency and 5mm amplitude

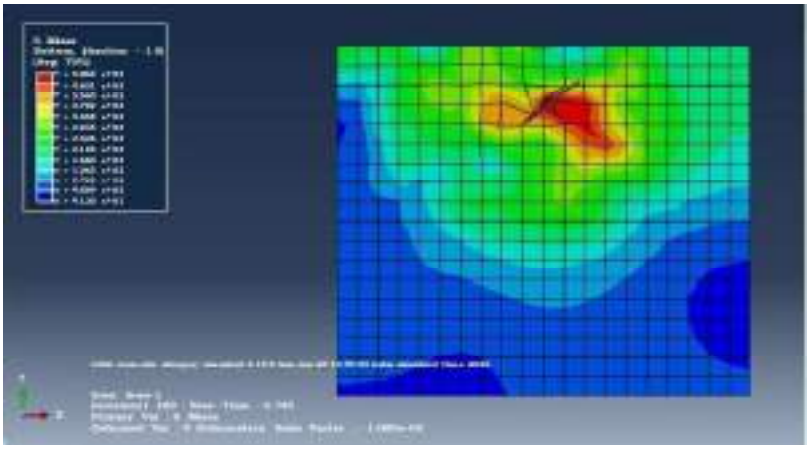

Fig. 4.488: Stress Contour for 50mm Square Plate with (H/B =3) at 30° inclination under 0.2 Hz frequency and 5mm amplitude

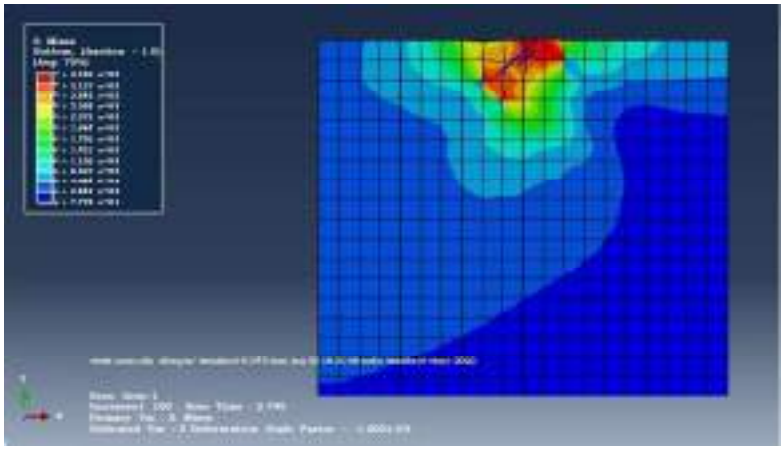

Fig. 4.489: Stress Contour for 50mm Square Plate with (H/B =1) at 45° inclination under 0.2 Hz frequency and 5mm amplitude

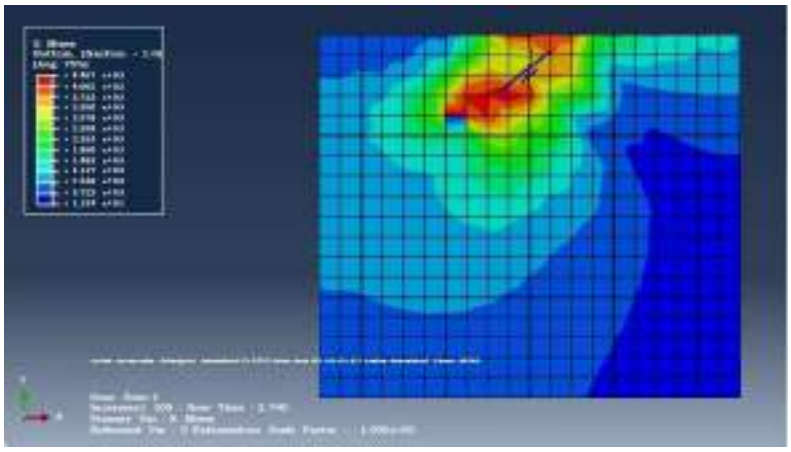

Fig. 4.490: Stress Contour for 50mm Square Plate with (H/B =2) at 45° inclination under 0.2 Hz frequency and 5mm amplitude

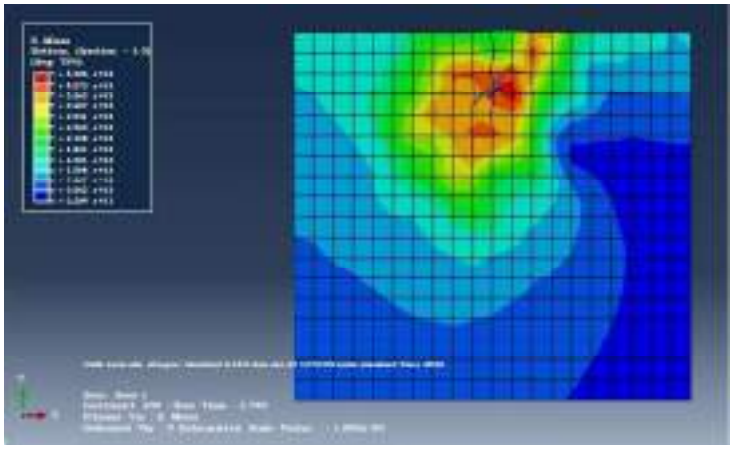

Fig. 4.491: Stress Contour for 50mm Square Plate with (H/B =3) at 45° inclination under 0.2 Hz frequency and 5mm amplitude

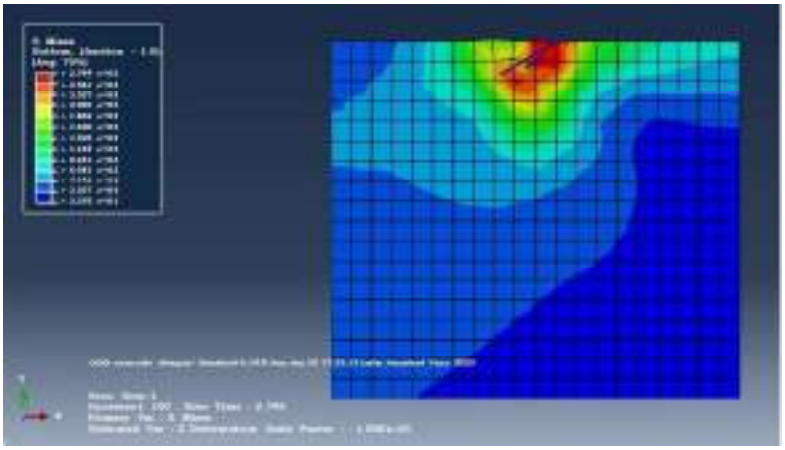

Fig. 4.492: Stress Contour for 50mm Square Plate with (H/B =1) at 60° inclination under 0.2 Hz frequency and 5mm amplitude

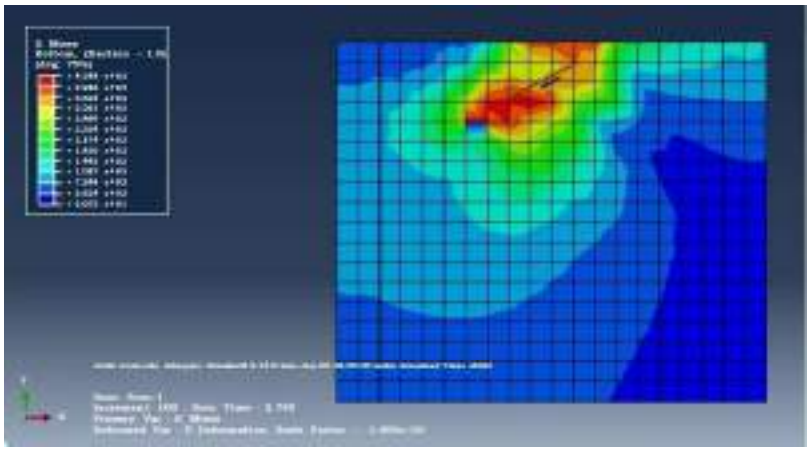

Fig. 4.493: Stress Contour for 50mm Square Plate with (H/B =2) at 60° inclination under 0.2 Hz frequency and 5mm amplitude

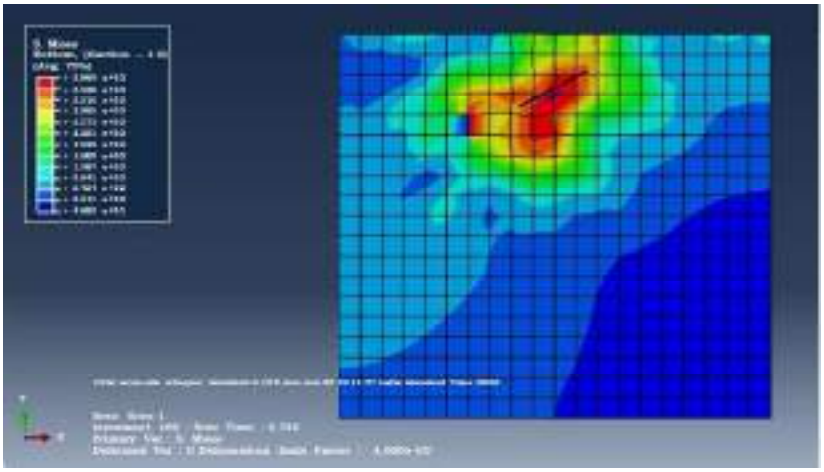

Fig. 4.494: Stress Contour for 50mm Square Plate with (H/B =3) at 60° inclination under 0.2 Hz frequency and 5mm amplitude

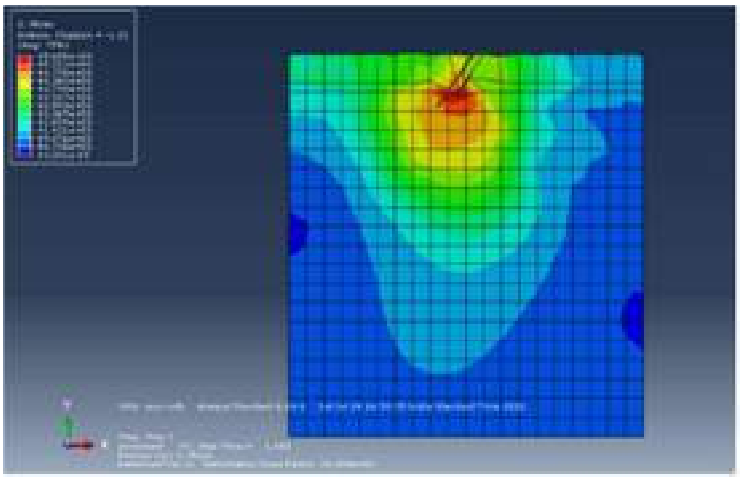

Fig. 4.495: Stress Contour for 75mm Square Plate with (H/B =1) at 30° inclination under 0.2 Hz frequency and 5mm amplitude

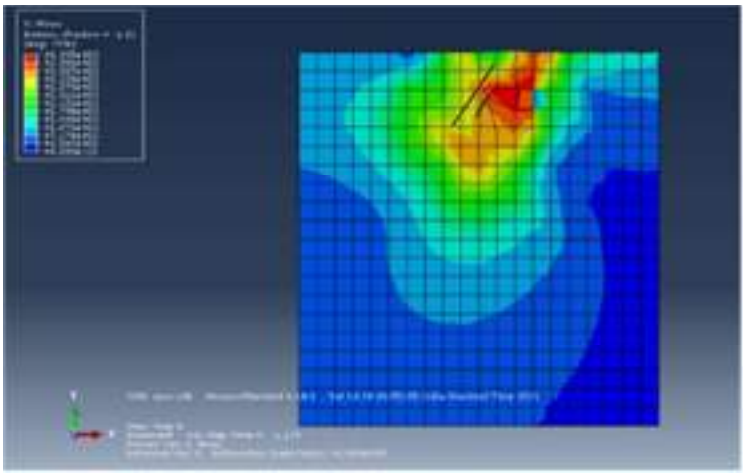

Fig. 4.496: Stress Contour for 75mm Square Plate with (H/B =2) at 30° inclination under 0.2 Hz frequency and 5mm amplitude

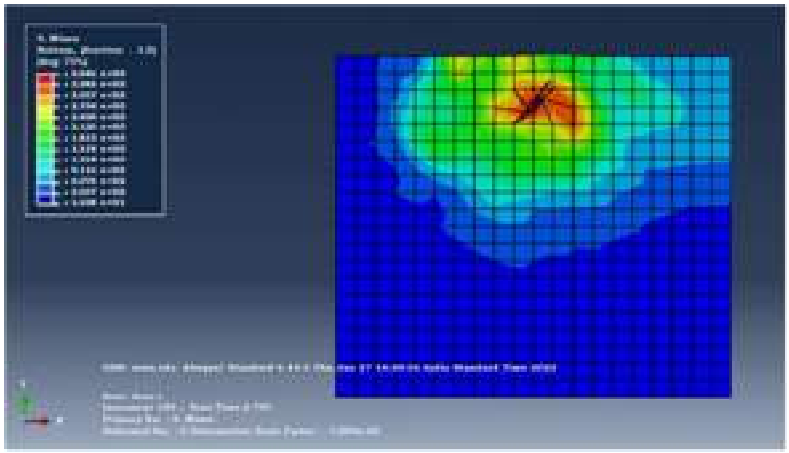

Fig. 4.497: Stress Contour for 75mm Square Plate with (H/B =3) at 30° inclination under 0.2 Hz frequency and 5mm amplitude

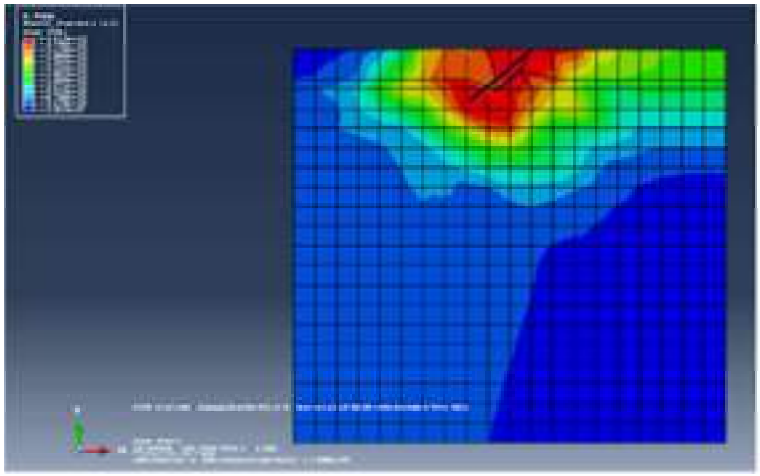

Fig. 4.498: Stress Contour for 75mm Square Plate with (H/B =1) at 45° inclination under 0.2 Hz frequency and 5mm amplitude

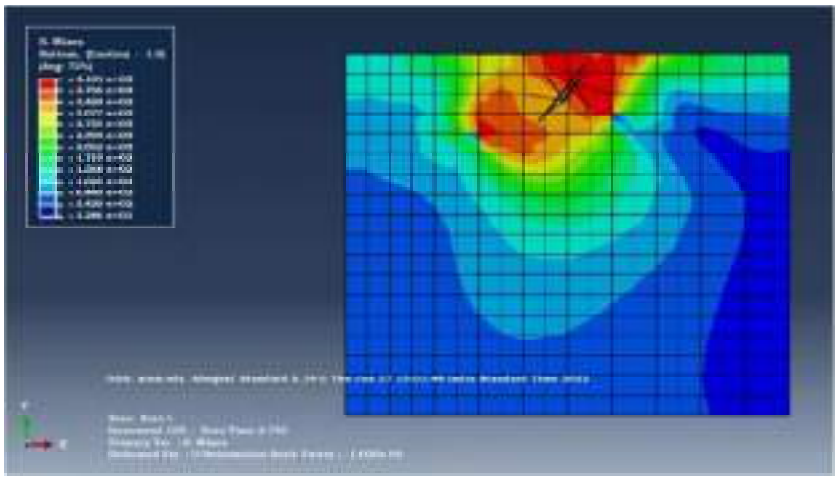

Fig. 4.499: Stress Contour for 75mm Square Plate with (H/B =2) at 45° inclination under 0.2 Hz frequency and 5mm amplitude

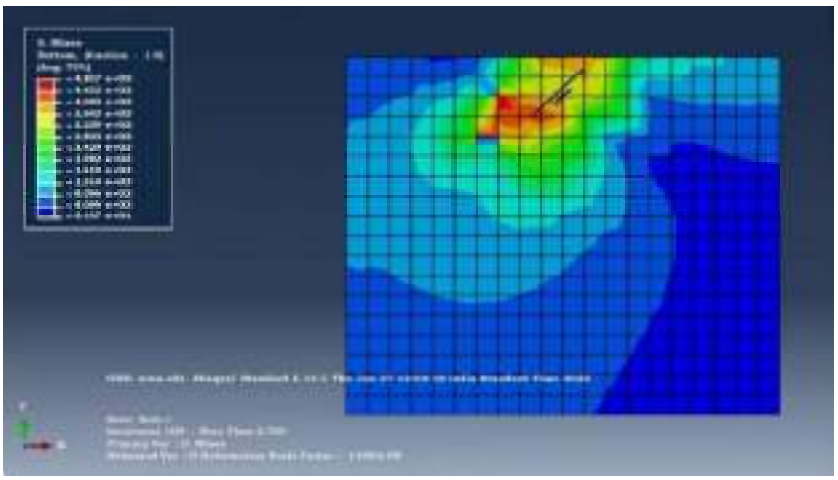

Fig. 4.500: Stress Contour for 75mm Square Plate with (H/B =3) at 45° inclination under 0.2 Hz frequency and 5mm amplitude

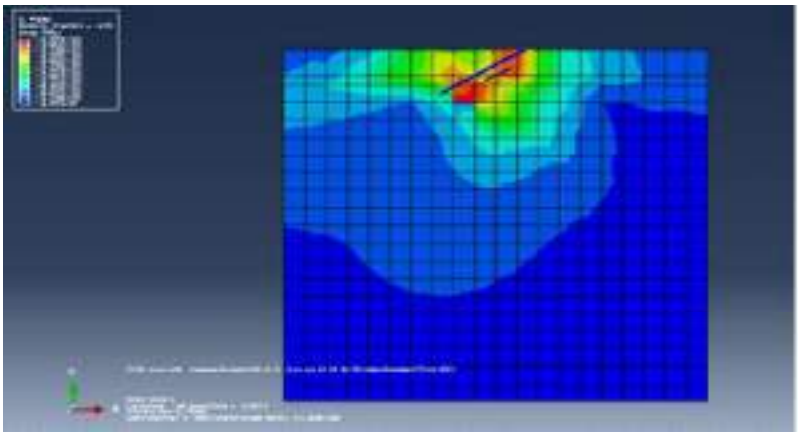

Fig. 4.501: Stress Contour for 75mm Square Plate with (H/B =1) at 60° inclination under 0.2 Hz frequency and 5mm amplitude

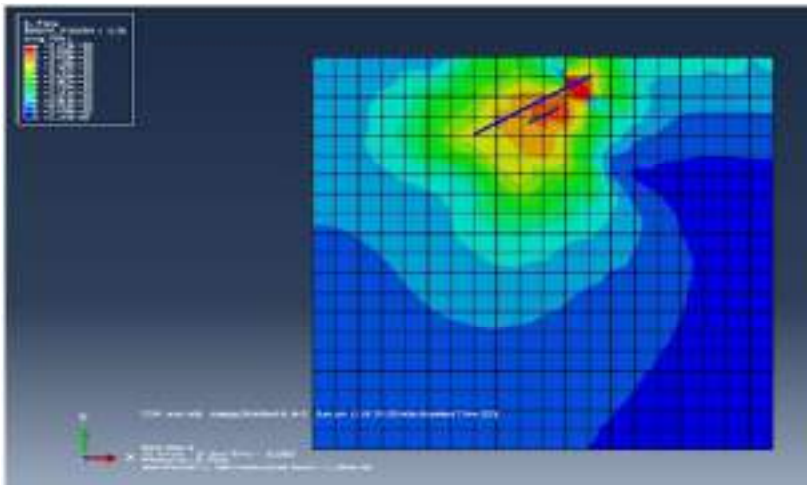

Fig. 4.502: Stress Contour for 75mm Square Plate with (H/B =2) at 60° inclination under 0.2 Hz frequency and 5mm amplitude

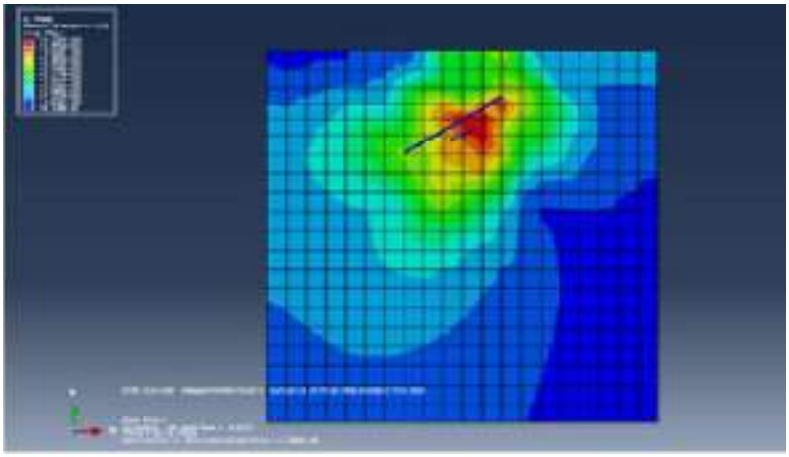

Fig. 4.503: Stress Contour for 75mm Square Plate with (H/B =3) at 60° inclination under 0.2 Hz frequency and 5mm amplitude

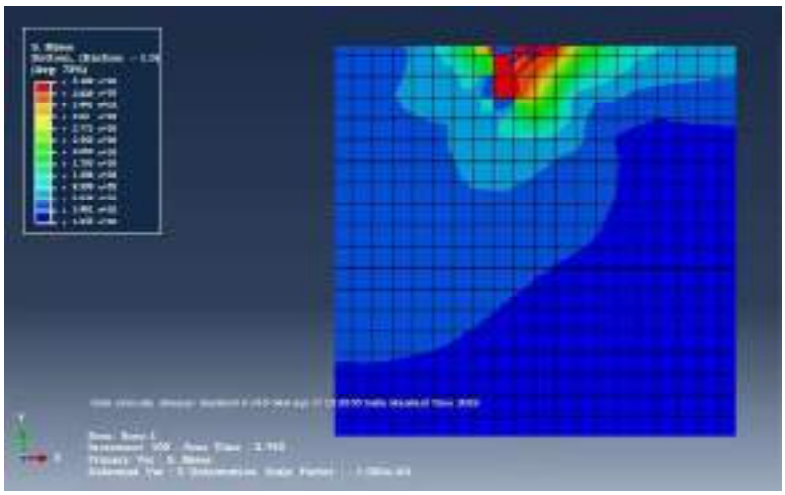

Fig. 4.504: Stress Contour for 25mm Square Plate with (H/B =1) at 30° inclination under 0.5 Hz frequency and 2mm amplitude

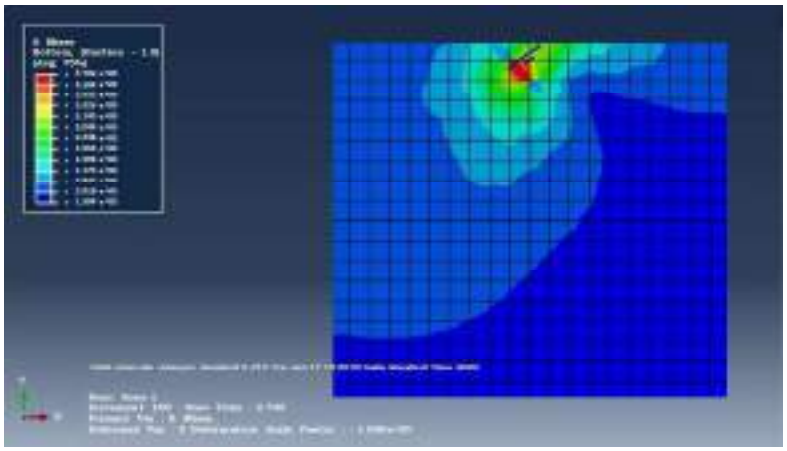

Fig. 4.505: Stress Contour for 25mm Square Plate with (H/B =2) at 30° inclination under 0.5 Hz frequency and 2mm amplitude

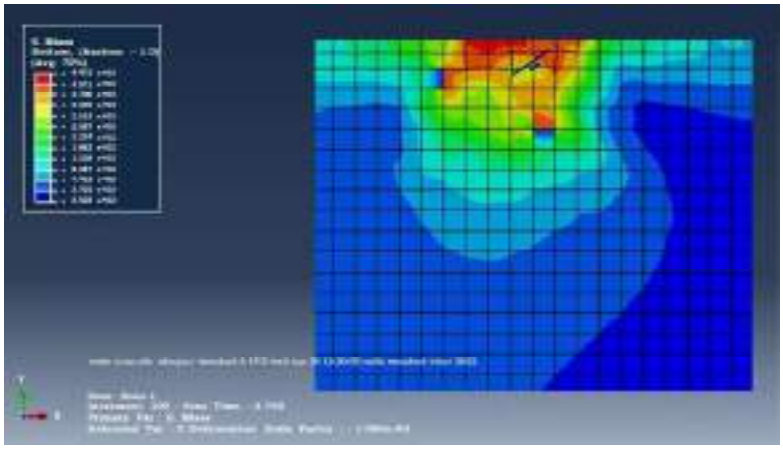

Fig. 4.506: Stress Contour for 25mm Square Plate with (H/B =3) at 30° inclination under 0.5 Hz frequency and 2mm amplitude

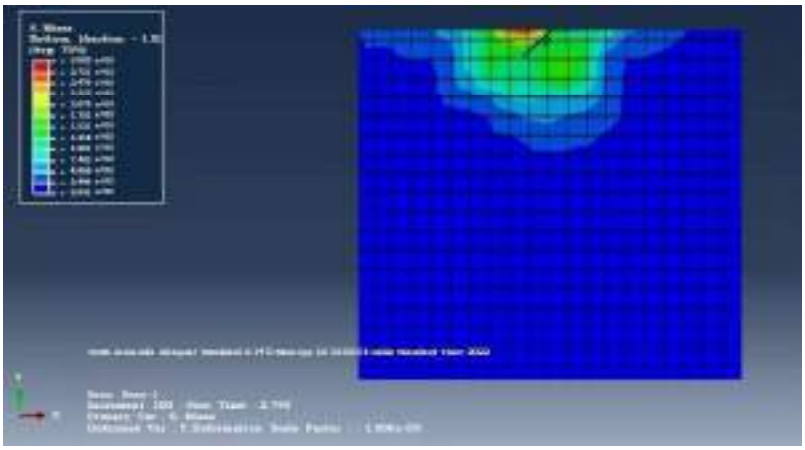

Fig. 4.507: Stress Contour for 25mm Square Plate with (H/B =1) at 45° inclination under 0.5 Hz frequency and 2mm amplitude

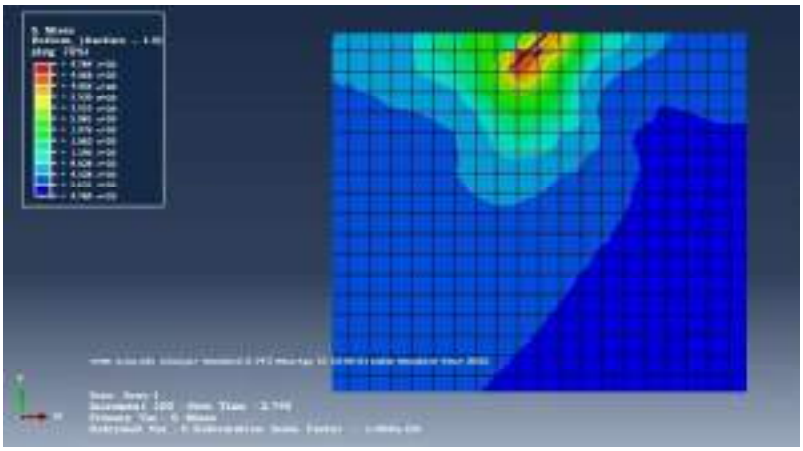

Fig. 4.508: Stress Contour for 25mm Square Plate with (H/B =2) at 45° inclination under 0.5 Hz frequency and 2mm amplitude

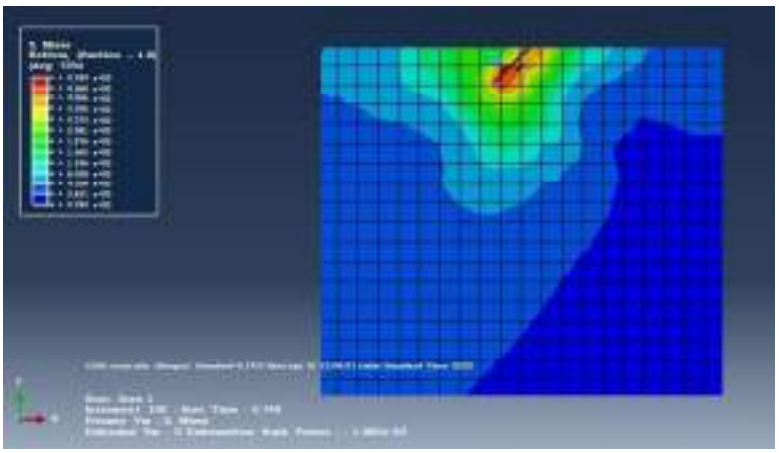

Fig. 4.509: Stress Contour for 25mm Square Plate with (H/B =3) at 45° inclination under 0.5 Hz frequency and 2mm amplitude

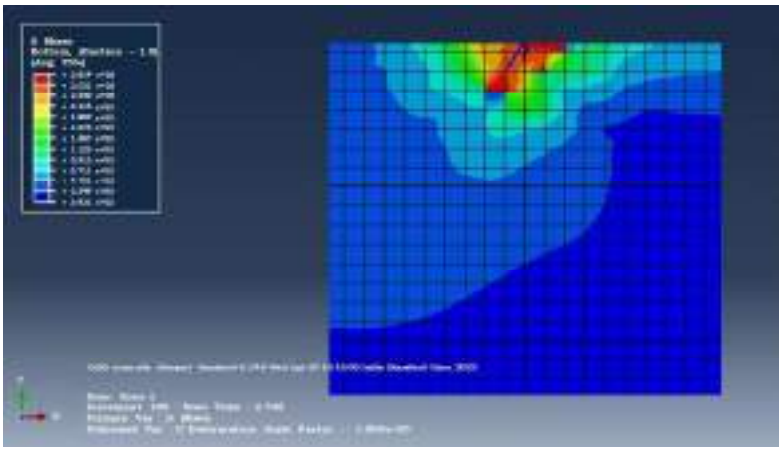

Fig. 4.510: Stress Contour for 25mm Square Plate with (H/B =1) at 60° inclination under 0.5 Hz frequency and 2mm amplitude

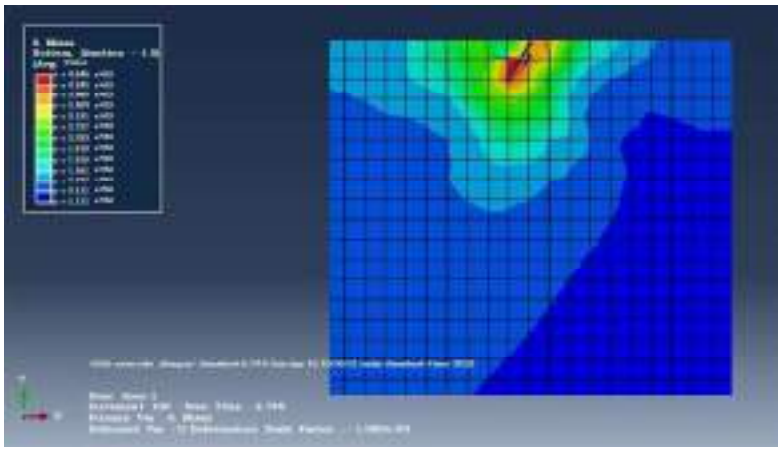

Fig. 4.511: Stress Contour for 25mm Square Plate with (H/B =2) at 60° inclination under 0.5 Hz frequency and 2mm amplitude

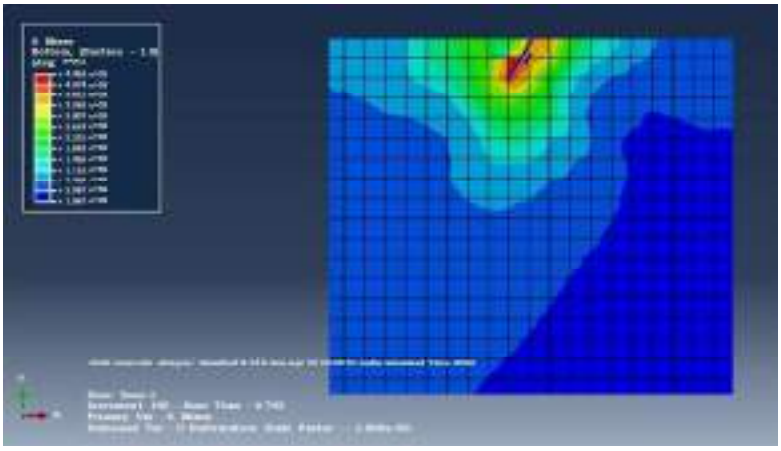

Fig. 4.512: Stress Contour for 25mm Square Plate with (H/B =3) at 60° inclination under 0.5 Hz frequency and 2mm amplitude

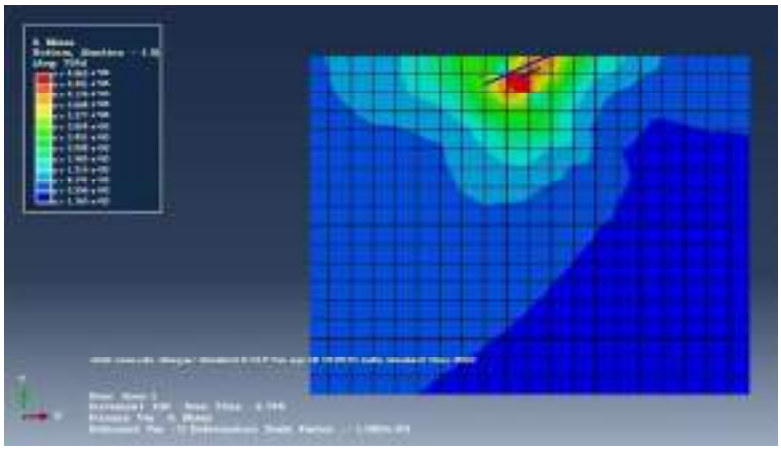

Fig. 4.513: Stress Contour for 50mm Square Plate with (H/B =1) at 30° inclination under 0.5 Hz frequency and 2mm amplitude

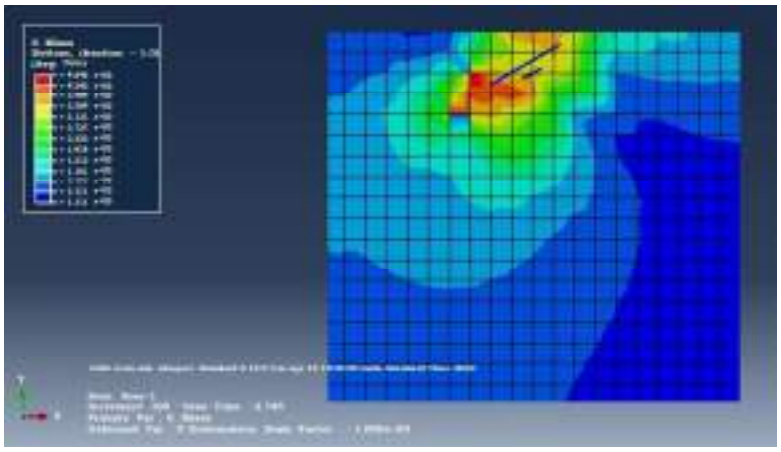

Fig. 4.514: Stress Contour for 50mm Square Plate with (H/B =2) at 30° inclination under 0.5 Hz frequency and 2mm amplitude

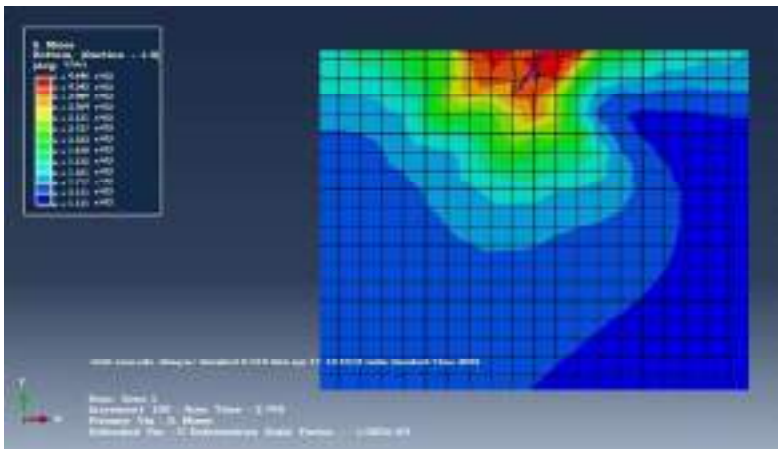

Fig. 4.515: Stress Contour for 50mm Square Plate with (H/B =3) at 30° inclination under 0.5 Hz frequency and 2mm amplitude

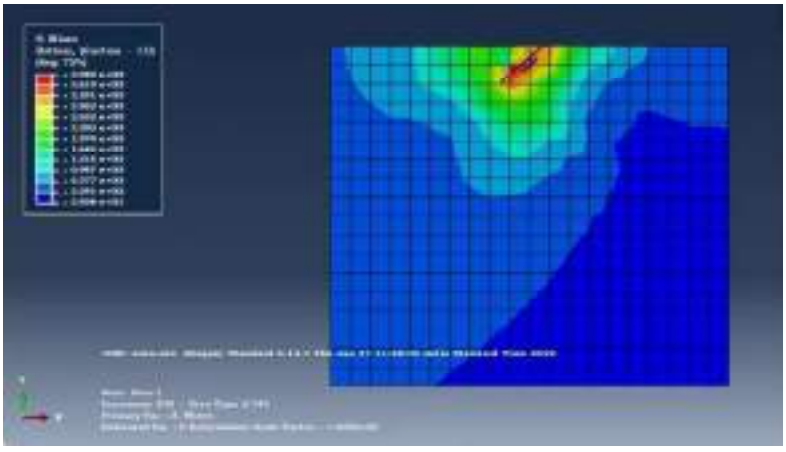

Fig. 4.516: Stress Contour for 50mm Square Plate with (H/B =1) at 45° inclination under 0.5 Hz frequency and 2mm amplitude

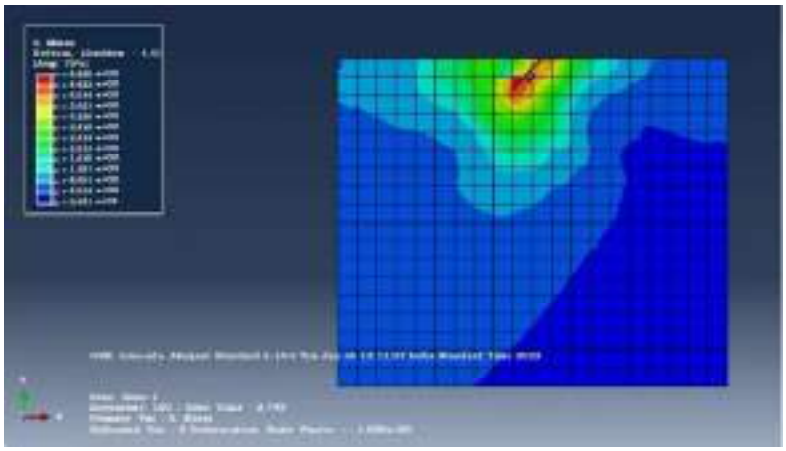

Fig. 4.517: Stress Contour for 50mm Square Plate with (H/B =2) at 45° inclination under 0.5 Hz frequency and 2mm amplitude

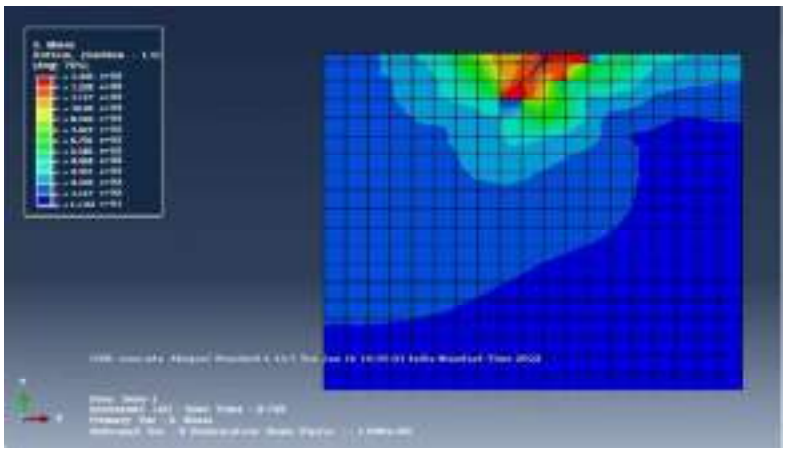

Fig. 4.518: Stress Contour for 50mm Square Plate with (H/B =3) at 45° inclination under 0.5 Hz frequency and 2mm amplitude

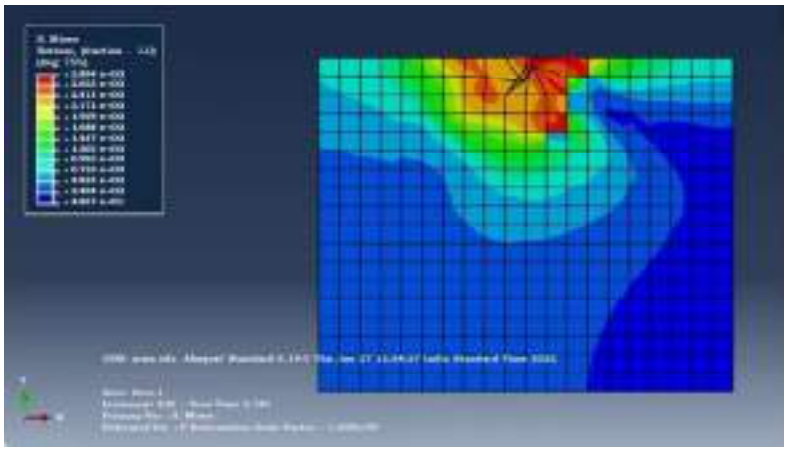

Fig. 4.519: Stress Contour for 50mm Square Plate with (H/B =1) at 60° inclination under 0.5 Hz frequency and 2mm amplitude

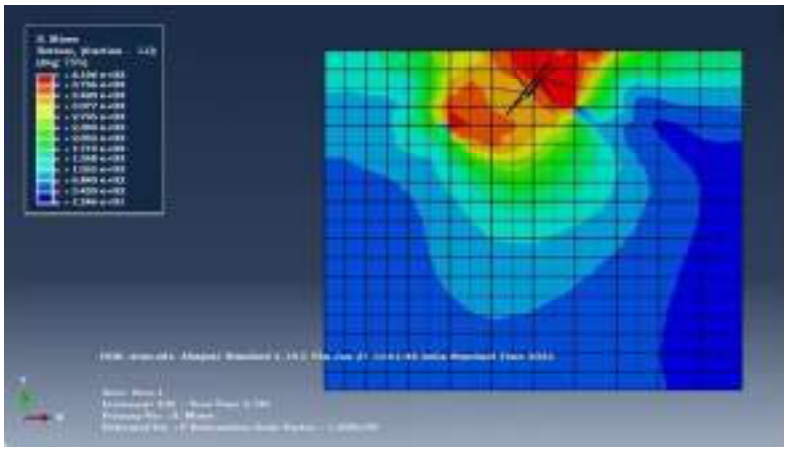

Fig. 4.520: Stress Contour for 50mm Square Plate with (H/B =2) at 60° inclination under 0.5 Hz frequency and 2mm amplitude

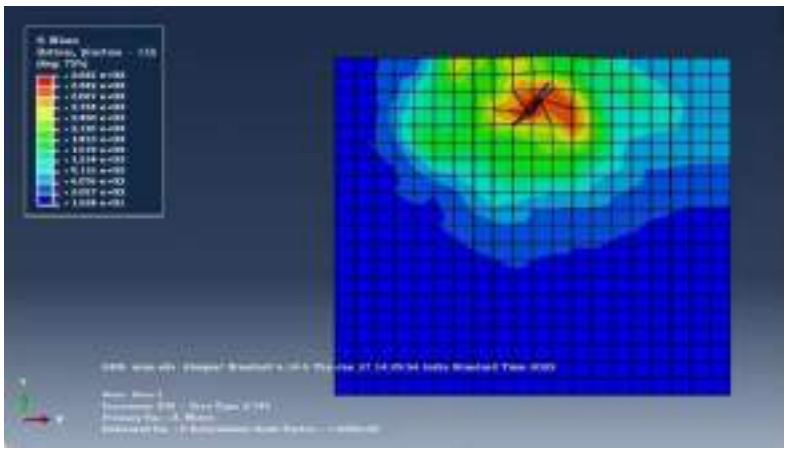

Fig. 4.521: Stress Contour for 50mm Square Plate with (H/B =3) at 60° inclination under 0.5 Hz frequency and 2mm amplitude

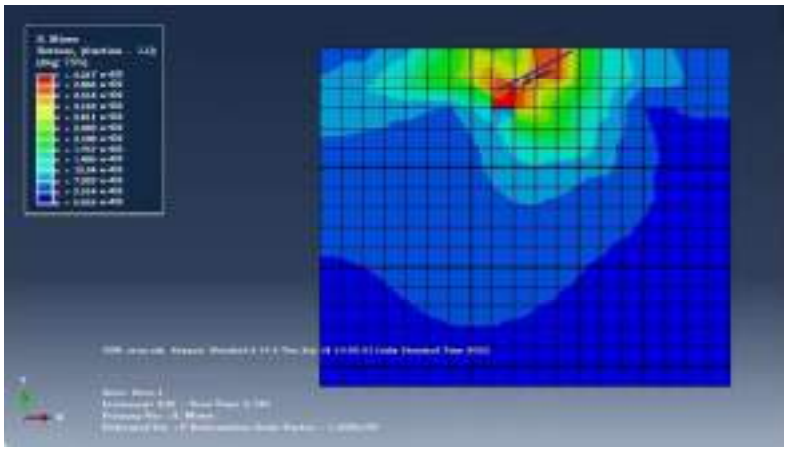

Fig. 4.522: Stress Contour for 75mm Square Plate with (H/B =1) at 30° inclination under 0.5 Hz frequency and 2mm amplitude

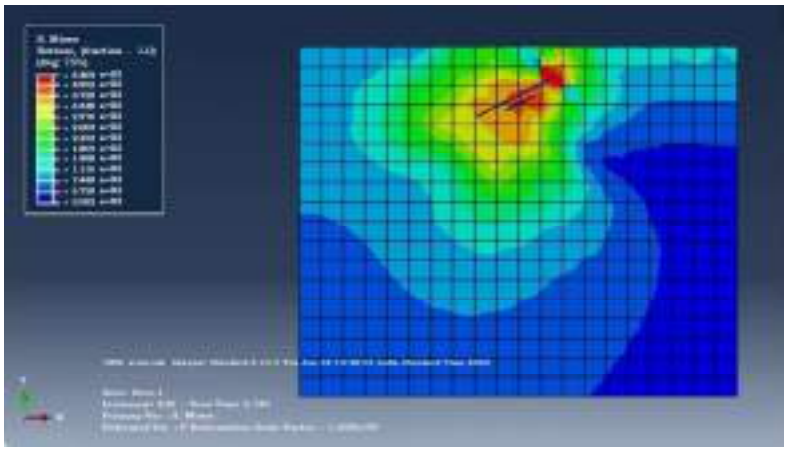

Fig. 4.523: Stress Contour for 75mm Square Plate with (H/B =2) at 30° inclination under 0.5 Hz frequency and 2mm amplitude

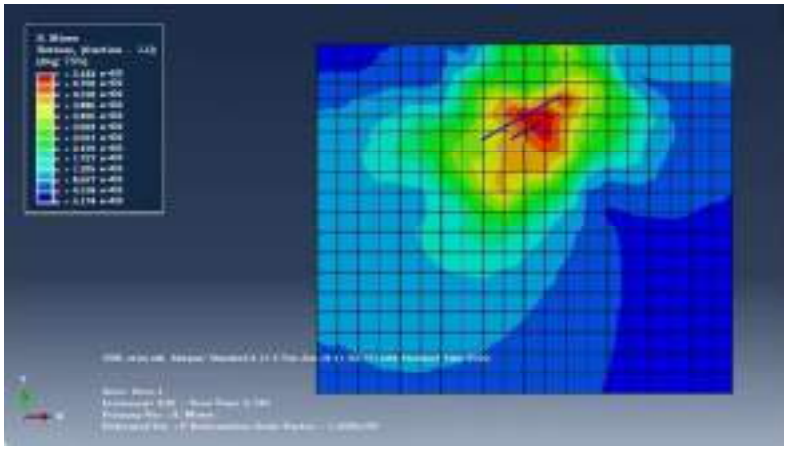

Fig. 4.524: Stress Contour for 75mm Square Plate with (H/B =3) at 30° inclination under 0.5 Hz frequency and 2mm amplitude

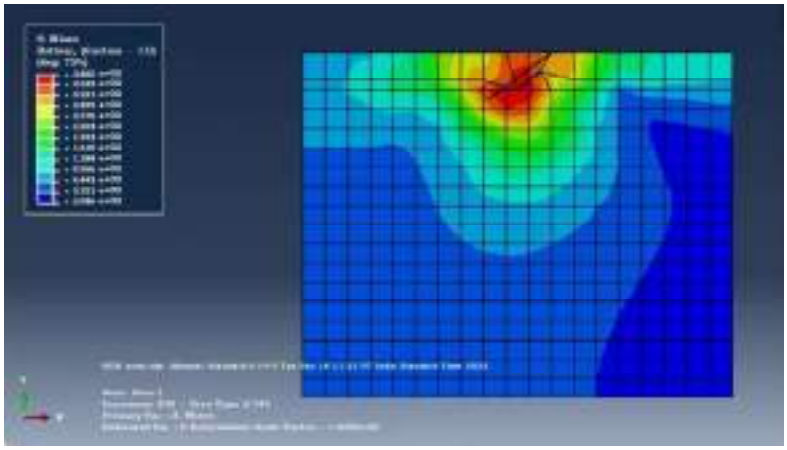

Fig. 4.525: Stress Contour for 75mm Square Plate with (H/B =1) at 45° inclination under 0.5 Hz frequency and 2mm amplitude

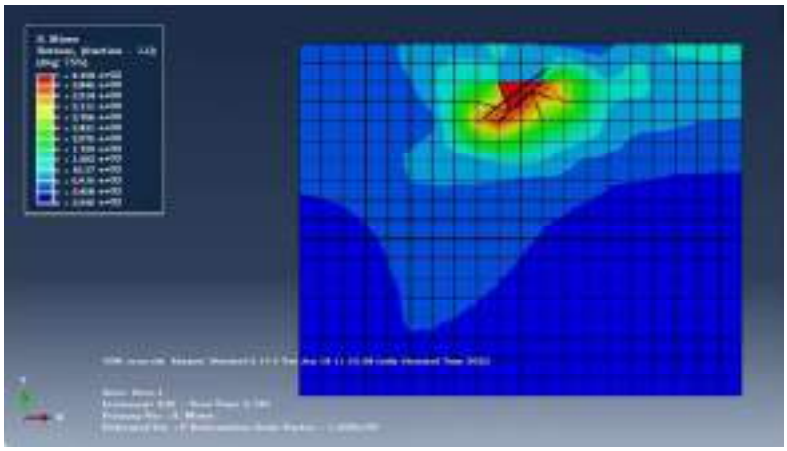

Fig. 4.526: Stress Contour for 75mm Square Plate with (H/B =2) at 45° inclination under 0.5 Hz frequency and 2mm amplitude

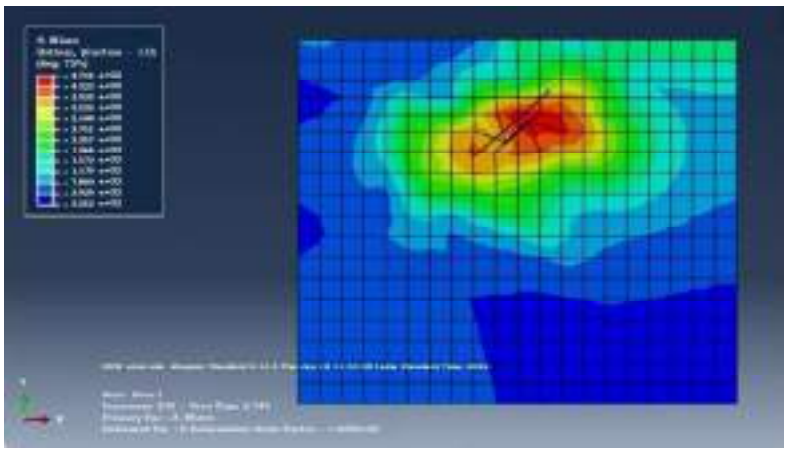

Fig. 4.527: Stress Contour for 75mm Square Plate with (H/B =3) at 45° inclination under 0.5 Hz frequency and 2mm amplitude

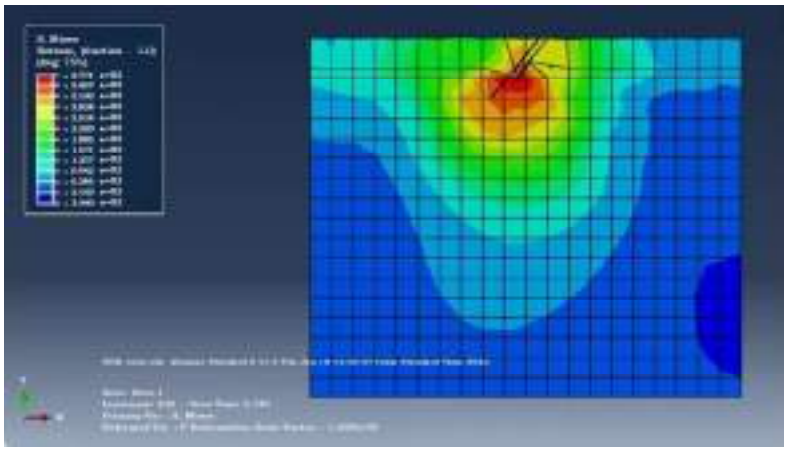

Fig. 4.528: Stress Contour for 75mm Square Plate with (H/B =1) at 60° inclination under 0.5 Hz frequency and 2mm amplitude

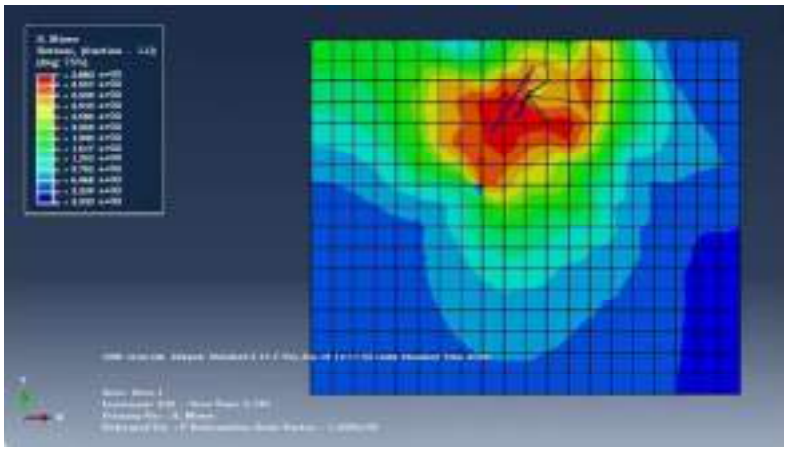

Fig. 4.529: Stress Contour for 75mm Square Plate with (H/B =2) at 60° inclination under 0.5 Hz frequency and 2mm amplitude

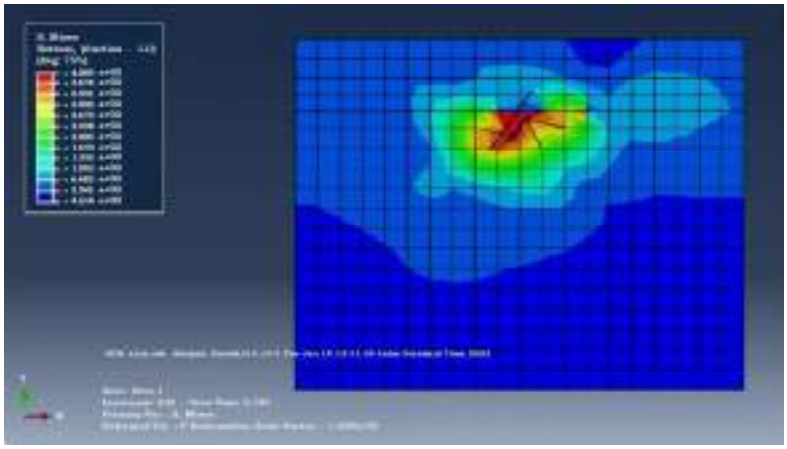

Fig. 4.530: Stress Contour for 75mm Square Plate with (H/B =3) at 60° inclination under 0.5 Hz frequency and 2mm amplitude

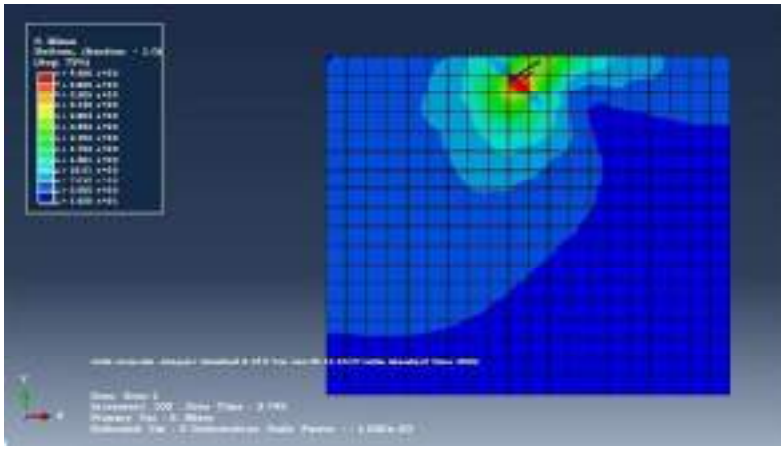

Fig. 4.531: Stress Contour for 25mm Square Plate with (H/B =1) at 30° inclination under 0.5 Hz frequency and 5mm amplitude

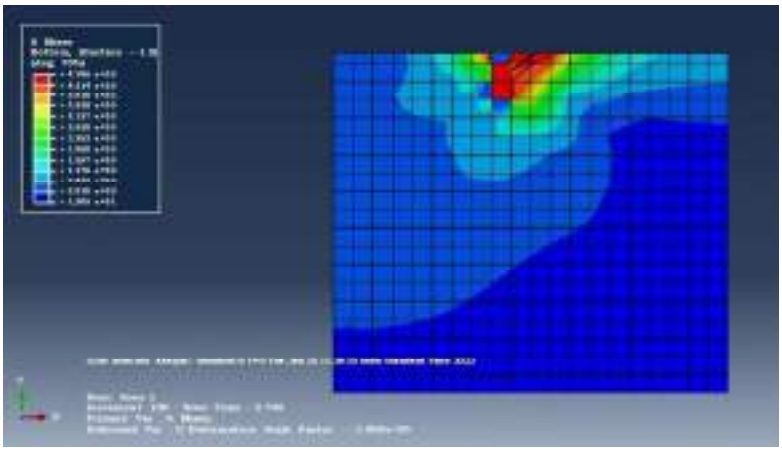

Fig. 4.532: Stress Contour for 25mm Square Plate with (H/B =2) at 30° inclination under 0.5 Hz frequency and 5mm amplitude

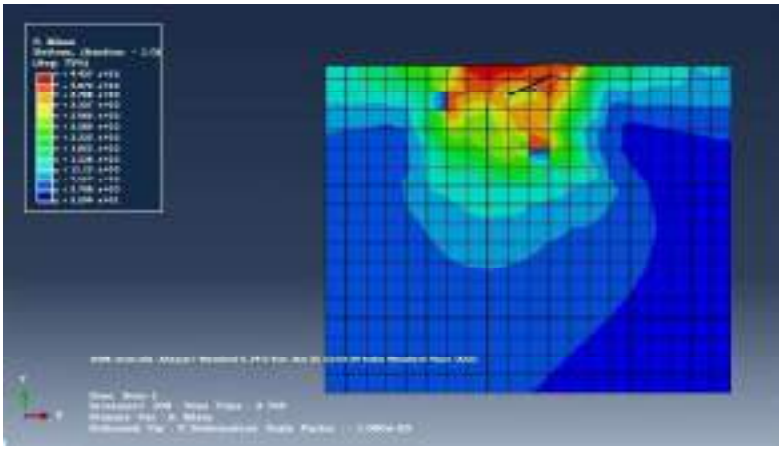

Fig. 4.533: Stress Contour for 25mm Square Plate with (H/B =3) at 30° inclination under 0.5 Hz frequency and 5mm amplitude

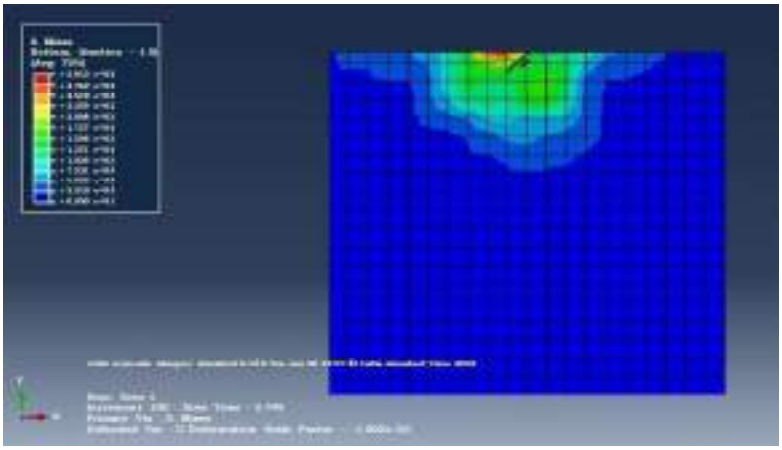

Fig. 4.534: Stress Contour for 25mm Square Plate with (H/B =1) at 45° inclination under 0.5 Hz frequency and 5mm amplitude

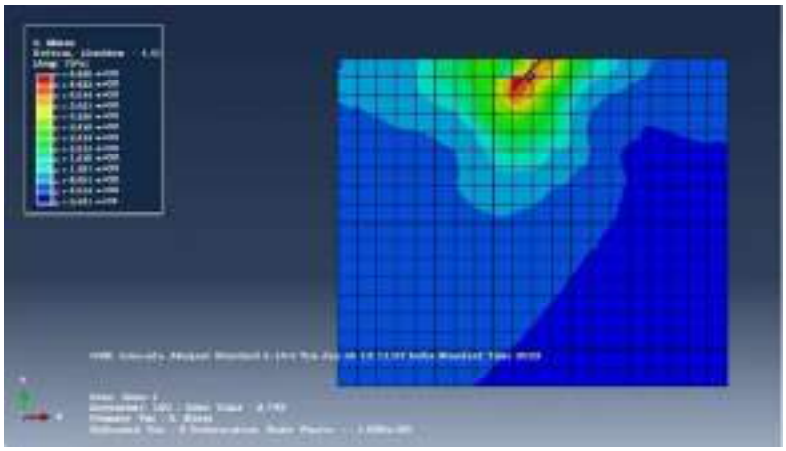

Fig. 4.535: Stress Contour for 25mm Square Plate with (H/B =2) at 45° inclination under 0.5 Hz frequency and 5mm amplitude

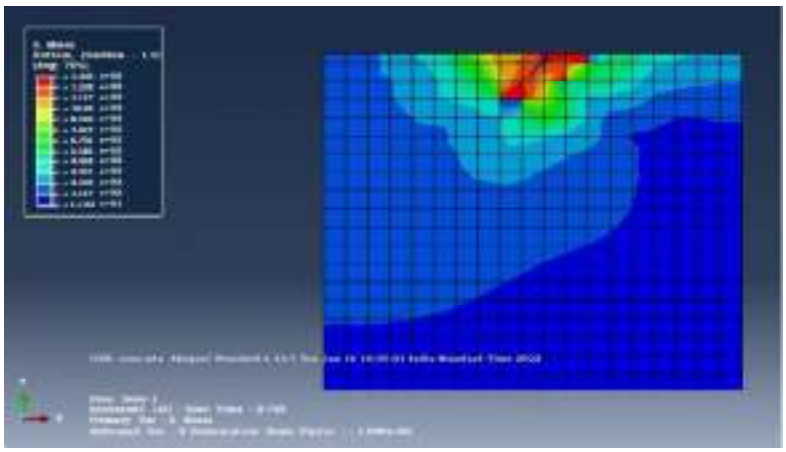

Fig. 4.536: Stress Contour for 25 mm Square Plate with (H/B =3) at 45° inclination under 0.5 Hz frequency and 5mm amplitude

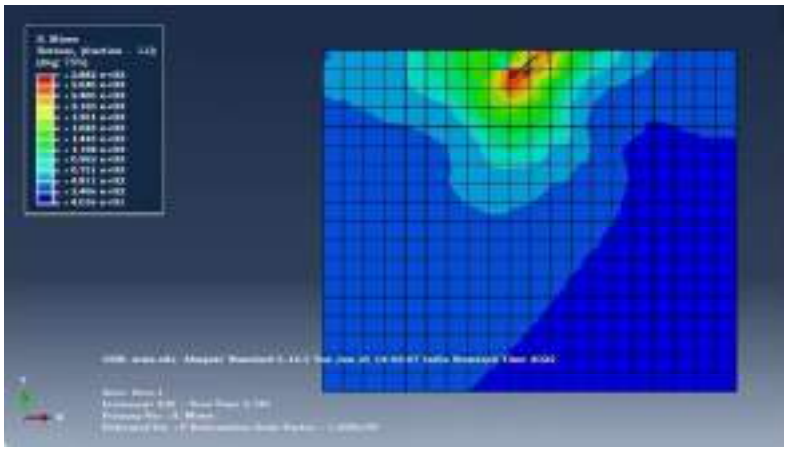

Fig. 4.537: Stress Contour for 25mm Square Plate with (H/B =1) at 60° inclination under 0.5 Hz frequency and 5mm amplitude

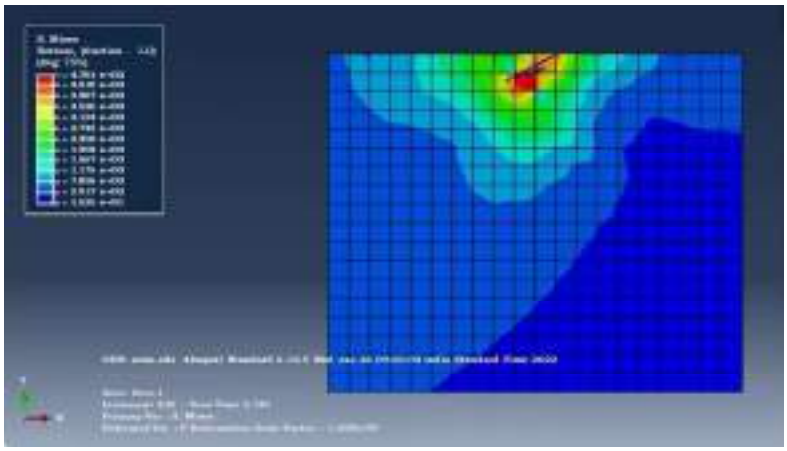

Fig. 4.538: Stress Contour for 25mm Square Plate with (H/B =2) at 60° inclination under 0.5 Hz frequency and 5mm amplitude

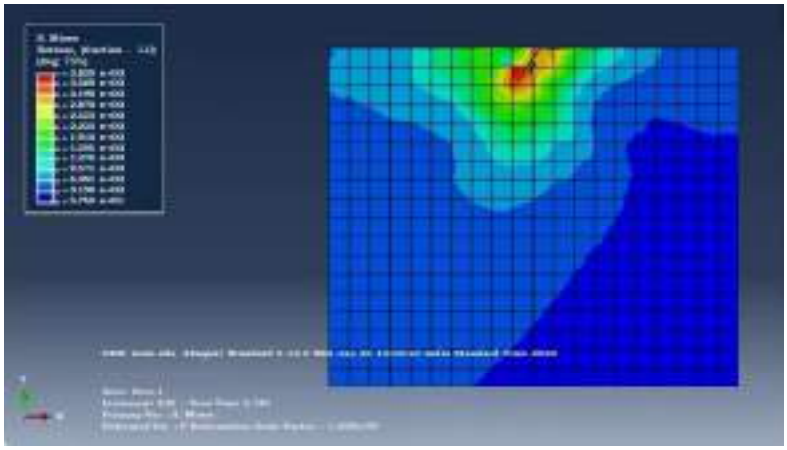

Fig. 4.539: Stress Contour for 25mm Square Plate with (H/B =3) at 60° inclination under 0.5 Hz frequency and 5mm amplitude

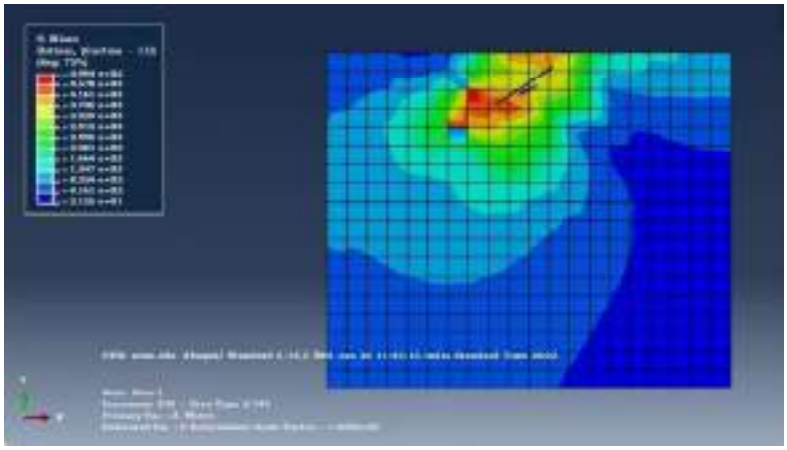

Fig. 4.540: Stress Contour for 50mm Square Plate with (H/B =1) at 30° inclination under 0.5 Hz frequency and 5mm amplitude

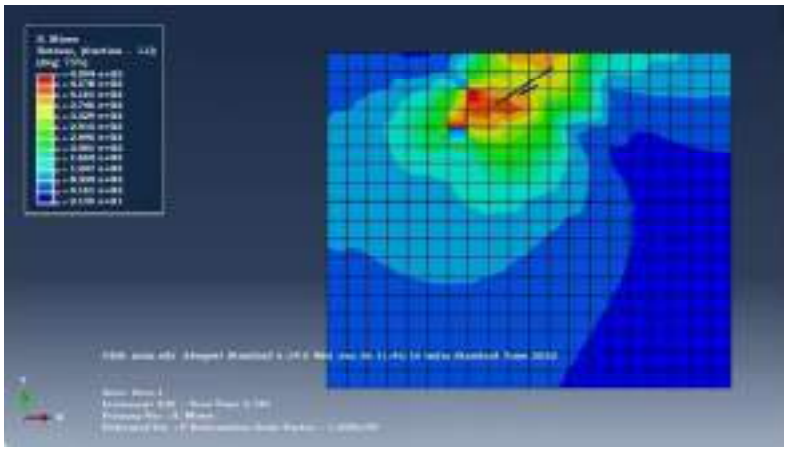

Fig. 4.541: Stress Contour for 50mm Square Plate with (H/B =2) at 30° inclination under 0.5 Hz frequency and 5mm amplitude

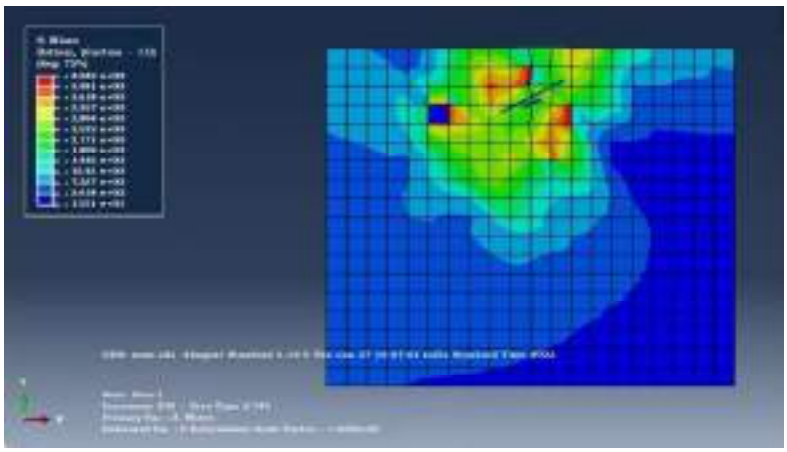

Fig. 4.542: Stress Contour for 50mm 50 mm Square Plate with (H/B =3) at 30° inclination under 0.5 Hz frequency and 5mm amplitude

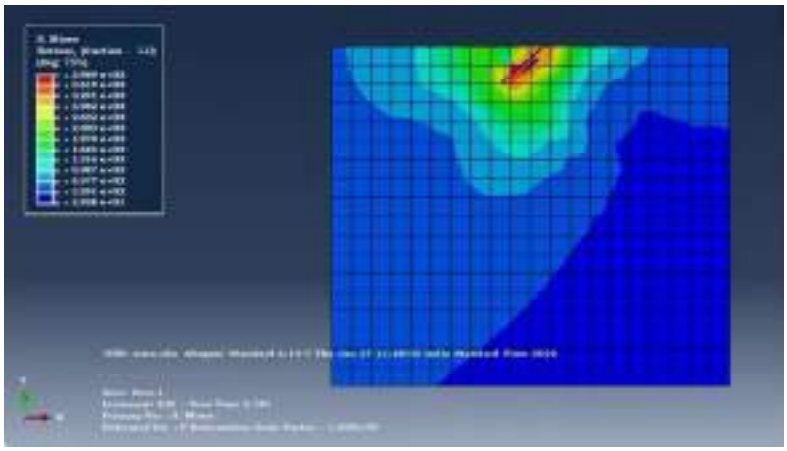

Fig. 4.543: Stress Contour for 50mm Square Plate with (H/B =1) at 45° inclination under 0.5 Hz frequency and 5mm amplitude

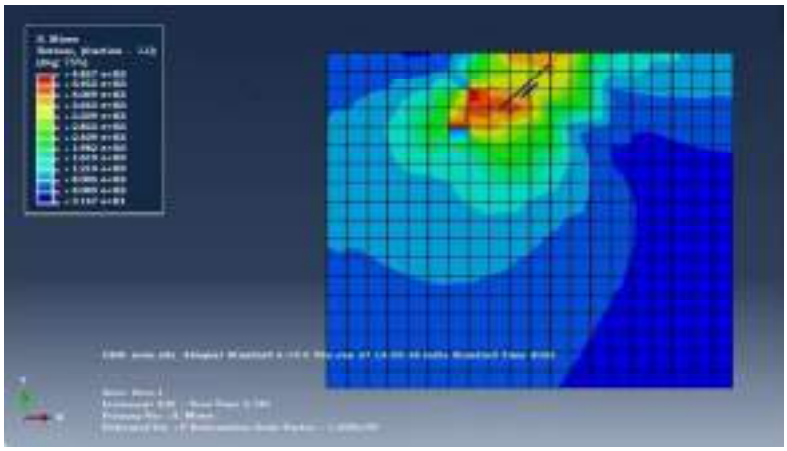

Fig. 4.544: Stress Contour for 50mm Square Plate with (H/B =2) at 45° inclination under 0.5 Hz frequency and 5mm amplitude

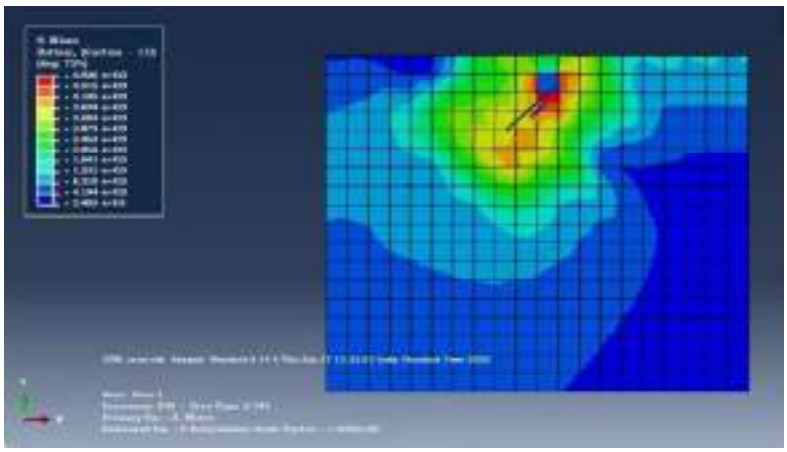

Fig. 4.545: Stress Contour for 50mm Square Plate with (H/B =3) at 45° inclination under 0.5 Hz frequency and 5mm amplitude

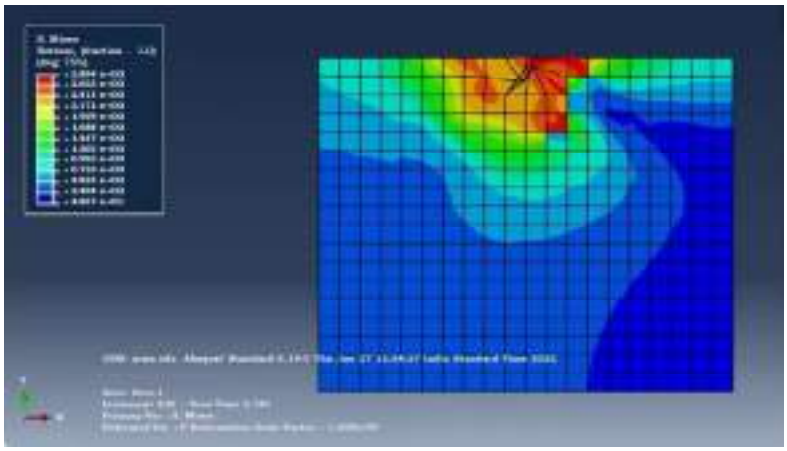

Fig. 4.546: Stress Contour for 50mm Square Plate with (H/B =1) at 60° inclination under 0.5 Hz frequency and 5mm amplitude

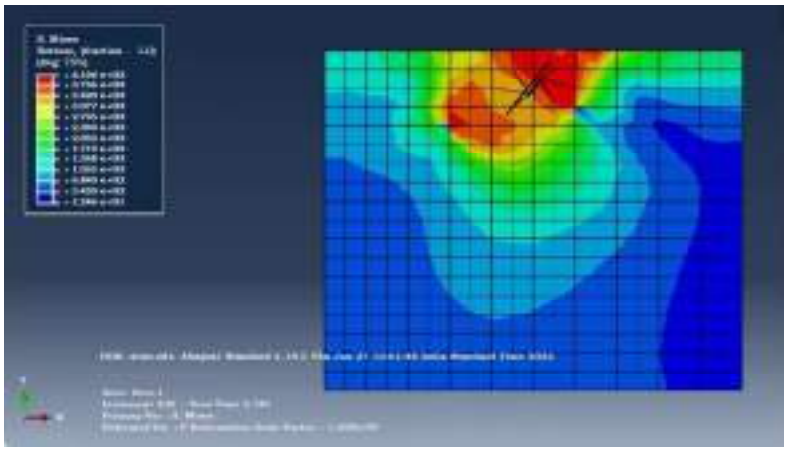

Fig. 4.547: Stress Contour for 50mm Square Plate with (H/B =2) at 60° inclination under 0.5 Hz frequency and 5mm amplitude

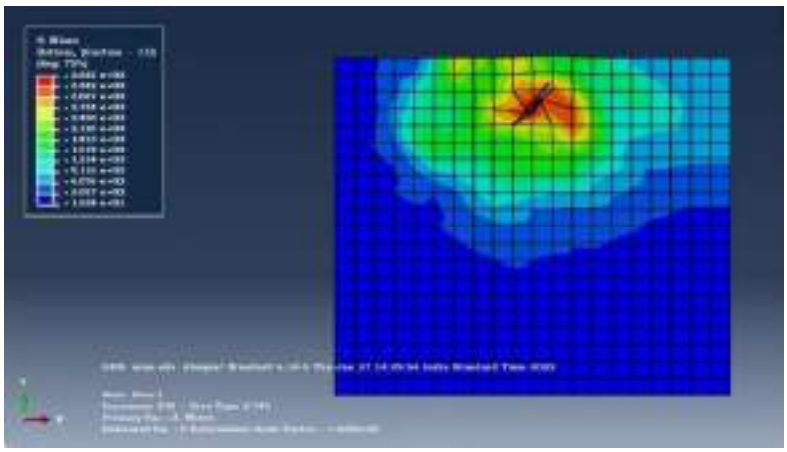

Fig. 4.548: Stress Contour for 50mm Square Plate with (H/B =3) at 60° inclination under 0.5 Hz frequency and 5mm amplitude

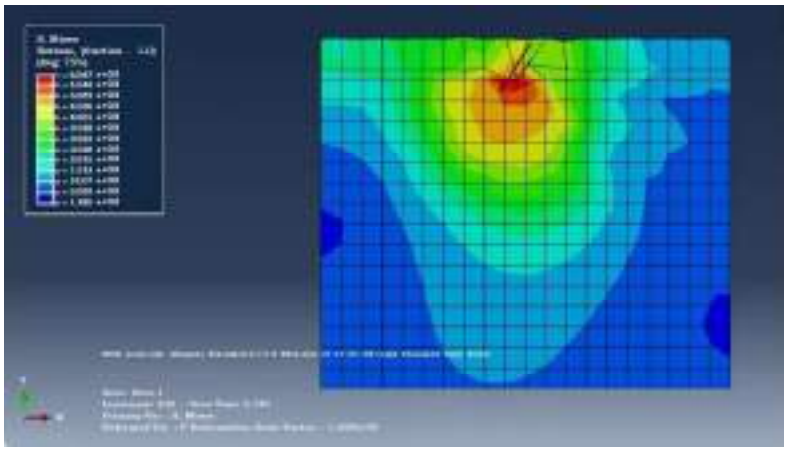

Fig. 4.549: Stress Contour for 75mm Square Plate with (H/B =1) at 30° inclination under 0.5 Hz frequency and 5mm amplitude

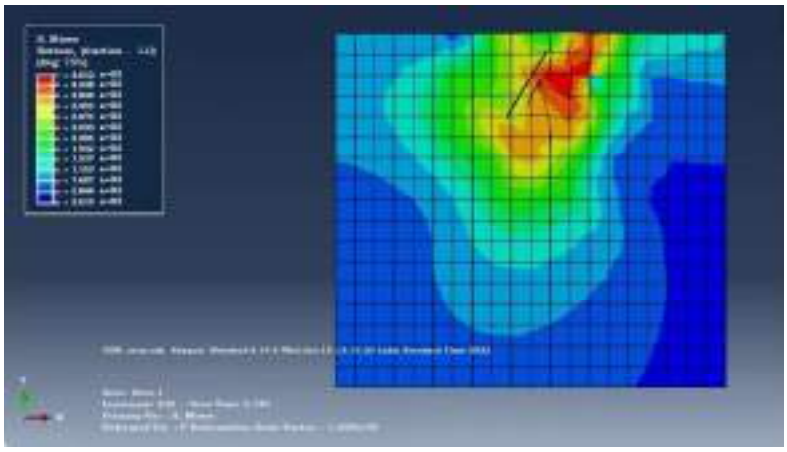

Fig. 4.550: Stress Contour for 75mm Square Plate with (H/B =2) at 30° inclination under 0.5 Hz frequency and 5mm amplitude

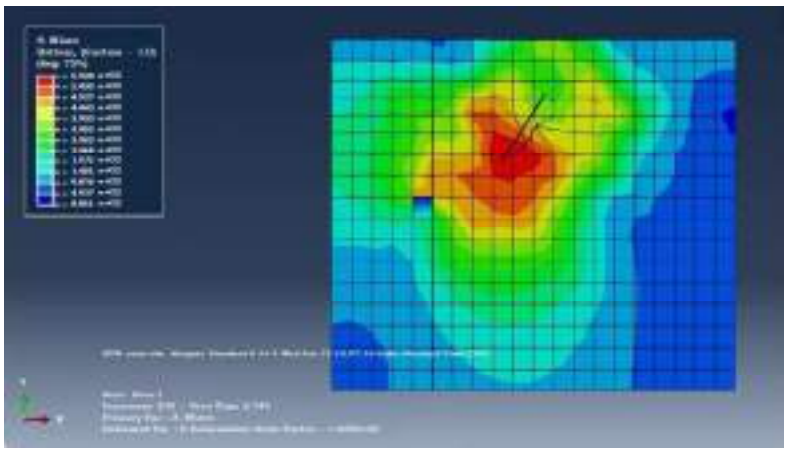

Fig. 4.551: Stress Contour for 75mm Square Plate with (H/B =3) at 30° inclination under 0.5 Hz frequency and 5mm amplitude

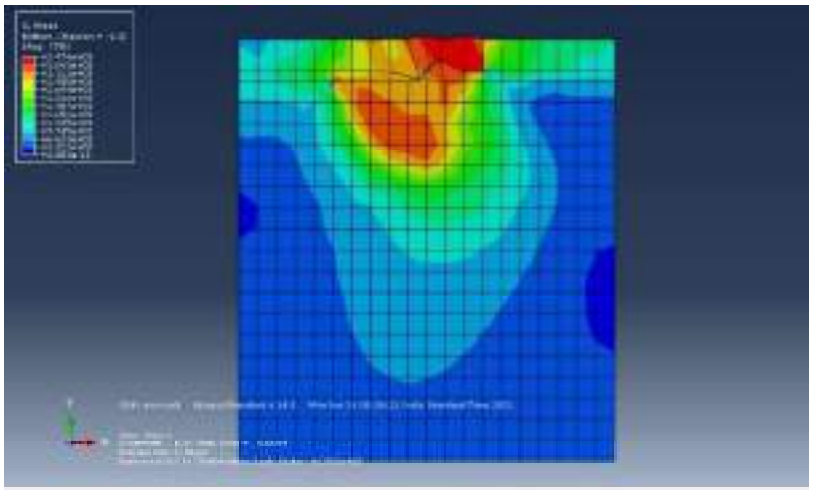

Fig. 4.552: Stress Contour for 75mm Square Plate with (H/B =1) at 45° inclination under 0.5 Hz frequency and 5mm amplitude

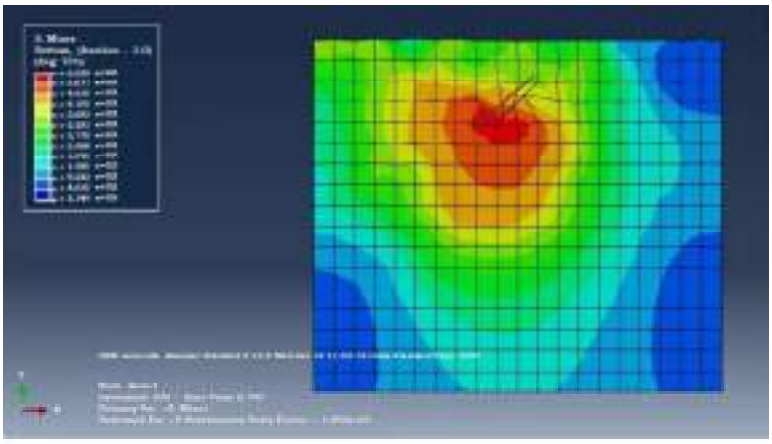

Fig. 4.553: Stress Contour for 75mm Square Plate with (H/B =2) at 45° inclination under 0.5 Hz frequency and 5mm amplitude

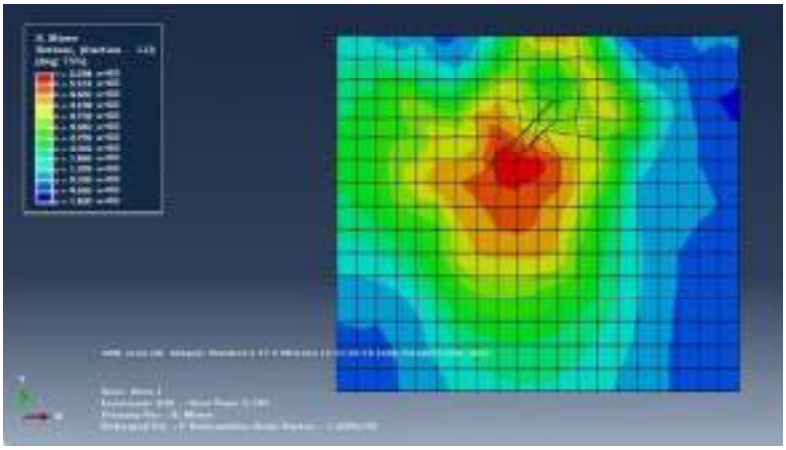

Fig. 4.554: Stress Contour for 75mm Square Plate with (H/B =3) at 45° inclination under 0.5 Hz frequency and 5mm amplitude

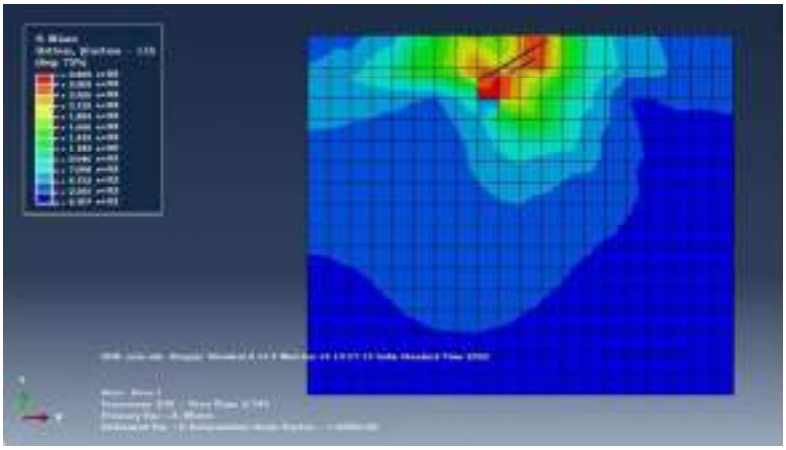

Fig. 4.555: Stress Contour for 75mm Square Plate with (H/B =1) at 60° inclination under 0.5 Hz frequency and 5mm amplitude

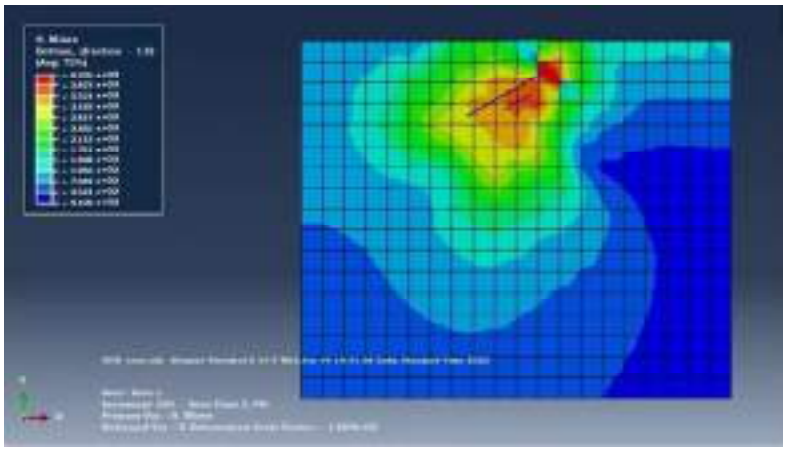

Fig. 4.556: Stress Contour for 75mm Square Plate with (H/B =2) at 60° inclination under 0.5 Hz frequency and 5mm amplitude

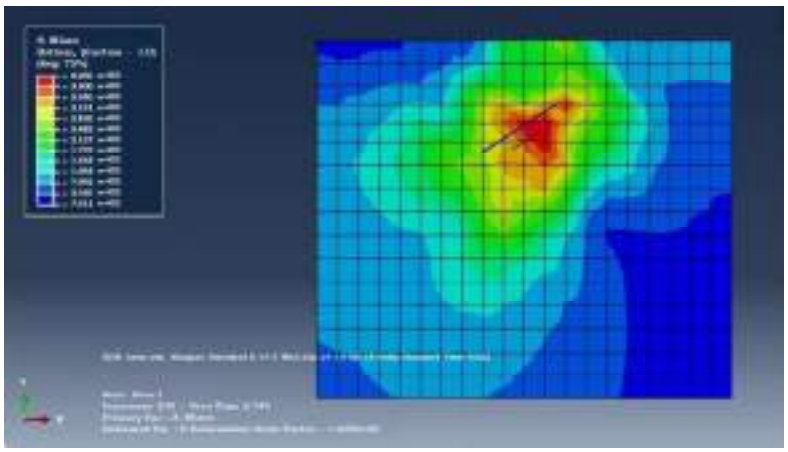

Fig. 4.557: Stress Contour for 75mm Square Plate with (H/B =3) at 60° inclination under 0.5 Hz frequency and 5mm amplitude

ANNEXURE -VI

PRESENTATION OF RESULTS OF EXPERIMENTAL STUDY (STATIC UNREINFORCED)

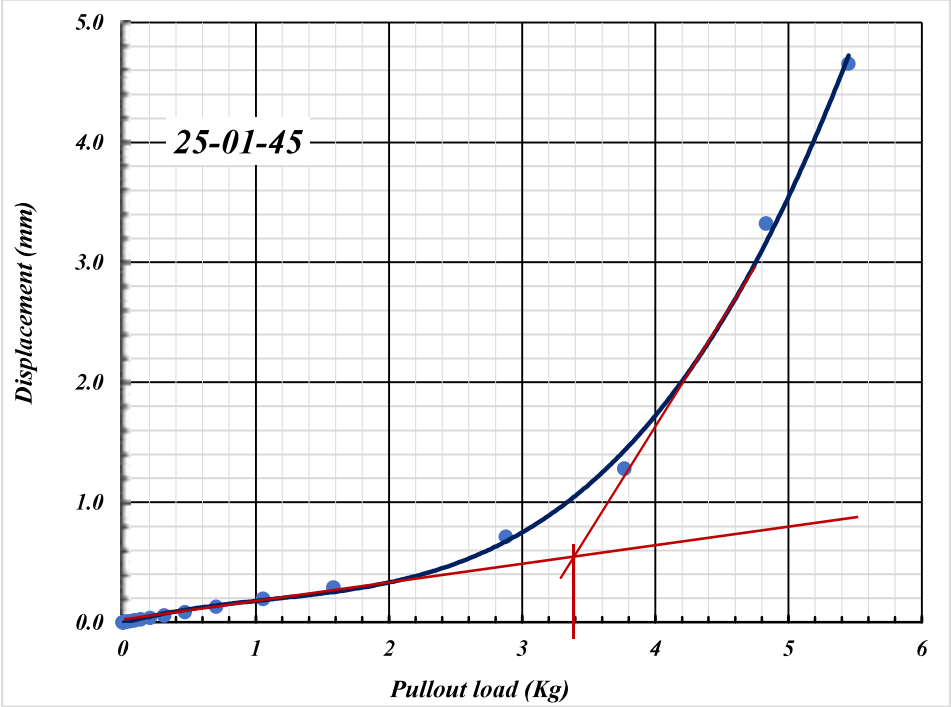

Fig. 5.10: Load vs Axial Movement for 25 mm Square Plate with (H/B =1) at 45^0 inclination

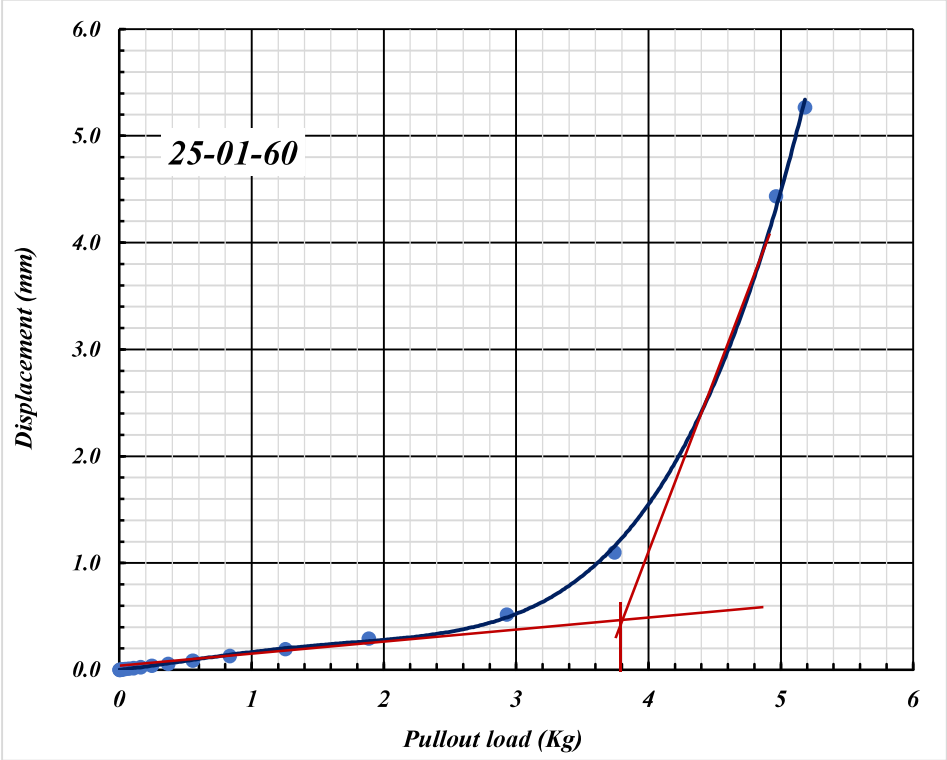

Fig. 5.11: Load vs Axial Movement for 25 mm Square Plate with (H/B =1) at 60^0 inclination

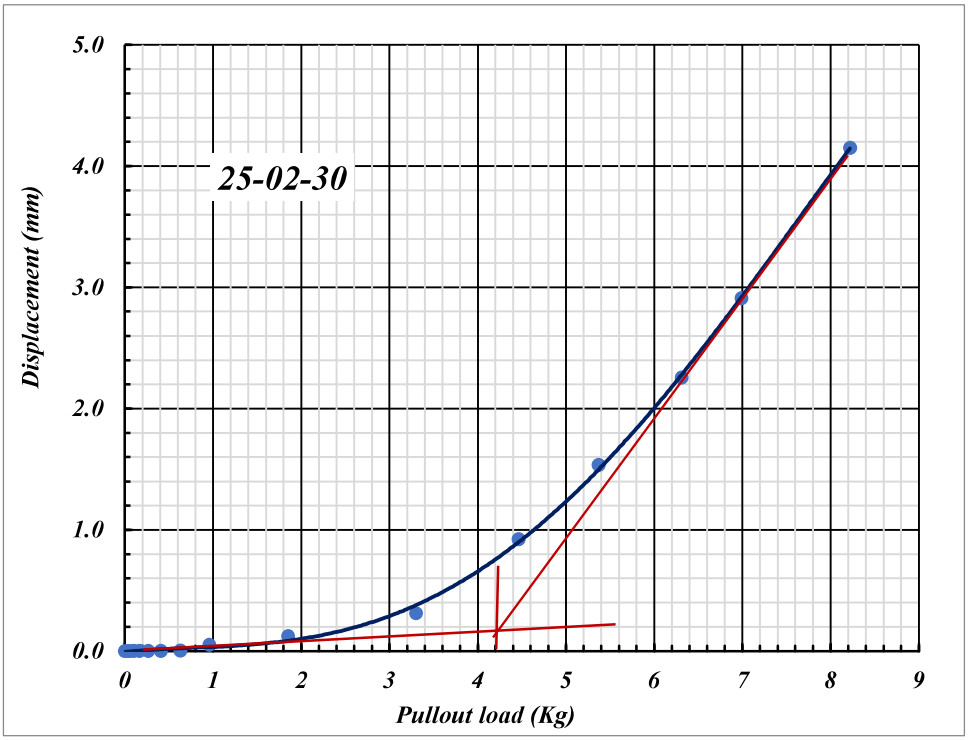

Fig. 5.12: Load vs Axial Movement for 25 mm Square Plate with (H/B =2) at 30^0 inclination

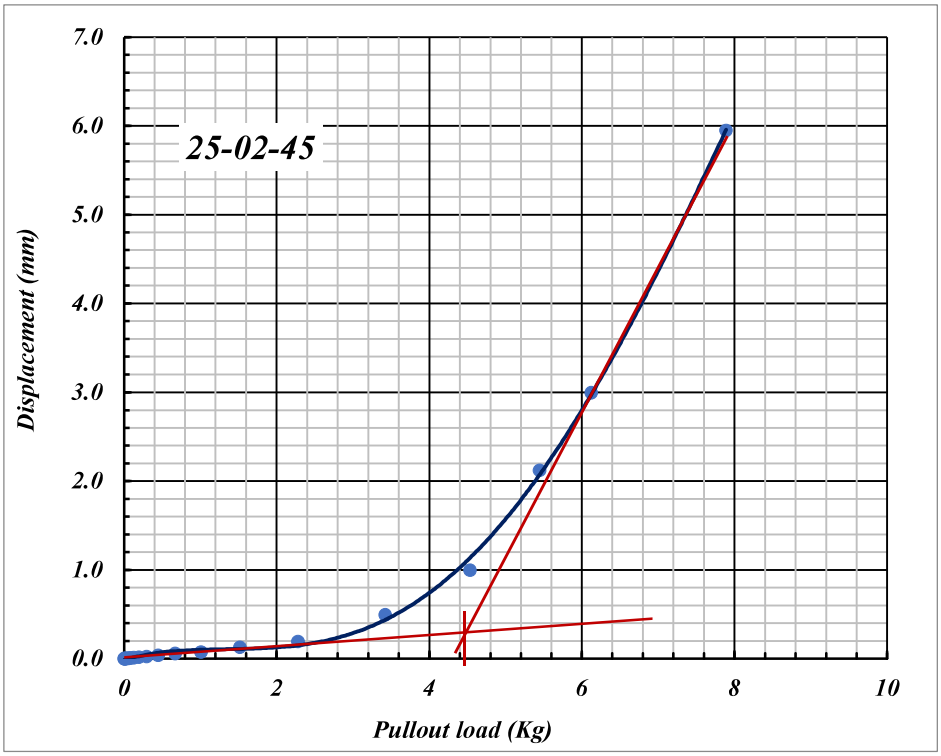

Fig. 5.13: Load vs Axial Movement for 25 mm Square Plate with (H/B =2) at 45^0 inclination

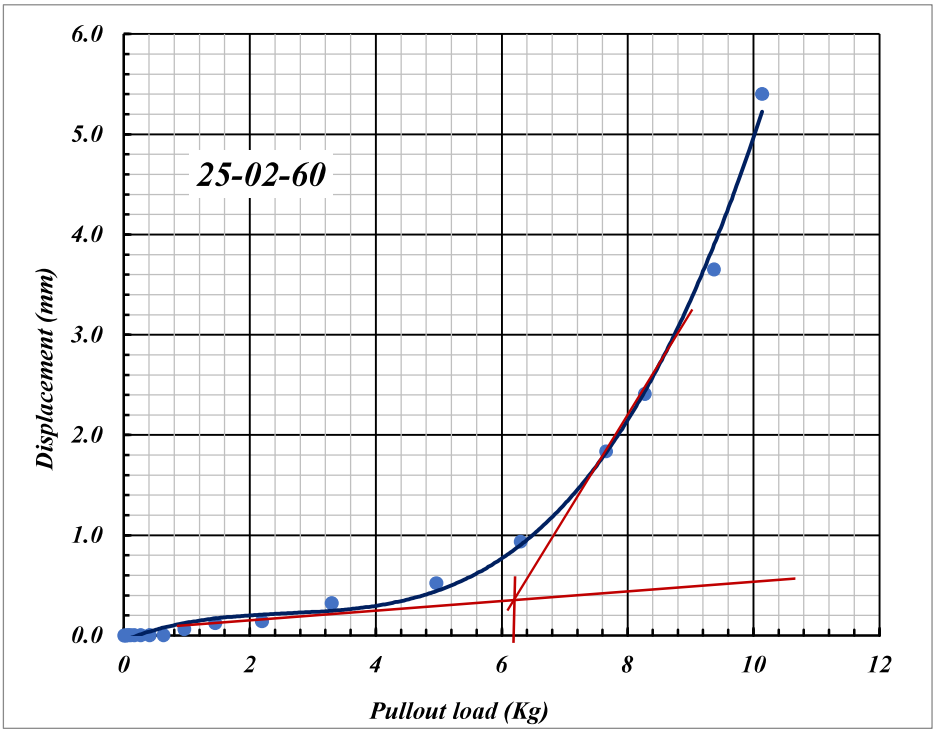

Fig. 5.14: Load vs Axial Movement for 25 mm Square Plate with (H/B =2) at 60^0 inclination

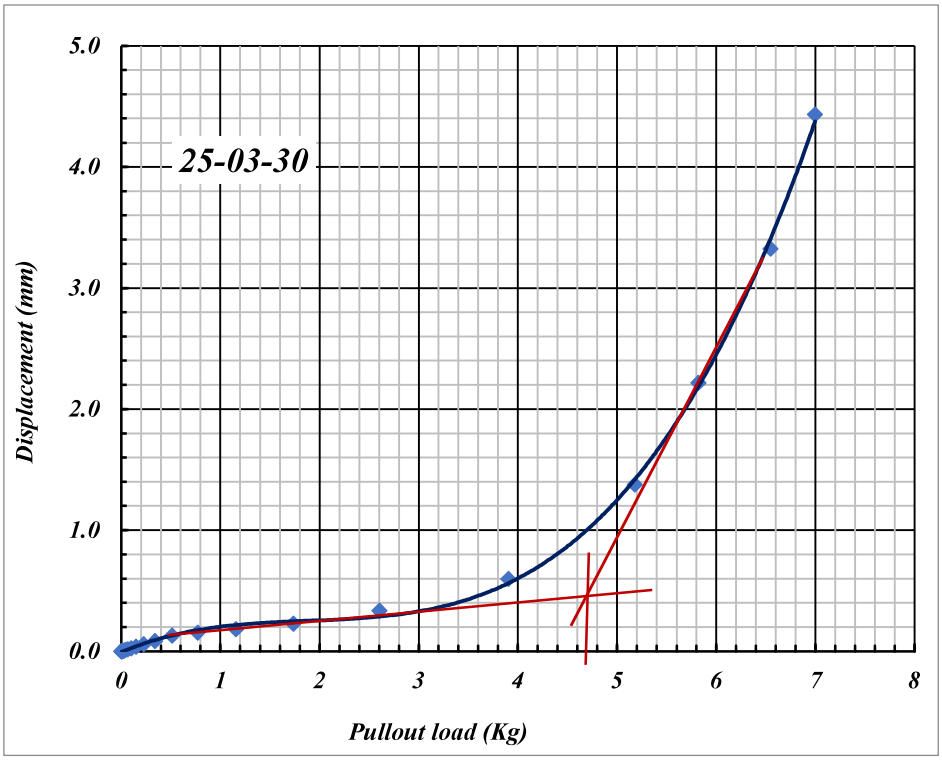

Fig. 5.15: Load vs Axial Movement for 25 mm Square Plate with (H/B =3) at 30^0 inclination

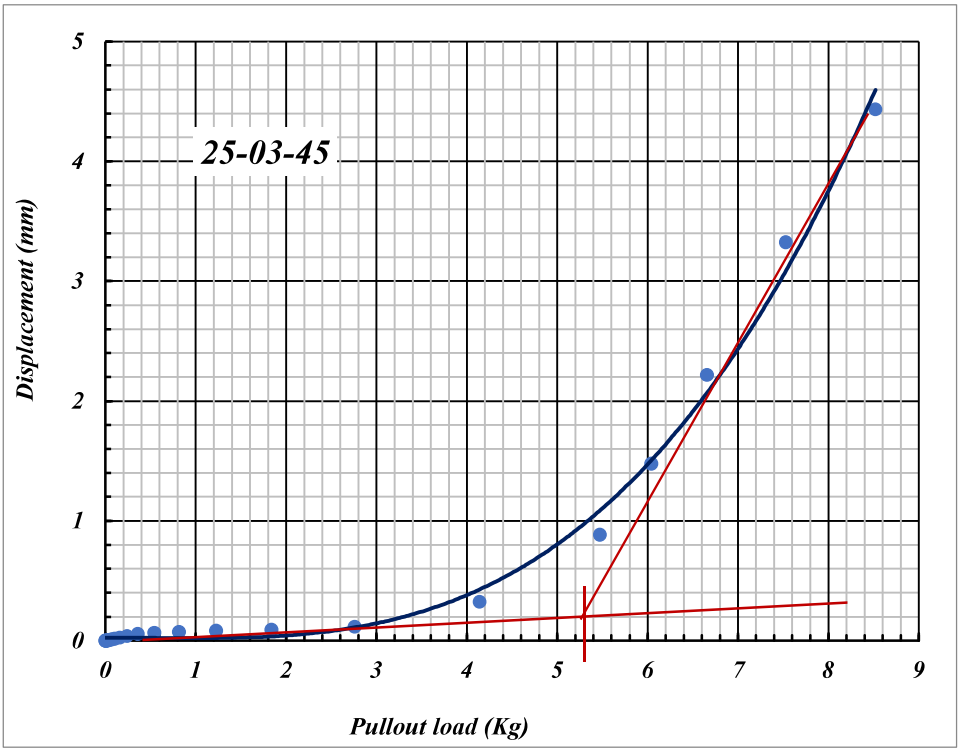

Fig. 5.16: Load vs Axial Movement for 25 mm Square Plate with (H/B =3) at 45^0 inclination

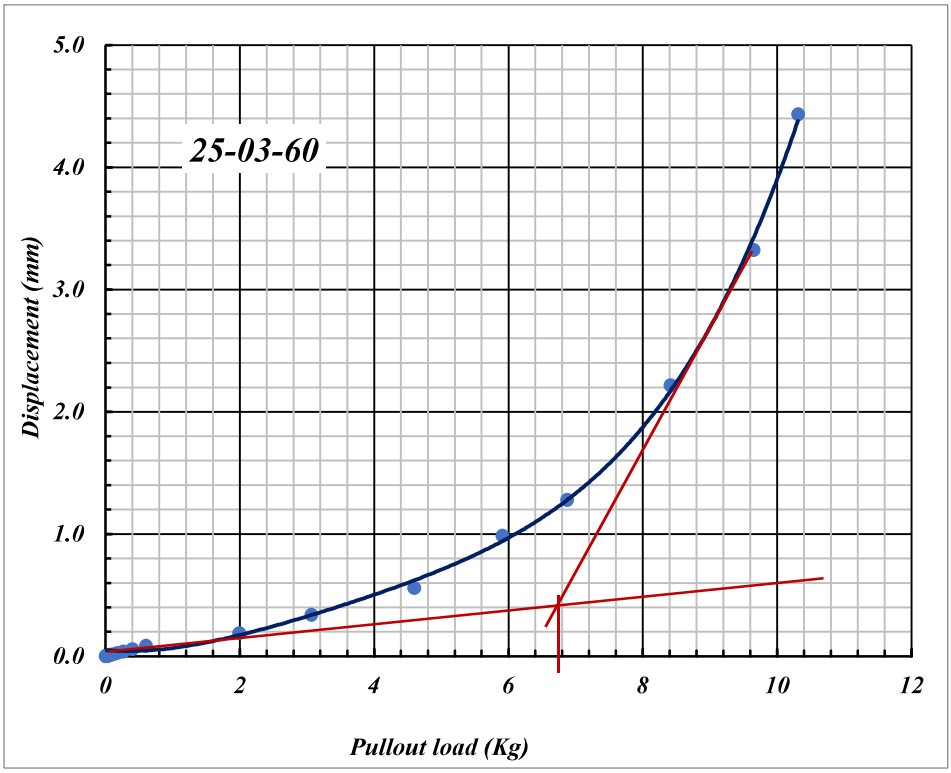

Fig. 5.17: Load vs Axial Movement for 25 mm Square Plate with (H/B =3) at 60^0 inclination

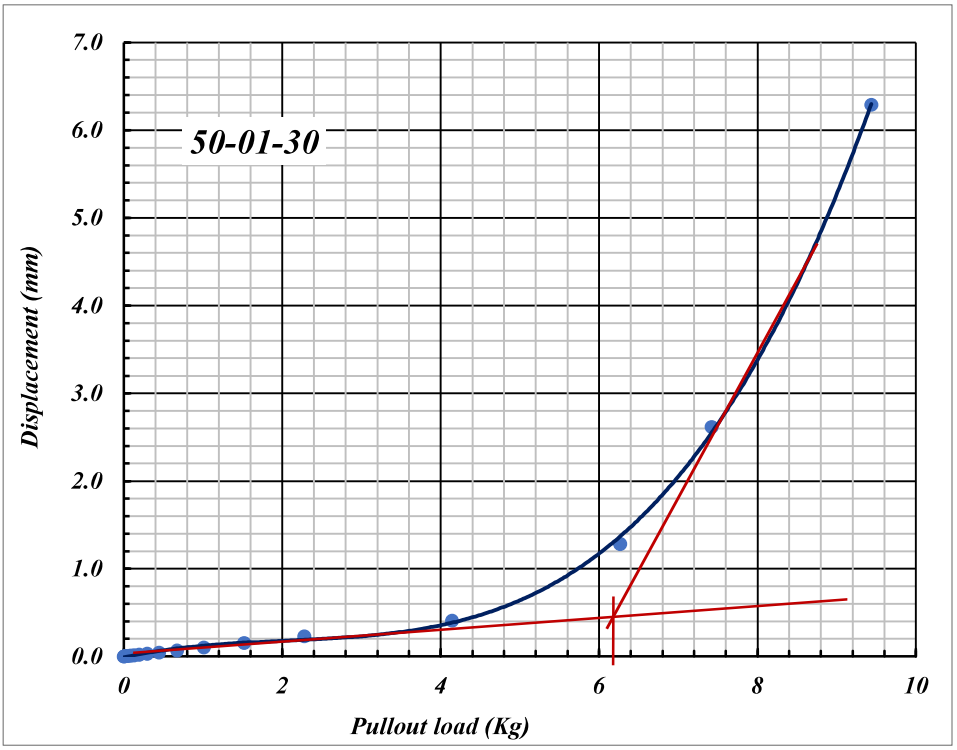

Fig. 5.18: Load vs Axial Movement for 50 mm Square Plate with (H/B =1) at 30^0 inclination

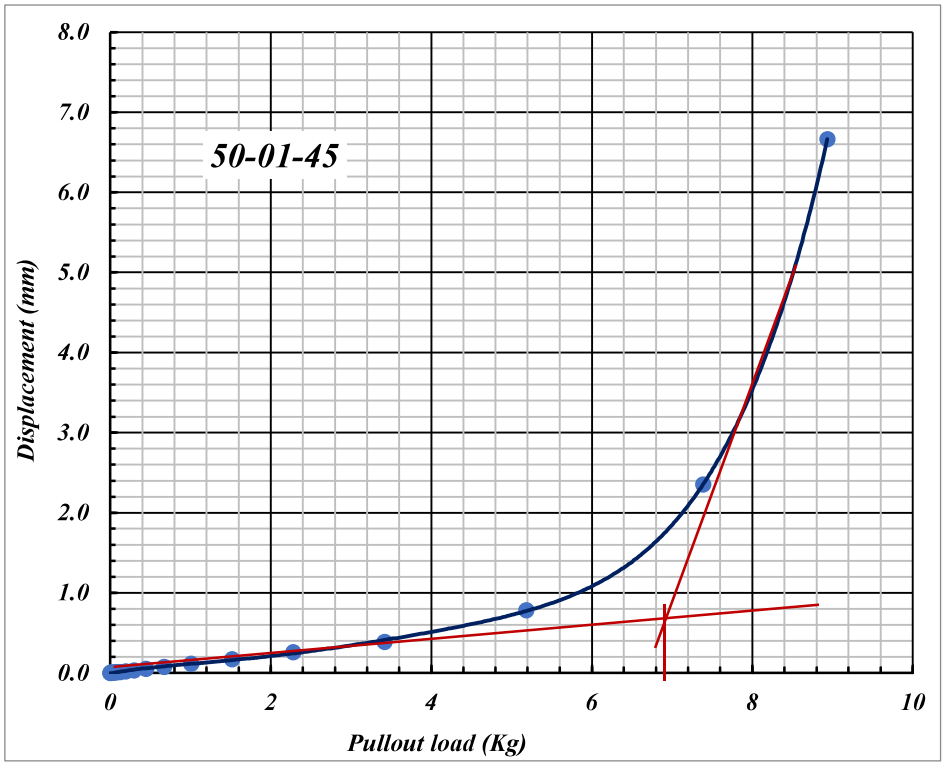

Fig. 5.19: Load vs Axial Movement for 50 mm Square Plate with (H/B =1) at 45^0 inclination

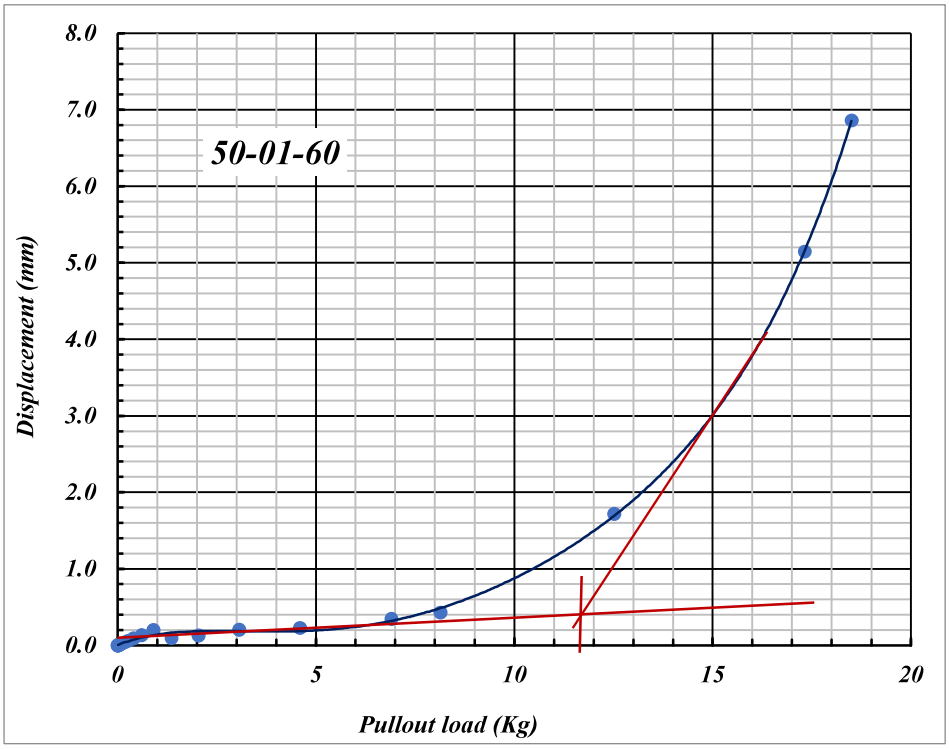

Fig. 5.20: Load vs Axial Movement for 50 mm Square Plate with (H/B =1) at 60^0 inclination

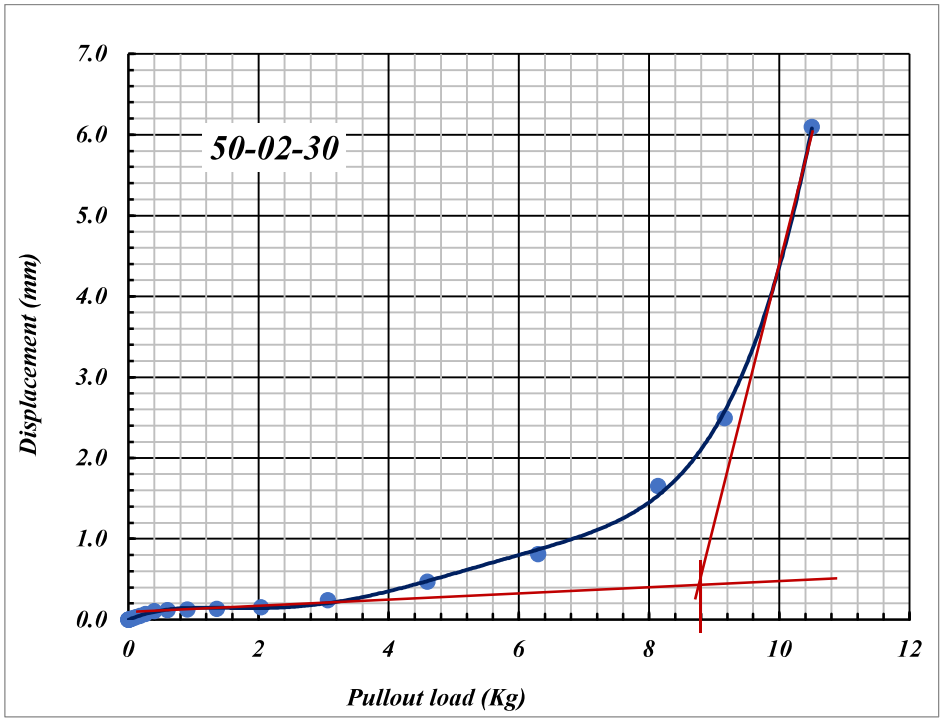

Fig. 5.21: Load vs Axial Movement for 50 mm Square Plate with (H/B =2) at 30^0 inclination

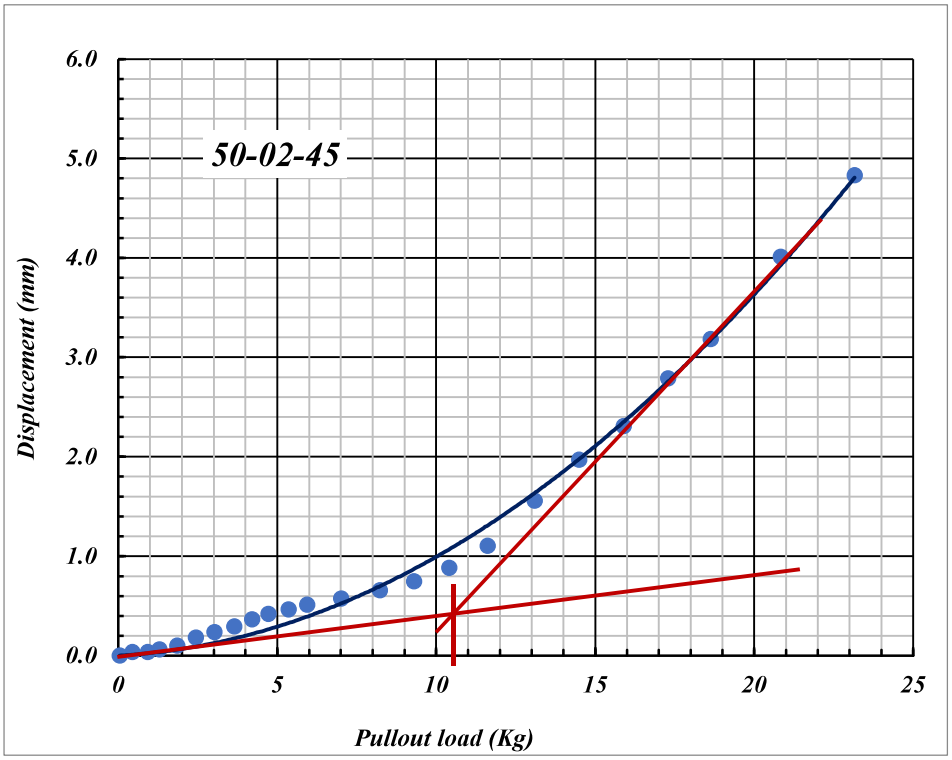

Fig. 5.22: Load vs Axial Movement for 50mm Square Plate with (H/B =2) at 45^0 inclination

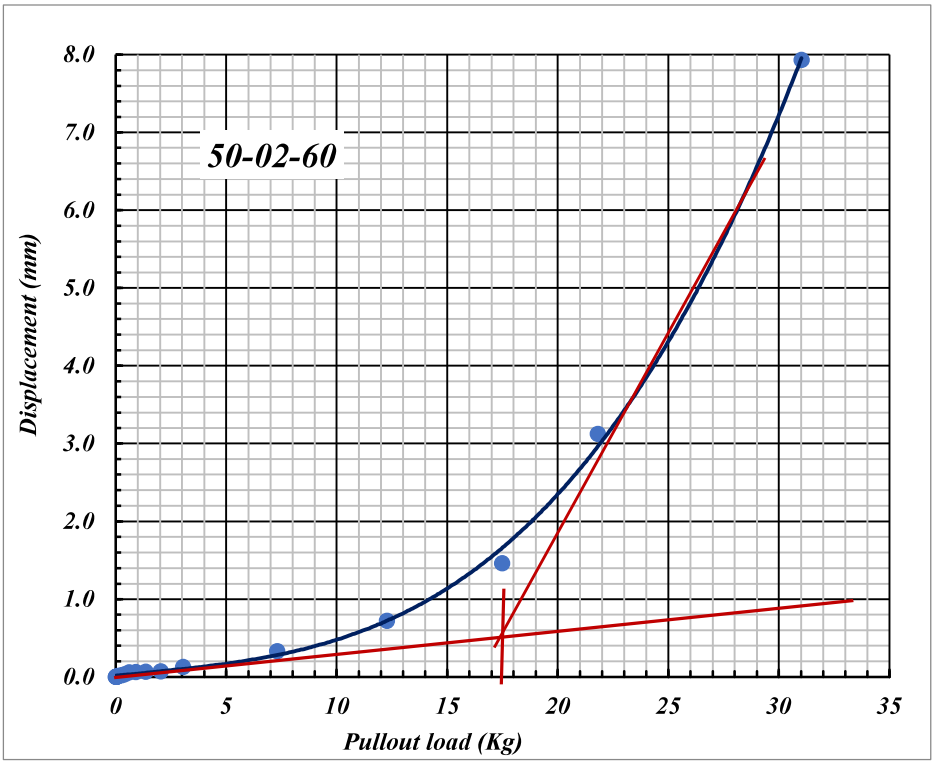

Fig. 5.23: Load vs Axial Movement for 50mm Square Plate with (H/B =2) at 60^0 inclination

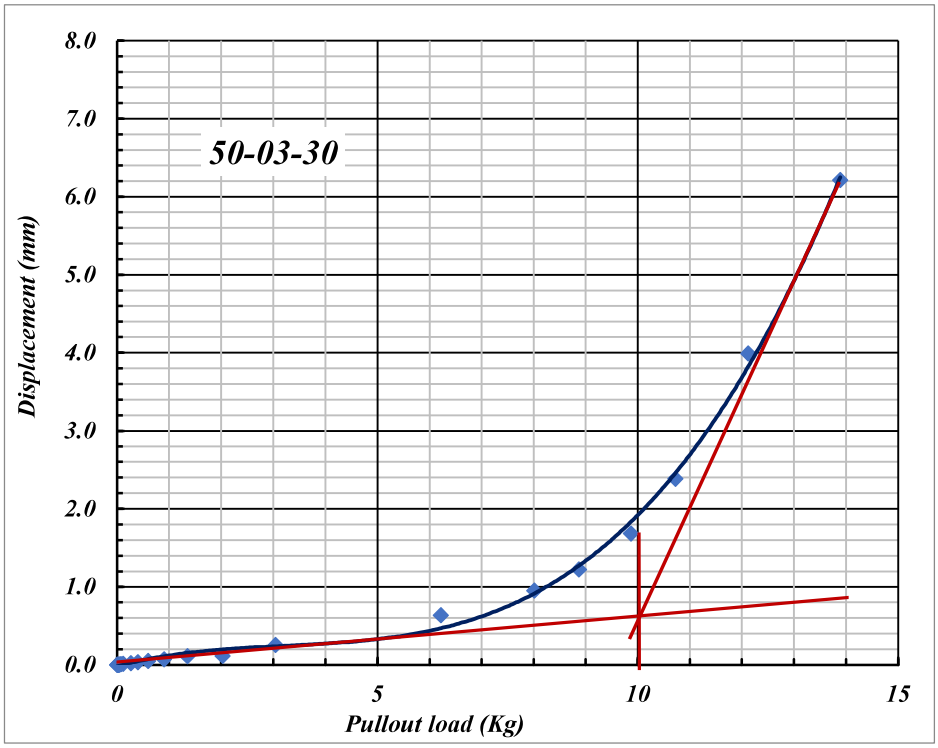

Fig. 5.24: Load vs Axial Movement for 50 mm Square Plate with (H/B =3) at 30^0 inclination

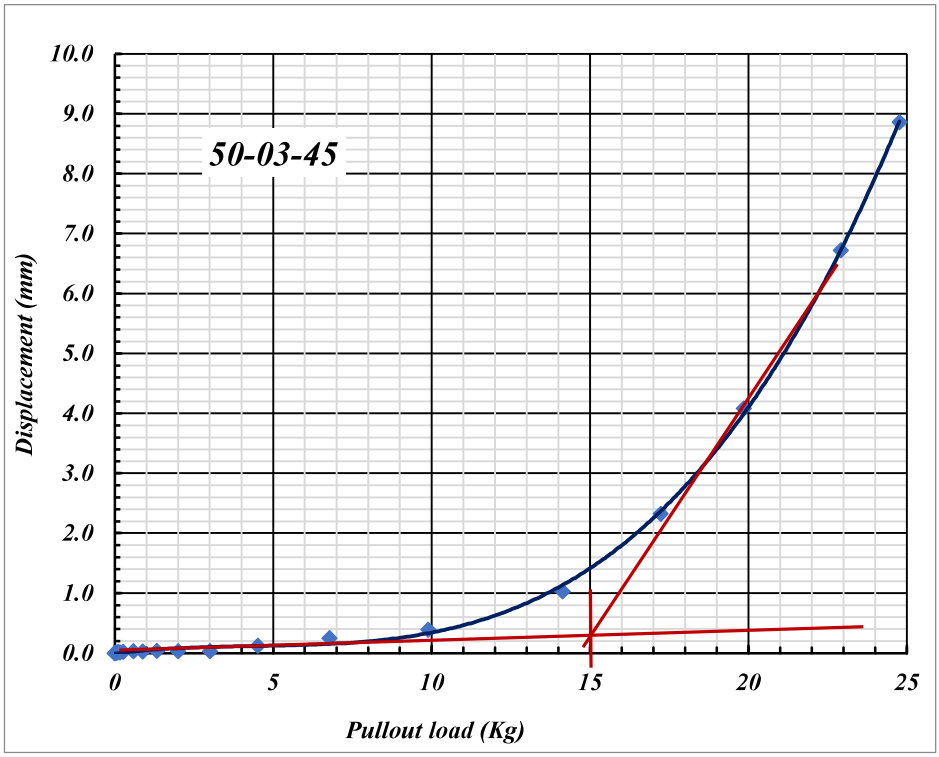

Fig. 5.25: Load vs Axial Movement for 50 mm Square Plate with (H/B =3) at 45^0 inclination

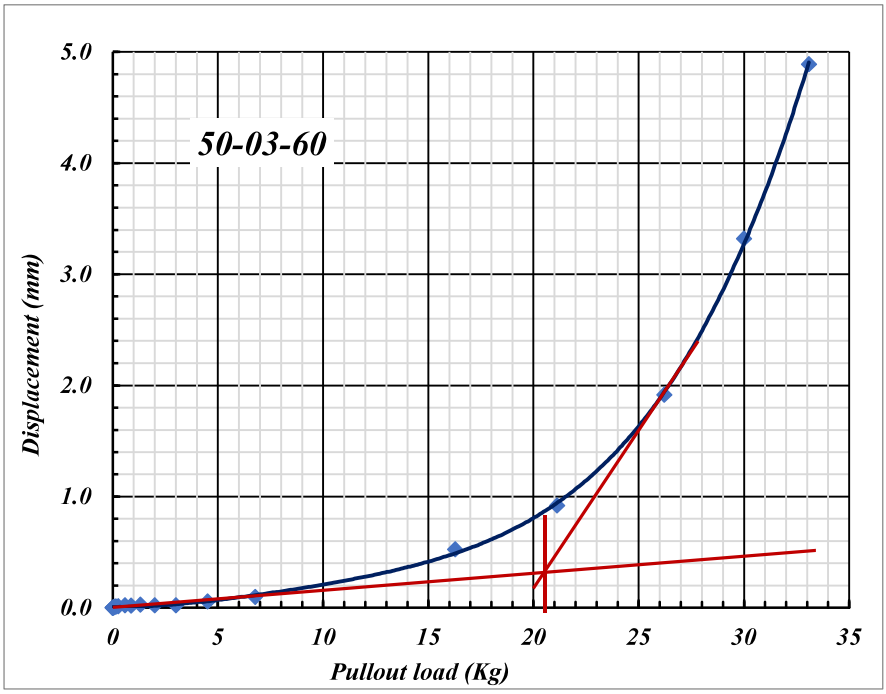

Fig. 5.26: Load vs Axial Movement for 50 mm Square Plate with (H/B =3) at 60^0 inclination

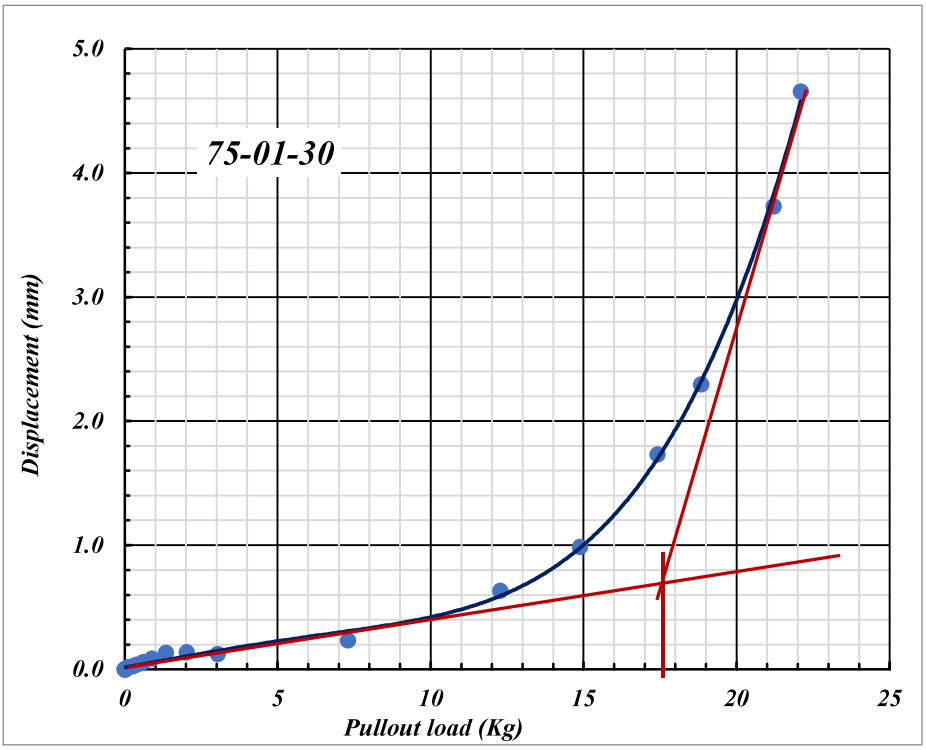

Fig. 5.27: Load vs Axial Movement for 75 mm Square Plate with (H/B =1) at 30^0 inclination

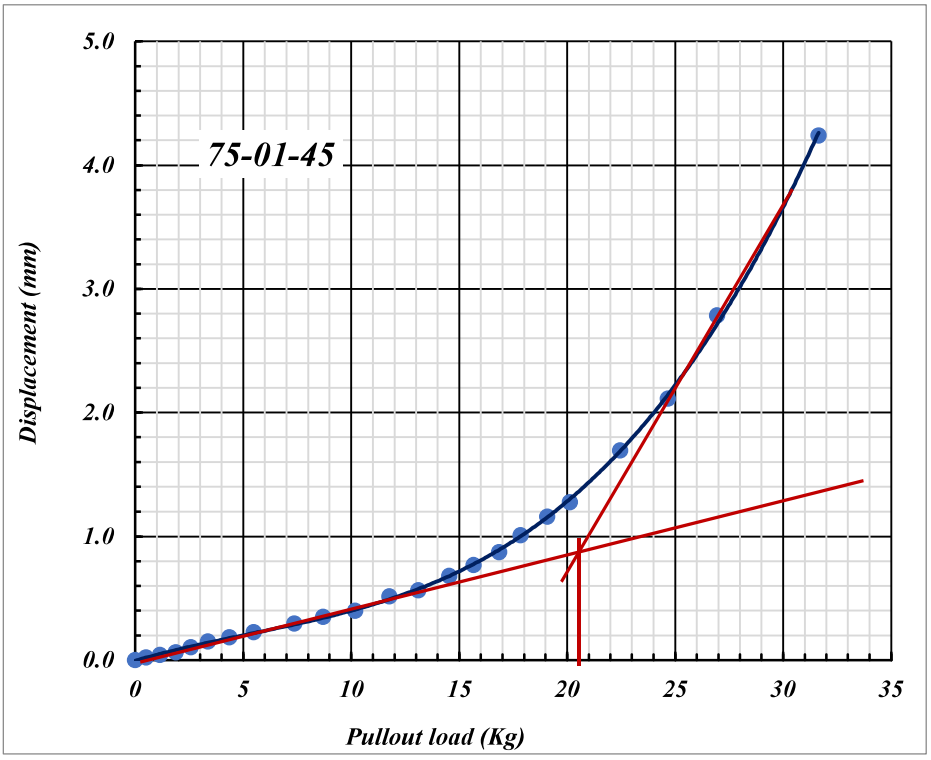

Fig. 5.28: Load vs Axial Movement for 75mm Square Plate with (H/B =1) at 45^0 inclination

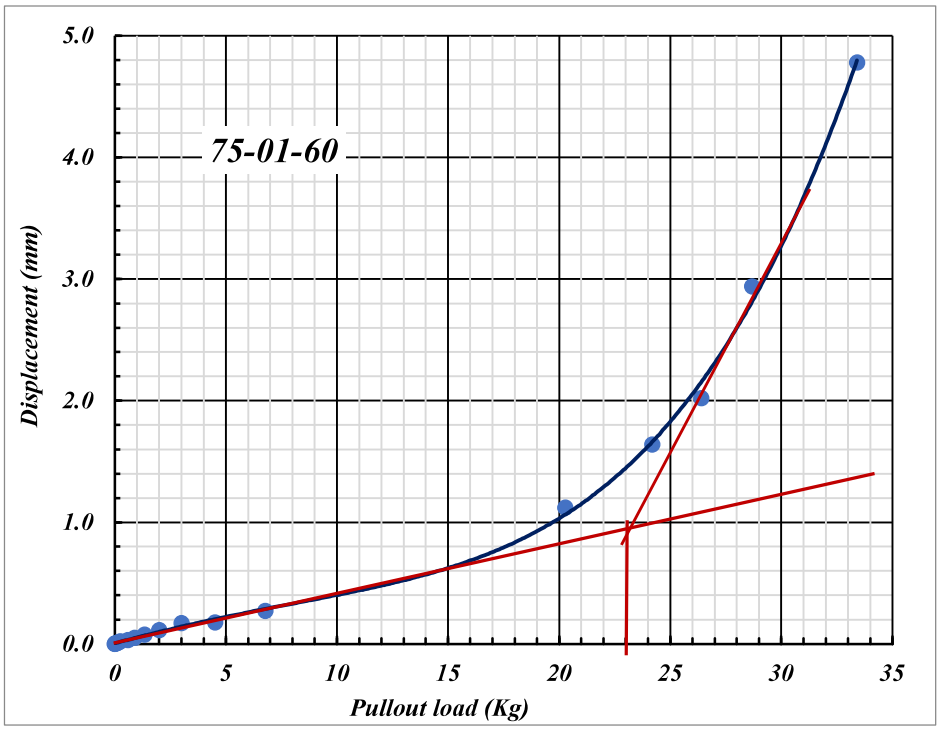

Fig. 5.29: Load vs Axial Movement for 75mm Square Plate with (H/B =1) at 60^0 inclination

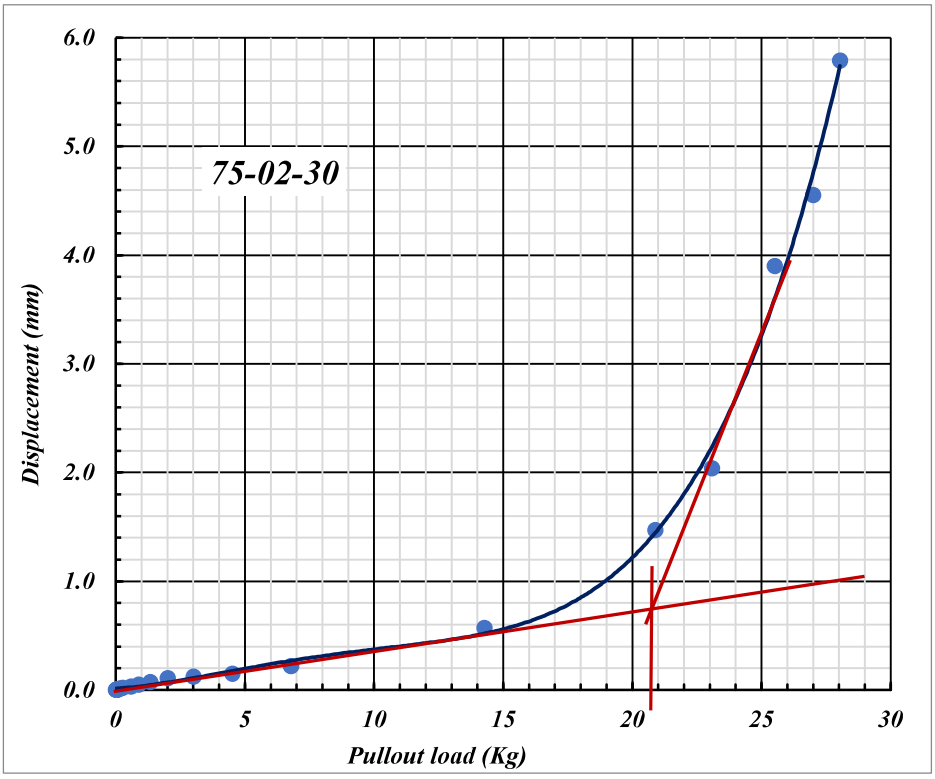

Fig. 5.30: Load vs Axial Movement for 75mm Square Plate with (H/B =2) at 30^0 inclination

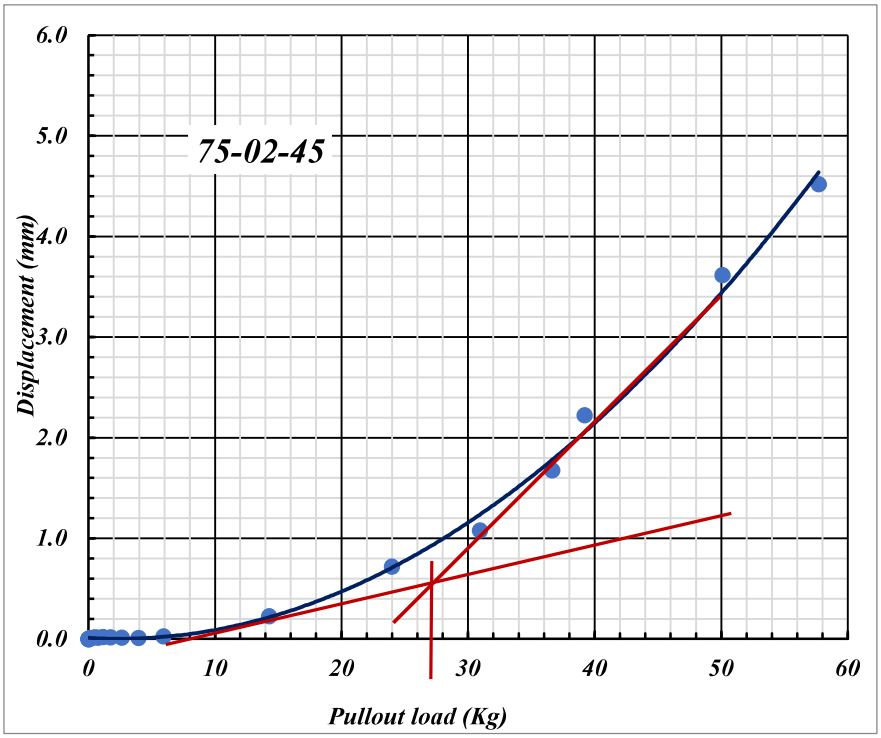

Fig. 5.31: Load vs Axial Movement for 75mm Square Plate with (H/B =2) at 45^0 inclination

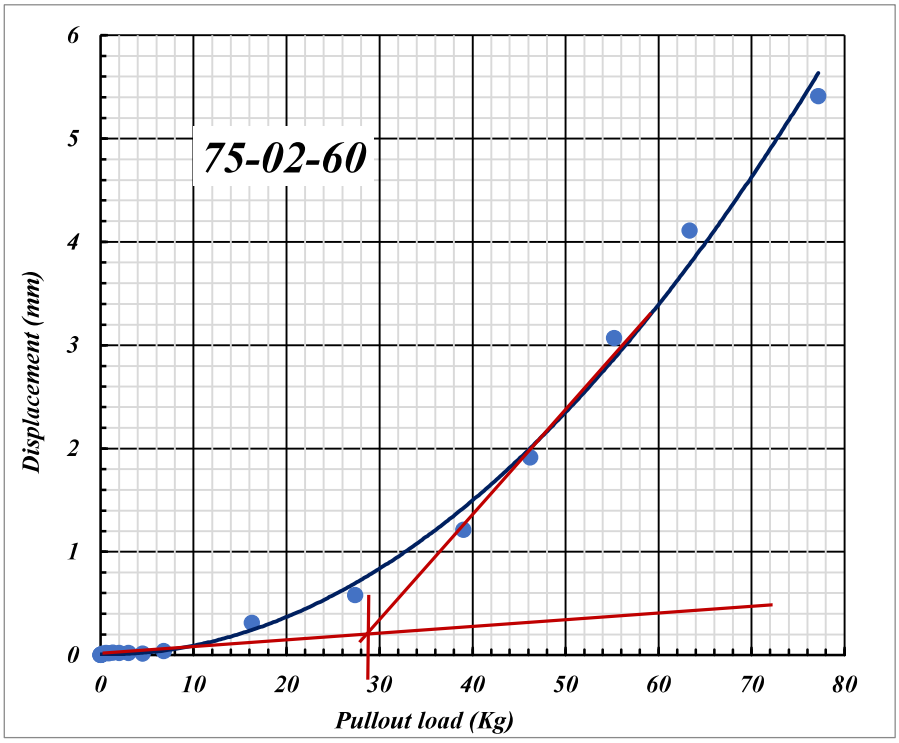

Fig. 5.32: Load vs Axial Movement for 75mm Square Plate with (H/B =2) at 60^0 inclination

ANNEXURE -VII

PRESENTATION OF RESULTS OF EXPERIMENTAL STUDY (STATIC REINFORCED)

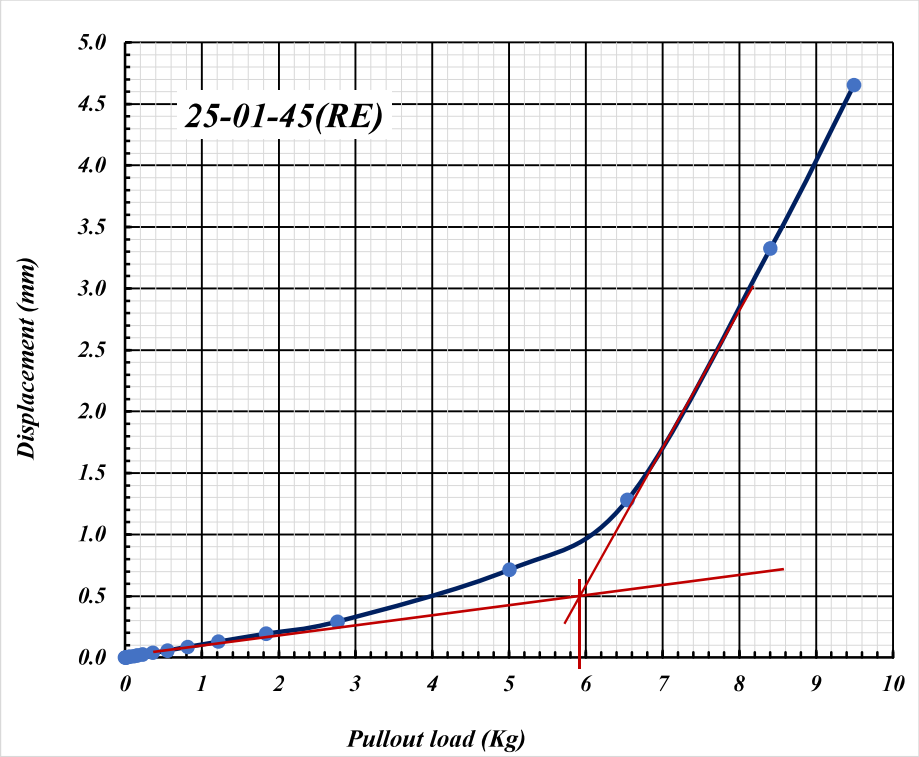

Fig. 5.35: Load vs Axial Movement for 25 mm Square Plate with (H/B =1) at 45^0 inclination

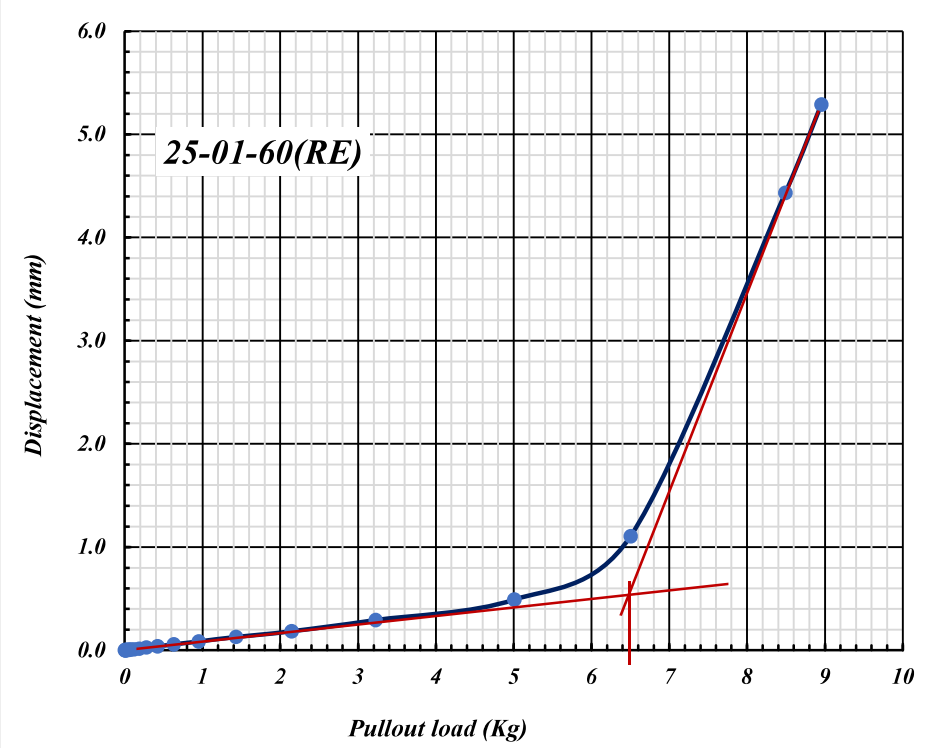

Fig. 5.36: Load vs Axial Movement for 25 mm Square Plate with (H/B =1) at 60^0 inclination

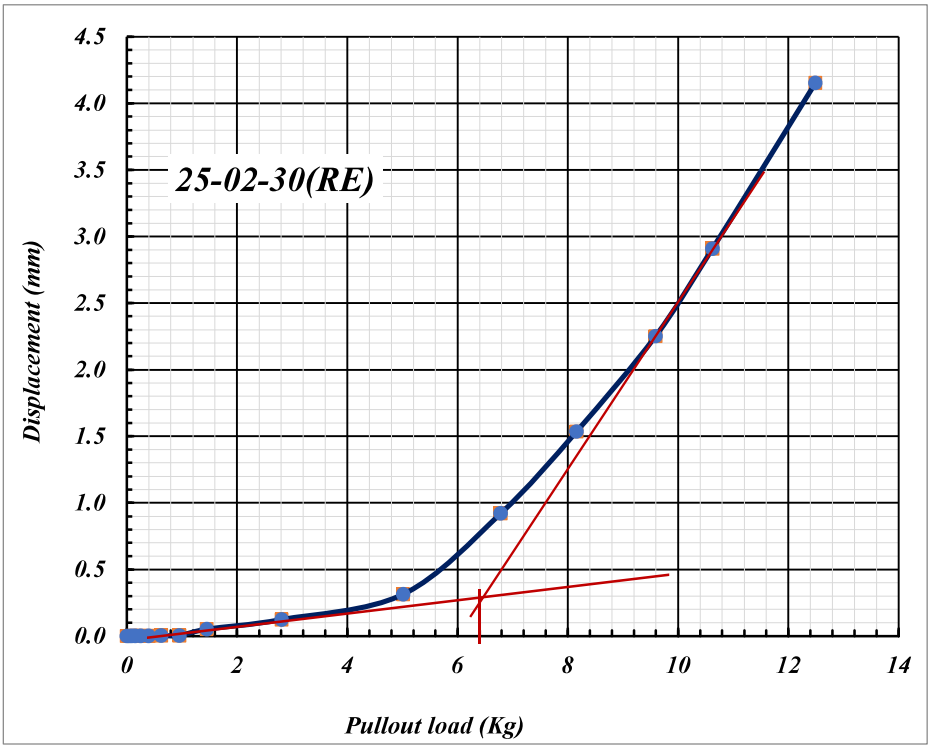

Fig. 5.37: Load vs Axial Movement for 25 mm Square Plate with (H/B =2) at 30^0 inclination

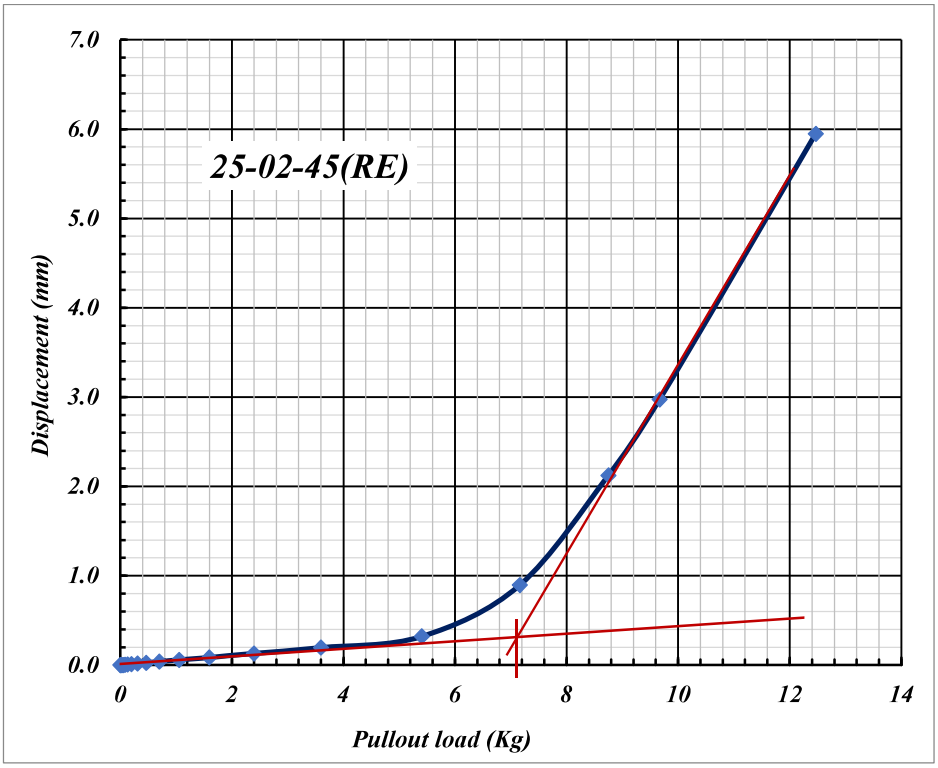

Fig. 5.38: Load vs Axial Movement for 25 mm Square Plate with (H/B =2) at 45^0 inclination

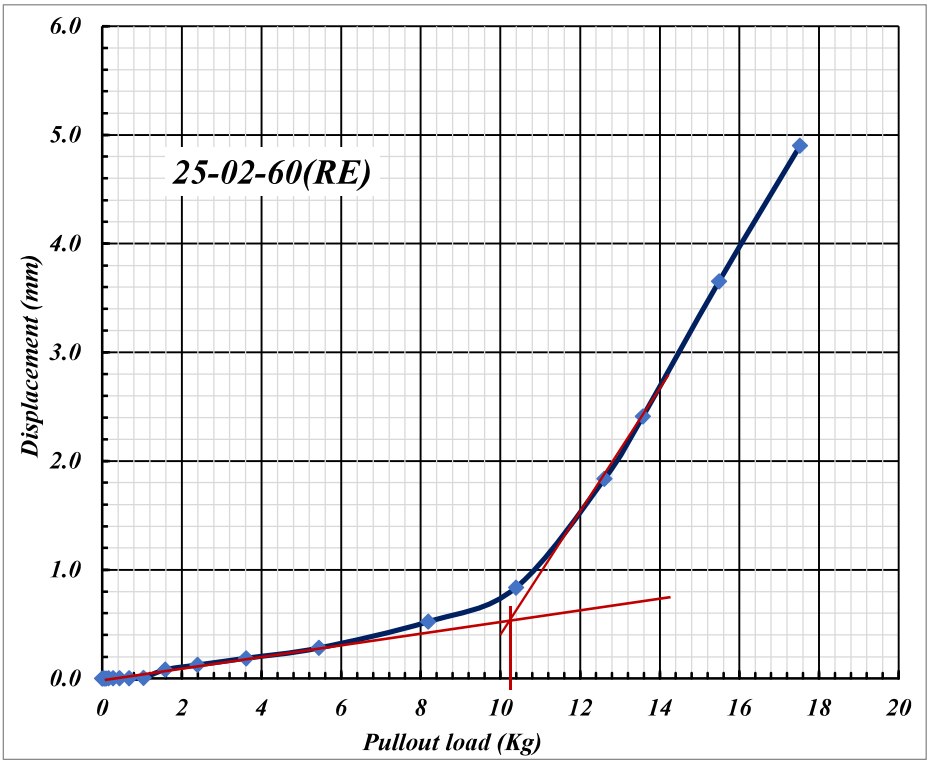

Fig. 5.39: Load vs Axial Movement for 25 mm Square Plate with (H/B =2) at 60^0 inclination

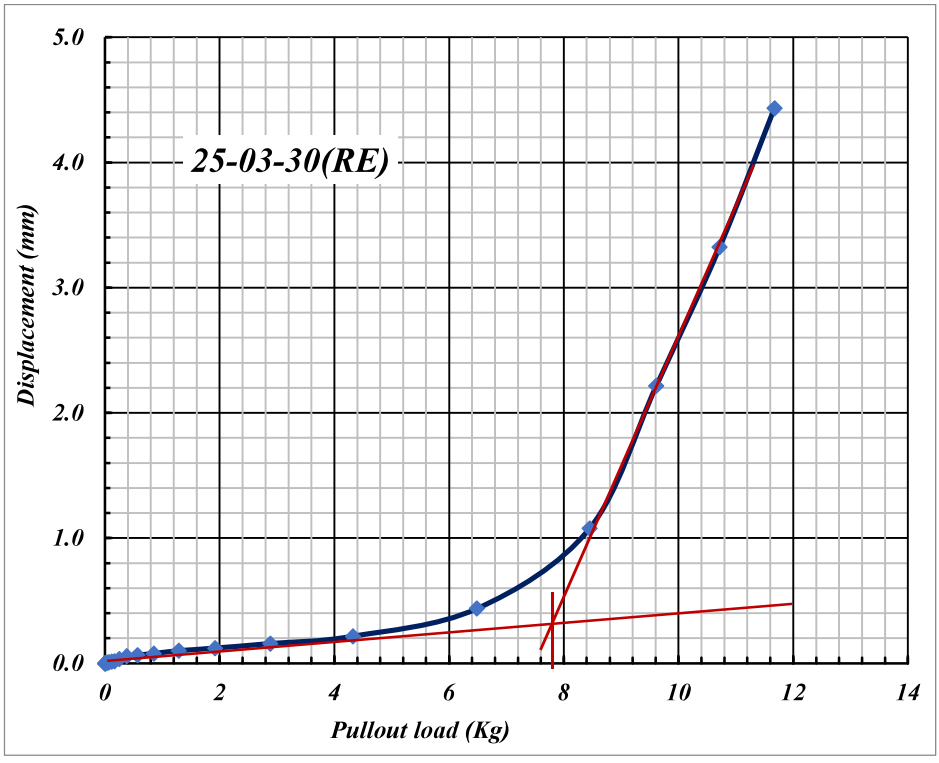

Fig. 5.40: Load vs Axial Movement for 25 mm Square Plate with (H/B =3) at 30^0 inclination

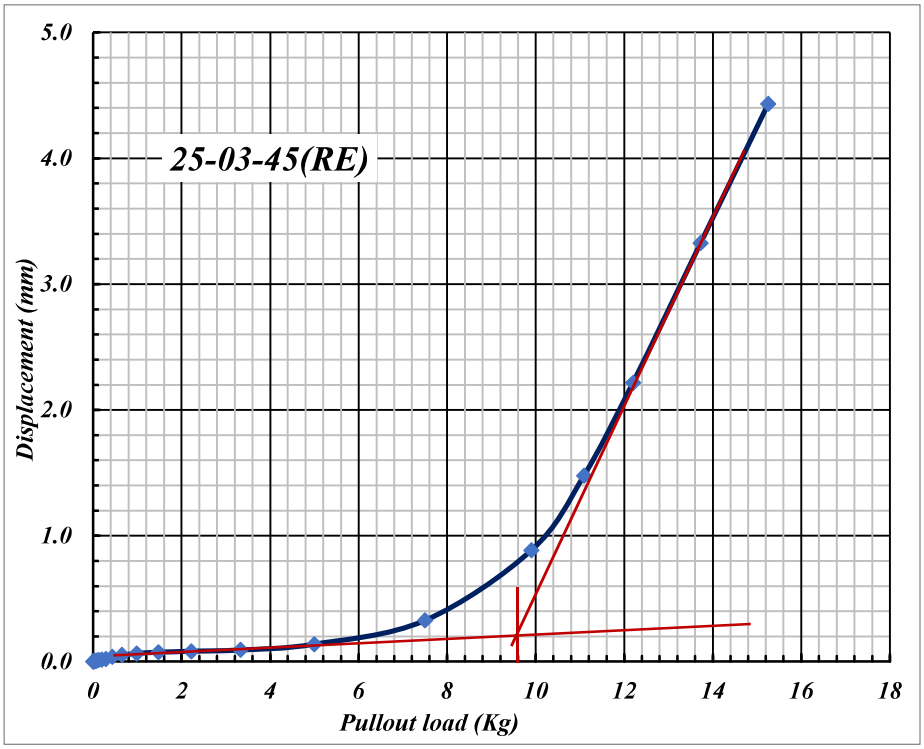

Fig. 5.41: Load vs Axial Movement for 25 mm Square Plate with (H/B =3) at 45^0 inclination

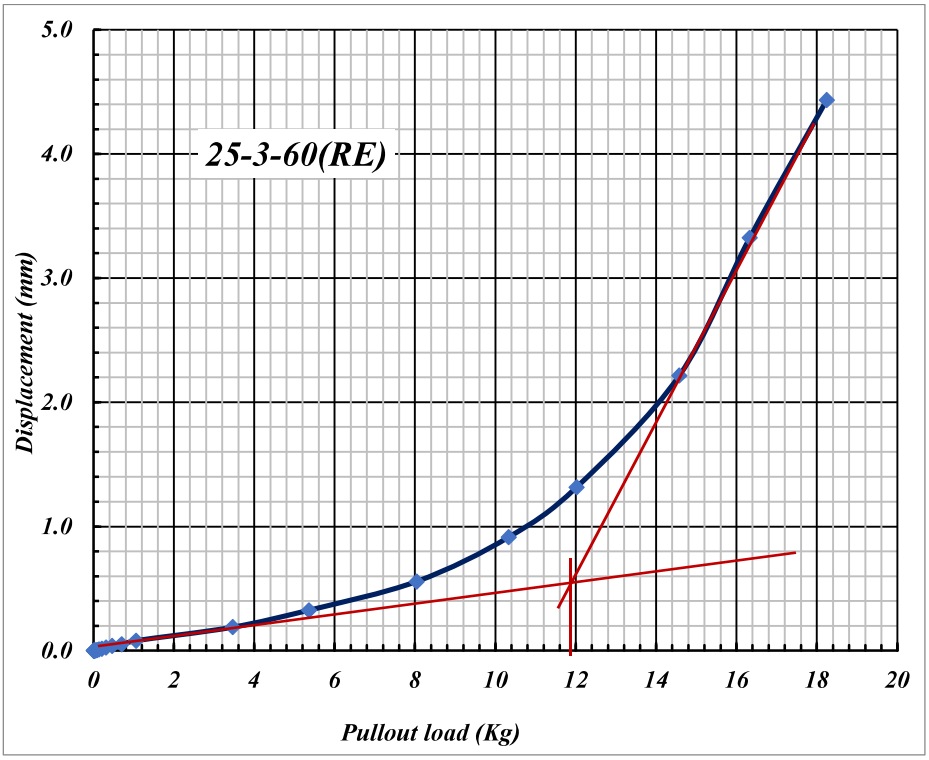

Fig. 5.42: Load vs Axial Movement for 25 mm Square Plate with (H/B =3) at 60^0 inclination

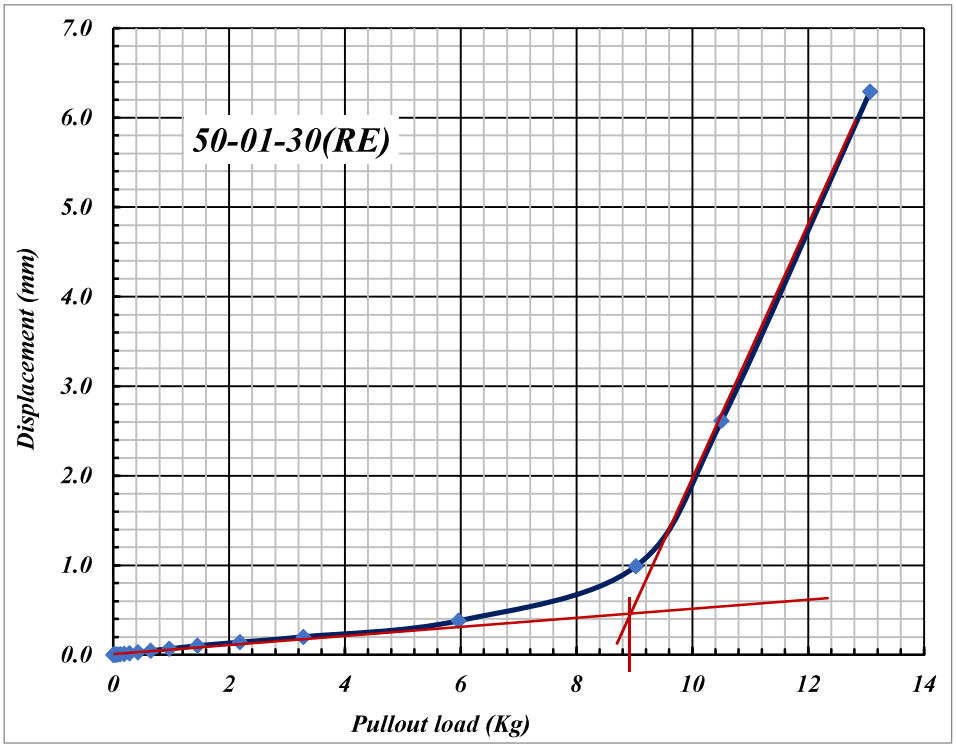

Fig. 5.43: Load vs Axial Movement for 50 mm Square Plate with (H/B =1) at 30^0 inclination

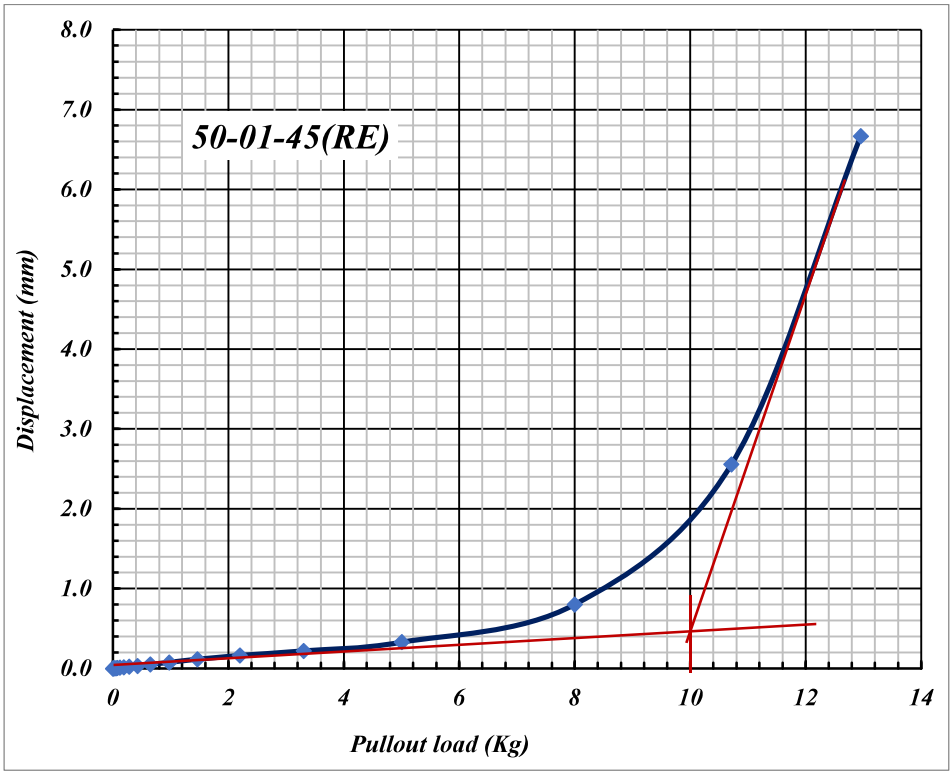

Fig. 5.44: Load vs Axial Movement for 50 mm Square Plate with (H/B =1) at 45^0 inclination

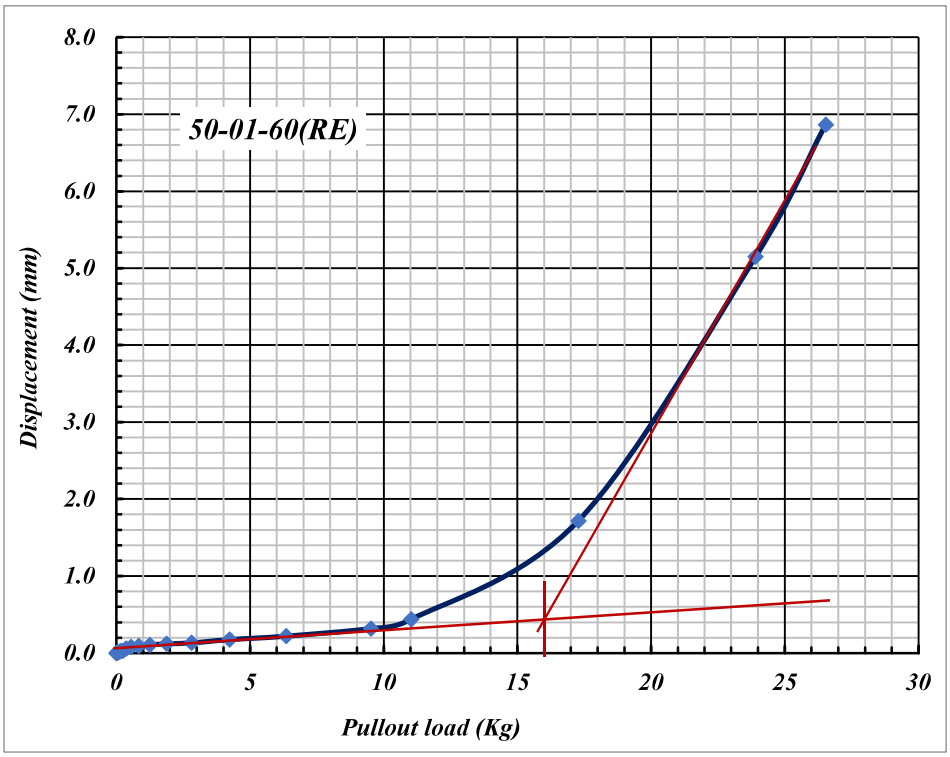

Fig. 5.45: Load vs Axial Movement for 50 mm Square Plate with (H/B =1) at 60^0 inclination

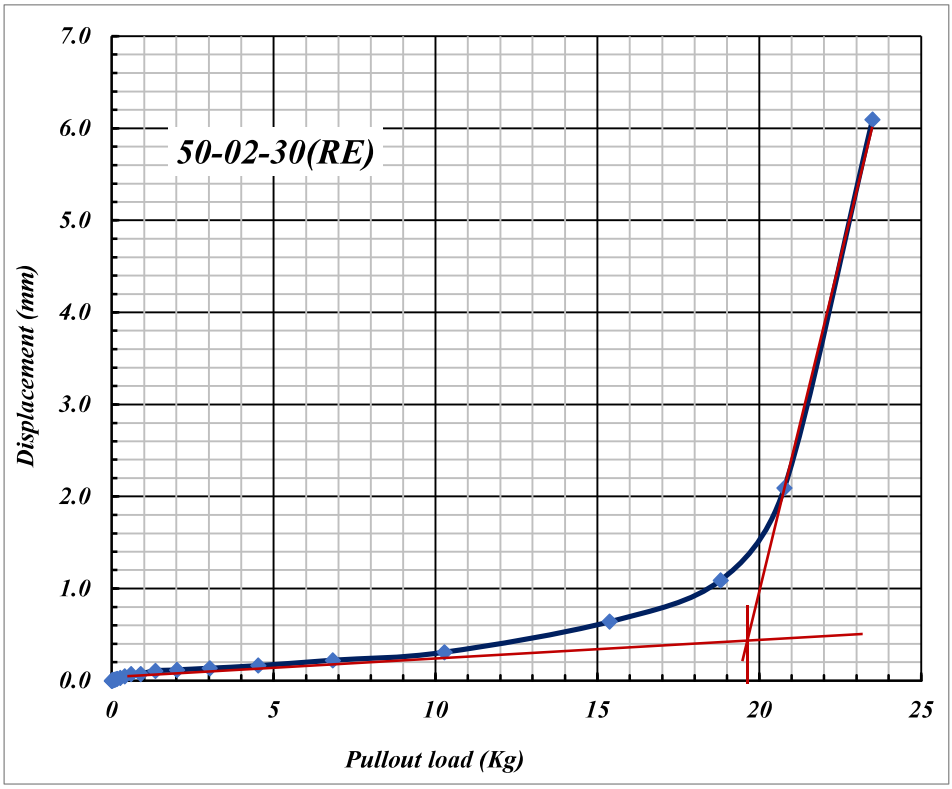

Fig. 5.46: Load vs Axial Movement for 50 mm Square Plate with (H/B =2) at 30^0 inclination

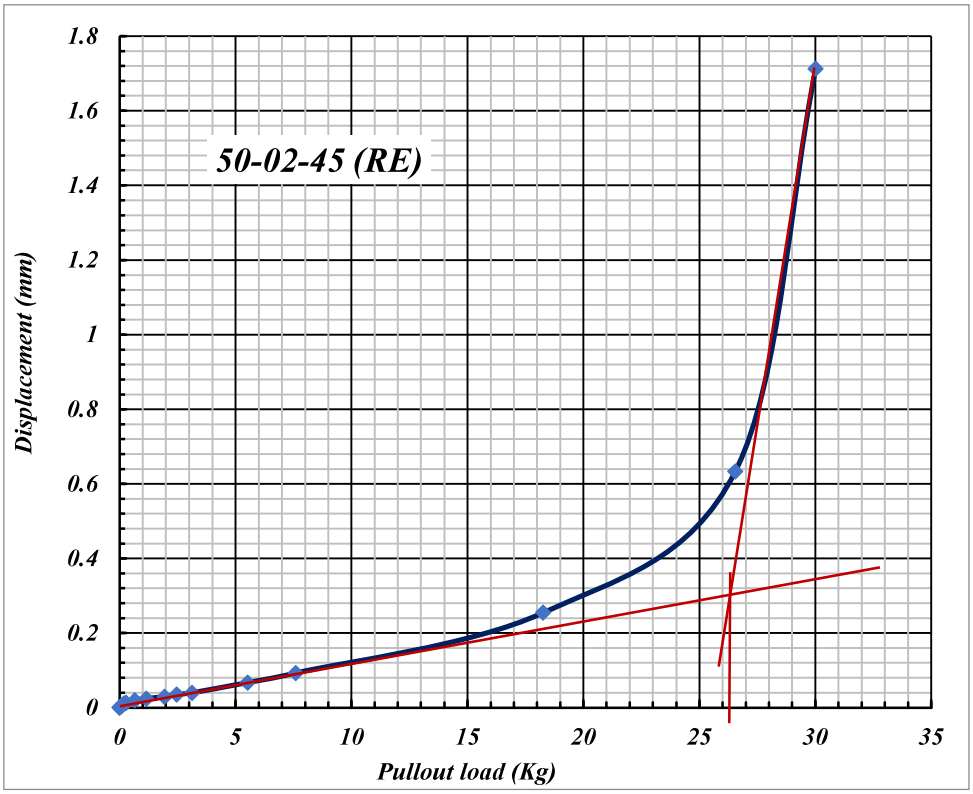

Fig. 5.47: Load vs Axial Movement for 50 mm Square Plate with (H/B =2) at 45^0 inclination

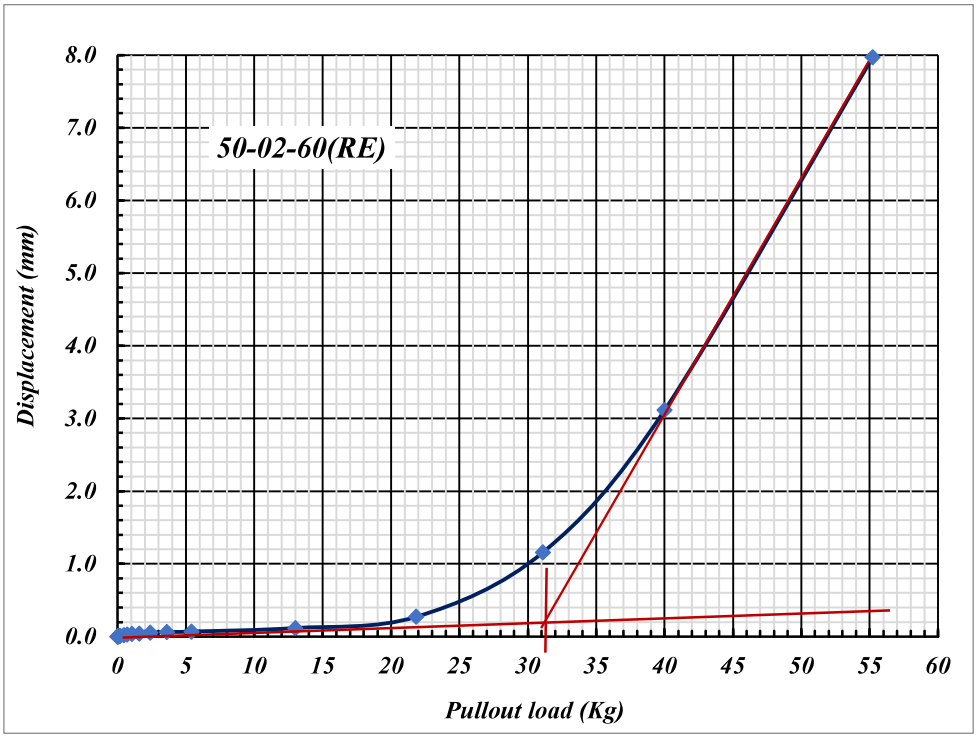

Fig. 5.48: Load vs Axial Movement for 50 mm Square Plate with (H/B =2) at 60^0 inclination

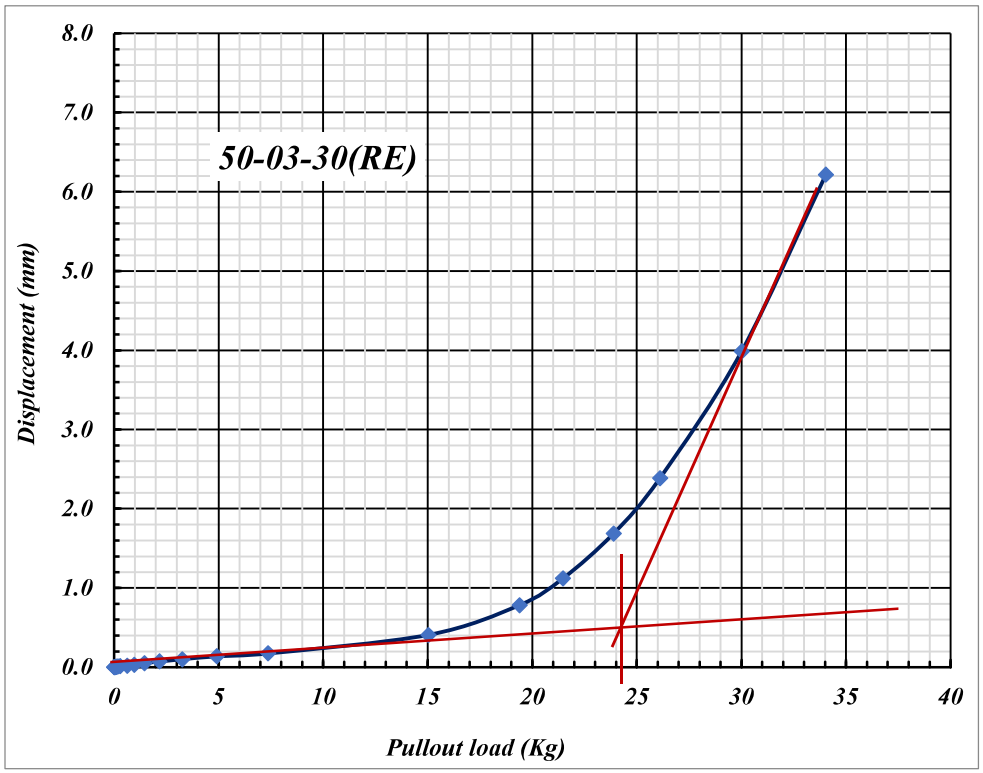

Fig. 5.49: Load vs Axial Movement for 50 mm Square Plate with (H/B =3) at 30^0 inclination

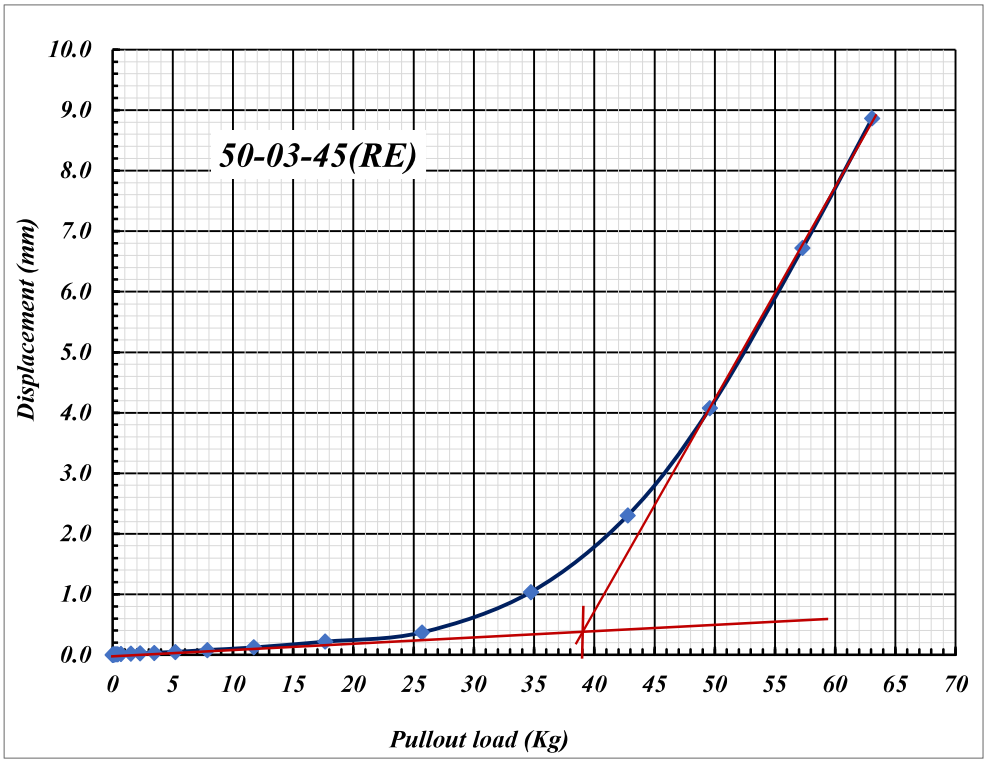

Fig. 5.50: Load vs Axial Movement for 50 mm Square Plate with (H/B =3) at 45^0 inclination

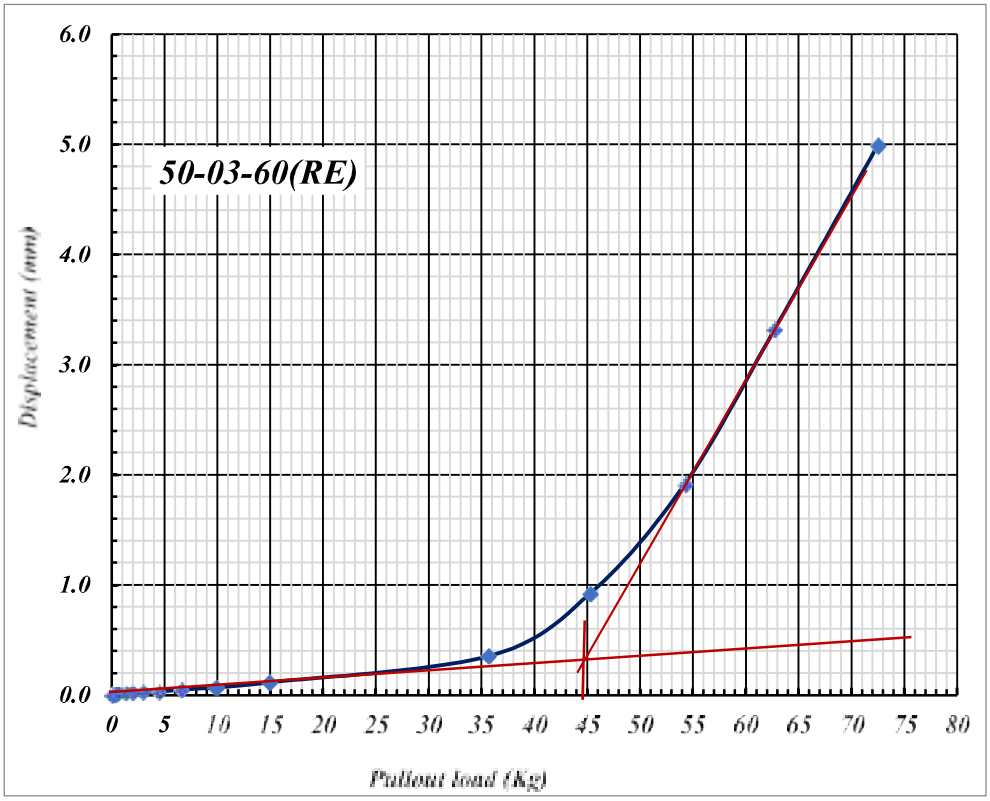

Fig. 5.51: Load vs Axial Movement for 50 mm Square Plate with (H/B =3) at 60^0 inclination

Arunashis Majumder
03/07/2024

Professor (Retd.)
CIVIL ENGINEERING DEPARTMENT
JADAVPUR UNIVERSITY
KOLKATA - 700 032

Associate Professor
Department of Civil Engineering
Jadavpur University
Kolkata-700 032

03/07/24

Dr. SUBHADEEP BANERJEE
Professor
Department of Civil Engineering
Indian Institute of Technology Madras
Chennai - 600 036